ZBORNIK RADOVA
CONFERENCE PROCEEDINGS

MATRIB 2006

HOTEL POSEJDON, VELA LUKA
OTOK / ISLAND KORČULA, HRVATSKA
22-24. lipnja / June 2006.

ORGANIZATORI / ORGANIZED BY:

HRVATSKO DRUŠTVO ZA MATERIJALE I TRIBOLOGIJU
CROATIAN SOCIETY FOR MATERIALS AND TRIBOLOGY
INSTITUTE OF MATERIALS AND MACHINE MECHANICS
(SLOVAK ACADEMY OF SCIENCES)
DUBLIN INSTITUTE OF TECHNOLOGY

SPONZORI / SPONZORS:

MINISTARSTVO ZNANOSTI OBRAZOVANJA I ŠPORTA
MINISTARSTVO ZAŠTITE OKOLIŠA, PROSTORNOG
UREĐENJA I GRADITELJSTVA
MINISTARSTVO GOSPODARSTVA, RADA I PODUZETNIŠTVA
INA INDUSTRIJA NAFTE – ZAGREB
PLINACRO d.o.o. - ZAGREB
PROPLIN o.o.o. - ZAGREB
AVE Automatska vrata d.o.o. - ZAGREB

IZDAVAČ / PUBLISHER:
Hrvatsko društvo za materijale i tribologiju
Croatian Society for Materials and Tribology
c/o FSB, Ivana Lučića 5, 10000 Zagreb
tel.: +385 1 61 68 389; fax: +385 1 61 57 126
e-mail: hdmt@fsb.hr, http://www.fsb.hr/hdmt

UREDNIK / EDITOR:
Krešimir Grilec

CIP - Katalogizacija u publikaciji
Nacionalna i sveučilišna knjižnica - Zagreb

UDK 620.1(063)(048)
621.89(063)(048)

SAVJETOVANJE o materijalima, tehnologijama, trenju i trošenju (11 ; 2006 ; Vela Luka)
MATRIB 2006, Vela Luka, 22. - 24. lipnja 2006. : zbornik sažetaka = abstracts book / organizatori Hrvatsko društvo za materijale i tribologiju = Croatian Society for Materials and Tribology, Dublion Institute of Technology, Institut of Materials and Machine Mechanics (Slovak Academy of Sciences) ; <urednik Krešimir Grilec>. - Zagreb : Hrvatsko društvo za materijale i tribologiju, 2006.

Tekst na hrv. ili engl. jeziku.

ISBN 953-7040-10-0
I. Materijali -- Ispitivanje -- Zbornik sažetaka
II. Tribologija -- Zbornik sažetaka

460609104

Svi radovi su tiskani u izvornom obliku.
All papers are printed in their original form

NAKLADA / ISSUE:
150

TISAK / PRINT:
Logo-press d.o.o., Zagreb

ORGANIZATOR / ORGANIZED BY:
HRVATSKO DRUŠTVO ZA MATERIJALE I TRIBOLOGIJU
CROATIAN SOCIETY FOR MATERIALS AND TRIBOLOGY
c/o FSB, Ivana Lučića 5, 10000 Zagreb
tel.: +385 1 61 68 581; fax: +385 1 61 57 126
e-mail: hdmt@fsb.hr, http://www.fsb.hr/hdmt
DUBLIN INSTITUTE OF TECHNOLOGY
INSTITUTE OF MATERIALS AND MACHINE MECHANICS
(SLOVAK ACADEMY OF SCIENCES)

SPONZORI / SPONSORS:
MINISTARSTVO ZNANOSTI OBRAZOVANJA I ŠPORTA
MINISTARSTVO ZAŠTITE OKOLIŠA, PROSTORNOG UREĐENJA I GRADITELJSTVA
MINISTARSTVO GOSPODARSTVA, RADA I PODUZETNIŠTVA
INA INDUSTRIJA NAFTE – ZAGREB
PLINACRO d.o.o. - - ZAGREB
PROPLIN d.o.o. - ZAGREB
AVE Automatska vrata d.o.o. - ZAGREB

ORGANIZACIJSKI ODBOR / ORGANIZING COMMITTEE:
Krešimir Grilec (Zagreb) - predsjednik / president
Darko Andreis (Vela Luka)
Denis Andreis (Vela Luka)
Suzana Jakovljević (Zagreb)
Dario Karlovčan (Zagreb)
Ivan Kramer (Zagreb)
Josip Lovričević (Vela Luka)
Željko Maričić (Vela Luka)
Gojko Marić (Zagreb)
Gorki Miletić (Vela Luka)
Želimir Oršanić (Zagreb)
Dinko Prižmić (Vela Luka)
Danko Žuvela (Vela Luka)
Krešo Žuvela (Vela Luka)

PROGRAMSKI ODBOR / PROGRAMME COMMITTEE:
Vinko Ivušić (Zagreb) – predsjednik / president
Tomislav Filetin (Zagreb)
Mladen Franz (Zagreb)
Maurice Grech (Msida, Malta)
Jaroslav Jerz (Bratislava, Slovak Republic)
David Kennedy (Dublin, Ireland)
Zoran Kožuh (Zagreb)
Slobodan Kralj (Zagreb)
Jan Meneve (Mol, Belgium)
Vedran Mudronja (Zagreb)
Ljiljana Pedišić (Zagreb)
Zdravko Schauperl (Zagreb)
František Simančik (Bratislava, Slovak Republic)
Ivo Štepanek (Pilsen, Czech Republic)
Toma Udiljak (Zagreb)
Dražen Živković (Split)

SADRŽAJ

DJELOVANJE EKOLOŠKIH INHIBITORA NA BRZINU KOROZIJE UGLJIČNOG ČELIKA U MORSKOJ VODI

V.Alar, I.Juraga, F.Kapor, V.Rede

Sažetak

U ovom radu istraživano je djelovanje inhibitora: Na- benzoata, Ca-glukonata i VCI 645 na brzinu korozije ugljičnog čelika u umjetnoj morskoj vodi. Djelotvornost inhibitora ispitana je elektrokemijskom metodom. Koristeći metodu Tafelove ekstrapolacije, određeni su sljedeći parametri: korozijski potencijal (E_{kor}), gustoća korozijske struje (j_{kor}), nagibi Tafelovih pravaca (b_a i b_k), te djelotvornost inhibitora (z).

Rezultati provedenog istraživanja ukazuju na mogućnost usporenja brzine korozije ugljičnog čelika u morskoj vodi primjenom ekoloških inhibitora.
Najveću djelotvornost pokazao je isparljivi inhibitor VCI 645.

Ključne riječi: korozija, inhibitor, ugljični čelik

UVOD

Unatoč relativno ograničenoj korozijskoj otpornosti, ugljični čelik je značajan konstrukcijski materijal (85% ukupne proizvodnje čelika). U velikim količinama se upotrebljava u pomorstvu, nuklearnim elektranama, petrokemijskoj proizvodnji i rafinaciji, cjevovodima, kemijskoj industriji, rudarstvu, te opremi za građevinarstvo i obradu metala. Iako je došlo do značajnog razvoja korozijski otpornih legura u posljednjih par desetljeća, ugljični čelik je najisplativiji, te je čak 3 do 5 puta jeftiniji od nehrđajućeg čelika.

Kada je morska voda u kontaktu s ugljičnim čelikom korozija je ubrzana. Da bi usporili brzinu korozije danas se sve više primjenjuju inhibitori. To su anorganske i organske tvari koje više ili manje usporavaju tijek korozijskih procesa. Svi ti spojevi, bez obzira da li se upotrebljavaju u otvorenim ili zatvorenim sustavima prema okolišu, prije ili kasnije dolaze u vodene tokove, rijeke, jezera i mora. Inhibitroske specije selektivno djeluju s obzirom na kemijski sastav i pH korozivne otopine, te vrstu metala ili legura. Velike količine inhibitora se primjenjuju u neutralnim otopinama, npr. u rashladnim sustavima, izmjenjivačima topline, te vodi u raznim granama industrije koja općenito sadrži otopljene soli , organske tvari i plinove, te ima pH neutralan ili slabo lužnat. Često prisutan kalcij hidrogenkarbonat stvara teško topive taloge kalcij karbonata koji utječe na djelovanje inhibitora. Inhibitori znatno smanjuju brzinu i učinak korozije na razne konstrukcijske materijale. Uspješno se mogu primjeniti kromati, nitriti i fosfati, međutim u novije vrijeme njihova upotreba je potpuno zabranjena zbog toksičnosti, rezistentnosti u vodenim tokovima ili što uzrokuju eutrofikaciju, tj. nagli rast nižih biljnih organizama, bakterija i alga, te tako onečušćuju velike vodene površine i obale rijeka i mora.

U ovom radu istraživanja su usmjerena na ispitivanje učinkovitosti djelovanja kemijskih spojeva niske toksičnosti i velike mogućnosti biorazgradnje. U tu svrhu ispitani su inhibitori Na-benzoat, Ca-glukonat i VCI (isparljivi inhibitor) na brzinu korozije ugljičnog čelika u morskoj vodi.

INHIBITORI

Inhibitori mogu smanjiti brzinu korozije na jedan ili više načina, ovisno kako utječu na pojedine elementarne reakcije u procesu korozije, što ovisi o vrsti metala i korozivnoj sredini. U približno neutralnoj sredini (pH= 5-9) za željezo i ugljični čelik je dominantan katodni proces redukcije kisika, te je prema tome brzina korozije pod utjecajem brzine prijenosa kisika prema površini metala.

Inhibitori su općenito klasificirani kao adsorpcijski ili stvaraoci filma; anodni, katodni ili miješani; sigurni ili opasni (dodani u premaloj količini za učinkovitu zaštitu uzrokuju lokalna oštećenja, najčešće rupičastu koroziju), oksidirajući ili neoksidirajući, organski ili anorganski. Navedene podjele jedna drugu ne isključuju. Najčešće se inhibitori ispituju s obzirom da li utječu na anodni ili katodni proces korozije. Stvaranje pasivnog filma na površini željeza i čelika pospješuju anodni inhibitori i tako sprečavaju anodno otapanje metala. Njihovo pasivirajuće djelovanje je popraćeno visokim vrijednostima korozijskog potencijala, reda veličine od 0 do – 250 mV (SCE). Anodni inhibitori mogu biti oksidirajući ili neoksidirajući već prema tome da li zahtjevaju prisutnost kisika u otopini da bi se razvio pasivitet. Među najpoznatijim anodnim inhibitorima su kromati i nitrati. Anodni inhibitori omogućuju stvaranje ili pomažu održavanje već stvorenog pasivnog filma na željezu da ne dođe do njegova razaranja putem loma u odsutnosti inhibitora na mjestima defekata rešetke Fe_2O_3 uz katodnu redukciju kisika. Može se zaključiti da se pasivni sloj također održava primjenom inhibitora koji osiguravaju zatvaranje inicijalno nastalih pora u oksidnom sloju bilo putem adsorpcije na ta aktivna mjesta, metala izloženog agresivnoj otopini, bilo netopivih spojeva inhibitorskog aniona i željeznih kationa. Najčešće su to Fe^{3+} ioni.

U neutralnim otopinama uz prisutnost kisika brzina korozije je određena brzinom redukciije kisika. Uloga katodnih inhibitora je smanjiti brzinu tog procesa stvaranjem netopivog sloja na površini, mnogo veće debljine od pasivnog, što onemogućava transport kisika prema površini. Netopivi slojevi se mogu stvarati reakcijom tvari iz otopine na površini metala nakon čega slijedi taloženje. Često se odvija više istovremenih procesa. Među katodnim inhibitorima najčešće se upotrebljavaju cinkove soli koje se talože kao cinkov hidroksid na katodnim mjestima površine metala, te fosfati koji stvaraju talog cink fosfata zaštitnih svojstava.

EKOLOŠKI NEPODOBNI INHIBITORI

Međunarodna tijela za kontrolu onečišćenja okoliša daju norme za primjenu inhibitora korozije sa naznačenom gornjom granicom koncentracije kemijskih spojeva; npr. na listi SAD USEPA (The United States'Environmetal Protection Agency) među štetnim teškim metalima krom i cink imaju prvenstvo dok je na listi Europske ekonomske zajednice (EEC) iz 1976. godine dodan i molibden kao zagađivač. Anorganski spojevi teških metala su otrovni i ne razgrađuju se biološki te iz otpadnih voda dolaze ne samo u površinske već i u podzemne vode. Potrebno je ipak naglasiti da je njihova opasnost limitirana koncentracijom.

NETOKSIČNI INHIBITORI

Pri upotrebi inhibitora u prirodnim vodama potrebno je uzeti u obzir sadržaj kationa, naročito kalcija, ali i magnezija i ostalih iona obično prisutnih u manjim količinama od kalcija. Oni uglavnom doprinose činu zaštite, npr. taloženjem kalcija karbonata i uz inhibiciju fosfatima, kalcij fosfata. Stvoreni slabo topljivi talozi nisu međutim potpuno jednoličnog sastava, tj. nepropusni, te dolazi do korozije, naročito one lokalnog tipa. Sastav i struktura taloga su pod utjecajem promjene parametara blizu metalne površine, npr. u izmjenjivačima topline uslijed lokalnog povišenja temperature, što opet utječe na topljivost soli i pH, pa može dođi do taloženja. Kontrola procesa korozije i stvaranja netopivih taloga mora se provoditi istovremeno. Osim primarne netoksičnosti od kemikalija koje dolaze u vodene tokove traži se da se brzo biološki razgrađuju. U novije vrijeme razvijeni su isparljivi inhibitori VCI (Volatile corrosion inhibitor) na bazi organskih spojeva koji su manje toksični i ekološki prihvatljivi.

EKSPERIMENTALNI DIO

Istraživano je djelovanje ekoloških inhibitora i to:Na-benzoata, Ca-glukonata i VCI-645 inhibitora na brzinu korozije ugljičnog čelika oznake Č0361 (1.0038) u umjetnoj morskoj vodi. Učinkovitost djelovanja navedenih inhibitora na ugljični čelik ispitana je elektrokemijskim metodama potenciostatičke polarizacije, odnosno metodom Tafelove ekstrapolacije i mjerenjem promjene korozijskog potencijala u vremenu izlaganja uzoraka korozijskoj otopini s i bez inibitora. Metoda potenciostatičke polarizacije provedena je snimanjem polarizacijskih krivulja u području potencijala ± 250 mV od korozijskog potencijala, E_{kor}, brzinom promjene potencijala 1 mVs^{-1}. Primjenom metode Tafelove ekstrapolacije određeni su slijedeći parametri: korozijski potencijal, E_{kor}, gustoća korozijske struje, j_{kor}, nagibi Tafelovih pravaca (b_a i b_k), te djelotvornost inhibitora , z.

REZULTATI I RASPRAVA

Istraživanje inhibitorskog djelovanja na brzina korozije ugljičnog čelika u umjetnoj morskoj vodi provedeno je elektrokemijskom polarizacijskom metodom uz dodatak sva tri inhibitora u koncentraciji od 0.5%. Na **slici 1**. prikazane su polarizacijske krivulje ugljičnog čelika u umjetnoj morskoj vodi s i bez inhibitora. U **tablici 1.** prikazani su kinetički parametri dobiveni Tafelovom metodom ekstrapolacije te stupanj djelovanja inhibitora.

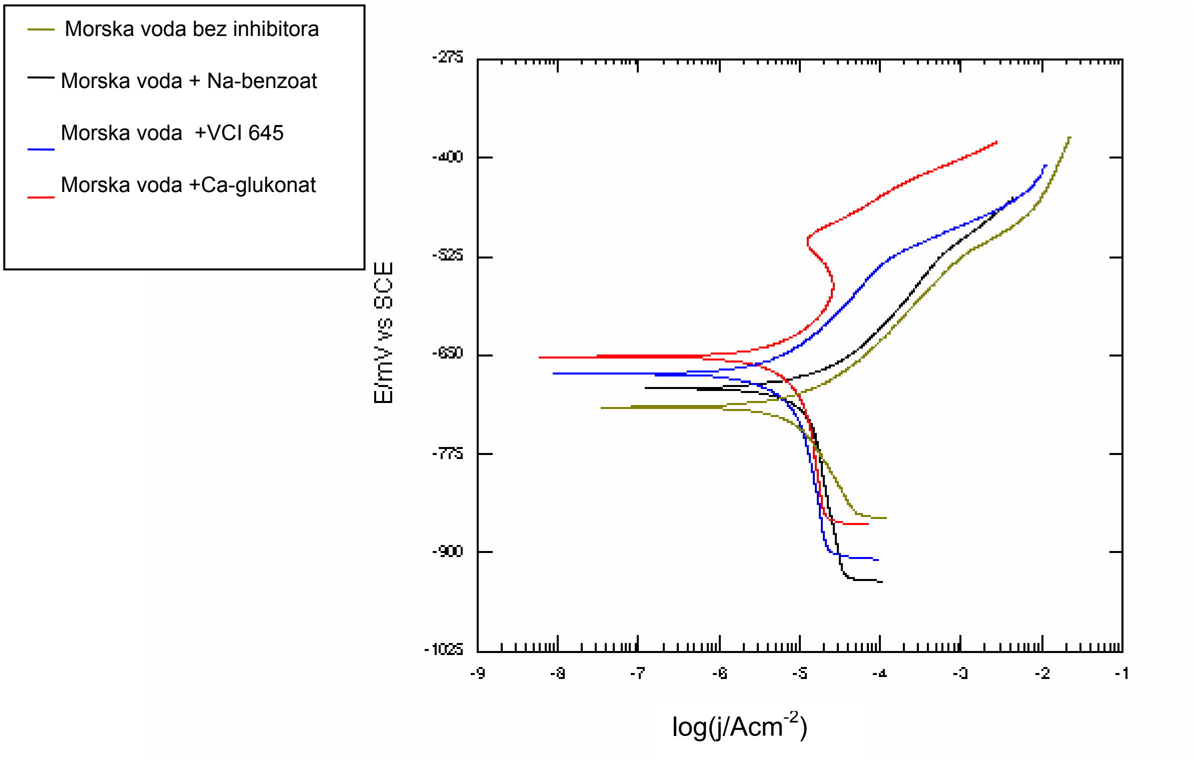

Slika 1. Polarizacijske krivulje ugljičnog čelika u umjetnoj morskoj vodi s i bez inhibitora.

Tablica 1. Usporedni prikaz korozijskih parametara ugljičnog čelika u umjetnoj morskoj vodi s i bez inhibitora.

Otopina	E_{kor}, mV	b_a, mVdek^{-1}	b_k, mVdek^{-1}	j_{kor}, μAcm^{-2}	Z,%
Morska voda bez inhibitora	-691	240	958	25.0	-
Morska voda s Na-benzoatom	-669	115	1000	23.8	4.8
Morska voda s VCI- 645 inhibitora	-653	144	870	11.7	53.2
Morska voda s Ca-glukonatom	-596	108	416	17.6	29.6

Na osnovu pregleda podataka iz literature i naših mjerenja učinkovitosti inhibicije elektrokemijskim metodama može se konstatirati da se organski inhibitori (VCI) mogu uspješno primjenjivati za zaštitu ugljičnog čelika u morskoj vodi.

ZAKLJUČCI

- Cilj ovog rada bio je ispitati djelotvornost različitih inhibitora na brzinu korozije ugljičnog čelika u umjetnoj morskoj vodi. Ispitivanja su provedena s Na-benzoatom, Ca-glukonatom i VCI-645 inhibitorom.
- Ispitivanja su provedena elektrokemijskom metodom linearne ekstrapolacije (Tafelove ekstrapolacije).
- Dobiveni rezultati metodom Tafelove ekstrapolacije pokazuju da najbolju djelotvornost na smanjenje brzine korozije pokazuje VCI inhibitor.
- Rezultati korozijskog potencijala E_{kor}, ovisno o vremenu pokazuju da Ca glukonat pomiče potencijal prema pozitivnijim vrijednostima.

11. Savjetovanje o materijalima, tehnologijama, trenju i trošenju
11. Conference on Materials, Processes, Friction and Wear
MATRIB'06, Vela Luka, 22-24.06.2006.

UTJECAJ STABILNOSTI SUSTAVA ZA OPTEREĆIVANJE NA REZULTATE UMJERAVANJA MJERILA SILE

THE INFLUENCE OF THE LOAD SYSTEM STABILITY ON THE FORCE MEASUREMENT RESULTS

Željko Alar, Mladen Franz, Tamara Aleksandrov
Sveučilište u Zagrebu, Fakultet strojarstva i brodogradnje
Ivana Lučića 5, 10000 Zagreb,
E-mail: zeljko.alar@fsb.hr;

Sažetak

Pri umjeravanju mjerila sile sustav za opterećivanje i prijenosni etaloni sile podvrgnuti su određenim okolišnim i radnim uvjetima koji tijekom ranog dana dovode do promjena njihovih karakteristika. Postavlja se pitanje da li je te promjene moguće procijeniti i uzeti u proračun ukupne mjerne nesigurnosti mjerenja dotičnog mjerila sile. U radu je provedeno praćenje promjena karakteristika kidalice EU-mod nazivne sile 400 kN tijekom jednog radnog dana. Ovo je provedeno kroz umjeravanje s prijenosnim etalonom sile klase 00 sukladno normi DIN EN ISO 7500-1 na početku, sredinom i na kraju radnog dana a u vremenu između ciklusa umjeravanja kidalica je bila konstantno u uporabi. Ovaj postupak je ponavljan više puta. Na temelju provedene analize dani su određeni zaključci.

Ključne riječi: sila, kidalica, prijenosni etalon sile, umjeravanje, mjerna nesigurnost

Abstract

During calibration of the force measuring equipment the travelling standards and the load system have been submitted to certain conditions which cause modification of their performances during the time. The question is, is it possible to evaluate those changes and include them in the calculation of the total measurement uncertainty. In this paper monitoring of the universal testing machine EU-40 mod characteristic variations during one day is carried out. Research is carried out on travelling force standard class 00 according to DIN EN ISO 7500-1 on the beginning, in the middle and at the end of the working day. Between the calibrations the universal testing machine was in frequently use. The procedure was repeated more than once. On the basis of the analysis certain conclusions are given.

Key words: force, universal testing machine, travelling standard, calibration, measurement uncertainty

1. UVOD

Mjerenje sile je osnova za određivanje mehaničkih svojstava nekog materijala ili proizvoda. Sila je matematički predstavljena kao vektor koji djeluje u određenoj točki, stoga mjerenje sile uključuje određivanje njene veličine i smjera djelovanja [1]. Samo ispitivanje sile provodi se na uređajima za mjerenje sile a najčešće su to kidalice različitih tipova i oblika. Tijekom uporabe ti uređaji gube na preciznosti a posljedice koje nastanu uporabom takovih uređaja mogu biti dalekosežne. Zbog toga se provodi sistematska periodična kontrola ili provjera (umjeravanjem) uređaja za mjerenje sile kroz jedno umjerno razdoblje, čija je najveća dopuštena vremenska granica propisana normama. Tijekom uporabe mjerila sile su izložena različitim utjecajima (okolišni uvjeti, djelovanje opterećenja, rukovanje više mjeritelja i itd.) što se kroz duži vremenski period odražava na njegova svojstva. Neki od ovih utjecaja su istraženi i dana je procjena te proračun njihova djelovanja na nesigurnost rezultata mjerenja sile. No neki još uvijek nisu u potpunosti istraženi te tako njihov utjecaj nije još kvantificiran.

Stanje mjerila sile odnosno kvaliteta njegova pokazivanja provjerava se umjeravanjem. Radni uvjeti pri umjeravanju i pri klasičnoj uporabi mjerila sile nisu identični. Oni se razlikuju po intenzitetu, vremenu trajanja, brzini prirasta opterećenja itd. Svakako bi tu treba uzeti u obzir i što se događa s mjerilom sile odnosno njegovim sustavom za očitanje prilikom loma ispitnog uzorka gdje se javlja udarno rasterećenja te koliko je vremena potrebno da se mjerilo smiri odnosno koliku pogrešku ćemo unijeti u slijedeće mjerenje ako odmah provodimo slijedeće mjerenje. Sve su to utjecaji koji djeluju na stabilnost mjerila sile i kao takvi stvaraju nesigurnosti mjernja sile. Ovomu još treba dodati da imamo različite sustave za opterećivanje i očitanje vrijednosti sile koji svakako različito reagiraju na pojedine ovakove uvjete pri mjerenjima.

Stoga je u ovom radu provedeno određeno istraživanje ponašanja univerzalne kidalice odnosno njene stabilnosti tijekom jednog radnog dana. Osnovna ideja je bila da se provode umjeravanje kidalice na početku radnog dana znači u hladnom stanju, u sredini i na kraju radnog dana. Cijelo vrijeme između faza umjeravanja kidalica je podvrgnuta opterećenjima od 50% do 90 % nazivne sile. Nakon dobivenih rezultata umjeravanja izvršena je analiza istih.

2. EKSPERIMENTALNI DIO

Eksperimentalna ispitivanja su provedena na kidalici EU 40/2 (slika 1) smještene u Laboratoriju za ispitivanje mehaničkih svojstava Fakulteta strojarstva i brodogradnje u Zagrebu. U tablica 1 dani su osnovni podaci o kidalici, okolišnim uvjetima te podaci o prijenosnom etalonu kojim je provedeno umjeravanje.

Umjeravanje je provodeno prema normama EN ISO 376 [2] i EN ISO 7500-1[3]. EN ISO 376 je norma po kojoj se provodi umjeravanje prijenosnih etalona sile koji se dalje koriste za umjeravanje kidalica. Kidalica EU 40/2 kao sastavni dio svog sustava za opterećivanje ima dinamometar preko kojeg se kontrolira opterećenje stoga je dio ispitivanja proveden sukladno EN ISO 376 normi. Norma EN ISO 7500-1 propisuje kako se provodi umjeravanje jednoosnih ispitnih kidalica za statička ispitivanja. Sam postupak umjeravanja sastoji se od postizavanja točno određenih induciranih sila, koje se očitavaju na uređaju za očitanje kidalice, a na prijenosnom etalonu se očitava deformacijska vrijednost X, mV/V koja odgovara stvarnoj vrijednosti koju je inicirala zadana poznata sila. Mjerenja su provedena prema slici 2, gdje je vidljivo da se provodi šest mjernih nizova (četiri pri porastu i dva pri opadanju vrijednosti sile).

Slika 1: Kidalica EU 40/2

Tablica 1: Osnovni parametri pri umjeravanju

Okolišni uvjeti:		
Temperatura	Tlak	Vlažnost
20 ± 1 °C	**1013 hPa**	**74% *rel.***
Kidalica:		
Tip	Mjerno područje	Rezolucija
EU 40/2	**0-400 kN**	**0,01 kN**
Prijenosni etalon:		
Mjerno pojačalo		*ML - 38*
Kabel	Dužina	**3 m**
	Priključak	**6 - žilni**
Očitavač		**AB12**
Dinamometar		
Tip	Mjerna sposobnost	Oznaka umjeravanja
Z4/400 kN	0,12 %	**0377 PTB 05**

Svaki mjerni niz sastoji se od pet mjernih točaka na kojima se očitava inicirana i stvarna vrijednost sile. Prva dva mjerna niza (X1, X2) su za slučaj kada se ne mijenja položaj prijenosnog etalona. Nakon toga se prijenosni etalon zakreće za 120^{o} i izmjeri se mjerni niz X3. Dostizanjem nazivne sile u nizu X3 nastavlja se mjerenje ali pod uvjetima opadajuće sile istim korakom, čime se dobije mjerni niz X4′. Sve to isto ponavlja za mjerne nizove X5 i X6′, s time da je prijenosni etalon sada zakrenut za 240^{o}.

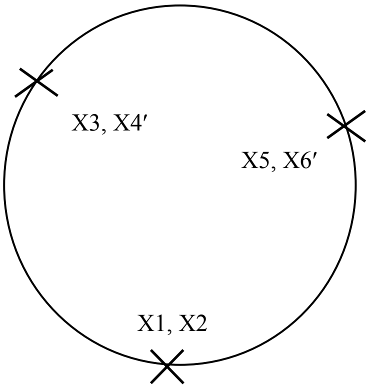

Slika 2: Raspored mjernih nizova pri umjeravanju kdalice [2]

Primjenom odgovarajućih izraza te statističkom obradom, provodi se usporedba dobivenih vrijednosti s poznatim uvedenim silama prilikom samog umjeravanja.

U jednom radnom danu provedena su četiri umjeravanja. Umjeravanja I i II su provedena na početku radnog dana i to jedno za drugim, a umjeravanja III i IV isto tako samo na kraju radnog dana. Između ove dvije grupe umjeravanja kidalica je bila konstantno opterećivana i rasterećivana u mjernom području između 50% i 90% nazivne sile u

vremenskom trajanju od četiri sata. S obzirom na obim posla koji je trebalo provesti u jednom radnom danu nije bilo moguće provesti umjeravanje u sredini radnog dana.
Kriteriji praćenja karakteristike kidalice bili su pogreške točnosti i ponovljivost rezultata pri istim i različitim ugradbenim položajima prijenosnog etalona sile te histerezna mjerenja. Izrazi za njihovo izračunavanje dani su u tablici 2. Sva mjerenja su provedena s relativnom mjernom nesigurnošću od 0,06%.

Tablica 2: Izrazi za izračunavanje pojedinih pogrešaka

Pogreške	Izraz
Relativna pogreška točnosti pri istim ugradbenim položajima	$q_{pon} = \frac{X_{sr-1,2} - X_{ref}}{X_{sr}} \times 100\ \%$
Relativna pogreška točnosti pri različitim ugradbenim položajima	$q_{rot} = \frac{X_{sr-1,3,5} - X_{ref}}{X_{sr}} \times 100\ \%$
Relativna pogreška ponovljivosti pri različitim ugradbenim položajima	$b = \frac{X_{\max} - X_{\min}}{X_r} \times 100\,\%$
Relativna pogreška ponovljivosti pri istim ugradbenim položajima	$b' = \frac{X_2 - X_1}{X_{wr}} \times 100\,\%$
Relativna pogreška histereznog mjerenja	$v = \frac{i' - i}{i} \times 100\,\%$

Tablica 3: Rezultati relativnih pogrešaka za sva četiri umjeravanja

Umjeravanje	*F*, kN	q_{rot}, %	q_{pon}, %	*b*, %	*b'*, %	*v*, %
I	80	-0,139	-0,151	0,019	0,016	0,54
	160	-0,110	-0,113	0,080	0,113	0,45
	240	-0,034	-0,036	0,052	0,054	0,39
	320	0,004	0,001	0,029	0,041	0,36
	400	0,048	0,044	0,023	0,016	-
II	80	-0,053	-0,151	0,062	0,012	0,46
	160	-0,052	-0,113	0,009	0,016	0,38
	240	0,012	-0,036	0,015	0,014	0,27
	320	0,047	0,001	0,019	0,008	0,33
	400	0,079	0,044	0,027	0,008	-
III	80	-0,195	-0,170	0,081	0,041	0,62
	160	-0,155	-0,130	0,081	0,033	0,54
	240	-0,104	-0,087	0,079	0,049	0,52
	320	-0,064	-0,041	0,077	0,028	0,46
	400	-0,020	-0,006	0,047	0,026	-
IV	80	-0,152	-0,140	0,063	0,059	0,57
	160	-0,105	-0,105	0,014	0,017	0,56
	240	-0,071	-0,077	0,035	0,022	0,56
	320	-0,033	-0,040	0,035	0,016	0,53
	400	0,006	0,001	0,037	0,003	-

3. ANALIZA REZULTATA

Na slici 3 prikazana je raspodjela svake pojedine karakteristike za četiri umjeravanja provedena u tijeku jednog radnog dana.

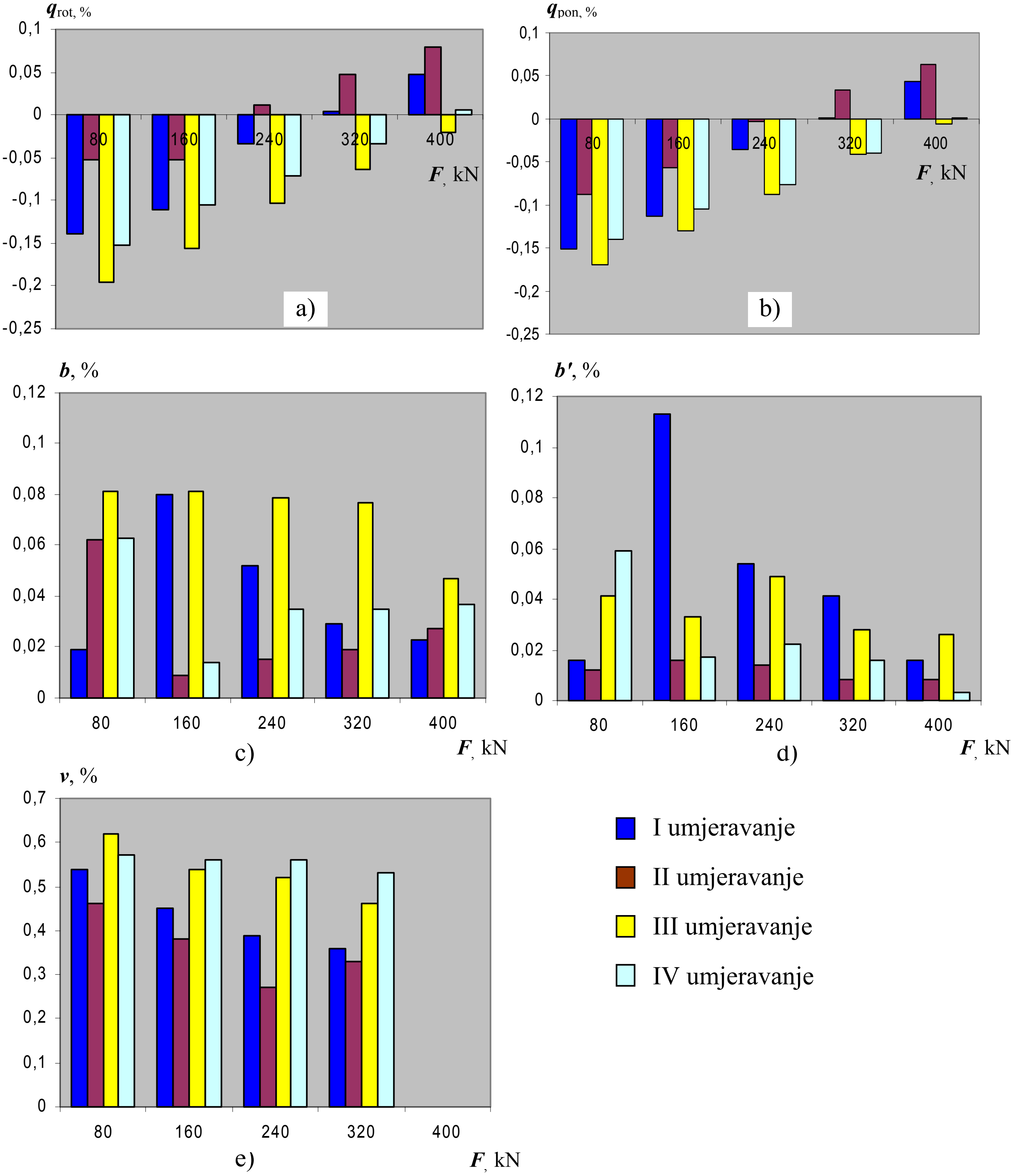

Slika 3: Prikaz rapodjele pogreške točnosti, ponovljivosti i histereze po mjernom području kidalice

Tijekom ispitivanja zamijećene su karakteristične pojave promjene pojedinih karakteristika. Sve relativne pogreške kidalice su u I umjeravanju veće nego u II što ukazuje da pri uprabi kidalice na početku radnog dana možemo unijeti znatnu pogrešku. Ova pojava je već od prije poznata [4] te je preporučljivo kidalicu prije uporabe pustiti da radi neko vrijeme (vrijeme ugrijavanja) te onda provesti opterećivanje do nazivne sile i to ponoviti više puta.

Općim pregledom svih dijagrama (slika 3) vidljivo je da III i IV umjeravanje imaju veće vrijednosti pogrešaka što nas dovodi do zaključka da sve karakteristike bivaju lošije nakon dugotrajnog rada kidalice.

Pogreška točnosti nakon dugotrajnog rada kidalice je u znatnom porastu i to znatno više kod rotiranog položaja prijenosnog etalona što je vidljivo porastom vrijednosti u III i IV nizu (slika 3a). Ovime proizlazi da nakon dugotrajnog rada dolazi do odmaka pokazivanja kidalice od stvarne (referentne) vrijednosti i to u značajnijem iznosu. U prosijeku to pogoršanje iznosi oko 0,1 %. Ovu pojavu bi svakako trebalo uzeti u obzir pri dugotrajnim mjerenjima. Također zanimljiva je progresija pogreške točnosti kroz mjerno područje jer poprima oblik pravca s određenim koeficijentom nagiba. Pogreška točnosti kod istog ali i kod rotiranog položaja dinamometra je u prvoj trećini nazivne sile znatno veća nego u ostale dvije trećine. Ovdje bi trebalo uvidjeti razlike pogreške točnosti u III i IV umjeravanju. U IV umjeravanju dolazi do smirivanja kidalice te time i manje vrijednosti pogreške.

Relativna pogreška ponovljivosti pri istom i pri različitom ugradbenom položaju također poprima lošije vrijednosti nakon dugotrajnog rada kidalice. No ovdje to pogoršanje nije moguće opisati nekim konstantnim iznosom. Posebno to pogoršanje dolazi do izražaja u III umjeravanju koje je provedeno odmah nakon konstantnog opterećivanja kidalice (slika 3c). U IV nizu je već došlo do određenog smirivanja rezultata te približavanje rezultatima II umjeravanja.

Dugotrajni rad kidalice se je najmanje odrazio na rezultate pogreške uslijed histereze (slika 3e). Ona također poprima oblik ostalih karakteristika ali u znatno manjoj mjeri. Isto tako vidljivo je da nakon dugotrajnog rada ona poprima približno konstantan iznos kroz cijelo mjerno područje.

S obzirom da su se pogreška točnosti i pogreška ponovljivosti pri različitim ugradbenim položajima prijenosnog etalona sile pokazale kritičnije nego ostale, stoga su one praćene kroz tri radna dana što je prikazano na slikama 4 i 5.

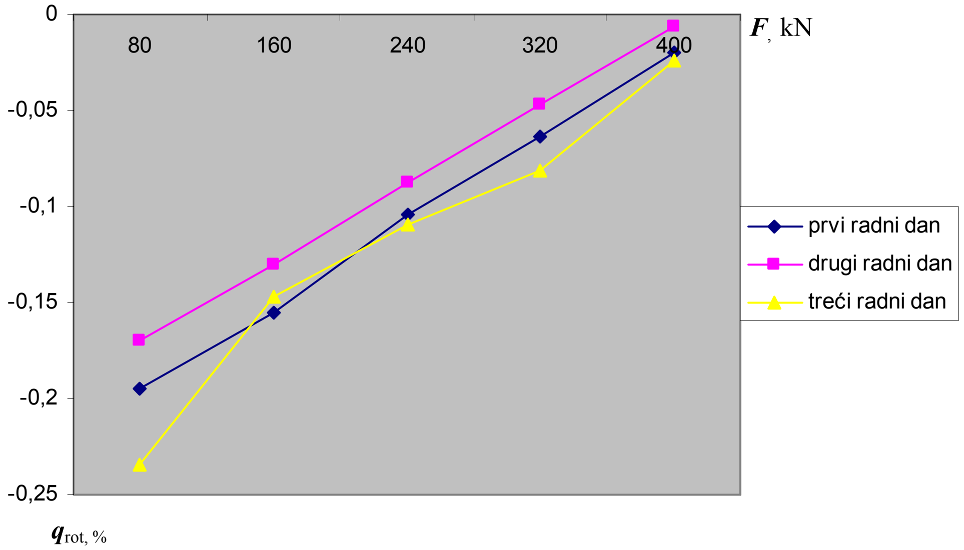

Slika 4: Promjene pogreške točnosti kidalice (III umjeravanje) kroz tri radna dana

Iz dijagrama na slikama 4 i 5 je vidljivo da promjene tih pograšaka imaju isti trend tijekom sva tri radna dana, što nam omogućuje da procijenimo pogreške kidalice pri takovim dugotrajnim mjerenjima.

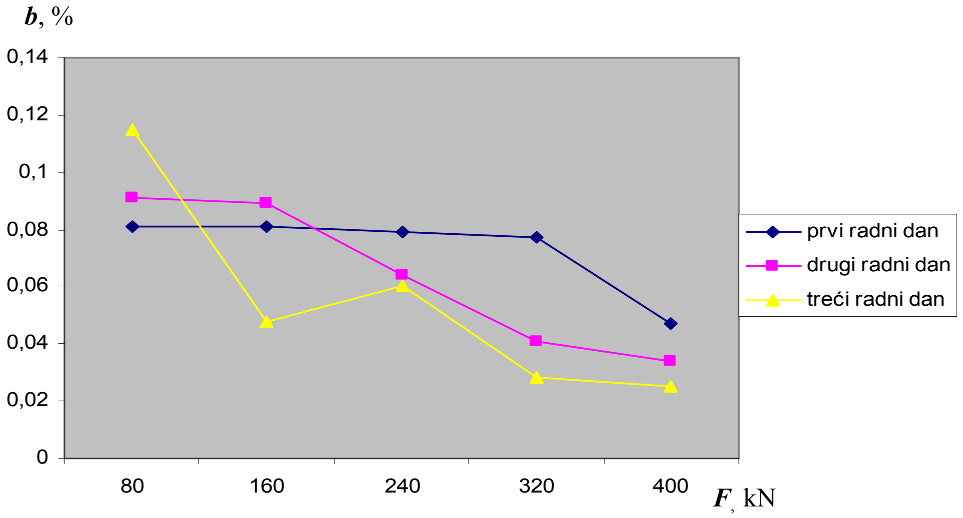

Slika 4: Promjene pogreške ponovljivosti kidalice (III umjeravanje) kroz tri radna dana

No da bi se mogla generalno provesti takova procjena te uvrstiti u cjelokupni proračun mjernih nesigurnosti mjerenja kidalica potrebno je više ovakvih ispitivanja na različitim tipovima kidalica.

4. ZAKLJUČAK

Na temelju provedenih istraživanja mogu se donijeti slijedeći zaključci:

- Dugotrajnim konstantnim radom kidalice odnosno njenog sustava za opterećivanje dolazi do promjene njenih karakteristika što bi svakako trebalo uzeti u obzir pri provedbi nekih dugotrajnih ispitivanja. Način za provjeru iznosa tih promjena je provođenje eksperimentalnih istraživanja na dotičnoj kidalici nekom od provjerenih metoda.
- Najveće promjene dolaze kod pogreške točnosti i ponovljivosti. Za kidalicu EU 40/2 ove pogreške se povećavaju približno do 0,1 % u odnosu na početno stanje.
- Prije prve uporabe u tijeku jednog radnog dana, potrebno je sustav za opterećivanje kidalice dovesti u njegovo radno stanje te provesti par probnih mjerenja sile što bliže nazivnoj vrijednosti ili ako postoji mogućnost izvršiti provjeru sile na barem jednoj mjernoj točki.
- Kod serijskih ispitivanja ostaviti određeni vremenski interval kako bi se kidalica smirila te time u slijedeće mjerenje unijeli što manju pogrešku nastalu utjecajem predhodnog mjerenja na mjernu stabilnost kidalice.

5. LITERATURA

[1] R.S. Figliola, D.E. Beasley: Theory and design for mechanical measurements, John Wiley & Sons, New York, 1991.

[2] EN ISO 376: Metallic materials – Calibration of force proving instruments used for the verification of uniaxial testing machines, 1999.

[3] EN ISO 7500-1: Metallic materials – Verification of static uniaxial testing machines – Verification and calibration of the force measuring system, 2004.

[4] Ž. Alar: Procjena mjerne nesigurnosti pri umjeravanju mehanizma opterećivanja kidalice, MATRIB 2000- Vela Luka

11. Savjetovanje o materijalima, tehnologijama, trenju i trošenju
11. Conference on Materials, Processes, Friction and Wear
MATRIB'06, Vela Luka, 22-24.06.2006.

MJERNA SPOSOBNOST REFERENTNOG ETALONA SILE INSTALIRANOG U LIMS-u

THE MEASUREMENT CAPABILITY OF THE REFERENCE FORCE STANDARD INSTALLED IN LIMS

Željko Alar, Mladen Franz, Tamara Aleksandrov
Sveučilište u Zagrebu, Fakultet strojarstva i brodogradnje, Zavod za materijale
Ivana Lučića 5, 10000 Zagreb
e-mail: tamara.aleksandrov@fsb.hr

Sažetak

Laboratorij za ispitivanje mehaničkih svojstva (LIMS) Fakulteta strojarstva i brodogradnje je nositelj državnog etalona za silu u mjernom području 50 N – 200 kN s mjernom sposobnošću <0,12%. Krajem 2005. u LIMS-u je instaliran referentni etalon sile nazivne vrijednosti 500 kN. U radu je opisana sljedivost mjerenja sile u RH prije i poslije instalacije referentnog etalona. Procjena mjerne sposobnosti dana je na temelju preliminarnih komparativnih mjerenja provedenih pomoću posredničkih etalona nazivnih sila 20 kN, 50 kN, 100 kN, 200 kN i 500 kN koji su sljedivi do nacionalnih etalona sile Republike Njemačke. Posrednički etaloni korišteni su u mjernom području 40 -100 % vrijednosti nazivne sile kako bi se dobila što manja nesigurnost mjerenja. Na temelju izvršenih mjerenja doneseni su određeni zaključci koji su ujedno i daljnje smjernice za poboljšanje mjerne sposobnosti referentnog etalona sile. Poseban naglasak je na utjecaju referentnog etalona na mjernu sposobnost LIMS-a, te na njegov položaj u europskim i svjetskim mjeriteljskim krugovima za mjernu veličinu sile.

Ključne riječi: referentni etalon sile, mjerna sposobnost, mjerna nesigurnost

Abstract

The Laboratory for testing mechanical properties of materials (LIMS) at the University of Mechanical Engineering and Naval architecture is the holder of the national force standard in measuring range 50 N – 200 kN with measurement capability <0,12%. Reference force standard with nominal value 500 kN at the end of 2005 is installed. In this paper measurement capability of Croatia before and after installation of the reference force standard is described. Evaluation of measurement capability is given on the basis of preliminary comparative measurements on transfer standards with nominal values 20 kN,50 kN, 100 kN, 200 kN and 500 kN which are traceable till German national force standards. The transfer standards in measuring range 40 – 100 % of nominal force are used. On the basis of measurements certain conclusions which are at the same time further directions for improvement of measurement capability of reference force standard are given. The emphasis is on the influence of the reference force standard on measurement capability of LIMS as well as on position of LIMS in European and global metrology.

Key words: reference force standard, measurement capability, measurement uncertainty

1. UVOD

Mjerenje sile je osnova za određivanje mehaničkih svojstava nekog materijala ili proizvoda. Mehanička svojstva materijala zauzimaju posebno mjesto među ostalim fizikalnim i kemijskim svojstvima, budući da se na osnovi njih dimenzioniraju dijelovi strojeva i uređaja. Pomoću mehaničkih svojstava može se objektivno ocijeniti kvaliteta materijala u prijamnoj kontroli poluproizvoda te u završnoj kontroli proizvoda. Samo ispitivanje sile provodi se na uređajima za mjerenje sile koji tokom uporabe gube na preciznosti, a razlozi tomu mogu biti različita oštećenja, kvarovi pojedinih sklopova, neadekvatna uporaba (preopterećenje), istrošenje pojedinih sklopova, itd. Posljedice koje nastanu uporabom takovih uređaja mogu biti dalekosežne. Zbog toga se javlja potreba za sistematskom periodičnom kontrolom ili provjerom (umjeravanjem) uređaja za mjerenje sile kroz jedno umjerno razdoblje čije su najveće dopuštene vremenske granice propisane normama. Sve dok zemlje članice EU početkom devedesetih godina nisu prihvatile novi Europski standard niza EN 10002, umjeravanje i klasifikaciju opreme za mjerenje sile nije bilo moguće provesti u Europi jednoobrazno.

Sila je matematički predstavljena kao vektor koji djeluje u određenoj točki. Stoga mjerenje sile uključuje određivanje njene veličine i smjera djelovanja. Mjerenje sile može se provesti direktnom ili indirektnom metodom.

Direktna metoda obuhvaća izravnu usporedbu sa poznatom gravitacijskom silom utega standardne mase. Vrijednosti mase i gravitacije moraju biti točno poznate. Ovu metodu koriste uređaji zvani vage za mjerenje sile. Njihova osjetljivost ovisi o konstrukcijskim parametrima.

Indirektna metoda obuhvaća mjerenje učinka sile na neko tijelo. Primjeri primjene ove metode su:

- mjerenja akceleracije tijela sa poznatom masom koje je izloženo djelovanju sile,
- mjerenje rezultantnog učinka (deformacije) kada se silom djeluje na elastično elemente.

2. SLJEDIVOST MJERENJA SILE U RH

Pod sljedivošću podrazumijeva se postupak kojim se pokazivanje mjerila može usporediti s nacionalnim etalonom dotične mjerne veličine u jednom ili više koraka (stupnjeva). Formalno sljedivost se određuje kao ***"svojstvo mjernog rezultata ili vrijednosti kojeg etalona po kojemu se on može dovesti u vezu s navedenim referencijskim etalonima neprekinutim lancem usporedaba koje imaju utvrđene nesigurnosti"***.[1] U svim tim stupnjevima umjeravanje se provodi etalonom čija je metrologijska kakvoća već određena umjeravanjem etalonom na višoj razini.

Sljedivost uređaja za mjerenje sile i njihovih rezultata mjerenja počinje od primarnog etalona za silu. Primarni etalon *(Primary standard)* definiran je kao etalon najviše mjeriteljske kakvoće u određenom području čije se vrijednosti prihvaćaju bez pozivanja na druge etalone iste kakvoće. On se nikad ne rabi izravno za mjerenje osim usporedbe s rezervnim etalonom ili referencijskim etalonom. Kako je jedinica za silu N izvedena jedinica SI sustavu proizlazi da nema međunarodnog primarnog etalona za silu, nego postoje primarni etaloni za silu za određenu državu, a nazivaju se nacionalni etaloni za silu. Nacionalni etalon *(National standard)* definiran je kao etalon prihvaćen državnom odlukom da bude u zemlji osnova za utvrđivanje vrijednosti svih ostalih etalona neke veličine. Nacionalni etaloni sile su uređaji s utezima preko kojih je ostvarena određena sila direktno bez intervenirajućih mehanizama, a relativna nesigurnost mjerenja iznosi 2×10^{-05} [2].

Slijedeća razina u mjeriteljskom lancu za silu su referentni etaloni. Referentni etalon (*Reference standard)* definiran je kao etalon najviše mjeriteljske kakvoće raspoloživ na nekom području, od kojega se izvode sva mjerenja na nekom području. Vrijednosti njihove nesigurnosti se deriviraju preko umjeravanja u nacionalnom etalonu. Referentni etaloni su stabilni uređaji za mjerenje sile, a nalaze se u akreditiranim umjernim laboratorijima te tako ostvaruju mjernu sljedivost između nacionalnog etalona i ostalih uređaja za mjerenje sile na nekom području. Očekivane najveće sposobnosti mjerenja postignute pomoću referentnih etalona ovise o tipu realizacije sile, a kreće se u rasponu od 5×10^{-05} do 5×10^{-03}. U tablici 1 su prikazani mogući tipovi mehanizama opterećivanja kod referentnih etalona sile te njihove najbolje mjerne sposobnosti.

Tablica 1 – Tipovi mehanizama opterećivanja kod referentnih etalona sile te njihove najbolje mjerne sposobnosti referentnih etalona [3]

Tipovi referentnih etalona prema mehanizmu opterećivanja	Najbolja mjerna sposobnost (proširena relativna mjerna nesigurnost)
Mehanizam opterećivanja direktno utezima	5×10^{-5} do 1×10^{-4}
Hidraulični mehanizam opterećivanja	1×10^{-4} do 5×10^{-4}
Polužni mehanizam opterećivanja	1×10^{-4} do 5×10^{-4}
Komparatorni sustav	do 5×10^{-3}

Prijenos sile između primarnog i referentnog etalona ostvaruje se posredničkim etalonom. Posrednički etalon (*transfer standard*) definiran je kao etalon, katkada posebne izvedbe, namijenjen prijenosu sile između različitih mjesta.

Pri prijenosu sile javlja se cijeli niz utjecajnih faktora koji se mogu klasificirati u tri skupine: okolišni uvjeti, konstrukcijska rješenja pri ostvarivanju prijenosa sile i mjerna sposobnost posredničkog etalona. Ovo djelovanje je potrebno procijeniti te provesti proračun mjerne nesigurnosti uslijed njihova djelovanja.

Laboratorij za ispitivanje mehaničkih svojstva (LIMS) Fakulteta strojarstva i brodogradnje postao je nositelj državnog etalona za silu 2005.godine. To je dobiveno na temelju akreditacije za umjeravanje mjerila sile od strane DAR/PTB/DKD (Deutsher Akkreditierungs Rat/Physicalische technische Bundesanstalt/Deutsche Kalibrierdiens i potpisivanja ugovora s Državnim zavodom za mjeriteljstvo (DZM). Najbolja mjerna sposobnost LIMS-a je <0,12% u mjernom području od 50 N do 200 kN. Jedne od glavnih smjernica razvoja LIMS-a su permanentno poboljšavanje mjeriteljske infrastrukture u Hrvatskoj i smanjenje mjerne nesigurnosti mjerenja sile, a iste su ujedno i odrednice sustava kvalitete LIMS-a. U skladu s tim, krajem 2005. u LIMS-u je instaliran referentni etalon sile. Na slici 1 prikazana je mjerna sljedivost LIMS-a nakon dobivanja akreditacije a prije instalacije referentnog etalona.

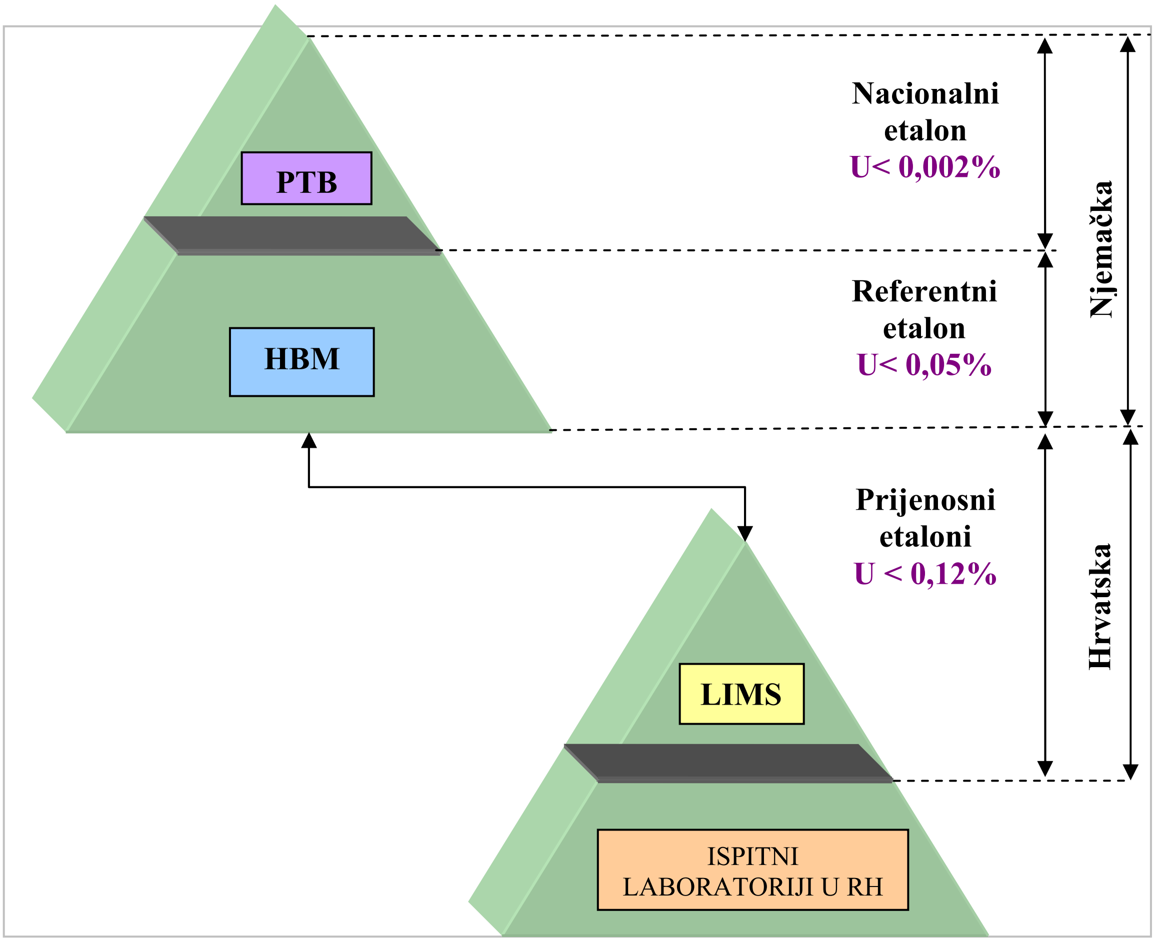

Slika 1 - Mjerna sljedivost LIMS-a prije instalacije referentnog etalona sile

Na vrhu piramide mjerne sljedivosti je krovna institucija u Njemačkoj PTB (Physikalische Technische Bundesanstalt) koja posjeduje nacionalne etalone sile čija je najveća mjerna sposobnost $\leq$ ***0,002 %***. LIMS je predstavljao umjerni laboratorij za mjerila sile s najvećom mjernom sposobnošću $\leq$ ***0,12 %***. Svoje prijenosne etalone umjeravao je u HBM-u ili PTB-u te je tako ostvarivao mjernu sljedivost za silu.

3. INSTALACIJA REFERENTNOG ETALONA U LIMS-U

Proces pripreme odgovarajućih okolišnih uvjeta pa sve do instalacije referentnog etalona sile trajao je 11 mjeseci. Pod osiguravanjem okolišnih uvjeta smatra se odgovrajući smještaj za uređaj, omogućavanje stalne kontrole i regulacije temperature, praćenje promjene vlage i tlaka. Posebno su morali biti pripremljeni antivibracijski temelji kako vibracije iz okoline ne bi utjecale na rezultate mjerenja. Instalacija referentnog etalona sile u LIMS-u završena je u listopadu 2005. Na slici 2 je prikazan referentni etalon sile a njegove osnovne karakteristike i tehničke mogućnosti dane su u tablici 2.

Mjerni sustav ovog etalona je komparatornog tipa što znači da ima odgovarajuće deformacijsko tijelo čiji se pomak (deformacija) pretvara u izlazni električni signal. Osnovne komponente ovog sustava su dinamometri i mjerno pojačalo. Kod ovog etalona karakterističan je novi model dinamometara (slika 3) koji je patentiran prije svega pet godina a omogućava šire mjerno područje. Radi se o modelu dvostruko složenih dinamometara koji se u ovom slučaju sastoji od visoko preciznih dinamometara KTN 100 kN i KTN 500 kN. Ovakav sustav omogućava mjernu sposobnost etalona sile < 0,05 %.

Slika 2 - Referentni etalon sile instaliran u LIMS-u

Tablica 2 - karakteristike referentnog etalona sile

KARAKTERISTIKE REFERENTNOG ETALONA SILE	
Proizvođač	GTM, Njemačka
Mjerno područje	10 – 500 kN
Nazivna sila	500 kN
Način opterećenja	hidraulički
Smjer opterećenja	Vlak, tlak
Ponovljivost	1×10^{-04}
Očekivana mjerna nesigurnost	< 0,05 %
Mjerni sustav	mjerno pojačalo, dvostruko složeni dinamometri

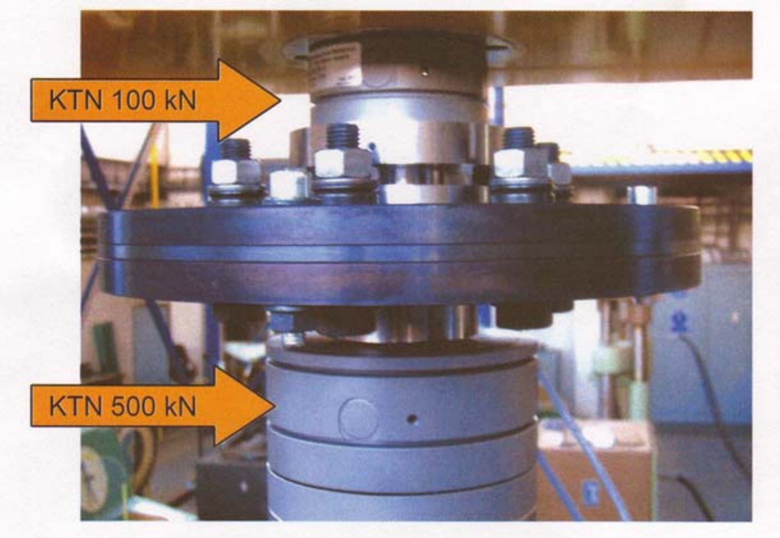

Slika 3 – Mjerni sustav referentnog etalona sile (dvostruko složeni dinamometri)

Značenje ovog uređaja može se sagledati iz više aspekata. Postavljanjem ovog stabilnog etalona u R. Hrvatskoj je temeljno promijenjena mjeriteljska infrastruktura za silu što je prikazano na slici 4.

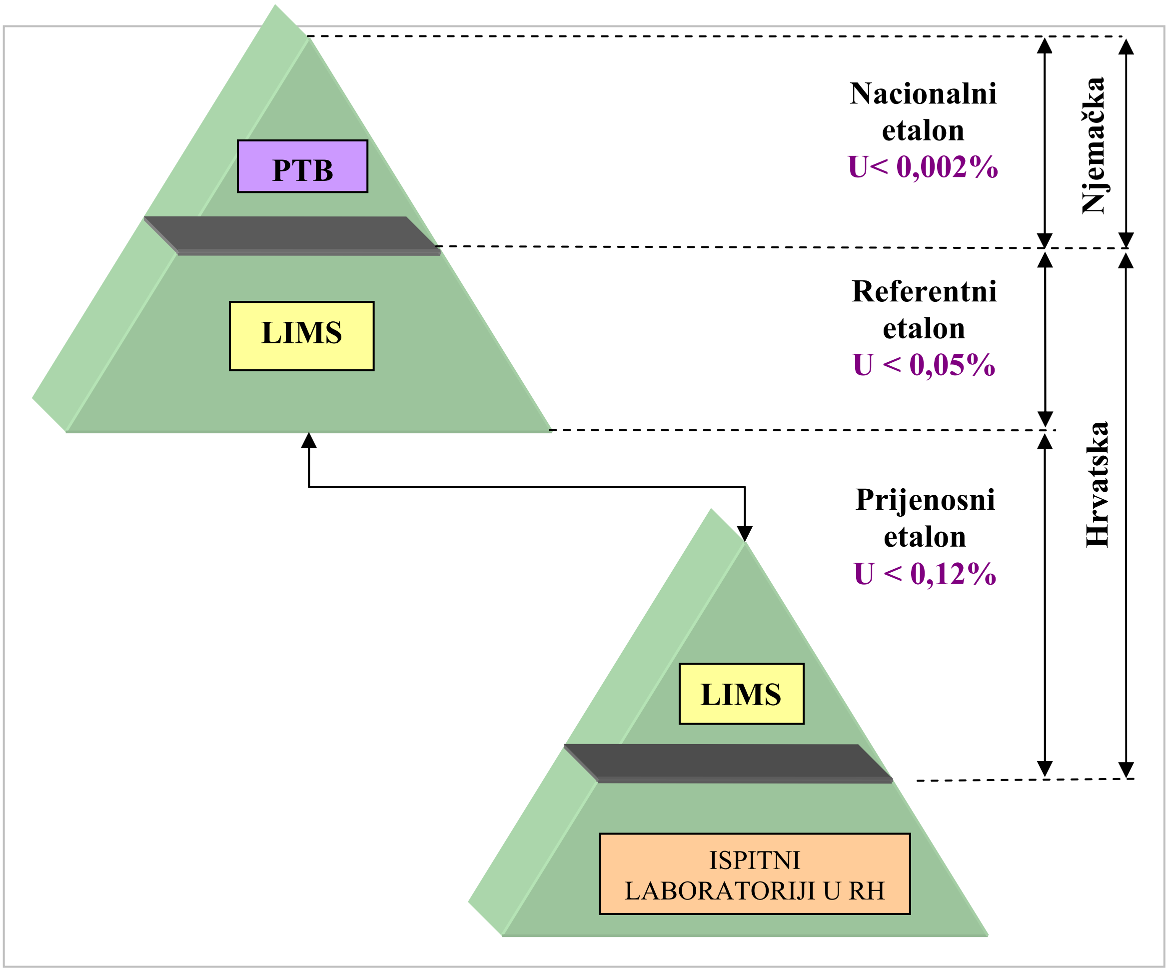

Slika 4 - Mjerna sljedivost LIMS-a nakon instalacije referentnog etalona sile

LIMS je instalacijom ovog referentnog etalona s mjernom sposobnošću < ***0,05%*** poboljšao svoju mjernu sposobnost te postao jedan od vodećih laboratorija u regiji. Svoje prijenosne etalone umjerava u vlastitom laboratoriju te time smanjuje troškove a ujedno je moguće stalno provoditi provjeru istih. Osim toga omogućeno je sudjelovanje u interkomparacijama s drugim nacionalnim laboratorijima i time potvrđivanje mjernih sposobnosti što je jedan od zahtijeva norme ISO/IEC 17025 za ispitne i umjerne laboratorije.

4. PRELIMINARNA MJERENJA

Na referentnom etalonu sile smještenom u LIMS-u izvršena su preliminarna mjerenja pomoću posredničkih etalona u njihovom mjernom području od 40 – 100% nazivne vrijednosti. Razlog zašto su korišteni u ovom mjernom području je u tome što dosadašnje spoznaje ukazuju da je najbolja mjerna nesigurnost ostvariva jedino u navedenom mjernom području [4]. Za ova ispitivanja korišteni su posrednički etaloni slijedećih nazivnih vrijednosti: 20 kN; 50 kN; 100 kN; 200 i 500 kN. Svi ovi etloni su vlasništvo tvrtke GTM a sljedivi su do nacionalnih etalona u PTB-u. Prosječno odstupanje od PTB-a, izraženo u ppm-ima (parts per million), pomoću posredničkih etalona prikazano je na slikama 5 i 6.

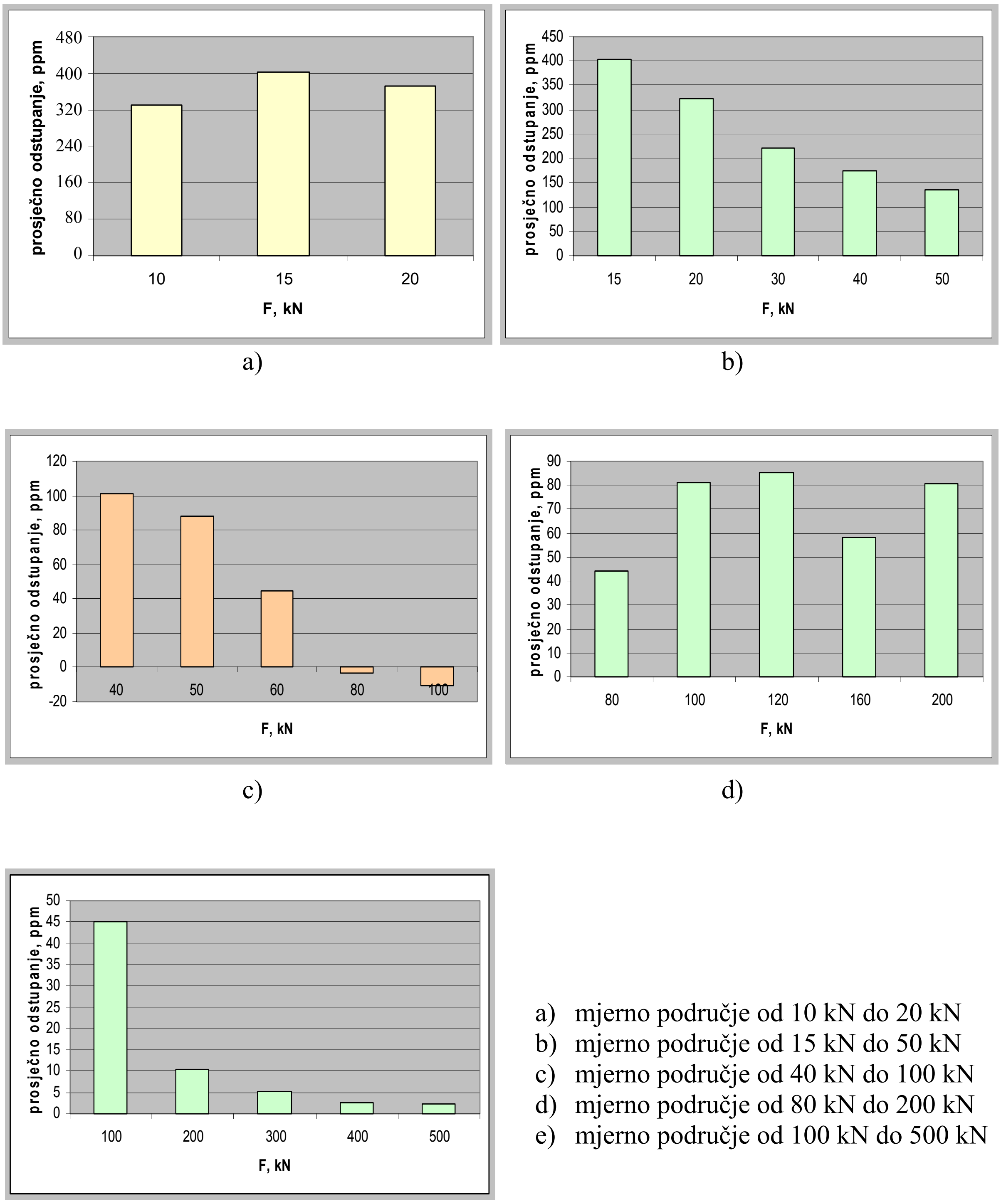

a) b) c) d) e)

a) mjerno područje od 10 kN do 20 kN
b) mjerno područje od 15 kN do 50 kN
c) mjerno područje od 40 kN do 100 kN
d) mjerno područje od 80 kN do 200 kN
e) mjerno područje od 100 kN do 500 kN

Slika 5 – Prosječno odstupanje od PTB-a

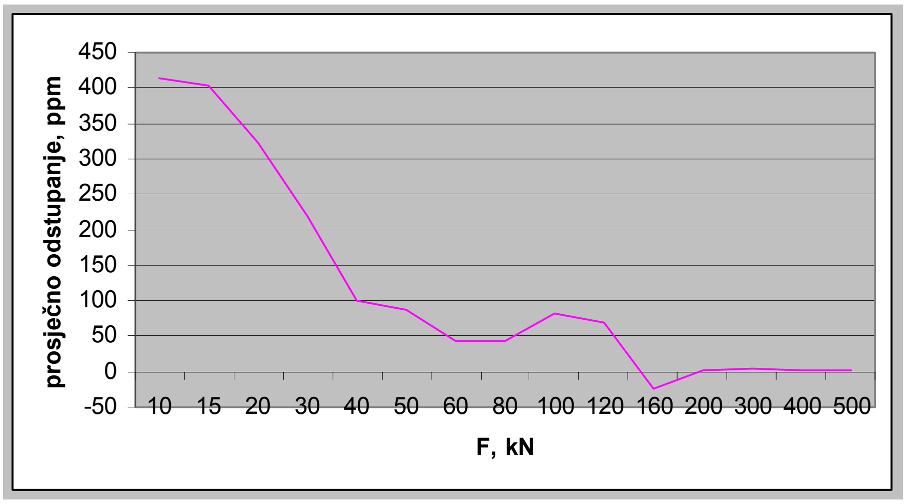

Slika 6 – Prosječno odstupanje od PTB-a za cijelo mjerno područje od 10 – 500 kN

Iz ovih preliminarnih mjerenja je vidljivo da će biti potvrđena očekivana mjerna sposobnost ovog referentnog etalona sile. Sada slijede usporedna mjerenja s PTB-om i to s posredničkim etalonima boljih karakteristika te je za očekivati da će ova odstupanja biti još i manja.

5. ZAKLJUČAK

Instalacijom referntnog etalona sile u LIMS-u poboljšana je sljedivost mjerenja sile u R. Hrvatskoj te omogućeno uključivanje LIMS-a u europsku i svjetsku infrastrukturu za mjernu veličinu sila. Osim toga omogućena je suradnja s drugim nacionalnim laboratorijima kroz interkomparacijska mjerenja a time održavanje i potvrđivanje mjeriteljske sposobnosti LIMS-a. Na znanstvenom polju ovim uređajem moguće je provoditi istraživanja doprinosa nekih dosad neutvrđenih utjecajnih veličina na nesigurnosti umjeravanja mjerila sile. Na temelju rezultata provedenih preliminarnih ispitivanja možemo zaključiti da će očekivana mjerna nesigurnost referentnog etalona sile biti < 0,05%. Time je znatno poboljšana mjerna sposobnost LIMS-a što je u skladu sa njegovim sustavom kvalitete.

6 . LITERATURA

[1] Međunarodni rječnik osnovnih i općih naziva u metrologiji, Državni zavod za normizaciju i mjeriteljstvo, Grafok, Zagreb, 1993.

[2] Ž. Alar: Procjenjivanje nesigurnosti rezultata mjerenja sile, Magistarski rad, Fakultet strojarstva i brodogradnje Sveučilišta u Zagrebu – Zagreb, 2001.

[3] EA-4/15 (EAL-G22):Uncertainty of Calibration Results in Force Measurement, 1996.

[4] A. Sawla: Guidance for the determination of the best measurement capability of force calibration machines and uncertainty of calibration results of force measuring devices, PTB-Mitteilungen 104 4/94, pp.237-242.

11. Savjetovanje o materijalima, tehnologijama, trenju i trošenju
11. Conference on Materials, Processes, Friction and Wear
MATRIB'06, Vela Luka, 22-24.06.2006.

UTJECAJ NANO PUNILA NA FAZNE PRIJELAZE I BUBRENJE EKSTRUDIRANIH POLIMERNIH MJEŠAVINA POLI(VINIL-KLORID)/KLORIRANI POLIETILEN

INFLUENCE OF NANO FILLER ON PHASE TRANSITIONS AND SWELLING OF EXTRUDED POLY(VINYL CHLORIDE)/CHLORINATED POLYETHYLENE BLENDS

Branka Andričić, Sanja Perinović, Ivana Karalić, Tonka Kovačić
Zavod za organsku tehnologiju, Kemijsko-tehnološki fakultet u Splitu, Teslina 10/V,
21000 Split, e-mail:sanja@ktf-split.hr

Sažetak: U ovom radu istraživan je utjecaj $CaCO_3$, čestica nano dimenzija (nano punilo) na fazne prijelaze i bubrenje polimerne mješavine poli(vinil-klorid)/klorirani polietilen (PVC/CPE). Mješavine su pripremljene ekstruzijom na jednopužnom laboratorijskom ekstruderu pri 170°C i 180 o/min uz dodatak toplinskog stabilizatora ($PbSO_4$) za PVC i omekšavala (dioktil-ftalata, DOP) radi bolje preradljivosti. Uočeno je da $CaCO_3$ pospješuje toplinsku razgradnju mješavina, što se očituje promjenom boje od bijele do smeđe. Očito je da dodatak nano punila uzrokuje razgradnju ili PVC-a ili CPE-a ili oba polimera, a razlog je najvjerojatnije termomehanička razgradnja zbog smičnog naprezanja u ekstruderu. Uzorci PVC/CPE/$CaCO_3$ analizirani su diferencijalnom pretražnom kalorimetrijom (DSC) u svrhu istraživanja utjecaja dodatka $CaCO_3$ na talište i toplinu taljenja CPE-a, te stakliště i specifični toplinski kapacitet PVC-a. Ustanovljeno je da nano punilo ne utječe na staklište PVC-a i talište CPE-a. S obzirom da je mješavina sastavljena od dva polimera, za određivanje značajki bubrenja odabrane su kapljevine u kojima se ni jedan polimer ne otapa (aceton, benzen, toluen). Stupanj bubrenja proporcionalan je dielektričnoj konstanti otapala, a konstanta bubrenja obrnuto proporcionalna dielektričnoj konstanti otapala.
Ključne riječi: PVC/CPE mješavine; $CaCO_3$; diferencijalna pretražna kalorimetrija; bubrenje

Abstract : In this work the influence of $CaCO_3$, nano particles (nano filler) on phase transitions and swelling of poly(vinyl chloride)/chlorinated polyethylene blends (PVC/CPE) was investigated. The blends were prepared by extrusion on single-screw laboratory extruder. The heat stabilizer ($PbSO_4$) for PVC and plasticizer (dioctylphthalate, DOP) as a processing aid were added. The optimum rotation speed was 180 rpm and the optimum temperature was 170 ºC. Color changes from white to brown shows that $CaCO_3$ accelerate degradation of the blends. Addition of the nano filler causes degradation of PVC or CPE or both polymers, and most probably reason was thermomechanical degradation, due to the shear arising from the mixing of polymers and filler in extruder. On the basis of DSC measurements it has been established that the nano filler has no influence on T_g of PVC and T_m of CPE. Considering that the blend consists of two polymers, determinations of swelling properties were performed in nonsolvents for both polymers (acetone, benzene and toluene). The swelling degree is proportional to dielectric constant of selected liquids while the swelling constant is reciprocal to the dielectric constant.
Keywords: PVC/CPE blends; $CaCO_3$; differential scanning calorimetry; swelling

Uvod

Poli (vinil-klorid) u komercijalnoj je uporabi već 70 godina. Sam po sebi toplinski je nepostojan i krt. Toplinska razgradnja PVC-a započinje pri relativno niskim temperaturama, već iznad staklišta (≈ 80 °C), pri čemu dolazi do njegove razgradnje uz nastajanje kloridne kiseline koja djeluje autokatalitički i polienskih struktura koje podliježu procesima oksidacije. Tijekom razgradnje poli(vinil-klorid) se obojava uz pogoršanje mehaničkih, fizikalnih, dielektričnih i drugih svojstava.

Uspješna uporaba PVC-a ne bi bila moguća bez različitih dodataka kao što su toplinski i svjetlosni stabilizatori, omekšavala, poboljšavala preradljivosti i toplinske postojanosti oblika te različita punila. Svi navedeni dodatci stalno se unaprjeđuju i uvode se novi. Tako npr. otrovni kadmijevi stabilizatori su izbačeni iz uporabe i koriste se novi Ca/Zn organski stabilizatorski sustavi; niskomolekulna omekšavala zamjenjuju se polimernima, neaktivna punila se modificiraju kako bi se poboljšala svojstva materijala, a ne samo snizila cijena koštanja itd.

Klorirani polietilen je kemijski modificiran PE sa statističkom raspodjelom klora uzduž lanca. Ovisno o stupnju kloriranja CPE polimeri mogu imati elastomerna ili termoplastična svojstva, te biti vrlo kompatibilni s nizom drugih polimera. Na svojstva CPE-a pored sadržaja klora utječu molekularna masa PE-a upotrebljenog za kloriranje, struktura lanca, te metoda kloriranja, a sve to ima značajan utjecaj na miješanje polimera i morfologiju mješavine.

CPE je modifikator žilavosti PVC-a. Takva mješavina mikroskopski je heterogena, a konačnim svojstvima doprinosi svaka komponenta mješavine. Modificiranjem PVC-a kloriranim polietilenom dobije se materijal prikladan za izradu geomembrana, fleksibilnih folija niske propustljivosti za kapljevine i paru koje se upotrebljavaju za oblaganje različitih speremnika, dna akumulacijskih jezera pitke vode, za otpadne vode, za vanjsku krovnu izolaciju itd.[1,2]

Precipitirani $CaCO_3$ jedan je od najčešćih sfernih nano punila koji se koristi za pripremu nanokompozita. Istraživanja PVC/$CaCO_3$ nanokompozita pokazuju da se dodatkom $CaCO_3$ povisuje staklište PVC-a[3], udarna žilavost po Izodu, produljenje pri lomu i Youngov modul elastičnosti.[4] Dodatkom $CaCO_3$ poboljšava se površinski sjaj izradaka od PVC-a što je važno kada se upotrebljavaju Ca/Zn stabilizatorski sustavi koji inače reduciraju površinski sjaj.[5] Dosadašnja istraživanja mehaničkih svojstava ternarnih mješavina PVC/CPE/nano $CaCO_3$ pokazuju da se udarna žilavost po Izodu, produljenje pri lomu i Youngov modul elastičnosti također povećavaju s porastom udjela nano punila .[4]

U ovom radu istraživana je mješavina PVC-a i CPE-a s različitim udjelima nano punila $CaCO_3$. Mješavine su pripremljene postupkom ekstruzije. Određen je utjecaj nano punila na fazne prijelaze polimera u mješavinama te na značajke bubrenja mješavina u acetonu, benzenu i toluenu.

Eksperimentalni dio

Za pripremu polimernih mješavina upotrijebljen je suspenzijski PVC prah (Ongrovil S-5064, Borsod Chem, Mađarska), praškasti CPE (Tyrin BH 9000, Dow, SAD) i precipitirani $CaCO_3$ (Socal U1, Solvay, Njemačka). Odnos PVC/CPE bio je 70/30. Maseni udio $CaCO_3$ bio je 2, 4, 6, 8, i 10% u odnosu na PVC. U svrhu bolje homogenizacije komponenata i lakše preradljivosti mješavine dodan je dioktil-ftalat, DOP (Vestinol AH, Chemische Verke Hüls AG, Njemačka) i to 10% u odnosu na PVC, a za sprječavanje toplinske razgradnje PVC-a dodan je toplinski stabilizator trobazni $PbSO_4$ (Ciba Geigy, Švicarska), 2 % u odnosu na

PVC. Priprema polimernih mješavina ekstruzijom provodena je na laboratorijskom jednopužnom ekstruderu (Dynisco, Qualitest North America).

Određivanje temperatura faznih prijelaza pripremljenih uzoraka, tj. stakilšta PVC-a (T_g) i tališta CPE-a (T_m) izvršeno je pomoću Perkin-Elmerovog diferncijalnog pretražnog kalorimetra (DSC – 4). Uzorci su zagrijani od 30 do 150 °C (RUN 1), ohlađeni na početnu temperaturu i ponovo zagrijani na 150 °C (RUN 2) sa brzinom zagrijavanja/hlađenja od 10 °Cmin^{-1}. Talište je određeno iz prvog zagrijavanja (RUN 1), a staklište iz drugog zagrijavanja (RUN 2).

Određivanje značajki bubrenja, ravnotežnog stupnja bubrenja (α_∞) i konstante A, u acetonu, benzenu (Kemika, Zagreb) i toluenu (Alkaloid, Skopje) provedeno je pomoću uređaja za volumetrijsko određivanje stupnja bubrenja na temelju dva mjerenja.[6]

Rezultati i rasprava

Usporedi li se boja uzoraka nakon ekstruzije, vidljivo je da se boja uzorka mijenja od bijele do smeđe s povećanjem sadržaja $CaCO_3$, slika 1. Očito je da dodatak $CaCO_3$ uzrokuje razgradnju ili PVC-a ili CPE-a ili oba polimera, a razlog je najvjerojatnije termomehanička razgradnja zbog smičnog naprezanja u ekstruderu. Razgradnja tijekom prerade je primijećena i kod pripreme drugih nanokompozita ekstruzijom.[7]

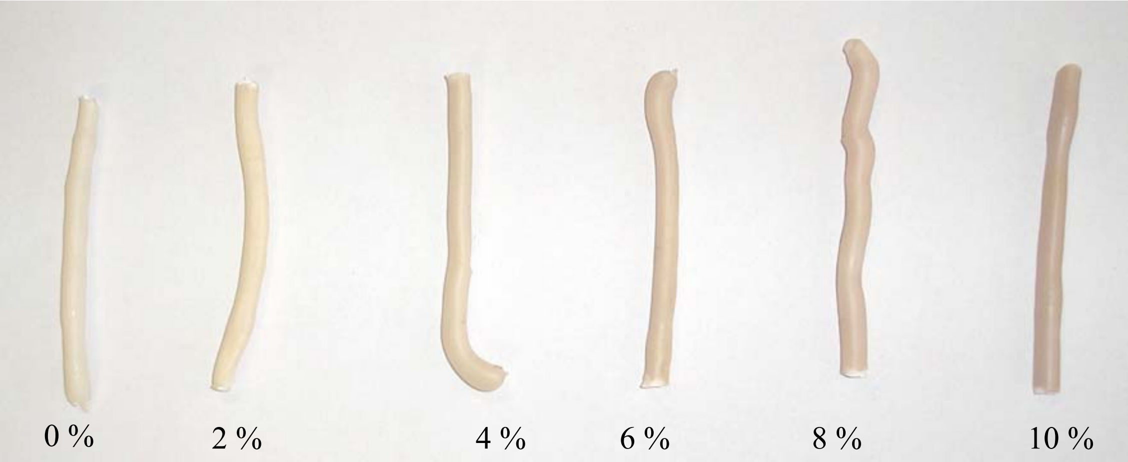

Slika 1. Obojenost uzoraka ovisno o sadržaju nano punila.

DSC krivulje mješavina PVC/CPE pokazuju dva prijelaza, od kojih je prvi (pri nižoj temperaturi) staklište PVC-a, a drugi talište CPE-a. Staklište PVC-a (79°C)[8] je sniženo zbog dodatka omekšavala, ali dodatak nano punila nema utjecaja na staklište PVC-a (tablica 1). Staklište PVC-a bez punila je 65,6 °C, a uz dodatak 2 do 10 % $CaCO_3$ više, 66,9±0,4 °C. Također, znatnije se ne mijenja ni vrijednost ΔCp u staklištu. Nano punilo $CaCO_3$ nema utjecaja na talište CPE-a, čije vrijednosti su, bez obzira na sadržaj punila, 107±0,4 °C.

Tablica 1. Rezultati DSC analize.

Sadržaj $CaCO_3$/ %	**Staklište PVC-a / °C**	**ΔCp / $Jg^{-1}°C^{-1}$**	**Talište CPE-a / °C**	**ΔCp / Jg^{-1}**
0	65,6	0,17	107,8	1,39
2	66,5	0,17	107,9	1,39
4	67,2	0,17	107,5	1,31
6	67,3	0,16	107,3	1,25
8	66,9	0,15	108,3	1,10
10	66,6	0,15	107,6	1,15

S obzirom da je mješavina sastavljena od dva polimera, za određivanje značajki bubrenja odabrane su kapljevine u kojima se ni jedan polimer ne otapa (aceton, benzen, toluen). Iz ovisnosti stupnja bubrenja o vremenu, te ovisnosti $d\alpha/dt$ o α određene su značajke bubrenja: ravnotežni stupanj bubrenja (α_∞) i konstanta A, ovisna o prirodi polimera i otapala. Ravnotežni stupanj bubrenja mješavina opada u nizu aceton > toluen > benzen (osim mješavine s 2 % $CaCO_3$), tablica 2. U istom nizu opada i polarnost tj. dielektrična konstanta otapala.[9]

Tablica 2. Ravnotežni stupanj bubrenja (α_∞) uzoraka bubrenih u acetonu, benzenu i toluenu

Sadržaj $CaCO_3$/%	**aceton α_∞/ mLg^{-1}**	**benzen α_∞/mLg^{-1}**	**toluen α_∞/mLg^{-1}**
0	2,05	1,13	1,30
2	2,06	0,85	0,70
4	1,47	0,81	0,90
6	2,05	0,86	0,98
8	1,66	0,87	0,96
10	1,60	0,72	1,04

Ravnotežni stupanj bubrenja mješavina ima uglavnom najveću vrijednost u mješavinama bez $CaCO_3$. Vidljivo je da se α_∞ snižava ukoliko se doda $CaCO_3$, ali to sniženje nije proporcionalno sadržaju nano punila. Ova pojava vjerojatno je rezultat i nejednolikog sastava mješavine dobivene ekstruzije. Vrijednosti konstante A, tablica 3, koja daje uvid u brzinu bubrenja pokazuju da mješavine najbrže bubre u benzenu zatim u toluenu, a relativno sporo u acetonu. Dakle, brzina bubrenja smanjuje se s povećanjem polarnosti otapala.

Tablica 3. Konstante A uzoraka bubrenih u acetonu , benzenu i toluenu

Sadržaj $CaCO_3$/%	**aceton A/ min^{-1}**	**benzen A/min^{-1}**	**toluen A/min^{-1}**
0	0,07	0,08	0,06
2	0,06	0,20	0,16
4	0,08	0,15	0,12
6	0,10	0,37	0,26
8	0,07	0,08	0,09
10	0,12	0,22	0,07

Zaključak

Mješavine PVC/CPE/nano punilo $CaCO_3$ pripremljene su ekstruzijom pri 170°C. Ekstrudat postaje tamniji porastom udjela nano punila što je rezultat termomehaničke razgradnje zbog povećanja smičnog naprezanja u sustavu koji sadrži čestice punila.

Podatci dobiveni DSC analizom pokazuju da nano punilo ne utječe na vrijednost stakljšta PVC-a i tališta CPE-a.

Stupanj bubrenja mješavina, α_∞, snižava se dodatkom $CaCO_3$ i opada u nizu aceton > toluen > benzen, a konstanta bubrenja, A, opada u nizu benzen > toluen > aceton. Značajke bubrenja, dakle, ovise o polarnosti medija za bubrenje.

Literatura

1. A.J. Varma, S.V. Deshpade i P. Kondapalli, *Polym. Degrad. Stabil.* **63** (1999) 1

2.H.D. Sharma i S.P. Lewis, *Waste Containtment Systems, Waste Stabilization and Landfill: Design and Evaluation,* John Wiley & Sons, N. York, 1994.

3. N. Chen, C. Van Y. Zhang and Y. Zhang, *Polym. Test.* **23**, (2004) 169-174

4. D. Wu, X. Wang, Y. Song and R. Jin, *J. Appl. Polym. Sci.* **92**, (2004) 2714-2723

5. M. Vučak i H.D. Stöver, *Kunstoffe,* **2**, (2005) 97-100

6. B. Pintarić, Polimeri, **6** (1985) 208

7. M.-A. Paul, M- Alexandre, M. Murariu i P. Dubois, *Biodegradable materials based on poly(L,L-lactide) and montmorilonite: Ageing and thermal degradation of poly(etrhylene glycol)-plasticized nanocomposites,* poster, MODEST, Lyon, 2004.

8. B. Andričić, T. Kovačić i I. Klarić, *J. Appl. Polym. Sci.* **100**, (2006) 2158-2163

9. www.blazelabs.com/dielectric-chart.pdf, 30.11.2005.

11. Savjetovanje o materijalima, tehnologijama, trenju i trošenju
11. Conference on Materials, Processes, Friction and Wear
MATRIB'06, Vela Luka, 22-24.06.2006.

CONSTRUCTION STRENGTH OF THE TRANSPORT BOX FOR FRUIT AND VEGETABLES

ČVRSTOĆA KONSTRUKCIJE TRANSPORTNE KUTIJE ZA VOĆE I POVRĆE

Babić, D., Lajić, B., Jurečić, D.
Faculty of Graphic Arts, Getaldićeva 2, 10000 Zagreb
Chair for Bookbinding, Packaging and Design of Graphic Products

Abstract:

Parameters which directly influence the construction strength of the transport box for fruit and vegetables have been investigated in this work. The whole series of demands must be fulfilled so that the transport box could be used for packing the determined kinds of provision. Transport, storage and distribution of fruit and vegetables represent a special problem today., because during the transport the boxes and their contents are often submitted to drastic changes of temperature and humidity. As the storage in the refrigeration plants demands pilling of boxes with the packed goods one above another, because of space saving, the dynamic loading is present, especially on the boxes which are underneath. Because of that the boxes have to be constructed so that they can endure all those burdens and atmosphere changes.

Key words: Construction, transport box, strength

Sažetak:

U radu se ispituju parametri koji direktno utječu na čvrstoću konstrukcije transportne kutije za voće i povrće. Cijeli je niz zahtjeva koji moraju biti ispunjeni da bi se transportna kutija primjenjivala za pakiranje određenih vrsta namirnica. Poseban problem danas predstavlja transport, skladištenje i distribucija voća i povrća jer tokom puta kutije i sadržaj u njima često budu izloženi drastičnim promjenama temperature i vlažnosti zraka. Obzirom da skladištenje plodova u hladnjačama zbog uštede prostora zahtijeva slaganje kutija sa upakiranim plodovima vrlo visoko jedna na drugu prisutno je i dinamičko opterećenje posebno donjih kutija u kupovima. Zbog toga kutije moraju biti tako konstruirane da mogu podnijeti sva ta opterećenja i promjene atmosfere.

Ključne riječi: Konstrukcija, transportna kutija, čvrstoća

Uvod

Poseban problem danas predstavlja transport, skladištenje i distribucija voća i povrća. S obzirom da nakon berbe voće i povrće nastavlja sa respiratornim procesima koji podrazumijevaju potrošnju kisika i otpuštanje ugljičnog dioksida, vode i energije potrebno ih je čuvati u hladnoj atmosferi gdje se fiziološke funkcije usporavaju ili zaustavljaju. Ovisno o kakvoj se vrsti povrća ili voća radi razlikujemo i različite postupke transporta i skladištenja te eventualnog izlaganja u prodajnom prostoru. Najlakše se čuvaju one vrste koje sadrže mali postotak vlage kao npr. korjenaste vrste povrća, bademi, lješnjaci i sl. Prilikom berbe i transporta voća i povrća potrebno je naročitu pažnju posvetiti zaštiti plodova od mehaničkih oštećenja koja mogu prouzročiti pogoršanje kvalitete i ubrzanu biološku razgradnju. Ako je vrijeme transporta do skladišta ili prodaje duže potrebno je osigurati vozilo sa strogo kontroliranim klimatskim uvjetima (CA – *controlled atmosphere*) za čuvanje. Suvremeno skladištenje podrazumijeva strogo kontroliranu temperaturu, vlagu i svjetlost u prostoriji gdje se čuva voće ili povrće. Temperatura kao osnovni faktor kreće se od nula do najviše pet stupnjeva čime se smanjuje aktivnost mikroorganizama (gljivica i bakterija) koji utječu na procese raspadanja organske materije. Što je temperatura viša to se proces degradacije ubrzava. Sljedeći jednako važni uvjet je strogo kontrolirana relativna vlaga prostora koja mora iznositi od 85 do 95 %. Ukoliko taj uvjet nije ispunjen može doći do kondenzacije vodene pare na površini proizvoda. Povišena vlažnost utječe na povišenje temperature što opet uzrokuje ubrzanu razgradnju biomaterije odnosno truljenja proizvoda ili ako djelovanje mikroorganizama nije toliko prisutno plodovi postaju smežurani, žilavi i time smanjene kvalitete. Svjetlost kao treći faktor može utjecati na povišenje temperature što ponovo dovodi do rasta mikroorganizama i truljenja. Općenito možemo reći da ambalaža za voće i povrće mora biti izrađena od lakog materijala i dovoljno čvrsta da se može slagati na potrebnu visinu u vozilu ili hladnjači,a u svrhu što boljeg iskorištenja prostora. Također mora biti izrađena od materijala koji nemaju u sebi nikakvih toksičnih tvari ili mirisa i koji nisu osjetljivi na vlagu. Konstrukcijski mora biti riješena tako da plodovi imaju dovoljnu prozračnost i da se mogu izložiti u prodajnom prostoru. Sljedeći važan uvjet je da prazna prije upotrebe zauzima što manje skladišnog prostora te da sklapanje po mogućnosti bude strojno. Osjetljivo voće i povrće se pakira u plitku ambalažu najviše do 3 reda, dok se otpornije može pakirati i u više redova s tim da treba paziti na mogućnost povišenja temperature u debelim slojevima zbog disanja i fermentacije. Cijena je također jedan od bitnih parametara odabira tipa i materijala od koje se izrađuje ambalaža za čuvanje i transport voća i povrća. Ambalaža koja najbolje odgovara svim tim zahtjevima je transportna kutija od valovitog kartona za transport voća i povrća. Naziv je vrlo nezgrapan i velik pa se u stručnim krogovima udomačio trgovački naziv tih kutija *holandez*. Kutije *holandez* za voće i povrće od valovitog kartona mogu se izrađivati u raznim modelima i od različitih kvaliteta materijala ovisno o: vrsti voća i povrća, dužini puta i uvjetima transporta, zahtjevu trgovačke kuće koja prodaje voće i povrće, klasi voća i povrća, visini slaganja u hladnjači, visini slaganja u prijevoznom sredstvu i visini slaganja na prodajnom mjestu, mogućnosti strojnog pakiranja na polju ili u sortirnici. Cijeli je niz zahtjeva koji moraju biti ispunjeni da bi se *holandez* kutija primjenjivala za pakiranje određenih vrsta voća i povrća. Istraživanje u ovom članku promatra čvrstoći *holandez* kutije u ovisnosti o vrsti materijala pa se drugi aspekti kvalitete i zahtjeva ne spominju. Skladištenje plodova u hladnjačama zbog uštede prostora zahtijeva slaganje kutija sa upakiranim plodovima vrlo visoko jedna na drugu. Pri transportu na velike udaljenosti brodom, vlakom ili kamionom gdje vladaju uvjeti kontrolirane atmosfere sa niskom temperaturom i povećanom relativnom vlagom zraka, prisutno je i dinamičko opterećenje posebno donjih kutija u kupovima. Može se zaključiti da je najveće opterećenje kutija upravo prilikom transporta. Zbog toga kutije moraju biti tako konstruirane da mogu podnijeti sva ta opterećenja i promjene atmosfere.

Metoda i materijal

Kutije *holandez* izrađuju se u mnogo različitih modela i iz različitih kvaliteta valovitog kartona. Nastoji se uvijek odabrati model i materijal koji će cijenom biti najniži, a da ambalaža zadrži fizikalno mehanička svojstva potrebna za dovoljnu zaštitu upakiranog proizvoda. Kako uglavnom proizvođači valovitog kartona upotrebljavaju svoje oznake a u istraživanju je upotrebljavan valoviti karton iz tvornice Belišće d.d. služili smo se upravo njihovim oznakama. Standardne gramature najviše korištenih vrsta papira: kraftliner (125 – 200 g/m^2), testliner (150 – 250 g/m^2), fluting (105 – 150 g/m^2), bijeli kraftliner (150 – 150 g/m^2), bijeli testliner (150 – 175 g/m^2). Najčešće se koriste peteroslojni materijali u proizvodnji *holandeza*, a smo ponekad troslojni kada se radi o lakšim plodovima, kada je put do kupaca kraći ili kada nije predviđeno duže čuvanje plodova što zahtijeva kontroliranu atmosferu. Najviše korišteni materijali za izradu kutija *holandez*: **2BŠ** - c/b val; **BKŠ** - c/b val; **BTŠ** - c/b val; **2KŠ** - c/b val; **2TŠ** - c/b val. Za potpuni opis kvalitete ljepenke pored oznaka vrste papira i visine valova bilo bi potrebno dopisati i gramature papira što je i propisano mnogim standardima međutim takva nomenklatura u Hrvatskoj još nije u primjeni prije svega iz komercijalnih razloga proizvođača U današnje vrijeme sve se manje koriste papiri izrađeni od primarnih sirovina (četinjače ili listače) tipa kraftliner i polukemijski fluting (do 90% primarnih vlakana) te se zamjenjuju papirima izrađenim od sekundarnih vlakana (starog papira). Testliner smeđi i bijeli načinjen od starog papira zamjenjuje kraftliner papire smeđe i bijele boje. Wellestoff (reciklažni fluting) papiri za izradu valovitog sloja izrađeni od starog papira zamjenjuju polukemijski fluting. Iako je razvoj novih tehnologija pridonio tome da se mogu proizvesti veoma kvalitetni papiri iz sekundarnih sirovina i njihova je potrošnja u razvijenim zemljama pa i kod nas premašila potrošnju papira načinjenih iz primarnih sirovina, za neke vrste ambalaže, još uvijek se koriste kraftliner papiri, a što je u velikoj mjeri prisutno kod ambalaže za voće i povrće. Sve vrste valovitog kartona bez obzira dali su izrađene od primarnih ili sekundarnih vlakana zahtijevaju poseban tretman u pogonima. Prije prerade mora se skladištiti u tamnom zatvorenom prostoru, na temperaturi 22 -24^o C i relativnoj vlažnosti 48-52 %. Ako materijal nije prije upotrebe čuvan u takvim uvjetima potrebno ga je 24 sata kondicionirati u uvjetima kakvi su u pogonu za preradu.(tempeatura 23 +/- 1^o C i RV 50+/- 2%). Za kvalitetno izrađenu kutiju potrebno je poznavati sljedeća fizikalno-mehanička svojstva materijala i kutije: otpor brida valovitog kartona na tlak (**Edge crush test – ECT** (N)), otpor valovitoga kartona na dinamičko probijanje (**Puncture test -PT** (J)), debljina valovitog kartona (**Caliper – CLP** (mm)), otpor valovitog sloja na tlak (**Concora medium test - CMT** (N)), otpor ravnine ploče valovite ljepenke na tlak (**Flat crush test - FCT** (kPa)), otpornost valovite ljepenke prema prskanju po Mullenu (**Bursting test - BT** (kPa)), otpor kutije od valovite ljepenke na tlak (**Box compression Test - BCT** (N)), otpornost valovite ljepenke na raslojavanje (**Internal bond test - BOND** (mJ)).

Iako se vidi koliko je potrebno ispitivati spomenute kutije, istraživan je samo odnos tipa kutije (**A** i **B**), vrste materijala od kojih su napravljene (**E2KŠ**, **2TŠ**, **2T** i **TŠ**) i to pomoću **BCT** i **PT** testa.

S obzirom da je udio papirne ambalaže u ukupnoj svjetskoj proizvodnji oko 40% to je pronalaženje kvalitetnih konstrukcijskih rješenja vrlo važan i odgovoran zadatak. U današnje vrijeme je trend sve većeg korištenja valovitog kartona proizvedenog iz starog papira pa iako je ta tehnologija znatno uznapredovala taj papir još uvijek nije jednako dobrih mehaničkih svojstava kao i papiri iste gramature dobiveni iz primarnih sirovina. Bolja kvaliteta takvih valovitih kartona može se postići većom gramaturom sastavnih slojeva što povećava potrošnju materijala, a time i težinu ambalaže. Isto možemo reći i za broj slojeva valovitog kartona. Fizikalno mehanička svojstva troslojnog ili peteroslojnog valovitog kartona nisu jednaka bez obzira o kakvim se kombinacijama papira radi. Tip **A** je lijepljena a tip **B** je složiva kutija *holandez*.

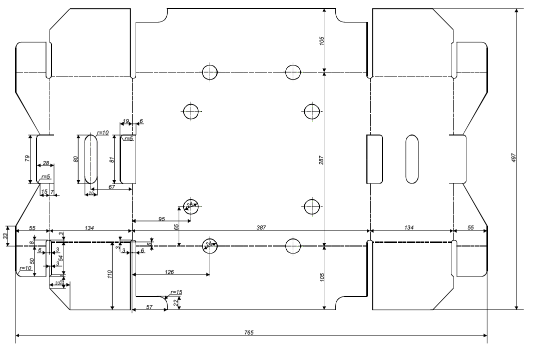

Slika 2. Nacrt lijepljene kutije *hlondez*
dimenzije: 385 x 285 x 130 mm

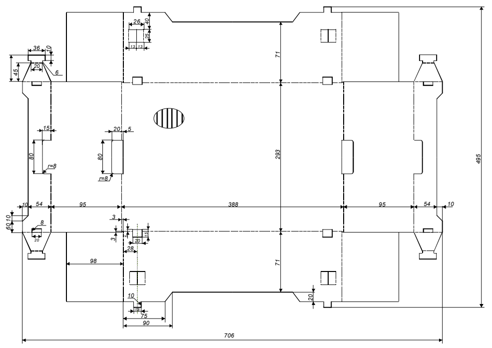

Slika 3. Nacrt složive kutije *holandez*
dimenzije: 385 x 290 x 90 mm

Dimenzije kutija su gotovo iste kako bi rezultati koji se dobiju bili usporedljivi u svim smjerovima i kvalitetama. Prikazani prirezi su zbog svoje specifične forme pogodni za izradu troslojnih (c-val) i peteroslojnih kutija (b/c val, e/b val ili e/c val).

Mjerenja

Sastav valovitog kartona i osnovna fizikalno-mehanička svojstva prema tvorničkoj specifikaciji

E2KŠ c/b val

Kraftliner,	175 g/m^2	+/- 3%
Belwell,	150 g/m^2	+/- 3%
Šrenc,	110 g/m^2	+/- 3%
Belwell,	150 g/m^2	+/- 3%
Kraftliner,	175 g/m^2	+/- 3%
Gramatura:	900-950 g/m^2	+/- 5%
Debljina:	6,20 – 6,70 mm	

2T c val

Testliner,	135 g/m^2	+/- 3%
Wellenstoff,	105 g/m^2	+/- 3%
Testliner,	135 g/m^2	+/- 3%
Gramatura:	430-460 g/m^2	+/- 5%
Debljina:	3,85 – 4,00 mm	

2TŠ c/b val

Testliner,	140 g/m^2	+/- 3%
Wellenstoff,	105 g/m^2	+/- 3%
Šrenc,	105 g/m^2	+/- 3%
Wellenstoff,	105 g/m^2	+/- 3%
Testliner,	125 g/m^2	+/- 3%
Gramatura:	670-700 g/m^2	+/- 5%
Debljina:	6,20 – 6,70 mm	

TŠ c val

Testliner,	135 g/m^2	+/- 3%
Wellenstoff,	105 g/m^2	+/- 3%
Šrenc,	105 g/m^2	+/- 3%
Gramatura:	410-430 g/m^2	+/- 5%
Debljina:	3,80 – 4,00 mm	

Mjerenje čvrstoće kutija tipa A i B na tlak (BCT)

Uređaj za ispitivanje otpora kutija od valovitoga kartona na pritisak konstruiran je tako da može tlačiti maksimalnu površinu dimenzije 1000 x 800mm silom od max. 20000 N. Maksimalna visina kutije koja se ispituje može biti do 1200 mm. Brzina gibanja ploče može varirati od 2 do 250 mm/min. Za ovaj pokus gibanje je regulirano na 10 mm/min. Stroj je tako konstruiran da kutiju najprije tlači sa određenim predotporom koji iznosi 220 N. Taj predotpor mora izdržati svaka ispitivana kutija inače nije moguće obaviti potrebno mjerenje. Rezultati ispitivanja izražavaju se u njutnima (N) za pritisak te u milimetrima (mm) i postocima (%) za deformaciju kutije. Ispitivanje je obavljeno na praznim kutijama. Ispitivano je po pet kutija tipa A i B od zadana četiri materijala što ukupno iznosi 40 uzoraka. Kod ispitivanja vrlo je važno odrediti vlagu i temperaturu jer direktno utječu na mehaničku čvrstoću materijala pa time i na rezultate mjerenja. Pokus je rađen na temperaturi od 23°C i relativnoj vlazi od 60%. Rezultati mjerenja BCT-a prikazani su u tablici 2. i dijagramima od 1. do 6.

Mjerenje otpornosti valovitog kartona na dinamičko probijanje (PT)

Uređaj za ispitivanje dinamičke otpornosti na probijanje pokazuje rad koji je potreban da se valoviti karton probije. Podatak je vrlo važan jer nam omogućuje odabir kvalitete materijala koji će zaštititi proizvod unutar ambalaže do onog nivoa kojeg zahtjeva proizvođač određene robe. Da bi se dobili što bolji rezultati ispitivanje se provodi s lica i naličja valovitog kartona. Ispitani svi kartoni od kojih su izrađeni *holandrzi* tipa **A** i tipa **B** po pet uzoraka, što je ukupno 40 ispitivanja.

Rezultati su dani u tablici 3. i u dijagramima 7. do 9.

Rezultati

Tablica 2. Rezultati mjerenja BCT - testa

E2KŠ- c/b

kutija **A**			
redni broj mjerenja	**N**	**%**	**mm**
1.	3810	5,89	8,20
2.	3540	6,54	9,10
3.	3850	6,76	9,40
4.	3250	6,54	9,10
5.	3050	6,04	8,40
srednja vrijednost	**3500**	**6,35**	**8,84**

kutija **B**			
redni broj mjerenja	**N**	**%**	**mm**
1.	3150	5,47	5,20
2.	3040	5,57	5,30
3.	3100	5,57	5,30
4.	3190	8,73	8,30
5.	3060	6,00	5,70
srednja vrijednost	**3108**	**6,27**	**5,96**

2TŠ- c/b

kutija **A**			
redni broj mjerenja	**N**	**%**	**mm**
1.	2940	6,52	9,00
2.	2510	4,92	6,80
3.	2790	7,31	10,10
4.	2820	7,24	10,00
5.	2630	6,66	9,20
srednja vrijednost	**2738**	**6,53**	**9,02**

kutija **B**			
redni broj mjerenja	**N**	**%**	**mm**
1.	1940	4,63	4,40
2.	3060	3,00	2,80
3.	2500	8,52	8,10
4.	3210	2,96	2,82
5.	1990	4,21	4,00
srednja vrijednost	**2540**	**4,66**	**4,42**

2T- c

kutija **A**			
redni broj mjerenja	**N**	**%**	**mm**
1.	1510	5,03	6,08
2.	1410	5,51	6,10
3.	1680	4,59	7,80
4.	1470	5,33	7,20
5.	1480	5,74	6,40
srednja vrijednost	**1510**	**5,24**	**6,72**

kutija **B**			
redni broj mjerenja	**N**	**%**	**mm**
1.	1390	5,15	4,90
2.	1470	5,47	5,20
3.	1410	4,52	4,30
4.	1370	5,26	5,00
5.	1400	4,94	4,70
srednja vrijednost	**1408**	**5,07**	**4,82**

TŠ- c

kutija **A**			
redni broj mjerenja	**N**	**%**	**mm**
1.	1180	2,59	3,50
2.	1100	4,59	6,20
3.	1460	5,18	7,00
4.	1280	2,88	3,90
5.	1180	2,51	3,40
srednja vrijednost	**1240**	**3,55**	**4,80**

kutija **B**			
redni broj mjerenja	**N**	**%**	**mm**
1.	1050	3,36	3,20
2.	920	2,63	2,50
3.	980	2,63	2,50
4.	980	2,84	2,50
5.	990	2,73	2,60
srednja vrijednost	**984**	**2,84**	**2,66**

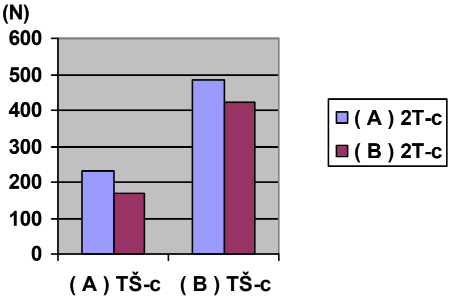

Dijagram 1. Odnos razlika otpora na tlak kutija A i B izrađenih od kartona TŠ-c i 2T-c.

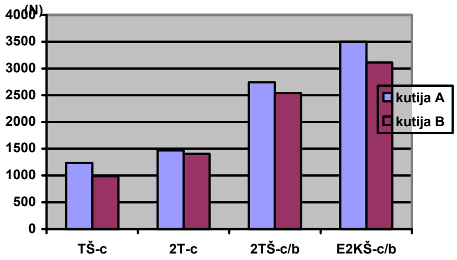

Dijagram 2. Prikaz odnosa vrijednosti sila gnječenja za četiri rste materijala i dvije vrste kutija

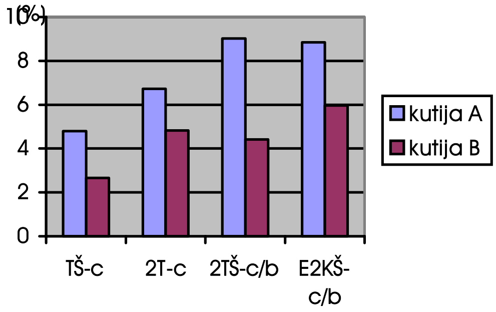

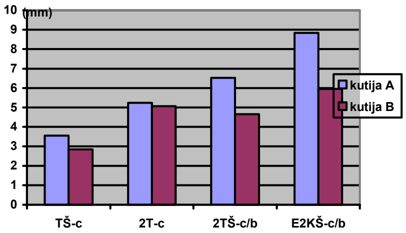

Dijagram 3. Prikaz odnosa vrijednosti deformacije kutija (mm).

Dijagram 4. Prikaz odnosa vrijednosti deformacije kutija (%).

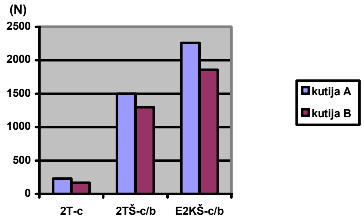

Dijagram 5. Odnos iznosa otpora na tlak kutije A izrađene iz valovitog kartona oznake TŠ-c i svih ostalih ispitivanih kombinacija modela i materijala osim kutije B izrađene iz kartona TŠ-c.

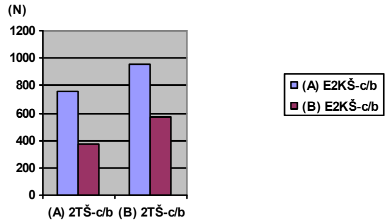

Dijagram 6. Odnos razlika otpora na tlak kutija A i B izrađenih od kartona E2KŠ-c/b i 2TŠ-c/b.

Tablica 3. Ispitivanje valovitog kartona na dinamičko probijanje (**PT**- Puncture test (J))

E2KŠ b/c val lice	
broj mjerenja	**J**
1	11,00
2	10,60
3	10,00
4	10,20
5	10,80
srednja vrijednost	**10,52**

E2KŠ b/c val naličje	
broj mjerenja	**J**
1	10,40
2	10,40
3	9,80
4	9,80
5	9,20
srednja vrijednost	**9,92**

2TŠ b/c val lice	
broj mjerenja	**J**
1	7,00
2	7,40
3	7,20
4	7,20
5	7,40
srednja vrijednost	**7,24**

2TŠ b/c val naličje	
broj mjerenja	**J**
1	7,20
2	7,60
3	7,40
4	7,40
5	7,40
srednja vrijednost	**7,40**

2T c val lice	
broj mjerenja	**J**
1	3,90
2	3,90
3	3,90
4	3,90
5	3,90
srednja vrijednost	**3,90**

2T c val naličje	
broj mjerenja	**J**
1	3,90
2	3,90
3	4,20
4	3,80
5	3,90
srednja vrijednost	**3,94**

TŠ c val lice	
broj mjerenja	**J**
1	3,80
2	3,80
3	3,80
4	3,70
5	3,60
srednja vrijednost	**3,74**

TŠ c val naličje	
broj mjerenja	**J**
1	3,60
2	3,90
3	3,70
4	3,70
5	3,70
srednja vrijednost	**3,72**

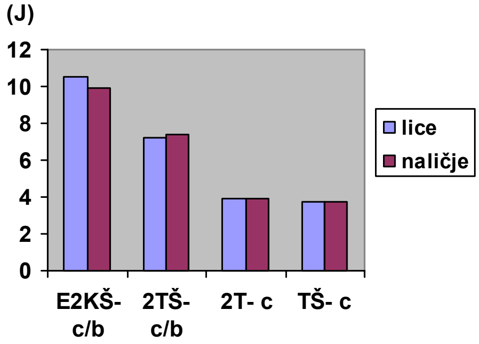

Dijagram 7. Odnosi vrijednosti otpora na dinamičko probijanje korištenih materijala

Analiza rezltata

Iz tablice 2. vidljivo je da kod kutija tipa A je potrebna veća sila gnječenja nego kod tipa B za sve ispitivane vrste valovitog kartona. Za ispitivane vrste materijala ta razlika iznosi: TŠ-c – 256 N = 20,00 %, 2T-c – 62 N = 4,20 %, 2TŠ-c/b –198 N = 7,20 %, E2KŠ-c/b – 392 N = 11,20 %. U prosjeku je to : 227 N = **10,65** %. Razlika između troslojnog i peteroslojnog materijala, bez obzira na A ili B tip kutije je najmanje 1070 N, pa možemo zaključiti da konstrukcijom ispitivanih kutija nije moguće kompenzirati toliku razliku u kvaliteti. Primjer takvog donosa vrijednosti prikazuje dijagram 5. Znatno manje razlike su između materijala sa istim brojem slojeva. Ako uspoređujemo različite modele i različite materijale tada dobivamo sljedeći redoslijed:

TŠ-c – model A ima veći BCT od **TŠ**-c – modela B za 20,65 %
2T-c – model A ima veći BCT od **2T**-c – modela B za 4,22 %
2TŠ-c/b – model A ima veći BCT od **2TŠ**-c/b – modela B za 7,23 %
E2KŠ-c/b – model A ima veći BCT od **E2KŠ**-c/b – modela B za 11,20 %

E2KŠ b/c val je otporniji na dinamičko probijanje od 2TŠ b/c vala za 31,18%.
E2KŠ b/c val je otporniji na dinamičko probijanje od 2T c vala za 62,93%.
E2KŠ b/c val je otporniji na dinamičko probijanje od TŠ c vala za 64,45%.
2TŠ b/c val je otporniji na dinamičko probijanje od 2T c vala za 46,13%
2TŠ b/c val je otporniji na dinamičko probijanje od TŠ c vala za 48,34%
2T c val je otporniji na dinamičko probijanje od TŠ c val za 4,10%

Iz dijagrama 1. vidimo da je najmanja razlika između kutije **A** izrađena iz TŠ-c i kutije **B** izrađene iz 2T-c (168 N ili 11,93 %) pa možemo zaključiti da koristeći model kutije **A** i kvalitetu valovitog kartona TŠ-c dobrim djelom kompenziramo slabiju kvalitetu kartona TŠ-c

dobivajući kutiju nešto slabije vrijednosti BTC-a od modela **B** izrađenog iz kvalitetnijeg i skupljeg materijala 2T-c. Zadovoljavaju li te vrijednosti traženu kvalitetu odabire se model kuitje A izrađen i TŠ-c.
Kod preostale tri kombinacije te razlike su veće:

2T-c model **A** - TŠ-c model **A** = 230 N (**15,65** %)
2T-c model **A** - TŠ-c model **B** = 486 N (**33,06** %)
2T-c model **B** - TŠ-c model **B** = 424 N (**30,11** %)

Uz to u dijagramu 7. prikazane vrijednosti otpora valovitog kartona TŠ-c i 2T-c na dinamičko probijanje razlikuju se za vrlo mali iznos (0,19 J ili 4,85 %). Valoviti karton 2T-c otporniji je na dinamičko probijanje od valovitog kartona TŠ-c što također govori u prilog zaključku o mogućnosti zamjene modela i kvalitete materijala. Kutije **A** i **B** izrađene iz dvije vrste peteroslojnog materijala pokazale su veće apsolutne razlike vrijednosti otpora na pritisak u odnosu na troslojne kutije, dok se u postocima te razlike neznatno razlikuju u odnosu na razlike između troslojnih materijala. Iz dobivenih rezultata je vidljivo da je najotporniji materijal na dinamičko probijanje onaj oznake E2KŠ b/c val . Slijede 2TŠ b/c val, 2T c val i TŠ c val kao najslabiji materijal u toj grupi.

6. ZAKLJUČAK

Kvaliteta kutija *holandez* određuje se na osnovu zahtjeva koje moraju ispunjavati kao što su npr. potrebna visina slaganja, težina i vrsta sadržaja, klasa proizvoda, i sl. Model kutije i vrsta valovitog kartona direktno određuju kvalitetu ambalaže. Zadatak svakog proizvođača ambalaže za voće i povrće je proizvesti što jeftiniju,a opet kvalitetnu kutiju za dovoljno pakiranje proizvoda kojima je namijenjena. To se postiže pronalaženjem optimalne kombinacije modela i valovitog kartona . Smanjenjem potrošnje materijala i većom upotrebom valovitog kartona čiji su slojevi papira dobiveni iz sekundarnih sirovina postižemo i pozitivni ekološki učinak jer se time smanjuje devastacija šumskog fonda, potrošnja vode itd. Iz provedenih istraživanja zaključujemo:

1. Veće površinske mase valovitog kartona daju bolje BCT i PT rezultate neovisno o tipu kutije.
2. Materijal E2KŠ- c/b (925 g/m^2) daje za 21,80 % bolje BCT rezultate od materijala T2Š- c/b (670 g/m^2) ili za čitavih 35,5 % od materijala TŠ- c (410 g/m^2). Isto je i sa PT i ECT testom.
3. Materijal E2KŠ- c/b (925 g/m^2) daje za 31,18 % bolje PT rezultate od materijala T2Š- c/b (685 g/m^2), 61,64 % od materijala 2T- c (430 g/m^2) i 64,45 % od materijala TŠ- c (410 g/m^2)
4. Materijal E2KŠ- c/b (925 g/m^2) daje za 28,76 % bolje ECT rezultate od materijala T2Š- c/b (685 g/m^2) 60,73 % od materijala 2T- c (430 g/m^2) i 62,55 % od materijala TŠ- c (410 g/m^2)
5. Smanjenjem gramature valovitog kartona dobivaju se veće površine ako je količina materijala ostala ista ,a to znači i veći broj kutija. Tako npr. za 1000 kutija **A** izrađenih iz E2KŠ- c/b (925 g/m^2) treba 98,59 kg više valovitog kartona nego da je izrađena iz T2Š- c/b (685 g/m^2). Ako taj broj podijelimo sa gramaturom materijala T2Š- c/b (685 g/m^2) dobivamo 144 m^2 valovitog kartona iz čega se može izraditi 350 kom. kutija.
6. Kutija model **A** ima 12,5 % manju površinu prireza od kutije model **B** što znači i 12,5 % manju potrošnju materijala .
7. Kutija model **A** je pokazala 11,2 % bolji rezultat BCT-testa od modela **B** u kvaliteti materijala E2KŠ- c/b (925 g/m^2), 7,23 % u kvaliteti materijala T2Š- c/b (685 g/m^2),

6,75 % u kvaliteti materijala 2T- c (430 g/m^2) i čak 20,6 % u kvaliteti materijala TŠ-c (410 g/m^2).

8. Najmanja razlika izmjerenih vrijednosti otpora kutija na pritisak je veća od 300 N.
9. Srednja vrijednost otpora valovitog kartona na dinamičko probijanje je za E2KŠ-c/b 10,22 J, a za 2TŠ-c/b je 7,32 J. Razlika je 2,9 J, ili **28,38** % što je iskustveno previše da bi mogli govoriti o sličnosti ta dva materijala.
10. Struktura valovitog kartona 2TŠ-c/b sa ugrađenim testliner papirima je bitno drugačija u odnosu na valoviti karton E2KŠ-c/b sa ugrađenim kraftliner papirima koji su u svakom pogledu bolji od testliner papira.
11. Srednja gramatura valovitog kartona E2KŠ-c/b je 900 gr/m^2,a valovitog kartona 2TŠ-c/b 670 gr/m^2. Razlika je **25,55** % .

Ako želimo mijenjati materijal za neku od kutija *holandez* koji će imati više vrijednosti PT i ECT tada toj kutiji povećavamo površinsku masu,a time i potrošnju valovitog kartona kao sirovine. Valoviti karton E2KŠ c/b (925 g/m^2) koji je pokazao najbolje rezultate prilikom mjerenja sadrži kao što je vidljivo iz njegove strukture i kraftliner papire koji se izrađuju iz primarnih sirovina (četinarsko ili liščarsko drvo) čija se upotreba nastoji smanjiti zbog visoke cijene, velike devastacije šumskog fonda, velike potrošnje vode za proizvodnju itd. Zamjena je moguća sa testliner papirima koji moraju biti veće gramataure zbog slabijih fizikalno mehaničkih svojstava u odnosu na kraftliner papire (znatno duža vlakanca i homogenija struktura u odnosu na testliner papire).

Literatura

1. www.fao.com
2. www.fefco.com
3. www.pbf.hr
4. www.belisce.hr
5. www.poljoprivreda.info
6. www.cooperprint.co.uk
7. www.valkarton.com
8. www.icp-lj.si
9. www.agr.hr
10. www.img-klett.com
11. www.ambalaza.hr
12. L. Roth, G. L. Wybenga: The Packaging Design Book of Patterns, New York, 1991.
13. V. Crnčević: Ambalaža za životne namirnice, Beograd, 1980.

HEAT RESISTANT ULTRA-FINEGRAINED AL PROFILES

Balog M.*, Nagy J., Simancik F., Izdinsky K.

Institute of materials and machine mechanics, SAS, Bratislava, Slovakia
*corresponding author: ummsbama@savba.sk

Abstract

Ultra-fine (d_{50} = 1.31 μm), monocrystalline, gas atomized Al 99.7 % powder was consolidated into profiles by means of common hot extrusion. Conventional approach, wherein complicated (i.e. expensive) procedure steps of powder encapsulating, degassing and hot isostatic pressing (HIP) are realized, was avoided. To keep potential expenses of following profiles competitive, powder was consolidated in loose or cold isostatically pressed (CIP) state. Structural stability of compacts and their enhanced mechanical properties at room and mainly at elevated temperatures were of paramount interest.

The effect of extrusion processing parameters on Al powder consolidation behavior and compact's mechanical properties is complexly presented. Extrusion yielded sound profiles with ultra-fine grained microstructures (grain size ~0.2 μm) consisting of fcc-Al matrix reinforced with α-alumina particles. Nano-scale dispersiods originated from broken surface oxide envelopes were homogenously redistributed within compact's structure where they effectively acted against dislocation movement and grain growth. The unique combination of ultra-fine grained structure and dispersion strengthening resulted in superior room temperature mechanical properties, where high tensile strength (up to 310 MPa) was accompanied with sufficient ductility (~10 %) and fracture toughness (K_{IC} ~ 40 Jcm^{-2}). Micro-structures were found to be intact to long term high temperature exposures, where even annealing at 350 °C for 20 hours led to no structural changes. Due to unique structural stability no pronounced strength decline was observed and compacts retained their relatively high strength even at testing temperatures of 500 °C (~70 MPa). Simple consolidation route without prior degassing resulted in the structure containing ultra-fine pores filled with entrapped and compressed gas. These pores had no negative effect on mechanical properties at room temperature. Moreover along with ultra-fine grained character and structural imperfections stress fields around these micropores yielded high structural damping behavior. However, at elevated temperatures attention has to be paid to expansion of gases entrapped within the closed pores, which may lead to the reduction of high temperature ductility.

This study further showed that ultra-fine Al powder possesses a great potential as matrix material in lightweight composites applications, especially where mechanical properties and structural stability at elevated temperatures are of prime interest.

1. Introduction

The large surface area of fine Al powders gives a rise to possibility to introduce relatively high amount of naturally formed surface oxide into the structure of subsequent compacts. Due to fine nature of surface oxides with thickness of ~5 nm [1], by nano-metric dispersion strengthened metal matrix composites (MMCs) can be produced in relatively easy way. It would be extremely technologically difficult to bring and redistribute evenly such a small dispersoids into structure intentionally if it were done by other techniques. Nano-metric dispersiods do not tend to act as micro-concentrators, are not susceptible to cleavage, do not cause formation of voids and good mechanical bonding is assured. As a result superior mechanical properties can be attained at substantially lower dispersion contents when compared to micro-metric sizes of dispersion particulates. Moreover oxide particles grain pinned the structure yielding unique structural stability of compacts even during high temperature long term exposures. To maintain desired ultra-fine grained microstructures and establish good metallurgical bonding between particles the consolidation is basically circumscribed to compaction routes based on introduction of shear deformation (mostly extrusion). It was expected that proper consolidation of fine Al powders would result in relatively easily prepared metal matrix composite profiles with superior mechanical properties especially at elevated temperatures, being in contrast to conventional high strength Al based alloys (based on precipitation strengthening). Al powder's compacts can be used as a promising candidate for non-degrading matrix material if connected with appropriate reinforcement in application where temperature strength and stability are of interest.

In order to desorb oxygen, water and other oxidizing gases absorbed on the surface of powder extrusion of encapsulated and degassed powder is wildly used. Otherwise it is recognized that shear deformation of powders introduced during consolidation gives rise to oxidation of newly "opened" surfaces yielding improper metallic bonding on powder interfaces [2]. Furthermore gasses being entrapped and compressed during consolidation lead to pronounced porosity and blistering and deteriorate mechanical properties of compacts at elevated temperatures. Moreover as a result of reaction between Al and water evolved hydrogen causes further pressure build-up within pores [2, 3]. All afore-mentioned phenomena are due to extreme powder surface area especially pronounced for herein studied ultra-fine size Al powders. On the other hand such a technologically difficult processing (degassing and encapsulating) of particles prior operation considerably surcharges the price of final compacts. In order to keep the expenses low and thus maintain potential industrial process feasible, compaction of loose (or CIPed) powder was established. Obviously profound interest is to be paid to maintain desired high temperature properties of compacts prepared in this way.

2. Experimental

1 μm Al powder of technical purity 99.7 % were prepared by gas atomization in N_2 atmosphere supplied by company MEPURA G.m.bH. [5]. Dimensional characterization of powder was determined by means of Helos analysis as follows: x_{50}=1.31 μm, x_{10}=0.66 μm, x_{90}=2.51 μm. Coarser 10 μm and 63-400 μm fraction Al 99.7 % powders were used for comparison.

Compaction was predominantly realized via conventional direct hot extrusion on pneu-hydraulical press. Different extrusion ratios (4:1, 11:1, 20:1, 44:1) with flat faced die shape were used for comparison. If not signed differently no flushing, degassing and canning were carried out prior extrusion. BN spray was used as a lubricant. Either loose or pre-compacted powder or mixture were filled into the preheated die (50 °C below extrusion temperature) and afterwards heated up to desired compaction temperatures for 30 min before extrusion. Load capacity limit during extrusion was set up to the value of 50 tons (i.e. stress of ~ 1.6 GPa) given by limitations of tool material. The ram speed during extrusion was adjusted to the lowest possible value. Nevertheless the particular value of the ram speed for each extrusion varied, depending on actual pressure demand. The average ram speed during extrusion within chosen compaction temperature range was ~1 $mm.s^{-1}$ (±0.8).

Structures of powders and extruded rods were examined by means of light microscopy, scanning electron microscopy (SEM) and transmission electron microscopy (TEM). To clearly demonstrate presence and distribution of nano-scale oxide dispersoids compacts were etched instead of ion bombarding during samples preparation for TEM. Relative density of the extrudates was measured via Archimedes route. The mechanical properties at room and at 300 °C (20 min to reach and stabilize desired temperature + 10 min dwelling prior experiment) were measured on specimens with the gauge of Ø4–32 mm (tension) and Ø5.5-10 mm (compression) using ZWICK tensile machine at the cross ram speed of 1 $mm.min^{-1}$. Vickers microhardness measurement were performed on compacts cross section with applied load of 10 g. Due to small dimension of final compacts, the unnotched fracture toughness specimens had non-standardized dimension 4x4x55 mm and were machined longitudinally to the extrusion axis. Regarding this restrictions, obtained nonstandard results of fracture toughness K_{CN} can not be compared to normalized values of K_C. Five fracture toughness specimens were machined for each extruded bar.

Dilatometry experiments of PM compacts were performed at the Technical university of Vienna using thermal–mechanical analysis equipment TMA 2940 CE, Thermal Instruments, USA [6]. In each test, the samples were positioned vertically on a quartz stage and a moveable probe was placed on the top of the sample with a negligible constant force ~7 kPa. It was filled with nitrogen (100 ml/min) during the test. 4 mm x 4 mm x 10 mm samples (two for each material) were heated up from room temperature up to 550 °C and cooled down to room temperature in three cycles at the rate of 3 $°C.min^{-1}$. The instantaneous coefficient of linear thermal expansion (CTE) at temperature T can be calculated from the measured dimension change as function of temperature $\Delta L(T) = L(T) - L_0$ divided by the initial specimen length at room temperature L_0. The repeatability of $\Delta L/L_0$ is given within ±0.01%, i.e., less than ±2 μm. Before derivation with respect to temperature, the $\Delta L(T)$ curve is smoothed within a width of 50 K, i.e., ±25 K around each temperature T using a least-square averaging method.

3. Results and discussion

3.1. Characterization of as-atomized powder

SEM observations revealed spherical morphology of as-atomized 1 μm powder (**Fig. 1**). Micrographs obtained by means of TEM confirmed the monocrystalline structure of 1 μm powder containing almost no dislocations (**Fig. 1**). Thanks to protective oxidic layer alongside with monocrystalline character of powder one does not have to be anxious about the lost of microstructural features of powder (coarsening, free sintering) during temperature exposures prior consolidation.

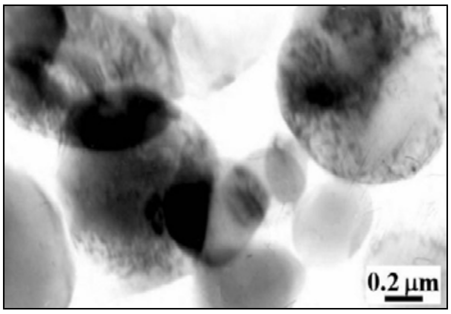

Figure 1 TEM - bright field micrograph of as-atomized 1 µm Al powder

3.2. Consolidation behavior during direct extrusion

Tab. 1 shows maximum pressures p_{max} needed for breakthrough during direct extrusion of Al powders at extrusion ratio R = 11:1. It covers also the lowest but still feasible extrusion temperatures (T_{ext}) for 1 µm, 10 µm and 63-400 µm Al 99.7 % powders at which sound compacts were succeeded to extrude (at R = 11:1). The lowest but still feasible T_{ext} for 1 µm powder was settled to value of 350 °C accompanied with p_{max} = 1376 MPa. Expected gradual pressure decrease was seen as coarser powders were used for extrusion at the same T_{ext}. The pressure p_{max} for 1 µm powder at 350 °C was more than twice higher than for 63-400 µm one. This was related to substantially higher volume fraction of surface oxides which had to be broken up due to obtain desired metallic bounds on interfaces of input powder particles. Higher volume fraction of surface oxides significantly increased the flow resistance of fine 1 µm powder. On the contrary extrusion of 10 µm powder at 350 °C accommodated only 13 % p_{max} decrease in comparison to extrusion of 1 µm powder. The coarser powders were managed to be pressed through a die at minimal T_{ext} of 300 °C and 250 °C for 10 µm and 63-400 µm powders, respectively.

Passing pressure peak p_{max} no sudden pressure fall connected with local temperature increase or dynamic recrystallization in just extruded 1 µm powder rods (R = 11:1) was observed [7]. Gradual pressure decrease after breakthrough, related to the reduction of overall friction in container as the extrusion proceeds, was similar for all powders. Expectedly, p_{max} decreased with increasing T_{ext} following $p_{max} = 2658 - 3.7\ T_{ext}$ tendency in studied temperature range (350 °C – 500 °C), **Tab. 1**. It is evident that the induced energy needed for plastic deformation of particles, cold welds, distortion and distribution of surface oxides is significantly higher as the powder mean size decreases and for lower extrusion temperatures.

Powder size [µm]	1				10		63-400	
T_{ext} [°C]	350*	400	450	500	300*	350	250*	350
p_{max} [MPa]	1376	1118	986	797	1506	1194	1274	648

Table 1 Breakthrough pressures during quasi-static extrusions of 1 µm, 10 µm and 63-400 µm Al 99.7 % powders. R = 11:1.
* - states for the lowest achievable T_{ext}

Evolution of p_{max} in hand with increasing R at 500 °C followed in studied range linear tendency $p_{max} = 698 + 9.2\ R$ (**Tab. 2**). Two fold increase of R led to ~10 % increase of p_{max} what was in good agreement with other works [8]. Similar behavior was observed either for T_{ext} = 500 °C wherein two fold R increase represented 13 % increase of p_{max}. R is a very powerful processing parameter where amount of induced plastic deformation (i.e. reduced porosity and better mechanical properties) can be enhanced with only marginal affect on required extrusion pressure or extrusion temperature.

Though in generally, to keep consolidation of powders technologically viable also at industrial scale, load demands shall not exceed p_{max} ~ 1000 MPa.

R	11:1	20:1	44:1
p_{max} [MPa]	797	885	1102

Table 2 Breakthrough pressures during quasi-static extrusions of 1 µm Al 99.7 % powder at 500 °C for different extrusion ratios R.

3.3. Microstructural characterization of powder compacts

Expectedly, as extrusion ratio increased during extrusion density of compacts increased. In **Tab. 3** is depicted continuing density improvement from 2.67 g.cm^{-3} to 2.69 g.cm^{-3} of 1 µm Al powder compacts extruded at 500 °C as R increased from 11:1 to 44:1. Extrusion performed at higher R more intensively closed up inner porosity. As seen from **Tab. 3** densities for given powder size remained approximately same within 350 °C – 500 °C regardless of T_{ext}. It is assumed to be caused by two competing phenomena. In spite of high resistance of Al powder to plastic deformation at low T_{ext}, severe work induced during extrusion maintained still acceptable density. On the contrary at high T_{ext} material was more viscous but rather low induced work could not provide equal gas press out and gas compression as at low T_{ext}. That is way the closed porosity remained same throughout of whole T_{ext} range. Expectedly smaller surface area of both coarser powders led to smaller internal porosity of their corresponding compacts (the effect of different Al_2O_3 content for different powders is neglected). Density of all compacts reached the values at the level of theoretical density (**Tab. 3**). Similar morphology of both powders, wherein coarser 63-400 µm powder particles were more or less conglomeration of smaller droplets, resulted in no major density differences between two coarser powders.

In case of 1 µm powder compacts and small engineering strains (R = 11:1) small pores (with diameter of ~0.5 µm) were found to be at grain / powder particle boundaries regardless of T_{ext}. That was in good agreement with density measurement. As densities measurements have indicated (**Tab. 4**), apparently smaller amount of micro-pores was determined within structure of 1 µm powder compacts extruded at higher extrusion ratios 20:1 and 44:1. As previously explained more intensive deformation improved both pressing of present gases away from compacted powder and close-up of micro pores.

Powder size [µm]	1				10				63-400
T_{ext} [°C]	350	400	450	500	350	400	450	500	350
ρ [g.cm^{-3}]	2.66	2.67	2.66	2.67	2.7	2.69	2.68	2.69	2.69

Table 3 Densities of compacts prepared via quasi-static extrusions of 1 µm, 10 µm and 63-400 µm Al 99.7 % powders. R = 11:1.

R	11:1	20:1	44:1
ρ [g.cm^{-3}]	2.67	2.68	2.69

Table 4 Densities of 1 µm Al 99.7 % powder compacts extruded at T_{ext} = 500 °C at different extrusion ratios.

TEM micrographs of extruded bars revealed deformation and fragmentation of initial powder particles of all studied powders into elongated grains mostly aligned along the extrusion direction even at the relatively small deformation (i.e. R = 11:1). As initially spherical powder particles elongated due to induced plastic deformation surface area enlarged what eventually led to oxide envelopes breakage. Where breakage of oxide envelopes took place newly "free" powder surfaces were created. Diffusion at these areas gave a rise to a formation of metallic bound "bridges" between individual powder particles. Incoherent plate-like oxide dispersoids in majority decorate former particles boundaries and

Extensive energy imposed to 1 µm powder during extrusion at low temperatures (350 °C) resulted in heavy deformed powder particles, superior fragmentation of surface oxides (whisker-like particles dark in contrast) and in homogeneous distribution of these fragments even inside of newly arose fine grains (**Fig. 2**). That was in contrast with microstructures obtained after extrusion carried out at higher T_{ext}. Extrusion held at T_{ext} = 500 °C did not ensured as fine microstructure as in case of T_{ext} = 350 °C and torn oxides were found predominantly at grain boundaries. Transversal grain size of extruded 1µm powder compacts was determined to be ~0.2 µm. A few small powder particles with initial diameter roughly similar to transversal grain size in the case of 1 µm powder compact (i.e. ~0.2 µm) remained non-deformed in 1 µm compacts, preserving their initial dislocation free structure.

Further increase of induced strain (i.e. higher R) on one hand led to reduction of residual porosity but on the other hand did not bring over additional structure refinement (**Fig. 3**). Microstructures of 1 µm Al powder compacts extruded at R = 20:1 and 44:1 at T_{ext} = 450 °C retained approximately same to those extruded at lower R = 11:1 and the same T_{ext}. Though, with careful look slight refinement contribution with R increase can be perceived. This grain refinement (at constant T_{ext}) is related partially to higher induced strain as well as to higher work required for breakthrough. Thus energy brought during consolidation was found to be more important parameter if homogenous oxide distribution and grain refinement are of interest. As the higher R was accommodated during extrusion at equal T_{ext} and extrusion speeds final grains tended to form more polygonized like microstructures. This might be attributed to the limits in reachable work grain refinement and the start of dynamic recovery processes. Moreover higher amount of heat developed during extrusion at higher R might accelerate dynamic recrystallization.

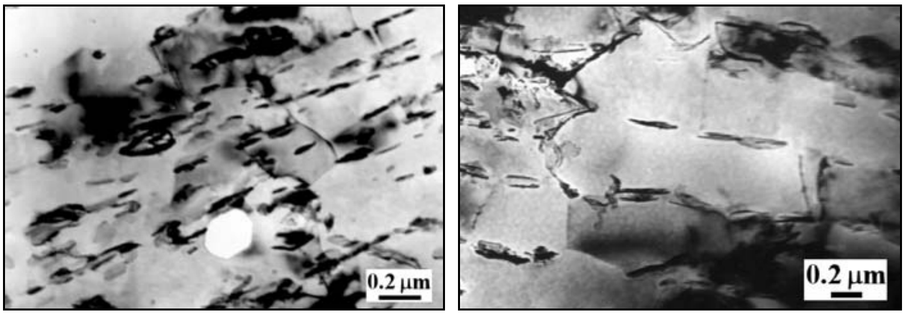

Figure 2 TEM cross-sectional micrographs (BF) of 1 µm Al powder compacts extruded at 350 °C (left) and 500 °C (right) at R = 11:1 (longitudinal to extrusion direction).

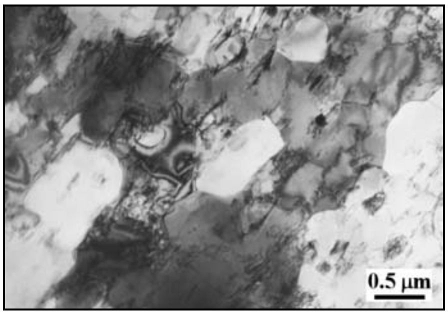

Figure 3 TEM cross-sectional micrographs (BF) of 1 µm Al powder compacts extruded at 500 °C at different R = 11:1 (left) and 44:1 (right). Longitudinal to extrusion direction.

Annealing experiments (350 °C @ 20 hours) proved the role of nano-scale oxides in preventing excessive grain growth at elevated temperatures of 1 µm and 10 µm powder compacts. These experiments accommodated no major microstructural changes, where microstructure of annealed compacts retained unchanged (**Fig. 4**). Further shift of annealing temperature towards higher values (500 °C @ 20 hours) led to clearly recognizable microstructural changes in case of 1 µm Al powder compacts (**Fig. 4**). Comparing to as-extruded state and to compacts annealed at 350 °C apparent grain growth already took place. As it is seen oxides dispersiods were drifted away by former powder interfaces during thermal exposure. Eventually they were exclusively found at the new grain boundaries. Moreover due surface area minimization govern by diffusional processes they became spherical in shape. Nevertheless massive coalescence of dispersed phase was avoided.

Generally, in respect to amount of reinforcing phase within structure of compacts, detected structural stability is far superior to conventional Al-based materials.

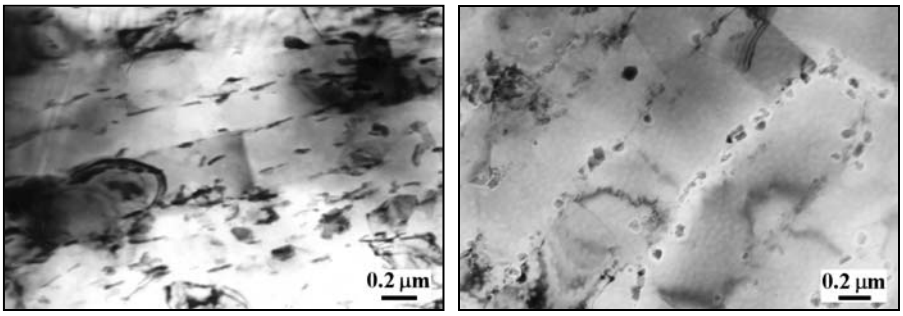

Figure 4 TEM micrograph (BF) of 1 µm Al powder compacts extruded at 350 °C after annealing at 350 °C (left) and 500 °C (right) for 20 hours

3.4. Effect of porosity and entrapped gasses within powder compacts

Simple consolidation route without prior degassing, where powders were consolidated in loose (or CIPed) state, resulted in compact's microstructures with higher amount of ultra-fine pores. The negative effect of gasses entrapped within pores on mechanical properties was in first step assessed by means of dilatometry tests.

Sharp deviation from near-to-linear CTE course was observed during the first heating cycle for compacts extruded at lowest T_{ext} = 350 °C (**Fig. 5**). It had onset at temperatures of ~100 °C below T_{ext}, reaching its maximum at ~500 °C and followed by steep CTE fall. Long cracks and interconnected micropores paths were observed within the structure of these samples, subjected to dilatometry tests (**Fig. 6**). This "foaming" phenomenon was clearly related to the entrapped gas compressed within the compacts volume, which massively expanded during first heating cycle and plastically deformed material until cracks formed. Eventually formed cracks enabled gas to release.

On the contrary compacts extruded at highest 500 °C showed an increase of the CTE during the first cycle (due to entrapped gas) but there was no failure observed at higher temperatures. It refers to the fact that the lower work induced during extrusion at higher T_{ext} along accommodated less gasses compression into the pores. Thus gas only expanded and did not lead to plastic fracture of compacts. That was supported by the fact that this increase was also observed in the subsequent cycles. No obvious cracks were determined in compacts volume.

Thermal expansion of compacts extruded at intermediate T_{ext} = 400 °C and 450 °C merged somehow behavior of two limiting cases. The higher T_{ext} was, the increase of the CTE due to the gas expansion was shifted towards higher temperatures.

Observed expansion of entrapped gas would be unambiguously inferior during potential service of this type of material at elevated temperatures. Especially it would concern extrudates prepared at low T_{ext}. Not to deteriorate desired high temperature mechanical properties service temperature of compacts shall not exceed particular temperature material has seen during consolidation (i.e. T_{ext}).

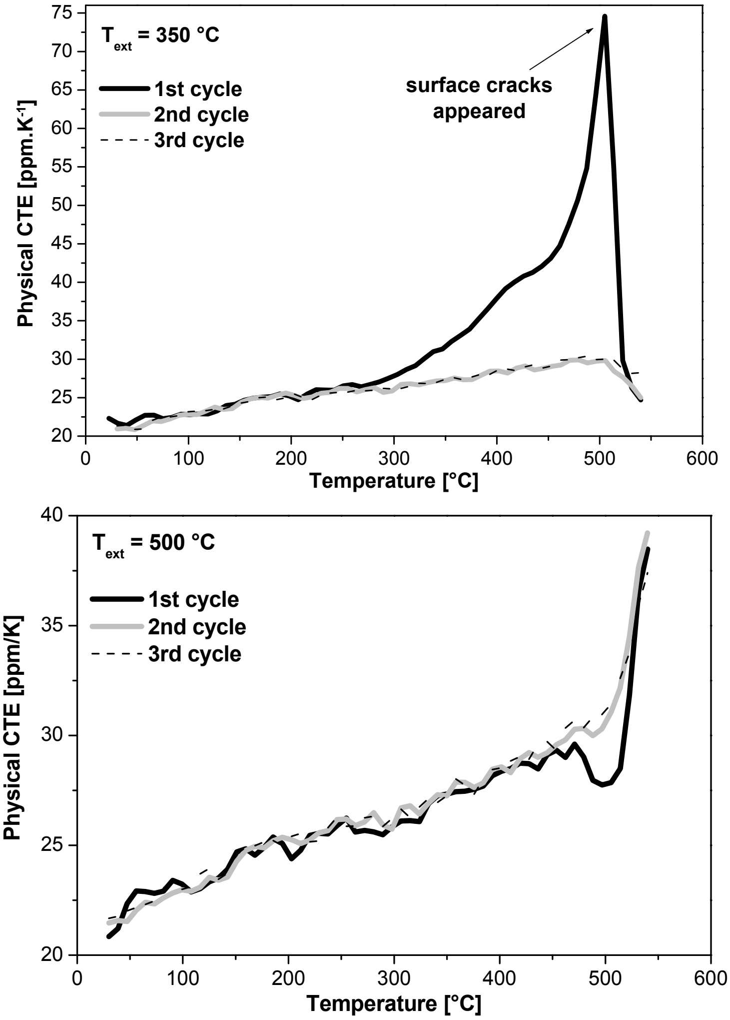

Figure 5 CTE course of 1 μm Al 99.7 % powder compacts extruded at R = 11:1 and different T_{ext} during three subsequent heating cycles (3 °C.min^{-1})

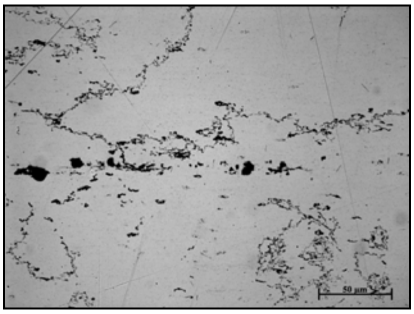

Figure 6 Detail of interconnected pores in volume of 1 μm Al 99.7 % powder compact extruded at R = 11:1 and T_{ext} = 400 °C subjected to dilatometry experiments.

Increase of deformation strain during extrusion of 1 μm Al powder had no substantial influence on expansion behavior of following compacts in studied R range from 11:1 to 44:1. Similar break-ups from linear CTE tendency at about the point of the particular T_{ext} were determined either for R = 20:1 as well as for R = 44:1.

Compacts made of coarser 10 μm powder extruded at T_{ext} = 350 °C and the same R = 11:1 accommodated similar "foaming" and gas realizing phenomena during first heating cycle. Again break-away from CTE course during first cycle is seen. The initiation of expansion is however shifted towards to higher temperature ~ 410 °C. This clearly refers to the less pronounced effect of expanding gas due to less specific powder surface and quantity of entrapped gases. On the contrary compacts prepared of the coarsest 63-400 μm powder expectedly accommodated no "gas foaming" phenomena behaving as an ideal bulk ingot material.

3.5. Mechanical properties of powder compacts

Tab. 5 summarizes mechanical properties obtained from tensile test measurements of powder compacts extruded at R = 11:1. Relatively high UTS values of 310 MPa accompanied with quite good ductility (A) of 9 % were determined for 1 μm powder compacts compacted at 350 °C. As the amount of work introduced during extrusion decreased (i.e. higher T_{ext}), UTS of compacts fell off gradually. This tendency was either confirmed by microhardness measurements on powder compacts. 20 % strength and HV increase as T_{ext} fell from 500 °C to 350 °C was attributed to finer microstructures with severely elongated powder particles. Moreover more homogenously redistributed oxide despersoids additionally strengthen powder compacts.

Considerably higher strength (at roughly similar A) of 1 μm powder compacts comparing to coarse powders can not be attributed only to higher oxide level in fine powder compact (**Tab. 5, Fig. 7**). Again this was mainly due to considerably finer microstructures and more appropriate redistribution of dispersoids within structure.

Powder size [μm]	1				10				63-400
T_{ext} [°C]	350	400	450	500	350	400	450	500	350
HV	102.2	96.1	87.3	85.9	75.7	66.3	64.9	63.6	-
$YS_{0.2}$ [MPa]	247	238	227	213	211	183	167	160	122
UTS [MPa]	310	305	290	280	261	234	219	204	149
A [%]	9	8.7	10.9	10.4	11.1	8.4	15	4.1	13.4
E [GPa]	63.9	64.3	63	64.5	65.4	65.4	65.8	62.4	62.2

Table 5 Room temperature mechanical properties of compacts prepared via quasi-static extrusions of 1 μm, 10 μm and 63-400 μm Al 99.7 % powders. R = 11:1.

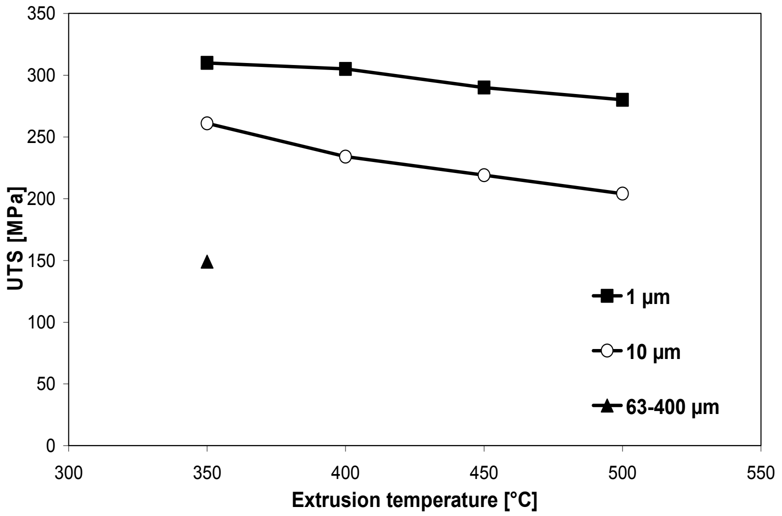

Figure 7 Room temperature ultimate tensile strengths of compacts extruded at 350 °C as function of powder size (R = 11:1, tensile tests).

Further increase of plastic strain induced during extrusion (higher R) yielded partial dynamic recrystallization and eventually did not lead to improved compacts strength (**Tab. 6**). That was in good correlation with corresponding micrographs of 1 µm Al powder extrudates. Extrudates prepared at higher R = 20:1 and 44:1 showed even slight decline in obtained UTS. Since herein described extrusion trails were performed at the same T_{ext} induced plastic work differentiated for each trails. That would even raise the diminishing effect of work recrystallization on obtained strength if compared with compacts extruded with equal plastic work (i.e. extrusion at R = 11:1 @ T_{ext} = 350 °C with R = 44:1 @ T_{ext} = 450 °C).

R	11:1	20:1	44:1
HV	87.3	87.2	89.4
UTS [MPa]	290	271	282
A [%]	9	8.9	9.2

Table 6 Room temperature mechanical properties of 1 µm Al 99.7 % powder compacts extruded at T_{ext} = 450 °C and different extrusion ratios R

Average values of non-standardized Charpy impact fracture toughness K_{CN} for all compacts extruded at R = 11:1 sufficiently exceeded values required by industrial applications and were at the level ~40 $J.cm^{-2}$ regardless of T_{ext}.

Room temperature tensile tests performed on annealed 1 µm Al compacts (350 °C @ 20 hours) confirmed superior grain pinning effect of nano-scale oxides preventing excessive grain growth of compact's microstructures at elevated temperatures (**Fig. 8**). Only slight ~5 % decrease in room temperature UTS after annealing was confirmed. It was attributed to stress relieve retained in compacts after extrusion. For the case of both coarse powder compacts decrease in UTS was more evident. Annealing of 10 µm and 63-400 µm powder compacts resulted in UTS declines of 9 % and 13 %, respectively. This was attributed to the lack of oxide pinning spots when comparing to 1 µm powder compacts.

Comparing 1 µm powder compacts extruded at 500 °C in as-extruded state and after annealing almost no alteration in room temperature UTS and A were observed (**Fig. 8**). It is seen that residual stresses concealed in compacts were proportional to induced plastic work and are not as pronounced as they were in this case of extrusion performed at 350 °C.

Long term annealing at extremely high temperatures (500 °C @ 20 hours) of 1 µm Al powder extrudates led to more significant room temperature strength decline. Strength deterioration after annealing at 500 °C comparing to as-extruded state represented ~50 MPa (**Fig. 8**). Again higher T_{ext} with less work induced responded in less absolute strength deterioration. Unlike the compacts annealed at 350 °C overall strength decline can not be explained solely by stress relief but it simultaneously acted in hand with obvious grain growth. Ductility of all compacts after 20 hours annealing at 350 °C and 500 °C retained approximately unchanged.

It should be pointed out that no blistering or cracking due released gas were recognized in the whole range of compacts prepared at R=11:1 exposed up to 500 °C for 20 hours.

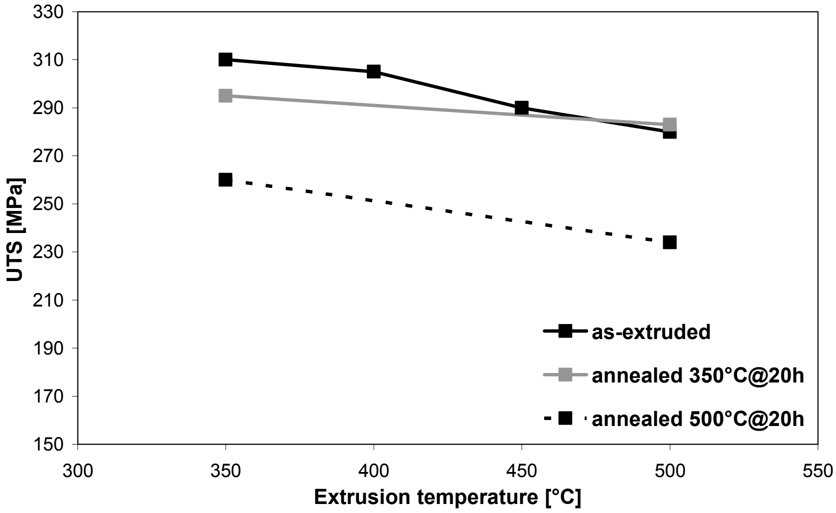

Figure 8 Room temperature UTS of extruded 1 μm powder compacts extruded at different T_{ext} in as-received state and after annealing at 350 °C and 500 °C for 20 hours (R = 11:1)

Tensile tests performed at 300 °C revealed favourably high values of UTS ranging from 186.7 MPa to 159.9 MPa for compacts extruded in T_{ext} range from 350 °C to 500 °C (R = 11:1), **Tab. 7**. With further increase of testing temperature compacts still preserved their very attractive strength (**Fig. 9**). That refers to the importance of oxide dispersoids embedded in grain boundaries regions. Beside of grain pinning effect, they acted by means of mechanical keying as a barrier to high temperature grains sliding.

On the other hand tensile loading of compacts at 300 °C resulted in substantial, approximately three fold decrease in ductility of all compacts (**Tab. 7**). Ductility increased from A = 1.7 % to 3.3 % with increasing T_{ext} value from 350 °C to 500 °C, respectively. Described ductility drop at elevated temperatures was governed by expanding gas entrapped within small pores. Small openings formed as a result of gas expansion initiated premature failure of compacts during tensile tests at 300 °C. Despite of rather similar residual porosities of 1 μm Al powder compacts extruded at different T_{ext}, gas expansion and crack creation at 300 °C were critical only for case of low T_{ext} (i.e. 350 °C). At low T_{ext} entrapped gas was close up and compress in more pronounced way comparing to higher T_{ext}. Moreover pressure build-up due to decomposition of absorbed humidity from powder surfaces acted in more pronounced way in case of compacts exposed to lower temperatures prior extrusion.

Powder size [μm]	1				10	63-400
T_{ext} [°C]	350	400	450	500	350	350
UTS [MPa]	186.7	181.7	168.9	159.9	147	79
A [%]	1.7	1.5	2.2	3.3	17.5	15.7
E [GPa]	45.7	39.2	41.3	47.2	45	48.6

Table 7 Mechanical properties of extruded Al 99.7 % powder compacts obtained from tensile tests performed at 300 °C (R = 11:1)

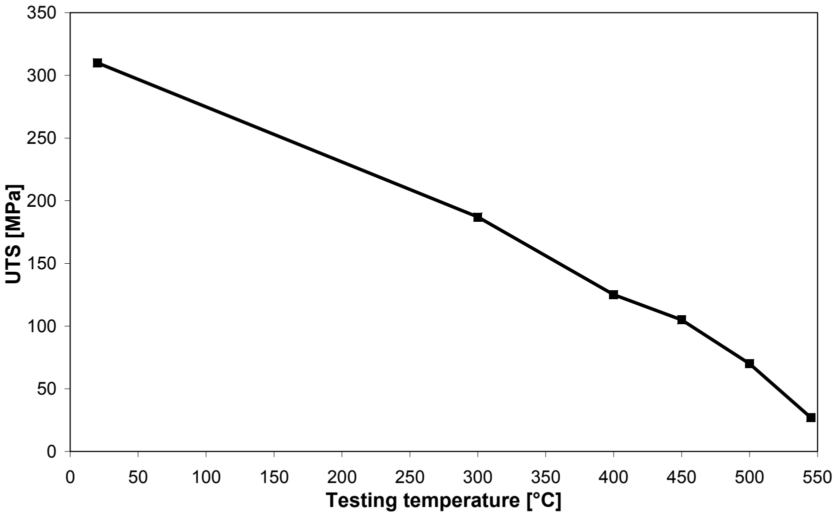

Figure 9 UTS evolution in hand with testing temperature of 1 µm Al 99.7 % powder compacts (T_{ext} = 350 °C, R = 11:1)

Alike room temperature tensile tests, compacts extruded at different deformation strains (i.e. R) showed very similar high temperature deformation behaviour (**Tab. 8**). UTS values of compacts extruded at R = 11:1, 20:1 and 44:1 tested at 300 °C remained approximately unchanged in the range 168.9 – 163.8 MPa. In spite of lower residual porosity reached by higher deformation rates, inferior high temperature ductility improved only marginally. In spite of promising results from dilatometry tests higher R did not sufficiently solved out the negative effect of entrapped gas on high temperature ductility.

R	11:1	20:1	44:1
UTS [MPa]	168.9	167.5	163.8
A [%]	2.2	3.7	3

Table 8 Mechanical properties obtained from tensile tests performed at 300 °C of 1 µm Al 99.7 % powder compacts extruded at T_{ext} = 450 °C and at different extrusion ratios.

Expectedly compacts of both coarser powders showed deeper relative decline in UTS obtained from tensile tests held at 300 °C (**Tab. 7**). Again, gradual increase of relative UTS decline as the size of Al powder increased was attributed to efficiency in disperse strengthening. Conversely, ductility of both coarser Al powders compacts at elevated temperatures 10 µm and 63-400 µm even increased, when compared to as-extruded state. This correlates with high theoretical relative densities of compacts of both coarser Al powders wherein expansion of entrapped gas did not affect so distinctly their high temperature ductility.

4. Conclusions

In presented work Al profiles with exceptional mechanical properties at room as well as at elevated temperatures, with superior structural stability at elevated temperatures were prepared using viable, relatively easy and inexpensive way. Herein commercially available atomized 1 µm 99.7 % powders were compacted in loose (CIPed) form via conventional hot PM extrusion performed at technologically feasible deformation strains. Thus commonly included processes of expensive HIP were avoided in presented approach. Consolidation process and compacts featured following characteristics:

Direct hot extrusion - processing

- sufficient straining and powder consolidation was already assured by extrusion ratio R = 11:1
- extrusion temperature (T_{ext}) had fundamental effect on pressure demand (p_{max}) and thus importantly influenced deformation work induced into compacted powder during extrusion (at R = 11:1 T_{ext} = 350 °C and 500 °C yielded p_{max} = 1376 MPa and 797 MPa, respectively)
- relation in between R and p_{max} followed linear tendency wherein in studied range $p_{max} = 698 + 9.2$ R

- due to higher content of surface α-Al_2O_3 extrusion of fine 1 μm Al 99.7 % powder accommodated significantly higher p_{max} when compared to coarser counterparts (at R = 11:1 and T_{ext} = 350 °C powders of 1 μm, 10 μm and 63-400 μm mean size yielded p_{max} = 1376 MPa, 1194 MPa and 648 MPa, respectively)

Density of compacts

- compacts featured high densities over 2.67 $g.cm^{-3}$ what represented relative densification over 97 %
- higher deformation strains led to slightly improved residual porosity (R = 11:1 and 44:1 for 1 μm Al powder at T_{ext} = 350 °C s yielded ρ = 2.67 $g.cm^{-3}$ and 2.69 $g.cm^{-3}$, respectively)
- T_{ext} did not affect obtained ρ of compacts in neither of powder's size

Microstructural characterization of compacts

- already extrusion at R = 11:1 enabled enough straining, where compact's microstructure consisted of heavily deformed grains elongated along extrusion direction
- deformation work had paramount influence on structure refinement, wherein severe work induced at low T_{ext} yielded superior ultra-fine grained microstructures (transversal grain size d_{trans} = 0.2 μm and 0.5 μm were attained after extrusion at T_{ext} = 350 °C and 500 °C, respectively)
- surface oxide's envelopes were torn by means applied shearing into nanoscopic dispersion flakes homogenously redistributed within compact's structure
- content of oxide dispersion phase was calculated to be roughly about 1.2 wt.%
- torn oxide's dispersoids predominantly decorated initial powder particles boundaries
- in compacts subjected to massive work during extrusion (i.e. low T_{ext} = 350 °C) dispersoids were found embedded even inside of grain areas
- by dispersoids grain pinned structure retained unchanged even after long term (20 hours) exposures at 350 °C
- long term annealings at 500 °C already accommodated moderate grain coarsening, coalescence and spheroidization of oxide's dispersion
- compact's microstructures prepared at higher R = 20:1 and 44:1 (T_{ext} > 450 °C) already experienced dynamic recrystallization and did not lead to further grain refinement
- extrusion of coarser 10 μm and 63-400 μm powders resulted in coarser microstructures (d_{trans} = 0.8 μm and 1 μm, respectively), more prone to grain coarsening under thermal exposures

Effect of porosity and entrapped gasses

- extrusion of loose (CIPed) undegassed powders resulted in gases entrapment and their compression in small pores which tended to expand during the service of all compacts at elevated temperatures
- onset of non-linear expansion due to compressed gases started at testing temperature which approximately equaled with particular T_{ext}
- expanding gas in case of compacts extruded at low T_{ext} (350 °C and 400 °C) led to formation micro and macroscopic cracks, which enabled gas to release at testing temperature ~500 °C
- compacts extruded at higher T_{ext} showed only marginal (T_{ext} = 450 °C) or none (T_{ext} = 500 °C) gas liberation (i.e. cracks formation)
- higher deformation strains (R = 20:1 and 44:1) diminished the effect of expanding gas
- usage of coarser 10 μm Al powder only marginally minimized the effect of entrapped gasses
- compacts extruded of 63-400 μm Al powder accommodated no "foaming" phenomena
- CTE for all 1 μm Al 99.7 % powder compacts regardless of T_{ext} tended to follow linear tendency and was found within range 22.10^{-6} - 30.10^{-6} K^{-1} in studied temperature range up to 550 °C

Mechanical properties

- regarding character of herein presented compacts (Al 99.7 %) and strengthening with small amount of α-Al_2O_3 dispersed phase (~1.2 wt.%) superior mechanical properties were attain in broad temperature range
- superior mechanical properties were defined by ultra-fine grained microstructure of pure Al, effective dispersion strengthening and grain-pinning with nano-scopic oxide dispersoids
- room temperature ultimate tensile strength (UTS) up to 310 MPa accompanied with good ductility (A) around 10 % were determined for extrudates prepared at R = 11:1
- higher deformation work induced to compacted powder (i.e. lower T_{ext}) yielded slightly improved strength values (UTS = 310 MPa for T_{ext} = 350 °C and UTS = 280 MPa for T_{ext} = 500 °C) at approximately unchanged A
- non-standardized Charpy impact fracture toughness K_{CN} in the range 38.3 $J.cm^{-2}$ – 53.7 $J.cm^{-2}$ was determined, what are values which meet goals for structural applications

- had experienced dynamic recrystallization during extrusion at higher deformation strains extrudates showed slightly inferior room temperature strength (UTS = 271 MPa for R = 20:1 and UTS = 282 MPa for R = 44:1, T_{ext} = 450 °C) at approximately unchanged A
- owing good structural stability long term (20 hours) annealing at 350 °C led to only marginal 5 % decline in room temperature UTS, though grain coarsening after extreme long term annealing at 500 °C yielded 15 % deterioration
- linear decrease in UTS at elevated temperatures was determined up to 550 °C, wherein compacts showed promising UTS = 187 MPa and 79 MPa at testing temperatures 300 °C and 500 °C, respectively
- expansion of entrapped and compressed gasses led to formation of interconnected micropaths and openings, where premature quasi cleavage failures were initiated at elevated temperatures leading do inferior high temperature ductility (A = 1.7 % for T_{ext} = 350 °C and A = 3.3 % for T_{ext} = 500 °C, R = 11:1, testing temperature 300 °C)
- higher deformation strains (R>20:1) assured slightly improved high temperature A
- compacts of coarser powders could not surpass superior strength values of their 1 μm Al 99.7 % "counterpart" at either of any testing temperature and their insensitivity to high temperature exposures
- owing to ultra-fine grained character, stress fields around high amount of tiny pores and structural imperfections compacts possessed desired high damping capacity (loss factor of 0.029 and 0.091 for testing temperature 25 °C and 300 °C, R = 11:1, T_{ext} = 350 °C)

5. Literature

[1] Nylund A., Olefjord I., Materials science and engineering, A134 (1991) 1225-1228

[2] Duszczyk J., Limit diagrams for the extrusion of 7XXX series P/M rapidly solidified aluminium alloy

[3] MEPURA G.m.b.H., http://www.mepura.at

[4] K. Xia, X. Wu, Scripta Materialia 53, 1225-1229 (2005)

[5] Nagy J., Balog M., Izdinsky K., Simancik F., Svec P., Janickovic D., International Journal of Materials and Product Technology, 79-90, Vol. 23, Nos. 1/2, (2005)

[6] Zhou J., Extrusion of Al-Si-X alloys prepared from RS powders, Dissertation thesis, (1991)

6. Acknowledgments

The financial support of the Slovak Agency for S&T Support under the projects APVT-51-021102 and APVT-51-031204 and State Project 2003 SO 51/03R 06 00/03R 06 03 is gratefully acknowledged. The authors thank Austrian company MEPURA GmbH for the supply of fine Al powders.

11. Savjetovanje o materijalima, tehnologijama, trenju i trošenju
11. Conference on Materials, Processes, Friction and Wear
MATRIB'06, Vela Luka, 22-24.06.2006.

PRAVCI RAZVOJA AKTIVNOSTI ZA SMANJENJE ILI UKLANJANJE ŠTETNOG DJELOVANJA ZAVARIVAČKOG DIMA

ACTIVITIES DEVELOPMENT DIRECTIONS FOR REDUCING OR REMOVING WELDING FUME HAZARDOUS EFFECTS

Mr. Razija Begić,
Univerzitet u Bihaću, Tehnički fakultet,
Bihać, BiH
Prof. Dr. Sead Pašić,
Univerzitet „Džemal Bijedić", Mašinski fakultet,
Mostar, BiH

Sažetak: Veoma štetno dejstvo zavarivačkg dima na zavarivača i okoliš, kao i sve stroži zakoni i propisi o dozvoljenom izlaganju štetnim supstancama zavarivačkog dima, iniciraju istraživače da svoje aktivnosti u ovom području usmjere u novim pravcima. Razvijaju se modeli za predviđanje i određivanje nivoa stvaranja isparavanja, kako bi proizvođači dodatnih materijala za zavarivanje mogli da razviju nove proizvode i procese koji će osigurati niži nivo štetnih isparavanja. Modeli za predviđanje mogu biti empirijski, teoretski ili kombinacija ova dva. Pored ovog pravca razvoja istovremeno se radi i na razvoju uređaja i pristroja koji će omogućiti mehaničko uklanjanje štetnih zavarivačkih dimova iz zone disanja zavarivača. Ovi pristroji se razvijaju u vidu navlaka koje pokrivaju područje zavarivanja, kod nekih postupaka, a služe za prikupljanje i odvođenje zavarivačkog dima iz zone zavarivanja. U radu su napravljena poređenja sastava okolnog zraka koji udiše zavarivač u zavisnosti od primjenjenog načina smanjenja količine zavarivačkog dima i štetnih supstanci u njemu.

Ključne riječi: zavarivački dim, štetne supstance, modeli stvaranja isparavanja, zaštitna navlaka

Abstract: Welding fume hazardous effects on welders and environment as well as more strict laws and regulations regarding to exposure to hazardous substances initiated investigators activities to new directions. Prediction models are developed for determining welding fume generation levels in order that manufacturers of materials can develop new products and processes which have lower welding fume levels. This models can be empiric or theoretic or combination these two models. Beside this investigators are developing apparatus which mechanical remove hazardous welding fume from welders' breathing zone. This apparatus are developed as hoods which cover welding zone in order to exhaust welding fume from welding zone. This study compares welders' breathing zone dependably of application of different methods for reducing welding fume hazardous substances.

Key words: welding fume, hazardous substances, welding fume generation models, shielding hood

1. UVOD

Zavarivački dimovi su, po definiciji, toksični metalni dimovi koji se generišu pri svim postupcima elektrolučnog zavarivanja. Sastoje se od teških metala, metalnih oksida, hemijskih jedinjenja i plinova. Hemijski sastav zavarivačkih dimova je različit i ovisi o sastavu osnovnog i dodatnog materijala za zavarivanje, kao i primjenjenom postupku zavarivanja. Prekomjerno izlaganje zavarivačkom dimu može da dovede do različitih neželjenih efekata po zdravlje zavarivača. U tabeli 1 su dati neki štetni sastojci zavarivačkog dima i zdravstvene smetnje koje oni izazivaju kod zavarivača.

Tabela 1. Opasni metali i metalni oksidi u dimu i njihovi efekti na ljudski organizam [4]

Metal	**Uzročni faktori**	**Potencijalni efekti**
Cr	Šestovalentna jedinjenja (kromat, Cr -VI)	Rastvorljivi Cr-VI: Iritativne i toksične efekte na kožu i sluzokožu,Nerastvorljivi Cr-VI: kancerogen za ljude (pluća, respiratorni trakt), alergijski efekti na koži
Ni	Jedinjenja sa niskom i visokom rastvorljivošću, NiO	Kancerogen za ljude (pluća, unutrašnjost nosa), alergijski efekti na koži
Mn	Metal i jedinjenja	Štetan za živce, kao oksid ima iritativan i toksičan efekat na respiratorni trakt, neurotoksičan
Zn	Oksid-sastojak dima	Izaziva metalnu groznicu uključujući Zastoje u disanju (nerazumljiv mehanizam, moguće imunološki), generalno nerazjašnjene štete
Cu	Oksid-sastojak dima	Izaziva metalnu groznicu uključujući Zastoje u disanju (nerazumljiv mehanizam, moguće imunološki), generalno nerazjašnjene štete
Co	Metal i jedinjenja	Kronični bronchitis, astmu (moguće toksičan i / ili izaziva alergijske reakcije), u tvrdim metalima fibrozu pluća, kancerogen u eksperimentima izvedenim na životinjama, alergijski efekti na koži
Ka	Metal i jedinjenja	Toksičan za bubrege(dugotrajni efekti trovanja), kao oksid ima jak toksičan efekat na respiratorni trakt i pluća, kancerogen u eksperimentima izvedenim na životinjama
Pb	Metal i neorganska jedinjenja	Anemija, štetan za živce i bubrege
Al	Metal i jedinjenja	Kao prašak izaziva fibrozu pluća,možda štetan za živce
Ba	Rastvorljiv u jedinjenjima	Štetan za živce i mišiće, utječe na poremećaj ravnoteže soli

Zbog kratkotrajnih i dugotrajnih negativnih efekata na zdravlje zavarivača, nacionalni instituti za sigurnost i zdravlje u industrijski razvijenim zemljama preporučuju da se nivo zavarivačkog dima strogo kontroliše, a da vrijeme boravka zavarivača, uz korištenje adekvatne zaštite, u tim uslovima bude ograničeno.

Iako su sastav zavarivačkih dimova istraživali mnogi znanstvenici, jako je teško za rezultate njihovih istraživanja donijeti jedinstvene zaključke. Jedan od problema je ograničena preciznost postignutih rezultata a također je komplicirana njihova interpretacija i korelacija zbog velikog broja varijabli. Mnogi od prvih radova iz ovog područja su bili usmjereni na rješavanje trenutnih problema na radnom mjestu. Studije o stvaranju isparavanja imaju veliki broj varijabli da ih je gotovo nemoguće bilo koristiti u teoretske svrhe. Većina istraživanja su napravljena tako da daju precizne rezultate u ograničenim uvjetima. I pored toga rezultati istraživanja su aplikativni u konkretnim uvjetima jer se zaključci izvode na osnovu kombinovanja teoretskih i eksperimentalnih rezultata.

2. PRAVCI RAZVOJA ZAŠTITE ZAVARIVAČA I OKOLINE OD ŠTETNOG UTJECAJA ZAVARIVAČKOG DIMA

Kontrola izlaganja zavarivačkom dimu je važno pitanje za zdravlje i sigurnost na radnom mjestu. *Occupational Safety & Health Administration* (OSHA), USA, je donio zaključke da postojeće metode kontrole zavarivačkog dima moraju biti unaprijeđene ili se moraju razviti nove metode i tehnike zavarivanja koje će sa ekološkog aspekta biti efikasnije, a prihvatljive u pogledu troškova [3]. Većina objavljenih istraživanja je usmjerena na unaprijeđenje postojećih tehnika zavarivanja uz prevenciju stvaranja zavarivačkog dima mjenjanjem hemijskog sastava žice i obloge elektrode ili prebacivanje na druge metode zavarivanja.

Napredak u istraživaju sastava zavarivačkog dima i njegovog utjecaja na zavarivača je postignut dizajniranjem izradom nove komore od strane AWS za skupljane isparavanja u toku zavarivanja. Ova fleksibilna komora je u odnosu na prethodne izvedbe komora nivo isparavanja mjerila sa velikom preiznošću i tačnoću. Premjestena je na novu lokaciju New England Welding Research Consortium-a (Harward school of Public Health) gdje se koristi za projekte koji uključuju isparavanja nerđajućeg čelika i uticaj na zdravlje radnika koji udišu takva isparavanja [5].

Jedan od nekonvencionalnih načina unapređenja uslova rada zavarivača, predviđa stvaranje modela za predviđanje nivoa generisanja zavarivačkog dima. Ovi modeli mogu biti empirijski ili teoretski ili kombinacija ova dva. Da bi sistem bio uspješan treba uspjeti predvidjeti nivo stvaranja dima uz korištenje kombiniranih parametara zavarivanja i karakteristika elektrode.

Također još jedan efikasan način eliminisanja zavarivačkog dima se oslanja na ideju kontrolisanja količine dima na izvoru njegovog nastajanja, odnosno njegovog efikasnog uklanjanja sa mjesta nastanka. Ove studije istražuju razvoj posebnih navlaka koje bi prekrivale gorionik za zavarivanje ili elektrodu i odstranjivale zavarivački dim direktno sa mjesta izvora njegovog nastanka.

2.1 Modeli za predviđanje nivoa stvaranja isparavanja

Teoretsko empirijski modeli za predviđanje nivoa isparavanja u funkciji od parametara zavarivanja, bi pomogli u razumjevanju mehanizma nastanka isparavanja. To bi bila veoma značajna pomoć u traženu boljih uslova rada za zavarivače. Postoji više takvih modela, a kao primjer se mogu navesti Deam i Dennis model, zasnovani na teorijskom radu Haidar-a. Novi model je formiran na onovu navedena dva modela [1]. Pomoću ovog modela moguće je predvidjeti koncentraciju Fe i Mn u isparavanju.

U globularnom i sprej načinu, isparavanja uglavnom nastaju isparavanjem metala iz kapljice na temperaturi od 2500 K. U ovom modelu je primjenjen gasni elektrolučni postupak zavarivanja GMAW za zavarivanje čelika srednje jačine. U razmatranje je uzeto samo isparavanje nastalo iz kapljice formirane na vrhu elektode prema Denis-ovom modelu. Dio isparavanja nastaje u električnom luku, dio nastaje iz prskanja mjehurića gasa iz kapljice, a dio iz kapljice koja je izbačena iz područja luka i tada lako oksidira sa kisikom iz okoline. Većina para metala se kondenzira bez stvaranja isparavanja ali ipak jedan dio para odlazi iz područje luka i reagira sa kisikom formirajući metalne okside.

Na osnovu Deam modela je procjenjena kondenzacija para metala osnovnog metala. Rezultati predviđanja modela su: temperatura kapljice, količina isparavanja nastala iz kapljice, količina isparavanja nastala nakon kondenzacije osnovnog metala i ukupnu količinu isparavanja itd. Model bi trebao da bude što prihvatljiviji i jednostavniji sa lako mjerljivim ulaznim veličinama. Model treba da predvidi nivo svaranja isparavanja uzimajući u obzir karakteristike primjenjenog postupka zavarivanja i karakteristike elektrode. Neke od tih karakteristika su: jačina struje, nivo kapanja, širina elektrode, dužina el. luka itd.

Dobivene jednačine novim modelom se odnose na: računanje prosječne temperature kaplice koja se odvojila sa vrha elektrode, količinu energije po jedinici volumena na kraju elektrode, temperaturu na površini kapljice, povećani volumen kapljice na temperaturi, gustoća kapljice, gubitak mase kapljice, gubitak radijacione energije iz kapljice, prenos konvekcione energije iz luka u kapljicu, brzina plazme, konvekciona sila gasa u zoni zavarivanja, isparavanja iz kapljice, gubitak energije zbog latentne topline isparavanja, vrijeme padanja kapljice, ubrzanje kapljice.

Masa isparenog Fe i Mn se ocjenjuje na osnovu sastava kapljice, nivoa punjenja žice i sastava žice. Jednačine za računanje nivoa stvaranja isparavanja metala u dimu (M_{FFR}) su:

$$M_{FFR} = M_{VGR} (1+ M_{VGR} / 2\alpha)^{-1} \quad [kg\ s^{-1}]\ [1], \qquad (1)$$

$$\alpha = U_0\, \pi\, (l_{mix})^2\, \rho_v \qquad [kg\ s^{-1}]\ [1], \qquad (2)$$

gdje su:
M_{VGR} – nivo stvaranja matalnog isparavanja
U_0 – brzina zaštitnog gasa na izlazu iz dovoda
l_{mix} – metalna isparenja u zaštitnom gasu
ρ_v – gustoća isparavanja

gustina isparavanja za element i je data jednačinom:

$$\rho_{vi} = M_i\, x_i\, P_i / (RT_{ds}) \quad [kg\ m^{-3}]\ [1], \qquad (3)$$

gdje su:
ρ_{vi} – gustoća isparavanja i-tog elementa
M_i – atomska masa elementa
x_i – frakciona masa elementa i u kapljici
P_i – pritisak elementa i u pari
R – konstanta univerzalnog gasa
T_{ds} – temperatura površine kapljice

Isparavanja kod GMAW zavarivanja imaju 65 % metala. Analizirani su samo sadržaj Fe i Mn, ostali elementi u tragovima npr. Si nisu analizirani. Pretpostavlja se da je zbir sadržaja Fe+Mn=const. približno 65 %. U tabeli 1 su prikazani uporedni eksperimentalni rezultati sadržaja Fe i Mn u zavarivačom dimu i rezultati sadržaja ova dva elementa dobiveni računski modeliranjem. Koncentracije Fe dobivene modeliranjem imaju nešto niže vrijednosti od vrijednosti dobivenih eksperimentalno, dok koncentracije Mn dobivene modeliranjem imaju nešto više vrijednosti od eksperimentalno dobivenih vrijednosti, uz napomenu da su vrijednosti jačine struje bile nešto više kod eksperimentalnih rezultata. Vrijednosti sadržaja Fe i Mn u isparenju rastu sa povećanjm jačine struje. Uočljive su razlike rezultata dobivenih eksperimentalno i modeliranjem. Postoje i tačniji rezultati dobiveni drugim modelima npr. Dennisov-im modelom. Ovaj pravac proučavanja isparavanja u zavarivačkom dimu se sve više razvija i za pretpostaviti je da će se razvijati modeli koji će davati sve tačnije rezultate i koji će biti sve bliže eksperimentalnim rezultatima.

Tabela br. 1 Poređenje sastava zavarivačkog dima dobivenog eksperimentalno i modeliranjem [1].

EKSPERIMENT			MODELIRANJE		
Jačina struje [A]	Fe masa %	Mn masa %	Jačina struje [A]	Fe masa %	Mn masa %
180	59	7,9	175	55,1	9,9
205	56	9,4	188	54,3	10,7
220	57	8,9	212	53,9	11,1
240	57	7,0	240	53,8	11,2
260	58	6,4	256	52,8	12,2
268	59	6,6	269	52,8	12,2
300	61	6,4	294	52,6	12,4

2.2 Odvođenje nastalih isparavanja mehaničkim načinom

Kod ručnog elektrolučnog postupka zavarivanja (REL), se primjenjuje mehanička navlaka koja usisava i odvodi isparavanja sa izvora nastanka. Ovim načinom se smanjuje nivo toka isparavanja, odvode se štetna isparenja, zavarivač se štiti u velikoj mjeri od UV zračenja i varnica nastalih tokom procesa zavarivanja. Efikasnost navlake je velika, u vazduhu ostaju nemjerljive količine štetnih satojaka zavarivačkog dima te nije potrebno nošenje maske niti zaštitne odjeće, a time se i potreba za ventilacijom prostora smanjuje. Smanjuje se i nivo buke. Također se smanjenjem disperzije zaštitnog gasa u okolinu smanjuje potrošnja zaštitnog gasa i do 50 %, a prilikom korištenja navlake uz niži nivo toka zaštitnog gasa dolazi do boljeg kvaliteta vara [2]. Ovakva navlaka prekriva cijelo područje zavarivanja. Praćenje procesa zavarivanja je omogućeno postavljanjem minijaturne kamere u navlaku. Time je omogućeno snimanje procesa zavarivanja u svrhu daljeg istraživanja specifičnosti ovakvog načina radai svrhu kontrole kvaliteta izvođenja procesa zavarivanja.

Nedostatak navlake je što povećava težinu zavarivačkog pištolja i zahtjeva dodatnu opremu za praćenje procesa zavarivanja, zatim ukoliko navlaka prekriva u potpunosti var, potrebno je obezbjediti hlađenje. Navlaka nesmije smetati distribuciji zaštitnog gasa u var. Princip rada navlake, kretanje zaštitnog zraka, zavarivačkog dima i okolnog zraka je prikazano shematski na slici 1 [2].

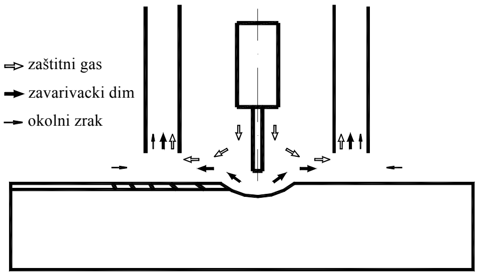

Slika 1. Ocekivani tok plinova

3. ZAKLJUČAK

Veoma je važno poznavati sastav zavarivačkg dima. Vrijednost koju susrećemo kao maksimalnu za ukupnu količinu isparenja u zavarivačkom dimu u svim standardima je 5 mg/m^3. Prema vrijednostima limita izlaganja štetnim supstancama, postavljaju se sve oštriji zahtjevi, provedeni kroz zakonske regulative, što je povoljno za zavarivače. Prijedlog je da se npr. trenutni OSHA limit za ZnO od 5 mg/m^3 za 8 sati promjeni na 5 mg/m^3 za 10 sati izlaganja.
OSHA i *American Conference of Governmental Industrial Hygienists* (ACGIH), poseban naglasak stavljaju na smanjivanje isparavanja koja sadrže okside Ni, Mn i heksavalentni Cr_{VI}.
U cilju smanjenja ovih materija predložene su sljedeće promjene:

- OSHA je predložila da se dozvoljeni limit izlaganja heksavalentnom hromu Cr_{VI} sa dosadašnjih 100 μg/m^3 kod kromata, reducira na osmosatni prosjek, *Time Weight Average* (TWA) standard osmočasovnog sigurnog izlaganja radnika, reducira na (0,5 do 5,0) μg/m^3 [6].
- ACGIH predlaže smanjenje dozvoljene količine mangana sa 1000 na 200 μg/m^3.
- ACGIH predlaže smanjenje dozvoljene količine nikla sa 1000 na 200 μg/m^3.

Zbog pooštrenih zakonskih propisa koji na zdravlje zavarivača i zaštitu okoline stavljaju prioritet, potrebno je razvijati što efikasnije načine za smanjenje ili uklanjanje zavarivačkog dima. Sve navedene aktivnosti u radu koje se provode u cilju što efikasnijeg smanjenja štetne emisije zavarivačkog dima u radnu okolinu, su veoma korisne i potrebno je i dalje vršiti slična istraživanja.

4. LITERATURA

[1] C.J. REDDING, *Fume Model for Gas Metal Arc Welding*, WELDING JOURNAL, JUNE 2002, 95-S, Bradford, UK, june 2002.

[2] NEDIM TURKEM, HARUN BILIRGEN, GUILLERMO A. VIECCO AND HUGO S. CARAM, *Development of a Lightweight Fume Hood forHandheld Welding Guns,* WELDING JOURNAL, february 2005.

[3] *Welding Fumes and Gases*, Occupational Safety &Healtg Administration (OSHA), Washington, USA, 2004.

[4] Welding Fumes and Gases, CPWR , NIOSH, 2003.

[5] B. J. QUIMBY and G.D. ULRICH, *Fume Formation Rates in Gas Metal Arc Welding,* WELDING JOURNAL, april 1999.

[6] „ESSENTIALLY SIMILAR“ to U.S. Department of Labor Form OSHA 20, Baltimore, Meryland, MSDS, 06/2004.

OTPORNOST NA TROŠENJE CRIJEVA PERISTALTIČKE CRPKE IZRAĐENIH IZ RAZLIČITIH MATERIJALA

WEAR RESISTANCE OF THE PERISTALTIC PUMP HOSE MADE FROM DIFFERENT MATERIALS

Srećko Brkić, PLIVA HRVATSKA D.O.O., 10000 Zagreb, Prilaz baruna Filipovića 25, Hrvatska

Sažetak:

U farmaceutskoj i kemijskoj industriji peristaltičke crpke se puno koriste. Izbor vrste materijala crijeva ovisi o mediju za koji se koristi. Crijeva izrađena iz različitih materijala posjeduju različitu otpornost na trošenje. To je i razlog radi čega im je radni vijek različit. U ovom radu testirana su 4 različita materijala na trošenje koji se koriste za izradu crijeva peristaltičke crpke i to: Silikon, Neopren, Tigon i Viton. Ispitivanje trajnosti obavljeno je pomoću prototipa peristaltičke crpke i električne bušilice koja se koristila za pogon.

Ključne riječi: peristaltička crpka, crijevo, izbor materijala

Abstract:

In the pharmaceutical and chemical industries peristaltic pumps are used a lot. Selection of the hose material depends on the liquid inside the hose. Different hose materials have defferent wear resistances. This is a reason why they have different life spans. In this work four different types material were tested on wear and all of them are commonly used for peristaltic pump hoses: Silica, Neopren, Tygon and Viton. For the longevity test a peristaltic pump and a manual electric machine, for power supply, were used.

Key words: peristaltic pump, hose, materials selection

UVOD

Najvažniji dio svake peristaltičke crpke je crijevo. U ovom radu opisan je postupak ispitivanja otpornosti na trošenje četiri različita materijala u podjednakim uvjetima ispitivanja. Uglavnom se koriste crijeva napravljena iz četiri vrste materijala i to: Silikon, Viton, Tygon i Neopren. Trajnost crijeva za ove materijale u peristaltičkoj crpki je različit. Dobivene vrijednosti mogu biti informativne naravi, jer su mjerenja otpornosti na trošenje dobivene uz osjetno veći broj okretaja (1/s) od onih koje preporučuje proizvođač crijeva.

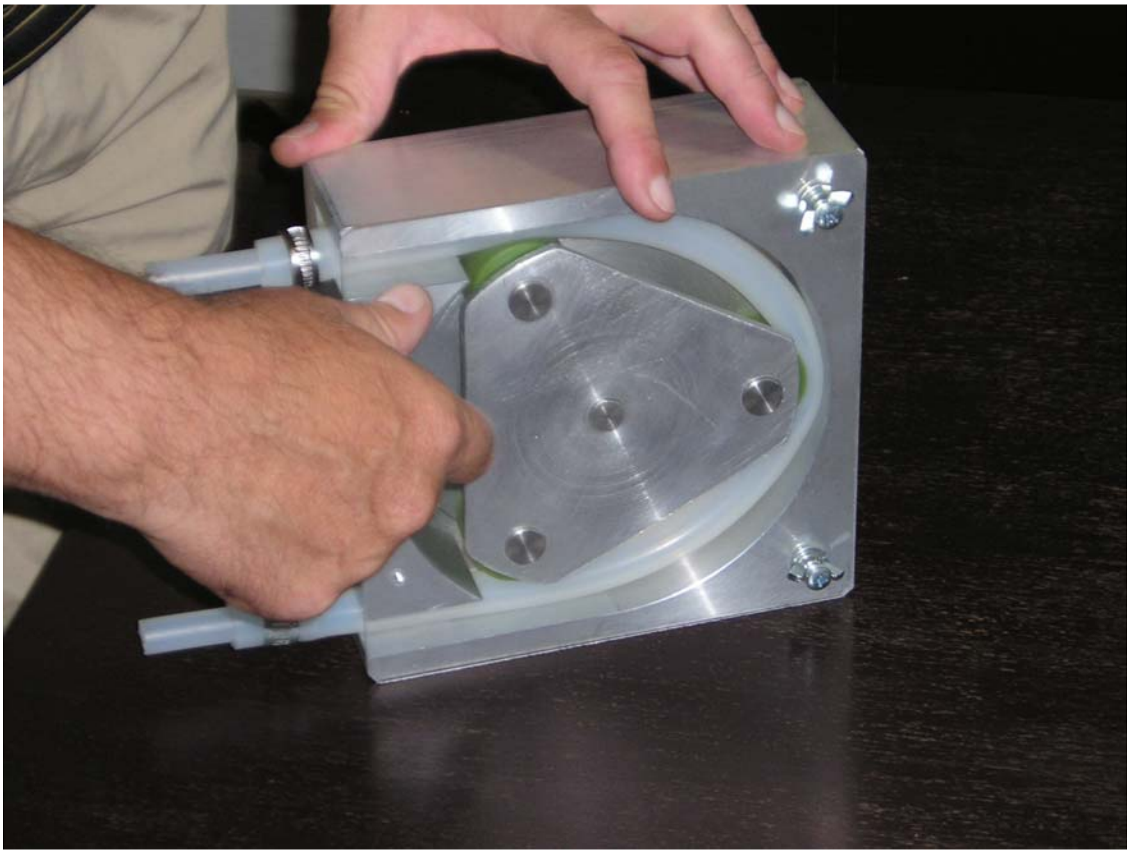

Slika 1. Fotografija peristaltičke crpke SB600

EKSPERIMENTALNI DIO

Trajnost crijeva u peristaltičkoj crpki ovisi prvenstveno o broju okretaja rotora (1/s). Proizvođač crijeva Masterflex (USA) ne daje garanciju za crijevo, jer ga smatra potrošnim materijalom. Proizvođač predlaže da prilikom rada peristaltičke crpke broj okretaja rotora (1/s) ne prelazi 8. Trajnost crijeva će se produžavati kako će se broj okretaja rotora smanjivati. Materijalu se treba ostaviti dovoljno vremena za relaksaciju, odnosno povratak u postojeći oblik. Elastičnost crijeva je prema tome vrlo bitno svojstvo. Najvažniji mehanizam trošenja crijeva je umor materijala. Ostali mehanizmi nemaju upliva, ako se za odgovarajući medij koristi primjereno crijevo. Proizvođač je u svojoj dokumentaciji specificirao na što su koji materijali kemijski otporni. Interesantno je napomenuti da ispitivanje kemijske otpornosti

crijeva na bilo koji medij može obaviti jednostavno svaka osoba. Postupak kemijskog ispitivanja je slijedeći. Odreže se komadić crijeva (oblik prstena) i izvaže na preciznoj vagi kojoj je mjerno područje u miligramima. Komadić odrezanog crijeva uroni se u medij za koji se mjeri kemijska otpornost. U mediju je potrebno držati izvagani komadić crijeva 48 sati. Nakon toga komadić crijeva se ispere, osuši i ponovno izvaga na istoj vagi. Ukoliko nije došlo do razlike u težini i obliku odrezanog crijeva smatra se da je crijevo kemijski otporno na ispitani medij te se može koristiti.
Prilikom ispitivanja trajnosti crijeva peristaltičke crpke koristio se veći broj okretaja rotora (1/s) od onoga što je preporučeno od strane proizvođača. Razlog je namjera da se jedino izvrši komparacija otpornosti na trošenje četiri različita materijala. Prilikom ispitivanja peristaltička crpka je radila na suho. Na usisnu stranu peristaltičke crpke ugrado se vakuum-metar. Tako se moglo odmah primijetiti trenutak kada je došlo do stvaranja prve pukotine na crijevu crpke.

Redni broj:	Vrsta materijala crijeva	Vrijeme do pucanja crijeva (s)
1	NEOPREN	721
2	SILIKON	343
3	TYGON	153
4	VITON	96

Tablica 1. Rezultati mjerenja

ZAKLJUČAK

Namjerno je korišten četiri puta veći broj okretaja rotora od preporuke proizvođača crijeva da bi se bitno skratilo vrijeme ispitivanja. Dobiveni rezultati ukazuju da ima smisla koristiti Neopren kao materijal crijeva na svim mjestima gdje je to moguće radi njegove najveće otpornosti na trošenje. Ovaj rad služi samo kao pokazatelj kako različiti materijali posjeduju različitu otpornost na trošenje. U konkretnom slučaju na umor materijala.

LITERATURA

/1/ V. Ivušić, Tribologija i materijali, Hrvatsko društvo za materijale i tribologiju, Zagreb 1993
/2/ T. Filetin, F. Kovačićek, J. Indof, „SVOJSTVA I PRIMJENA MATERIJALA“, FSB, Zagreb 2002
/3/ Masterflex, TUBING PUMP SYSTEMS-REFERENCE BOOK, Chicago 1992

KINETICS OF THE THERMAL DEGRADATION OF AN EPOXY / POLY(OXYPROPYLENE)DIAMINE / OCTADECYLAMMONIUM MODIFIED MONTMORILLONITE SYSTEM

Ivan Brnardić, Jelena Macan, Marica Ivanković & Hrvoje Ivanković
Faculty of Chemical Engineering and Technology, Marulićev trg 19, Zagreb, Croatia

Abstract: Thermal degradation kinetics of organic-inorganic nanocomposites based on organically modified montmorillonite and a commercial epoxy resin have been investigated by thermogravimetric analysis (TGA). For organic modification of montmorillonite octadecylamine was used. Commercial poly(oxypropylene) diamine (Jeffamine®D230) was used as a curing agent for epoxy resin. Energy of activation for degradation of the epoxy-amine system and nanocomposites with different inorganic content was determined by isoconversional Kissinger-Akahira-Sunose method. The process of degradation was described by appropriate empirical kinetic model.

Key words: kinetic, thermal degradation, nanocomposite

1. Introduction

Thanks to its special properties, epoxy resin has various applications in construction, electronics, adhesion and coatings. Addition of organically modified montmorillonite into epoxy resin results in marked improvement of its properties. Homogeneity of distribution and degree of layering have a direct influence on barrier properties and thermal stability of resulting nanocomposite. Although a lot of research has been done in the area of nanocomposites based on epoxy matrix and layered silicate in the last decade [1-5], only several researchers investigated the influence of nanofillers on thermal degradation and its kinetics [2, 6].

In this work the organic-inorganic nanocomposites based on organically modified montmorillonite and a commercial epoxy resin were prepared and kinetics of thermal degradation was studied.

2. Experimental

Epoxy resin, diglycidyl ether of bisphenol A (DGEBA, DER 331), with the epoxy equivalent weight of 187 g/mol, was obtained from Dow Chemicals. Poly(oxypropylene) diamine, provided under the trade name Jeffamine® D230 by Fluka, with N-H equivalent weight of 57.5 g/mol, was used as a curing agent. The clay used was a Wyoming type montmorillonite provided by M. I. Drilling Fluids Co. Octadecylamine provided by Kemika, with N-H equivalent weight of 134.7 g/mol was used as modifier for montmorillonite. The materials were used as received.

Montmorillonite clay was purified by standard sedimentation methods and converted to Na-montmorillonite form with dilute NaCl aqueous solution. The cation exchange capacity (CEC) was determined by ammonium acetate method to be 101 meq/100g. The organically modified montmorillonite was prepared by ion-exchanging the inorganic cations with the protonated form of octadecylamine. Stoichiometric amount of the amine calculated from the CEC and dilute aqueous HCl in small excess of the ion-exchange capacity of the clay was used to ensure the formation of the protonated amines. The ion-exchanged montmorillonite was separated by centrifugation, washed and dried.

Stoichiometric amount of curing agent (30 phr) was added to DGEBA. Mixture was stirred at room temperature in a closed vessel for 60 min. To prepare the composite system, epoxy resin was mixed with desired amount of octadecylamine-modified montmorillonite, OMMT, (5 and 10 g of OMMT per 100 g of epoxy, WO5 and WO10) at 75 °C for 24 h and sonicated for 15 min. After cooling the mixture to room temperature, a stoichiometric amount of the curing agent was added with thorough mixing. The mixtures were poured into molds and cured at 80 °C for 3 h, followed by postcuring at 120 °C for 1 h.

Weight loss of fully cured samples, weighing approximately 15 mg, was measured by thermogravimetric analysis (TGA). The TGA measurements were done on a Perkin Elmer thermobalance TGS-2. The samples were heated from room temperature to 1000 °C at four different heating rates ($5\,^{o}$, $10\,^{o}$, $15\,^{o}$ and $20\,^{o}$C/min) in a nitrogen gas flow of 150 cm^3/min.

3. Results and Discussion

When modeling kinetics of nonisothermal processes, a problem of separating temperature dependence of rate or reaction constant from that of kinetic model *f(α)* is encountered, since both temperature and conversion are functions of time. Isoconversional methods of kinetic analysis represent a solution for this basic problem of determining the kinetic parameters from TGA measurements.

As thermogravimetric analysis (TGA) was used to determine the kinetics of degradation of composites, the results were integral curves showing weight loss dependence on temperature. Thus integral isoconversional method such as Kissinger-Akahira-Sunose (KAS) method [7-9] is commonly used. Differential isoconversional methods are not the most suitable for analysis of TGA curves because of the need for numerical derivation of experimental results, which contributes to the experimental error. In this work the KAS method was chosen for isoconversional calculation of E_a.

The conversion, α, was calculated according to the equation (1), in which m_0 is the initial and m_∞ is the final weight of the sample, ignoring the initial loss at temperatures under 300 °C, which is a result of evaporation of adsorbed moisture.

$$\alpha(T) = \frac{m_0 - m(T)}{m_0 - m_\infty} \tag{1}$$

E_a, was calculated from KAS equation (2) for conversions in the range of α = 0.05-0.90, where β is the heating rate, T the thermodynamic temperature, k_0 the pre-exponential factor, R general gas constant (8.314 J mol^{-1} K^{-1}), and *G(α)* the integral form of the kinetic model *f(α)*. Figure 1 shows an example of isoconversional plots for epoxy-amine system.

$$\ln\left(\frac{\beta}{T^2}\right) = \left[\ln(k_0 R / E_a) - \ln G(\alpha)\right] - \frac{E_a}{RT} \tag{2}$$

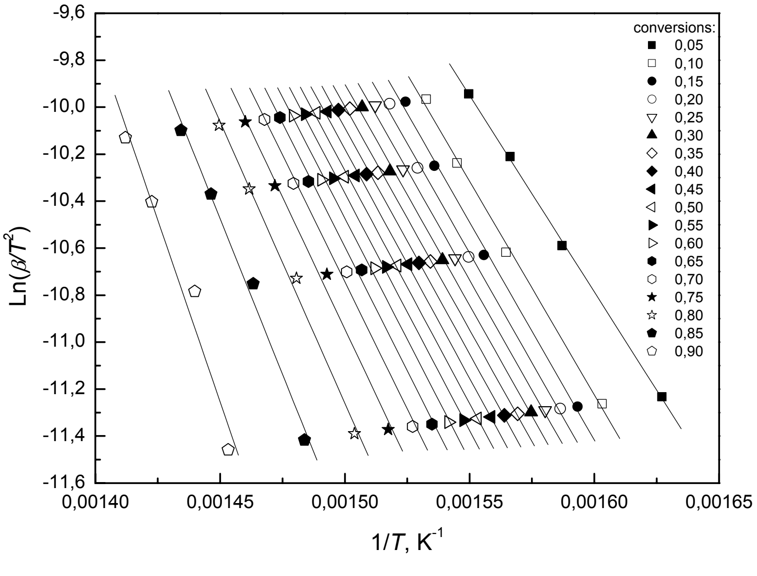

Figure 1. Isoconversional plots used to calculate activation energy at listed conversions using Kissinger-Akahira-Sunose method, for epoxy-amine system.

The dependence of E_a on conversion, for all investigated systems, is given in Figure 2. The inorganic phase was expected to enhance E_a of the epoxy-amine matrix in composite systems, both acting as flame retardant and by increasing char formation. For the composite WO5 the E_a is higher in comparison with epoxy-amine system but the sample WO10 has the lowest activation energy that may indicate an inhomogeneous distribution of the filler in the matrix.

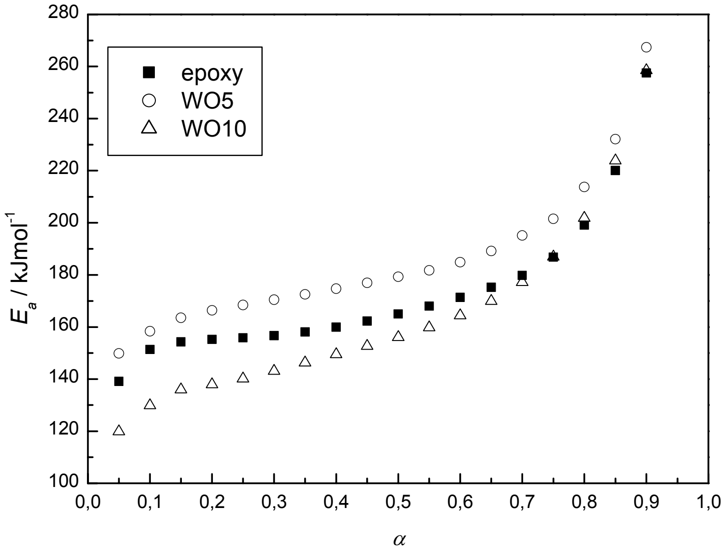

Figure 2. Dependence of activation energy, E_a, on the extent of conversion, α, as determined by KAS method, for all investigated systems.

If the energy of activation does not vary greatly with conversion, it is possible to describe the whole interval of degradation by a single kinetic model. To describe the thermal degradation kinetics of investigated systems the autocatalytic model (3) was chosen:

$$\frac{d\alpha}{dt} = k_0 \exp(-E_a / RT)\alpha^m (1-\alpha)^n \qquad (3)$$

were $d\alpha/dt$ is the rate of reaction, and m and n are empirical coefficients.

Parameters of the model were calculated by simultaneous analysis of experimental curves for all four heating rates using Wolfram Mathematica 5.0 program. The values of the parameters of the kinetic model had been optimized by minimizing the mean square difference between the calculated and experimental conversions. The average values of $E_{a,KAS}$ (in the interval $\alpha = 0.15 - 0.75$) were used as initial values. The results of kinetic modeling are displayed in Table 1 and Figure 3. Higher values of E_a and parameter k_0 mean that the degradation reaction is harder to start but proceeds faster. As fitted values of $E_{a,fit}$ are significantly higher than $E_{a,KAS}$ it can be postulated that reaction mechanism of these systems is quite complex

Table 1. *Activation energy (E_a), pre-exponential factor (k_0) and empirical exponents m and n for given systems and model, Eq. 3.*

System	$E_{a,fit}$/kJ mol^{-1}	$E_{a,KAS}$/kJ mol^{-1}	k_0/s^{-1}	*m*	*n*
Epoxy	179	165	exp(28.8)	0.55	1.90
WO5	214	179	exp(35.3)	0.52	2.15
WO10	177	155	exp(28.3)	0.42	1.76

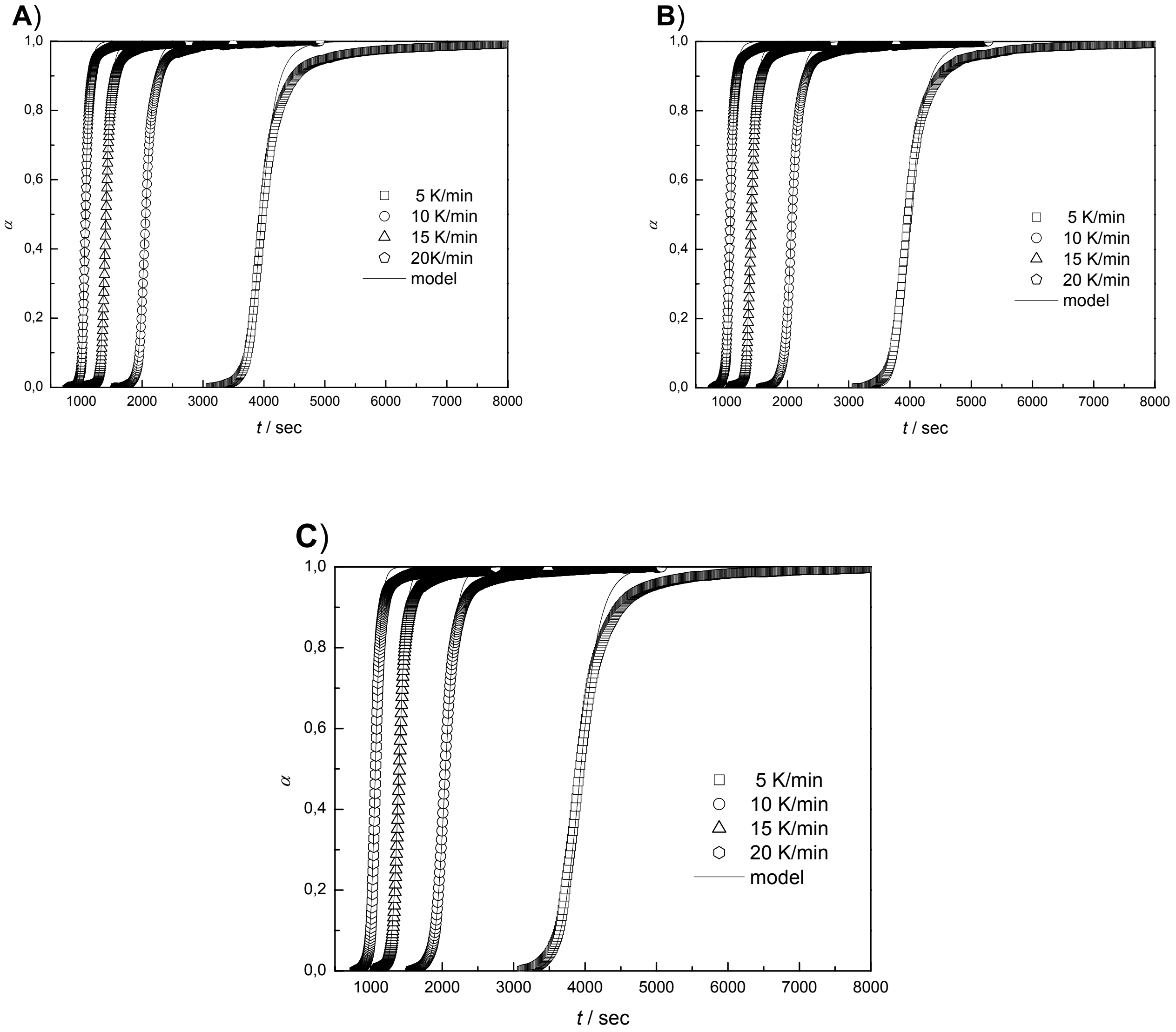

Figure 3. Comparison of experimental data with the kinetic model data obtained for investigated systems for all heating rates: (A) epoxy-amine system; (B) WO5 system; (C) WO10 system.

To elucidate the degradation mechanism for investigated systems and to explain kinetics thoroughly, more powerful experimental methods should be used. But, if the degradation is studied in order to ascertain the processing and appropriate working conditions for materials, the use of TGA and simple empirical models in kinetic analysis is justified.

4. Conclusion

Thermogravimetric analysis (TGA) was used to determine the kinetics of thermal degradation of nanocomposites based on epoxy resin and organically modified montmorillonite, OMMT. Energy of activation, E_a, for these reactions was calculated using isoconversional KAS method and kinetics was described with empirical autocatalytic model. For the composite with 5 g of OMMT per 100 g of epoxy the E_a is higher in comparison with the epoxy-amine system. The composite with 10 g of OMMT per 100 g of epoxy has the lowest activation energy that may indicate an inhomogeneous distribution of the filler in the epoxy-amine matrix.

References

1. M.S. Wang, T.J. Pinnavaia, *Chem. Mater.*, **6** (1994) 468.
2. P.B. Messersmith, E.P. Giannelis, *Chem. Mater.*, **6** (1994) 1719.
3. T. Lan, T.J. Pinnavaia, *Chem. Mater.*, **6** (1994) 2216.
4. J.M. Brown, D. Curliss, R.A. Vaia, *Chem. Mater.*, **12** (2000) 3376.
5. X. Kornmann, H. Lindberg, L.A. Berglund, *Polymer*, **42** (2001) 1303.
6. A. Gu, G. Liang, *Polymer. Degrad. Stabil.*, **80** (2003) 383.
7. H.E. Kissinger, *Anal. Chem.*, **29** (1957) 1702.
8. T. Akahira, T. Sunose, *Res. Report Chiba Inst. Techn.*, **16** (1971) 1622.
9. Z.M. Gao, M. Nakada, I. Amasaki, *Thermochim. Acta*, **369** (2001) 137.

ALKALINE FUEL CELL ENGINEERING AND TESTING

J.Brunton[1], D.M. Kennedy and E.Coyle.
Faculty of Engineering
Dublin Institute of Technology
Dublin 1.
[1]james.brunton@dit.ie

Abstract: A fuel cell is a device that directly converts the chemical energy of reactants (a fuel and an oxidant) into low d. c. electricity [1]. Used in conjunction with other sustainable energy options, hydrogen and fuel cell technology can provide a realistic alternative to fossil fuels. Although research is continuing in many areas we are no closer now to commercialisation than ten to twenty years ago. This is due to a number of key reasons, some of which include efficiency, scale, accessories and power output.
This paper outlines the benefits that could be derived from switching to a hydrogen based economy and the commercialisation of hydrogen fuel cells as a clean and environmentally friendly alternative. It looks in general at the fuel cell, outlines its origin, how it operates, and the wide range of fuel cells available. The paper also compares the alkaline fuel cell (AFC) with the proton exchange membrane fuel cell (PEMFC) as options for low temperature applications. In particular, the paper focuses on the research being conducted by the Dublin Institute of Technology into alkaline fuel cell technology and outlines the systems capabilities and limitations.

Keywords: Alkaline Fuel Cells, Electrode, Electrolyte, Low Temperature Fuel Cell

1. Introduction

Peak oil means the end of cheap oil. In contrast to this, demand for oil is increasing as energy intensive industrialised economies are cornering available supplies and pushing up fuel prices. In the last four years the price of oil has jumped drastically from 20 dollars to over 70 dollars a barrel with no signs of a fall off in this rising trend. Another major economic concern centres on the fact that fossil fuel reserves are located in volatile areas of the world and oil is being used as a political and economic weapon that could result in world recession as demand increases and supplies decrease.

Environmentalists would suggest that economic problems with the carbon economy coupled with rising emissions concerns resulting in climate change, global warming and the greenhouse effect, should spell a new beginning for the hydrogen based economy and other alternative energy options for the production of electricity, such as wind, solar, wave, and renewable sustainable supplies.

It was with this in mind that the European Commission Research Directorate-General in March 2004 called for deeper co-operation between research groups through co-ordination of resources, cross fertilisation of ideas, and sharing of results in an effort to speed up commercialisation of hydrogen and fuel cell technology. It is recognised at European level that hydrogen and fuel cell technologies are core long-term technologies for realising global sustainable energy. Hydrogen compliments electricity and together they represent the most promising mass market energy sectors for delivering sustainable energy for stationary heat, power and transport in the long term [2].

1.1 Overview

William Groves invented the fuel cell in 1839, years before the internal combustion engine was invented. His experiments centred on the use of platinum electrodes connected in series, immersed in sulphuric acid and the process of reverse electrolysis. In the 1960’s one of Groves successors, Francis Bacon a pioneer of alkaline fuel cell development found prominence when NASA decided to used fuel cell technology to power its Apollo space program [1]. The alkaline fuel cell was selected because of its power generating efficiency that approached 70% [3]. A cell with a high efficiency uses less fuel to generate the same amount of electricity [4]. Another advantage was the cells low cost (use of non-noble metal catalysts) and also by maintaining the pH of the water exiting the cell between 6 and 8 the water was drinkable, this was a major weight saving consideration [1]. As part of this program the alkaline fuel cell powered 106 missions and clocked up more than 82,000 service hours for NASA [5].

All this development should have spelt the beginning of the hydrogen economy but with cheap and abundant fossil fuel readily available and fuel cells still experiencing technical difficulties the opportunity to switch to a renewable, sustainable, and environmentally friendly energy alternative was set aside.

As the space program pioneered most investment into fuel cell research, when NASA switched allegiance from the alkaline fuel cells to the dry electrolyte Solid Polymer Fuel Cell (SPFC) developed by General Electric, American interest in alkaline fuel cell technology ceased. Later in the 1990’s Ballard Technologies with its newly named Proton Exchange Membrane Fuel Cell (PEMFC) scored great success in financing its technology development program and attracting big automakers as strategic partners. This left only a few players remaining in the AFC field world wide, mainly based in Europe [6].

1.2 Fuel Cells

A fuel cell converts chemical energy into d .c. electrical energy [7]. This can be achieved by various ways and means depending on the fuel and oxidant, direct or indirect fuelling or type of electrolyte and temperature of operation [8]. Table 1. is a compilation of existing fuel cell solutions, and lists fuel type, electrolyte, efficiency and application. The efficiency stated is the percentage figure the fuel cell manages to convert of the fuel energy in the hydrogen to electrical energy.

Fuel Cell Type	Electrolyte	Anode Gas	Cathode Gas	Electric Power	Efficiency	Applications
Proton Exchange Membrane, (PEM)	Ion Exchange Membrane	Hydrogen	Pure or Atmospheric Oxygen	50 to 250 kW	35-60%	Vehicle Applications
Direct Alcohol Fuel Cell, (DAFC)	Polymer Membrane	Methanol Solution in Water	Atmospheric Oxygen	Up to 10 kW	35-40%	Vehicle Applications and small Heat and Power
Alkaline Fuel Cell (AFC)	Potassium Hydroxide	Hydrogen	Pure Oxygen	5 to 20 kW	45-65%	Military, Space and Vehicle Applications
Phosphoric Acid Fuel Cell, (PAFC)	Immobilised liquid Phosphoric Acid	Hydrogen	Atmospheric oxygen	200 kW to 1 MW	35-50%	Medium combined Heat and Power
Solid Oxide Fuel Cell, (SOFC)	Ceramic	Hydrogen, Methane	Atmospheric oxygen	Up to 200kW	45-60%	Large and small combined Heat and Power. Vehicle Applications
Molten Carbonate Fuel Cell (MCFC)	Immobilised liquid Molten Carbonate	Hydrogen, Methane	Atmospheric oxygen	Up to 2 MW	40-55%	Large combined Heat and Power

Table 1. Range of Fuel Cells

Figure 1. illustrates the operating temperature ranges of the six fuel cells in common use. Fuel cells are categorised as high or low temperature cells and this dictates their suitability for various applications, stationary, transport or heat/plant.

The electrolyte used in a cell can be either solid or liquid. For temperatures below 100°C, aqueous acid, alkaline or a solid electrolyte may be used. Between 100 and 200°C it is necessary to use highly concentrated solutions of acids such as phosphoric acid. Between 200 and 400°C, one may use molten alkaline hydroxides and from 600 to 1000°C molten carbonate or salt mixtures may be used. Above 1000°C solid electrolytes can also be used [9].

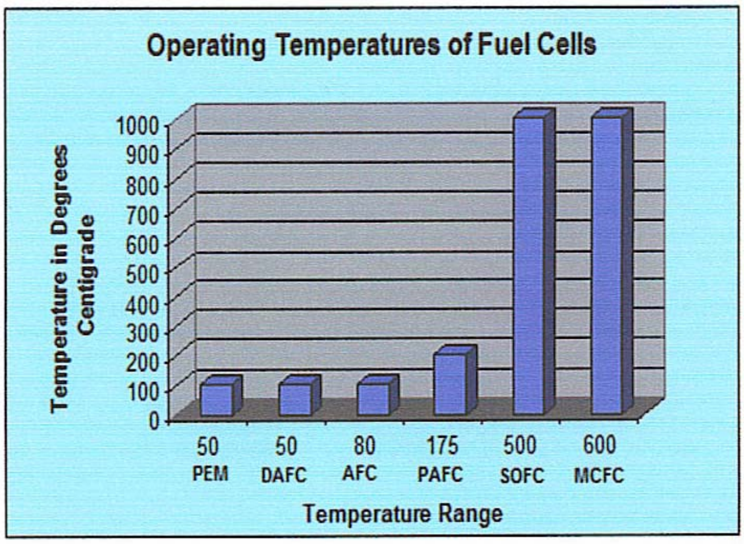

Figure 1. Operating temperatures of the six most common fuel cell.

The very popular Proton Exchange Membrane (PEM) cell employs a solid electrolyte that allows positively charged ions to travel unimpeded across the polymer membrane while rejecting negatively charged ions forcing them to flow through an external circuit in the form of electrical current. The preference for acidic or alkaline electrolytes is dependant on the desired application, for a mobile situation (e.g. buses, trucks, cars) alkaline electrolytes would be suitable but the acidic PEM cell is the one most vehicle manufacturers involved in fuel cell research prefer. Advantages of using an alkaline electrolyte compared to an acidic electrolyte are that electrode materials other than noble metals (platinum) can be utilised. Other cell materials that form part of the cells casing and construction can also be produced from inexpensive material with less risk of aggressive attack, these are important factors to the longevity and cost of the fuel cell. Also oxygen reduction reaction is faster in alkaline solutions than in acids.

1.3 Fuel Cell Type and Operation

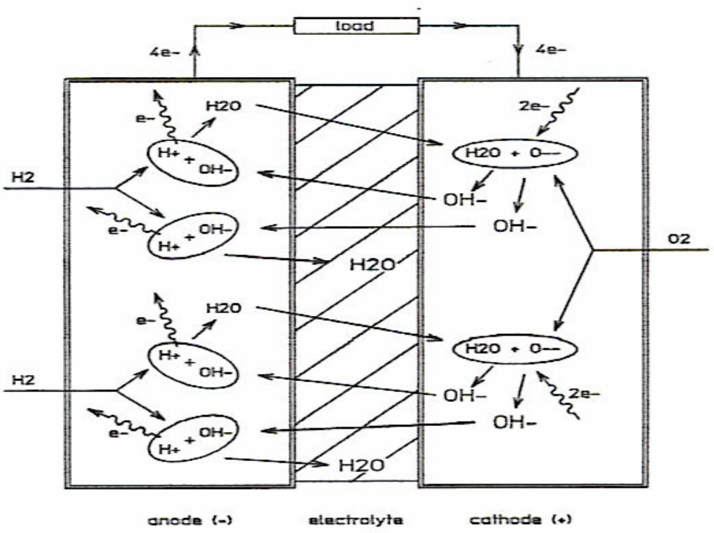

Figure 2. Alkaline Fuel Cell

The Alkaline Fuel Cell (AFC) is shown in Figure 2. this cell utilises the migration of Hydroxyl ions (OH-) from the cathode to the anode to create a reaction. At the anode the hydrogen gas (H_2) combines with the hydroxyl ions (OH-) to form water (H_2O) and electrons (e-). Because the electrons cannot pass through the electrolyte they are forced out at the anode supplying current to external loads. Water formed at the anode then migrates back to the cathode where it joins up with oxygen (O_2) and returning electrons to regenerate the hydroxyl ions (OH-) and the cycle repeats itself. Most reaction water leaves at the anode (H_2) side but a small amount is removed via the electrolyte causing the electrolyte's molar concentration to be weakened affecting the cell output. The remedy for this is to periodically replace the Potassium Hydroxide electrolyte.

Oxidation at Anode: $\mathbf{2H_2 + 4OH^- \rightarrow 4H_2O + 4e^-}$

Reduction at Cathode: $\mathbf{O_2 + H_2O + 4e^- \rightarrow 4OH^-}$

Overall Reaction: $\mathbf{2H_2 + O_2 \rightarrow 2H_2O}$

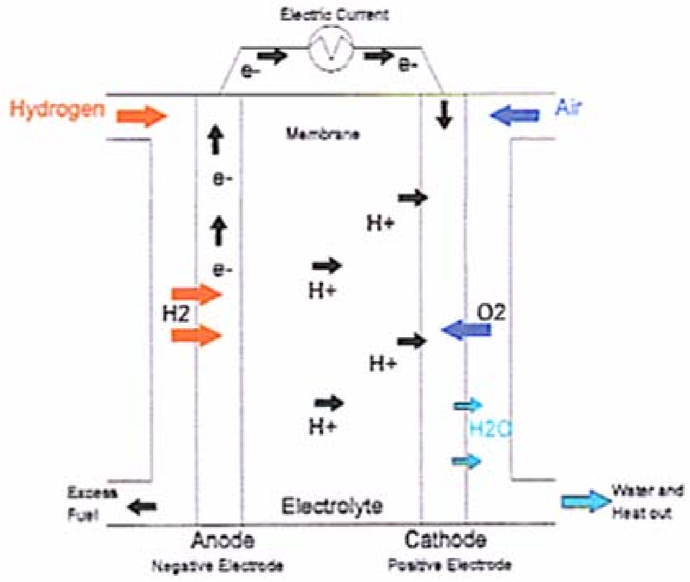

Figure 3. The PEM Fuel Cell.

The acronym PEM refers to **Polymer Electrolyte Membrane** or **Proton Exchange Membrane** and refers to the solid acid electrolyte used by the PEM fuel cell illustrated in Figure 3. As hydrogen gas (H_2) enters the cell at the anode side it comes into contact with a precious metal catalyst and breaks down into protons (H+) and electrons (e-). The catalyst is a substance usually platinum that accelerates a chemical reaction. The protons can pass unimpeded through the thin plastic membrane while the electrons travel in the form of current to supply the external loads before returning to the cell at the cathode. The protons that have diffused through the membrane reunite with the electrons and react with the oxygen fed in at the cathode to produce water (H_2O). This process produces no pollution and the only by-products are water and heat.

Oxidation at Anode: $2H_2 \rightarrow 4H^+ + 4e^-$

Reduction at Cathode: $O_2 + 4H^+ + 4e^- \rightarrow 2H_2O$

Overall Reaction: $2H_2 + O_2 \rightarrow 2H_2O$

The PEM fuel cell is finding most favour with Motor Manufacturers and is believed in some quarters to be most suitable for transportation and small stationary applications. Compared to other types of cell the PEM generates more power for a given volume or weight of fuel cell. There is also the added advantage that it uses air as opposed to pure oxygen and does not require a corrosive fluid to operate [10]. The Canadian company Ballard Power Systems and the American company UTC Fuel Cells are acknowledged as two of the leading companies in the industry and both are developing PEM fuel cells for the mass market, especially the transportation sector. Other important US companies include Fuel Cell Energy, which is developing large-scale fuel cell power plants and Plug Power, which is developing smaller units to power residential and commercial premises, [11]. The commercial potential of the PEM fuel cell and the continued investment has lead to the development of ion conducting plastic film membranes that generate electric current more easily, operate across a broader temperature range and cost less than incumbent materials, which are mainly sulfonated fluoropolmers [12]. This allows for a compact, low cost and quick responding cell technology more suited to the various application demands of industry. However some of the main problems that still impair the dominance of the PEM fuel cell are Carbon Monoxide poisoning, affecting the long-term performance of the membrane. The PEM fuel cell requires pure hydrogen as a fuel and therefore is not suited to on-board reforming of hydrocarbons (natural gas, gasoline etc.). Also it's use of precious metal catalysts especially platinum which is rare and costly. PEM fuel cell technology has been targeted for transportation applications because it operated efficiently on pure hydrogen with the result being zero emissions. But converting from a Carbon based economy to a Hydrogen economy is a future aspiration, and realistically reforming of fossil based fuels to extract hydrogen would be required in the interim to bridge the gap.

1.4 Direct Methanol fuel cells (DMFC) are relatively new and similar to the PEM cell in that it uses a polymer membrane as an electrolyte. However, in the DMFC the anode catalyst draws the hydrogen from the liquid methanol, eliminating the need for a fuel reformer. The liquid Methanol is oxidized in the presence of water at the anode and produces CO_2, hydrogen ions and electrons. The hydrogen ions pass through the membrane and the electrons travel through the external circuit as current, reuniting to react with the oxygen from the air to form water at the anode and complete the circuit, [13]. Initially the DMFC was ignored because of its high catalyst costs (platinum), fuel crossover effect, poisonous fuel, low efficiency and power density problems. But it now seems that new technology has resolved these matters and interest in the DMFC has resurfaced for very small to mid size applications like laptops, cellular phones and motor vehicles, because it offers low temperature operation without the need for a reformer.

1.5 The Phosphoric Acid Fuel Cells (PAFC) is considered the first generation of modern fuel cells and was one of the first to be commercialised. Its typical use is stationary power generation and also to power large vehicles like city buses. As the name suggests the electrolyte is liquid phosphoric acid (H_3PO_4) at nearly 100% concentration and it is most conductive at a temperature of 150 to 200^oC. It operates similar to a PEM fuel cell, as the hydrogen (H_2) enters the cell at the anode, the catalyst causes it to split into protons (H^+) and electrons (e^-). The protons migrate through the electrolyte to the cathode side where they combine with the electrons from the external circuit and oxygen (O_2) from the air to form water and another by-product, heat [14].

1.6 Solid Oxide Fuel Cells use a solid ceramic electrolyte and operate at very high temperatures. The high temperature operation is considered an advantage because of the cells flexibility to use more types of hydrocarbon fuel (natural gas, diesel, gasoline, alcohol, coal gas) be tolerant of impurities and use inexpensive catalysts, but a disadvantage in that high temperatures enhance the breakdown of cell components. Because of its high efficiency output, 60% approx., the SOFC is mainly used for power generation with a potential also to power vehicles [15].

The solid electrolyte structure of the SOFC is impervious to gas crossover from one electrode to another, with the charge carrier being the oxygen ion (O^{2-}). At the cathode the oxygen molecules from the air are split into oxygen ions with the addition of four electrons. The oxygen ions are conducted through the electrolyte and combine with the hydrogen at the anode, releasing four electrons. The electrons exit the cell as current to supply the external circuits and return to the cathode to continue the cycle. The by-products are heat and water that exits the cell on the anode side.

1.7 Molten Carbonate Fuel Cells (MCFC) are high temperature fuel cells operating at temperatures in excess of 650^o C. This implies high fuel to electricity efficiencies of up to 60%, increasing to 85% if the waste heat is utilised.

The MCFC uses a molten carbonate salt mixture as its electrolyte; the two commonly used compositions are lithium carbonate and potassium carbonate, or lithium carbonate and sodium carbonate. The mobility of the Carbon Trioxide ion is dependent on the conductive mobility of the melted salt (a liquid at 650^oC). At the anode a reaction occurs between hydrogen and carbonate ions (CO_3^{2-}) that have migrated across the electrolyte from the cathode that produces water, carbon dioxide (CO_2) and electrons. The electrons are routed through the external system as current and return to the cathode to combine with oxygen (O_2) and carbon dioxide (CO_2) to produce carbonate ions to continue the process. The bi-products of producing electricity in this fashion are water and heat with carbon dioxide being collected at the anode exhaust and mixed with the cathode feed stream [16].

2.0 Alkaline Fuel Cell Research

Research at Dublin Institute of Technology (DIT) has centred on developing alkaline fuel cell engineering with a view to promoting this technology and steering it towards commercialisation. In conjunction with a German industrial partner, Gaskatel GmbH, DIT has built a single cell test bed for education and research purposes to enhance its research potential in this area and assist in refining Gaskatels alkaline fuel cell and system.

In an alkaline cell, fuel oxidation occurs at the anode. The single fuel cell unit, as shown in Figure 4. has two hydrogen electrodes made of Raney-nickel which have a high catalytic activity at low temperature for hydrogen oxidation and at the cathode oxidant reduction is accomplished by two oxygen electrodes made of silver. The supply for the gases and electrolyte are situated at the bottom of the cell and the exit for both gases and the electrolyte are at the top of the cell. This allows the cell to benefit from the fact that both hydrogen and oxygen will flow freely up through the cell of their own accord. The gases also move quicker through the cell on start-up, which helps to expel any trapped bubbles, inert gases and reaction water that may lodge in the cell on shutdown and re-start.

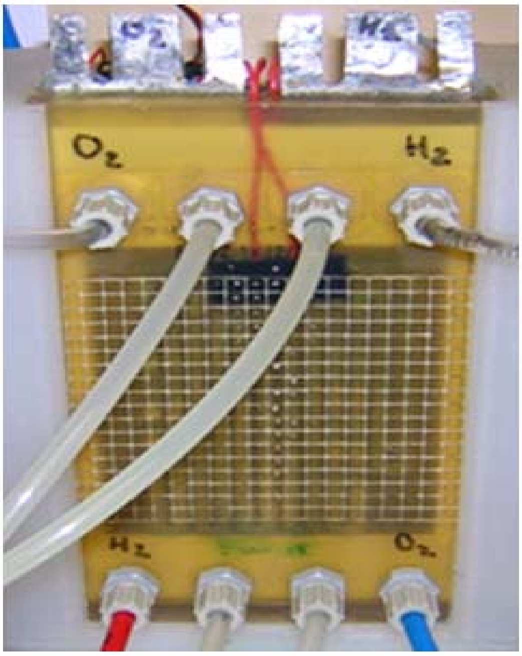

Figure 4. Alkaline Fuel Cell

The cells output is most efficient at a constant temperature of 55° C. As part of the cells construction two heating elements are fitted between the positive and negative poles of the cell and connected in series (24 VDC, 1A) to speed up the heating process. This method of heating the cell is only effective if the electrolyte is immobile, when electrolyte circulation commences the cell temperature drops quickly and drastically affecting the cells potential. The conclusion gathered from this is that the mobilisation of the electrolyte, although beneficial should be controlled, becoming more intermittent than constant. The temperature of the cell is monitored to prevent damage of overheating by a Pt. 100 resistor also positioned inside the cell in close proximity to each heating element.

The gas pressure within the cell also requires regulating and monitoring at a set 0.5 bar above atmospheric pressure to prevent cross-over between the electrolyte and the gas. When the electrodes are being constructed a two-pore system is created, the hydrophobic pores through which the gas flows and the hydrophilic pores through which the electrolyte flows. Capillary forces keep the electrolyte in the small pores when an over pressure of the gas with respect to the electrolyte is applies (as referred to above). In the alkaline fuel cell the gas diffused porous electrodes are very important and the contact zone where reactant, electrolyte and catalyst meet is called the three-phase zone [17].

The cell has one active separator and two passive separators. A thin porous plastic film or active separator is critically used to separate the anode and cathode electrodes from each other. This separator also facilitates the migration of the hydroxyl ion from the cathode to the anode and the water return in the opposite direction. The passive separators only separate the KOH and gas chambers from each other.

In alkaline fuel cell systems, the preferred electrolyte is usually the aqueous potassium hydroxide (KOH), which has a higher conductivity than most other alternatives. Sodium hydroxide (NaOH) was envisaged as a potential option but on balance its performance characteristics were less interesting than that of KOH, and the cost advantage was not really that important because the KOH electrolyte can be used for a longer time in the fuel cell so that its cost to the overall cost is almost negligible [18].

2.1 Testing

Automotive vehicles are the biggest users of oil and one of the major polluters so if a breakthrough is to be made in the development of the hydrogen economy and fuel cell technology it is they who will take the lead in developing this renewable and environmentally friendly energy source. The challenges facing the alkaline fuel cell being considered as a realistic option for automotive manufacturers is:

- Dispelling the suggestion that the cell requires pure oxygen as an oxidant and cannot operate on air. It has been quoted in many journals that the AFC needs its air supply virtually CO_2 free, as the ingress of CO_2 into the electrolyte reduces the electrolytes the current carrying capacity [19].
- Finding an electrolyte that is less aggressive and still has the very good conductivity that the alkaline solution provides [19].

As part of the research program conducted by DIT in collaboration with Gaskatel GmbH an alkaline fuel cell operating with air was tested under a variety of conditions. In order to facilitate these tests the cell was modified by increasing the size of the air intake compartment to suit the new conditions. Air contains approximately 77% nitrogen and only 21% oxygen with trace gases making up the remainder. Because the cell requires oxygen as an oxidant the air supply was adjusted to provide a higher gas flow through the cell [20]. The purpose of these tests was to simulate different electrolyte concentrations and observe the build up of potassium carbonate inside the cell. The general perception is that the formation of these carbonate particles will block up the pores of the electrode, causing the cell to mal-function and that this will happen rather quickly.

The results were quiet different, the cell operated for more than 5000 hours with un-scrubbed air. With a constant current density of $100mA/cm^2$ there was a decrease of potential of approximately 10% and this was reversible by changing to a fresh electrolyte solution [20]. This would suggest that the perception that an alkaline fuel cell cannot operate with air is dated and if a suitable air scrubber (a type of air filter) were used as part of a systems construction the cell should operate efficiently.

Figure 5. Single Alkaline Fuel Cell Test Bed.

Another part of the research program currently in progress at DIT involved the construction of a single alkaline fuel cell test bed, Figure 5. Constructing the system gave researchers at DIT a valued insight into the complexities of a basic fuel cell system. As a result of collaboration between researchers at DIT and Gaskatel GmbH a suggestion was made to change the gas and electrolyte supply from the top of the cell to the bottom of the cell and this has been incorporated into the new cells construction. The new configuration allows both the hydrogen (H_2) gas and the oxygen (O_2) gas to flow freely through the cell as opposed to being pushed. This has a positive effect on relieving the build up of inert gas and trapping of bubbles inside the cell, allowing them to rise by natural progression towards the exit lines.

Constructing the test bed also identified and solved another problem with the system involving the hydrogen and oxygen gas supply to the cell. It was reported to the researcher that the test bed required constant monitoring because the system pressure varied with the change in volume of gas in each cylinder. As the level of the gas dropped inside the external gas cylinder the system pressure also dropped and this affected the pressure balance inside the cell between the pores of the electrode resulting in crossover and cell malfunction. The solution was to fit a Multi-stage gas regulator to the external hydrogen and oxygen gas supply bottles.

At the anode of an AFC the hydrogen gas (H_2) combines with the hydroxyl ions (OH-) to form water (H_2O) and electrons (e-). As part of this process water builds up in the electrolyte and also leaves the cell in the exiting hydrogen stream. As reported as part of the Apollo space missions this water having been treated (the pH of the water maintained at between 6 and 8) was used as drinking water for the mission [1]. One of the problems encountered with the operation of the single cell test bed was the build-up of water in the exit lines of the system after shutdown. This water was alkaline and corrosive and is undergoing various tests to establish if it is reaction or crossover water, (the results of these tests are not available for this paper). With the old cell configuration (gas and electrolyte supply at the top of the cell) water was building up at the supply side of the cell, interfered with the gas supply and corrosively attacking the gas regulator. To prevent this a one-way valve was incorporated into the system but because potassium hydroxide molecules are tiny corrosive water did get past this valve and attach the hydrogen gas regulator. In a system incorporating a multi cell stack this problem would be amplified tenfold. The new design puts the hydrogen gas stream water at the exit side of the cell, which is more beneficial and easier to rectify. In a fuel cell stack system the hydrogen gas can be re-circulated towards the inlet side of the stack and this H_2 gas could be run through a condenser to extract the water. The separated water would be gathered in a sedimenter (water separator), made ph neutral and could be drained off when full.

Tests have also being carried out to check the cells recovery time.

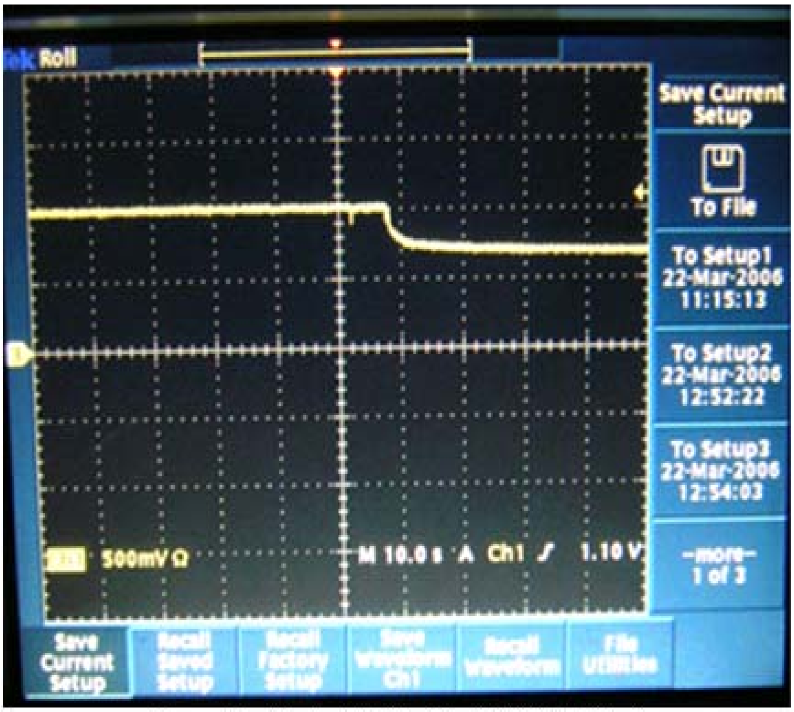

Figure 6. Single Alkaline Fuel Cell Test Bed.

Results to date have suggested that the single cell takes up to 4 minutes to reach its start-up open circuit potential of 1.05 volts depending on cell temperature conditions. If the cell is at 50°C it takes less time to reach 1.05 volts, but time is taken up warming the cell so the time factor evens out. When operating under load if the load is increased the cell voltage drops immediately but if the load is decreased the cell takes up to 6 ~ 8 seconds (depending on the load applied) to recover its voltage and even out as shown in Figure 6. This would suggest that the fuel cell is more suited to constant loads as opposed to snap load situations similar to those associated with driving an automotive vehicle. The tests suggest that fuel cells operated in an automotive environment require a secondary power source to assist and smooth out vehicle start up and other periods of excessive loading on the cell, (acceleration etc). Hybrid situation were not available in the early years of fuel cell development but the results from these tests would suggest that their use in an automotive application are well justified. It should also be mentioned that when a fuel cell is on activated stand, without load, the fuel cell electrodes and catalysts degrade more than under load [21].

The performance of the single alkaline fuel cell fitted to the test bed is most efficient at 55°C but controlling the temperature of the cell with a circulating electrolyte requires constant monitoring and control. When initially heating the cell on start-up it is best to leave the KOH immobile until the operating temperature is reached. When the pump is activated (the pump in this situation is externally powered) and circulation begins the cells potential starts to drop off as the cell temperature decreases. If the electrolyte is left to circulate it takes a long time to bring the cell back to its most efficient operating temperature (55°C) and effects cell efficiency. A circulating electrolyte is very desirable for cooling the cell and replenishing the electrolyte concentration. But it is hard to maintain an accurate cell temperature with a continuous circulating electrolyte. The solution adopted for the single cell system (with internal cell heating coils) was to monitor the cell heating times and control the KOH circulation intervals, but other options, such as externally heating the KOH are being looked at as part of the process of refining the system.

Conclusions

In conclusion, tests have shown that an alkaline fuel cell can operate on un-scrubbed air for an extended period exceeding 5000 hours, with any decrease in its potential being rectified by changing to fresh electrolyte. The cell and its operating system have also displayed enough reliability and durability during testing to suggest that the misconceptions relating to alkaline fuel cells and its use of a corrosive electrolyte (KOH) can be resolved using modern technology. The new cell configuration has also allowed for an easier passage through the cell for gas and electrolyte prompting trapped bubbles, water and inert gases to exit the cell making the system and external subsystems easier to operate and design. Constructing this test bed and conducting various tests to examine the system and the cells potential has highlighted the need for expertise across a wide range of disciplines if the refinements necessary to bring the alkaline fuel cell to commercialisation is ever to be realised.

References

[1] G. Hoogers, E. Chen, Fuel Cell Technology Handbook. 2003.
CRC Press.
[2] J. Metthey, Integrating and Strengthening the European Research Area. 2004.
European Commission Research Directorate-General.
[3] M.Cifrain, K. Kordesch, Hydrogen/oxygen (Air) fuel cells with alkaline electrolytes. 2003. Handbook of Fuel Cells John Wiley & Sons Ltd.
[4] K. Kordesch, Fuel Cell Comparisons. 2004.
http://www.electricauto com/contents/fc_compare.html
[5] B. Cook, An Introduction to Fuel Cells and Hydrogen Technology. 2001.
Heliocentris, Canada.
[6] Jiri K.Nor, Alkaline Fuel Cell Technology for the 21st Century. 2000.
Astri Energi Website www.astri.ca.
[7] R. Stobart, Fuel Cell Technology for Vehicles. 2001.
Society of Automotive Engineers.
[8] N.K. Bansal, Indian Strategy for Fuel Cell Development. 2003.
Forschungszentrum Julich GmbH.
[9] D.P. Gregory, Fuel Cells. 1972.
Mills & Boon Ltd. Library Ref. 621 . 359.
[10] Concurrent Technologies Corporation, Proton Exchange Membrane Fuel Cells.
2003. http://www.fctec.com/fctec_types_pem.asp
[11] The Future of Fuel Cells. 2004
http://www.benwiens.com/energy4.html.
[12] Online Article. Plastic Technology. 2004.
file://C:\Temp\4Q70Q96R.htm.
[13] Direct Methanol Fuel Cells (DMFC). 2004.
http://www.cfdrc.com/bizareas/power/fuel_cell/dmfc.html.
[14] Phosphoric Acid Fuel Cells (PAFC). 2004
http://fuelcells.si.edu/phos/phos3.htm.
[15] Online Article, Vision Engineer-Solid Oxide Fuel Cell. 2004.
http://www.visionengineer.com/env/so.shtml
[16] FCTec, Molten Carbonate Fuel Cells (MCFC). 2004.
http://www.fctec.com/fctec_types_mcfc.asp.
[17] K. Kordesch, V.Hacker, Stack Materials and Design.. 2003. Handbook of Fuel Cells John Wiley & Sons Ltd.
[18] L.J. Blomen, M.N. Mugerwa, Fuel Cell Systems. 1993.
Plenum Press, New York.
[19] R.H. Thring, G. Sauer, O. Carlisle, Fuel Cells for Automotive Applications. 2004.
Professional Engineering Publishing.
[20] E. Coyle, D. Kennedy, H-J Kohnke, S. Schudt, G. Sauer, J.P. Hamilton,
H. Smith-Walter. Long-Term Operation of an Alkaline Fuel Cell with Air. 2006.
REMIC2.
[21] Advantages of Alkaline Fuel Cell Systems for Mobile Applications.
Hacker et al.

KARAKTERIZACIJA NITROKARBURIRANOG SLOJA

CHARACTERIZATION OF NITROCARBURIZED LAYER

Franjo Cajner, Darko Landek, Sanja Šolić

Fakultet strojarstva i brodogradnje, Sveučilište u Zagrebu
Ivana Lučića 1, 10000 Zagreb, Hrvatska
E-mails: franjo.cajner@fsb.hr, darko.landek@fsb.hr, sanja.solic@fsb.hr

Sažetak:
U radu su prikazani načini karakterizacije nitrokarburiranog sloja. Način određivanja osnovnih svojstava (debljina zone spojeva, dubina nitrokarburiranja, površinska tvrdoća) propisan je normama DIN 6773:2001, EN 10052:1993., DIN 50190:1979. Za detaljniju procjenu kvalitete nitrokarburiranog sloja koriste se i dodatna ispitivanja: mikrostrukture, hrapavosti, topografije površina, triboloških svojstva i korozijske postojanosti.

Ključne riječi:
nitrokarburiranje, TENIFER, mikrotvrdoća, otpornost na trošenje, korozijska otpornost

Abstract:
This paper presents methods for the characterization of nitrocarburized layer. Testing methods for base properties (compound layer thickness, nitrocarburizing depth, surface hardness) are described according to current standards DIN 6773:2001, EN 10052:1993., DIN 50190:1979. Detailed estimation of quality of the nitrocarburized layer is performed by additional testing of: microstructure, surface roughness and topography, tribological properties and corrosion resistance.

Key words:
nitrocarburizing, TENIFER, microhardness, wear resistance, corrosion resistance

1. UVOD

Nitrokarburiranje (u solnim kupkama, plinu ili plazmi plinova) je često primjenjivan postupak toplinsko kemijske obrade kojim se površinski sloj dijelova i alata od čelika ili željeznih ljevova difuzijski obogaćuje dušikom i ugljikom (slika 1). Ovaj postupak je znatno kraćeg trajanja (2 do 4 sata) u odnosu na postupke klasičnog (plinskog) nitriranja (više od 10 sati) i može se primijeniti na većini čelika pri čemu one zakaljive treba odgovarajuće prethodno toplinski obraditi (kaliti i visokotemperaturno popustiti). Postupkom nitrokarburiranja (kao i nitriranjem) postiže se povećanje: tvrdoće, dinamičke izdržljivosti, otpornosti na trošenje (posebno adhezijsko), otpornosti na koroziju (u atmosferi i slanoj vodi), na povišene temperature (do 550ºC) uz male ili zanemarive deformacije obratka. Uz postupke nitriranja i nitrokarburiranja u industrijskoj su primijeni i postupci u kojima u površinu čelika uz dušik i ugljik difundira kisik (oksinitriranje, oksinitrokarburiranje) ili sumpor (sulfonitriranje, oksisulfonitriranje) [1 - 6].

U ovom radu opisati će se karakterizacija nitrokarburiranog sloja prema EN i DIN normama, koja obuhvaća određivanje površinske tvrdoće, tvrdoće i debljine zone spojeva, rasporeda tvrdoće po dubini difuzijske zone, te određivanje dubine nitrokarburiranja. Uz normama propisana ispitivanja prikazati će se i uobičajena laboratorijska ispitivanja kao što su ispitivanje hrapavosti, otpornosti na trošenje te metalografska ispitivanja. Sve navedene metode i postupci karakterizacije nitrokarburiranog sloja vrijede i za ostale prije spomenute površinske slojeve: nitrirane, oksinitrirane, sulfonitrirane i dr.

2. NORMAMA PROPISANA KARAKTERIZACIJA I OZNAČAVANJE NITROKARBURIRANOG SLOJA

Na slici 1 prikazan je dijagram postupka nitrokarburiranja u solnoj kupki sa i bez naknadne oksidacije s uobičajenim vrijednostima radnih parametara. U slučaju naknadne oksidacije u solnoj kupki AB1 nitrokarburirane obratke treba prethodno polirati (tzv. postupak QPQ).

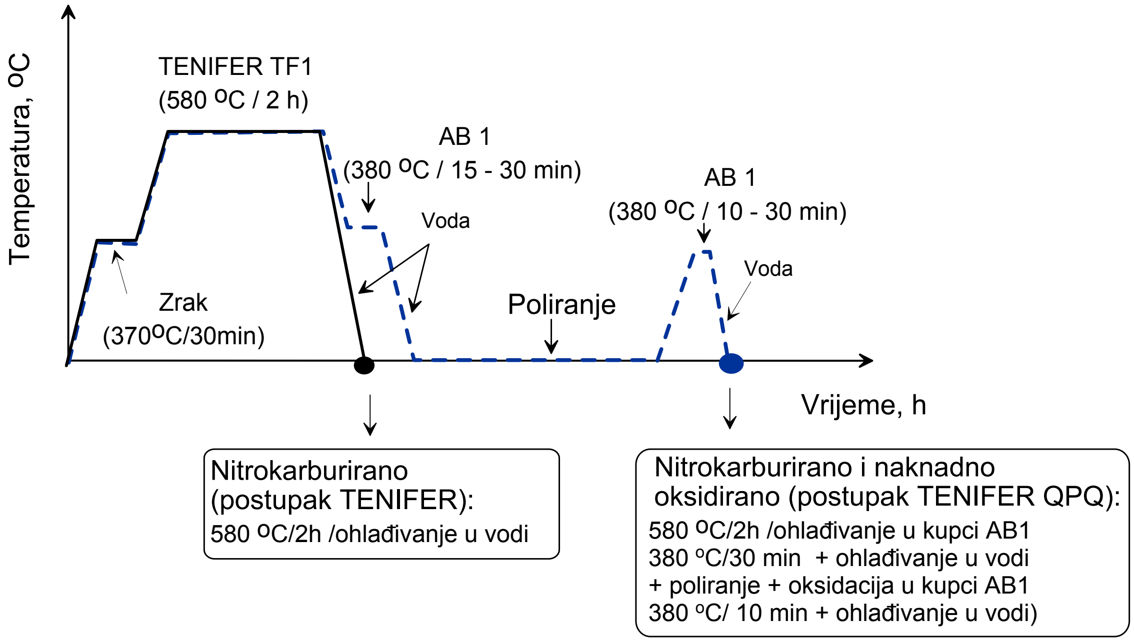

Slika 1. Dijagram postupka nitrokarburiranja sa i bez naknadne oksidacije

Nitrokarburirani sloj općenito se sastoji, idući od površine prema jezgri, od **zone spojeva** (debljine 15 do 20 µm) i **difuzijske zone** (slika 2). Treba napomenuti da je nekim postupcima (npr. nitriranjem ili nitrokarburiranjem u plazmi) moguće postići samo difuzijsku zonu bez zone spojeva. Prisutnost zone spojeva na nitrokarburiranim predmetima moguće je jednostavno i brzo utvrditi kemijskim ispitivanjem pomoću tzv. Haynove otopine (otopina bakrenog klorida, $CuCl_2NH_3Cl\ \ 2H_2O$)[7].

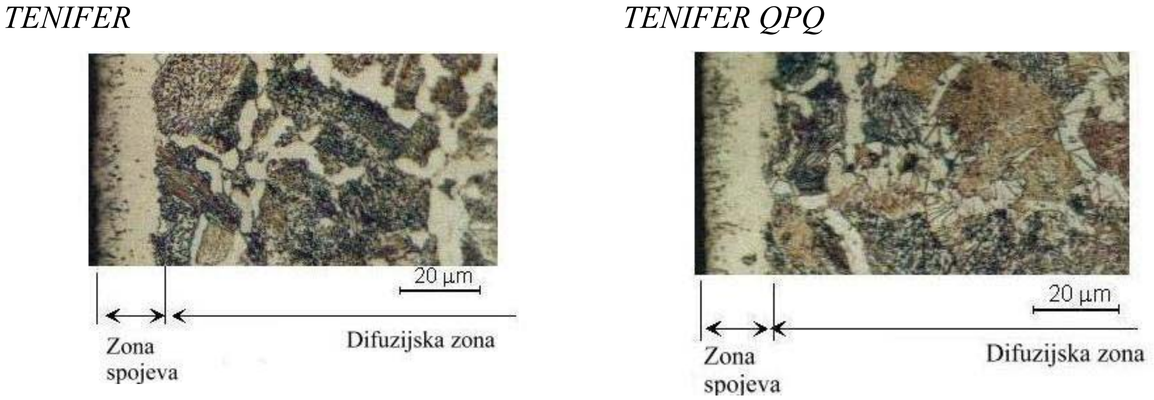

a) b)

Slika 2. Mikrostruktura rubnog sloja čelika Ck45 u nagriženom stanju (3% NITAL) nakon:
a) nitrokarburiranja postupkom TENIFER (TF1 580 ºC / 2 h / voda)
b) nitrokarburiranja i naknadne oksidacije (postupak TENIFER QPQ, slika 1)

U zoni spojeva su zbog visokog sadržaja dušika prisutni karbonitridi i/ili nitridi (Fe_4N, $Fe_{2\text{-}3}N$, $Fe_x(C,N)$) u tolikoj mjeri, da se struktura tog sloja bitno razlikuje od ostalog područja (kemijskim sastavom, svojstvima, izgledom) (slika 2).

Difuzijska zona nastavlja se na zonu spojeva i sadrži osim elemenata N,C,O u čvrstom ili djelomično precipitiranom stanju, dovedene u materijal tijekom nitrokarburiranja i nitride. Sporim hlađenjem s temperature nitrokarburiranja ili naknadnim ugrijavanjem čelika (namjerno ili u postupku postoksidacije) moguće je difuzijsku zonu uočiti zbog izlučivanja igličastih nitrida i karbonitrida (slika 2.b).

Karakterizacija nitrokarburiranog sloja sastoji se u ispitivanju u sljedećih veličina [5]:

- površinske tvrdoće
- tvrdoće zone spojeva
- rasporeda tvrdoće po dubini difuzijske zone
- debljine zone spojeva (ako je prisutna poroznost onda i njene dubine i intenziteta)
- dubine nitrokarburiranja

Sve navedene veličine, osim površinske tvrdoće, ispituju se na metalografski pripremljenom poprečnom presjeku nitrokarburiranog predmeta.

Debljinu zone spojeva moguće je odrediti i nerazornim ispitivanjima. Uglavnom se koristi ultrazvučna metoda impulsnog odjeka pri kojoj je raspon mjerenja debljina površinskih slojeva je 10 do 500 µm uz točnost od 1 µm te metoda mjerenja debljine zone spojeva primjenom vrtložnih struja [7, 8].

Tvrdoća zone spojeva ispituje se na metalografski pripremljenom uzorku i po iznosu se razlikuje od tvrdoće površine. Za ispitivanje tvrdoće zone spojeva primjenjuju se metode prema Vickersu (HV 0,1; HV 0,05; HV 0,01) ili Knoopu (HK 0,1; HK 0,2) sa malim opterećenjima zbog male debljine i velike krhkosti sloja [6].

Površinska tvrdoća nitrokarburiranog obratka ovisi o tvrdoći zone spojeva i difuzijske zone, dubini nitrokarburiranja (nitriranja) i primijenjenom opterećenju indentora (veće opterećenje daje niže iznose tvrdoće i obratno). Stoga je normama propisano maksimalno dopušteno opterećenje za ispitivanje površinske tvrdoće Vickers-ovom metodom ovisno o minimalnoj dubini nitrokarburiranja (nitriranja) i očekivanoj tvrdoći površine [5].

Debljina zone spojeva je okomita udaljenost od površine nitrokarburiranog predmeta do granice difuzijske zone (gdje je vidljiv prijelaz iz jednog strukturnog stanja u drugi) (slika 2). Može se dovoljno točno izmjeriti do sada poznatim mjernim metodama (npr. svjetlosnom mikroskopijom) samo na metalografski pripremljenom uzorku pri dovoljnom povećanju (npr. 500:1 prema normi SAE J423). Na tehničkim crtežima navodi se u **milimetrima** te joj se pripisuje maksimalna moguća, no ipak funkcijski primjerena tolerancija u plusu [5]. Dubina poroznosti zone spojeva**,** prisutne u nekim postupcima poput nitrokarburiranja u solnim kupkama, također se određuje na metalografski pripremljenom uzorku svjetlosnom mikroskopijom s povećanjima od 200:1 i većim. Pri tome se može izraziti dubina prisutne poroznosti zone spojeva (u milimetrima) i procijenjen intenzitet (u %).

Dubina nitrokarburiranja (nitriranja), Nht (skraćenica od Nitrierhärtetiefe – dubina tvrdoće nitriranja - kod nas uvriježeno nazvana efektivna dubina nitriranja) okomita je udaljenost od površine nitrokarburiranog predmeta do mjesta na kojem tvrdoća odgovara utvrđenoj graničnoj vrijednosti [4]. Pri tome treba razlikovati ukupnu dubinu nitrokarburiranja (ukupna dubina do koje je dušik difundirao u čelik) od dogovorene (efektivne) dubine nitrokarburiranja Nht.

Sukladno normi DIN 50190:1979 dubina nitrokarburiranja (Nht) određuje se na slijedeći način (slika 3):
Na metalografski pripremljenom uzorku (polirano stanje) poprečnog presjeka nitrokarburiranog dijela mjeri se tvrdoća, od ruba prema jezgri. Tvrdoća se mjeri Vickers-ovom ili Knoop-ovom metodom, sa silom utiskivanja **4,9 N (HV 0,5)**. Prema potrebi moguće je upotrijebiti i druge sile utiskivanja od 2,9 N do 19,6 N (HV 0,3 do HV 2). Potrebno je izmjeriti **dva niza** tvrdoće na **istom** uzorku. Dobiveni rezultati ucrtavaju se u dijagram, i potom se određuje dubina nitrokarburiranja Nht na način da je to okomita udaljenost od ruba do mjesta gdje je granična tvrdoća jednaka tvrdoći jezgre + 50 HV [6].

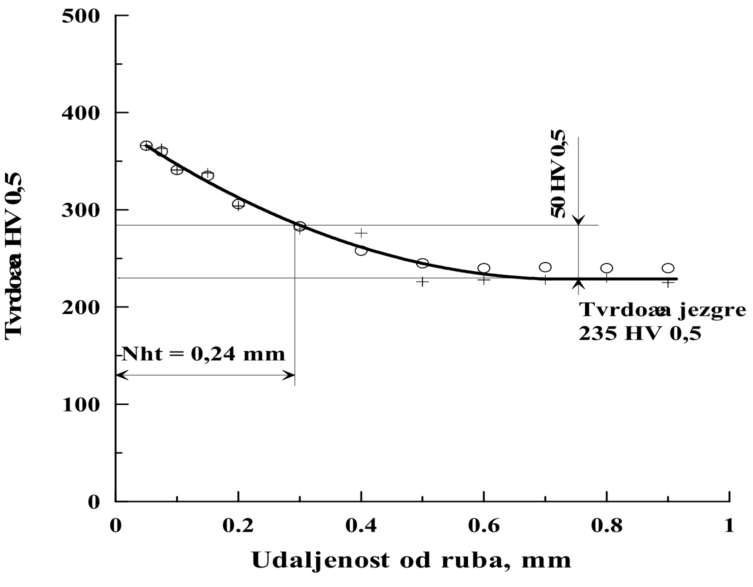

Slika 3: Raspored mikrotvrdoće u rubnom sloju čelika Ck45 nitrokarburiranog postupkom TENIFER(TF1 580ºC / 2h / voda) s određenom dubinom nitrokarburiranja (Nht)

Zadavanje zahtijeva za nitrokarburiranjem (nitriranjem**) na tehničkoj dokumentaciji** sastoji se od propisivanja samo najnužnijih (ne i svih gore navedenih) veličina. Navedene veličine ovisiti će o postupku nitrokarburiranja i potrebi propisivanja vrijednosti svojstava koja se od sloja traže u eksploataciji. Najčešće se propisuje **dubina nitrokarburiranja** (rjeđe ukupna, a češće Nht) te **površinska tvrdoća**. Važno je napomenuti da se svi navodi na tehničkoj dokumentaciji (crtežima), riječima i brojevima, odnose na **završno stanje** [5, 9]. Dubina nitrokarburiranja navodi se u milimetrima i njoj se pripisuje najveća moguća funkcijski odgovarajuća tolerancija u plusu. Prema DIN 6773:2001 na slici 4 prikazan je uobičajeni zahtjev za nitrokarburiranje u tehničkoj dokumentaciji (crtežu) uz pojašnjenje oznake (efektivne) dubine nitrokarburiranja.

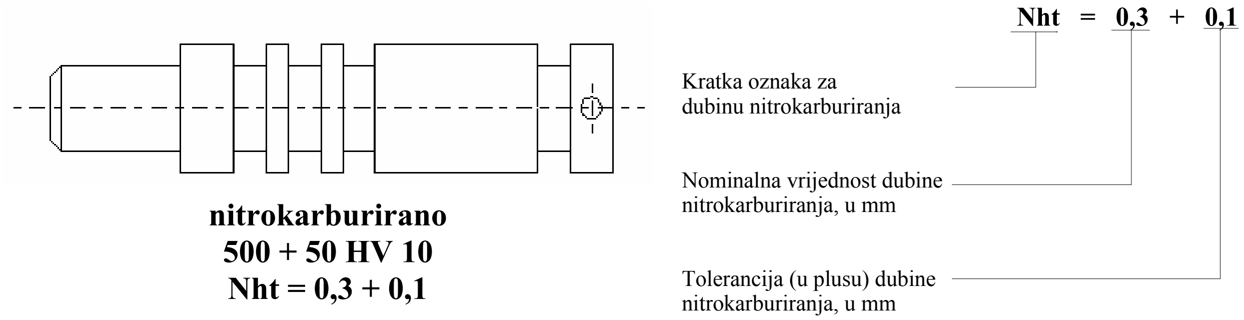

Slika 4: Primjer označavanja zahtjeva za nitrokarburiranje cijelog predmeta i pojašnjenje oznake za dubinu nitriranja (Nht) [5]

Prikazani navod 500 + 50 HV 10 na slici 4 označava zahtijevanu površinsku tvrdoću uz uvjet da je navedena tvrdoća površine minimalna koju treba ostvariti (min. 500 HV 10). Ukoliko je potrebno, konkretno mjerno mjesto ispitivanja površinske tvrdoće može se označiti strelicom. Norma [5] propisuje i preporučeno stupnjevanje vrijednosti dubine nitriranja, Nht, kao i vrijednosti tolerancija, kojih se treba pridržavati. Ako se pri utvrđivanju dubine nitriranja primjenjuje **sila ispitivanja** tvrdoće koja **odstupa od norme** primijenjeno opterećenje mora se navesti u oznaci, iza Nht. Ukoliko se ne radi o nitrokarburiranju cijelog predmeta, područje koje je potrebno **djelomično nitrokarburirati** obilježava se širokom crta-točka-linijom (u neobilježenom području ne smije biti prisutna niti zona spojeva, niti difuzijska zona).

3. DODATNA ISPITIVANJA NITROKARBURIRANOG SLOJA

Osim ispitivanja nitrokarburiranog sloja svjetlosnom (i elektronskom) mikroskopijom te određivanja mikrotvrdoće postoji niz metoda (tablica I.) koje se uglavnom primjenjuju pri znanstvenim istraživanjima, razvoju i usvajanju novih parametara postupka nitrokarburiranja, kod analize dotrajalih i oštećenih nitriranih dijelova, te pri ispitivanju eksploatacijskih karakteristika nitrokarburiranog (nitriranog) sloja. Od metoda navedenih u tablici I u nastavku će se ukratko opisati ispitivanja hrapavosti površina, kemijskog sastava sloja, otpornosti na trošenje te otpornosti na koroziju.

Tablica I. Pregled metoda za ispitivanje karakteristika nitrokarburiranog (nitriranog) sloja [8, 9]

Svrha ispitivanja	***Metode ispitivanja***
Određivanje kemijskog sastava rubnog sloja	- rendgenska difrakcija - Auger-ova elektronska spektroskopija - optička spektrometrija tinjajućeg pražnjenja (GDOS)
Određivanje kemijskog sastav osnovnog materijala	- spektroskopija - mokra kemijska analiza
Određivanje debljine sloja	- nerazorne metode - razorne metode
Ispitivanje hrapavost i topografije površine nitrokarburiranog obratka	- mjerenja hrapavosti površine elektro-mehaničkim uređajem s ticalom - 3D profilometrija
Analiza mikrostrukture	- svjetlosna mikroskopija - elektronska mikroskopija (SEM, TEM) - rendgenska analiza
Ispitivanje unutrašnjih naprezanja sloja	- rendgenska difrakcija
Određivanje gustoće sloja	- gravimetrija - volumetrija
Ispitivanje triboloških svojstava sloja	- ispitivanje prionjivosti zone spojeva - ispitivanje faktora trenja - ispitivanje otpornosti na trošenje (adhezijsko, abrazijsko)
Ispitivanje mehaničkih svojstava sloja	- metode utiskivanja (mikrotvrdoća, nanotvrdoća)
Ispitivanje korozijske postojanosti (otpornosti) sloja	- ispitivanja u slanoj komori (SS test) - elektrokemijska ispitivanja

3.1 Ispitivanje hrapavosti površine

Hrapavost i topografija površine bitna su svojstva sa aspekta trenja i trošenja. Različitim elektro-mehaničkim uređajima sa ticalom ispituje se profil površine na zadanoj referentnoj duljini. Pri tome se može mjeriti niz tzv. horizontalnih i vertikalnih parametara [7]. Najčešće se određuju dva (vertikalna) parametra (slika 5):

R_t – najveća visina neravnina, µm,
R_a – srednja aritmetička udaljenost profila, µm

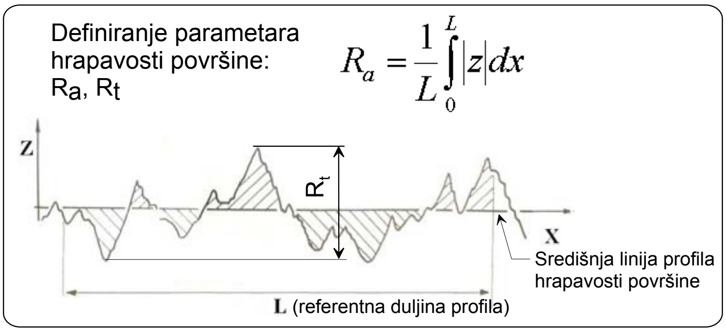

Slika 5. Shematski prikaz određivanja parametara hrapavosti površine

Nitrokarburiranjem se hrapavost površine povećava zbog stvaranja zone spojeva (slika 6). Ako se obratci nitrokarburiraju i naknadno oksidiraju (npr. postupak TENIFER QPQ) hrapavost se zbog međufaznog poliranja značajno smanjuje u odnosu na nitrokarburirano stanje. Naknadna oksidacija u solnoj kupki AB1 uopće ne utječe na hrapavost površine [10, 11].

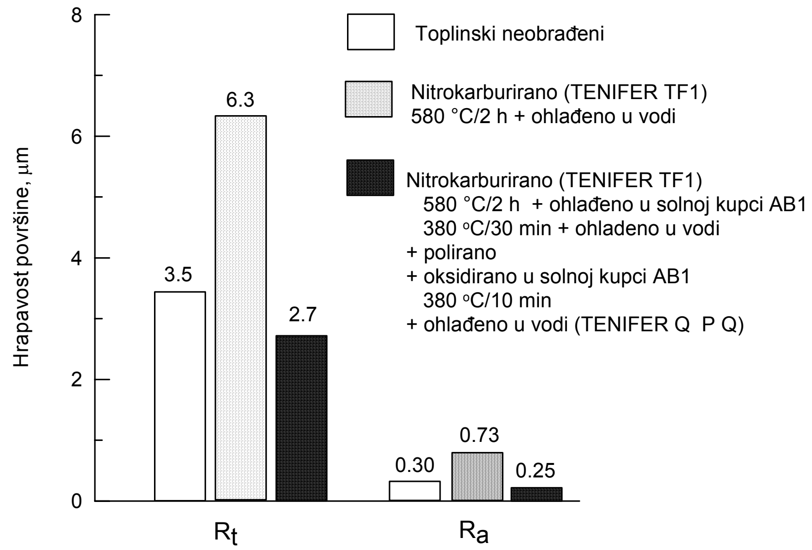

Slika 6. Vrijednosti parametara hrapavosti površine (R_{max}, R_a) ispitnih uzoraka od čelika Ck45 u toplinski neobrađenom stanju te nakon nitrokarburiranja postupkom TENIFER i nitrokarburiranja s naknadnom oksidacijom (postupak TENIFER QPQ)

3.2 Ispitivanje kemijskog sastava nitriranog sloja

Osim dubine i mikrostrukture, nitrokarburiranom sloju se može ispitivati i kemijski sastav nitrokarburiranog sloja po dubini sloja. Metode analize površine rade na principu međusobnog djelovanja čestica visoke energije (elektrona, iona) s površinom ispitivanog uzorka, i registriranju nastalog povratnog zračenja. Za ispitivanje kemijskog sastava najčešće se koriste slijedeće metode [7]:

- **Elektronska mikroanaliza** (EPMA – Electron Probe Microanalysis)
    - rendgenska energijskodisperzijska analiza
    - (EDX – Energy Dispersive X- Ray Microanalysis)
    - rendgenska valnodisperzijska analiza
    - (WDX – Wavelenght Dispersive X – Ray Microanalysis)
- **Auger-ova elektronska spektroskopija** (AES – Auger Electron Spectroscopy)
- **Fotoelektronska spektroskopija** (ESCA – Electron Spectroscopy for Chemical Analysis)
- **Optička spektrometrija tinjajućeg pražnjenja** (GDOS – Glow Discharge Optical Spectrometry)

3.3 Ispitivanje otpornosti na trošenje

Otpornost na trošenje nije jednoznačno definirano svojstvo, već se mora specificirati na koji se dominantni mehanizam ono odnosi. Nitrirani i nitrokarburirani slojevi nosioci su prvenstveno otpornosti na adhezijsko trošenje i tribokoroziju, a posjeduju i određenu otpornost na abraziju. Nitrokarburiranjem se također smanjuje faktor trenja u odnosu na nenitrirani čelik [12, 13, 14] .

Otpornost na adhezijsko trošenje određuje se uvijek za tarni par, npr. nitrokarburirani ispitni uzorak – prsten od kaljenog i popuštenog čelika. Osnovni kriterij za ocjenu otpornosti na adhezijsko trošenje materijala triboparova je njihova tribološka kompatibilnost. Nitrokarburirani (i nitrirani) sloj ima drugačiji tip kristalne rešetke od željeznih materijala, pa je stoga kompatibilan za rad u triboparovima sa čelikom. Za ispitivanje otpornosti na adhezijsko trošenje postoji niz metoda od kojih su često korištene slijedeće [12, 13]:

- test "četiri kuglice" (ASTM D 2783)
- ispitivanje u triboparu ispitni uzorak (kvadar ili valjak) – klizni prsten od kaljenog i popuštenog čelika za kotrljajuće ležajeve (slika 7.a)
- ispitivanje u triboparu ispitni uzorak (konus ili valjak) - čelični disk

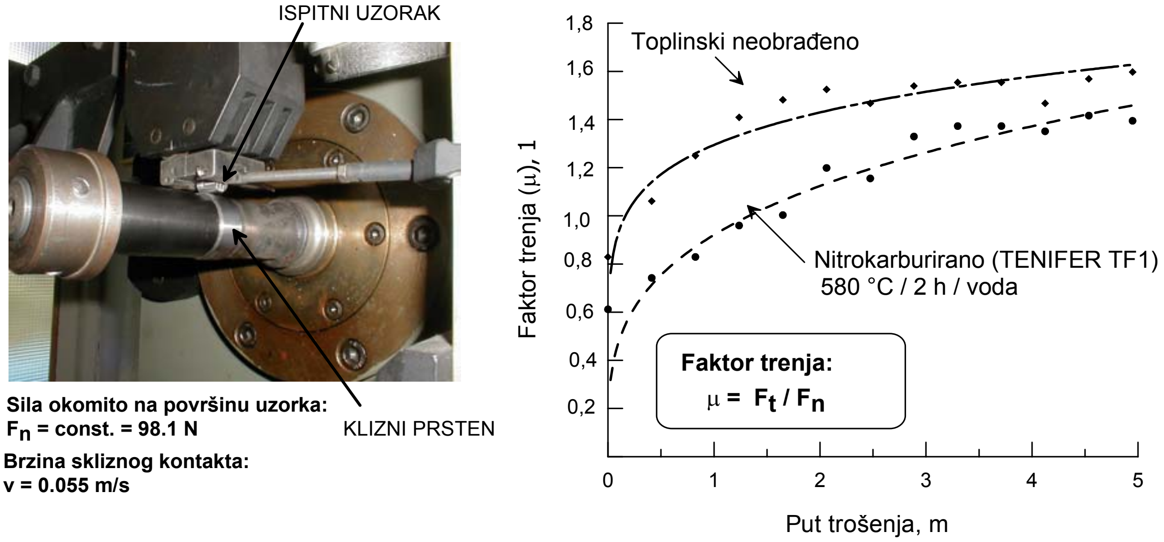

Slika 7. a) Tribopar ispitni uzorak – klizni prsten na istoimenom uređaju
b)Promjena faktora trenja s putem trošenja ispitnog uzorka od čelika Ck45, nitrokarburiranog postupkom Tenifer (TF1 580 ºC/2h/voda) u odnosu na toplinski neobrađeni uzorak od istog čelika [9, 11].

Osim za ispitivanje otpornost na adheziju uređaj ispitni uzorak – klizni prsten može poslužiti i za ispitivanje faktora trenja. Na slici 7. b prikazana je promjena faktora trenja s putem trošenja, na ispitnim uzorcima od čelika Ck45 toplinski neobrađenim i nitrokarburiranim u solnoj kupki Tenifer (snimljeno na uređaju ispitni uzorak – klizni prsten - bez podmazivanja).

Otpornost na abrazijsko trošenje povezana je s međusobnim odnosom tvrdoća abraziva i materijala odnosno površinskog sloja trošene podloge (npr. nitrirani ili nitrokarburirani sloj). Površinski modificirani sloj pokazuje nultu abraziju kad su čestice abraziva manje tvrdoće od površinske tvrdoće sloja. Otpornost na abraziju također se ispituje nizom metoda koje oponašaju eksploatacijske uvjete. Uobičajena metoda ispitivanja otpornosti na abraziju metalnih materijala jest "suhi pijesak – gumeni kotač" (ASTM G 65-85) pri čemu treba primijeniti pijesak što manje granulacije [12, 13, 14].

3.4 Ispitivanje otpornosti na koroziju

Za određivanje otpornosti na koroziju nitrokarburiranog sloja uobičajeno se koristi ispitivanje u slanoj komori (SS test prema normi DIN 50025), ali i normama još neobuhvaćena elektrokemijska ispitivanja (određivanje brzine korozije Tafelovom ekstrapolacijom, određivanjem polarizacijskog otpora) [10, 15, 16].

Pri ispitivanju u slanoj komori (SS test) simulira se djelovanje kapljica morske vode (5% vodena otopina NaCl) na površinu čelika. Nakon izlaganja ispitnih uzoraka slanoj atmosferi u trajanju od 100 do 1000 sati nastali korozijski produkti mehanički se uklanjaju vodenim mlazom ili četkom. Brzina korozije (g/m^{2}h) ispitnih uzoraka određuje se gravimetrijski (vaganjem) prije i poslije izlaganja slanoj atmosferi [15]. U tablici II. prikazan je izgled ispitnih uzoraka od čelika Ck45 toplinski neobrađenih te nitrokarburiranih postupkom TENIFER s i bez naknadne oksidacije nakon 96 sati izlaganja koroziji u slanoj komori u 5 %-tnoj vodenoj otopini NaCl. Iz izgleda ispitnih uzoraka vidljiva je značajno bolja otpornost nitrokarburiranog i naknadno oksidiranog uzorka (TENIFER QPQ) u odnosu na samo nitrokarburirani (TENIFER) uzorak i toplinski neobrađeni uzorak.

Tablica II. Ispitni uzorci od čelika Ck45 u različitih polaznih stanja nakon izlaganja slanoj magli 5 %-tne otopine NaCl u vodi

Toplinski neobrađeno stanje	Nitrokarburirano postupkom TENIFER (TF1 580ºC / 2h / ulje)	Nitrokarburirano i oksidirano postupkom TENIFER QPQ (TF1 580ºC/2h/AB1 390ºC / 15min / voda / polirano / AB1 340ºC /30 min / voda)
		

Kod elektrokemijskog određivanja brzine korozije ispitivanja se provode u elektrokemijskoj ćeliji sastavljenoj od tri elektrode: radne (ispitni uzorak), referentne (zasićena kalomel elektroda) i pomoćne (od platine ili grafita). Elektrode se spajaju na potenciostat ili galvanostat i programirano se mijenja električni potencijal ili struja. Pri metodi Tafelove ekstrapolacije snimaju se krivulje promjene električnog potencijala ispitnog uzorka (katodna i anodna polarizacija) ovisno o gustoći struje (slika 8) [10, 16].

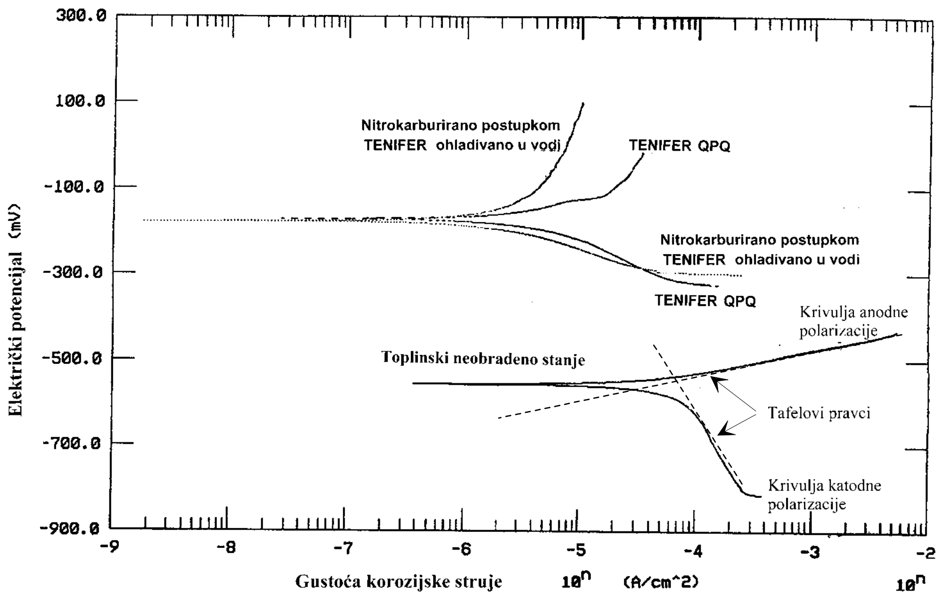

Slika 8. Određivanje gustoće korozijske struje Tafelovom ekstrapolacijom za različita stanja površinski modificiranog čelika Ck45 (toplinski neobrađeno, nitrokarburirano i nitrokarburirano s naknadnom oksidacijom)

Ekstrapolacijom Tafelovih anodnih i katodnih pravaca u njihovom sjecištu se određuje vrijednost gustoće korozijske struje (A/cm^2) i korozijski potencijal. Iz istih krivulja određuje se i polarizacijski otpor ispitnog uzorka definiran nagibom krivulje «potencijal – gustoća struje» u neposrednoj blizini korozijskog potencijala. Snimanje potencio-dinamičkih krivulja i određivanje gustoće korozijske struje, odnosno polarizacijskog otpora ispitnog uzorka automatizirano je i provodi se specijaliziranim mjernim uređajima uz računalnu obradu i prikaz rezultata mjerenja.

4. ZAKLJUČAK

Preduvjet za postizanje odgovarajućeg nitrokarburiranog (ili nitriranog) sloja na konkretnim obradcima jest potpuno i jednoznačno propisivanje njegovih svojstava na tehničkoj dokumentaciji prema kojoj se provodi postupak nitrokarburiranja.

Karakterizacija nitrokarburiranog sloja definirana je važećim europskim normama, a sastoji se od ispitivanja: površinske tvrdoće, profila tvrdoće po poprečnom presjeku, debljine zone spojeva i dubine nitrokarburiranja (nitriranja).

Ostala svojstva nitrokarburiranih (ili nitriranih) slojeva kao što su ispitivanje: hrapavosti, kemijskog sastava, otpornosti na trošenje i koroziju daju detaljniju sliku o ovim slojevima i mogućnostima njihove primjene te se obavezno provode u znanstveno istraživačkim, razvojnim i eksploatacijskih istraživanjima.

5. LITERATURA

[1] B. Liščić, M.Stupnišek, F. Cajner, T. Filetin: ¨Toplinska obrada – praktikum¨, Fakultet strojarstva i brodogradnje Sveučilišta u Zagrebu, 1992

[2] M. Novosel: ¨Osnove toplinske obradbe – Inženjerski priručnik¨, I. sv ur. A. Mulc, D. Taboršak, I. Budin, Školska knjiga, Zagreb, 1998

[3] D. Krumes: ¨Toplinska obradba¨, Strojarski fakultet Sveučilišta u Osijeku, Slavonski Brod, 2000

[4] EN 10052:1993.

[5] DIN 6773:2001

[6] DIN 50190:1979

[7] ...¨Handbook of analytical methods for materials¨, Materials Evaluation and Engineering, 2001.

[8] J. Büchler, T. Pagel: ¨High Precision Coating Measurement with Ultrasound¨, NDTnet, 2000.

[9] F. Cajner, D. Landek, S. Šolić: "Definiranje i karakterizacija nitriranog sloja", Zbornik savjetovanja "Novi postupci modificiranja i prevlačenja površina", Zagreb, 21.04.2004., 55-64

[10] F. Cajner, D. Landek, E. Stupnišek-Lisac: Improvement of properties of steels applying salt bath nitrocarburizing with post-oxidation", Materiali in tehnologije, 37 (2003) 6, 333-339.

[11] F. Cajner, D. Landek: Influence of oxidation of nitrocarburized steel upon the resistance to wear and corrosion", Proceed. of the 9th Seminar IFHTSE, Warsaw, Poland, 23.-25. 09. 2003, 371-378

[12] K. Holmberg, A. Matthews: ¨Coatings Tribology- Properties, Techniques and Applications in Surface Engineering¨, Elsevier Science B.V., Amsterdam, 1994.

[13] ... ASM Handbook Vol. 18 Friction, Lubrication and Wear Technology, ASM International, Metals Park, Ohio, 1995.

[14] V. Ivušić: ¨Tribologija¨, Fakultet strojarstva i brodogradnje Sveučilišta u Zagrebu, 1998.

[15] DIN 50025

[16] ... ASM Handbook Vol. 13 Corrosion, ASM International, Metals Park, Ohio, 1995.

INFLUENCE OF JOINING METHODS ON MICROSTRUCTURE AND PROPERTIES OF DENTAL MATERIALS

Carek A.(1), Živko-Babić J.(1), Schauperl Z.(2), Jakovac M.(1)

(1)Department for Prosthodontics, School of Dental Medicine, University of Zagreb,
Gundulićeva 5, 10000 Zagreb, Croatia
(2) Faculty of Mechanical Engineering, University of Zagreb,I.Lučića 5, 10000 Zagreb,
Croatia

Abstract:

The reconstructive disciplines are faced with an increasing number of different functional, aesthetic and prophylaxis criteria that must be satisfied. Therefore, numerous technical materials of different composition and properties are currently being used.

Due to some technological failures or combining prosthetic reconstructions there is a need for joining together parts of metallic construction either of same composition or those of different compositions. For this purpose different technologies and different conditions are used.

The aim of this study was the analysis of microstructure and microhardness of the soldered or welded joints.

The analysis involved two Ni-Cr and two Co-Cr alloys. Samples (25 x 10 x 1.5 mm) were cast. Two halves of each sample were joined by soldering, laser welding and electric arc welding (TIG). Joining was performed either by adding materials or without additions. The quality of joints and heat affected zone was examined with optical microscopy and SEM. Microstructure was qualitatively and quantitatively analyzed with a special regard to porosity. Microhardness was measured by Vickers method.

Soldering gives the best results. Welding is advantageous if all the procedures are performed properly. Otherwise, there are lot of cold cracks.

Keywords: base alloys, soldered and welded joints

INTRODUCTION

The reconstructive disciplines are faced with an increasing number of different functional, aesthetic and prophylaxis criteria that must be satisfied. Therefore, numerous alloys of various composition and properties are currently being used.

Consequently, it is of utmost importance to be familiar with composition and structure of metallic constructions as well as with their essential mechanical and technological properties. Because of technical failures, interruptions of functional and technical durability of prosthetic work, or in newly combining work pieces there is often a need for joining metallic parts of same or different composition. Joining includes heating metals at high temperature and applying different work technologies in various atmospheric conditions. Since on today's market there are over 2000 alloys based on different metals and from different manufacturers, the number of possible combinations of materials and joining procedures is immeasurable [1-3].

The use of base alloys in the USA for metalloceramic works increased in 1968/69, whereas Europe saw their more frequent use in the last four decades. Base alloys are more resistant to high temperatures, technologically are more sensitive, show great contraction with cooling (2.4%), are colour platinum, can be modelled thinner, have low viscosity in liquid condition, even the thinnest parts of a work piece are well cast, guarantee high rigidity of construction, are less elastic, but have high hardness and flexural strength.

Their modulus of elasticity is twice higher than that of noble alloys (200000 N/mm^2). They are corrosion resistant, make small galvanic elements, have low density, which saves up to 40% of an alloy in large constructions. They have low prices and are weak protectors from plaque. They are not good electricity and heat conductors; five times worse than noble alloys, which causes small or no stimulus of the pulp [1-10].

Laboratorial procedures of joining parts of metal constructions include: soldering, laser welding and TIG-welding. Soldering is a standard heating procedure of joining two equal metals with the help of a third which is being melted between them, without reaching the solidus temperature of the parent material. In stomatology the technical terms of welding and soldering are often being interchanged, whereas in metallurgy these two processes are differentiated. Laser welding is a process of joining metal construction of same or different material. For welding of prosthetic constructions is used neodymium YAG laser (Nd:YAG-yttrium aluminium garnet), which has active YAG crystals with addition of neodymium ions. Neodymium laser emits light with a wavelength of 1064 nm, and acts in pulses which last a few milliseconds. Pulse duration, power, and the area (0.3-2.0 mm) can be regulated depending on the type of material and length of joint.

Welding with electric arc (TIG) is a procedure with which direct current makes an electric arc between tungsten electrode and the sample which is spot welded. The electric arc's temperature is very high and because of this the alloy melts instantly. At the same time, there is a risk of alloy's overheating and burning of some of the components [4, 11]. According to the instructions of machine manufacturers, each new spot weld must cover at least 50 % of the previous weld. Welding can be performed with or without additional material depending on the width of joint. As a consequence of the contraction of material sagging occurs at the place of weld. Each of the parameters involved in this process considerably affects the structure and composition of the jointed materials. The consequences are worsened properties and corrosion stability of jointed parts of reconstructions. Effects of the Heat Influence Zone are not to be disregarded. In the end they could be reflected on the whole prosthetic therapy. The aim of this study was the evaluation of soldered and welded joints of four base as-cast alloys.

Material and methods

Two as-casts of Co-Cr and two of Ni-Cr alloys from different manufacturers were used as testing materials. The decleared composition and certain properties of alloys are shown in Table 1.

Table 1. Composition and properties of base alloys

Name	Alloys	Composition (wt. %)												Density g/cm^3	Melting interval °C	HV 10	Elongation %	Modulus of elasticity N/mm2
		Ni	Co	Cr	Mo	C	Si	Nb	N	W	Fe	Ce	Mn					
I-BOND O2	Ni-Cr	65		22.6	9.6		1	1			0.5	0.3		8.2	1250-1310	180	25	205000
WIRO-BOND C	Co-Cr		61	26	6	max 0.02	1			5	0.5	0.5		8.5	1270-1380	310	6	210000
WIRON 99	Ni-Cr	65		22.5	9.5	Max 0.02	1	1			0.5	0.5		8.2	1250-1310	180	25	205000
VI-COMP	Co-Cr		61	32	5.5		0.7						0.7	8.3	1360-1398	320	7.7	200000

Co-Cr alloys, Wisil and Vi-Comp, were centrifugally cast, sandblasted with Al_2O_3 fragments, size 10 µm and mechanically polished. Other two alloys were vacuum-pressure cast, sandblasted with Al_2O_3 fragments, size 250 µm and electrolitically polished.

For metallographic analysis the samples were embedded in acrylic resin Varidur, grounded, polished and etched. The grinding was performed automatically on abrasive papers of several grit: 120, 320, 600, and 1000, with water cooling and obligatory bathing of casts after each change of papers. The casts were then polished with polishing fabric and pastes with diamond abrasives, dimension 3 µm and 1 µm respectively. A device Lubricant blue (Stuers, Rodovre, Denmark) for lubricating samples was used for polishing. After polishing the sample structure was obtained by etching in a water solution 30 ml HCl, 15 ml HNO_3 and 10ml HOH, for 5 seconds. Each sample was cut in the middle, and their parts were joined together using the procedures of soldering, laser welding and electric arc welding (TIG). Soldering and laser welding were performed by adding certain materials or without adding any material. The microstructure of as–cast, joints and the Heat Affected Zone were examined by light microscopy and SEM. Vickers microhardness was measured with "PMT-3", with loading of 200 g (HV 0.2). Ten measurements were performed for each sample along the length of weld and horizontally along the cross section including thus the parent material (PM), Heat Affected Zone (HAZ) and welding material. The measurement was made in a zigzag line with space between individual prints 10µm along the height and length. Along the cross section 10 prints were made with a 10µm space between them. Spot welding time was almost the same in both methods (TIG – 18 msec, laser 19.4 msec). The pressure of argon was different**.** In electric arc welding the pressure was 1 bar and in laser welding it was 2-3 bar. In all compounds wire Wiroweld NC was used as an additional material.

Results

Figures 1 to 12 show welds made with TIG procedure and laser, and solders of casts Ni-Cr and Co-Cr alloys for metalloceramic system.

Figure 1. Ni-Cr alloy, *I – Bond O2* TIG

Figure 2. Ni-Cr alloy, *I – Bond O2* laser

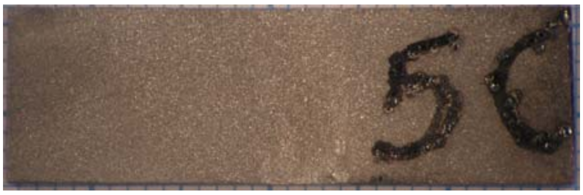

Figure 3. Ni-Cr alloy, *I – Bond O2* soldered

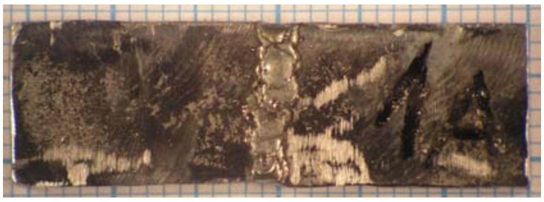

Figure 4. Ni-Cr alloy, *Wiron 99* TIG

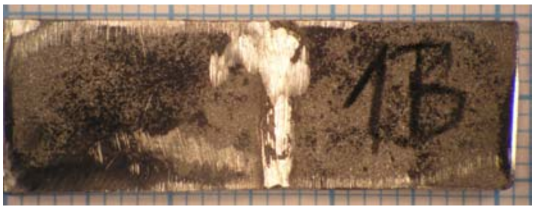

Figure 5. Ni-Cr alloy, *Wiron 99* laser

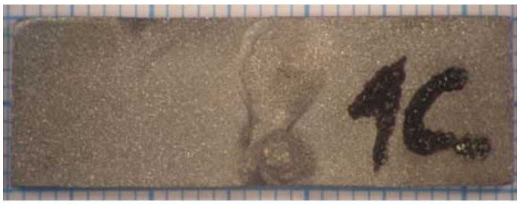

Figure 6. Ni-Cr alloy, *Wiron 99* soldered

TIG welded as-cast Ni-Cr, I-Bond 02, shows great porosity at the beginning and the end of the weld, while the rest is homogeneous (Fig.1). In the middle of the laser weld there is a crack extending along the whole weld that is probably as consequence of bending during control. There is also melted part on the place of weld as well as insufficient overlap of individual welds. Porosity is visible on the edges (Fig. 2). Soldered joint is neat and homogeneous (Fig. 3). The sample cast Wiron 99, TIG welded (Fig. 4), shows a horizontal crack in the middle of weld face, probably as a consequence of quenching and the resulting internal tension that extends along the whole length of the weld. Overlapping of welds is visible which indicate excess material. At the beginning of the weld there is a 1mm deep area of melted material. Laser welded material (Fig. 5) is homogeneous, without visible cracks and porosity, with significantly smaller depth of melted material at the place of weld's beginning. Soldering (Fig. 6) resulted in the greatest joint width, homogeneous material at the place of joint, without visible joint defect.

Figure 7. Co-Cr alloy, *Wirobond C* TIG

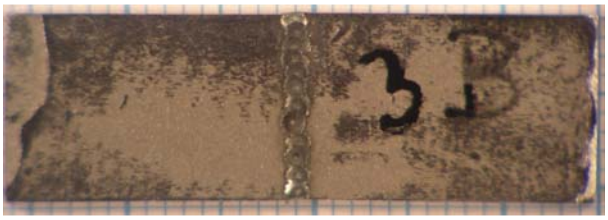

Figure 8. Co-Cr alloy, *Wirobond C* laser

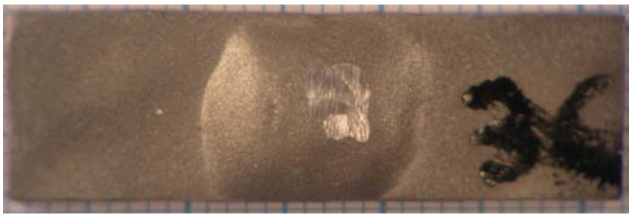

Figure 9. Co-Cr alloy, *Wirobond C* soldered

Figure 10. Co-Cr alloy, *Vi-Comp* TIG

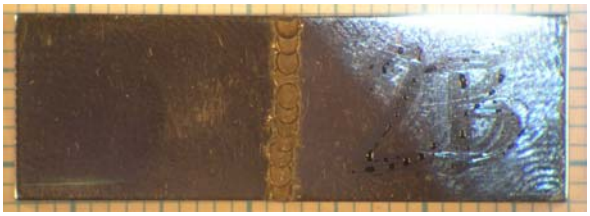

Figure 11. Co-Cr alloy, *Vi-Comp* laser

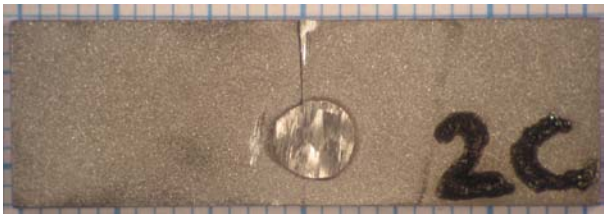

Figure 12. Co-Cr alloy, *Vi-Comp* soldered

TIG welded as-cast of Co-Cr alloy (Fig. 7) shows no cracks, but only porosity at some places. The laser-joined sample is similar (Fig. 8). Soldering resulted in a homogeneous joint which covers a larger part of sample's material (Fig. 9).

Figure 10 shows TIG welded Co-Cr alloy with a visible longitudinal crack in the middle of weld face, and a local smaller cracks. Laser welded joint (Fig. 11) is homogeneous with a small longitudinal crack at the place of weld's beginning. Soldering was performed only locally, in the middle of the sample whereas edges of the surface were not joined. There is a crack which might also be an unsoldered part (Fig. 12).Results of measuring microhardness are shown in Table 2.

Table 2. Mean values of measuring microhardness (HV=0.2)

Method	Measurement place	HV0,2			
		Ni-Cr Wiron 99	Co-Cr I-Bond =O2	Co-Cr Wirobond C	Ni-Cr Vi-Comp
TIG	As-cast	238	346.8	352	236.3
	HAZ	289	349.7	330.3	247
	Welded joints	255.6	343.8	359.3	246
LASER	As-cast	200	326	356.2	244.2
	HAZ	216.3	365.5	353.3	248.7
	Welded joints	238.2	338.7	381.7	259.2
SOLDERING	as-cast l	236.8	334.7	365.6	210.8
	HAZ	298.5	379.7	375.7	279
	Soldered joints	324,5	345,6	323,5	265,4

As-casts of Co-Cr alloys are significantly harder than as-casts of Ni-Cr alloy. TIG and laser joints have approximately equal microhardness values as well as parent material casts, with the exception of joints' interfaces being somewhat harder comparing to the parent material. The microstructure of the based, and welded materials created with TIG and laser procedures were analyzed.

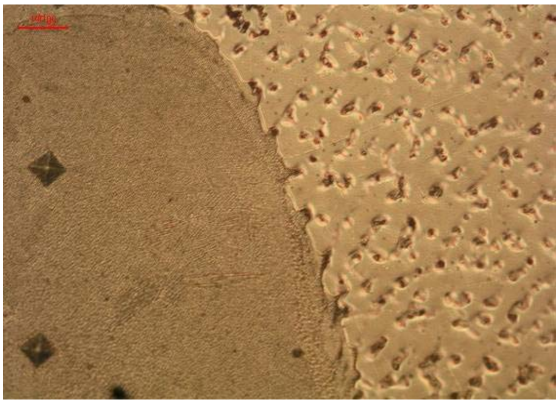

Figure 13. Wiron99, Ni-Cr alloy, TIG

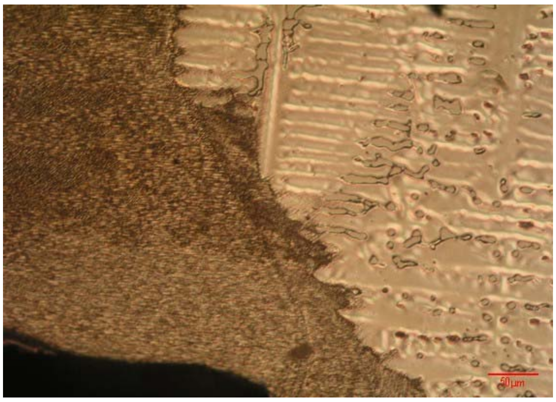

Figure 16. Vi-Comp, Co-Cr alloy, TIG

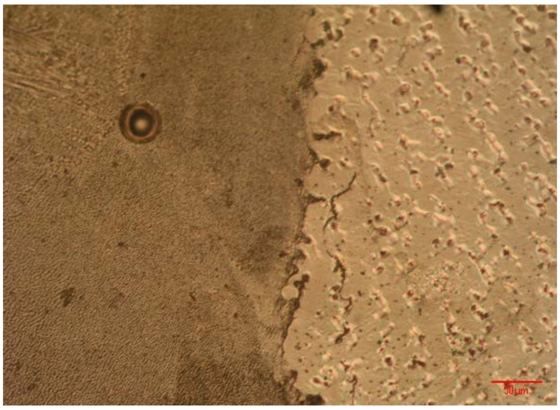

Figure 14. Wiron99, Ni-Cr alloy, laser

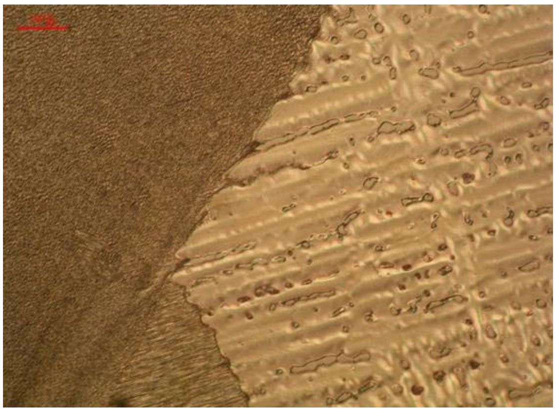

Figure 17. Vi-Comp, Co-Cr alloy**,** laser

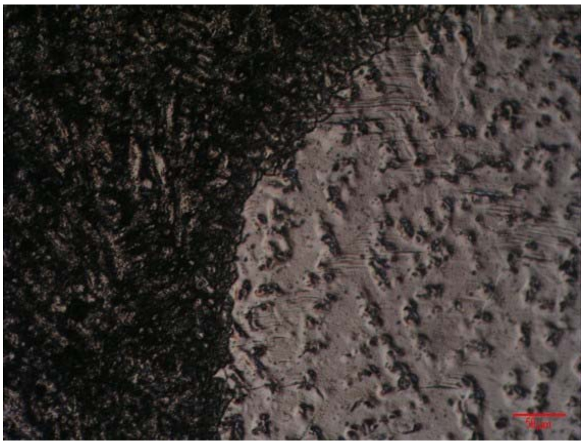

Figure 15. Wiron99, Ni-Cr alloy, soldered

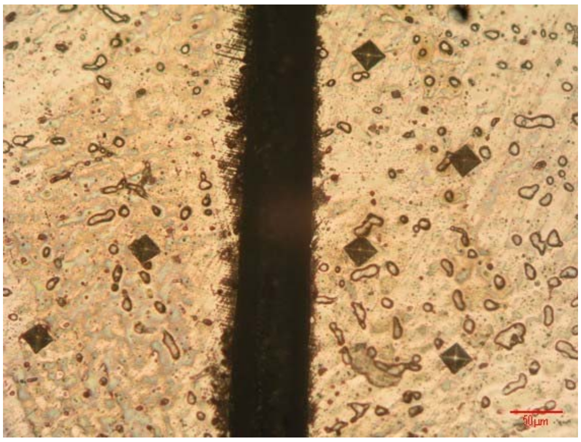

Figure 18. Vi-Comp, Co-Cr alloy, soldering

In as-cast material it was not proved that different way of casting had an influence on the micrographs of as-cast. The weld of Ni-Cr sample made with TIG, is dendritic, fine grained; the heat affected zone is not visible (Fig. 13). The fusion line indicates that the joint is satisfactory.

Laser weld is more ramified with structural transformations in the heat affected zone (Fig. 14). The weld itself is of fine dendritic structure.

As opposed to weld, surface shows somewhat coarser dendritic structure, similar to the as-cast (Fig. 15). A large part of white phase was noticed in the as-cast.

Laser and TIG welded base alloys reveal cracks and porosity in the largest number of samples. With TIG procedure the coarser structure of dendritic shape was obtained and irregular lines of fusion (Fig. 16). In laser weld, the fusion line is more clearly marked, obviously as a consequence of smaller input of heat (Fig. 17). In the main material there is a second additional phase visible. Soldering area shows successful results (Fig.18).

SEM micrographs are shown in Figures 19. and 20.

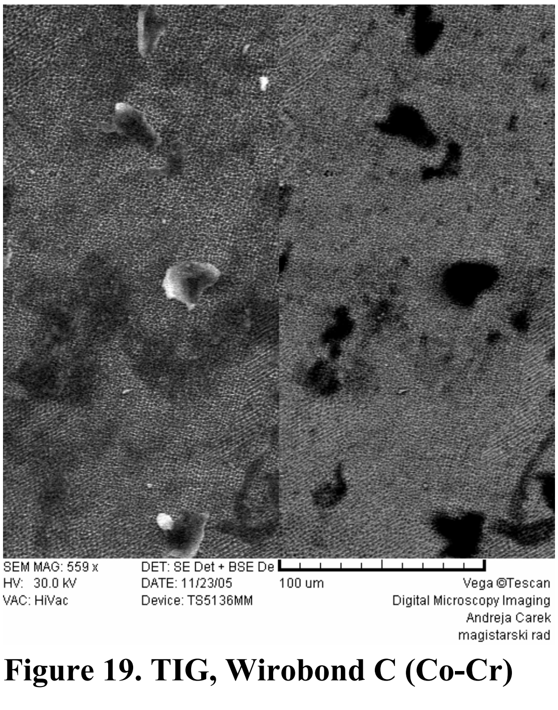

Figure 19. TIG, Wirobond C (Co-Cr)

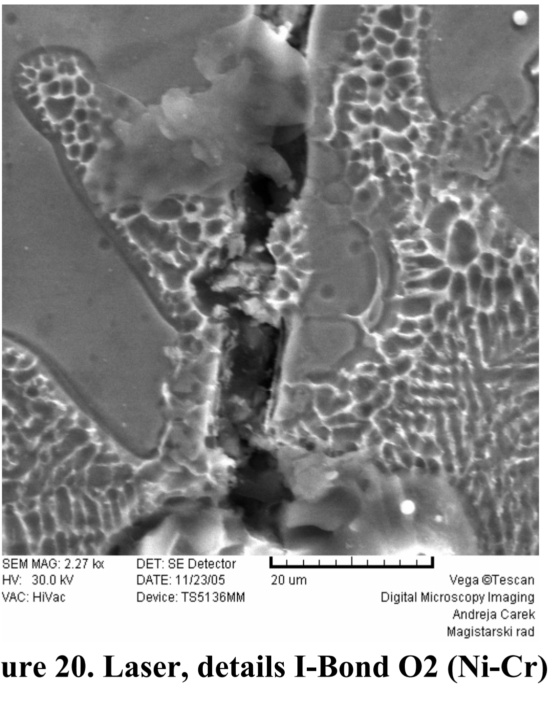

Figure 20. Laser, details I-Bond O2 (Ni-Cr)

SEM images show dendritic structure. Wirobond C sample shows porosity. On the sample I-Bond O2 width and depth of crack in the laser weld are visible, as well as excess material in some places. Obtained results are very interesting from scientific and clinical point of view. Since construction materials conform to the Drug Law, the knowledge of impact of laboratory procedure is very important.

Soldering in furnace gives the best results both in soldered and Heat Affected Zone.

Welding is advantageous if all the procedures are performed correctly. Otherwise, there might be cracks and corrosion. Nickel alloys have, like Co-Cr alloys, dendritic microstructure of cast. Besides a lower melting interval, these alloys are also somewhat softer (HV0.2=220) comparing to Co-Cr alloys (HV0.2=340). Technical literature says that inhomogeneity of surfaces causes intercrystalline corrosion, and at the same time tension could occur between parent material and surface. These are the most frequent reasons why objects break at the soldering place during chewing function [4, 11]. However, the results of this research have shown that, with regard to homogeneity of material structure and quality of joint, soldering is a much more successful joining procedure than TIG-welding or laser welding.

Cheng et al. proved that heating technique with infra red light can be an alternative to flame soldering technique in case of base alloys, and especially Co-Cr alloys (12).

Increased values of HAZ and surface micro hardness with regards to parent material imply a potential precipitation hardening. The soldering time was probably too short, and the soldering temperature too low to achieve optimal diffusion of atoms [13]. The samples should be fixed firmly during joining, i.e. secured in a vice/clip or another holder so as to keep their mutual positions constant. Hand-held samples could be moved. Moving of samples during joining and incorrectly defined space between adjoining surfaces are probably some of the reasons of frequent crack occurrences on most samples, especially in case of TIG and laser joining [14,15]. The condition that laser joining should cover 80%, and TIG at least 50% of the previous weld was not satisfied in the most of the samples analyzed in this research, which was also one of the reasons of crack occurrences [11]. Since the samples had not been microscopically analyzed right away after joining, it was hard to differentiate whether they were warm or cold cracks [15]. However, their appearance, position and spreading indicated they were cold cracks caused by internal tensions created during the cooling of materials.

The risk of deformity is smaller in electric arc joining than in laser joining because of the way of handling and the amount of input heat. In electric arc welding, one part of the sample is fixed with electrode, and the other is fixed in the holder during joining, whereas in laser welding samples are being held with hands and thus the connection of the welding materials is questionable [11,16,17]. The success of joining was also probably a result of samples' dimensions since in practice much smaller pieces need to be joined with one of the described techniques. Furthermore, all the alloy joints' surfaces were parallel while laser joining prefers V-shape or the shape of a groove.

The obtained results indicate the need for a more detailed and thorough determination of parameters of welding, handling materials, defining joint's shape and optimal depth with the purpose that laboratory joined metals satisfy functional and technical durability in a biological medium.

Acknowledgment
This paper has been supported by The Ministry of Science, Technology and Sport.

References

1. Rogers BA. The nature of materials. Zagreb: Technical book,1962.(Croat)

2. Kovačićek F, Španiček Đ. Materials. Osnove znanosti o materijalu. Zagreb: FSB, 2000.(Croat)

3. Dental alloys used in Prosthodontics. Based information about metals and alloys.

4. Živko-Babić J, Jerolimov V. Metals in Prosthodontics. Zagreb: Školska knjiga, 2005.(Croat)

5. Combe EC. Notes on the metal materials. Edinburg: Cherchill Livingston, 1998.

6. Bakarat MM, Asgar K. Mechanical properties and soldering of some cobalt base metal alloys. Dent Mater 1986; 2: 272-274.

7. Craig RG, Hanks CT. Citotoxicity of experimental casting alloys evaluated by cell culture tests. J Dent Res 1990; 69: 1539-1542.

8. Wagner E. Werkstoffkunde der Dentalmetallegierungen. Munchen: Neuer Merkur,1980.

9. Espevik S. Corrosion of base metal alloys in vitro. Acta Odontol Scand 1978; 36: 113-117.

10. Gil FJ, Sanchez LA, Espias A, Pianell JA. In vitro corrosion behaviour and metallic ion release of different prosthodontic alloys. Int Dent J 1999; 49:
361-367.

11. Wulfes H. Precision Milling and Partial Denture Constructions. 1st Bremen academia, Dental International School BEGO Germany, 2004.

12. Cheng AC, Chai JY, Gilbert J, Jameson LM. Mechanical properties of metal connectors soldered by gas torch versus an infrared technique. Prosthodont 1993; 2: 103-109.

13. Bumgardner JD, Doeller J, Lucas LC. Effect of nickel-based dental casting alloys on fibroblast metabolism and ultrastructural organization. J Biomed Mater Res 1995; 29: 611-617.

14. Leinfelder KF, Lemons JE. Clinical restorative materials and techniques. Philadelphia: Lea & Febiger, 1988.

15. Juraga I, Ljubić K, Živčić M. Pogreške u zavarenim spojevima. Zagreb: Kratis,1995.

16. Hoffman J, Lindigkeit J. Laserschweißen kombinierter Arbeiten. Dent Labor 1999; 8: 1285-1288.

17. Bertrand C, Le Petitcorpe Y, Albingre L, Dupuis V. The laser welding technique applied to the non precious dental alloys procedure and results. Br Dent J 2001; 10: 255-257.

11. Savjetovanje o materijalima, tehnologijama, trenju i trošenju
11. Conference on Materials, Processes, Friction and Wear
MATRIB'06, Vela Luka, 22-24.06.2006.

KARAKTERIZACIJA KOMPOZITNOG MATERIJALA ZA IZRADU BESPILOTNE LETJELICE "MARICA"

Danko Ćorić	Fakultet strojarstva i brodogradnje
Daniel Filković	Ivana Lučića 5, Zagreb, Hrvatska

Sažetak: U radu je proveden izbor i karakterizacija materijala za izradu konstrukcije bespilotne letjelice "Marica". Na temelju zahtjeva koji se postavljaju na materijal konstrukcije, u prvom redu visoke čvrstoće, krutosti i male mase, prednost je dana polimernim kompozitima koji se odlikuju visokom specifičnom čvrstoćom (omjer čvrstoće i gustoće) i specifičnim modulom elastičnosti (omjer modula elastičnosti i gustoće). Kompoziti ojačani staklenim i ugljičnim tkaninama pokazali su se vrlo podesnim materijalom za izradu konstrukcije letjelice. Ovisno o materijalu ojačanja, vrsti tkanja i plošnoj masi tkanine te volumnom udjelu vlakana u strukturi kompozita i smjeru djelovanja opterećenja s obzirom na položaj vlakna utvrđene su različite vrijednosti vlačne čvrstoće i modula elastičnosti ispitivanih kompozita. Za oplatu letjelice najpovoljnijim se pokazao kompozit epoksidne matrice i staklenog ojačanja (tkanina "twill", plošne mase 163 g/m^2) s praktički jednakim mehaničkim svojstvima u oba smjera vlakna, a za ramenjače, koje moraju biti čvršće i kruće, kao najbolji izbor pokazao se materijal ojačan ugljičnom tkaninom usmjernog tkanja plošne mase 254 g/m^2 i matricom od epoksidne smole uz uvjet polaganja tkanja u smjeru najvećih naprezanja ramenjače.

Ključne riječi: Bespilotna letjelica, Marica, polimerni kompozit, epoksidna smola, staklena vlakna, ugljična vlakna

1. UVOD

Projekt izrade bespilotne letjelice pokrenut je početkom 2004. godine od strane studenata zrakoplovstva Fakulteta strojarstva i brodogradnje, članova Hrvatske udruge studenata zrakoplovstva.

Danas u svijetu sve više zemalja koristi bespilotne letjelice, posebice zemlje u tranziciji koje su uočile isplativost takovog sustava nadzora i obavješćivanja. Bespilotne letjelice i zemaljske baze iz kojih se upravlja letjelicama implementirane su u sustave za nadzor direktno povezane s npr. vatrogasnim operativnim centrima, gorskom službom spašavanja, policijom, obalnom stražom itd. Glavne prednosti bespilotnih letjelica u odnosu na postojeće zrakoplove jesu: isplativost (mali troškovi izrade, održavanja, eksploatacije), sigurnost, visoka uporabna prilagodivost, neuočljivost, domet, trenutna raspoloživost podataka izviđanja (slika u realnom vremenu).

Primjena bespilotnih letjelica moguća je na mnogim područjima kao što su:

- otkrivanje i suzbijanje šumskih požara u ranoj fazi;
- nadzor državne granice;
- otkrivanje unesrećenih tijekom spašavanja;
- nadzor prometa i otkrivanje akcidentnih situacija na kopnu i moru;
- otkrivanje ekoloških zagađenja;
- nadzor biljnog i životinjskog svijeta;
- procjena štete nastale elementarnom nepogodom;
- geološka i meteorološka istraživanja ;
- nadzor naftovoda i cjevovoda i sl.

Stoga se ukazala potreba za takvom letjelicom i u R. Hrvatskoj. Do sada je provedeno dimenzioniranje letjelice, a nakon izbora materijala slijedi njena izrada. Letjelica je dimenzionirana s obzirom na maksimalnu poletnu težinu 30 kg. U proračunu je pretpostavljena težina prazne letjelice 20 kg, brzina krstarenja 100 km/h i maksimalna visina krstarenja 3000 metara. Određena je geometrija krila pravokutno-trapeznog oblika sa dihedralom trapeznog dijela. Na slici 1 prikazan je model letjelice u FLUENTU /1/.

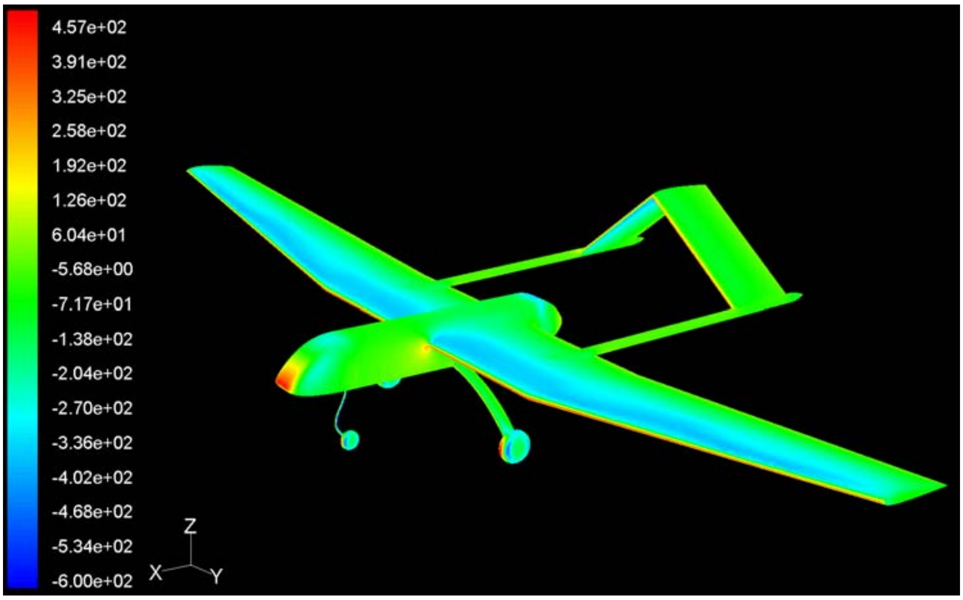

Slika 1. FLUENT model letjelice sa rasporedom statičkog tlaka

Na temelju aerodinamičkih koeficjenata pretpostavljenog oblika letjelice, korištenjem 6DOF računalnog paketa, letjelica se pokazala stabilnom i upravljivom te je određen konačan oblik, slika 2.

Slika 2. Oblik bespilotne letjelice nakon aerodinamičkog dimenzioniranja

2. ANALIZA MATERIJALA

Do nedavno, u zrakoplovstvu su se većinom koristile legure aluminija ("duraluminij") zbog relativno visoke čvrstoće i modula elastičnosti te male mase. Duraluminijski lim je vrlo savitljiv te je tehnologija izrade konstrukcije relativno jednostavna.

Međutim, za izradu konstrukcije bespilotne letjelice prednost je ipak dana kompozitim materijalima ponajprije zbog toga što su to danas najučestaliji materijali u malom nekomercijalnom zrakoplovstvu, no naravno tu su i druge prednosti kao npr.: odnos čvrstoće i gustoće koji je za polimerne kompozite s ugljičnim vlaknima 5 puta veći nego kod čelika te tehnologija izrade koja omogućava dobivanje izradka proizvoljnog oblika.

Kompoziti su općenito materijali dobiveni umjetnim spajanjem dvaju ili više materijala različitih svojstava s ciljem dobivanja materijala takvih svojstava kakva ne posjeduje niti jedna komponenta sama za sebe /2/.

Primjenom polimernih kompozita pokušali su se zadovoljiti zahtjevi za čvrstoćom i krutošću uz istovremeno bitno smanjenje težine letjelice čime ostaje više prostora za gorivo. Zahtjevi koji se postavljaju na materijal konstrukcije proizlaze iz analize raspodjele naprezanja gdje je vidljivo da je glavno opterećenje uzrokovano savijanjem krila uslijed čega dolazi do:

1. deformiranja krila i deformiranja oplate uslijed rasporeda naprezanja na gornjaci (gornji dio krila) i donjaci (donji dio krila). Savojna deformacija krila čak je manji problem od deformacije same oplate pri čemu se mijenja oblik aeroprofila i karakteristike letjelice.
2. izvijanje krila na gornjaci gdje je tlačno naprezanje;
3. pojava velikih vlačnih odnosno tlačnih naprezanja na ramenjači (glavnom nosivom elementu krila) uslijed savijanja krila.

Očito je da polimerni kompozit, uz zadovoljavajuću čvrstoću, prvenstveno mora jamčiti dovoljnu krutost jer je teže zadovoljiti problem krutosti nego čvrstoće. Kako polimerni kompoziti posjeduju visoku specifičnu čvrstoću (omjer čvrstoće i gustoće) i specifični modul elastičnosti (omjer modula elastičnosti i gustoće) pokazali su se vrlo podesnim materijalom za izradu konstrukcije letjelice /3/.

Polazeći od činjenice da je ukupno ponašanje kompozita određeno svojstvima osnove (matrice) i ojačala te veličinom, oblikom i rasporedom konstituenata, njihovim volumnim udjelom i prirodom (jakošću) veze među konstituentima odabran je kompozit s epoksidnom smolom kao matricom koja je dodatno ojačana da bi se modificirala njena svojstva. Budući da je efikasnost ojačanja najveća kod kompozita ojačanih vlaknima jer se opterećenje prenosi i distribuira na vlakna i to putem matrice, koja je općenito duktilna, ojačanje je ostvareno korištenjem staklenih odnosno ugljičnih vlakana. Da bi ojačanje bilo značajnije veza vlakno-matrica mora biti vrlo jaka /4/. Za oplatu letjelice izabran je kompozit epoksidna smola/staklena vlakna, a za ramenjače koje moraju biti čvršće i kruće odabrana je epoksidna smola ojačana ugljičnim vlaknima.

Kako je općenito poznato da raspored vlakana u strukturi kompozita bitno utječe na njegova svojstva ojačanje nije ostvareno "klasičnim" vlaknima već tkaninom da bi svojstva materijala bila ujednačenija. Time se željela izbjeći anizotropnost mehaničkih svojstva česta kod kompozita s usmjerenim vlaknima kada je u smjeru vlakana čvrstoća maksimalna, dok je okomito na vlakna čvrstoća minimalna. Na slikama 3 i 4 prikazane su tkanine korištene za ojačanje. Slika 3 prikazuje tkaninu tzv. keper-veza (eng. twill), a slika 4 tkaninu jednosmjernog tkanja (eng. unidirectional - UD).

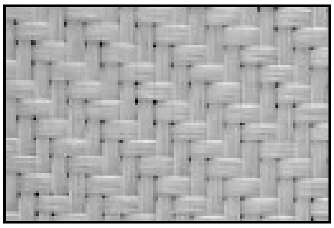

Slika 3. "Twill" tkanje

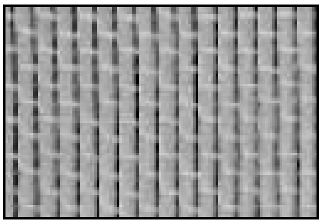

Slika 4. "UD" tkanje

"Twill" tkanina je satkana od staklenih vlakana. S ciljem optimiranja mehaničkih svojstava uporabljene su "twill" tkanine oznake završne obrade I 550 (proizvođač: R&G, Njemačka) odnosno "twill silan" tkanine od firme R&G, odnosno Keltex, Hrvatska /5/, /6/. Plošna masa ovih tkanina iznosila je 163 g/m^2. Među tkaninama "UD" tkanja satkanim od ugljičnih vlakana korištene su tkanine različitih plošnih masa: 140 g/m^2 (proizvođač: R&G,) i 254 g/m^2 (proizvođač: Keltex). Glavna razlika između ove dvije vrste tkanja je u tome što je "twill" tkanje deformabilnije pa je pogodnije za zaobljene površine, a osim toga ima i nešto bolja svojstva zbog manjeg presavijanja vlakna.

Za materijal matrice korištene su dvije epoksidne smole: jedna od firme Novapox, Hrvatska, a druga od R&G-a, Njemačka /7/.

S ciljem poboljšanja krutosti letjelice njeni konstruktivni elementi bit će izvedeni u obliku sendvič konstrukcije sastavljene od dva čvrsta i kruta sloja laminata između kojih se nalazi porozna (šuplja) jezgra, slika 5.

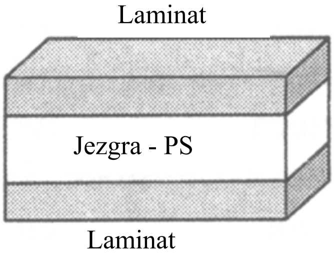

Slika 5. Sendvič konstrukcija

Jezgru sendvič konstrukcije činit će ekspandirana polistirenska pjena (PS) općenito poznata pod trgovačkim nazivom Stiropor. Radi se o poroznom materijalu (pjenasti materijal) male toplinske provodnosti i dobre sposobnosti prigušenja vibracija. Predviđena je debljina ekspandiranog polistirena 5 mm što bi trebalo biti dovoljno da se postigne relativno visoka čvrstoća i krutost uz relativno nisku gustoću.

3. TEHNOLOGIJA IZRADE

U izradi konstrukcije letjelice koristit će se dvije tehnologije: kalupljenje i laminiranje. Tehnologija kalupljenja sastoji se od dvije faze:

1. Izrada pozitiva: Pozitiv se izrađuje iz ekspandirane polistirenske pjene koja se reže na zadani oblik i dimenzije užarenom žicom na CNC stroju. Dobiveni oblik prevlači se slojevima staklenih vlakana i epoksidne smole (3 sloja staklenog tkanja plošne mase 163 g/m^2) i zatim popunjava kitom i "špric" kitom te lakira bojom i polira. Na taj način postiže se vrlo glatka površina pozitiva.

2. Izrada kalupa (negativa): Kalup se vadi iz pozitiva tako da se na površinu pozitiva nanese sredstvo koje daje visoku otpornost na trošenje i tvrdoću, a nakon toga slijedi laminiranje staklom, s time da je potrebno više slojeva i ukruta kako bi se smanjnila elastičnost kalupa. Kalup je izrađen od jednog sloja finog staklenog tkanja (163 g/m^2) i tri sloja grubljeg staklenog tkanja (400 g/m^2) zatim dolazi stiropor i opet jednaka kora kompozita.

Nakon toga slijedi laminiranje unutar kalupa čime se dobiva konstrukcijski element traženog oblika i dimenzija. Danas postoji više tehnologija laminiranja među kojima su najraširenije: mokro laminiranje i laminiranje u vakuumu kojim se postiže znatno veći udio vlakana u matrici. Kod izrade kalupa, ali i materijala ispitnih uzoraka laminiranje je provedeno na zraku, a nakon toga slijedilo je vakuumsko laminiranje kojim se, za razliku od uobičajene metode, ne istiskuje višak smole podtlakom nego se laminat zatvara u čvrstu i nepropusnu polietilensku foliju i spaja na vakuum pumpu koja isisava suvišni zrak dok se mehaničkim putem istiskuje višak smole iz laminata, slika 6.

Slika 6. Istiskivanje suvišne smole uz istovremeno vakuumiranje u plastičnoj foliji

Iz ovako dobivenih kompozitnih laminatnih ploča izrezuju se, za potrebe ispitivanja, epruvete određenog oblika i dimenzija.

Istovjetna tehnologija laminiranja bit će primjenjena i kod izrade kontrukcijskih elemenata bespilotne letjelice.

4. ISPITIVANJE I REZULTATI

Ispitivanja su provedena na kompozitnim epruvetama s matricom od epoksidne smole dva različita proizvođača i staklenim odnosno ugljičnim vlaknima kao ojačanjem. S ciljem optimiziranja mehaničkih svojstava ispitivani laminati sadržali su različite tkanine za ojačanje: ugljične "UD" tkanine različitih plošnih masa (140 g/m^2, 254 g/m^2), te staklene "twill" tkanine različite završne obrade (I 550, "silan"), plošne mase 163 g/m^2. Epruvete su sadržale 4 do 8 slojeva ojačanja.

Mehanička svojstva određena su statičkim vlačnim ispitivanjem. Kidanjem epruveta na kidalici utvrđene su vrijednosti vlačne čvrstoće i modula elastičnosti. Postupak određivanja modula elastičnosti sastojao se od postupnog povećanja sile te određivanja pripadnog produljenja epruvete pomoću mehaničkog ekstenzimetra s dva mjerna sata. Produljenje je određeno za početnu mjernu duljinu epruvete L_0=50 mm. Crtanjem dijagrama sila-produljenje i povlačenjem tangente na linearni dio krivulje (proporcionalni odnos sile i produljenja), slika 7, određena je vrijednost modula elastičnosti prema izrazu:

$$E = \frac{L_0}{a \cdot b} \cdot \frac{\Delta F}{\Delta X}, \text{N/mm}^2$$

gdje je:

a - širina epruvete;
b - debljina epruvete.

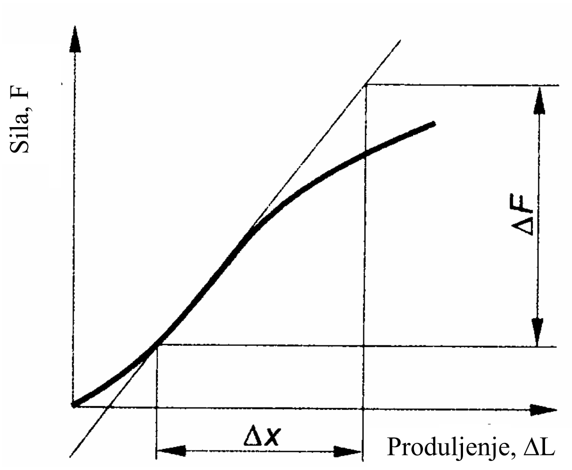

Slika 7. Postupak određivanja modula elastičnosti

Vlačna čvrstoća (R_m) proizlazi iz omjera masimalne sile (F_m) i početne površine poprečnog presjeka epruvete (S_0):

$$R_m = \frac{F_m}{S_0}, \text{N/mm}^2.$$

Epruvete su ispitane za dva različita smjera opterećenja s obzirom na položaj vlakna u strukturi. Epruvete s ugljičnim ojačanjem "UD" tkanja vlačno su opterećivane u smjeru vlakna (smjer 1) te okomito na vlakna (smjer 2). Kod kompozita ojačanih staklenim tkaninama "twill" tkanja nije moguće točno razgraničiti ova dva smjera zbog ortogonalne strukture tkanja.

Rezultati ispitivanja mehaničkih svojstava sažeti su u tablicama 1 i 2 . Tablica 1 sadrži vrijednosti mehaničkih svojstava kompozita epoksidna smola/staklena tkanina, a tablica 2 epoksidna smola/ugljična tkanina.

Tablica 1. Vrijednosti R_m i E polimernog kompozita epoksidna smola/staklena vlakna

Vrsta ojačanja	Vrsta smole	Broj slojeva	Vol. udio vlakna %	Gustoća ρ_k kg/m^3	Smjer vlakna	Oznaka epruv.	Početna površina presjeka S_0 mm^2	Max. sila F_m N	**Vlačna čvrstoća R_m N/mm^2**	**Modul elastičnosti E N/mm^2**
Staklena tkanina; 163 g/m^2; "twill" I 550; R&G	Epoksidna smola; Novapox	7	0,44	1761	1	13	12,73	3120	**245**	**24708**
						14	12,11	2460	**203**	**24744**
						15	14,00	3680	**263**	**23887**
					2	16	11,97	2960	**247**	**23439**
						17	12,64	2980	**236**	**25612**
						-	-	-	**-**	**-**
Staklena tkanina; 163 g/m^2; "twill" I 550; R&G	Epoksidna smola; R&G	8	0,41	1705	1	19	16,56	4760	**287**	**23627**
						20	16,20	4380	**270**	**25048**
						21	15,00	4500	**300**	**26646**
					2	22	14,52	4100	**282**	**22841**
						23	15,07	4500	**299**	**28083**
						24	15,96	4340	**272**	**22536**
Staklena tkanina; 163 g/m^2; "twill silan"; R&G	Epoksidna smola; Novapox	6	0,29	1525	1	109	15,36	2600	**169**	**12383**
						110	16,74	3260	**195**	**13431**
						111	16,38	2880	**176**	**13500**
					2	112	16,90	3580	**212**	**16123**
						113	15,88	4480	**282**	**15400**
						114	15,48	3740	**242**	**15740**
Staklena tkanina; 163 g/m^2; "twill silan"; Keltex	Epoksidna smola; Novapox	6	0,36	1640	1	301	11,07	3680	**332**	**18567**
						302	13,20	3580	**271**	**15742**
						303	13,31	3780	**284**	**14314**
					2	304	12,90	3645	**283**	**16929**
						305	13,00	3960	**305**	**17159**
						306	10,80	3200	**296**	**16520**

Tablica 2. Vrijednosti R_m i E polimernog kompozita epoksidna smola/ugljična vlakna

Vrsta ojačanja	Vrsta smole	Broj slojeva	Vol. udio vlakna %	Gustoća ρ_k kg/m^3	Smjer vlakna	Oznaka epruv.	Početna površina presjeka S_0 mm^2	Max. sila F_m N	**Vlačna čvrstoća R_m N/mm^2**	**Modul elastičnosti E N/mm^2**
Ugljična tkanina; 254 g/m^2; "UD"; Keltex	Epoksidna smola; Novapox	6	0,65	1537	1	401	7,45	7649	**1027**	**-**
						402	7,55	8336	**1104**	**-**
						403	8,41	8630	**1026**	**128140**
					2	115	21,14	1080	**51**	**8468**
						116	20,40	1200	**59**	**10350**
						-	-	-	**-**	**-**
Ugljična tkanina; 140 g/m^2; "UD"; R&G	Epoksidna smola; Novapox	6	0,51	1440	1	601	16,00	16181	**1011**	**102153**
						602	19,68	18142	**922**	**107548**
						-	-	-	**-**	**-**
					2	100	11,20	1120	**100**	**13978**
						102	12,16	1170	**96**	**13500**
						103	12,87	1280	**99**	**11433**
Ugljična tkanina; 140 g/m^2; "UD"; R&G	Epoksidna smola; R&G	4	0,53	1457	1	501	15,19	15789	**1039**	**97083**
						502	14,99	15495	**1034**	**109035**
						-	-	-	**-**	**-**
					2	101	7,50	790	**105**	**-**
						104	8,97	690	**77**	**10119**
						105	8,40	710	**85**	**10710**

Volumni udio vlakana određen je mikrostrukturnom analizom na uređaju za analizu slike.

Na temelju volumnog udjela vlakna i matrice, te poznavajući njihovu gustoću izračunata je gustoća kompozita koristeći se zakonom miješanja:

$$\rho_k = V_m \cdot \rho_m + V_v \cdot \rho_v \text{, gdje je:}$$

ρ_k – gustoća kompozita;
V_m – volumni udio matrice;
ρ_m – gustoća matrice;
V_v – volumni udio vlakana;
ρ_v – gustoća vlakna.

Za neke materijale navedene u tablicama 1 i 2 nije bilo moguće ispitati po tri epruvete za svaki smjer opterećenje/vlakno zbog male količine raspoloživih laminata. Kod epruveta oznake 101, 401 i 402 nije određena vrijednost modula elastičnosti zbog problema koji su nastali klizanjem ekstenzimetra s tijela izrazito tankih epruveta.

Ispitivanja polimernih kompozita ojačanih staklenim tkaninama provedena su na kidalici čiji je proizvođač Werkstoffprüfmaschinen, Njemačka; vrsta: 2132; serijski broj: 11/942; razred točnosti: 1; mjerno područje: 0-4800 N, dok su kompoziti ojačani ugljičnim tkaninama ispitani na kidalici veće nazivne sile proizvođača: Zwick, Njemačka; vrsta 1162; razred točnosti 1.

5. RASPRAVA I ZAKLJUČAK

Budući da materijal konstrukcije letjelice mora, osim male mase, posjedovati i zadovoljavajuću čvrstoću te dovoljnu krutost da bi se izbjeglo nepoželjno deformiranje krila uslijed savijanja i stim u vezi deformiranje oplate, izvijanje krila na gornjaci te pojava velikih naprezanja na ramenjači, za materijal konstrukcije odabrani su polimerni kompoziti vlaknima ojačani. Kod ovih kompozita dolazi do izražaja poboljšanje čvrstoće i krutosti te povećanje omjera čvrstoća/gustoća, modul elastičnosti/gustoća uslijed ugradnje čvrstih vlakana u mekaniju, duktilniju matricu. Budući da se opterećenje prenosi i distribuira na vlakna i to putem matrice, vlakna nose najveći dio opterećenja čime se postiže značajno ojačanje. Vlaknima ojačani kompoziti upravo se "dizajniraju" s ciljem postizanja neuobičajenih kombinacija čvrstoće, krutosti i male mase.

U izradi laminatnog kompozitnog materijala korištena je modificirana tehnologija vakuumskog laminiranja koja sadrži zatvaranje laminata u čvrstu i nepropunu foliju i isisavanje zraka pomoću vakuum pumpe te mehaničko odstranjivanje viška smole čime je postignut vrlo dobar volumni udio vlakana od preko 40 %.

Za konstrukciju letjelice odabrani su kompoziti s epoksidnom matricom i staklenim odnosno ugljičnim vlaknima kao ojačanjem budući da su se već ranije pokazali vrlo pogodnim za primjenu u zrakoplovstvu. Za ojačanje je korištena tkanina koja u usporedbi s "klasičnim" usmjerenim vlaknima daje ujednačenija svojstva materijala.

Ispitivanja su pokazala da tkanina "twill" tkanja daje vrlo slična svojstva materijala u oba smjera vlakna, u usporedbi s "UD" tkaninom koja sadrži više usmjerenu strukturu tkanja. Kod kompozita ojačanih tkaninom "twill" I 550 vrijednosti vlačne čvrstoće i modula elastičnosti gotovo su istovjetne za oba smjera djelovanja opterećenja. Nešto veća razlika mehaničkih svojstava zabilježena je jedino kod kompozita ojačanog "twill silan" tkaninom čiji je proizvođač R&G kada je u jednom smjeru čvrstoća veća za 36,1%, a modul elastičnosti za 20,2%. S tog stanovišta "twill silan" tkanina dobavljena od firme Keltex pokazala se kvalitetnijom, a kako je njena cijena niža od istovjetnih R&G-evih tkanina predstavlja vrlo vjerojatan izbor pri odabiru materijala.

Mehanička svojstva kompozita ojačanog ugljičnom "UD" tkaninom izrazito su anizotropna. Ukoliko opterećenje djeluje u smjeru vlakna postiže se vrlo visoka čvrstoća i krutost. Efikasnost ojačanja tada je puno veća nego kod kompozita sa staklenim vlaknima. Međutim, ako opterećenje djeluje okomito na vlakna vrijednosti mehaničkih svojstava višestruko su niže. Čvrstoća, ovisno o ispitivanom kompozitu, iznosi samo 5% do 10 % čvrstoće zabilježene u smjeru vlakna. Istovjetna tendencija uočena je i kod modula elastičnosti. U smjeru okomitom na vlakna ovaj je modul tek 7% do 12% vrijednosti elastičnog modula uzduž vlakna. Najveća anizotropnost mehaničkih svojstava zabilježena je kod kompozita ojačanog ugljičnom "UD" tkaninom plošne mase 254 g/m^2. Kod kompozita s "UD" tkaninom manje plošne mase 140 g/m^2 anizotropnost je nešto manja, ali još uvijek vrlo dominantna.

Što se tiče kvalitete epoksidne smole dva različita proizvođača vidljivo je da smola od R&G-a doprinosi porastu ukupne čvrstoće kompozita. Uporabom ove smole i staklene tkanine "twill" I 550 zabilježen je porast čvrstoće od 18,8% dok je kod kompozita s ugljičnom "UD" tkaninom čvrstoća viša za 7,2% u poredbi s kompozitom epoksidne matrice drugog proizvođača. S druge strane, smole različitih proizvođača ne utječu značajno na vrijednost modula elastičnosti ispitivanih materijala.

Iz navedenog proizlazi da je za materijal oplate najpodesniji kompozit ojačan staklenom tkaninom "twill silan" plošne mase 163 g/m^2 (proizvođač: Keltex) i epoksidnom smolom od Novapoxa jer posjeduje najveću čvrstoću među staklom ojačanim kompozitima te krutost koja je nešto niža ali još uvijek zadovoljavajuća. Uz to ne treba zaboraviti da se radi o domaćem i jeftinijem materijalu. Svojstva ovog kompozita vrlo su ujednačena u oba smjera vlakna. Za ramenjače od polimernog kompozita s ugljičnim vlaknima kao najbolji izbor pokazao se materijal ojačan ugljičnom tkaninom usmjernog tkanja plošne mase 254 g/m^2, uz uvjet da je tkanje položeno u smjeru najvećih naprezanja ramenjače.

LITERATURA:

/1/ D. Filković i suradnici: Projektna dokumentacija izrade bespilotne letjelice "Marica"
/2/ T. Filetin, F. Kovačiček, J. Indof: Svojstva i primjena materijala, Fakultet strojarstva i brodogradnje, Zagreb, 2002.
/3/ Grupa autora: Materijali u strojarstvu – Tendencije razvoja i primjene, Hrvatsko društvo za materijale i tribologiju, Zagreb, 1993.
/4/ Robert M. Jones: Mechanics of composite materials, 1975.
/5/ http://www.r-g.de/
/6/ http://www.kelteks.hr/
/7/ http://www.nova-karlovac.hr/

SIMPLE EXPERIMENTAL METHOD OF CHARACTERIZATION OF THIN-FILM REVERSE OSMOSIS AND NANOFILTRATION MEMBRANES

Davor Dolar, Krešimir Košutić
University of Zagreb, Faculty of Chemical Engineering and Technology,
Marulićev trg 19, HR-10001 Zagreb, Croatia

Abstract: The objective of this study was to show how two distinctive experimental RO/NF membrane characteristics could be used to describe the porosity of the membrane's active layer without resorting to theoretical models. Two characteristic parameters: the susceptibility of the active layer structure under pressure $\boldsymbol{\alpha}$ and the membrane's pure water permeability ***K'***, were determined from the membrane's flux dependency on pressure. The significance of the characteristic parameters was confirmed by relating them to the pore size distributions (PSD) and to the effective number of pores, N in the active membrane layer. The examined RO/NF membranes were classified into three groups according to the values of the characteristic parameters.

Keywords: Reverse osmosis; Nanofiltration; Characterization; Membrane porosity parameters

1. INTRODUCTION

The applicability of membrane separation processes, reverse osmosis (RO) and nanofiltration (NF), for water treatment is well known. Membrane separation technology has been widely used for desalination of sea and brackish waters [1,2] and industrial effluents treatment [3].

The reverse osmosis performance parameters, rejection factor and permeate flux, are known to be influenced by membrane characteristics, by physicochemical properties of the system, and by operating variables such as solute concentration and operating pressure. An important characteristic of a separation membrane is its porosity, expressed by the pore size, pore size distribution (PSD) and effective number of pores in membrane's upper layer (skin).

Every membrane manufacturer gives nominal characteristics of its products but membrane porosity is never specified. As it directly affects efficiency and execution of any separation process it is necessary to have some data on the membrane's porosity. The porosity of a membrane can be generally measured by several direct methods like thermoporometry, gas adsorption/desorption, electron or atomic force microscopy, bubble pressure/solvent permeability or chronoamperometry. Unfortunately, none of them can be employed in case of membranes with average pore radii in the sub-nanometer (0.2-1 nm) range. Therefore an indirect RO/NF membrane's skin characterization method based on selective solute permeation data has to be used. The porous structure containing narrow pores in size range 0.2-1 nm can be characterized by measuring the membrane's water flux and the rejection of a series of selected uncharged organic molecules of the known size.

The appearance of a distribution of pore sizes in the membrane's skin has been recently reviewed [4]. However, the exact nature of the pore size distribution in NF membranes is unknown because of the limitations of the available measurement techniques. In addition, all available methods of porosity determination are complex and time consuming. The main objective of this work was therefore to determine the membrane porosity by a simple experimental method and to relate the results to the known and established procedures.

The theoretically expected proportional dependence of the membrane water flux on the applied pressure:

$$J_w = K \cdot \Delta P \quad \text{or} \quad \frac{J_w}{\Delta P} = K$$

is rather an exception than a rule, and a deviation from proportionality for cellulose acetate membranes was observed [2] and also found [5] to be valid for some RO/NF polyamide membranes. The proposed [2] asymptotic exponential relationship could be used:

$$J_w = K \cdot e^{-\alpha P}$$

For easier comparison the data on J_w vs. pressure are linearized by calculating the reduced flux J_w/P and by plotting it in the logarithmic form against pressure:

$$ln \frac{J_w}{P} = K' - \alpha P$$

The resulting relationship includes two compound parameters ***K'*** and ***α***. ***K'*** generally depends on the pore radius, the membrane tortuosity, the water viscosity and the skin thickness [6], and ***α*** represents a measure of the susceptibility of the skin's structure under pressure. These experimental parameters determined by measuring the changes of a membrane water flux with pressure variations are not related to any theoretical model neither to the resulting mathematical expressions that describe the membrane skin porosity. They can be used to characterize independently the porosity of the membrane's skin. Their significance is recognized when they are related to the measured PSD of the membrane's skin that reflects its specific structure and its influence on the water flux and the solutes rejection.

2. EXPERIMENTAL

Three types of commercial RO thin-layer composite membranes: HR95PP and XLE from Dow/FilmTec, Midland MI, and , and nanofiltration thin-layer composite membranes: NF90 and NF270 from Dow/FilmTec, and HL and DK from Desal, Osmonics, GE Infrastructure Water Process & Technol., Vista, CA, were used throughout the work.

The membranes were tested in a laboratory set-up illustrated schematically in Fig. 1. Flow rate of the feed solution to home-made RO cells of the same type and dimensions was 350 ml min^{-1}. The surface area of the membranes investigated was 13.2 cm^2.

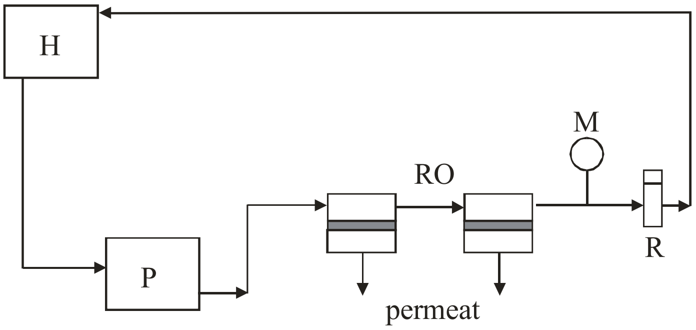

Figure 1. Schematic representation of the reverse osmosis set-up. H – holdup tank, P – high pressure pump, M – manometer, RO – reverse osmosis cells, R – back pressure regulator

The membranes were pressurized at 25 bar for 8 hours before the pure water flux measurements. The membrane water fluxes were measured at various pressures up to 22 bar. The NF/RO experiments with the sodium chloride and the organic markers' solutions were of the short-run type, each lasting for about three hours; they were carried out at laboratory temperature and various pressures. The concentration of the feed in the case of the sodium chloride solution was 300 mg l^{-1}, and in the case of the organic markers solutions, 100 mg l^{-1}. The reported permeate flow rates, J_w /l m^{-2} h^{-1} referring to the membrane permeated solution are the values measured at the laboratory temperature and corrected to 25 ºC using the relative viscosity and density data for pure water.

The retention factor R, defined as

$$R = 1 - \frac{C_p}{C_f}$$

with C_p and C_f as permeate and feed concentrations (mg l^{-1}), respectively, was determined in each experiment.

The membranes' PSDs and effective numbers of pores in the membranes' upper layer (skin) were determined by the method described in detail previously [6]. Seven organic reference solutes (markers) were used for the pore size distribution analysis. All the markers are listed in Table 1. The concentrations of sodium chloride were determined by conductivity measurements, and those for the markers' solutions were determined by a carbon analyzer, Ionics Inc, model 1555.

Table 1. Organic reference solutes (markers)

Name	Formula	Molecular mass
Ethanol	C_2H_5OH	46.07
Trimethylene oxide	C_3H_6O	58.08
1,3-Dioxolane	$C_3H_6O_2$	74.08
1,4-Dioxane	$C_4H_8O_2$	88.11
12-Crown-4 (1,4,7,10-tetraoxacyclododecane)	$C_8H_{16}O_4$	176.21
15-Crown-5 (1,4,7,10,13-pentaoxacyclopentadecane)	$C_{10}H_{20}O_5$	220.27
18-Crown-6 (1,4,7,10,13,16-hexaoxacyclooctadecane)	$C_{12}H_{24}O_6$	264.32

3. RESULTS AND DISCUSSION

The results of the examined membranes' water flux and its dependence on the pressure measurements are presented in Fig. 2 and the numerical values of the described typical membrane parameters are listed in Table 2.

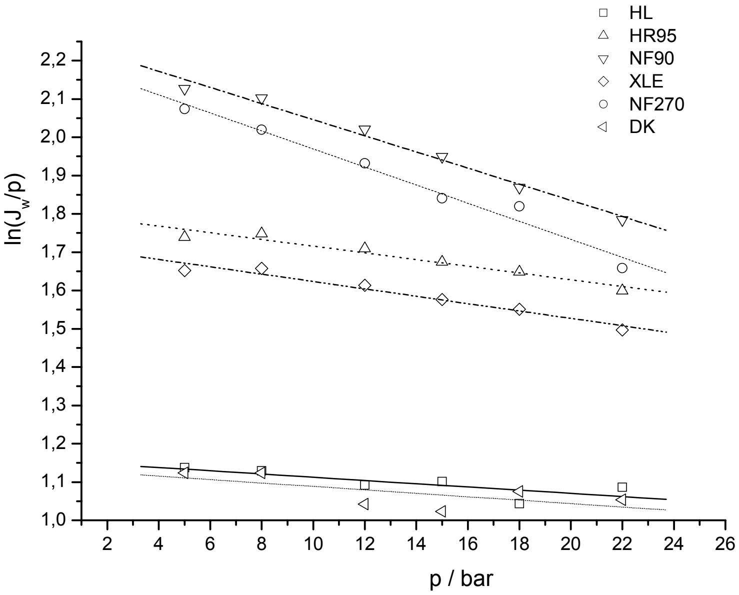

Figure 2. Effect of operating pressure on membrane water permeability constants

Table 2. Compound experimental porosity parameters together with the pure water flux of the examined membranes at 8 and 15 bar

	$\alpha\cdot10^4$	K'	J_w (8 bar) / l m^{-2} h^{-1}	J_w (15 bar) / l m^{-2} h^{-1}	J_w/K' (8 bar)	J_w/K' (15 bar)
RO						
HR95	87.7	1.803	43.97	73.34	24.4	40.7
XLE	96.2	1.720	35.17	59.61	20.4	34.7
NF loose						
DK	44.7	1.133	26.62	–	23.5	–
HL	42.2	1.155	30.67	56.97	26.6	49.3
NF tight						
NF270	209.0	2.179	85.70*	–	39.3	–
NF90	210.6	2.256	51.26	75.48	22.7	33.5

*10 bar

The obtained values of the parameters ***α*** and ***K'***, characterizing the structure and porosity of the membranes, show that the skin structure of all the examined membranes is less and more affected by the applied pressure. The presented numerical values point to the parameter ***α*** as a distinguishing feature for the skin structure of the examined membranes, and for their separation into three groups: RO, tight NF and loose NF membranes. The lowest ***α*** values of up to $50\cdot10^{-4}$ are found for the loose NF membranes supposedly having the widest pores. The steeper slope values of up to $100\cdot10^{-4}$ are obtained for the examined reverse osmosis membranes having expectedly the narrowest pores in the skin. And the steepest slope values of approximately $200\cdot10^{-4}$, pointing to the most sensitive skin structure, are found for the tight NF membranes, those at the narrow pore end of the NF separation range.

The numerical values of parameter ***K'*** of the examined membranes do not differ so clearly and cannot be immediately connected to the proposed membrane grouping. However, the significance of the ***K'*** values is best seen from the data of the J_w/K' ratio, given in the last columns of Table 2, and showing in fact the similar proportionality of ***K'*** values to the water permeability for the majority of the membranes. This finding indicates that both quantities must originate from the same morphological features of the membranes' skin.

All these findings and the proposed grouping of the membranes according to their measured characteristics, ***α*** and ***K'***, are supported and can be explained by the PSD's curves obtained for all the membranes. The pore size distributions in the membranes' skin are presented in Fig. 3, and the corresponding calculated "effective numbers of pores" together with the water permeation rate values are listed in Table 3 and Table 4.

The results of the pore size and pore size distribution for the investigated membrane samples (Fig. 3) show obvious differences in the PSD curves. The PSDs of the typical RO membranes (HR95, XLE) at lower operating pressure as shown in Fig. 3 are practically unimodal with the most pores at the pore size of 0.67-0.78 nm. In case of the HR95 membrane PSD shows additionally a small peak at 1.28 nm. The loose NF membrane (HL) is unimodal with the pores at the size of 0.90 nm. The highest peak for the DK type membranes is at 1.1 nm followed by significant amount of pores between 1.4 and 2.2 nm. The PSDs of two tight NF membrane, as seen in Fig. 3, have the main peak at pore size 0.69 nm for NF90 and 0.90 nm for NF270 type membrane and there is also an additional peak at 1.24 nm for NF90 and 1.56 nm for NF270 nm.

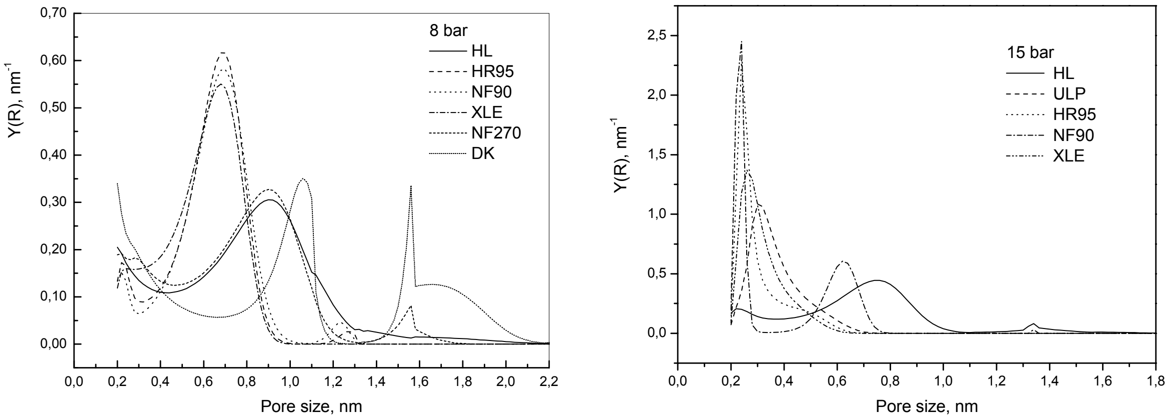

Figure 3. Pore size distribution of the membrane samples at 8 and 15 bar

The pronounced dissimilarity PSD between RO and NF membranes at the higher operating pressure of 17 bar (Fig. 3) is more obvious. The PSDs of RO membranes shift to lower pores sizes. An important divergence between the RO membranes also appears: the main maximum of HR95 membrane is one around 0.23 nm, XLE around 0.26 nm. All the observed changes of PSDs with operating pressure are significant, and their importance is emphasized by the data obtained for the effective number of pores in examined membranes samples.

The calculated "effective" number of pore values of the examined membranes, N, are shown in Table 3 and 4 together with the membranes' water flux data, and their ratio giving the calculated average water flux through a single pore, a value pointing to the average pore size in a membrane. The results show that all the N-values grow with an increase of the operating pressure, and the calculated effective number of pores in the upper layer of some membranes changes with pressure.

Table 3. The effective number of pores together with membrane water fluxes at 8 bar

	J_w (8 bar) / l m^{-2} h^{-1}	N (8 bar) / 10^{16} m^{-2}	J_w/N / 10^{-16} lh^{-1}
RO			
HR95	43.97	2.181	20.16
XLE	35.17	2.069	17.00
ULP	8.29	0.316	26.23
NF loose			
DK	24.60	0.217	122.67
HL	30.67	0.519	59.09
NF tight			
NF270	85.70*	1.457	58.82
NF90	51.26	2.291	22.37

*10 bar

Table 4. The effective number of pores together with membrane water fluxes at 15 bar

	J_w (15 bar) / l m^{-2} h^{-1}	N (15 bar) / 10^{16} m^{-2}	J_w/N / 10^{-16} l h^{-1}
RO			
HR95	73.34	8.246	8.89
XLE	59.61	7.532	7.91
ULP	13.41	0.767	17.48
NF loose			
HL	56.97	0.760	74.96
NF tight			
NF90	75.48	2.724	27.71

It is evident from this table that the RO and tight NF membranes contain much more pores in the skin than loose NF membranes. It is also confirmed by the J_w/N ratios that the average pores in the RO membranes are smaller than those in the NF tight membranes, and that the NF loose membranes contain the larger pores in the skin.

4. CONCLUSION

Two characteristic membranes' skin parameters were experimentally determined in this study. The experimental parameters were obtained from the membrane water flux dependency on pressure. Their values especially the value of parameter $\boldsymbol{\alpha}$, representing a measure of the skin's structure susceptibility under pressure, are suitable to classify the membranes into RO, loose NF and tight NF. The PSDs at higher operating pressure shift to lower pores sizes and the membranes contain much more pores in the skin. Results of this research can be used in prediction of separation behavior of investigated membranes.

References

1. G. Belfort, Synthetic Membrane Processes, Fundamentals and Water Applications, Academic Press, Orlando, FL, 1984
2. S. Sourirajan, T. Matsuura, Reverse Osmosis/Ultrafiltration Process Principles, National Research Council Canada, Ottawa 1985
3. C.A. Buckley, C.J. Brouckaert, C.A. Kerr, Reverse osmosis application in brackish water desalination and in the treatment of industrial effluent, in: Z. Amjad (Ed.), Reverse Osmosis, Van Nostrand Reinhold, New York , 1993. pp. 275-299
4. W.R. Bowen, J.S. Welfoot, Chem. Eng. Sci. **57** (2002) 1393-1407
5. K. Košutić, L. Kaštelan-Kunst, B. Kunst, J. Membr. Sci. **168** (2000) 101-108
6. B. Van der Bruggen, C. Vandecasteele, Water Res. **36** (2002) 1360-1368

Acknowledgement

This work has been supported by the Croatian Ministry of Education, Science and Sport (Project No. 0125017), and by EU project EMCO (INCO CT 2004-509188)-Reduction of environment risks, posed by Emerging Contaminants, through advanced treatment of municipal and industrial wastes.

UČINAK CIJEPLJENJA NA MIKROSTRUKTURNA SVOJSTVA AL-SLITINE 5083

EFFECT OF INOCULATION ON MICROSTRUCTURE PROPERTIES OF AL-ALLOY 5083

N. Dolić1), A. Markotić1), F. Unkić1), J. Prgin2), K. Terzić1)
1)Metalurški fakultet Sveučilišta u Zagrebu
Aleja narodnih heroja 3
44 103 Sisak
Republika Hrvatska
2)TLM d.d.
Narodnog preporoda 12
22 000 Šibenik
Republika Hrvatska

Sažetak: Provedena su ispitivanja mikrostrukture Al – bloka lijevanog na rekonstruiranoj i moderniziranoj liniji za lijevanje vertikalnim DC («direct–chill») postupkom u ljevaonici TLM –a Šibenik. Naglašena je važnost kontroliranja uvjeta lijevanja i cijepljenja u dobivanju finozrnate i ujednačene strukture. Poluautomatskom metodom mjerenja duljine presijecanja zrna izmjerene su veličine zrna, odnosno broj zrna po jedinici ispitivane površine teško gnječive aluminijske slitine 5083 po presjeku bloka, što daje uvid u uspješnost obrade taline cijepljenjem i ispravnost primijenjenih parametara procesa lijevanja DC postupkom. Iz dobivenih rezultata uočava se da u mikrostrukturi prevladavaju istoosna zrna sa većim brojem zrna (manja zrna) na rubovima bloka, što je rezultat većeg intenziteta odvođenja topline sa rubova bloka. Morfologija raspodjele veličina zrna po presjeku bloka upućuju na učinkovito cijepljenje taljevine. Za gnječive legure, struktura zrna u lijevanom (primarnom) stanju ima izravan utjecaj na kasniju obradu deformacijom i svojstva konačnog proizvoda.
Ključne riječi: slitina 5083, veličina zrna, DC lijevanje, cijepljenje, lijevana struktura

Abstract: Microstructural analysis has been performed on Al–slab casted on reconstructed and modernized line for casting by vertical DC («direct–chill») process in TLM Cast house in Šibenik. An importance of control of cast conditions and refining of melt in gaining fine-grained and uniform structure has been underlined. Semiautomatic method by the length intercept of the grain has been used for grain size measuring, i.e. grain number per unit of examined surface of the hard wrought 5083 aluminium alloy on the slab cross intersection. This has provided an insight in the efficiency of the melt treatment by the inoculation and correctness of the applied parameters of the DC casting process. From the obtained results it could be noticed that equiaxed grains have dominated in the microstructure with the greater grain number (smaller grains) on the slab edges, due to higher intensity of heat extrication from the slab edges. Morphology of grain size distribution per cross intersection of the slab refers to efficient inoculation of the melt. Grain structure in as-cast (primary) state of the wrought alloys has a direct influence on the following deformation treatment and the final product properties.
Key words: 5083 alloy, grain size, DC casting, inoculation, as-cast structure

UVOD

Lijevanje izravnim hlađenjem (Direct-Chill Casting) je polukontinuirani postupak lijevanja kod kojeg se skrućivanje taljevine odvija u vodom hlađenoj kokili, a pojavljivanje bloka na donjoj strani te kokile prati izravno prskanje vodom [1]. Ovaj postupak, te njegove varijante, praktički su jedine metode izrade blokova i trupaca. Izrada kvalitetnog odljevka, u obliku blokova i trupaca, igra bitnu ulogu u kvaliteti završnog proizvoda [2].

Osnovne proizvodne operacije koje određuju kvalitetu izlivenih blokova i trupaca su: taljenje - kemijski sastav, usitnjavanje zrna, odplinjavanje, filtriranje, lijevanje, te homogenizacija [3]. Da bi osigurali visoku kvalitetu gotovih proizvoda vrlo ja važno lijevanje bloka, kao poluproizvoda, i povezano s tim dobra kvaliteta taline, što je važan dio prakse lijevanja za gotovo sve aluminijske legure.

Kemijski dodaci u talinu tj. cjepiva (sredstva za usitnjavanje zrna) povećavaju broj aktivnih centara kristalizacije što vodi finijoj i ujednačenijoj strukturi po cijelom presjeku bloka. Danas se najčešće upotrebljavaju sredstva za usitnjavanje zrna na bazi Al-Ti-B i Al-Ti-C. Usitnjavanje zrna olakšava (potpomaže) lijevanje blokova DC postupkom: to omogućuje veće brzine lijevanja smanjujući sklonost nastanku napuklina na bloku, poboljšava mehanička svojstva bloka za naknadnu plastičnu deformaciju ili izvlačenje žice. Al-Ti-B sredstva osjetljivija su na okrupnjavanje (aglomeraciju) čestica nukleanata, ali su vrlo otporna na slabljenje učinka jer su čestice TiB_2 vrlo stabilne. Al-Ti-C sredstva ne pokazuju aglomeraciju (općenito otpornija su na «trovanja», ali pate od slabljenja djelovanja pri višim temperaturama taline, jer nukleacijske čestice TiC nisu stabilne). Općenito, cilj usitnjavanja zrna nije vrlo sitno zrno već ujednačena struktura zrna po presjeku bloka.

Još uvijek nije potpuno jasan sam mehanizam nukleacije, mehanizam djelovanja sredstva za usitnjavanje zrna, iako se izvode brojna istraživanja i postoje razne teorije [4-6]. U posljednje vrijeme izvode se istraživanja s tehnikom metalnog stakla gdje je ipak pomoću TEM slika moguć detaljniji pogled na mehanizam nukleacije u ovisnosti o sadržaju titana.

Dugoročno gledano moguće je da će se sve manje i manje upotrebljavati sredstva za usitnjavanje zrna na bazi Al-Ti-B i biti zamijenjena drugim sredstvima, barem za najkritičnije proizvode. Al-Ti-C sredstvo će se sve više upotrebljavati, a i vjerojatno će se poboljšavati njegova kvaliteta.

Ispitivanje mikrostrukture je jedno od glavnih pomoći u procjeni slitina i proizvoda pri određivanju utjecaja proizvodnih varijabli i toplinskih obrada kao i analizi uzroka grešaka. U eksperimentalnom dijelu rada prikazani su rezultati metalografskih ispitivanja (mjerenja veličine zrna) uzetih sa kraja bloka aluminijske slitine 5083, prema EN 573-3 [7] označene EN AW-5083, šarže 3121 što daje uvid u uspješnost obrade taline i lijevanja bloka DC postupkom.

EKSPERIMENTALNI DIO

Metodologija ispitivanja

U eksperimentalnom dijelu ovoga rada ispitivana je mikrostruktura kvantitativnom metalografskom analizom na aluminijskom bloku lijevanom na moderniziranoj liniji za lijevanje vertikalnim DC postupkom (VDC) u ljevaonici TLM –a Šibenik. Prikazani su rezultati ispitivanja veličine zrna, odnosno broja zrna aluminijske slitine EN AW-5083, šarže 3121, koja se koristi za daljnju preradu plastičnom deformacijom.

Taljevina je prije lijevanja rafinirana smjesom argona i klora u ALPUR-u. Usitnjavanje zrna provedeno se dodatkom predlegure AlTi5B1 u obliku polugica i u obliku žice, kemijskog sastava danog u tablici 1.

Tablica 1. Kemijski sastav sredstva za cijepljenje (modifikatora)

	Kemijski sastav modifikatora [%]					
	Si	Fe	Zn	Ti	B	Na
Polugice	0,15	0,11	0,005	5,05	0,84	0,0008
Žica	0,11	0,06	0,005	5,00	0,84	0,0006

Polugice dimenzija oko 35x30x840 mm dodaju se u ljevačku peć neposredno pred početak lijevanja, u prosječnoj količini 0,45 kg/t taljevine, slika 1a. Žica promjera oko 9,5 mm dodaje se u žlijeb neposredno ispred ALPUR-a u prosječnoj količini od 2,16 kg/t taljevine, slika 1b.

a) polugice b) žica

Slika 1. Dodatak sredstva za cijepljenje u obliku
a) polugica
b) žice

Ispitivanje mikrostrukture

Uzimanje, priprema i nagrizanje uzoraka

Uzorci za ispitivanje mikrostrukture uzeti su sa poprečnog presjeka izrezanog sa (kraja) bloka, lijevanog vertikalnim DC postupkom. Dimenzije presjeka lijevanog bloka iznose 1680x520 mm. Poprečni presjek tj. ploča debljine 3 cm, tzv. „šajba“ podijeljena (razrezana) je na 12 manjih segmenata, čije su pozicije u presjeku označene rednim brojevima 1-12. Po pravcu x tj. po širini presjeka bloka uzeto je 7 uzoraka, i to dva sa ruba „šajbe“ oznaka 7R i 12R, a ostalih 5 uzoraka sa sredine: 7S, 8, 9, 10 i 11, slika 2. Oznaka R označava rub, a S sredinu „šajbe". Po pravcu y tj. po debljini presjeka bloka uzeta su 4 uzorka, dva sa ruba (4R i 10R) i dva bliže sredini „šajbe" (4S i 10S). Prikaz „šajbe" izrezane na segmente i raspored uzimanja uzoraka za metalografska ispitivanja prikazan je na slici 2.

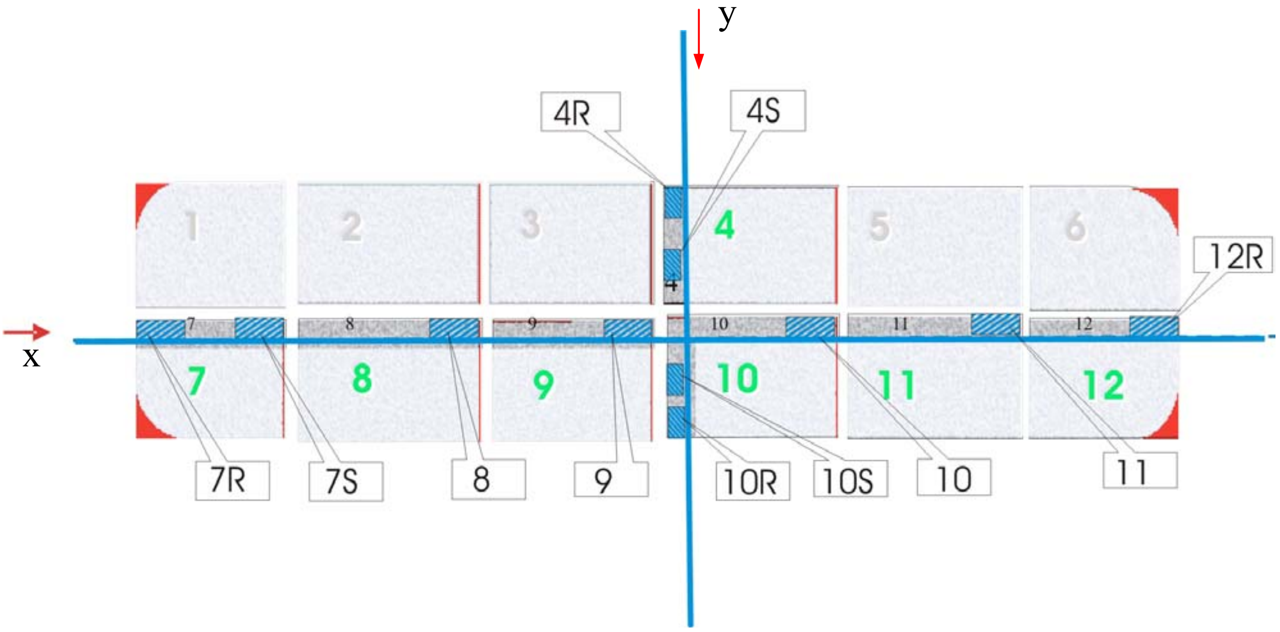

Slika 2. Mjesta uzimanja uzoraka za metalografska ispitivanja i označavanje uzoraka

Da bi se mogla provesti automatska priprema (brušenje i poliranje) uzorci moraju biti u obliku valjčića promjera 30 mm [8, 9]. U tu svrhu uzorci se postavljaju u kalupe i ulažu u masu. Uzorci su brušeni pod mlazom vode na uređaju za automatsku pripremu uzoraka Vector LC sa brusnim papirom gradacije 600 i 800. Na svakoj gradaciji brusnog papira uzorak je brušen 10 minuta kod sile opterećenja od 10 N i brzine okretanja rotacijskog diska 150 o/min. Nakon brušenja na najfinijoj gradaciji uzorci su polirani na platnu za poliranje Microcloth vodenom otopinom glinice granulacije 0,3 μm. Poliranje uzoraka provedeno je na istom uređaju kao i brušenje, pri istim uvjetima. Polirana površina mora biti dovoljno velika da omogući mjerenja najmanje pet područja kod potrebnog povećanja [10].

Radi otkrivanja granice zrna uzorci su nagrizani elektrolitički (anodizacija) istosmjernom strujom (U= 20 V), 6-8 min. u Barker-ovom reagensu [11]. Anodizacija je postupak elektrolitskog nagrizanja radi nanošenja tankog oksidnog filma na površinu metala koji je nadgrađen na strukture zrna. Taj tanki oksidni film kod upotrebe polariziranog svjetla i tintnog filtra na mikroskopu svako zrno oboji drugom bojom.

Kvantificiranje mikrostrukture optičkim mikroskopom

Metalografska ispitivanja uzoraka provedena su na svjetlosnom mikroskopu Olympus GX51 sa digitalnom kamerom Olympus DP70 i sustavom za automatsku obradu slike («AnalySIS Materials Research Lab»), sa povećanjem od 100 i 200X. Za određivanje prosječne veličine zrna, odnosno broja zrna ispitivanih uzoraka upotrijebljena je **poluautomatska metoda mjerenja veličine zrna mjerenjem duljine presijecanja zrna (intercept procedura)** [9, 10, 12].

REZULTATI I DISKUSIJA REZULTATA

Slitina EN AW-5083 spada u teško gnječive, toplinski neočvrstive slitine aluminija sa magnezijem, koje se odlikuju malom specifičnom masom, visokim mehaničkim svojstvima i otpornošću prema koroziji u uvjetima obične i morske atmosfere, uz uvjet da su prisutne nečistoće svedene na dopuštene vrijednosti. Kemijski sastav slitine EN AW-5083 je dan u tablici 2., a uzorci za kemijsku analizu su uzimani tijekom lijevanja kod dužine blokova od oko 0,5 m.

Tablica 2. Kemijski sastav ispitivane aluminijske slitine EN AW-5083, šarža 3121

Šarža	Kemijski sastav slitine EN AW-5083 (%)								
	Cu	Mn	Mg	Si	Fe	Cr	Be	Ti	Na
3121	0,01	0,43	4,365	0,13	0,38	0,10	0,0045	0,0295	0,0003

Kemijski sastav ispitivane slitine EN AW-5083 određen je optičkim emisionim spektrometrom (OES) firme ARL.

Ispitivane Al-Mg slitine sadrži dodatke željeza, kroma, mangana ili titana, pojedinačno ili u kombinaciji, u ukupnoj količini od 0,25 do 1 % (tablica 2.) u cilju poboljšanja vlačnih svojstava i tehnoloških značajki [13]. Pored Mg koji u obliku Al_3Mg_2 precipitira po granicama zrna, u mikrostrukturi se najvjerojatnije pojavljuju i željezom bogate kompleksne faze kao $(Fe,Cr)_2Mg_3Al_{18}$ i/ili $(Fe,Mn)Al_6$ tipa. Legiranje berilijem dodatkom predslitine AlBe5 u ljevačku peć, u prosječnom iznosu od 0,6 kg/t taljevine provedeno je radi smanjenja odgora magnezija, te povećanja kvalitete površine blokova. Učinkovitost pročišćavanja taljevine u ALPUR-u bila je dobra (Na=0,0003%).

Mikrostrukturna analiza ispitivanih uzoraka aluminijske slitine 5083

Na slikama 3. i 4. prikazane su mikrostrukture nagriženih uzoraka Barker-ovim sredstvom, gledane uz dodatak polarizacijskog svjetla i tintnog filtra.

Iz slike 3. i 4. vidi se da smo dobili dobru razlučivost zrna kao različite nijanse odgovarajućih boja. Da bi mogli precizno i bez dvojbi razlikovati zrna operater sam «namješta» boje dok se ne dobije najbolja razlučivost između različito obojenih zrna. Ipak kod nekih uzoraka bilo je poteškoća kod dobivanja jasnih granica zrna pa je bilo potrebno duže nagrizanje Barker-ovim reagensom što je dovelo do «otapanja» intermetalnih faza na granicama zrna, ali se ipak zrna bez dvojbi razlikuju, npr. slika 4d. Većinom su to istoosna zrna, štapićasta zrna nisu primijećena.

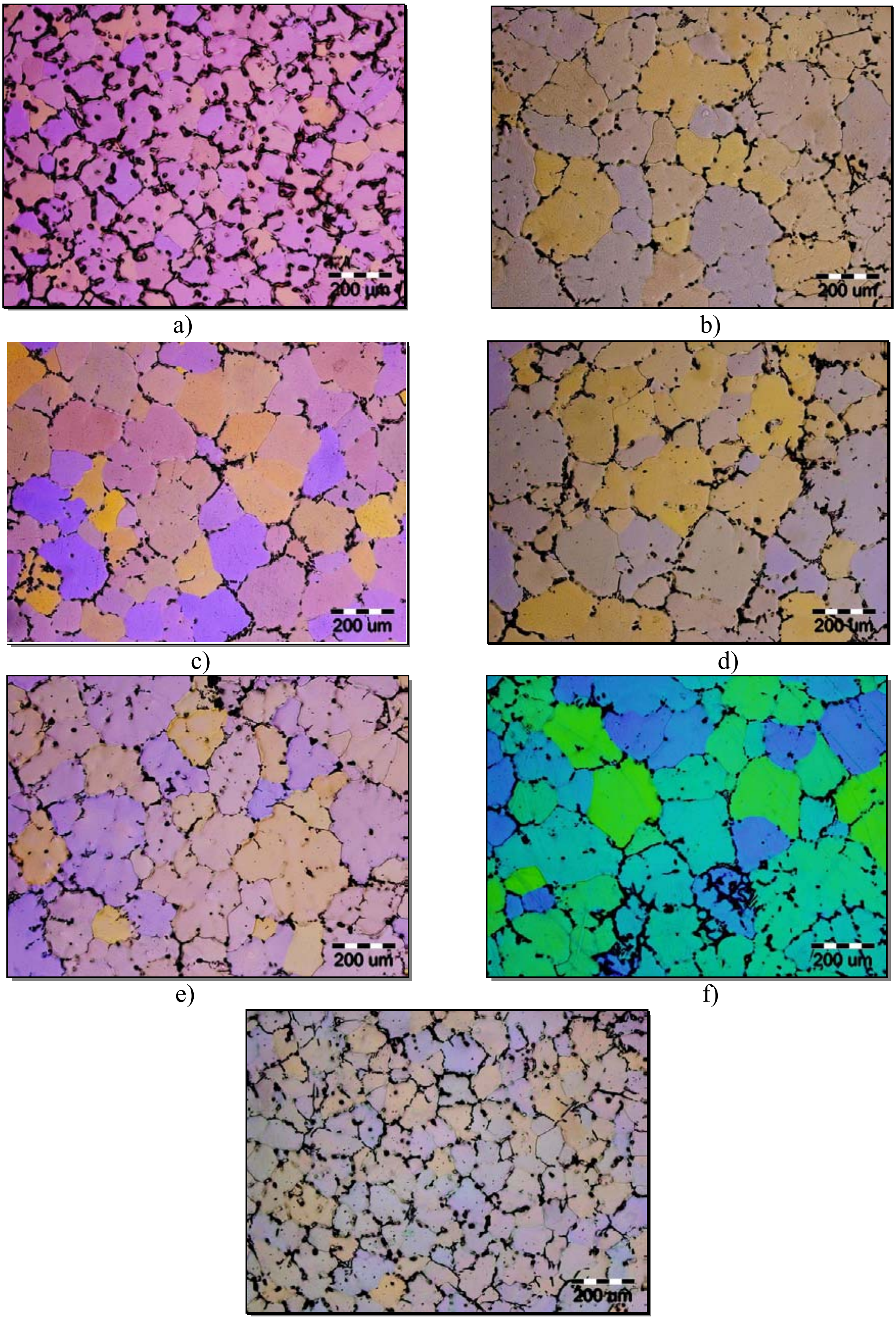

a) b) c) d) e) f) g)

Slika 3. Mikrostruktura slitine EN AW-5083 nagrižene Barker-ovim reagensom, promatrane sa polarizacijskim svjetlom i tintnim filtrom, pri povećanju mikroskopa 100X
a) uzorak 7R, b) uzorak 7S, c) uzorak 8,
d) uzorak 9, e) uzorak 10, f) uzorak 11, g) uzorak 12R

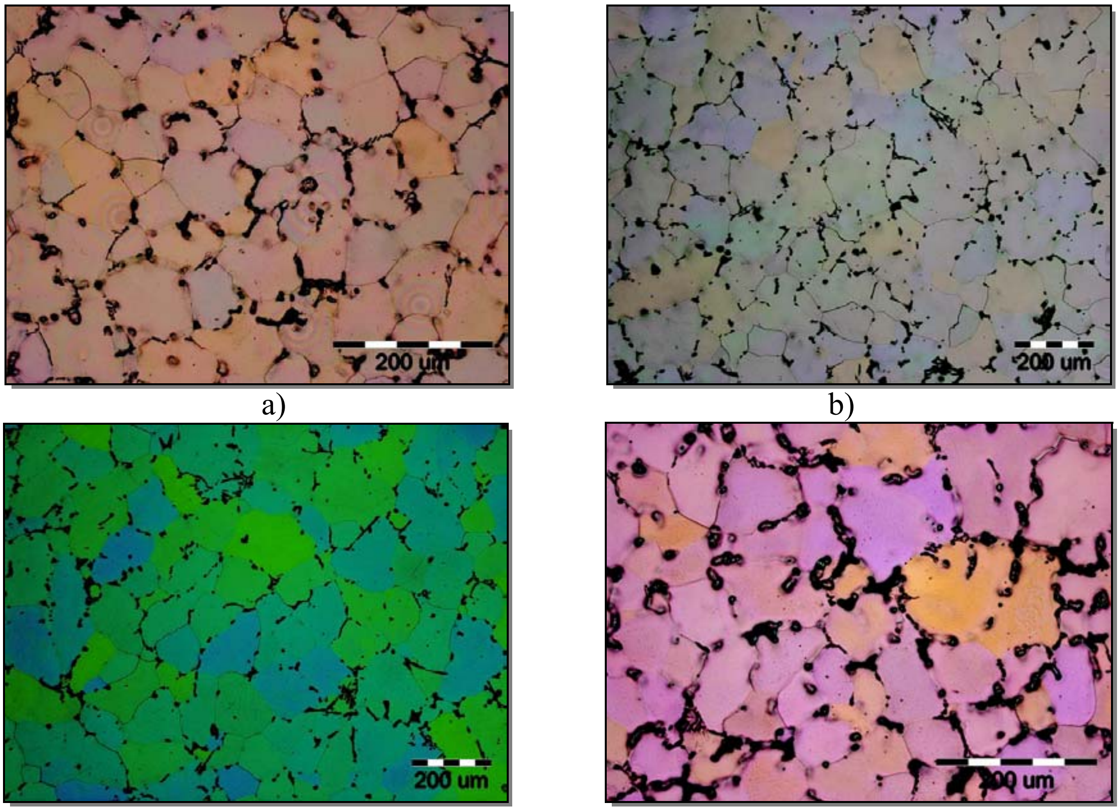

a) b)

c) d)

Slika 4. Mikrostruktura slitine EN AW-5083 nagrižene Barker-ovim reagensom, promatrane sa polarizacijskim svjetlom i tintnim filtrom
a) uzorak 4R, pri povećanju mikroskopa 200X
b) uzorak 4S, pri povećanju mikroskopa 100X
c) uzorak 10S, pri povećanju mikroskopa 100X
d) uzorak 10R, pri povećanju mikroskopa 200X

Rezultati određivanja veličine zrna poluautomatskom metodom mjerenja veličine zrna metodom mjerenja duljine presijecanja zrna na 11 ispitivanih uzoraka slitine EN AW-5083, šarže 3121 dani su u tablicama 3. i 4. Software automatski računa prosječnu (srednju) duljinu presijecanja, $\bar{l}$ [µm], iz koje se linearnom aproksimacijom (tablica 2. u [14]) izračuna srednji broj zrna po jedinici ispitivane površine $\overline{N_A}$ (No./mm^2) ili *G–broj* za mjerenih *n* područja. Da bi rezultat statistički bio opravdan postupak ručnog određivanja presjecišta granica zrna se ponavlja dok se ne izmjeri najmanje 500 duljina presijecanja zrna.

Tablica 3. Rezultati mjerenja veličine zrna slitine EN AW-5083 dobiveni metodom mjerenja duljine presjeka zrna, po pravcu x

Oznaka uzorka	$\bar{l}$ **[µm]**	**Broj presjeka**	**G - broj**	$\overline{N_A}$ **[No./mm^2]**
7R	83,64	529	3,88	115,24
7S	131,79	506	2,56	46,14
8	137,12	519	2,45	42,52
9	129,21	494	2,62	48,33
10	148,21	497	2,23	36,94
11	123,65	527	2,75	53,05
12R	75,49	533	4,18	142,24

Tablica 4. Rezultati mjerenja veličine zrna slitine EN AW-5083 dobiveni metodom mjerenja duljine presjeka zrna, po pravcu y

Oznaka uzorka	$\bar{l}$ **[μm]**	**Broj presjeka**	**G - broj**	$\overline{N}_A$ **[No./mm^2]**
4R	62,38	505	4,73	208,76
4S	105,38	535	3,21	73,01
10S	103,24	522	3,27	76,07
10R	69,74	495	4,40	165,49

Grafički prikaz promjene veličine zrna po pravcu x i y dan je na slikama 5. i 6.

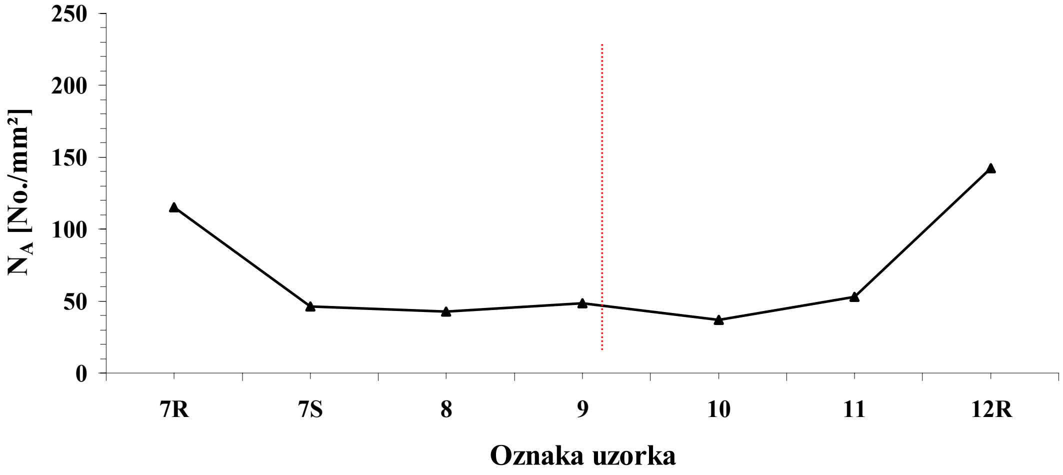

Slika 5. Grafički prikaz promjene veličine zrna po pravcu x

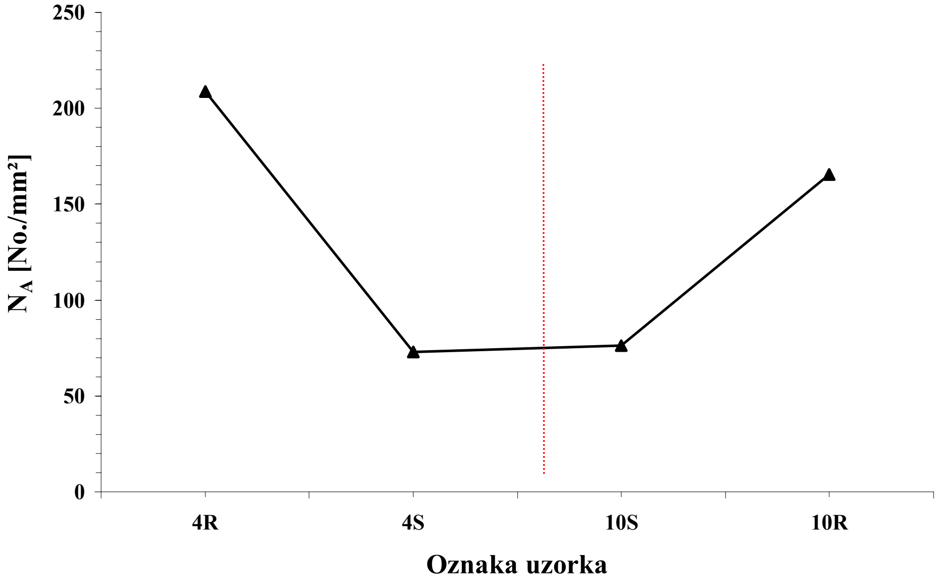

Slika 6. Grafički prikaz promjene veličine zrna po pravcu y

Iz dobivenih rezultata ispitivanja mikrostrukture po pravcu x, tj. po širini bloka (tablica 3. i slika 5.) vidi se da je veličina zrna manja na rubovima bloka (G = 3,88 - 4,18 tj.

$\overline{N_A}$ = 115,24 – 142,24 No./mm^2), dok je u sredini prisutna grublja struktura (G = 2,23 – 2,75 tj. $\overline{N_A}$ = 36,94 – 53,05 No./mm^2).

Prisutna je sličnost promjene veličine zrna po pravcu y, tj. po debljini bloka (tablica 4. i slika 6.), gdje se kod rubno uzetih uzoraka 4R i 10R veličina zrna kreće od G = 4,73 tj. $\overline{N_A}$ = 208, 76 No./mm^2 (za uzorak 4R), tj. G = 4,4 odnosno $\overline{N_A}$ = 165,49) (za uzorak 10R), za razliku od uzoraka uzetih bliže sredini bloka gdje su vrijednosti G relativno niže, tj. zrna su sitnija u odnosu na rub bloka.

Veličina zrna mjerena po „visini šajbe“, odnosno po debljini bloka je mnogo veća nego po „širini šajbe“ tj. bloka što ukazuje na veći intenzitet odvođenja topline po debljini bloka nego po širini.

Uzorci koji su uzeti po sredini presjeka „šajbe“ po pravcu x, bez rubno uzetih uzoraka 7R i 12R, pokazuju jednoliku raspodjelu zrna (G=2,56 – 2,75), bez velikih odstupanja. To je posljedica učinkovitosti cijepljenja i ograničenja rasta djelovanjem magnezija kao legirajućeg elementa i djelovanja legirajućih elemenata u okviru mehanizma konstitucijskog podhlađenja, premda nema podataka koji bi odredili učinak interakcije između otopljenih elemenata i faktora restrikcije rasta [1]. Obzirom da se prije valjanja bloka odstranjuju njegovi rubovi glodanjem, može se zaključiti da je dobivena ravnomjerna veličina istoosnih zrna po presjeku bloka., što govori o korektno primijenjenoj tehnologiji cijepljenja i lijevanja ispitanog bloka slitine EN AW-5083.

ZAKLJUČCI

Na temelju provedenih ispitivanja uzoraka bloka Al slitine kvalitete EN AW-5083 mogu se izvesti sljedeći zaključci:

1. Elektrolitsko nagrizanje (anodizacija) Barker-ovim reagensom i promatranja uzoraka pri polariziranom svjetlu i sa tintnim filtrom daje dobru razlučivost kontrasta boja različitih zrna.
2. Poluautomatska metoda mjerenja duljine presijecanja zrna upotrebom softverskog paketa olakšava i ubrzava mjerenje veličine zrna, kao i promatranje i komentiranje mikrostrukture.
3. Prema dobivenim rezultatima možemo reći da je na rubovima bloka finija mikrostruktura - manje je zrno tj. veći je broj zrna (115,24 – 208,76 No./mm^2) nego u ostatku bloka (36,94 – 76,07 No./mm^2), zbog veće brzine odvođenja topline.
4. Veličina zrna mjerena po „visini šajbe“, odnosno po debljini bloka je mnogo veća nego po „širini šajbe“ tj. bloka što ukazuje na veći intenzitet odvođenja topline po debljini bloka nego po širini.
5. U mikrostrukturi prevladavaju istoosna zrna, značajna zona štapićastih (stubičastih) zrna nije zapažena.
6. Obzirom da se prije valjanja bloka odstranjuju njegovi rubovi glodanjem može se zaključiti da je dobivena ravnomjerna veličina istoosnih zrna po presjeku bloka. To govori o korektno primijenjenoj tehnologiji cijepljenja i lijevanja ispitanog bloka slitine EN AW-5083.

LITERATURA

[1] Quested, T. E., Ph. D. Thesis: Solidification of Inoculated Aluminium Alloys, Departement of Materials Science and Metallurgy, University of Cambrige, Cambrige UK 2004.

[2] D. G. Altenpohl: Aluminium: Technology, Applications, and Enviroment, A Profile of a Modern Metal, The Aluminum Association and The Minerals, Metals & Materials Society (TMS), Warrendale, Pennsylvania, USA, 1999, pp. 77-125.

[3] J. Prgin, Neophodna poboljšanja kvalitete blokova i trupaca u TLM-u, 4th INTERNATIONAL FOUNDRYMEN CONFERENCE: Recent Developments in the Casting Productions, Opatija, 2004.

[4] A. L. Greer: Grain Refinement of Aluminium Alloys, Solidification of Aluminium Alloys, The Minerals, Metals & Materials Society (TMS), Warrendale, Pennsylvania, USA, 2004, pp. 131-145.

[5] D. G. Altenpohl: Aluminium: Technology, Applications, and Enviroment, A Profile of a Modern Metal, The Aluminum Association and The Minerals, Metals & Materials Society (TMS), Warrendale, Pennsylvania, USA, 1999, pp. 33-59.

[6] M. Easton and D. StJohn: Factors Affecting the Development of a Fine Grained Solidification Microstructure in Aluminium Alloys, Solidification of Aluminium Alloys, The Minerals, Metals & Materials Society (TMS), Warrendale, Pennsylvania, USA, 2004, pp. 147-56.

[7] prEN 573-3: 2003: Aluminium and aluminium alloys – Chemical composition and form of wrought products - Part 3: Chemical composition, European Comitee for Standardization, 2003.

[8] E 3 – 01: Standard Guide for Preparation of Metallographic Specimens, American National Standard Institute/ASTM, 2001.

[9] N. Dolić, K. Terzić, J. Prgin, A. Markotić, F. Unkić, Kvantitativna metalografska analiza Al-slitina 5083, 6th INTERNATIONAL FOUNDRYMEN CONFERENCE: Innovative Foundry Materials and Technologies, Opatija, 2005.

[10] E 1382 – 97: Standard Test Methods for Determining Average Grain Size Using Semiautomatic and Automatic Image Analysis, American National Standard Institute/ASTM, 1997.

[11] http://www.aluminium.org/education/TALAT/index.htm

[12] N. Dolić, K. Terzić, J. Prgin, A. Markotić, F. Unkić, Structural Analysis of Al Alloy 5083 Cast By Vertical DC Process, MATRIB, 2005.

[13] John E. Hatch, Aluminum, Properties and Physical Metallurgy, American Society for Metals, Metals Park, Ohio, 1988, pp. 58-104.

[14] E 112 – 96: «Standard Test Methods for Determining Average Grain Size», American National Standard Institute/ASTM, 1996.

Napomena: Rad je izrađen u okviru složenog projekta «Poboljšani postupak lijevanja blokova i trupaca teško gnječivih aluminijskih legura», (TP – 02-0124-04), HITRA – TEST.

AL-FOAM PARTS FOR ENHANCED PASSIVE SAFETY AND COMFORT

R.Florek, F.Simancik, P. Tobolka; M. Nosko; J.Jerz

Institute of Materials and Machine Mechanics SAS, Racianska 75 SK-83102 Bratislava, Slovakia

The application of lightweight materials in car body structures decreases fuel consumption thus saving cost and environment, reduces wear of i.e. brakes and tires or enables making cars larger and thus safer at same weight, and finally creates the space and weight reserve for additional devices like air condition, various servo systems etc.

Al-foam structures possess besides the lightness also excellent damping ability, convenient stiffness-to-weight ratio and very efficient crash absorption ability. Based on these features Al-foam parts are able to improve comfort and passive safety for passengers as well as for surroundings.

The main aim of the paper is to suggest the ways for realistic use of foams in lightweight structural components. It will be shown that Al-foam parts are serious candidates for this purpose.

Keywords: Aluminium foam, lightweight, vibration damping, crash absorption, passive safety

Introduction

Demands on higher safety, economy and comfort of vehicles require use of new material concepts which will be able to reduce weight, vibrations and in one hand to enhance crash absorption ability. To fulfil these requirements a quite new point of view on lightweight designing is needed. Bulk aluminium alloy parts have already found very wide application range in transport industry and their share get continuously wider. The lightness enhancement can be further improved by additional modification of bulk aluminium by foaming technologies. Recent foaming techniques are able to produce 3-D net shape foamed structural parts made of aluminium alloys. Such parts can subsequently join the advantages of the foam structure to one functional component that can combine, besides the weight reduction, functionality, load-bearing ability, noise and vibration damping as well as the crash absorption capability [1]. Additional benefits of the foams are incombustibility and very good temperature stability within the vehicle common operation temperature range.

Aluminium foam structure and its properties

There were already done a lot of attempts to find the real applications of Al-foams especially in automotive industry. However, such attempts considered the foam mostly as a filler of hollow profile in order to avoid premature buckling and to increase resulting bending strength. Comparing the ratio costs vs. obtained benefits, these applications of aluminium foams were too expensive even though the properties enhancement was significant [1]. A proper designing approach which allows use together most of the above mentioned properties in one functional Al-foam part able to improve lightness, passive safety or comfort is needed.

In order to better understand these properties of foamed structure the crash absorption, stiffness-to-weight ratio as well as damping ability will be presented separately.

Parts of Al-foam are able to absorb deformation energy more efficiently than bulk Al-profile [3]. If the bulk and foamed part are compared different deformation behaviour is apparent. While the bulk part deforms by folding making maximum first stress peak with rather decreasing subsequent ones, the foam part does not loose its compression strength during deformation and due to deformation plateau is thus able to absorb much more energy. Figure 1 presents the compression curves of bulk as well foamed Al part. The tested samples are listed in Table 1. Comparing these results, the foam was 30% lighter than bulk Al whereas the amount of absorbed deformation energy was in case of Al foam significantly increased.

Table 1: Tested profiles; weight, density and dimensions.

	Length weight (kg/m)	Density (g/cm^3)	Cross-section (mm)
Al-alloy foam - heat treated	**1,35**	**0,7**	**55 x 35**
Al-alloy hollow profile	1,75	2,7	60 x 90 x 2,5

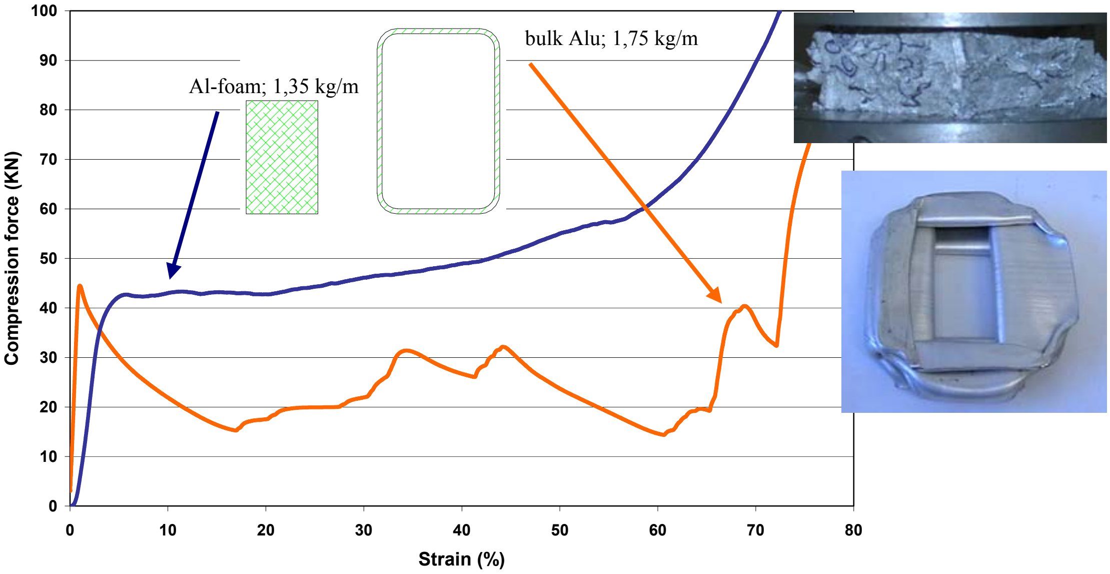

Figure 1: Compression-strain curves of Al-foam and bulk Al-hollow profile according to table 1. Right: Al-foam and bulk Al-profile after deformation

The crash absorption ability can also be expressed by efficiency *Eff* calculated according to following formula:

$$Eff = \frac{100 \cdot E_X}{F\max_{0-X} \cdot d_X}(\%)$$

Whereas: E_x is absorbed deformation energy up to deformation d_x
F_{max} is maximal compression force up to deformation d_x

Graphic expression of this formula can be seen in Figure 2. From this figure it is apparent, that the Al-foam possesses much better crash absorption efficiency compared to bulk Al-alloy hollow profile in spite of lower weight and smaller dimensions.

However, the demands on crash absorption ability are rather contending, on one hand there is a requirement on absorption of huge amount of crash energy in case of vehicle accident with i.e. rigid wall in order to protect passengers, on the second hand there are also pedestrians, who have only got very little protection if crashed by vehicle. The problem how to protect the passengers is being solved by means of many car safety systems; more or less complicated. The less complicated one is to use the crash absorbers with low compression strength (up to 2 MPa) which deform easily under crash with human body and thus eliminate serious injuries. Using of Al-foam for this purpose is possible if the low compression strengths are available. These strengths can only be reached at low densities up to 0,3 g/cm^3. With increasing density the compression strength also increases; from about 4 MPa at 0,4 g/cm^3 up to 6 MPa at 0,5 g/cm^3. Recently, the foaming technologies at IMMM SAS are able to produce Al-foams with density between 0.2 and 0.3 g/cm^3 which possess low strength (about 2MPa) and maintain this strength almost at same level during whole deformation. In Figure 3 the deformation behaviour of Al-foam cylinders (D x L= 25x30 mm) with density 0.22 g/cm^3 is presented. As can be seen, the compression strength is about at 2 MPa, and crash absorption ability at this load is almost up to 80% deformation.

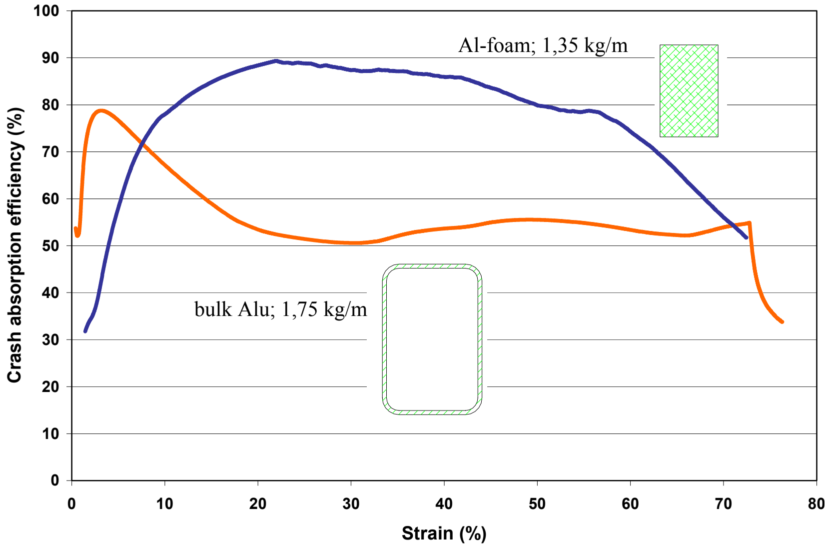

Figure 2: Difference in crash absorption efficiency; Al-foam vs. Al-hollow profile listed in table 1; significant higher efficiency of Al-foam is apparent.

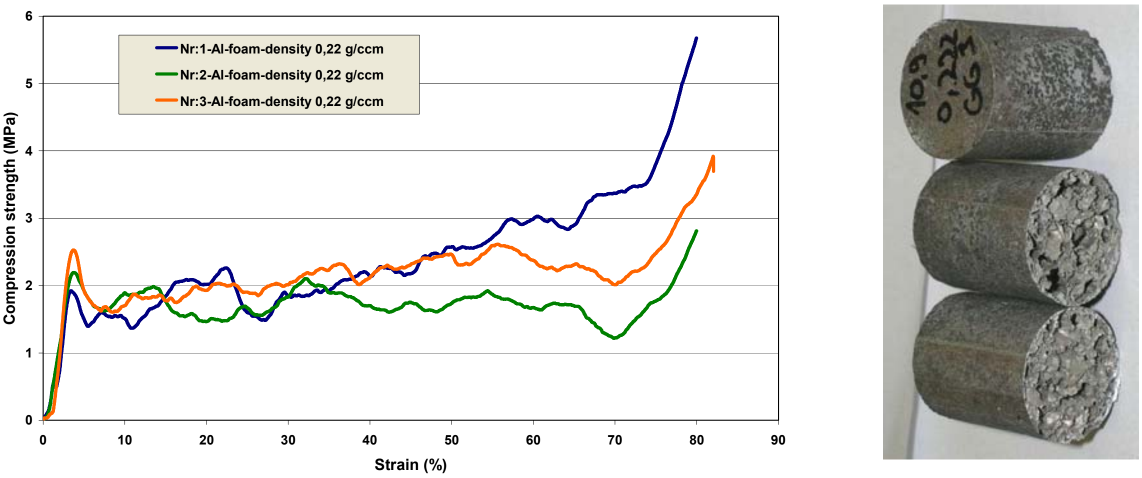

Figure 3: Compression test on Al-foam samples with low density 0.22 g/cm^3. Low compression strength acceptable for pedestrian protection was reached.

Stiffness-to-weight ratio

Another feature of Al-foam which can contribute to improvement of lightness is its good stiffness-to-weight ratio. By foaming the cross-sectional moment of inertia and thus also the stiffness increase. In order to present this property two Al-sheets and one Al-foam panel were compared. The panels (see The test have shown that 25 mm Al-foam panels have significant higher stiffness compared to 3 mm Al-sheet of similar weight and even better than considerably heavier 5 mm Al-sheet. In Figure 4 are presented loading and unloading curves of tested Al-foam panel and Al-sheets together with slope of the straight line *k*. The coefficient *k* expresses the stiffness and one can see that Al-foam panel is about 60 times stiffer than 3 mm Al-sheet of similar weight. However, beside high stiffness also high strength is necessary if load bearing applications are considered. Al-foams have generally much lower strength in tension than bulk aluminium due to premature fracture in weakest sections, which makes serious drawback in structural design.

Table 2) were loaded by surface pressure up to 37 kPa. For better understanding, 30 kPa corresponds to about 750 kg load per area 500 x 500 mm.

The test have shown that 25 mm Al-foam panels have significant higher stiffness compared to 3 mm Al-sheet of similar weight and even better than considerably heavier 5 mm Al-sheet. In Figure 4 are presented loading and unloading curves of tested Al-foam panel and Al-sheets together with slope of the straight line *k*. The coefficient *k* expresses the stiffness and one can see that Al-foam panel is about 60 times stiffer than 3 mm Al-sheet of similar weight. However, beside high stiffness also high strength is necessary if load bearing applications are considered. Al-foams have generally much lower strength in tension than bulk aluminium due to premature fracture in weakest sections, which makes serious drawback in structural design.

Table 2: List of tested samples: Al-foam and bulk Al-sheets.

	Weight (kg)	Dimensions (mm)	Slope of a straight line *k* $y = k \cdot x$	
25 mm Al-foam	2	500 x 500	171	
3 mm Al-sheet	1,9	500 x 500	3	
5 mm Al-sheet	3,3	500 x 500	7	

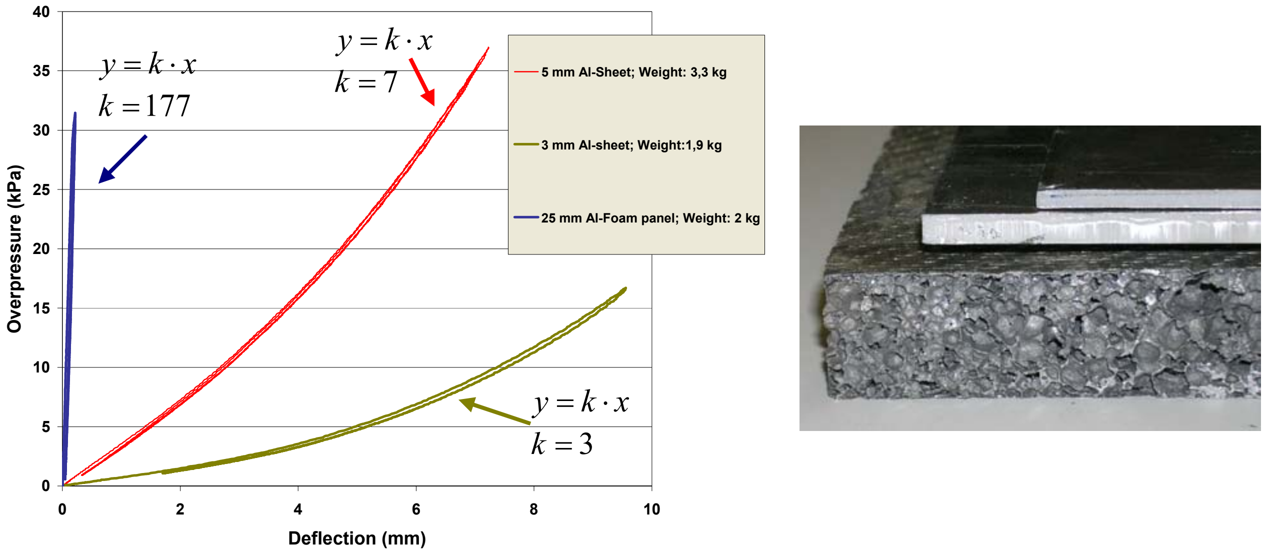

Figure 4: Loading and unloading curves of 25 mm thick Al-foam panel vs. 5 mm and 3 mm Al-sheet; right detail view on the measured foam panel and Al-sheets.

Foamed parts therefore need additional reinforcing e.g. by steel meshes which avoid premature brittle failure and also further enhance the bending strength and stiffness at negligible weight increase. The bending strength can be further or alternatively enhanced also by proper heat treatment if heat-treatable Al-alloy is used for foaming. In order to determine these effects the 4-point bending tests on reinforced and non-reinforced hollow Al-foam profiles 50x7x325 mm (see also Figure 5) manufactured of heat treatable Al-alloy were performed. The tested samples are listed in Table 3. The arrangement of test apparatus is shown in Figure 5. The results from bending tests are presented in Figure 6. It can be seen on the chart that heat treatment as well as steel reinforcement affect bending behaviour significantly. The deformation mode of the specimens is presented in Figure 7. It is visible that the failure starts primarily in foam structure and subsequently; after certain deformation;

tears up the reinforcing steel mesh. In case of reinforced and heat treated profile the deformation of the foam structure is not visible and the tested profile failed due to steel reinforcement failure at significant higher bending force and lower deflection compared to the reinforced and non-heat treated profile, because of higher compression strength of heat treated Al-alloy foam. The hollow profile without reinforcement and heat treatment fractures very soon without any visible foam yielding.

It must be noted that the reinforcement should be optimized according to Al-foam compression strength. Weaker foams require considerably lover portion of reinforcements.

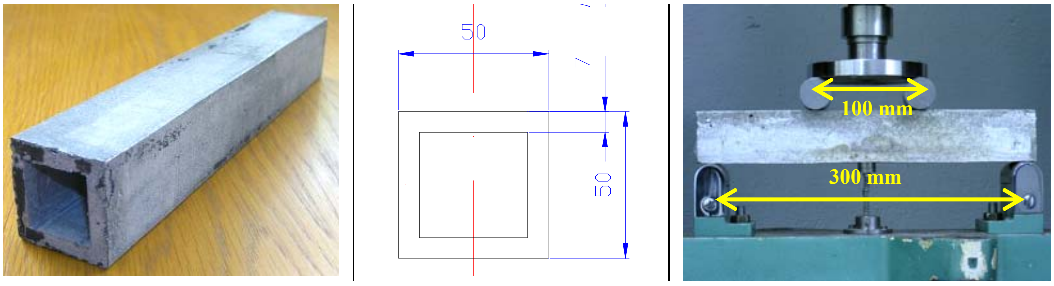

Figure 5: Hollow profile of heat treatable Al-alloy foam and arrangement of test apparatus.

Table 3: List of tested samples for 4-point bending test. (the values of E-Modul are only informative; for calculation the formulas for isotropic materials have been used).

	Weight (g)	E-Modul (GPa)	Ultimate strength (N)
reinforced + heat treated	348	8	9400
reinforced ; non-heat treated	333	8	7400
non-reinforced; non-heat treated	233	5	3800

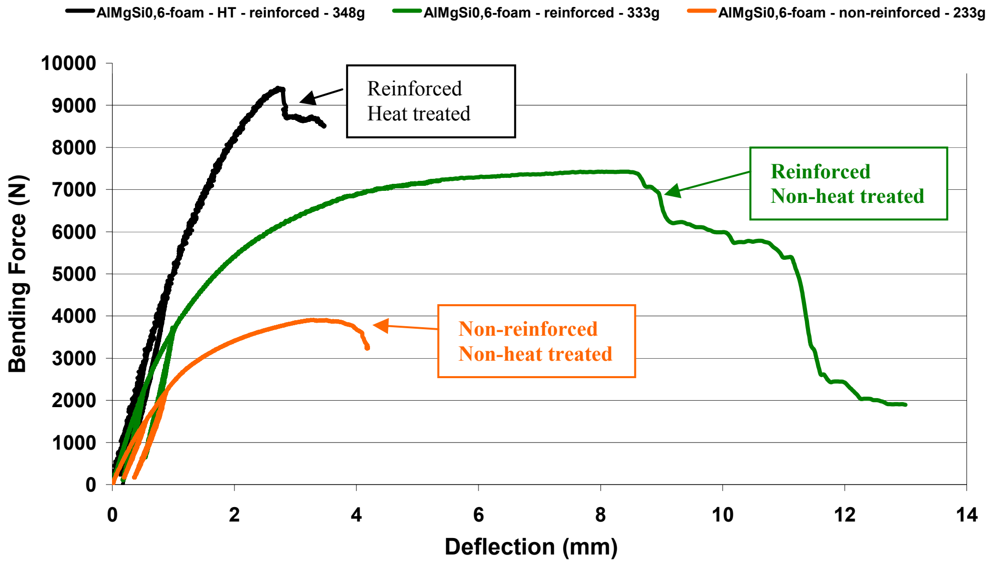

Figure 6: Bending force vs. deflection curves of 50x7x325 hollow profiles made of heat treatable Al-alloy foam.

a) reinforced + heat treated | **b)** reinforced ; non-heat treated | **c)** non-reinforced; non-heat treated

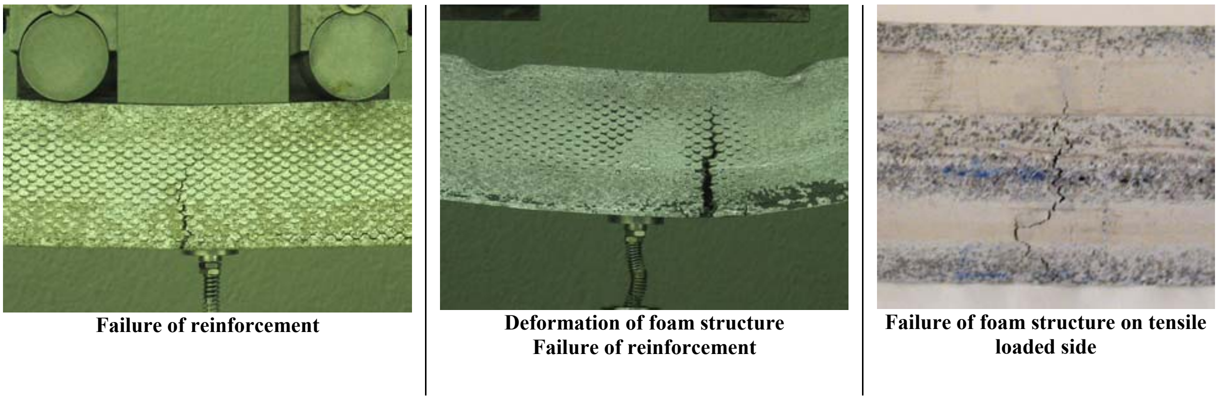

Failure of reinforcement

Deformation of foam structure
Failure of reinforcement

Failure of foam structure on tensile loaded side

Figure 7: Tested Al-foam hollow profiles from table 3 after 4-point bending test.

Damping ability

Another very interesting property of Al-foam is its damping ability. It was well documented in [3], that the i.e. cast aluminium engine covers (front cover, valve cover and the other cast components) contribute strongly to the total engine noise. The acoustic measurements [3] have also confirmed that the acoustic response is primarily caused by resonance of the cover. The noise is induced in the similar way as in case of loudspeaker if the cover wall starts to vibrate at its resonance frequencies. The vibrations can be damped by many methods i.e. applying layer damping treatments on lightly damped surface [3]. However, this method is only unpractical "repair" solution if the vibrations occur. In order to avoid the vibrations already in designing stage more sophisticated approach e.g. use covers of materials with better damping ability should be applied. The possibility to utilise an excellent damping of aluminium foam structure will be discussed in this part. The damping ability of aluminium foam panel will be compared to bulk Al-sheets.

The tests were performed on Al-foam panel and Al-sheets which are listed in
Table 4. The panels were tested using a frequency response analysis in free-free arrangement presented in

Figure 8. The test apparatus consists of impact hammer with force sensor, acceleration sensor and frequency analyzer. The frequency response was acquired in the middle of the panel in order to determine the oscillation response as well as the damping ability [4].

Table 4: List of tested panels.

	Weight (kg)	Dimensions (mm)	
25 mm Al-foam	2,0	500 x 500	
3 mm Al-sheet	1,9	500 x 500	

5 mm Al-sheet	3,3	500 x 500	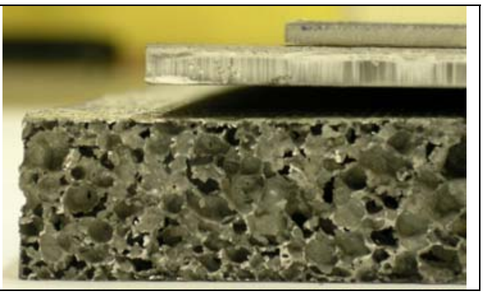

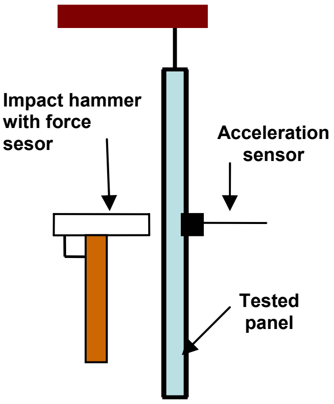

Figure 8: Arrangement of test apparatus for vibration damping measurements

The frequency response functions for Al-foam panel and bulk Al-sheets are presented in Figure 9. The difference in number of oscillation frequencies is significant. Both 3 mm and 5 mm Al-sheets showed considerably higher inertance peaks and also higher number of oscillation frequencies than the Al-foam panel. Also damping factor (decay) computed from resonance peaks at three different oscillation frequencies showed the damping of Al-foam one order higher than bulk aluminium (10^{-3} vs. 10^{-4} –see Figure 10). Time dependence of the surface acceleration damping after impact by impact hammer is presented in Figure 11. As can be seen, Al-foam is able to damp the surface acceleration after impact within 250ms, which was considerably shorter than in case of both bulk Al-sheets.

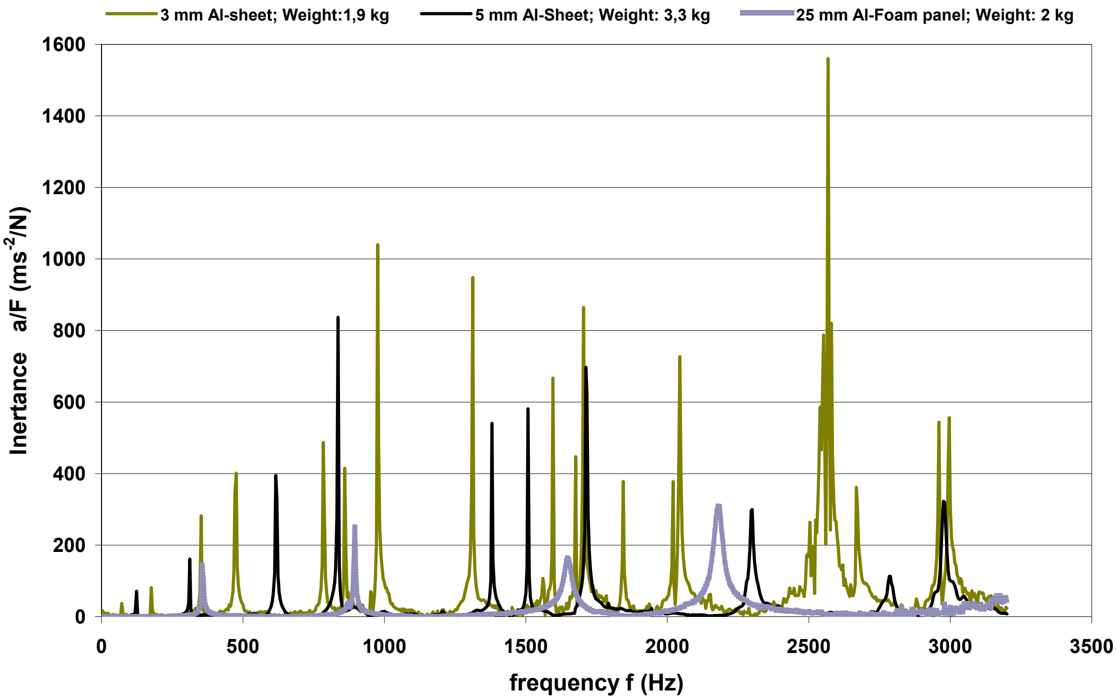

Figure 9: Frequency responce curves after impact by impact hammer; 25 mm Al.foam panel, 5 mm Al-sheet; 3 mm Al-sheet.

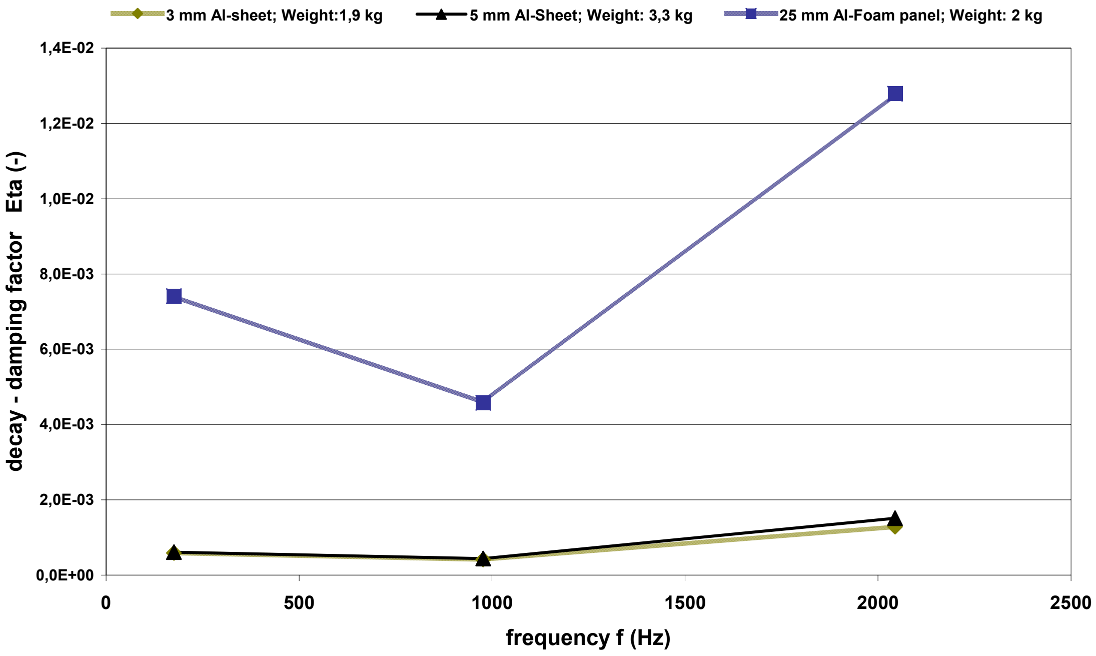

Figure 10: Damping factor (decay) of 25 mm Al.foam panel, 5 mm Al-sheet and 3 mm Al-sheet.

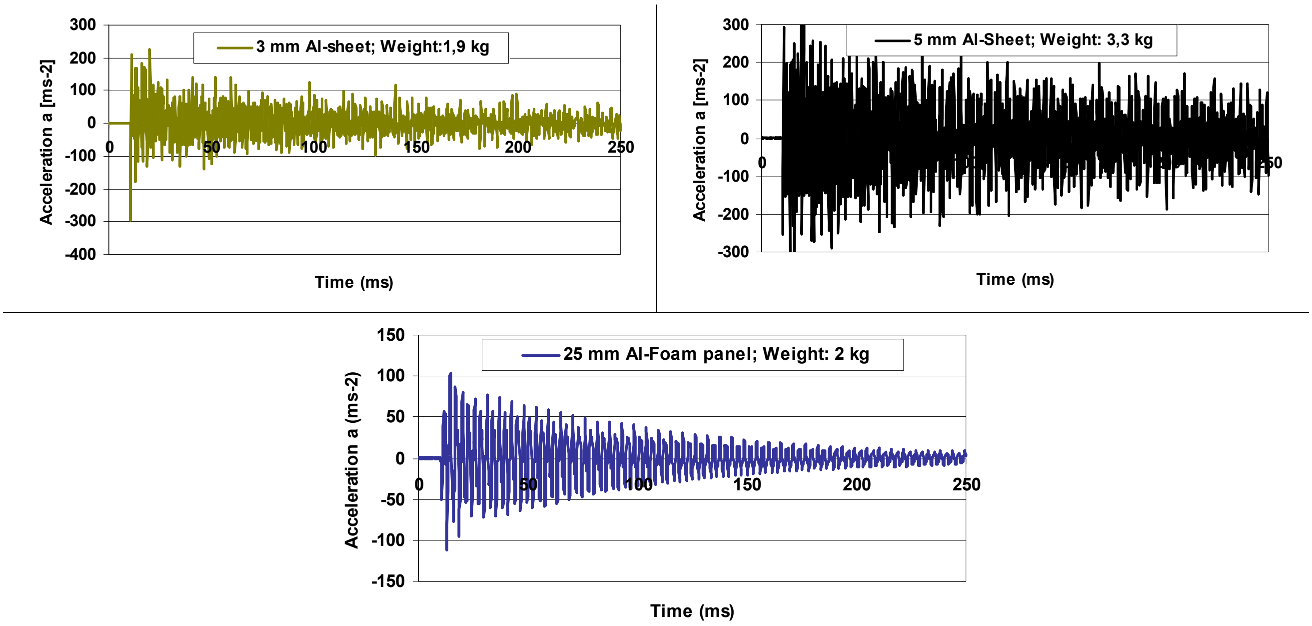

Figure 11: Time vs. surface acceleration dependance, ability to damp vibration after impact by impact hammer;

Conclusion

The damping ability of the aluminium foam structure is very important property which will strongly reduce the noise induced by vibrations. Together with above mentioned good stiffness-to-weight ratio as well as crash absorption efficiency aluminium foam seems to be suitable for new progressive applications focused on lightness, passive safety and comfort improvement. Recent state of art in foaming technology is already able to produce complex 3-

D prototype parts at reasonable price and time. The difficulties with joining of foams to other materials can nowadays also be overcome by in-situ foaming of bulk Al-inserts, which offer the possibility to cut threads or perform welding. Even and oil tight surface for i.e. sealing can be obtained in this way as well. However, significant reduction of manufacturing costs of aluminium foams still remains the main objective of further development activities regarding their wide industrial application.

References

[1] Jaroslav Kováčik, František Simančík, Jaroslav Jerz, Peter Tobolka: REINFORCED ALUMINIUM FOAMS; Institute of Materials and Machine Mechanics, Slovak Academy of Sciences, Bratislava, Slovakia; International Conference "ADVANCED METALLIC MATERIALS" 5 – 7 November, 2003, Smolenice, Slovakia

[2] František Simančík; R.Florek: Reinforced aluminium foams – promising solution for lightweight load-bearing parts; Institute of Materials and Machine Mechanics, Slovak Academy of Sciences, Bratislava, Slovakia - International Conference Metfoam 2005, 21-23.9.2005 Kyoto; Japan

[3] N.J. Oosting; J. Hennessy; D. T. Hanner; D. Fang: Application of a constrained layer damping treatment to a cast aluminium V6 engine front cover - Roush Industries Inc; General Motors corp. – 2005-01-2286 (SAE international 2004)

[4] P. Tobolka; F.Simančík: Meranie elastických a tlmiacich vlastností ohybovo kmitajúcej vzorky z hliníkovej peny; UMMS SAV, Bratislava; Konferencia: Experimentálna mechanika – aplikovaná optika 10-11. 10. 1995, Kočovce

11. Savjetovanje o materijalima, tehnologijama, trenju i trošenju
11. Conference on Materials, Processes, Friction and Wear
MATRIB'06, Vela Luka, 22-24.06.2006.

MEHANIČKA SVOJSTVA I MIKROSTRUKTURA 42CrMo ČELIKA

MECHANICAL PROPERTIES AND MICROSTRUCTURE OF 42CrMo STEEL

Mirko Gojić[1], Ladislav Kosec[2] i Stjepan Kožuh[1]

[1] Metalurški fakultet Sisak, Aleja narodnih heroja 3, 44103 Sisak
[2] Naravoslovnotehniška fakulteta, Univerza v Ljubljani, Aškerčeva 12, 1000 Ljubljana

[1] Faculty of Metallurgy, University of Zagreb, Aleja narodnih heroja 3, 44103 Sisak, Croatia
[2] Faculty of Natural Sciences and Enginnering, University of Ljubljana, Aškerčeva 12,
1000 Ljubljana, Slovenia

Sažetak: U radu su prikazani rezultati ispitivanja mehaničkih svojstava i mikrostrukture cijevi iz niskolegiranog krom-molibdenskog čelika. Čelik dobiven u industrijskim uvjetima valjan je u toplovaljane bešavne cijevi (promjera 159 mm i debljine stijenke 8 mm). Nakon toga cijevi su se postupkom hladnog pilgerovanja reducirale na vanjski promjer 130 mm i debljinu stijenke 6,2 mm te su odžarene na 700^{o}C u peći pod zaštitnom atmosferom. Mehanička i mikrostrukturna analiza provedene su na uzorcima nakon žarenja. Mikrostruktura je analizirana pretražnom elektronskom mikroskopijom (SEM) uz primjenu energetsko disperzijske spektralne analize. Utvrđena je bainitna mikrostruktura s izlučenim karbidnim česticama cementitnog tipa. Oko pukotina uz vanjsku stijenku cijevi zapažena je prisutnost kompleksnih oksidnih uključaka.

Ključne riječi: čelik, mikrostruktura, mehanička svojstva, karbidi

Abstract: In this work the results both of mechanical properties and microstructure pipes made from low-alloyed chromium-molybdenum steel are shown. The steel obtained in industrial conditions was rolled in hot-rolled seamless pipes (diameter of 159 mm and wall thickness of of 8 mm). After that the pipes are reduced up to the diameter of 130 mm and wall thickness of 6,2 mm by cold pilgern procedure. The pipes are annealed at 700^{o}C in the furnace with protective atmosphere. After annealing the mechanical properties and microstructural testing were carried out. Microstructure was analysed by scanning electron microscope (SEM) using energy dispersive spectrum analysis. Bainite microstructure with precipitated carbide particles of cementite type are founded. About cracks near to the outher thickness observed the presence of complex nonmetallic inclusions.

Key words: steel, microstructure, mechanical properties, carbides

UVOD

Niskolegirani krom-molibdenski čelici zbog svojih odličnih svojstava imaju široko područje primjene [1-3]. Primarno se koriste za izradu različitih strojnih dijelova čija se toplinska obrada najčešće sastoji od kaljenja i popuštanja [4]. Iz 42CrMo4 čelika izrađuju se i različiti cijevni proizvodi, koji se najčešće isporučuju u žarenom stanju. Da bi se postigla zadovoljavajuća svojstva prema tehničkim uvjetima kupca često se kombinira hladna prerada cijevi i njihova toplinska obrada. Stoga su u ovom radu navedeni rezultati istraživanja mehaničkih svojstava i mikrostrukture cijevi nakon postupka hladnog pilgerovanja i žarenja u industrijskim uvjetima.

EKSPERIMENTALNI DIO

Izrada taline za eksperimentalni dio ovog rada provedena je u čeličani Željezare Sisak. Talina niskolegiraniog Cr-Mo čelika oznake Č4732 proizvedena je u 30-t elektrolučnoj peći (tablica 1). Uložak (format 276) je zagrijavan u kružnoj peći (I zona=900^{o}C, II zona=1270^{o}C i III zona=1260^{o}C) u vremenu od 6 sati i 40 minuta. Postupkom toplog valjanja dobivene su cijevi koje su nakon valjanja imale vanjski promjer od 159 mm i debljinu stijenke 8 mm. Poslije toplog valjanja cijevi su hladno pilgerovane na ϕ130 mm i debljinu stijenke 6,2 mm. Određivanje mehaničkih svojstava je provedeno na Instron kidalici. Udarna radnja loma u uzdužnom smjeru valjanja je provedena na standardnim uzorcima Charpy metodom kod sobne temperature. Tvrdoća uzoraka ispitana je Brinell metodom. Mikrostrukturna analiza odabranih uzoraka provedena je skenirajućim elektronskim mikroskopom (SEM) JEOL JSM-5610 i EDS IXRF SISTEMS Inc. 500 pri naponu od 50 kV. Korišteni SEM omogućava i energetsku x-ray spektrometriju (EDS).

Tablica 1. Kemijski sastav čelika, mas.%.

C	Mn	P	S	Si	Cu	V	Mo	Cr	Al	Sn	Ni
0,39	0,80	0,010	0,019	0,28	0,22	0,01	0,24	1,19	0,03	0,011	0,08

REZULTATI I DISKUSIJA

U tablici 2 navedene su srednje vrijednosti mehaničkih svojstava nakon toplog valjanja te nakon hladnog pilgerovanja i žarenja na 700^{o}C. Vrijednosti granice razvlačenja i vlačne čvrstoće su relativno visoke nakon toplog valjanja. Nakon hladnog valjanja one su se još i povećale. Nakon žarenja u prolaznoj peći s brzinom od 10 m/h postignuta su mehanička svojstva cijevi prema traženim tehničkim uvjetima kupca. Mikrostruktura cijevi u uzdužnom i poprečnom smjeru je bainitna s izlučenim karbidnim česticama cementitnog tipa (slika1). Sastav miješanog cementitnog karbida je: 64,52 mas. % Fe – 0,74 mas. % Cr – 33,10 mas. % C. U neposrednoj blizini vanjske površine hladno pilgerovanih cijevi zapažene su pukotine (slke 2 i 3). EDS analiza je pokazala da je vjerojatni početak nastajanja pukotina na nemetalnim oksidnim uključcima sastava: 63,21 mas. % Fe – 27,56 mas. % O, te 70,47 mas. % Fe – 14,02 mas. % O.

Tablica 2. Rezultati mehaničkih svojstava cijevi

Stanje cijevi	Granica razvlačenja, MPa	Vlačna čvrstoća, MPa	Istezanje, %	Udarna radnja loma, J	Tvrdoća, HB
Toplovaljano	701	1062	10,5	5,3	341
Žareno	584	829	15,1		

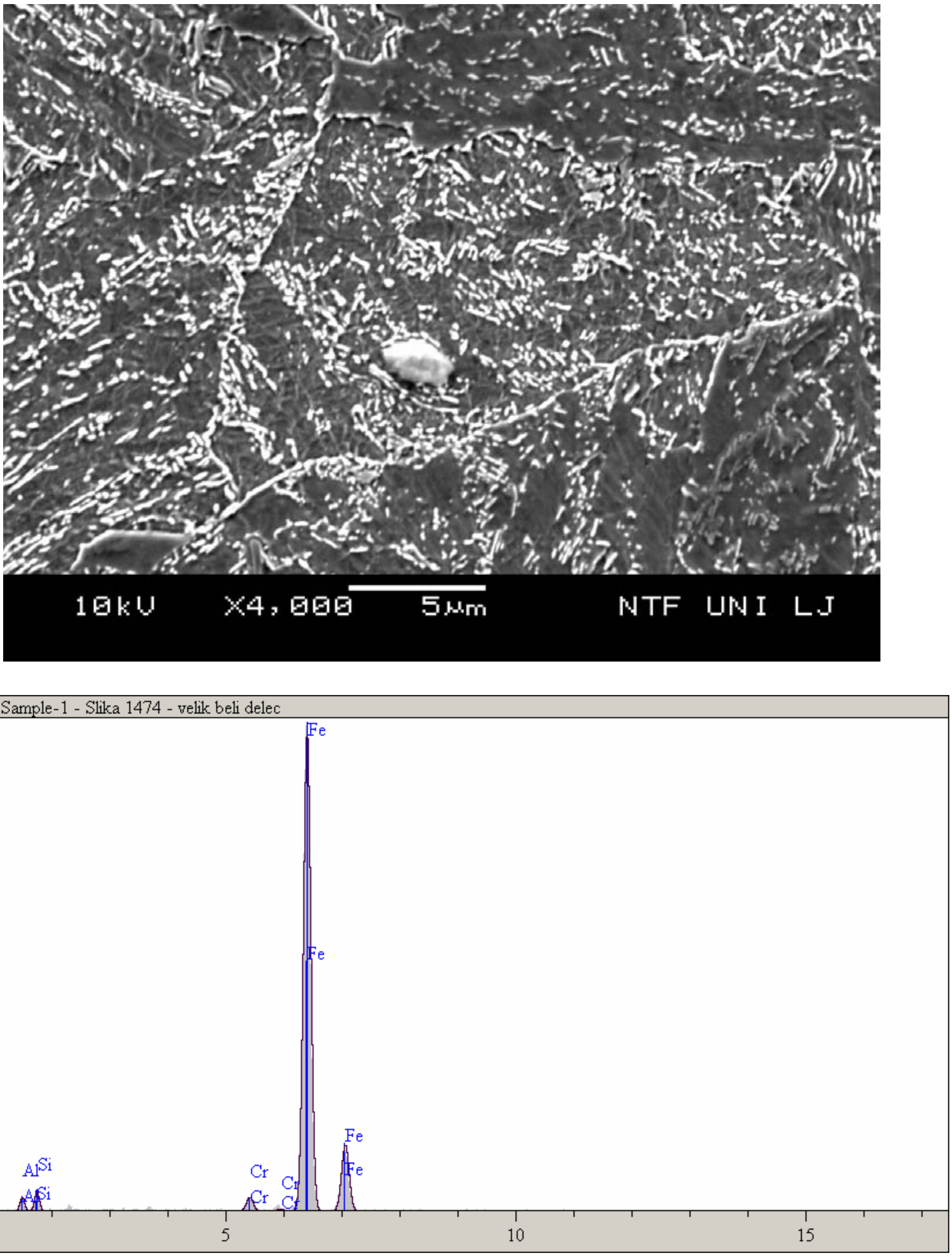

Slika 1. SEM mikrostrukturni snimak s odgovarajućim EDS spektrom karbidne čestice

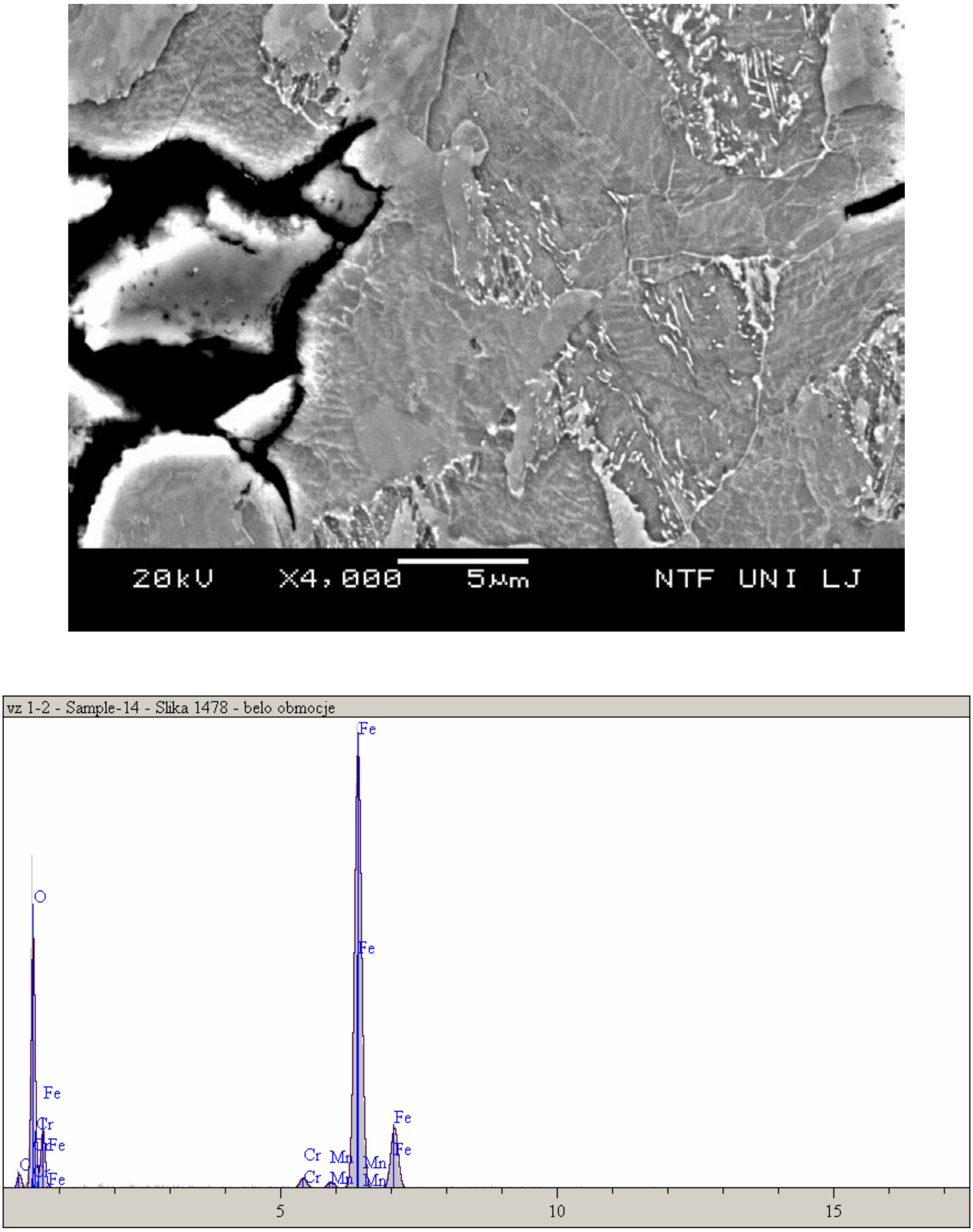

Slika 2. SEM mikrostrukturni snimak blizu vanjske površine cijevi s odgovarajućim EDS spektrom nemetalnog uključka, pozicija 1

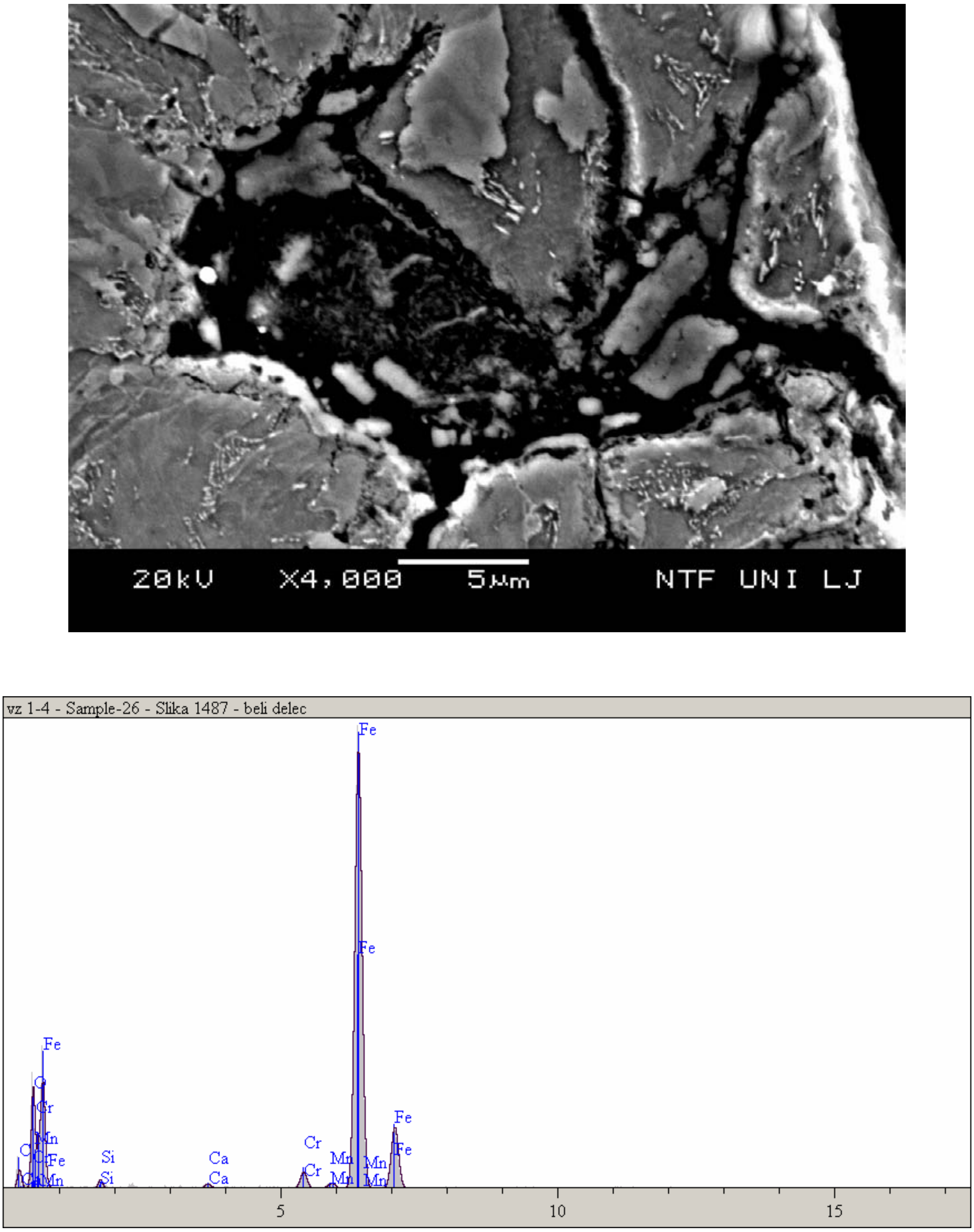

Slika 3. SEM mikrostrukturni snimak blizu vanjske površine cijevi s odgovarajućim EDS spektrom nemetalnog uključka, pozicija 2

ZAKLJUČAK

Na temelju provedenih istraživanja na cijevima iz niskolegiranog CrMo čelika može se zaključiti sljedeće:

1. Postignuta mehanička svojstva cijevi nakon hladnog pilgerovanja i žarenja na 700°C zadovoljavaju propisanim tehničkim uvjetima kupca.
2. Mikrostruktura cijevi je bainitna s izlučenim karbidnim česticama cementitnog tipa.
3. Na određenom broju cijevi u blizini vanjske površine zapažena je pojava pukotina. EDS analizom je utvrđeno da je raspucavanje započelo na međupovršinama nemetalni uključci/metalna osnova.

LITERATURA

[1] T. Filetin, F. Kovačiček, J. Indof: Svojstva i primjena materijala, Fakultet strojarstva i brodogradnje, Zagreb, 2002.
[2] M. Gojić: The Effect of Tempering on Mechanical Properties of Cold-Rolled 42CrMo4 Steel Pipes, Kovové Materiály, 39 (2001) 2, 85-92.
[3] M. Gojić, L. Kosec, P. Matković: The Effect of Tempering Temperature on Mechanical Properties and Microstructure of Low Alloy Cr and CrMo Steels, Journals of Materials Science, 33 (1998) 2, 395-403.
[4] V. E. Thelning: Steel and its Heat Treatment, Butterworths, London, 1984.

11. Savjetovanje o materijalima, tehnologijama, trenju i trošenju
11. Conference on Materials, Processes, Friction and Wear
MATRIB'06, Vela Luka, 22-24.06.2006.

THE GENERAL OVERVIEW ON TITAN AND ITS ALLOYS, PHYSICAL, MECHANICAL CHARACTERISTICS AND THE USE OF TITAN AND ITS ALLOYS

Lutvo Haznadarević, MA.Sci.
„Džemal Bijedić" University of Mostar, Faculty of Mechanical Engineering
USRC "Midhat Hujdur Hujka", 88104 Mostar, BiH

Abstract: We decided to give the general overview on a common phenomenon of titan, to analyze its physical and mechanical characteristics in a comparison to characteristics of other the most frequent constructive materials in use (aluminium, copper, iron, magnesium, nickel). The main reason for that is the notable growth of the use of titan and its alloys. This work deals with the basic aspects and reasons for the use of titan alloys what is given in short overview.

Key words: titan and its alloys, physical and mechanical characteristics, the use of titan alloys.

1. INTRODUCTION

Titan is the ninth element on Earth cortex, considering its spreading, and it takes 0,6% of the Earth cortex. On the level of constructive metals and their spreading, titan takes the fourth place and comes after aluminium, magnesium and iron, but it s spread is higher than the one of chromium, nickel, copper, lead and many other metals. Raw materials obtained from titan are very much spread and they provide lengthy exploitation. The most important minerals of titan for the commercial purpose are: ailment – $FeO–TiO_2$ and retile TiO_2.

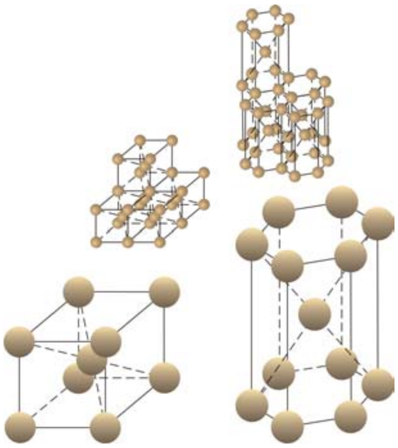

Alpha: a = 2,9504 A C = 4,683 A c/a = 1,587
Beta: a = 3,3065 A

Picture no.1. Crystal grids of titan modifications

Advanced titan production process was necessary because of its affinity for oxygen, nitrogen and carbon. Titan produces reaction with these elements, but it even melts them in considerable quantity while it is in a liquid state, and a high quantity of nitrogen and oxygen keeps in a hard solution, as well. Titan also produces tumultuous reaction with a high number of fire-proof oxides in a condition of rising temperature.

Rapid growth of titan metallurgy began with the invention of Kroll's process in 1939. By Kroll's process, titan has been given by reduction of titanchlorida $TiCl_4$ with the help of magnesium. Tetrachloride can be easily got from ore by process with neutral atmosphere in iron pot.

Reduction with the help of magnesium gives titan with a different cleanliness and it depends on operative conditions. Oxygen and nitrogen are the most common contamination of air and iron in the pot in which the reaction is produced. Usual percentage of contamination is: 0,05÷0,25% for the air 0,01÷0,20 for nitrogen and 0,05÷0,25 for iron. Titan got on this way "spongy titan" is not good for the practical use, but in order to refine it further titan has been pressed into joists and has been exposed to the process electrolytic divergence or melting in electrical stoves with the highly power vacuum. Such titan is relatively clean of oxygen and nitrogen, but it can have some kind of metal contamination.

Titan belongs to the fourth group of periodic table. Ordinal numeral of titan is 22, atomic weight is 47,9, atomic volume is 10,64 cm^3/g atom, radius of atom 1,46 Å.

There are two allotropically titan modifications: a low-temperature modification (alpha) with a hexagon solid plumped grid that is stable to the temperature of 1155 K and a high-temperature modification (beta) with a cubic grid centered in the area and that is stable on the temperature above 1155 K.

Titan goes through the one polymorphous change on a temperature of 1155 K while the crystal grid is being changed, or it can be said that it comes alpha – beta transformation. During this kind of transformation the change of volume is insignificant and the sum is 0,1 %. The speed of cooling has no influence on a formation of alpha grid while titan is technically and commercially clean during beta-alpha transformation and we can conclude that clean titan cannot be exposed to the thermo process.

2. Physical characteristics of clean titan

Titan has a high melting point, but it is not suitable for the use in a condition of high temperature exposed to the air because of his tendency to the absorption of nitrogen and oxygen on a temperature above 946 K.

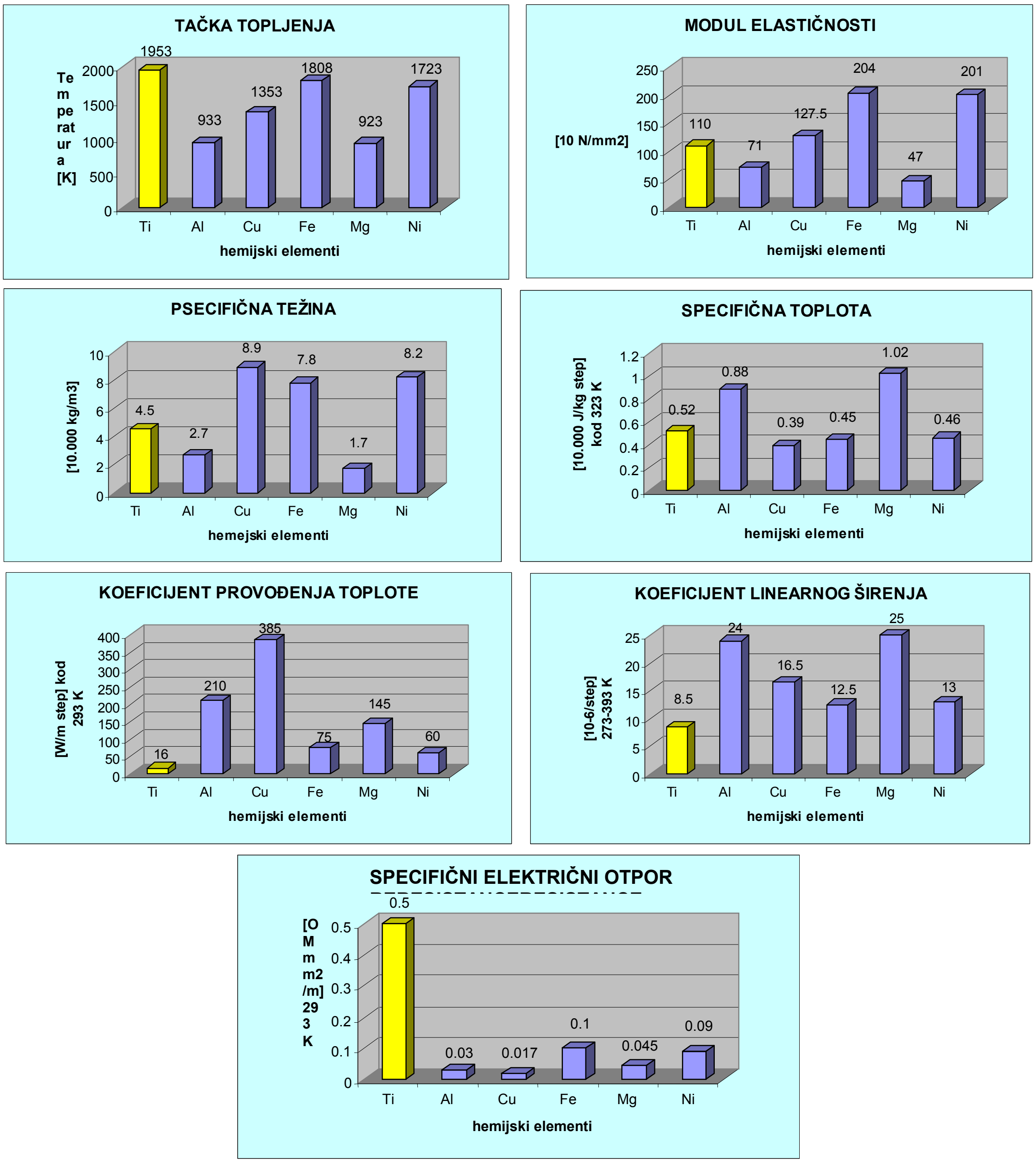

Picture no. 1.2. Physical characteristics of the most common used constructive metals

Clean titan is not good as a constructive metal. The reason is his relative softness and flexibility in such a condition. Titan with the commercial quality that contains certain quantity of inter-crystal elements, such as oxygen, nitrogen is much stronger and it can serve as a good constructive material. Electrical and thermal conductivity are quite low, and it is unsuitable in use on objects that need thermal or electrical conductivity.

Low coefficient of thermal expansion enables its use in constructions with periodical thermal fluctuation. Titan is closer to the light metals with its specific weight up to 4,5 gr/cm, until it is closer to stainless steel by its thermal and electrical characteristics. Titan is non-magnetic, what is advantage in its use in geophysics and at electrical conections.

3. Mechanical characteristics of titan that is clean technically

Clean titan is relatively soft and elastic. In such a clean condition titan is not suitable as a constructive material. Titan with commercial quality that contains certain quantity of inter-crystal elements as an oxygen, nitrogen and carbon is stronger and can serve as a good constructive material. Mechanical characteristics of titan first of all depend on cleanliness; on quantity of admixtures after ekstraction. Today we have production of clean titan and titan with commercial quality that ca be either low or high hardness.

Mechanical characteristics of titan depend on quantity of elements that are melted on an inter-crystal way such as carbon, oxygen and nitrogen. This is shown on the picture no. 1.8.

Titan has high affinity to hydrogen, oxygen and nitrogen and it is not suitable for the use in the condition oh high temperatures. Oxide film is being formed on unalloyed titan below the temperature of 773 K and that film reduces intensity of oxidation in a certain time period. This protective film is being destroyed above the temperature of 773 K and oxygen brakes through it, than oxygen makes duration of a construction smaller very soon.

Protective film is being formed in the big part of titan alloys, so the stability is bigger or the same to the one of unalloyed metal. In order to use titan on a temperature above 773 K, before that must be formed stabile film of oxide. Maximal temperature for the constant work is 623 K, and the one for the part-time work is 1273 K, which is the temperature of final limit. Alloys of titan have established relationship of hardness and specific weight.

Titan with commercial quality is generally ductile And is not insensible on cuts, but sharp cuts make ductility smaller on a low temperatures. Alpha alloys have smaller ductility and they are more sensitive on a cuts' appearance. Alpha – beta alloys in a condition of live coals conduct like iron. They are suitable for the use in a condition of stale air-temperature and they become sensitive on lower temperatures. Alpha – beta alloys are sensitive on cut if they are in a state of thermo process, especially with hardness above 100 (N/mm^2). Sensitivity on cuts depends on presence some of interstictions Alloyed elements. Carbon, nitrogen and oxygen are little dangerous, but hydrogen is highly dangerous, especially on a temperature below 373 K.

Striking toughness is the most effective test for a determination of a level of tendency to a hard trash.

It is noticed that by getting the temperature lower it does not come to the rush fall of toughness even it is noticed mild growth of soft sorts. The content of hydrogen of 200 ppm may cause low toughness. Titan with commercial quality has the content of hydrogen to 200 ppm. Titan and alloys used for a work in a condition of low temperatures, as for equipment of titan for underwater research must have higher striking toughness than titan for other use. Titan with an exceptionally low content of interstictions Alloyed elements are being produced for this kind of use.

Table 1.2. The basic mechanical characteristics of the clean and commercial titan

Characteristic	Clean titan	Commercial titan	
		Low hardness	High hardness
Elasticity module (10 N/mm^2)	11.000	11.000	11.000
Skating module (N/mm^2)	45000	45000	45000
Tighten hardness (10 N/mm^2)	20-30	45-55	60-70
Limit of stretching (10 N/mm^2)	12-18	30-40	50-60

Characteristic	Clean titan	Commercial titan	
		Low hardness	High hardness
Extension (%)	40-60	20-30	20-25
Reduction of cutting (%)	70-90	40-70	40-50
Hardness (HV)	80-100	160-180	200-220
Striking toughness (10 N/cm^2)	4-12	4-12	4-12

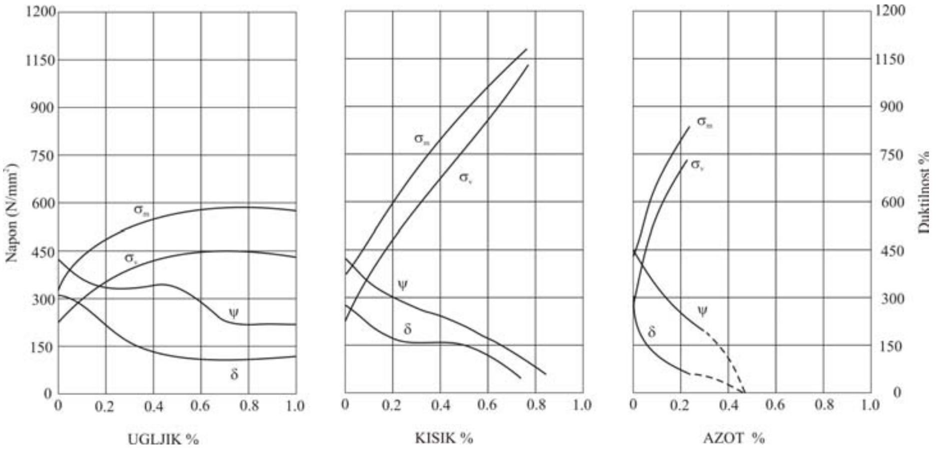

σ_m – tighten hardness δ - Relatively expansion

σ_v – limit of stretching ψ - Relatively narrowing

Picture 1.8. Influence of oxygen, carbon and nitrogen on the mechanical characteristics of titan

Mechanical characteristics of titan and its alloys fall down while the contamination and oxidation are in a condition of high temperatures (Picture no.1.5.).

Influence of interstictions alloyed elements is very important especially in a construction of welded elements of titan. Influence of hydrogen is very expressive during the all phases of process for construction of one machine of titan, beginning from cleaning and further to the final processing. The content of hydrogen in the alloys of commercial quality has not important influence on tighten hardness, but its presence is one of the basic reasons for the appearance of hard break during the striking action. The content of hydrogen in titan sheets can become partly lower by stirring in vacuum stoves. In alloys of titan of aluminium and tin can be tolerated bigger content of hydrogen than in titan with commercial quality. Carbon, oxygen and nitrogen appear themselves as backward tilt in all alloys of titan as well as in commercial clean titan.

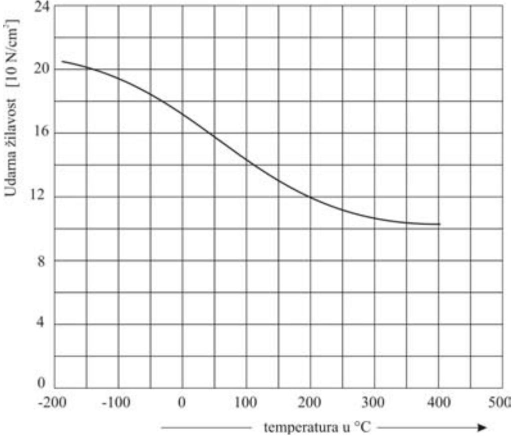

1.9.

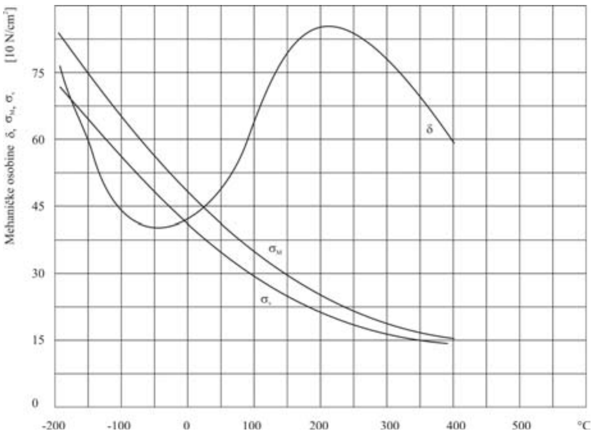

1.10.

Picture 1.9. Dependence of striking toughness on temperature by unalloyed titan

Picture 1.10. Influence of temperature on mechanical characteristics of titan with commercial quality

4. The use of titan and its alloys

We find titan in all usual ways of delivery of metal such as sheet metal, pipes, rods, wires, unchained pieces, etc. Chemical and petrochemical industry, refineries, food industry, plastic industry, aerial, rocket and nuclear industry use titan more and more as a constructive material. Titan is known to the big part of producers of dishes under pressure.

Chlorine atmosphere – tile and pipe products of a change, spiral pipes, valves, pumps, dishes and pipelines that work in (exceptional corrosive stability in moist chlorine).

See water – tile and pipe products of change, sailor's condensers and condensers in energetic factories, pumps, pipelines and metal frameworks, submarine weapon, yacht's and submarine's equipment (exceptional corrosive and erosive stability and hardness in a clean and polluted see water, even if it is the case oh high content of firm substance).

Metal chloride – tile and pipe products of change in dishes, pipelines, pumps and metal frameworks for the work with Fero-chloride and chloride of other metals, evaporators of salt water with NaCl and KCl, platinum – titan anode (chemical and electro-chemical corrosive resistance).

Nitric acid – tile and pipe products of change in dishes, pipelines, pumps, metal frameworks (corrosive stability in all kinds of concentration except in puny acid).

Oxidized acid – dishes and pipelines (corrosive stability).

Reductive acid: sulfuric acidsumporna, hydrogen chloride acid – dishes and pipelines (exceptional corrosive stability).

Whitening liquid hypo chloride chlorine dioxide – warehouses, rollers, elements of heating (corrosive stability higher than the one of black steel, especially in paper mush and factories for the textile whitening).

Artificial fertilizers pesticide – the parts of equipment (corrosive stability in nitric acid, ammonium nitrate, in a complex organic pesticide and herbicide).

Factories for the artificial fiber, terilen, nylon and liquid cellophane – a different parts of machine (corrosive stability).

Food industry, soups, vegetables, juices – different parts of machine (corrosive stability and prevention of product's contamination).

Color’s production – dishes, spiral pipes, the things that cause the change in temperatures (corrosive stability and avoiding of contamination, it is being used solely in a presence of hydrogen chloride acid or sulfuric acid).

Sulfur, sulfur dioxide – gas filter, lines (corrosive stability).

Pharmaceutical industry – different parts of equipment (corrosive stability, prevention of product's contamination).

Human body – surgical implants – prosthesis (the relationship between hardness and weight, corrosive stability, unpoisonousness).

Solutions for production of layers of and polished solutions - tanks, tubs, spirals, traps (electro-chemical corrosive stability).

Electrical equipment – different parts, bipods, grids, components of the ionic pump (unmagnetic and electrical characteristics plus absorption of oxygen).

Armament – bulletproof vests and helmets (mechanical characteristics).

Automobile industry „sport's cars“ –oscillated parts, connecting rod, framework capacity, coils (high hardness).

Equipment foe under water research – parts of equipment (high hardness and corrosive stability).

Turbine – disks and shoulder blade (high hardness, small specific mass).

Pumps and propellers for a great speed – rotated parts (high hardness and corrosive resistance and erosion in the sea water).

Conclusion

Titan becomes more and more explored constructive material because of its good physical and mechanical characteristics. The following table will show advantage and disadvantage of Ti alloys.

Advantages	Disadvantages
✓ The fourth place considering its spread between constructive elements ✓ Ductile, insensible on cuts ✓ Corrosive stability ✓ High resistance on erosion ✓ Relationship between hardness and weight ✓ It is not magnetic	✓ Tempestuous reaction of titan on high temperature with the big part of fireproof oxide (above 946 K) ✓ Clean Ti can not be used because of Ti flexibility and softness ✓ Conductor of electricity and thermal capacity is low ✓ With a temperature growth there is rush fall of Ti mechanical characteristics

LITERATURE

[1] Jovičevič M.: *Osvrt na istraživanja procesa obrade brušenjem*, Saopštenje IAMA, br. 18, 1973.
[2] Werner G.: *Influence of Work material on Grinding Forces*, Anaals of CIRP, Vol. 27/1, 1978.
[3] Zdenković R.: *Obrada metala skidanjem.* Sveučilište u Zagrebu, FSB, Zagreb, 1976.
[4] Cebalo R.: *Verbessern der Schleifqualität durch geeignetes Abrichten*, Werkstaat und Betrieb 123 (1990) 10.
[5] Cebalo R.: *Suvremena tehnologija brušenja – Priručnik oznaka jedinica i pojmova*, Vlastito izdanje, Zagreb, 1993.
[6] Cebalo R.: *Optimalno područje brušenja u puno vatrootpornih Ni-legura za plinske turbine*, Doktorska disertacija, Zagreb, 1985.
[7] Haznadarević L., Mijanović K.: *Appendix to the study of thermal condition by process of grinding*, Naučni skup "MATRIB '05", Vela Luka, 2005.

11. Savjetovanje o materijalima, tehnologijama, trenju i trošenju
11. Conference on Materials, Processes, Friction and Wear
MATRIB'06, Vela Luka, 22-24.06.2006.

THE ROLE AND FUTURE OF NANOTECHNOLOGY IN RESEARCH, INDUSTRY AND EDUCATION

David. M. Kennedy
Department of Mechanical Engineering
Dublin Institute of Technology
David.kennedy@dit.ie

Abstract: Major developments in Nanotechnology have taken place across the world over the last few years. From a humble beginning, Ireland inc. became a leader in the Microelectronics industry and now has to face the challenge of developing a strategic plan to maintain its lead position in the nano field which in most cases will supersede the micro phase. Most countries are taking a similar path of development all be it alone or in collaboration with other countries. This process is expensive and requires market drivers and experts to lead and deliver demands from the industries of the future. The approach may be driven from a top down or bottom up, i.e. from macro to micro to nano or from sub nano to nano components and machines. What are the development areas and implications for nano Biotechnology, nanoelectronics and nanomaterials, how are the industries developing and how are we educating our undergraduates and postgraduates in this technology. This paper will discuss some of the key areas of development and the associated industries and research centres and how the knowledge may be transferred to our educational programmes.

The paper provides a summary of the work developed in a number of key reports on Nanotechnology [1-3], combined with the authors views and opinions on developments in the nanotechnology field.

Keywords: Nanotechnology, Biomaterials, Nanomaterials,

1 Introduction

Nanotechnology is a term to define a wide range of technologies concerned with structures and processes on the scale of a nanometer (one billionth of a meter, 10^{-9}m). It is a collective term for a set of tools and techniques that permit the atoms and molecules that comprise all matter to be manipulated. Nanoscience and nanotechnology are new approaches to research and development that aim to control the fundamental structure and behaviour of matter at the level of atoms and molecules. Applications of nanotechnology are emerging and will impact on the life of every citizen. Nanoengineering represents the extension of the engineering fields into the nano- scale realm (nanofabrication, nanodevices, etc.) and concerns itself with the fabrication of objects which are anywhere from hundreds to tens of nanometers in size.

Nanoscience is the science for nanotechnology. Materials produced on a nanometer scale behave differently from the same materials produced on a larger scale. Nanotechnology is therefore regarded as a key technology which will not only influence technological development in the near future, but may also have decisive economic, ecological and social implications.

Using nanotechnology tools and techniques, it is possible to exploit the size-dependent properties of materials structured on the sub-100 nanometer scale, which may be assembled and organised to yield nanodevices and nanosystems that possess new or improved properties. These tools and techniques, materials, devices and systems present companies in all sectors of the Irish economy with opportunities to enhance their competitiveness by developing new and improved products and processes[4]. Nanotechnology is also an enabling technology which can impact on other fields leading to new developments and challenges (examples range from enabling efficient thermal to electrical energy conversion systems to enabling molecular manufacture on an industrial scale). Table 1. gives a brief summary of the history and innovations in nanotechnology.

1931 Knoll and Ruska develop the electron microscope – subnanometer imaging
1959 Richard Feynman "There's plenty of room at the bottom" – concept of atomic engineering
1968 Cho and Arthur, Bell Labs – technique to deposit single atomic layers on a Surface
1974 Taniguchi coins the word "nanotechnology" – machining less than a micron Tolerance
1981 Binnig and Rohrer invent the Scanning Tunnelling Microscope – ability to image and drag individual atoms
1985 Curl, Kroto and Smalley discover "buckeyballs" – nanometer in diameter
1986 Drexler publishes "Engines of Creation" –
1989 Eigler writes the letters IBM - using individual xenon atoms
1991 Iijima, NEC – discovers carbon nanotubes
1993 Robinett and Williams connect a VR system to an STM – see and touch Atoms
1998 Dekker, Delft University - creates a transistor from a carbon nanotube
1999 Tour and Reed - demonstrate how single molecules can act as switches
2000 Clinton administration announces the National Nanotech Initiative (NTI) – large funding ($497m) and increased visibility
2000 Eigler creates a quantum mirage – possible means of transmittimg information without wires
2001 Scientific America issues special Nanotech report
2002 Bush administration and congress give $604.4m budget to NTI
2003 NTI budget increased to $679m, $180m going to Dept. of Defence

Table 1. The History of Ten to the Power of Minus Nine

2. Terminology

NanoBiotechnology is an interdisciplinary field of research based on the cooperative work of chemists, physicists, biologists, medical doctors and engineers. At the interface between biotechnology and nanotechnology, nanobiotechnologists carry out research on the phenomena of self-assembly or self-organisation of biomolecules such as cell membranes or virus particles, in order to adapt these principles to the technical production of nanostructures.

Nano-to-Bio designates the use of nanotechnological tools to study the molecular mechanisms behind various biological processes at the single molecule level. From this perspective, nanoanalysis, nanomanipulation techniques for biological structures and objects, nanotechnologically produced active ingredients for living organisms, nanocarriers for transporting active ingredients, nanomachines, nanobots for research, diagnostics and therapy, nanotechnologically coated implants and nanoelectronic (particularly neurological) implants are possible applications.

Bio-to-Nano refers to bio(techno)logical materials and designs for producing technical nanosystems. These could be exploited in information and communication, energy, environment and many other areas for technical applications. These include e.g. nanotechnology applications based on biological paradigms (biomimetics), the use of biological components on the nanometer scale for technical systems, or nanoelectronics and nanoinformatics using biological components, functional or organisational principles. Nanotechnology and nanoscience are seen as;

(i) dealing with structures smaller than 100 nm in at least one dimension and
(ii) as describing the deliberate manufacture and/or manipulation of individual nanostructures.

Research into nanoS&T and its materials typically adopts one of two fundamental strategies:

(i) the “top-down” approach in which, starting from microtechnology, structures and components are more and more miniaturised. For example, components can be physically reduced in size through etching.
(ii) the “bottom-up” approach.

2.1 Top-down Fabrication

Top-down methods start with large area blocks of a material and carve out structures by selectively patterning and processing well-defined areas on the block surface. Continued miniaturisation of transistor devices over the last 40 years has resulted in exponential increases in both processor speed and also the number of transistors per chip (Moore’s Law), thus enabling greater functionality. Processor chips for modern PCs are fabricated using short wavelength (193 nm) light sources and optical lithography processes which produce transistors with feature sizes as small as 70 nm across wafer slices of silicon crystals up to 300 mm in diameter. These methods are amenable to mass manufacturing, which has resulted in reduced costs (per transistor) for high-end electronics products. However, exponentially increasing fabrication costs and fundamental physical limitations remain significant challenges for continued top-down miniaturisation over the next decade.

2.2 Bottom-Up Nanofabrication

Bottom-up processes use chemically- or biologically-inspired routes for synthesis and assembly of nanoscale building blocks into complex nano architectures with novel electronic or optical properties. Self- and directed-assembly mechanisms are often found in nature, from the growth of crystals to the formation of complex functional biotechnological systems – including the cells of the human body. The advantages of bottom-up processes include drastically reduced fabrication costs; however development of controlled assembly strategies for integration of bottom-up nanostructures and nanoarchitectures into electronic devices and circuits remains a significant long-term challenge. In the medium term, development of hybrid top-down/ bottom-up fabrication strategies for electronics represents a key opportunity.

3. Research Developments in Nanotechnology

Nanotechnology and Nanoscience can pervade virtually all technological sectors. The expected level of impact of nanotechnology on the various technology areas, are given in Figure 1. While nanoelectronics will be pervasive in all of the areas identified the level of impact will vary with the sector.

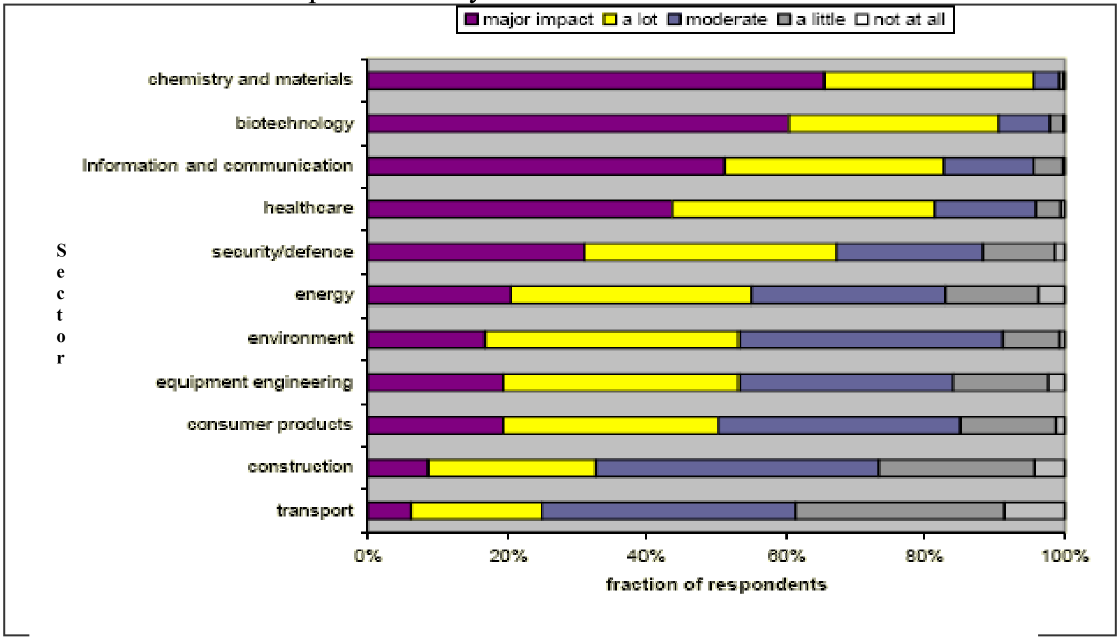

Figure 1. Expected impact of nanotechnology on economic sectors.

Figure 2. shows Japan's governmental nanotechnology budget by research field (fiscal 2001). The red and green areas indicate amounts for non-competitive national funds and competitive individual ones, respectively. Allocation of nanotechnology budgets by research field shows that basic technologies for metrology and manufacturing coupled with nanomaterials occupy some 50% of the total, indicating the government's resolve to strengthen Japan's position in the nanomaterials sector.

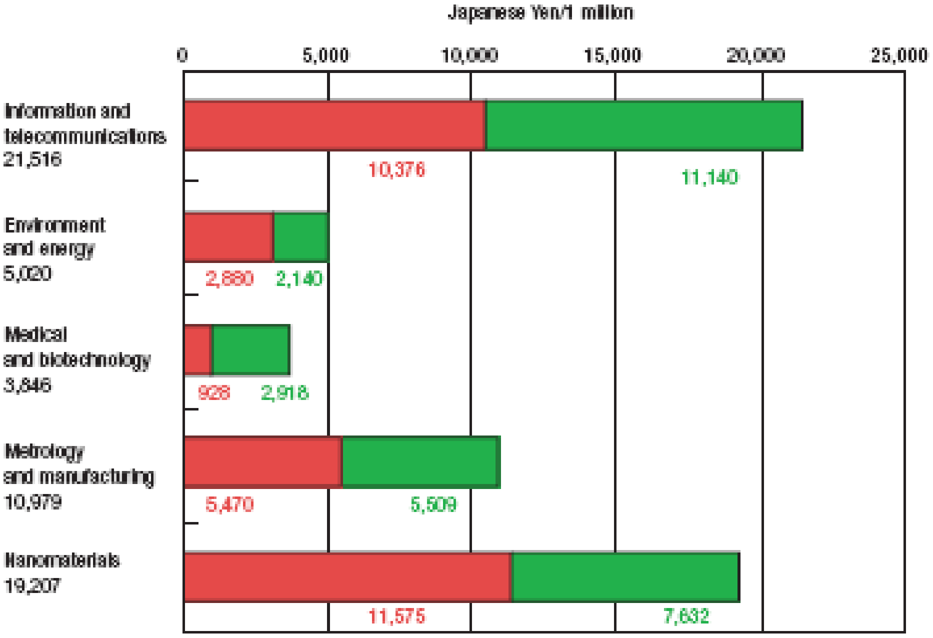

Figure 2. Japan's governmental nanotechnology budget by research field (2001).

Each **new technological generation** requires a steep increase in the level of investment needed to conduct research and build production plants – the European electronics industry currently spends 20% of turnover on research and a typical fabrication facility today costs around €2.5 billion.
NanoMarkets, a leading advanced technology analyst firm based in the US, forecasts that the market for nano-enabled electronics will reach US$10.8 billion (€8.6 billion) in 2007 and grow to US$82.5 billion (€66 billion) in 2011. Figure 3. shows the range of applications for nanotechnology in Europe.

EU infrastructure – activities by area

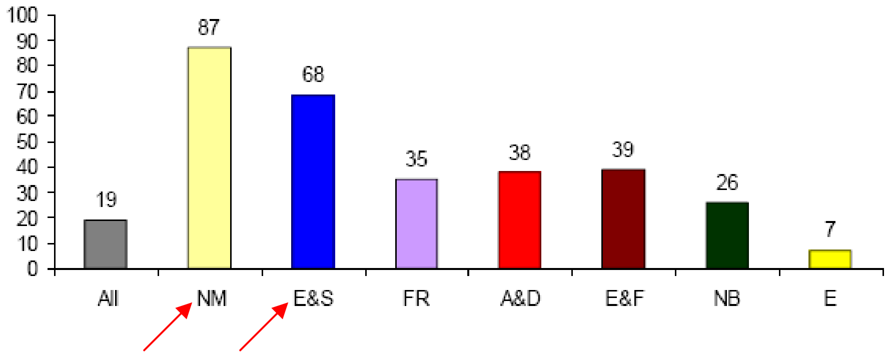

N&N infrastructure in the EU and associated states (by area): **NM** nanomaterials, **E&S** electronics and systems, **FR** fundamental research, **A&D** analytical and diagnostics, **E&F** engineering and fabrication, **NB** nanobiotechnology, **E** energy.

Figure 3. - Nanoscience and Nanotechnology infrastructure in the EU and associated states [7].

4.1 Industrial Applications

Atomic force microscope (AFM) technology (which can move single atoms about) is being used to create smaller and more sensitive microarrays for use in diagnostics and drug discovery. AFMs can also be used to nanostructure surfaces, and for example make them more biocompatible. Nanoparticles such as fullerenes, dendrimers, and quantum dots (complexes of semi-conductor material that have unique fluorescent properties) are being exploited in many areas including imaging such as enhancement of magnetic resonance imaging [MRI] and ultrasound and drug delivery.
Formulating drugs with nanoparticles can also improve their solubility. Many drugs are not marketed because they are not very water-soluble. Other problems concern ways to increase their resistance to stomach acid and enzymes (allowing better uptake from the small intestine), and allow controlled release (e.g. over days rather than minutes and hours). Nanotubes represent another mechanism for drug delivery, both as a "container" and potentially a system for "nano-injection" into cells.
In hyperthermic therapy, magnetic particles are covered with biological species and injected into cancerous areas. The molecular structure of the coating forces the cancer cells to absorb the particles, while the healthy cells do not. Using an external magnetic field, the particles are then activated, causing the cancer cells to heat up and die. This is one of the more promising treatments for cancer diseases over the next few decades. Nanocomposites of titanium alloys, for example, can be used to improve the

biocompatibility and longevity of surgical devices and implants. Nanostructuring surfaces can improve cellular attachment (e.g. etching surfaces with nanoscale grooves or using instruments such as an AFM to imprint surfaces with cell attachment molecules), and direct cells to grow into defined structures. By incorporating biodegradable polymers to act as a scaffolding, these structures can be assembled into 3-dimensional "tissues". Nanostructuring can also be used to provide an anti-microbial coating on implants. Antimicrobial agents based on nanomaterials (e.g. silver incorporated into polymer tubes or titanium dioxide coated surfaces) can be used to sterilise medical equipment or other items.

New medical treatments are expected over the medium time scale, e.g. self-organizing hollow spheres that will transport drugs in the bloodstream to a specific area of the body. External control may even be possible via an additional coupling of magnetic particles or antibodies. Drugs that are presently injected may be taken orally with the aid of nanomaterials. The potential of such nanoscale drug delivery systems is estimated at $50 million by 2007.

4.2 Food and Agriculture

Nanotechnology also has applications in the agri-food sector. Many vitamins and their precursors, such as carotinoids, are insoluble in water. However, when formulated as nanoparticles, these substances can easily be mixed with cold water, and their bioavailability in the human body also increases. Many lemonades and fruit juices contain these specially formulated additives, which often also provide an attractive colour. The world market potential of such micronized compounds is estimated at $1 billion. Bio and gas sensors could gain importance in food production. These sensors could be integrated into packaging materials to monitor the freshness of the food. Spoiling of the food could be indicated by a colour change of the sensor. Several concepts have already been developed for such applications based on silicon or polymer thin film sensors.

4.3 Energy and Environment

Energy research is increasingly important, particularly as regards the role it plays in support of a wide range of key EU policies. Nanotechnology shows promising potential in all segments of the energy sector: production, storage, distribution and use with the potential to change the way we convert, store and utilize the world's energy supply. Trends in nanotechnology will contribute to cleaner industrial production processes or products, mainly through reducing the use of raw materials and energy. Nanotechnology in conjunction with biotechnology and new materials research can help develop products that require less energy to recycle and produce.

Better energy generation, conservation and storage was identified as the most promising area of nanotechnology research in a survey of 63 specialists worldwide (April 2005). Energy research priorities are identified in the report of the interagency workshop on *Nanoscience Research for Energy Needs* (2004). Key areas include:

1. Highly selective catalysts for clean and energy efficient manufacturing;
2. Energy efficient, resource-saving building materials / lighting / glazing;
3. Nanocomposites for energy efficient vehicles and engines;
4. Low cost fuel cells and batteries;
5. Lightweight, efficient solar cells (power collectors and storage); and
6. More efficient (1 gigawatt) power transmission lines.

Renewable energy areas apart from solar cells include hydroturbines, wind turbines and biomass burners. Other opportunities occur in energy end-use – innovative building design, low consumption heating and lighting and smart energy controls.

While Ireland is not a global producer of energy, it has the potential to contribute in energy storage and transmission technologies through engineering and energy technologies.

4.4 Construction

Construction is important for the economy of Ireland. Construction output as a percentage of GNP had increased from 13 per cent in 1994 to over 20 per cent in 2001 and that level was sustained and even increased slightly to 21 per cent in 2003. In GDP terms, construction output was 18 per cent of GDP in 2003 (compared with an average of 10.4 per cent of GDP in 2003 for construction across Western Europe). The value of output in the construction industry in 2004 is estimated at € 28.2bn in 2004 , compared with €21.3bn in 2002.

Many applications of nanomaterials in construction derive from the distribution of nanoparticles in a ceramic, metallic or polymer matrix. Introducing nanoscale particles in metals improves the mechanical properties, which can contribute substantially to lightweight construction. Material properties such as hardness, compressive strength, ductility and wear resistance can be enhanced. Examples include:

1. Silicon dioxide nanoparticles in synthetic silicic acid (nanosilica) used as an additive for sprayed and high-performance concrete to help improve bond tensile strength and bond shear strength between concrete and reinforcing steel.
2. Nanometer multilayer coating from conducting polymers for corrosion protection of carbon steel or stainless steel construction materials.
3. Thermal insulation for buildings (e.g. windows with an invisible silver nanocoating forming a transparent thermal insulation)
4. Façade design (e.g. self-cleaning, anti-graffiti protection or high scratch and wear resistance in plastics through appropriate coatings) and
5. interior (e.g. titanium dioxide nanoparticle additives to coatings to protect from discoloration under artificial and natural light).

4.5 Electronics and ICT

Over 300 overseas ICT companies develop, market and manufacture a wide range of leading edge products in Ireland. 45,000 people are employed here by overseas companies alone (including IBM, Intel, Hewlett Packard, Dell and Microsoft). In 2003, Irish exports in this sector exceeded €21 billion, representing 26 per cent of all exports.

To date, much of the global nanotechnology activity in the electronics and ICT areas has been focused on miniaturisation of components but nanoelectronics and nanoengineering may also lead to new production processes including self assembly of circuits and systems. Areas of development in the industry include design and simulation of materials; synthesis, growth, deposition and processing of materials; high throughput characterization and analysis and device prototyping, integration and analysis. Materials feature in all of these, even potentially in the analysis and testing stages of prototyping.

Much of the miniaturisation of computer chips to date has involved nanoscience and nanotechnologies, and this is expected to continue in the short and medium term. The storage of data, using optical or magnetic properties to create memory, will also depend on advances in nanoscience and nanotechnologies.

Alternatives to silicon-based electronics are already being explored through nanoscience and nanotechnologies, for example plastic electronics for flexible display screens. Other nanoscale electronic devices currently being developed are sensors to detect chemicals in the environment, to check the edibility of foodstuffs, or to monitor the state of mechanical stresses within buildings. Much interest is also focused on quantum dots, semiconductor nanoparticles that can be ‘tuned’ to emit or absorb particular light colours for use in solar energy cells or fluorescent biological labels.

4.6 Materials for medical applications

Biomaterials and medical devices represent a fast emerging market that was estimated at about 260 billion € world-wide for the year 2000 alone, with Europe's share being about 30%. Biomaterials research in Europe is of very high quality and in strong competition with the USA who are still the world leader. On the other hand, Europe holds its position of excellence in specific areas like tissue engineering.

The new and active life-style of citizens and the ageing European population need multidisciplinary materials research, which are strongly oriented towards promising developments. An example is hybrid tissue engineering that can satisfy the ever-growing demand of tissue and organ replacements or repair avoiding dependence on human donors or xenotransplantation, and all related risks of rejection, infection or transmission of diseases.

Technologies aiming at the improvement of the biocompatibility of all types of implants through, for example, bio-active coatings and nano-structures or newly designed or bio-mimicking materials should be strengthened. NB approaches are also required within the development of materials for new targeted drug delivery systems to fight against diseases that have been so far incurable. Related technologies like minimally invasive surgery, non–invasive diagnostic systems, including reliable biosensors, also need further continuing support.

4.7 Nanoelectronics

The term nanoelectronics refers to electronics at the sub-micron scale. Many chip components in manufacture already feature sizes at the nanoscale. However nanoelectronics also encompasses molecular electronics. This make use of individual molecules in electronics as shown in Figure 4. Up until recently, the size of the smallest electronic circuit element was expressed in microns. Continuous evolution in technology over the years has shrunk circuits so that these dimensions are now less than 65 nanometers. At this scale, some of the classical laws of physics no longer apply and give way to properties defined by quantum physics. Such effects may present challenges for conventional semiconductor technology but also offer opportunities for new technologies. Advances in nanotechnology with applications in electronics include carbon nanotubes that can be used in both chips and displays. Other nanomaterials that can be used in very thin films make smaller, more flexible displays and improved computer hard disks.

Since the 1970’s, the microelectronics industry has followed Moore’s law, doubling processing power every 18 months. This performance increase has been obtained mainly by decreasing the size of circuit features obtained by optimisation and improvement of existing technology. The minimum feature size is approaching 10 nm for the next decade.

CMOS technology currently dominates manufacture of integrated circuits. Its energy efficiency makes it possible to integrate many more CMOS gates on a chip than those made with alternative technologies, so offering much higher functionality. As a result, CMOS is currently the mainstream technology for microprocessors, memory and logic circuits on silicon wafers. Due to its advantageous characteristics and future development potential, experts predict that CMOS will remain the mainstream technology for many years and improvements will continue until at least 2016.

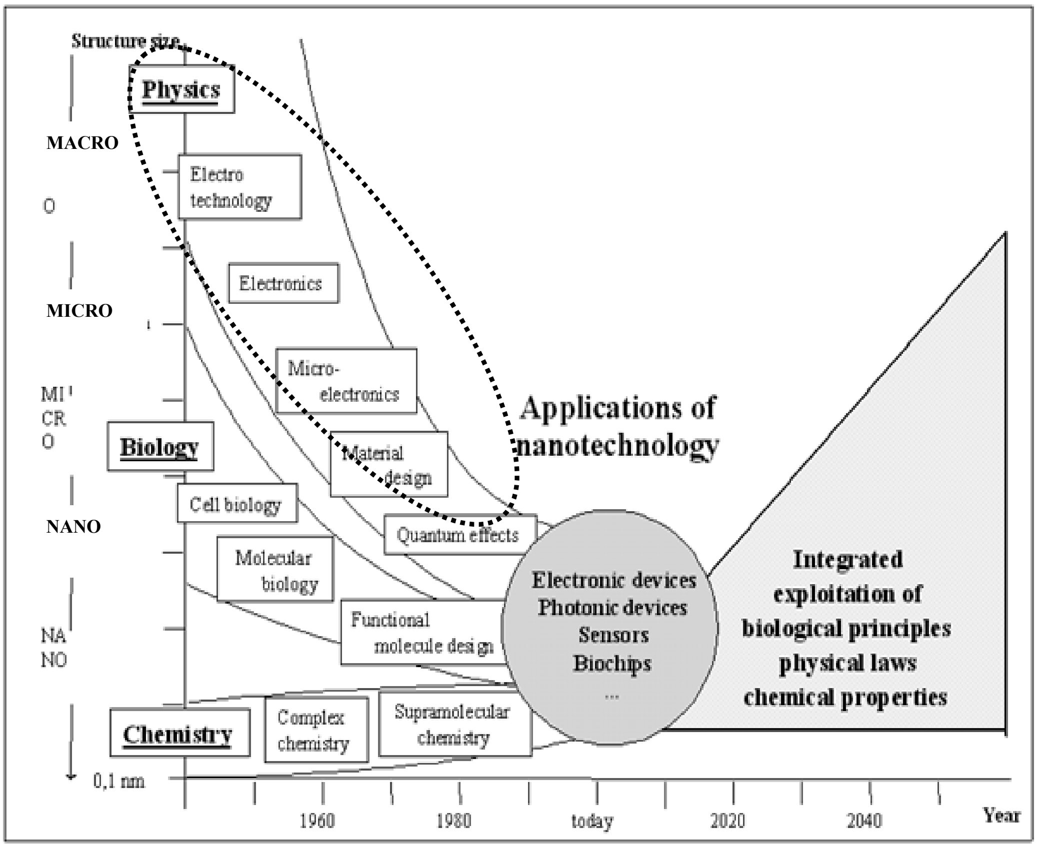

Figure 4. - Position of Nanoelectronics in the Nano Landscape [5].

While CMOS continues to dominate the semiconductor industry, it appears that several **nanoelectronic devices** originally conceived as successors to CMOS, are now finding their way into niche markets. It is also clear that the Moore's Law exponential increases in density and that the performance that CMOS has enjoyed for over thirty years cannot be maintained for ever. Eventually the increase in density, power consumption and volume of silicon chips will require all the energy in the universe to allow operation [6].

As the result of industry's adoption of new materials / technology platforms - such as spintronics, plastic electronics, molectronics and nanotubes / nanowire electronics, low- and high-k materials, a new demand for novel manufacturing modes is now emerging. **Current investment in electronics accounts for** some 30% of overall industrial investment in the developed world. The **market size** of the nanoelectronics business chain (manufacturers, related industries such as the equipment and material suppliers, the designers, system builders and integrators, etc.) represents currently nearly 1% of the world wide GDP with a strong annual average growth rate of approximately 15%. When considering the leverage effect of this enabling technology (telecom operators, consumer products, internet services, automotive, defence, space, etc.), its **global value** can be increased to an estimated €5,000 billion. Furthermore, the nanoelectronics sector is also a significant generator of highly qualified jobs, given its manufacturing dimension.

In Europe some 40% of the **annual sales** of the semiconductor manufacturers are reinvested in R&D and improved production processes. The worldwide annual market for electronics at just under €800 billion is now bigger even than the global automotive market. Alternatives or complements to CMOS, such as spinelectronics, molecular electronics and quantum computing, also exist and are in the early stages of research and development. Molecular electronics are the most futuristic devices among all discussed so far. They have a large potential, but there are huge obstacles that must be overcome. For the moment it seems of the utmost importance that chemists, biologists, physicists and engineers develop an interdisciplinary platform for communicating the needs of the electronics industry in one direction and the possibilities of chemical synthesis and self-assembly concepts in the other.

European Nano-electronics Initiative Advisory Council (ENIAC) has stated that for Europe to become the world's most competitive powerhouse, Europe must lead the transition of the micro-electronics sector to the next generation of nano-electronics, with co-ordinated public and private investments of at least €6 billion per year. This is the message from CEOs of leading companies and research organisations also emphasised that smarter and smaller electronics at the nanometer scale, managing vast amounts of data, are becoming key components for many applications, from household appliances and consumer goods to automotive transport, health care and security, and ultimately ambient intelligence.

4.8 Design Technology

Demands on systems design will increase with the adoption of new nanoelectronics technologies and the resultant increase in complexity of the devices and heavily integrated applications. There will be a need for new design approaches that make it possible to reuse designs easily when new generations or families of products appear. These approaches should be coupled with automatic translation of the resulting high-level designs into device manufacture.

Advanced research into **manufacturing process technology** is a driving force behind Europe's significant scientific and manufacturing economies. Going to smaller circuit feature sizes in the nanometer range down to 22nm or even lower, the process technology for nano-lithography, as well as for the deposition and etching of device layers, also needs to be improved. Certain of the device layers will have a thickness of only one or a few atomic layers and their deposition process needs to be very well controlled and take place in an ultra-clean environment. Obtaining the fundamental insights that will lead to acceptable manufacturing yields for the resulting billion transistor devices will be extremely demanding..

4.9 Other Applications

Ambient intelligence: Moving from micro- to nanometer dimensions allows chips to become so small and cheap that they can be integrated almost anywhere and interact with each other, making everyday activities systematically smarter and more reactive. Typical applications could centre on personal health, entertainment and leisure delivered through networked multifunctional appliances.

Nano-scale medical diagnostics and treatment: Nanoelectronics-based biosensors will speed and simplify measurements at molecular level. This will allow us to design and fabricate ultra-sensitive sensors creating new insights into our health as well as offering better diagnostics and treatments.

Cleaner, safer and more comfortable transport: Highly reliable, smart and interactive low-cost devices will be created, able to withstand harsh environments, cut pollution, increase safety, navigation systems and in-car environment and entertainment systems.

Anti-terrorism and security applications: Nanoelectronics applications range from surveillance to personal identification and access control.

NanoMarkets [8], a leading advanced technology analyst firm in the US, forecasts developments in three key areas:
The emergence of a large market for **nanomemory** products. The market for such products is expected to grow to US$8.6 billion (€6.9 billion) by 2007 and US$65.7 billion(€52.6 billion) by 2011, with the main driver being demand for high-performance, non-volatile memories for mobile communications and computing.
nano-engineered display technology. Roll-up displays using plastic electronics and other platforms are expected areas with strong opportunities and have attracted leading electronic firms such as Xerox and Philips.
carbon nanotubes as a platform for High Density TV monitors at 42 inches and above. The total nano-enabled display market is expected to grow to US$1.6 billion (€1.3 billion) in 2007 and reach US$7.5 billion (€6.0 billion) by 2011.

Plastic electronics [9] holds out the prospect of new products with reasonable times-to-market and large revenue potential. One of the key advantages of plastic electronics is in its ability to create products of a kind that really have never existed before such as electronic paper, roll-up displays, photovoltaic cell or sensor laden laminates and coating, and low-cost optical interconnects. They can be printed using techniques similar to those of ink jet printing or rubber stamping which would reduce the need for building giant fabs. There is also considerable industry push behind this technology. Several of the largest materials and electronics firms - DuPont, Lucent, Philips, Siemens, Sony and Xerox, for example - are either already selling, or are developing, plastic electronics products. Even big pharma is getting in on the act - Merck just bought a small U.K. plastic electronics company. A recent report "Emerging Nanoelectronics Markets” by NanoMarkets, forecasts the market for nano-enabled electronics will reach US$10.8 billion (€8.6 billion) in 2007 and grow to US$82.5 billion (€66.0 billion) in 2011.

5. Nanomaterials

Bulk materials for manufacturing are generally uncontrolled and disordered at small scales. By controlling the nanostructure of materials, novel mechanical, thermal, electrical, magnetic and other properties can be engineered. For instance, metal alloys are made of crystals whose size and shape is only crudely controlled. In comparison, a carbon nanotube (a tiny, hollow tube of carbon atoms) can be perfectly formed, is remarkably strong, and has useful electrical and thermal properties.
Using nanoparticles in composite materials can enhance their strength, reduce weight, increase chemical and heat resistance and change their interaction with radiation. Coatings made from nanoparticles can be unusually tough or slippery, or exhibit unusual properties, such as changing colour when a current is applied or cleaning themselves when it rains. Examples of the uses of nanoparticles are given in Table 2.

Electronic, optoelectronic magnetic applications	Biomedical, pharmaceutical cosmetic applications	Energy, catalytic structural applications
Chemical–mechanical polishing Electro-conductive coatings Magnetic fluid seals Magnetic-recording media Multilayer ceramic capacitors Optical fibres Phosphors Quantum optical devices	Antimicrobials Bio-detection and labelling Bio-magnetic separations Drug delivery MRI contrast agents Orthopaedics and implants Sunscreens Thermal spray coatings	Automotive catalyst Ceramic membranes Fuel cells Photo-catalysts Propellants Scratch-resistant coatings Structural ceramics Solar cells

Table 2. Current and emerging applications of nano-particles [10]

Although hard to quantify, it has been estimated that nanostructured materials and processes can be expected to have a market impact of over \$ 1 trillion (\$ 10^{12}) by 2015 [11].

Some existing applications include:

1. clay nanoparticles in packaging materials, where reduced porosity leads to less gas entering (e.g. less gas such as oxygen that spoils foods);
2. rolled graphite nanotubes used in coatings on car bumpers that better hold their shape in a crash;
3. carbon nanotubes which are sources of field-emitted electrons and create enhanced phosphorescence e.g. in "jumbotron" lamps used at many athletic stadiums
4. nanoparticles of zinc oxide in sunscreens, more efficient at absorbing UV than more traditional white titanium dioxide lotions and leaving the lotion smooth and transparent;
5. textiles which are dirt and crease resistant due to nanocoatings;
6. nanoparticles used as antiseptics, for abrasives and in paints;
7. nanocoatings for spectacle glasses (making them scratchproof and crack resistant)
8. nanocoatings for tiles to reduce slipping;
9. electrochromic or self-cleaning nanofilm coatings on windows, which in sunshine breaks down dirt and helps the water falling on it to carry the dirt away;
10. nanofilms with non-stick properties used as anti-graffiti coatings for walls;
11. ceramic coatings for solar cells to improve scratch and erosion resistance;
12. glues containing nanoparticles with variable optical properties are used in optoelectronics (e.g. for coupling fibres to other optical components); and
13. conductive nanofilms used in casings for electronic devices, such as computers, to provide shielding against electromagnetic interference.
14. Applications under development, some of which are close to market, include:
15. "smart" fabrics that can change their physical properties according to surrounding conditions, or even monitor vital signs;
16. drug delivery mechanisms including antibacterial and antiviral nanoparticles;
17. nanoceramics for more durable and better medical prosthetics;
18. improved catalysts for fuel production; and
19. nanoengineered membranes for energy efficient water purification.

Commentators highlight the importance of nanomaterials to industry by looking at the technical barriers to commercialism, principally mass production and the cost of nanomaterials. Improvements in production will dramatically decrease the cost of materials. For example, 1 gram of low-grade carbon nanotubes cost $1000 five years ago. Today, they cost just $30 due to increased manufacturing efficiencies and greater processing know-how.

6. General Healthcare

In addition to the topics covered under medical devices, there is a wealth of opportunity to use nanotechnology in the healthcare field, another important industry for Ireland.

The following healthcare uses of nanomaterials have been identified [12]:

1. Remote health monitoring / non-invasive diagnosis;
2. Nano-based imaging and drug targeting and delivery for early identification and minimally toxic treatment of disease.
3. Drug / hormone delivery on a needs-basis using electronics-derived technology.
4. Patient-friendly, 'smart' cochlear and retinal implants.
5. Medical textiles, with health monitoring, transmission of information and therapeutic capabilities;
6. Nanostructured bandages, surfaces and textiles that encourage cell growth, reduce infection; and
7. Nano-enabled technologies for quality of life for the elderly or infirm (lightweight, flexible interactive displays / robot 'helpers') activated verbally, by minimal movement or even thought.

7. Educational implications and opportunities

The main points that can be summarised for the developments of nanotechnology within the educational system include:

1. Need relevant courses and multidisciplinary teams developing these courses.
2. Educational Institutes must emphasize for this revolution in nano and biotechnology fundamental science and engineering - short term educational strategies are dangerous
3. Commercialisation issues must be understood by students
4. European Research funding could be centralised in major counties
5. Drift in high tech industry is inexorably to low income counties in Far East
6. Need to train highly qualified manpower. Such manpower was a decisive advantage in past but if manpower is running low Industries will have a problem – strategic training is even more important
7. Funding in the Irish context through Enterprise Ireland 'pathways' in 1990s and precursors were laid down
8. High tech start-up companies supported
9. Science Foundation Ireland(SFI) established to link with other state agencies HEA-Enterprise Ireland-IDA etc. and develop specialist centres which can compete for EU funding (Clearly this is a vital national policy)
10. IDA are seeking nano based industries and helping upgrade existing industries
11. FP6 + etc.
12. Need to develop greater collaborations between Researchers- academics- industry – and funding agencies.

Conclusions

Nanotechnology is forecast to be a $Trillion industry by 2015 (Electronics and communications $300bn; Materials and processing $340bn; Life sciences $180bn; Sensors and instrumentation $22bn). The Main beneficiary will be medical diagnostics, implants and drug delivery, materials and sustainable/ renewable energy

As outlined by Stewart Brand:

"The science is good, the engineering is feasible, the paths of approach are many, the consequences are revolutionary-times-revolutionary, and the schedule is in our life time."

References

[1] Dr. Imelda Lambkin, NanoBiotechnology, Background Paper, NanoIreland Forfas, October 2005
[2] Dr Jos Evertsen, Nanoelectronics, Background Paper, NanoIreland, NanoIreland_NanoElectronics_consultation_, Forfás 2006.
[3] Dr. Jacqueline Allan, NanoMaterials, Background Paper, NanoIreland, Forfás October 2005,
[4] Irish Council for Science Technology and Innovation (ICSTI, 2004)
[5] Source: **www.sigda.org/iwls/iwls2002/elena.ppt**
[6] Compaño R., L. Molenkamp and D.J. Paul. 1999. Technology Roadmap for Nanoelectronics. MELARI NANO - Microelectronics Advanced Research Initiative. European Commission, IST programme, Future and Emerging Technologies.
[7] Source: Nanoforum. 2004.
[8] NanoMarkets Report Predicts $10.8-Billion Nanoelectronics Market by 2007, Posted on Thursday, October 28, 2004.
[9] Nanotechwire.com. New Report Examining Key Areas of Emerging Nanoelectronics Market. 2/10/2005
[10] Business Communication Corporation
[11] US, National Nanotechnology Initiative, http://www.nano.gov/).
[12] Nanotechnology – a Key Technology for the Future of Europe, 2005

UTJECAJ KLIZANJA TLA NA KARAKTERISTIKE MATERIJALA PLINOVODA

D.Kolednjak(1), B.Radošević(2), D.Kamenečki(2), Z.Schauperl(3)

(1) INP d.o.o., SR Njemačke 10, Zagreb
(2) PLINACROd.o.o., Savska cesta 88, Zagreb
(3) FSB, Ivana Lučića 5, Zagreb

Sažetak:

Na međunarodnom plinovodu Rogatec-Zabok DN 500 (20") u mjestu Strmec Humski došlo je do pomaka zemljišta na padini (klizišta), koji su utvrđeni nakon iskopa za novu cestu 1992. godine. Pomaci zemljišta su uzrokovali značajna vlačna naprezanja materijala cijevi koja je položena u dijelu terena gdje se nalazi klizište.

Klizište je sanirano obavljanjem radova prema odgovarajućem projektu, ali plinovod je zbog pomaka terena ostao pod značajnim kontinuiranim opterećenjem. Radi otklanjanja tog opterećenja i izbjegavanja moguće havarije, plinovod je rezan na dva mjesta kako bi se materijal rasteretio i omogućio pomak plinovoda u prvobitno stanje.

Provedenim laboratorijskim ispitivanjem izrezanog materijala cijevi plinovoda istražio se utjecaj dugotrajnog opterećenja na karakteristike materijala s posebnim naglaskom na kritična mjesta i zavarene spojeve. Provedena je vizualna analiza vanjske i unutarnje površine cijevi, statički vlačni pokus, ispitana žilavost materijala te analizirana mikrostruktura na kritičnim mjestima.

Rezultati su uspoređeni sa deklariranim svojstvima materijala novog plinovoda te doneseni zaključci o stanju materijala plinovoda izloženog klizanju tla.

Ključne riječi:
Plinovod, ispitivanje materijala, mikrostruktura

1. UVOD

Plinovod Rogatec-Zabok zasad je jedini međunarodni plinovod u Republici Hrvatskoj i jedini uvozni pravac kojim se uvozi plin iz Rusije, te transportira više od jedne trećine ukupne godišnje potrošnje plina u Republici Hrvatskoj. Početak plinovoda je u Sloveniji u mjestu Rogatec a završetak u plinskom čvoru Zabok (PČ Zabok) iz kojeg je moguće plin usmjeravati u smjeru Zagreba i Ludbrega, tj. Varaždina. Kapacitet plinovoda je oko milijardu prostornih metara prirodnog plina godišnje. Iz tih podataka očita je strateška važnost plinovoda Rogatec-Zabok za transportni plinski sustav odnosno opskrbu plinom Republike Hrvatske.

Tijekom iskopa za novu cestu u mjestu Strmec Humski u području na kojem je položen plinovod uočen je pomak zemljišta na padini, tj. klizište, koje je uzrokovalo značajna opterećenja materijala cijevi na dijelu trase na kojem plinovod prolazi kroz zonu utjecaja klizišta. Klizište je sanirano obavljanjem radova prema odgovarajućem projektu, ali je plinovod, zbog pomaka terena, ostao pod značajnim kontinuiranim opterećenjem. Radi otklanjanja tog opterećenja i izbjegavanja moguće havarije, plinovod je rezan na dva mjesta kako bi se materijal rasteretio i omogućio pomak plinovoda u prvobitno stanje. Nakon rezanja cijevi ustanovljeno je produljenje cijevi čak i do 6 cm, što govori o opterećenju koje je djelovalo na materijal plinovoda. Ovim radom istražio se stvarni utjecaj dugotrajnog opterećenja na karakteristike materijala s posebnim naglaskom na kritična mjesta i zavarene spojeve cijevi.

2. ISPITIVANJE MATERIJALA

Radni tlak prirodnog plina u cjevovodu je 30 do 50 bara. Materijal cijevi plinovoda je API 5L X52, promjera 508 mm i debljine stjenke 7,1mm. Osnovne karakteristike materijala cijevi prikazane su u tablici 1.

Tablica 1. Karakteristike materijala cijevi

C, %	Mn, %	Si, %	P, %	S, %	R_m, N/mm^2	R_e, N/mm^2	A, %	CE
0,28	<1,25		0,04	0,05	455	358	22	<0,49

Iz plinovoda su izrezani dijelovi cijevi namijenjeni laboratorijskom ispitivanju materijala. Posebna je pažnja posvećena načinu izrezivanja kako ne bi došlo do dodatnog oštećenja materijala. Isto tako pazilo se da izrezani dio cijevi bude reprezentativan i da se na temelju stanja materijala tog dijela mogu donijeti zaključci o materijalu kompletnog plinovoda.

2. 1. Vizualna analiza

U vrijeme izgradnje plinovoda stanje tehnike je bilo takvo da se antikorozivna zaštita cijevi, uz katodnu zaštitu, izvodila direktno na gradilištu namatanjem dvoslojne polietilenske trake na površinu cijevi koja je prije toga bila očišćena od korozije mehaničkim četkanjem.

Na mjestu izrezanog uzorka, ulijed pomicanja zemljanog materijala došlo je do pomicanja, pucanja i odvajanja PE trake pa je metalna cijev bila direktno izložena zemljanom tlu, a uslijed

pomicanja tla uz plinovod je trajno protjecala voda od izvora koji su i potaknuli klizište, što je sve zajedno pogodovalo razvoju vanjske korozije.
Vizualnom analizom vanjske strane analiziranog djela plinovoda vidljivo je da je površina bez zaštitne folije zahvaćena općom korozijom dubine do 1mm, slika 1a. Osim korozije na analizirnom dijelu plinovoda vidljiva je i mjestimična deformacija kao posedica djelovanja sile tijekom klizanja tla.
S unutarnje strane cijevi također je prisutna opća korozija dubine do 0,5mm. Osim deformirane stijenke cijevi mjestimično su vidljive i greške u zavarenom spoju, slika 1b.

a) b)

Slika 1. Plinovod: a - Vanjska površina plinovoda s vidljivom korozijom vanjske i deformacijama.
b - Unutarnja površina plinovoda. Vidljive greške u zavarenom spoju, strelica.

a) b)

Slika 2. Epruvete za statički vlačni pokus: a - izrezane iz osnovnog materijala plinovoda
b - izrezane na mjestu zavara.

Osim ispitivanja čvrstoće provedeno je i ispitivanje udarne radnje loma materijala plinovoda. Uzorci su izrađeni prema normama za tu vrstu ispitivanja s V utorom, KV. Tri uzorka su izrađena iz osnovnog materijala plinovoda, a tri na mjestu zavara.

Na slici 3 prikazani su izrađeni uzorci za ispitivanje udarne radnje loma.

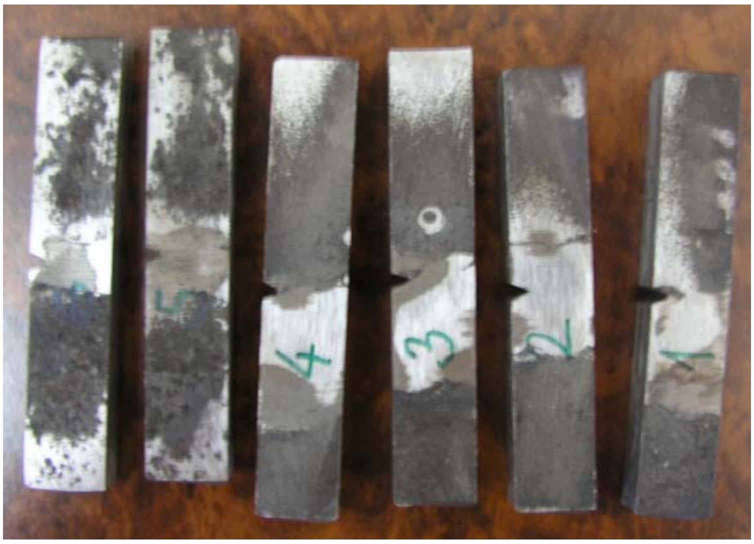

Slika 3. Uzorci za ispitivanje žilavosti materijala plinovoda.

Ispitivanje čvrstoće i žilavosti materijala provedeno je u Laboratoriju za ispitivanje mehaničkih svojstava Fakulteta strojarstva i brodogradnje u Zagrebu.
Statički vlačni pokus proveden je na kidalici slijedećih karakteristika:

proizvođač:	VEB Werkstoffprüfmaschinen, Njemačka;
vrsta:	EU 40 mod;
serijski broj:	990.06/35;
mjerno područje:	20 - 400 kN;
razred točnosti:	0,5.

Ispitivanje je provedeno sukladno normi DIN EN 10002-1 pri temperaturi od 20 ± 1°C. Grafički prikaz rezultata ispitivanja statičkog vlačnog pokusa nalazi se na sl.4.

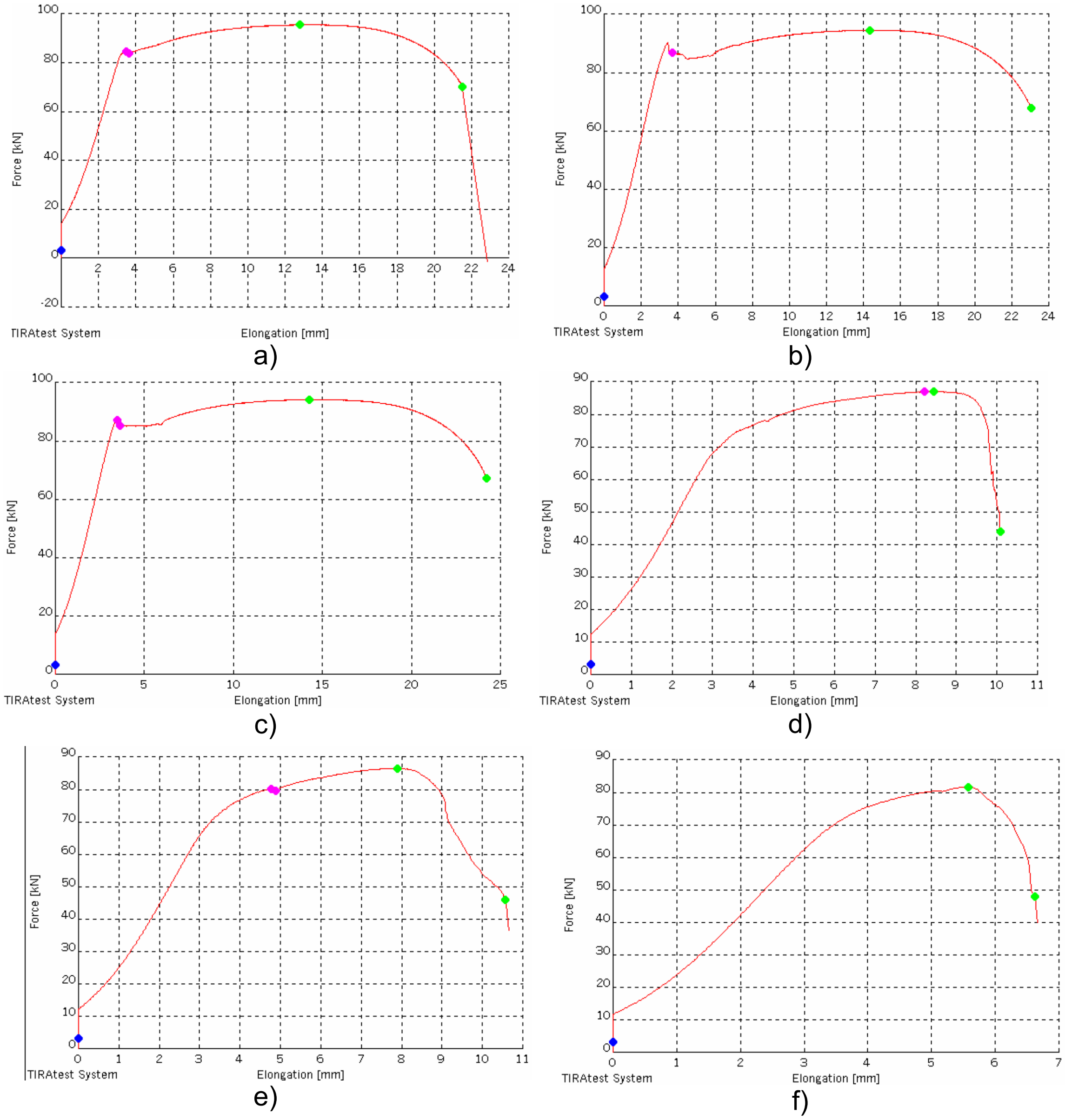

a)

b)

c)

d)

e)

f)

Slika 4. Rezultati SVP materijala plinovoda: a, b, c – osnovni materijal
d, e, f – materijal zavara.

Rezultati statičkog vlačnog pokusa za svih šest epruveta prikazani su u tablici 2, a rezultati ispitivanja žilavosti u tablici 3.

Tablica 2. Rezultati SVP

Epruveta	Statički vlačni pokus											Napomena
	D_0 a_0*b_0,mm	S_0 mm^2	L_0 mm	F_e kN	F_m kN	L_u Mm	d_u a_0*b_0, mm	R_e N/mm^2	R_m N/mm^2	A, %	Z, %	
A1	7,3x25,1	183,2	80	84,15	95,37	96,50	3,2x19,6	459,3	520,5	20,63	66,27	Osn.mat.
A2	7,3x24,8	181,0	80	87,40	94,43	97,55	3,1x19,1	482,9	521,1	21,94	67,76	Osn.mat.
A3	7,3x24,8	181,0	80	86,53	94,07	98,99	3,2x18,9	477,6	519,2	23,74	66,58	Osn.mat.
B1	6,8x24,7	168,0	60	69,32	86,84	67,30	6,0x21,4	411,9	516,0	12,17	23,85	Zavar
B2	6,8x24,7	168,0	60	70,77	86,36	67,32	5,9x21,8	421,4	514,2	12,20	23,78	Zavar
B3	6,8x24,7	168,0	60	69,77	81,57	63,90	6,0x23,2	405,9	474,6	6,50	19,04	Zavar

Tablica 3. Rezultati ispitivanja žilavosti materijala plinovoda

Epruveta	Ispitivanje udarcem			Napomena
	a_0*b_0*55, mm	S_0, mm^2	KV, J	
1	10x6	60	128	Osn. mat.
2	10x6	60	136	Osn. mat.
3	10x6	60	98	Osn. mat.
4	10x6	60	70	Zavar
5	10x6	60	77	Zavar
6	10x6	60	72	Zavar

2.2. Analiza mikrostrukture materijala plinovoda

Karakterizacija materijala plinovoda uključuje i analizu njegove mikrostrukture. U tu svrhu iz plinovoda su izrezani uzorci materijala dimenzija 10x10mm. Izrezivanje je obavljeno uz intenzivno ohlađivanje i podmazivanje kako bi se izbjegla deformacije i rekristalizacija strukture.
Tako izrezani uzorci pripremljeni su za analizu u skladu s preporukama za tu vrstu materijala: grubo i fino brušeni, polirani te nagriženi u nitalu.

Mikrostrukture materijala prikazane su na slikama 5-9.

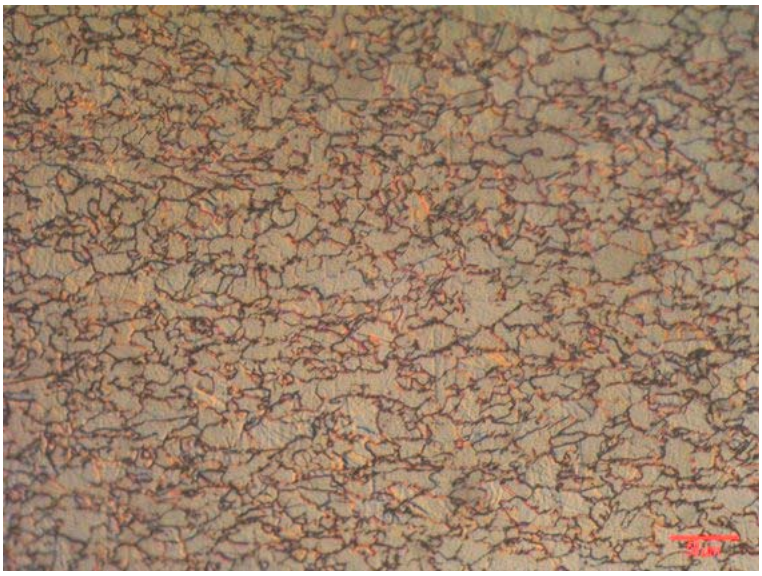

Slika 5. Mikrostruktura materijala plinovoda, sredina stijenke.

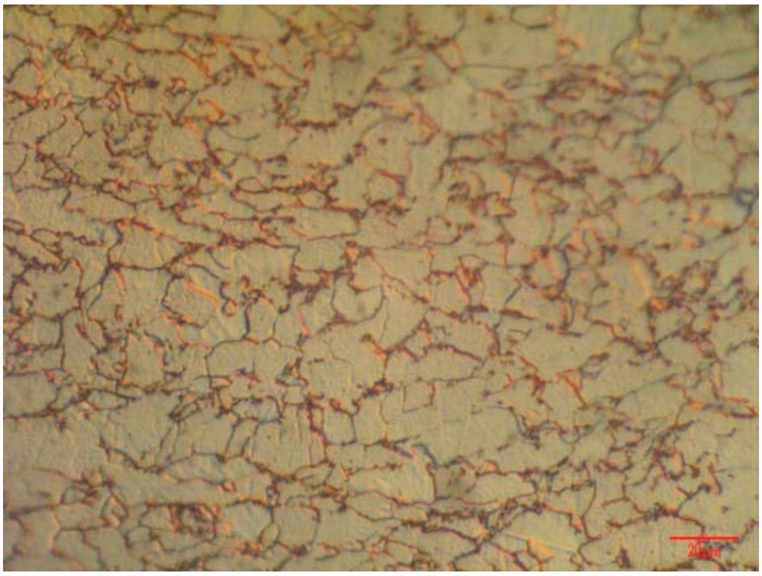

Slika 6. Mikrostruktura materijala plinovoda, sredina stijenke. Veće povećanje.

Slika 7. Detalj mikrostrukture uz vanjsku površinu materijala plinovoda.

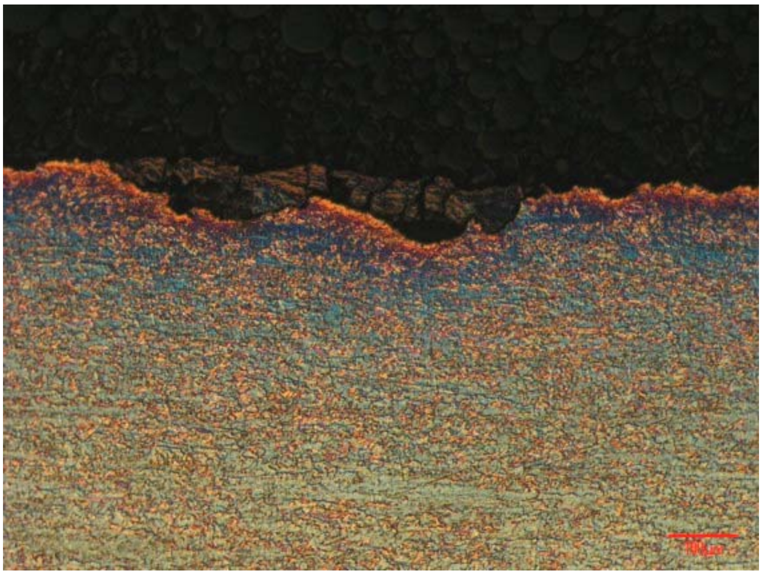

Slika 8. Mikrostruktura uz vanjsku površinu materijala plinovoda.

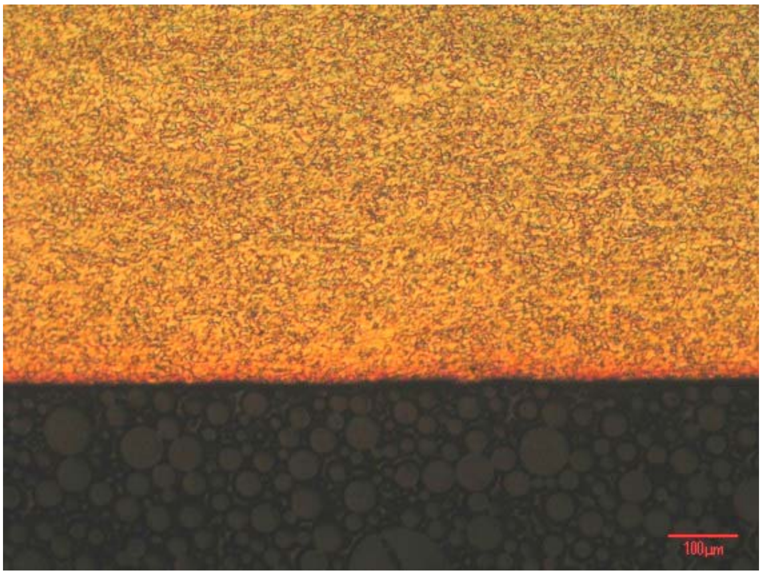

Slika 9. Mikrostruktura uz unutarnju površinu materijala plinovoda.

Mikrostruktura u sredini materijala cijevi, prikazana na slikama 5 i 6 je feritno-perlitna s vro malim udjelom perlitne faze. Struktura je izrazito usmjerena što može biti posljedica tehnologije izradbe cijevi, ali dijelom i tečenja materijala uslijed dugotrajnog opterećenja. Tik ispod vanjske površine materijala mjestimično su vidljive nemetalne uključine u materijalu, slika 7.
Vanjska površina cijevi je izrazito zahvaćena općom korozijom, slika 8, tako da korozijski produkti mjestimično prodiru duboko u osnovni materijal. S unutarnje strane cijevi struktura je na analiziranom mjestu homogena, djelomično rekristalizirana bez značajnijih nepravilnosti.

ZAKLJUČAK:

Sanacijom klizišta i rezanjem cijevi na dva mjesta ponovno je uspostavljeno normalno stanje plinovoda: cijev je rasterećena od vlačnih naprezanja i uklonjen je uzrok tih naprazenja, tj radijalni pritisak zemljanog materijala, te je plinovod vraćen u prvobitno stanje čime je omogućena daljnja sigurna eksploatacija.

Dio cijevi izložen klizištu bio je bez PE zaštitne trake do čijeg je odvajanja došlo uslijed pomicanja zemljanog materijala. Stoga je metalna cijev bila direktno izložena zemljanom tlu, a uslijed pomicanja tla uz plinovod je trajno protjecala voda od izvora koji su i potaknuli klizište, što je sve zajedno pogodovalo razvoju vanjske korozije dubine i do 1mm.

Mehanička ispitivanja svojstva materijala pokazala su značajne razlike u svojstvima osnovnog materijala i materijala zavara cijevi plinovoda. Granica razvlačenja, vlačna čvrstoća i žilavost materijala cijevi se ne razlikuju značajno od deklariranih svojstava za tu vrstu materijala. Medjutim primijećen je značajan pad vrijednosti tih svojstava kod zavarenih spojeva. Osim što granicu razvlačenja (Re) nije moguće jasno definirati, vlačna čvrstoća je značajno niža od čvrstoće osnovnog materijala. Također je velika razlika uočena i ispitivanjem udarne radnje loma. Dok prosječna vrijednost KV pri 20°Cza osnovni materijal iznosi oko 115J, za materijal zavara ta vrijednost pada na nešto više od 70J.

Mikrostruktura osnovnog materijala cijevi nije pretrpjela značajne promjene. Mjestimično je izrazito usmjerena što može biti posljedica tehnologije izradbe cijevi, ali i tečenja materijala uslijed dugotrajnog opterećenja. Tik ispod vanjske površine materijala mjestimično su vidljive nemetalne uključine u materijalu.

Provedena ispitivanja pokazuju djelomičnu degradaciju materijala cijevi plinovoda uzrokovanu klizištem tla. Posebno su zahvaćeni materijal zavara i zone utjecaja topline što se očituje u padu mehaničkih svojstava. Stoga je potrebno u budućnosti, prilikom zahvata na plinovodu, obratiti pažnju na svojstva materijala na tim kritičnim mjestima.

VERY HIGH CONDUCTIVE METAL MATRIX COMPOSITES FOR THERMAL TRANSPORT APPLICATIONS

Juraj Koráb, Karol Iždinský, Stanislav Kúdela,jr., Pavol Štefánik, Štefan Kavecký,
*** Táňa Šrámková**
Institute of Materials and Machine Mechanics, Slovak Academy of Sciences, Bratislava, Slovak republic
*Institute of Physics, Slovak Academy of Sciences, Bratislava, Slovak republic
ummskora@savba.sk

Introduction

The continuously increasing degree of chip integration within the semiconductor industry has inevitably led to very high power densities. These result in significant temperature increase that can be prevented only by introducing of efficient ways for heat dissipation. Thermal conductivities of required novel heat sinks significantly exceed the conductivities of traditionally used aluminium and copper. The only reasonable way how to improve this fundamental material property is by forming a composite material based on the addition of more conductive component to the metal matrix.

New types of pitch-based high modulus carbon fibres exhibit significantly higher thermal conductivity in the axial direction than that of copper (*e.g.* Thornel K1100 - Table 1). Embedding these fibres into the metal matrix is expected to increase the thermal conductivity of the material considerably. Such fibres can be important for the most demanding thermal management applications where very high performance and weight reduction are to be achieved.

Material systems

Previous experience with the Cu/C system confirmed that there is very poor wetting and no reaction between carbon fibre and copper [1, 2]. Therefore only mechanical bonding due to CTE mismatch between both constituents exists at the fibre-matrix interface. However, this type of bonding does not provide sufficient heat transfer from matrix to fibres and thus the potential of highly conductive K-1100 fibres cannot be effectively utilised. In order to reduce the interfacial thermal resistance alloyed matrices in three following different material systems were subjected to investigation in this work: Cu/C, Al/C and Mg/C.

Tab. 1 Properties of Thornel K1100 pitch based C fibres (data published by Cytec Industries Inc.)

Tensile Strength	3.10	GPa
Tensile Modulus	965	GPa
Density	2.2	g/cm^3
Filament Diameter	10	μm
Carbon Assay	99+	%
Surface Area	0.40	m^2/g
Electrical Resistivity	1.1 - 1.3	micro-ohm-m
Thermal Conductivity	900-1000	W/mK
CTE at 21°C	-1.45	ppm/°C

There are principally two techniques for manufacturing of metal matrix composites (MMC) reinforced with multifilament carbon fibres. The first is based on galvanic or PVD coating of C-fibre tows with matrix metal and their subsequent consolidation into bulk bodies by vacuum diffusion bonding. However, this technique is not appropriate for high modulus K1100 fibres due to their brittleness and excessive fracturing that occurs during pulling through a coating line.

The other well-adopted technique for preparation of C-fibre reinforced MMC is gas pressure infiltration (GPI), whereas the fibrous preform is infiltrated with molten matrix metal. In this case two different technological problems appear: lack of wetting behaviour between carbon fibres and molten metal (e.g. Cu, Mg), which does not allow proper infiltration of multifilament tow even at high infiltration pressures and in the contrary severe reaction of carbon fibres with some of molten metals (e.g. Al, Fe, Ni,..) leading to deterioration of fibre properties.

In case of copper matrix some carbide forming elements are added to overcome the first difficulty. Cr and Zr are typically used for this purpose. They usually do not form a solid solution with copper but precipitate to the matrix and increase the metal strength. This reduces pollution of the matrix and tends to keep high electrical and thermal conductivity. Chromium in small amounts does not reasonably decrease the thermal conductivity of copper but improves wetting and the fibre-matrix interfacial bonding due to the mutual reaction with carbon.

In the case of Al based matrix chemical reaction between molten Al and C fibres takes place forming highly unstable hygroscopic aluminium carbide - Al_4C_3 at the interface. Therefore the C-fibre/Al-matrix composite undergoes rapid corrosion in the aqueous environment. Suitable coatings can be deposited on fibres by various methods – *e.g.* titanium diboride that both aids wetting and protects the fibre from chemical attack at elevated temperatures. However, the brittleness of high modulus C-fibres makes the application of coating techniques extremely difficult or even impossible. The reaction between constituents can be retarded also by alloying of Al with elements like Si or Mg that change the solubility of the fibre atoms in a metal matrix.

In the Mg/C system there is no reaction between pure Mg matrix and carbon fibres - magnesium does not form carbides with fibres. That is why interfacial bonding is poor - similar to the Cu/C system. Some controlled reaction at the fibre-matrix interface may help to solve this problem e.g. if carbide forming elements like Al or Zr are added to matrix metal.

Therefore the effect of matrix alloying on the infiltration quality and on the thermal conductivity of composite reinforced with Thornel K1100 three different matrix alloys were investigated: CuCrZr, AlMg3 and MgAl2.

Manufacturing technology

For infiltration experiments graphite moulds with a cylindrical hole with the diameter of 12 mm and the length of 50 mm were prepared and filled with continuous unidirectionally aligned tows of K1100 carbon fibres. Fibre tows were pretreated in the water dispersion of TiN particles (fraction size 1 – 2 µm) in order to deposit some of these particles on the fibre surface. The particles were aimed to act as separators of monofilaments in fibre yarn and provide enough free space for the penetration of molten metal in the fibrous preform. The mould was evacuated and immersed into a graphite crucible that was filled with molten alloy. Then the gas pressure was applied on the liquid metal surface and in this way metal was forced to penetrate fibres and to form the composite material. After infiltration the mould was withdrawn from the crucible and molten metal within the fibrous perform was allowed to solidify under the pressure of the surrounding gas. Finally, the infiltrated fibre preform (composite) was machined-out of the graphite mould.

Results

Microstructure of Cu-C

In spite of generally very poor wetting in the pure Cu/C system the gas pressure infiltration with the CuCrZr alloy yielded a composite with homogeneous fibre distribution. Typical structure in cross-sectional views is shown in Fig.1. The fibre volume fraction was determined to 60 vol. %. However, fine pores can be observed at high magnification between some fibres. Investigation of fracture surfaces confirmed lack of bonding at the fibre-matrix interface. C-fibres with smooth surfaces neighbouring the plastically deformed matrix can be well distinguished as shown in Fig. 2.

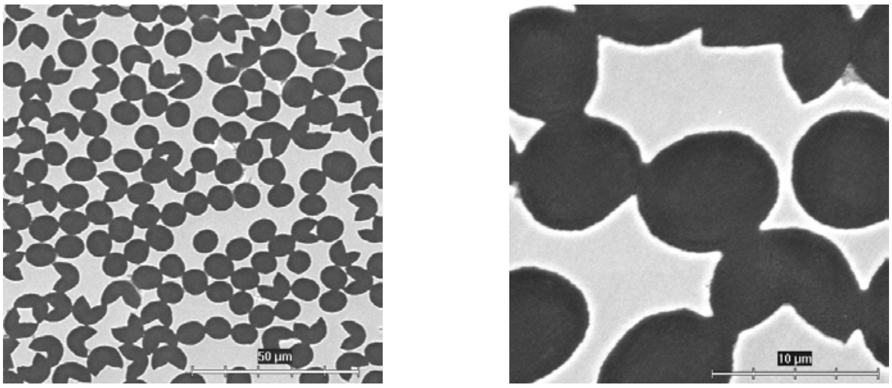

Fig.1: Structure of CuCrZr/C composite with pores between adjacent fibres (secondary electron micrographs)

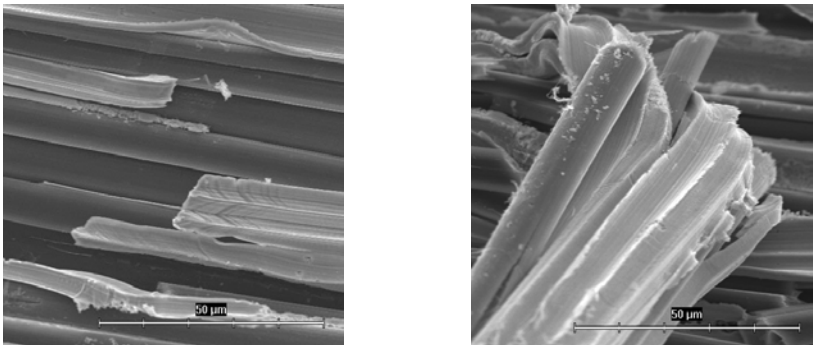

Fig.2: Fracture surface of CuCrZr/C composite revealing poor interfacial bonding (secondary electron micrographs)

Microstructure of Al-C

The gas pressure infiltration of K1100 fibres with AlMg3 alloy yielded the pore-less composite material with homogeneous fibre distribution (Fig.3). The aim of infiltration trials was to achieve the material with some limited interfacial reaction, not destroying carbon fibres. Here chemical compositions of the matrix alloy, structural stability of C fibres, as well as kinetic factors play the dominant roles. The particular effect of these factors has to be established later. The fibre volume fraction was determined close to 55 vol. %.

As shown in Fig.4 some interfacial reaction took place and islands of adhered matrix can be found on the fibres by examination of sample fracture surfaces. TiN particles were easily observed in the structure as well as on fracture surfaces providing thus only limited reaction with the matrix metal.

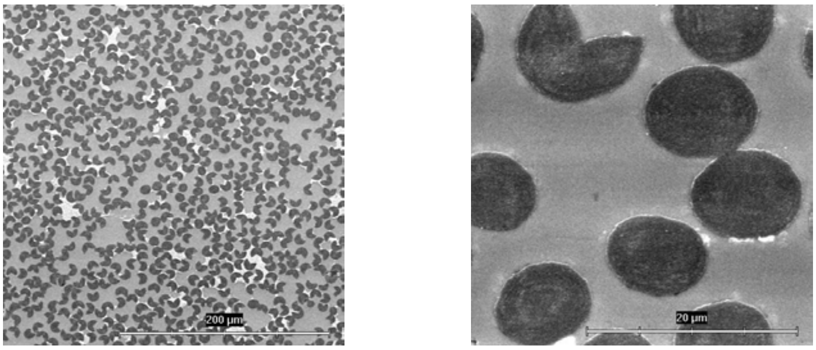

Fig.3: Structure of AlMg3/C composite with white islands of TiN particles (secondary electron micrographs)

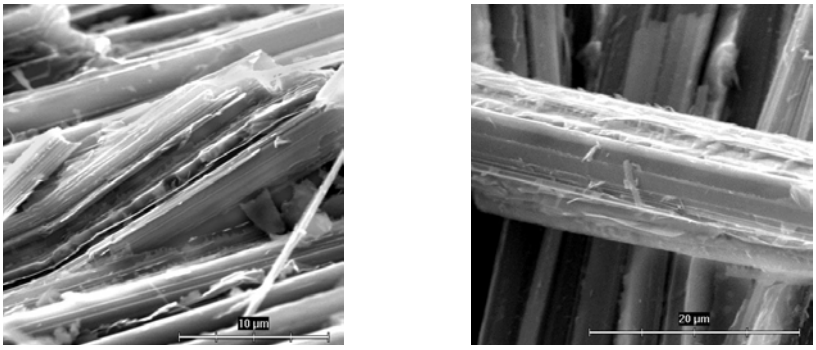

Fig.4: Fracture surface of AlMg3/C composite revealing traces of fibre-matrix reaction (secondary electron micrographs)

Microstructure of Mg-C

The gas pressure infiltration of K1100 fibres with MgAl2 matrix also produced samples with homogeneous fibre distribution and fibre volume fraction at the level of 55 vol. % (Fig.5). White appearing areas are again TiN particles that served as fibre separator obviously not reacting with both the matrix and fibres.

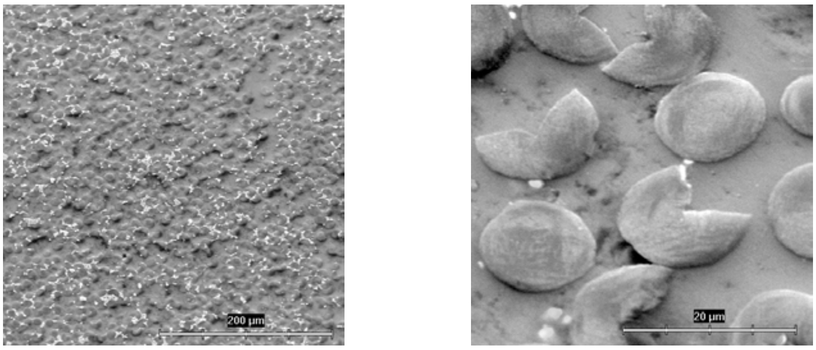

Fig.5: Structure of MgAl2/C composite with white islands of TiN particles (secondary electron micrographs)

Observation of fracture surfaces revealed the lack of interfacial reaction. Debonding takes place at the fibre-matrix interface as shown in Fig.6. Interface improvement is the precondition for better performance of the composite (e.g. thermal cycling load). This could be achieved by the further alloying optimization.

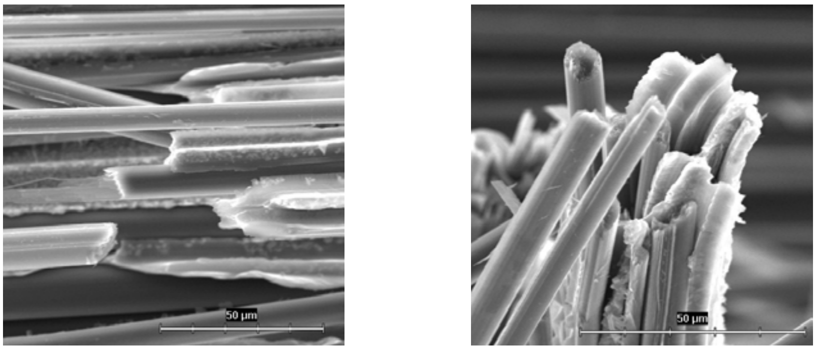

Fig.6: Fracture surface of MgAl2/C composite revealing lack of interfacial bonding (secondary electron micrographs)

Thermal conductivity results

The thermal conductivity of MMC samples was calculated from the experimentally determined thermal diffusivity, density and specific heat values. The density was calculated from the volume and mass measurements with the assumption of void free composite material. The specific heat values were calculated from the data of individual components. The thermal diffusivity was measured by widely used “flash” method [3]. The samples were disc shaped of diameter 10 mm and thickness 3-5 mm. Heat flux was applied parallel to the fibre direction. To obtain a relevant value for thermal diffusivity by the flash method, the tested material should be homogeneous enough for the propagating thermal wave. First results with thinner samples revealed that the thickness of 3 mm is not sufficient enough to get a reliable value of the effective thermal diffusivity. Therefore the thermal diffusivity measurements were performed also on 5 mm thick composite samples and these results were used for the calculation of thermal conductivity values (table 2). The thermal conductivities obtained from diffusivity measurement were compared with theoretical values calculated from rule of mixture using properties of particular constituents (some were obtained experimentally) listed in table 3.

From the obtained results one can see that the implementation of K1100 carbon fibres into suitable metallic matrix significantly improves its thermal conductivity. All investigated systems attained higher value of thermal conductivity than that of pure copper, especially in direction parallel to fibre orientation. Although the transverse conductivity is expected to be significantly lower [4] the unidirectional K1100 carbon fibres composites are very promising for applications where extremely high heat flow in one direction has to be arranged.

Tab. 2: Thermophysical properties of prepared composites (thermal conductivity was calculated theoretically from rule of mixture (ROM) and from experimentally obtained diffusivity using values given in table 3)

Composite	**Sample thickness**	**Fibre vol. fraction**	**Density**	**Diffusivity**	**Thermal conductivity** [W / m .K] calculated from	
	[mm]		[kg/m^3]	[m^2/s]	ROM	diffusivity
MgAl2+C-fibres+TiN	5	0.55	2120	2.500E-04	604	414
AlMg3+C-fibres+TiN	5	0.55	2450	2.684E-04	627	523
CuCrZr+C-fibres+TiN	5	0.60	4810	2.844E-04	673	651

Tab. 3: List of property values used for thermal conductivity calculations

Component	**Cp [J/kgK]**	**Density [kg/m^3]**	**Thermal conductivity [W/mK]**
MgAl2	1020	1740	120
AlMg3	900	2700	170
CuCrZr (non hardened)	380	8900	182
K1100	710	2200	1000

Conclusions

Generally, current study proved the expectations regarding the technological feasibility of gas pressure infiltration technique for preparation of metal matrix composites based on copper, aluminium and magnesium alloys containing higher portion of carbon fibres. Measurements confirmed the substantial increase in the thermal conductivity of all three tested matrices due to the employment of K-1100 fibres - they all overcome the thermal conductivity of copper.

In the case of copper based matrix the fundamental contribution of this work is the knowledge that high modulus C-fibres can be infiltrated by copper alloy containing some carbide forming elements.

Al based composite suffering from the undesired fibre-matrix reaction also showed interesting potential if the detrimental Al_4C_3 carbide formation is retarded due to the superficial activity of Mg diffusing preferentially to the interface.

Mg based composite is attractive due to the simplicity of interfacial reactions restricted to the wetting of fibres with the matrix. However, the successful performance of the composite requires improved interface what can be achieved again by proper alloying.

It should be noted that properties of unidirectionally reinforced composites are anisotropic and need to be tailored accordingly to the individual application requirements.

Acknowledgement:

This work has been performed within the framework of the Integrated European Project „ExtreMat“ (contract NMP-CT-2004-500253) and with financial support by the European Community. It only reflects the view of the authors and the European Community is not liable for any use of the information contained therein.

References:

[1] Schweighofer A. Kúdela S.: Developnment of gas pressure infiltration technology of copper into porous carbon bodies, *Research report of the Institute of Materials and Machine Mechanics*, Bratislava, Slovak republic, 1979, (in Slovak)

[2] Šebo,P. and Štefánik,P.: Copper matrix – carbon fibre composites, *Int.J.Mat.Prod.Tec.*, 18 (1-3), 2003, p.141-159

[3] Šrámková T., Log T.: Using nonlinear CHI-2 fit in flash method. *Int. J. Heat Mass Transfer*, 38 (15), 1995, p.2885-2891

[4] Štefánik,P., Hudcovič,P. and Šebo,P.: Influence of volume fraction and orientation of carbon fibres on heat transfer in unidirectional copper matrix composites, *Kovove mater. (Metallic materials)*, 42, 2004, p.329-337

11. Savjetovanje o materijalima, tehnologijama, trenju i trošenju
11. Conference on Materials, Processes, Friction and Wear
MATRIB'06, Vela Luka, 22-24.06.2006.

FRICTION STIR WELDING OF FOAMABLE MATERIALS AND FOAM CORE SANDWICHES

I.Kramer[1], F.Simancik[1], R.Florek[1]; M. Nosko[1]; K.Müllerová[1]; P.Tobolka[1], O. Mishina[2]

[1] *Institute of Materials and Machine Mechanics SAS, Racianska 75 SK-83102 Bratislava, Slovakia*
[2] *Sapa Technology, SE-612 81 Finspång, Sweden*

Abstract

Because of exceptionally high stiffness-to-weight ratio aluminium foams are very promising materials for lightweight construction, especially for use in large and complex lightweight panels or similar structures. One of the promising ways for they manufacturing is powder metallurgical process, where powders of aluminium alloy and foaming agent, e.g. TiH_2, are mixed and compacted via extrusion, thus creating so called foamable precursor, which expands on melting. However extrusion process does not allow manufacturing of precursor in the form of large or complex 3D-structures and this fact makes a foaming process significantly more difficult.

Main aim of this work is to show that joining of such foamable precursor profiles into large parts is feasible via friction stir welding (FSW). As this welding is performed in solid state no premature foaming of precursor was observed and foaming ability of both precursor and welds was preserved without any changes. Since FSW generates only low amounts of heat no thermal distortion or other geometry changes were observed on welded materials. It will be shown, that FSW is suitable technique also for welding of foam-cored sandwiches if appropriate distance profile between opposite coversheets is used. The coversheets are welded together without affecting foam core, which leads to excellent mechanical properties of welded joint. Even sandwiches made by gluing of coversheets onto foamed core can be welded by this method without destroying glued interface.

Keywords: sandwich plates, aluminium foam, friction stir welding

Introduction

FSW is relatively novel joining technique which has been invented by TWI (The Welding Institute, 1991). Material is joined during stirring and mixing of metal in solid state. Schematic display of FSW process is shown below /1/.

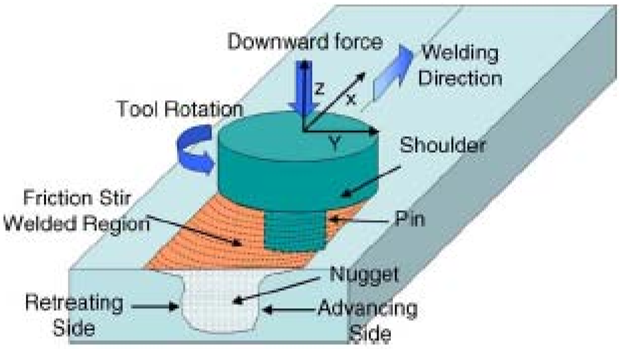

***Figure 1**. Schematic display of FSW process /1/.*

FSW technique is very simple. Pin of the rotating tool is inserted into interface between workpieces to be welded and moved along weld centerline. Heat is generated by friction between rotating tool and both material surfaces. Because of generated heat material is softened and easily stirred by rotating pin. Due to the shoulder attached directly to the upper surface of welded parts, stirred material cannot flow out of the weld and the original geometry of the welded cross section is thus retained. At first sight it is noticeable that tool design plays very important role and is decisive for the performance of whole FSW process. Other very important welding parameters are: tool rotating rate, tool traverse speed and upper force applied on a tool.

This technique is nowadays predominantly used for joining of metals with higher affinity to oxygen, such as aluminium, magnesium, zinc, lead and copper without need to apply any protecting atmosphere. The stirring efficiently disintegrate the surface oxides on both counterparts and provides thus optimum conditions for sound welds. Also joining of dissimilar alloys and even dissimilar materials is possible. Some of the other main advantages of FSW process are: low energy input into welds and thus lower thermal stresses and geometry distortion, harmless processing for the environment, fine grain microstructure in weld area, no need for additional weld material, low cost (no consumables, low energy), etc.

Within this work three types of experiments have been performed: FSW of foamable precursor material, FSW of aluminum foam which has inserts made of bulk aluminium and FSW of glued aluminium foam sandwich plates.

FSW of foamable precursor

Powder metallurgical route is one of the mostly used processing techniques for aluminium foam production. In this method the metal and foaming agent (TiH_2, ZrH_2, etc.) powders are mixed together and extruded creating so called foamable precursor. On heating the foaming agent evolves gas, thus creating foam with desired porosity. Due to extrusion the foamable precursor cannot be produced in the form of large or complex 3D-structures and thus joining of precursor is sometimes needed. In this case FSW is probably only welding technique which can be used without destroying the foamability of the precursor.

Main danger is decomposition of TiH_2 which starts at about 450°C and premature foaming of precursor due to the high amount of involved energy during welding. This can affect quality of the weld and significantly reduce the attainable porosity in subsequent foaming. The exact temperature during FSW process is very hard to measure, even impossible, because of the nature of this technique. Some estimates (based on temperature measurements near to the weld line) give the temperature range between 400-480° C in case of aluminium alloys. It is clearly noticeable that this temperature is well below melting point of any commercial aluminium alloys, although the upper limit of this range can already lead to partial decomposition of foaming agent.

Welding experiments were performed on precursor material made of **AlMg1Si0,6** alloy with addition of **0,4% ZrH_2**. Thickness of material was 5 mm and FSW parameters were: tool rotating rate - **1000 rpm** and tool traverse speed - **112 mm/min.**

The both surfaces of the weld and its microstructure are given in Figure 2 and 3 respectively.

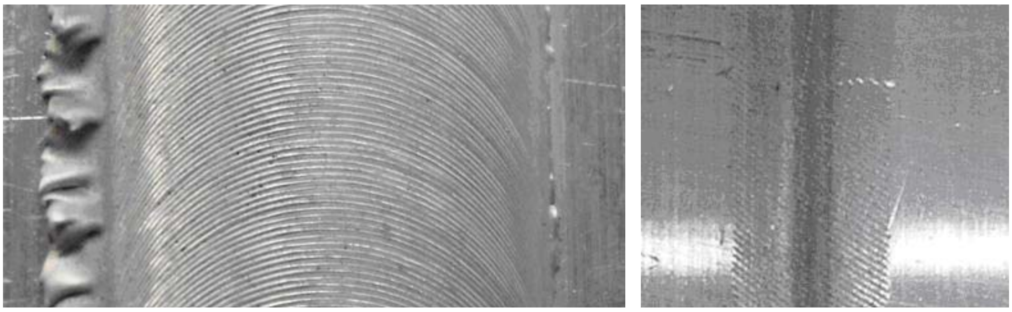

a) **b)**

Figure 2: Weld surfaces after friction stir welding of foamable precursor (thickness 5 mm):
a) upper part under shoulder; b) bottom part under pin

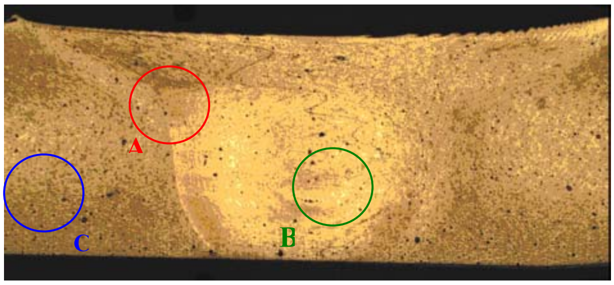

Overall weld (magnification 12,5x)

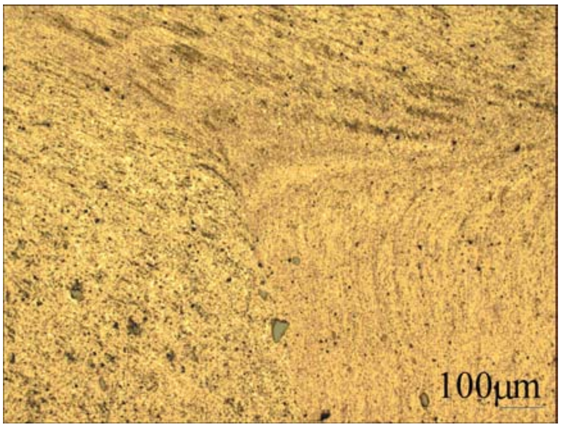

Detail A

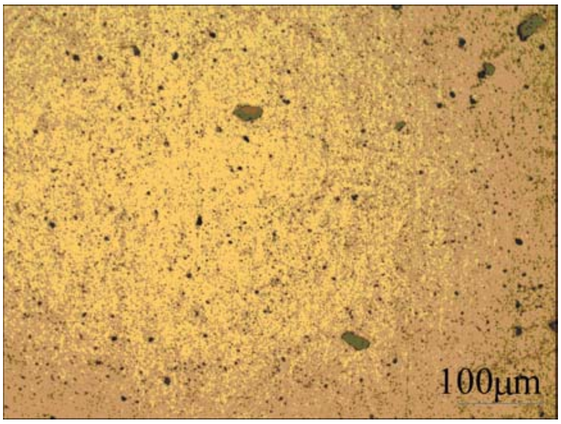

Detail B

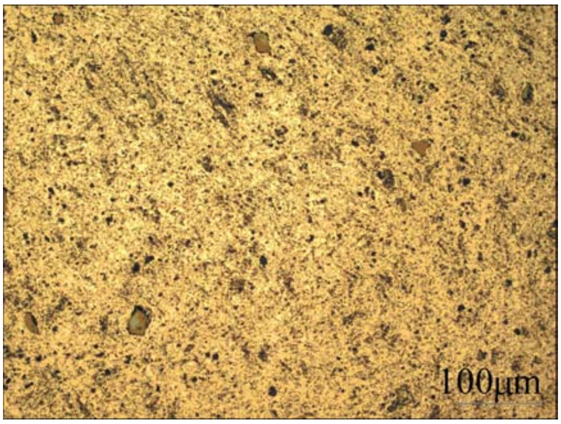

Detail C

Figure 3: Microstructure of precursor material after welding: border area between base material and weld (detail A); microstructure of a weld zone (detail B) and of a base material (detail C).

Fig. 3 confirms the assumption that FSW leads to smaller grain size in weld area compared to the base material [2]. Question is how this smaller grain size and overall FSW process affects the foamability of precursor.

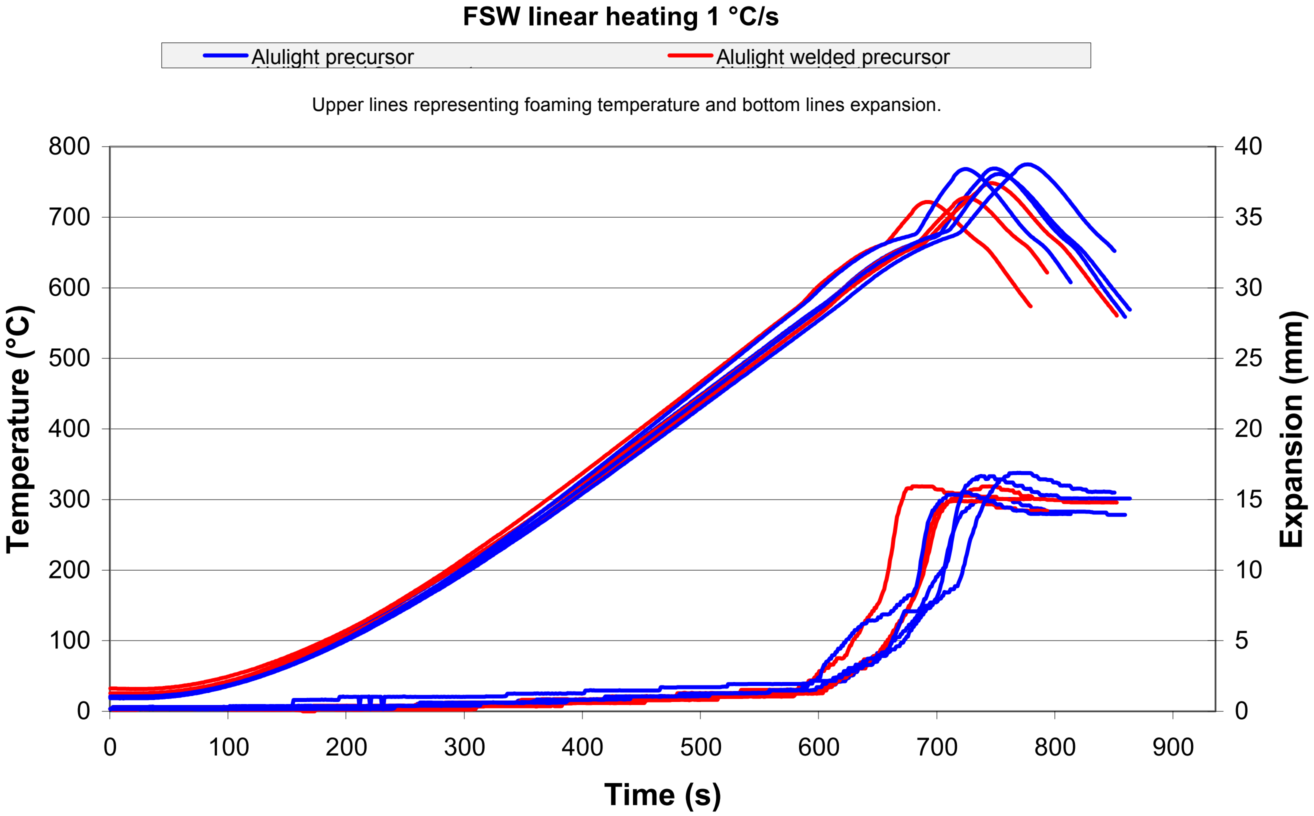

Figure 4. Results of the foaming experiments.

Therefore several foaming experiments were performed with both original as well as welded precursor materials at linear heating rate of 1°C/s. Figure 4 shows expansion kinetics (bottom lines) with corresponding temperature profiles (upper lines). Blue line represents original material (outside the weld) and red one the welded part of the same precursor. Generally, it can be seen that the foaming ability of precursor material after friction stir welding remains almost unchanged. Slight shift of expansion towards shorter foaming times can be attributed to improved heat transfer within fine grained stirred zone. However these differences are negligible from practical point of view.

Figure 5 shows structure of welded precursor samples after foaming experiment. As it could be expected from results of foaming kinetics, there is no significant difference between foam structure obtained from the welded zone and from both original precursors.

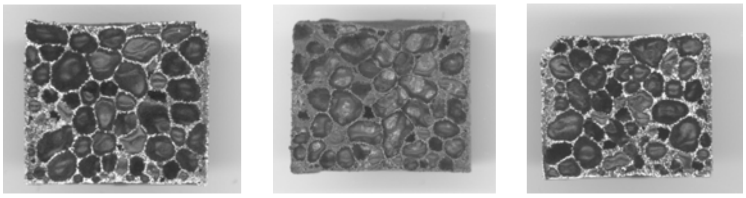

Figure 5: Structure of foams made from original precursors (left and right) and from the welded zone (middle).

The experiments have shown that FSW is really very promising method for joining of foamable precursors. Premature foaming was not observed at all and the fine structure of stirred zone has not resulted in any significant difference concerning the foaming ability of both precursor and weld.

FSW of aluminium foam

The joining of foams is still very tricky task, especially when permanent metallurgical bonding has to be obtained [3]. In this case simple FSW is not possible, because foams are compressible and thus pressure necessary to create sufficient frictional forces between rotating tool and cell wall material does not arise after inserting a pin into the porous structure. One possibility is to insert a bulk aluminium profile made of alloy with higher melting point than the foamable precursor into the foaming mould before foaming and then to use this profile as a base material for final FSW. Fig. 6 shows an example, where such an insert was foamed-in AlSi10 foam and then used for welding with the similarly manufactured counterpart. The advantage against simple welding is significantly lower thermal loading of the part during welding and thus lower thermal stresses at the foam – insert interface. Moreover a part of foamable precursor, which was not allowed to foam (e.g. cooled edge) can be used instead of inserts which considerably simplify the manufacturing of foams for subsequent welding..

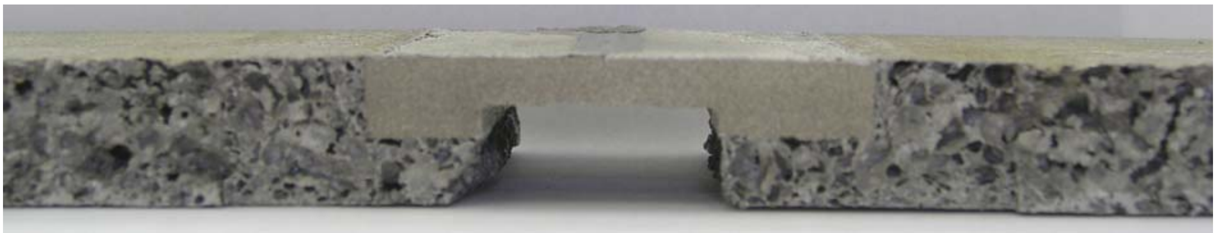

Figure 6: FSW of two AlSi10-foam samples using bulk inserts made of plain Al..

FSW of foam-cored sandwiches

If glued sandwiches are to be welded, the involving heat may not destroy the adhesive layer between core and coversheets also in the vicinity of the weld. This is very difficult (even almost impossible) to achieve with traditional welding techniques. Furthermore if hardened coversheets are used, their properties cannot be redressed via after treatment, because of low thermal stability of adhesive. As it was already mentioned, FSW produces significantly less heat than traditional welding, as the material is not melted at all, and provides therefore very promising method also in this case. The main problem to utilise FSW for this purpose is the low indentation resistance of the foam core. When the pin is inserted between two adjacent coversheets the material is partially pressurised into the pores below the pin and the frictional forces enabling good stirring and thus metallurgical bonding do not come up. Therefore some kind of support must be inserted between coversheets prior to FSW to provide stable base to rotating tool. Figure 7 shows several types of such inserts between sandwich plates.

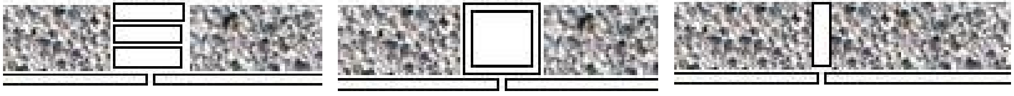

Figure 7: Various inserts between coversheets enabling FSW of sandwich plates.

If the welding is performed properly the supporting profiles are also welded to both adjacent coversheets in one operation, which significantly improves the mechanical properties of the joint. The experiments have shown that satisfactory bonding can be attained for coversheets thicker than 1 mm. During welding no degradation of adhesive properties was observed. Heat generated in weld area is very quickly dissipated in the coversheet (without significant temperature rise), because of its very good thermal conductivity. For smaller pieces some kind of cooling can be optionally applied. The properties attained after thermal treatment of coversheets before joining can be preserved in this way as well.

Conclusions

It has been shown that FSW technique is very successful tool for joining of foamable materials. No degradation of foaming ability was observed in foaming of welded AlSi10 precursors. Next step should be the optimisation of the process (tool rotating rate, tool traverse speed, pin designs) for foamable precursors made of other alloys. The earlier start of foaming of stirred material if compared with original precursor needs also more profound explanation.

Joining of aluminium foam core sandwich plates via FSW has also proven its feasibility. Heat generated during welding did not harm the properties of adhesive and interfacial bonding strength stayed preserved. Further research is needed to optimise the tool and joint design for FSW of thin coversheets and to investigate systematically the mechanical properties of obtained joints.

Reference

1. R.S.Mishra, Z.Y.Ma: ″Friction stir welding and processing″, Materials Science and Engineering R 50 (2005) 1-78, 2005 Elsevier Science Ltd.
2. C.G.Rohdes, M.W.Mahoney, W.A.Bingel, M.Calabrese: ″Fine-grain evolution in friction stir processed 7050 aluminium″, Scripta Material 48(2003) 1451-1455, Elsevier Science Ltd.
3. F. Simančik., W. Rajner, R. Laag.: “Reinforced Alulight for structural use”, Proceeding of the conference “Processing and Properties of Lightweight Cellular Metals and Structures (TMS Annual Meeting)”, Seattle, 2002, p. 25.

11. Savjetovanje o materijalima, tehnologijama, trenju i trošenju
11. Conference on Materials, Processes, Friction and Wear
MATRIB'06, Vela Luka, 22-24.06.2006.

STUDY OF PET/HDPE BLENDS WITH EPDM COMPATIBILIZER
PET/HDPE POLIMERNE MJEŠAVINE S EPDM KOMPATIBILIZATOROM

Ljerka Kratofil, Zlata Hrnjak-Murgić, Jasenka Jelenčić
Faculty of Chemical Engineering and Technology, P.O. Box 177, Zagreb, Croatia
E-mail: zhrnjak@marie.fkit.hr

Abstract: Ecological concerns provided the need for intensive research of waste polymers recycling. Poly(ethylene terephthalate), PET, is one of polymers which can be successfully recycled by several methods. It is very interesting to study mechanical recycling of PET through preparation of different polymer blends. Collected PET usually contains some high-density polyethylene (HDPE) impurities. Simultaneous recycling of PET and HDPE simplifies the recycling process and brings economical benefits. To obtain compatibile PET/HDPE blends it is necessary to use suitable types of compatibilizers. In this work PET/HDPE blends and PET/HDPE blends with ethylene-propylene diene (EPDM) compatibilizer were studied. PET/HDPE polymer blends were prepared by mixing in ratio of 97/3, 95/5, 94/6 and 90/10. EPDM compatibilizer was prepared as EPDM/HDPE masterbatch (EPDM-M). In the other step this compatibilizer was mixed with PET/HDPE blend 95/5 to obtain blends with compatibilizer. All prepared blends were characterized by scanning electron microscopy (SEM) in order to study the morphology of blends and characterized by FTIR spectroscopy. Free surface energy of all blends was also measured to study the influence of compatibilizer on the interactions at the interface in polymer blends. It can be concluded that when PET/HDPE blends were prepared with EPDM-M masterbatch two step mixing process shows significant achievement in compatibility. The results show that higher interactions between phases in polymer blends are obtained when the compatibilizer is used, which is reflected on blend properties.

Key words: compatibilizer, ethylene-propylene-diene rubber (EPDM), high density polyethylene (HDPE), mechanical recycling, poly(ethylene-terephthalate) (PET), polymer blends

Sažetak: Briga za zaštitu okoliša nalaže potrebu za intenzivnim istraživanjem mogućnosti recikliranja otpadnih polimernih materijala. Poli(etilen-tereftalat), PET, jedan je od polimera koji se može uspješno reciklirati različitim metodama, a ispituje se i recikliranje PET-a pripremom različitih polimernih mješavina. Sakupljeni PET često sadrži onečišćenja polietilenom visoke gustoće (HDPE) jer su od njega izrađeni čepovi za boce. Recikliranje PET-a u prisutnosti HDPE-a čini proces recikliranja jednostavnijim i jeftinijim. Da bi se dobile kompatibilne polimerne mješavine PET/HDPE, nužna je upotreba prikladnih vrsta kompatibilizatora. U ovom su radu proučavane PET/HDPE polimerne mješavine te polimerne mješavine s etilen-propilen-dienskim kopolimerom (EPDM) kao kompatibilizatorom. PET/HDPE polimerne mješavine pripremljene su u omjeru 97/3, 95/5, 94/6 and 90/10. EPDM kompatibilizator pripremljen je kao EPDM/HDPE *masterbatch* (EPDM-M). Zatim je ovako pripremljen kompatibilizator pomiješan s polimernom mješavinom PET/HDPE 95/5 te je tako pripremljena serija polimernih mješavina s kompatibilizatorom. Sve pripremljene polimerne mješavine karakterizirane su skenirajućom elektronskom mikroskopijom (SEM) da bi se istražila njihova morfologija. Provedena je i karakterizacija FTIR spektroskopijom. Slobodna energija površine polimernih mješavina izmjerena ja da bi se ispitao utjecaj kompatibilizatora na interakcije komponenata u ispitivanim polimernim mješavinama. Može se zaključiti da proces pripreme polimernih mješavina u dva stupnja, koji je proveden pri pripremi polimernih mješavina s EPDM-M kompatibilizatorom, ima utjecaj na poboljšanje kompatibilnosti. Rezultati pokazuju da upotreba kompatibilizatora utječe na povećanje interakcija između komponenata polimernih mješavina što se odražava na poboljšanje svojstava polimernih mješavina.

Ključne riječi: etilen-propilen-dienski kopolimer (EPDM), kompatibilizator, mehaničko recikliranje, poli(etilen-tereftalat) (PET), polietilen visoke gustoće (HDPE), polimerne mješavine.

INTRODUCTION

Poly(ethylene-terephthalate) (PET) is extensively used in packaging of consumer goods and industrial products. The main packaging applications of PET are bottles used for storing juices, mineral water, oil and many other liquids. This is the reason why these bottles represent the highest content in total quantity of collected waste PET. Due to the enormous growth of plastic waste materials the environmental policy of many countries encourages the recycling of plastics[1]. Recycling of plastic is a ecologically friendly method because it results with new polymer material instead of waste accumulation in our environment. Recycling of waste PET is one of the most spread and developed methods of polymer recycling. Recently, recycling of PET with presence of other polymers is also developing. This is a effective approach to produce materials with a new range of properties and to decrease the cost of recycling process, which usually always includes high cost procedures of impurities separation. However, most polymer pairs are unfortunately immiscible and blended together result in phase separation, which leads to poor mechanical properties and undesirable performance for target end uses. In spite of this, a wide range of new useful materials with improved and unique properties have been obtained from such immiscible and incompatible polymer pairs either, by the addition of a third component, usually a graft or block copolymer, or by in situ formation of such copolymers during the blend preparation[2].

In our study PET was mechanically recycled with presence of HDPE impurities. HDPE is commonly used for caps for PET bottles. Recycling of PET with present HDPE impurities simplifies the recycling process because there is no removing of HDPE impurities from PET before recycling. However, since PET and HDPE are extremely immiscible from thermodynamic point of view, the interfacial interactions between PET and HDPE are poor and the blend compatibility was not achieved. The objective of the present study is to improve the compatibility between PET and HDPE using ethylene-propylene-diene rubber (EPDM) as compatibilizer, which was prepared as EPDM/HDPE masterbatch (EPDM-M).

EXPERIMENTAL

Materials. Materials used for preparation of PET/HDPE polymer blends were poly(ethylene terephthalate), PET (waste bottles), high density polyethylene, HDPE (waste bottles), ethylene-propylene-diene copolymer, EPDM (Keltan 312, DSM, Netherlands; 55 wt.-% ethylene, 4 wt.-% diene, Mooney viscosity = 33 °M).

PET pre-treatment. The waste PET and HDPE bottles were collected, sorted, washed and dried. Bottles were sorted by colour and any undesirable parts, like paper labels and caps, were removed. The bottles were washed at 80 °C in NaOH solution, dried at room temperature, cut into small flakes (cca 6x6 mm) and dried for 24 hours (PET at 120 °C, HDPE at 80 °C) to eliminate moisture.

Blend preparation

Blend preparation was carried out in Brabender plasticorder internal mixer. Composition of PET/HDPE blends is given in Table 1. Blends were prepared without compatibilizer and with EPDM masterbatch. All PET/HDPE blends were mixed at the temperature of 255 °C. Blends with EPDM masterbatch were prepared in two steps. First EPDM-M masterbatch was prepared by mixing as EPDM/HDPE blend containing 10 mass.-% of HDPE (blending temperature: 210 °C). The EPDM/HDPE masterbatch was then mixed with PET/PE5 and blended at 255 °C to obtain PET/PE5/EPDM-M blends. The speed of the screws for preparation of all blends was 30 rpm and the residence time was 5 minutes.

Table 1. Composition of blends.

Samples PET/HDPE	**PET bottles mass.-%**	**HDPE bottles mass. -%**	**Compatibilizer phr**
PET/PE10	90	10	-
PET/PE6	94	6	-
PET/PE5	95	5	-
PET/PE3	97	3	-
	PET/PE5 mass.-%		**EPDM–M mass.-%**
PET/PE5/EPDM-M50	50		50
PET/PE5/EPDM-M30	70		30
PET/PE5/EPDM-M15	85		15
Masterbatch EPDM-M	EPDM mass.-%		HDPE mass. -%
	90		10

Characterization

Scanning electron microscopy (SEM)

Morphology of studied blends was characterized from a cross-section of cryogenically fractured surfaces of pressed samples (2 mm thick) using a Philips XL 30 Scanning Electron Microscope. Samples were immersed in liquid nitrogen for more than 15 min to cool down and then fractured immediately. The dried samples were sputter-coated with gold prior to scanning electron microscopy (SEM) examination.

FTIR spectroscopy

FTIR spectra of PET and HDPE as well as spectra of PET/HDPE blends with and without compatibilizer were recorded on Perkin Elmer Spectrum One FTIR spectrometer in the range of 4000 to 450 cm^{-1}. Samples for this purpose were ground into fine powder and prepared as pellets with KBr.

Contact angle measurements

Surface free energies of materials were determined throughout the measurements of contact angles on DataPhysics OCA 20 Instrument. The contact angles of standard test liquids (water, formamide and diiodometane) on the polymers have been measured at temperature T = 23°C ± 0.2 and humidity of 60% RH. Parameters of surface free energy were determined in order to study the interactions of components in polymer blends using Lewis acid/base theory.

RESULTS AND DISCUSSION

SEM studies

The basic idea of this work was to study potential compatibilizer for PET/HDPE blends, which should enhance interactions between PET and HDPE. In SEM micrographs of PET/PE10, PET/PE6 and PET/PE3 blends it is observed that PET/HDPE blends produce two phase morphology because of their incompatibility. In studied samples the fraction of HDPE was low (3, 6, 10 mass.-%) and HDPE forms dispersed phase in PET matrix. From the micrographs (Figure 1 a), b), c)) it can be seen that the morphology of blends is finer as fraction of HDPE (dispersed phase) decreases. The average particle size is 9.9 μm for blend with 3 mass.-% of HDPE, 12.7 μm for 6 mass.-% and 18.3 μm for 10 mass.-%. It has been known from literature[3] that the ratio of polymers in blend has significant effect on blend properties. It is possible that partially miscible polymers may form completely miscible blends when one of the polymers is present in very low concentration. The poor adhesion between the continuous and the dispersed phases is indicated by the presence of the holes in PET matrix formed by the pullout of HDPE particles[4], which could be seen in micrographs. The reason for such behaviour is big interfacial tension between polymers in blends.

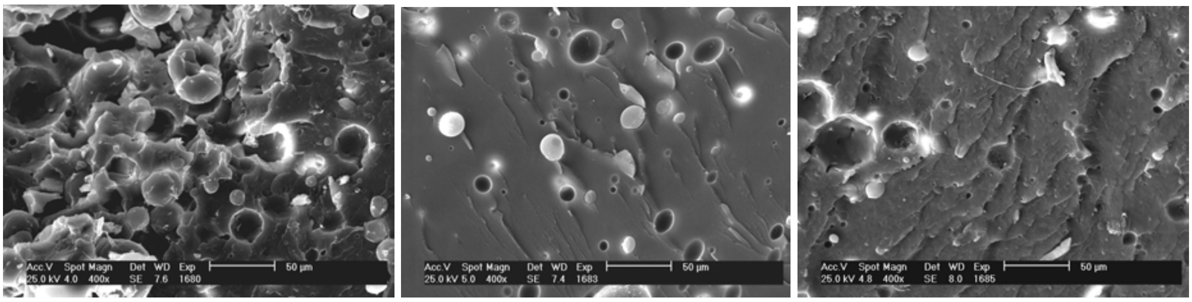

a) b) c)

Figure 1. SEM micrographs of a) PET/PE10, b) PET/PE6 and c) PET/PE3 blends.

The morphology of blends and efficiency of the studied compatibilzers could be best seen in micrographs (Figure 2 a), b), c)). It was assumed that the compatibilized PET/HDPE blends will show a reduction in interfacial tension between the two phases resulting in finer particle size of the dispersed phase. PET/HDPE blends were prepared with EPDM-M masterbatch to improve the compatibility. Due to present ethylene sequences in EPDM it is supposed that EPDM rubber will establish interactions with HDPE and PET matrix. At the same time it is expected that HDPE from masterbatch will additionally contribute to compatibility of the PET/HDPE blend. From the micrographs of PET/HDPE blends with EPDM-M masterbatch it is obvious that these blends show completely different morphology because of high fraction of EPDM elastomer. As the fraction of EPDM decreases finer morphology is observed because fraction of EPDM in EPDM-M masterbatch is high (90 mass.-%) and masterbatch is added in blends in fraction of 50, 30 and 15 mass.-%. Furthermore, it is supposed that PET is dispersed in EPDM when the concentration of EPDM is approximately equal to those of PET, micrograph 2a). In micrographs 2b) and 2c) it can be seen that HDPE makes spherical dispersed particles and EPDM and PET polymers make co-continuous phase where HDPE particles are encapsulated by the rubber phase. Particles size of HDPE is significantly decreased and it is in the range from 3.5 to 6.0 μm. In comparison to PET/HDPE blends without compatibilizer it can be concluded that used EPDM-M masterbatch causes better dispersion of HDPE and higher compatibility of blends. It can be concluded that the optimal content of masterbatch in blend is 15 mass.-% (sample PET/PE5/EPDM-M15, Figure 2c). Preparation of blend with masterbatch was two step process. This type of blend preparation also contributes to compatibility. The results of some other authors also showed that some premixing processes can improve blend properties in comparison to one step mixing process[5].

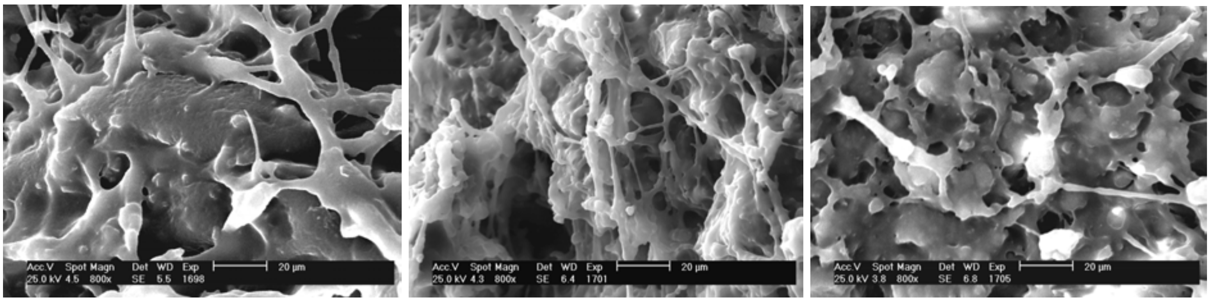

a) b) c)

Figure 2. SEM micrographs of a)PET/PE5/EPDM-M50, b) PET/PE5/EPDM-M30 and c) PET/PE5/EPDM-M15 blends.

FTIR Analysis

FTIR analysis in this study was not suitable for characterization of miscibility. It was used for identification of components and for detection of changes caused by degradation during processing at high temperatures. Spectra of PET, HDPE and PET/HDPE blend PET/PE6 are shown in Figure 3. It could be seen that the spectra of PET/HDPE blend reveals characteristic vibrations of both polymers.

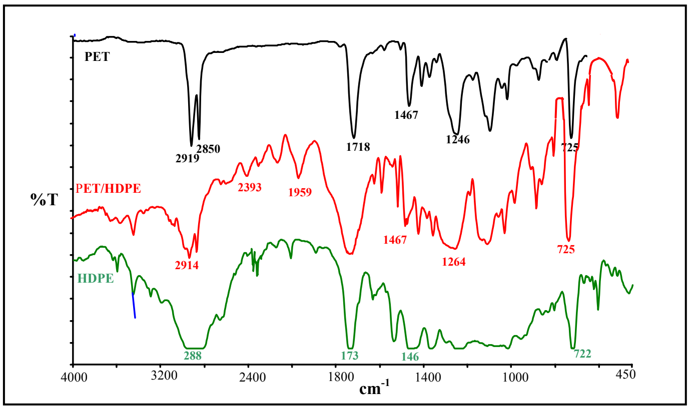

Figure 3. FTIR spectra of PET, HDPE and PET/HDPE polymer blend PET/PE6.

The changes between PET/HDPE blends without compatibilizer and with EPDM-M masterbatch were also studied. When PET/HDPE polymer blends are prepared at elevated temperatures certain depolymerization occured, which is detected through absorbance intensity of hydroxyl end groups (cca 3400 cm^{-1}). In blends with compatibilizer the absorbance intensity of that groups is decreased, which could be explained by better compatibilization and chain bonding (Figure 4).

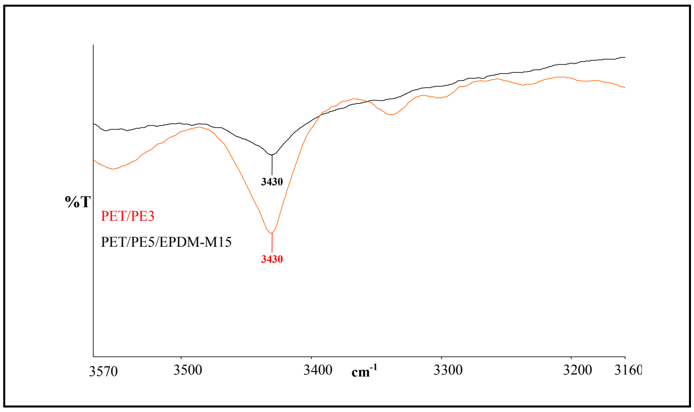

Figure 4. Decrease of carboxyl groups vibration intensity in blend with EPDM-M compatibilizer.

Contact angle measurements

Miscibility and compatibility of polymers in blend are strongly affected by the interface and/or interphase. The knowledge about the surface free energy of polymers is essential for optimising the interface and/or interphase to improve adhesion of polymers in blends. Because of the critical importance of the interface and interphase in blends, the study of adhesion is relevant for predicting of blend properties.[6] The calculation of adhesion parameters enables us to predict the intensity of interactions at the polymer/polymer interface and to correlate them with the other properties of polymer blends. The results in Table 2 illustrate the adhesion phenomena at the interface in studied PET/HDPE polymer blends.

Table 2. Surface free energies of PET/HDPE polymer blends, calculated according to Lewis acid-base theory.

	Surface free energy (mJ m^{-2})				
Samples	γ^{LW}	γ^{A}	γ^{B}	γ^{AB}	γ^{total}
PET	41,45	0,07	9,41	1,56	**43,01**
HDPE	38,12	0,17	8,62	2,40	**31,00**
EPDM	32,44	0,57	2,40	6,83	**21,60**
PET/PE10	35,57	1,05	3,18	3,65	**39,22**
PET/PE6	37,97	1,51	0,02	0,37	**38,34**
PET/PE3	36,02	1,53	9,69	7,71	**43,73**
PET/PE5/E-M50	23,79	5,34	7,58	12,73	**36,52**
PET/PE5/E-M30	32,16	1,34	0,60	1,80	**33,96**
PET/PE5/E-M15	26,66	0,87	7,87	5,23	**31,89**

The better adhesion in polymer blends leads to better properties. From the results it can be seen that PET/HDPE polymer blends show values of surface free energy between surface free energy of pure polymer components. Polymer blends prepared with EPDM-M masterbatch show further changes of surface free energy to lower values, which confirm better interactions of components in polymer blends. All these conclusions confirm the increase of homogeneity in blends, which is result of higher interactions.

CONCLUSION

From the results it can be seen that studied EPDM-M masterbatch enhances compatibility in PET/HDPE polymer blends. It can be concluded that the optimal content of masterbatch in blend is 15 mass.-%. Furthermore, it is observed that two step mixing process used for preparing of PET/HDPE blends with EPDM-M masterbatch also contributes to significant achievement in compatibility.

REFERENCES

1. *Scheirs, J.:* Incineration of plastic waste with energy recovery, in: Polymer Recycling: Science, Technology and Applications. *Scheirs, J.*, p. 508, John Wiley & Sons, New York (1998)
2. *Paul, D.R., Barlow, J. W., Keskkula*, H.: Polymer blends, in: Encyclopedia of Polymer Science and Engineering. *Mark, H. F., Bikales, N. M., Overberger, C. G., Menges, G.*, vol. 12, p. 399, John Wiley & Sons, New York (1985)
3. *Fox, D. W., Allen, R. B.*: Compatibility, in: Encyclopedia of Polymer Science and Engineering. *Mark, H. F., Bikales, N. M., Overberger, C. G., Menges, G.*, vol. 3, p. 758, John Wiley & Sons, New York (1985)
4. *Kim, D. H., Park, K. Y., Kim, J. Y., Suh, K. D.:* J. Appl. Polym. Sci. 78, p. 1017 (2000)
5. *Pracella, M., Rolla, L., Chionna, D., Galeski, A.:* Macromol. Chem. Phys. 203, p. 1473 (2002)
6. *Mittal, K. L.* in: Adhesion Science and Technology, *Le, L. H.,* vol. A, Plenum Press, New York (1975)

SPECIJALNE TISKARSKE BOJE

Vesna Kropar-Vančina[1], Darko Babić[1], Jana Žiljak Vujić[2]
Contact: babic@grf.hr

Grafički fakultet Sveučilišta u Zagrebu, Getaldićeva 2, 10000 Zagreb[1]
Tehničko veleučilište u Zagrebu, I. Lučića 3, 10000 Zagreb[2]

Sažetak: U sklopu rada opisane su neke od mnogobrojnih specijalnih boja koje se otiskuju konvencionalnim tehnikama tiska. Opisane su boje za specijalne namjene kao što su elektronske boje, boje za membranske dodirne sklopke, fosforescentne boje, strojno "čitljive" boje, sterilizacijske boje, boje koje mijenjaju obojenje, srebrne boje za struganje (strugalice), boje s mirisima u kapsulama i termokromatske boje. Opisane su i boje za zaštitu, magnetske boje te "nevidljive boje".

Ključne riječi: boje koj mijenjaju obojenje, elektronske boje, fosforescentne boje, nevidljive boje, srebrne strugalice, sterilizacijske boje, strojno čitljive boje, termokromatske boje, zaštitne boje

Abstract: In this work printing inks for special applications such as electronics inks, inks for membrane touch switches, phosphorescent inks, machine readable inks, sterilisation inks, colour change inks, oblitering silvers, inks with encapsulated fragnances and thermochromic inks are described. Description of security, magnetic and nonvisible inks is given too. All these inks are printed by conventional printing processes.

Key words: Colour Change Inks, Electronics Inks, Inks for Membrane Touch Switches, Inks with Encapsulated Fragnances, Machine Readable Inks, Oblitering Silvers, Phosphorescent Inks, Sterilisation Inks, Thermochromic Inks

1 UVOD

Tiskarske boje su komleksni koloidni i/ili molekularni disperzni sustavi sastavljeni od: pigmenti i/ili bojila, punila, veziva (ulja, smola, otapala), sušila i dodataka. Boje se formuliraju za različite tehnike tiska konvencionalne i digitalne/NIP, a u sklopu pojedine tehnike boje se razlikuju ovisno o vrsti tiskarskog stroja, tiskovnoj podlozi i brzini otiskivanja. U osnovi boje se dijele na pastozne ili guste i tekuće, rijetke odn. fluidne. [1-4]

2 OPĆI DIO

SASTAVNICE TISKARSKIH BOJA

PIGMENTI su krute tvari koje daju obojenje tiskarskim bojama, a o njima ovise reološka i druga svojstva tiskarskih boja kao npr. opacitet/transparentnost, svjetlostalnost, otpornost na toplinu, kemikalije, vodu itd. Pigmenti su netopljivi u vodi i/ili vezivima u kojima se raspršuju/dispergiraju, s kojima se trebaju dobro močiti i tvoriti koloidne disperzije.

Pigmenti se mogu podijeliti prema podrijetlu (prirodni i umjetni), kemijskom sastavu (anorganski i organski), boji (kromatski i akromatski), strukturi (kristalni i amorfni) i uporabi (za obojenje i sa specijalnim svojstvima).

Osnovna svojstva pigmenata su: veličina, raspodjela veličina čestica i oblik čestica, pokrivnost, izdašnost, svjetlostalnost, tekstura i ostala svojstva. [1-7]

BOJILA su krute tvari koje daju obojenje tiskarskim bojama, ali se za razliku od pigmenata, uglavnom, otapaju u otapalu (organskom i vodi) s kojim tvore prozirne molekularne disperzije. Otopine bojila rabe se za izradbu boja konvencionalanih i digitalnih/NIP tehnika tiska.

Bojila su zbog finog/molekularnog disperziteta sjajna, velike izdašnosti i transparentna. Bojila pokrivaju znatno veći kolor gamut od pigmenata, zbog mnogobrojnosti i specifičnih fizikalnih svojstava. Velika transparentnost je temeljni zahtjev za uspješan višebojni tisak s procesnim bojama (CMYK).

Bojila su po kemijskom sastavu organski spojevi, a dijele se na: direktna/izravna, disperzna, taložna, VAT, reaktivna, kisela ili anionska i lužnata ili kationska.

Zbog jednoznačne klasifikacije i identifikacije 600 pigmenata i 8000 bojila se označavaju šifrom prema COLOUR INDEXu (CI) koji propisuju Society of Dyers and Colourists i American Association of Textile Chemists and Colorists. [5-7]

PUNILA su krute anorganske tvari koja djelomično zamjenjuju skupe pigmente, ali i mijenjaju reološka svojstva tiskarskih boja. Punila su kao i pigmenti netopljiva u vodi i/ili vezivima u kojima se raspršuju/dispergiraju i s kojima se trebaju dobro močiti.

Vodene disperzije punila su neprozirne, a uljne veće ili manje prozirnosti ovisno o indeksu loma punila i veziva. Što je indeks loma punila bliži po iznosu indeksu loma ulja/veziva disperzija je prozirnija. Indeks loma punila i močenje punila vezivom ovise o: kemijskom sastavu, čistoći i veličini/finoći čestica punila. Srednja veličina čestica punila iznosi od 0.01 do 1,00 μm.

Najpoznatija punila su: barijev sulfat, milovka, kaolin, magnezijev karbonat, hidratiziran aluminijev hidroksid, kalcijev karbonat precipitiran, glina i silicijev dioksid. [5-10]

VEZIVA TISKARSKIH BOJA su tekuće tvari s kojima se pigmenti moče i u kojima se pigmenti dispergiraju. Vezivo treba u potpunosti obavijati fine čestice pigmenta kako bi nastala jednolika/homogena smjesa/disperzija.

Vezivo nosi pigment kroz prijenosne mehanizme tiskarskih strojeva, osigurava prijenos boje na tiskovnu podlogu i veže boju na podlogu. Vezivo daje boji reološka svojstva, sušiva svojstva i pogodnost za tisak. Odabir veziva ovisi o: tehnici tiska, vrsti tiskarskog stroja, brzini otiskivanja i tiskovnoj podlozi. [5-9]

Ulja - sastavnice veziva tiskarskih boja su viskozne tekuće tvari koje se prema podrijetlu dijele na biljna, životinjska, mineralna i umjetna, a prema sušivosti na sušiva, polusušiva i nesušiva. Sušivost ulja izravno ovisi o nezasićenosti odn. broju dvostrukih kovalentnih veza u molekuli ulja. Sušiva i polusušiva ulja se suše oksipolimerizacijom koja se može katalizirati sušilima. Biljna/vegetabilna ulja su esteri viših masnih kiselina i glicerola. Proizvode se prešanjem ili ekstrakcijom otapalima iz sjemenki, plodova i lišća biljaka. Pojedinipredstavnici biljnih ulja tiskarskih boja su: laneno ulje, tungovo ili kinesko drvno ulje, dehidrirano ricinusovo ulje, sojino ulje i ulje od repice. Mineralna ulja se proizode frakcionom destilacijom nafte. Vrelište mineralnih ulja je pri 350 ^{o}C ili više. To su smjese organskih spojeva pa im svojstva ovise o sastavu smjese. Uglavnom se rabe za izradbu jeftinih crnih roto boja i knjigotiskarskih boja. [2,5-7,11]
Smole - sastavnice veziva tiskarskih boja su organske viskozne tekuće ili amorfne krute tvari relativno velike molekularne mase. Smole se dijele na prirodne, modificirane i umjetne, a prema podrijetlu na biljne, životinjske i mineralne. Smole tiskarskim bojama poboljšavaju: adheziju, čvrstoću, savitljivost/fleksibilnost i sjaj suhog otiska. Od poluprirodnih smola za izradbu veziva tiskarskih boja najviše se rabe modificirani kolofonij i derivati celuloze. Modificiranjem kolofonija dobivaju se: metalni rezinati, esteri kolofonija, maleinske smole, fumarinske smole i dimerizirani kolofonij. Derivati celuloze se proizvode modificiranjem celuloze, a kako su promjene svojstava celuloze izrazito velike derivati celuloze se mogu svrstati u grupu umjetnih smola. Za veziva fleksografskih i boja za duboki tisak te sitotiskarskih boja rabe se derivati celuloze: nitro celuloza (NC), etil celuloza (EC), etil hidroksi etil celuloza (EHEC), celulozni acetat butirat (CAB), celulozni acetat propionat (CAP). [5-8] Umjetne smole veziva tiskarskih boja su: kolofonij fenolne smole, alkidne smole, ugljikovodične smole, urea i melamin formaldehidne smole, poliamidi, klorirana guma, ciklizirana guma, vinilne smole, ketonske smole, akrilne smole i epoksi smole. [2-10]
Otapala - sastavnice veziva tiskarskih boja su tekuće organske tvari koje otapaju smolu/smole tiskarskih boja. Otapala zadržavaju smolu u stabilnoj otopini tijekom proizvodnje, skladištenja i tiska do sušenja otiska. Nakon otiskivanja otapalo se, u pravilu, treba što brže ispariti osim otapala koja služe kao omekšivači/plastifikatori tvrdih filmova otisaka koji se u suhom filmu nalaze neodređeno vrijeme. Otapala se prema vrelištu dijele na otapala: niskih ($T_v<100$ ^{o}C), srednjih ($100 >T_v<150$ ^{o}C) i visokih vrelišta ($T_v<225$ ^{o}C). Otapala viših vrelišta su omekšivači/plastifikatori tvrdih filmova. Najvažnija svojstva otapala su "jakost" otapala

i brzina isparavanja otapala. Brzina isparavanja se određuje uspoređivanjem brzine isparavanja otapala s brzinom isparavanja iste količine etera, a označava kao broj brzine isparavanja (BBI). Otapala se prema brzini isparavanja dijele na otapala koja se brzo (BBI<10), srednje (10<BBI<35) i sporo (BBI>35) isparavaju ili "suše". Ponekad se miješanjem više otapala dobivaju specifične smjese otapala tzv. azeotropne smjese koje jednoliko isparavaju što je povoljno za tvorbu optimalne površine filma/otiska. Najviše otapala sadrže brzosušeće boje kojima se brzo otiskuje. Otapala su otrovna, zapaljiva (osim kloriranih ugljikovodika), a često i eksplozivna pa u pogonima treba imati "monitoring" isparavanja i koncentraciju para otapala u zraku te brzine sušenja otisaka zbog protupožarne prevencije i zaštite okoliša. U pogonima se ugrađuju rekuperatori pomoću kojih se pare otapala kondenziraju i vraćaju u tisak pa se tako smanjuju troškovi proizvodnje, a štiti se i okoliš. Prema kemijskom sastavu otapala se dijele na: ugljikovodike, alkohole, ketone, etere, estere, nitroalkane i terpene. [2,4,7]

SUŠILA su tvari koje ubrzavaju sušenje tiskarskih boja na tiskovnim podlogama odn. sušenje otisaka koji se suše oksipolimerizacijom. Po kemijskom sastavu sušila su oleati rezinati i naftenati, kobalta, mangana i olova. Sušenje katalizira kation/metalni ion, a topljivost sušila u vezivu ovisi o anionu/kiselinskom ionu.

Brzina sušenja tiskarske boje ovisi o: vrsti i količini sušila, temperaturi te udjelu vlage. Sušiva i polusušiva ulja vežu kisik iz zraka, tvore neastabilne perokside koji se brzo raspadaju na reaktivne radikale, a nakon oksidacije dolazi do izravne ili neizravne polimerizacije. Tijekom sušenja vezivo je, isprva, viskoznije i ljepljivije, zatim se stvara tanki film/kožica na površini otiska nakon čega otisak prosušuje u potpunosti te postaje netopljiv i otporan na toplinu.

Sušila ubrzavaju sušenje jer "daju" nascentni kisik. Samo optimalne količine sušila ubrzavaju sušenje otisaka tiskarskih boja. Kobaltno sušilo je najjače i najbrže, otisak se brzo suši, a na površini se stvara tvrda kožica ispod koje je mekana boja. Manganovo sušilo je slabije i sporije pa se otisak sporije suši, ali se suši u cijelom sloju. Olovno sušilo najmanje ubrzava sušenje, ali se otisak suši jednoliko u cijelom sloju. U višebojnom tisku u prvu boju treba dodati najmanje najslabijeg sušila, a u zadnju boju najviše najjačeg sušila. [3,6-9]

DODATCI poboljšavaju određena svojstva tiskarskih boja ili otklanjaju nepoželjne pojave u tisku. Dodaci se trebaju lako povezati s vezivom ili gotovom tiskarskom bojom. Dodatci tiskarskih boja su: voskovi, ulja, masti, antioksidansi, sapuni, mirisi itd. [4-8]

3 STRUČNI DIO

3.1 ELEKTRONSKE BOJE

Otisnuta pločica strujnog kruga u početku je tanka bakrena folija na temeljnom izolacijskom laminatu. Specijalnom tiskarskom bojom otpornom na otopinu za jetkanje otiskuju se sitotiskom vodljive vrpce/trake na bakrenoj foliji. Zatim se kiselinom otopi bakar s površina koje ne trebaju biti vodljive, a boja koja pokriva vodljive vrpce bakra, otopi se organskim otapalom ili razrjeđenom alkoholnom otopinom kako bi se "oslobodile" vodljive vrpce/trake bakra.

Na pločici se izbuše rupice u koje se pričvrste elektronske komponente na izolacijskoj strani, a žice prolaze kroz rupice do bakrenih traka/vrpca. Kontaki se učvrste/spoje lemljenjem samo na spoju pa je potrebno otiskivati s bojom koja je otporna na lemljenje. Takve boje temeljene su na dvokomponentnim polimernim sustavima epoksi poliamida ili epoksi akrilata koji se suše pomoću UVa.

Ponekad treba formirati električne kontakte između dviju strana ploče elektroplatiniranjem ili taloženjem vodljivog sloja metala kroz rupice. Za takve pločice rabi se boja otporna na elektroplatiniranje koja zaštiti preostale površine od metala za platiniranje. Pločica se označi bojom koja se suši toplinom, a temeljena je na epoksi smoli.

3.2 BOJE ZA MEMBRANSKE DODIRNE SKLOPKE

Membranske dodirne preklopke odn. prekidači na dodir s membranom rabe se sve više od uređaja u domaćinstvima do profesionalnih uređaja gdje uspješno zamjenjuju mehaničke preklopke/prekidače.

Temeljne sastavnice membranske dodirne preklopke su: prvi sloj ili sloj na vrhu s otisnutim simbolima, prvi ili gornji strujni krug, tanki sloj između strujnih krugova,
drugi ili donji strujni krug i podložna pločica. Kad se prstom pritisne gornji strujni krug uspostavlja se kontakt, a kad se prst makne kontakta više nema.

Strujni krugovi otiskuju se s vodljivim bojama na poliesterskoj osnovi. Na mjestima gdje se križaju vodljive vrpce/trake rabi se dielektrični premaz kao izolator. Simboli se također otiskuju specijalnim bojama. [2,6-9]

3.3 FOSFORESCENTNE BOJE

Fosforescentne boje, kao i fluorescentne apsorbiraju i reemitiraju svjetlo. Fluorescentne boje reemitiraju svjetlo odmah pri različitim valnim duljinama pa su takve boje vrlo sjajne. Fosforescentne boje reemitiraju svjetlo i dva sata nakon osvjetljavanja pa su vidljive (sjaje) u mraku. Aktivirani ZnS je temeljna sastavnica fosforescentnih boja koje se otiskuju u sitotisku s mrežicama velikih okanaca jer su čestice cink sulfida velike/grube. [5,7]

3.4 STROJNO "ČITLJIVE" BOJE

Strojno čitljivim bojama ili bojama koje se mogu "čitati" optičkim čitačima (engl. Optical Character Recognition Inks) otiskuju se crni magnetski znakovi - brojke i slova. Boje su temeljene na magnetskom željeznom oksidu koji daje stalan magnetski "odgovor" na "čitaču". Pravilan položaj znakova za čitanje osigurava se pomoću crta vodilica. Zbog učinkovitosti znakovi se otiskuju crnom ili nekom tamnom bojom, ali crte vodilice ne smiju biti vidljive "čitaču", a trebaju biti vidljive korisnicima.

Optički "čitači" (engl. Optical Character Readers, OCRs) mogu "pročitati" i nemagnetske znakove, ako su na određenom mjestu, određenog oblika i određene boje. Bilo koja boja može se "čitati" optičkim čitačem, ako je OCR čitač dovoljno osjetljiv na boju otiska. Najviše se rabe čitači bar kodova, a OCR tehnologija rabi se za sortiranje dokumenata, čekova, predračuna, pošte, ali i za skaniranje dokumenata na kojima konvertira otisak u digitalne signale za računalo.

Tiskarski stroj treba temeljito očistiti prije tiska boje koja se ne "čita" jer i najmanja kontaminacija crnom bojom može prouzročiti odgovor na nekom scaneru. Također ne smije biti mrljanja čitljive boje otisnute bilo gdje na obrascu jer ako boja uđe u područje čitanja može "zbuniti" scaner. Papiri koji se rabe ne smiju sadržavati optička bjelila i tamne točkice koje, također, mogu interferirati sa čitačima. [4-7]

3.5 STERILIZACIJSKE BOJE

Pakirane kirurške i medicinske proizvode treba streilizirati u autoklavima pri povišenom tlaku i temperaturi (T>100 ^{o}C) u vlažnoj atmosferi ili pomoću etilenoksida. Boje otisnute u dubokom i fleksografskom tisku promjenom obojenja od bijelog do crnog potvrđuju uspješno obavljenu sterilizaciju. [5-7]

3.6 BOJE KOJE MIJENJAJU OBOJENJE

Boje koje mijenjaju obojenje često se rabe kao elementi zaštite otisaka pri sigurnosnom tisku. Rabe se boje koje mijenjaju obojenje u dodiru s odgovarajučim olovkama. Reverzibilne boja su bezbojne, u dodiru s olovkama mijenjaju obojenje, a stajanjem izblijede odn. obezboje se. Ireverzibilne boje od bezbojnih postanu crne i više se ne mijenjaju obojenje. [2,4-7]

3.7 SREBRNE BOJE ZA STRUGANJE

Kartica instant lutrije ima niz simbola, dobitnih ili gubitnih, koji se otkrivaju kad se ostruže površina otisnuta srebrnom bojom za struganje odn. "strugalicom". Kod takvih otisaka najvažnije je da prodavač i kupac ne mogu identificirati dobitnu karticu prije struganja otiska. U kartice su ugrađeni elementi osiguranja, a sastavnice kartica su: temeljni karton, otisnuti uzorak sa simbolima, sloj prozirnog laka ili folije, otisak srebrne boje za struganje i otisak na vrhu. Uzorak i simboli otiskuju se offsetnim bojama, a otisak se treba potpuno prosušiti prije tiska ostalih slojeva. Sloj prozirnog laka ili prozirna folija na otisku daje glatku površinu jednolike upojnosti na kojoj se otiskuje srebrna boja za struganje kroz koju se ne može vidjeti otisak, a istodobno to je površina s koje se "strugalica" lako struže bez mrljanja.

Najvažniji element osiguranja je srebrna boja otisnuta u sitotisku, kako bi otisak bio potpuno neproziran kada se kartica osvjetli jakim izvorom svjetla s donje strane. U bojama za struganje nalazi se veliki udjel aluminijskog praha kako bi dobili potrebnu pokrivnost, a kao vezivo najviše se rabi lateks jer dobro veže aluminij i lako se ukloni struganjem. Pri formulaciji "strugalica" valja precizno izbalansirati adheziju boje i lakoću struganja. Srebrna boja se ne smije otirati tijekom daljne obrade, transporta i skladištenja, ali treba se lako strugati noktom ili novčićem bez prašenja boje. [4-7]

3.8 BOJE S MIRISIMA U KAPSULAMA

Tehnika kapsuliranja mirisa je ista kao i kapsuliranje bojila. Svaki miris može se spremiti u kapsule koje se inkorporiraju u vezivo temeljeno na vodi i otiskuju sitotiskom preko izabranog otiska. Suhi otisak je praktički nevidljiv, a miris je stabilan u kapsulama do trenutka kad se otisak (npr. tester parfema ili prehrambenog proizvoda) zagrebe noktom. [2,4-7]

3.9 TERMOKROMATSKE BOJE

U kapsulama se može pohraniti i termokromatska boja temeljena na tekućim kristalima koji mijenjaju obojenje s promjenom temperature. Promjena boje započinje u intervalu od -30 do 70 ^{o}C, a interval promjene može biti mali 1 ^{o}C ili veliki 20 ^{o}C. Termokromatske boje rabe se za industrijske i reklamne potrebe, na etiketama zapakiranih proizvoda u deep freezu kako bi bili sigurni da su pohranjene pri odgovarajučoj temperaturi, na etiketama boca s vinom gdje potvrđuju kako je vino spremno za posluživanje ili na majicama (engl. T shirts) gdje mijenjaju boju promjenom topline tijela. [1-2, 5-7]

3.10 BOJE ZA ZAŠTITU (ZAŠTITNE BOJE)

Zaštitnim bojama (engl. Secutity Inks) otiskuju se čekovi i drugi dokumenti koji se mogu unovčiti. Iznos novca piše se preko čeka otisnutog zaštitnom bojom. Brisanje ili bilo koji pokušaj izmjene brojeva/znamenki uništava ili oštećuje boju. Zaštitne boje su, uglavnom, topljive u vodi pa se lako otapaju u dodiru s tekućim brisačem boja ili kemikalijama u sklopu boje za brisanje otisaka.

Za tisak osobnih iskaznica, putovnica, vozačkih dozvola i sl. rabe se specijalne color-shift boje koje imaju "pomak obojenja". Na otisku se vidi promjena boje ovisno o kutu gledanja. Boje se tiskaju u dubokom tisku, motivi su jednostavni i lako prepoznatljivi, ali zbog color-shifta nemoguće je krivotvoriti otisak odn. dokument. Boje s dva stupnja zaštite temeljene su na tekućim kristalima pa imaju color-shift i polarizaciju svjetla za koju je potreban specijalni dvostruki filtar. Gledana s jedne strane filtra boja je intenzivna i svjetla, a s druge strane se mijeja ili nestaje. [2-7]

3.11 MAGNETSKE BOJE

Magnetske boje (engl. Magnetic Inks) rabe se za tisak serijskih brojeva i ostalih informacja na čekovima kao bi se sa čekovima rukovalo pomoću uređaja koji mogu prepoznati otiske otisnute magnetskim bojama (MICR i. e. Magnetic Ink Character Recognition). Magnetski željezni oksid rabi se kao pigment magnetskih boja. To je pigment s kojim je teško formulirati kvalitetnu boju odn. boju potrebne tečljivosti, s kojom se može otiskivati i koja se dobro suši te na kraju daje otisak koji se lako očitava MICRom. Tiskari ne smiju mijenjati boju dodavanjem različitih dodataka koji mogu promijeniti magnetičnost otiska i njegovu čitljivost na MICRu. [3-10]

3.12 NEVIDLJIVE BOJE

Nevidljive boje s glinom rabe za tisak na vrlo sjajnim premazanim papirima. Otisci su skoro nevidljivi kad se boja osuši. Kako je glina osjetljivija na "struganje olovkom" od premazanog papira, nakon "struganja" otisak postaje vidljiv.

Transparentne nevidljive boje imaju tvari koje svjetlucaju kad u izložene "crnom svjelu" odn. UV zračenju i rabe se za tisak različitih kartica za lutriju, dobitnih kupona i sl. pa pri isplati blagajnik može lako uređajem s UV zračenjem provjeriti/pročitati nevidljivi zaštitni (engl. Security) dizajn.

Rabe se i nevidljive boje s bezbojnim, transparentnim tvarima koje brzo potamne kad se otisak zagrijava. Otisci ostalih nevidljivivih boja postanu vidljivi nakon obrade s kemikalijama ili njihovim parama koje reagiraju s određenim sastavnicama boja i tvore vidljivi otisak. [3-9].

4 RASPRAVA I ZAKLJUČCI

Tiskarske boje su komleksni koloidni i/ili molekularni disperzni sustavi
sastavljeni od: pigmenta i/ili bojila, punila, veziva (ulja, smola, otapala), sušila i dodataka. Tiskarske boje se prema konzistenciji dijele na pastozne/guste i tekuće/rijetke. Prema tehnikama tiska dijele se na boje za konvencionalne tehnike tiska i boje za alternativne tehnike tiska (NIP).

Elektronske boje rabe se za tisak pločica strujnog kruga. Kao tiskovna podloga rabi se bakrena folija na temeljnom izolacijskom laminatu. Tehnikom sitotiska otiskuju se vodljive trake/vrpce na bakrenoj foliji, a boja mora biti otporna na kiseline koje otapaju bakar s neotisnutih površina te topljiva u organskom otapalu kako bi se vodljive vrpce bakra mogle "osloboditi". Takve boje temeljene su na vrlo kiseloj smoli otopljenoj u glikol eteru. Za pločice strujnog kruga rabe se i boje koje su otporne na lemljenje, a temeljene su na dvokomponentnim polimernim sustavima epoksi poliamida ili epoksi akrilata koji se suše UV zračenjem. Ako se pločice obrađuju elektroplatiniranjem rabe se boje temeljene na epoksi aminskom polimeru.

Za tisak strujnih krugova membranskih dodirnih preklopki rabe se vodljive boje na osnovi poliestera, a simboli se mogu otisnuti konvencionalnim vinilnim bojama ili specijalnim bojama.

Fosforescentne i fluorescentnim boje apsorbiraju i reemitiraju svjetlo. Fluorescentne boje reemitiraju svjetlo odmah pri različitim valnim duljinama pa su boje vrlo sjajne, a forescentne boje nastavljaju reemitirati svjetlo i dva sata nakon osvjetljavanja pa sjaje u mraku. Aktivirani ZnS je temeljna sastavnica ovih boja. Kako su čestice cink sulfida velike potrebno je takvim bojama otiskivati u sitotisku, a mrežice trebaju imati velika okanca.

Strojno "čitljive" boje su temeljene na magnetskom željeznom oksidu koji daje stalan magnetski "odgovor" na čitaču. To su crni magnetski znakovi - brojke i slova otisnuti na čekovima i dokumentima koji se automatski sortiraju. Međutim magnetski znakovi nisu jedini čitljivi na čitaču. Optički čitači (engl. Optical Character Readers, OCRs) mogu "čitati" nemagnetske znakove, ako su na određenom mjesu, definiranog oblika i obojenja. Pravilan položaj znakova za čitanje osigurava se pomoću crta vodilica. Zbog učinkovitosti znakovi se otiskuju crnom ili nekom tamnom bojom. Crte vodilice ne smiju biti vidljive "čitaču", ali trebaju biti vidljive ljudima pa "čitači" imaju "čitače glave" s različitim "odgovorima" na različite valne duljine u odnosu na karakteristike ljudskog oka.

Kirurške i medicinske proizvode treba nakon pakiranja streilizirati pa se za tisak takve ambalaže rabe boje koje promjenom obojenja otiska od bijelog do crnog. ukazuju na uspješno obavljenu sterilizaciju.

Boje koje mijenjaju obojenje često se rabe pri sigurnosnom tisku, a njihov sastav treba ostati tajna jer u suprotnom gube vrijednost u sustavu osiguranja. Rabe se boje koje mijenjaju obojenje u dodiru s odgovarajučim olovkama. Reverzibilne boja su bezbojne, u dodiru s olovkama mijenjaju obojenje, a stajanjem se obezboje. Ireverzibilne boje od bezbojnih postanu crne i više se ne mijenjaju. Ako original dodirnemo s vlažnim prstom stvara se obojena mrlja, a na falsifikatu takvih mrlja nema.

Kartica sa srebrnom strugalicom sastoji se od pet dijelova, a to su: temeljni karton, otisnuti uzorak sa simbolima, sloj prozirnog laka ili prozirne laminatne folije, otisak srebrne boje za struganje i otisak na vrhu. Uzorak i simboli (na 2. sloju) otiskuju se, uglavnom, offsetnim bojama, a sloj prozirnog laka ili prozirna folija na otisku je temeljna sastavnica osiguranja kartice jer tvori potpuno glatku površinu jednolike upojnosti na kojoj se otiskuje boja za struganje, kroz koju se ne može vidjeti otisak i površinu s koje se boja za struganje lako struže bez mrljanja. Boja za struganje otiskuje se u sitotisku jer otisak treba biti nevidljiv i onda kada se kartica osvjetli jakim izvorom svjetla s donje strane. Temeljne sastavnice srebrnih strugalica su auminijski prah i lateks. U bojama se treba precizno izbalansirati adhezija boje i lakoća struganja. Otisak se treba lako strugati noktom ili novčićem bez stvaranja prašine od boje koja bi mogal zamrljati prste ili odjeću osobe koja sudjeluje u igri.

Boje s mirisima u kapsulama imaju miris u kapsulama koje se inkorporiraju u vezivo temeljeno na vodi i otiskuju sitotiskom preko izabranog otiska. Suhi otisak je praktički nevidljiv, a miris je stabilan u kapsulama do trenutka kad se otisak zagrebe noktom.

Termokromatske boje temeljene na tekućim kristalima mogu se pohraniti u kapsulama, a mijenjaju obojenje s promjenom temperature kroz cijeli spektar boja. Promjena boje može biti bilo gdje između –30 i 70 ^{o}C, a interval promjene može biti mali 1 ^{o}C ili veliki 20 ^{o}C. Termokromatske boje rabe se za industrijske i reklamne potrebe.

Zaštitnim bojama otiskuju se čekovi i drugi dokumenti koji se mogu unovčiti. Iznos novca piše se preko čeka otisnutog zaštitnom bojom. Brisanje ili bilo kakav pokušaj izmjene brojeva/znamenki uništava ili oštećuje boju. Zaštitne boje su, uglavnom, topljive u vodi pa se lako otapaju u dodiru s tekućim brisačem boja ili kemikalijama u sklopu boje za brisanje otisaka. Za tisak osobnih iskaznica, putovnica, vozačkih dozvola i sl. rabe se specijalne color-shift boje koje imaju "pomak obojenja". Na otisku se vidi promjena boje ovisno o kutu gledanja. Boje se tiskaju u dubokom tisku, motivi su jednostavni i lako prepoznatljivi, ali zbog color-shifta nemoguće je krivotvoriti otisak odn. dokument. Boje s dva stupnja zaštite temeljene su na tekućim kristalima pa imaju color-shift koji je lako vidljiv i polarizaciju svjetla za koju je potreban specijalni dvostruki filtar. S jedne strane filtra boja je intenzivna i svjetla, a s druge se mijeja ili nestaje.

Magnetski željezni oksid rabi se kao pigment magnetskih boja. To je pigment s kojim je teško formulirati kvalitetnu boju potrebne tečljivosti, s kojom se može otiskivati, koja se dobro suši i na kraju daje otisak koji se lako očitava MICR uređajem. Strojno "čitljive" boje su temeljene na magnetskom željeznom oksidu koji daje stalan magnetski "odgovor" na čitaču. To su crni magnetski znakovi brojke i slova otisnuti na čekovima i sličnim dokumentima koji se automatski sortiraju.

Rabi se nekoliko vrsta "nevidljivih boja". Boje s glinom koja pokriva otisak, a struganjem olovkom otisak postaje vidljiv. Transparentne nevidljive boje imaju tvari koje svjetlucaju kad u izložene "crnom svjelu" - UV zračenju i rabe se za tisak različitih kartica za lutriju, dobitnih kupona i sl. Rabe se i nevidljive boje s bezbojnim tvarima koje potamne zagrijavanjem. Otisci ostalih nevidljivivih boja postanu vidljivi nakon obrade s kemikalijama ili njihovim parama koje reagiraju s određenim sastavnicama boja i tvore vidljivi otisak. [3-9].

5 LITERATURA

[01] R. M. Romano and F. J. Romano (Eds.), The GATF Encyclopedia of Graphic Comunications, GATF Press, Pittsburgh, 1998.
[02] G. A .Stevenson, Graphic Arts Encyclopedia, McGraw Hill, New York, 1991.
[03] P. J. Hartsuch, Chemistry for the Graphic Arts, Graphic Arts Technical Foundation, Pittsburg, 1983.
[04] C. H. Williams, The Printer's Ink Handbook, Maclean Hunter Ltd, Hertfordshire, 1992.
[05] N. R. Eldred, What the Printer Should know about Ink, 3rd edition, GATF; Pittsburgh, 2001.
[06] R. E. Todd, Printing Inks, Pira International, Leatherhead, 1994.
[07] N. R. ELDRED, Package Printing, Jelmar Publishing Co., Inc. New York, 1993.
[08] B. Thompson, Printing Materials, Science and Technology, 2nd edition, Pira International, Leatherhead, 2004.
[09]. C. H. Williams, Printing Ink Technology, Pira International, Leatherhead, 2001.
[10] V. Vančina, Predavanja iz predmeta: Tiskarske boje, Grafički fakultet Sveučilišta u Zagrebu, akad. god. 2005./2006.
[11] V. Vančina i M. Mikota, Materijali u grafičkoj proizvodnji – boje, priručnik za vježbe, Grafički fakultet Sveučilišta u Zagrebu, Zagreb 1992.

ISOTHERMAL CRYSTALLIZATION KINETICS OF BULK GAHNITE GLASS-CERAMICS

KINETIKA KRISTALIZACIJE KOMPAKTNE GANITNE STAKLOKERAMIKE U IZOTERMNIM UVJETIMA

Stanislav Kurajica, Emilija Tkalčec and Ivan Simčić
University of Zagreb, Faculty of Chemical Engineering and Technology, Marulićev trg 19, HR-10000 Zagreb, Croatia

Abstract: Crystallization behavior and kinetics of bulk glass, with the composition: 55.6 mol% SiO_2, 22.8 mol% Al_2O_3, 17.7 mol% ZnO and with 3.84 mol% of TiO_2 as nucleating agent, has been studied by differential thermal analysis (DTA) and X-ray diffraction (XRD) in isothermal conditions.

It was determined that the isothermal DTA scans are characterized with two overlapped exothermal crystallization peaks. According to XRD data, two crystalline phases: zinc-aluminosilicate s.s. with high-quartz structure, $Zn_{x/2}Al_xSi_{3-x}O_6$, and gahnite, $ZnAl_2O_4$, are formed after isothermal heat treatment. The high degree of overlapping disabled the kinetic analysis using DTA scans, therefore X-ray diffraction method was employed for the crystallization path determination and kinetic parameters calculation. It was determined that crystallization of zinc-aluminosilicate s.s. and gahnite are competitive processes. The crystallization process of Zn-aluminosilicate is much slower compared to gahnite. The occurrence of Zn-aluminosilicate is possible due to a long induction period for gahnite crystallization. After commence of the gahnite crystallization process, sudden retardation and halt of Zn-aluminosilicate crystallization process occurs.

The activation energies of zinc-aluminosilicate s.s. and gahnite crystallization have been determined by fitting the Johnson-Mehl-Avrami (JMA) equation to experimental XRD data and by application of Arrhenius equation. The differentiated JMA curves are than compared with DTA curves and very good match has been observed. The activation energies for zinc-aluminosilicate s.s. and gahnite crystallization have been determined to be 449±59 and 334±42 $kJmol^{-1}$, respectively. The obtained values are in concordance with previously determined values for powder sample in non-isothermal conditions and literature data.

Keywords: crystallization, DTA, gahnite, isothermal kinetics, zinc-aluminosilicate, XRD.

Introduction

Transparent glass-ceramics with gahnite, $ZnAl_2O_4$, as the main crystalline phase can be prepared from the glass system of ZnO-Al_2O_3-SiO_2, with TiO_2 as nucleating agent[1-6].

The important potential application area of gahnite glass-ceramics are displays with liquid crystals, since gahnite glass-ceramics is characterized, beside transparency, with the expansion coefficient close to silicon, good thermal stability and chemical resistivity[3]. Based on the mentioned properties it is possible, after CVD deposition of amorphous silicon on glass-ceramics, to conduct the crystallization using high temperatures. Obtained polycrystalline silicon enables reduction of TFT size and faster response in each pixel.[4] Gahnite glass-ceramics is appropriate matrix for luminescence activators, which makes it useful for the solar collectors, and laser production.[7-9] Glazes with gahnite as the main crystalline phase are interesting because this is phase with high scratch hardness and high refraction index.[10]

In this work crystallization of glass system ZnO-Al_2O_3-SiO_2, with TiO_2 as nucleating agent has been investigated. The crystallization path has been studied on bulk samples in isothermal conditions. The kinetic parameters of isothermal crystallization process have been determined.

Experimental procedure

The mixture of oxides with the composition (mol%) 55.6 % SiO_2, 22.8 % Al_2O_3, 17.7 ZnO and 3.9 % TiO_2 has been prepared using p.a. grade chemicals. The sample was melted in platinum crucible for 2 h at 1600°C. The obtained glass was crushed and re-melted at the same conditions. The re-melted glass was annealed at 600°C and cooled down at a cooling rate of the furnace. The glass was crushed in corundum mortar in order to produce particles with approximate size of 5 mm.

Differential thermal analysis of the samples was conducted by NETZSCH STA 409 device. The Pt crucibles and Al_2O_3 as reference were used. Thermal treatment of the samples was conducted in a computer controlled furnace. Thermally treated samples were analyzed using X-ray diffraction, (PHILIPS PW 1710, CuKα irradiation and graphite monochromator). For semi-quantitative analysis, the amount of 10 wt% of silicon was added to the samples as internal standard.

The Johnson-Mehl-Avrami equation for the nucleation and growth process in isothermal conditions was used to describe the crystallization process:[11]

$$\alpha(t) = 1 - exp[- k^n (t - \tau)^n] \qquad [1]$$

Where k is rate constant, t is elapsed time, τ is incubation time and n is Avrami exponent. Avrami exponent depends on reaction mechanism, the growth dynamics and nucleation process and can be given by equation:[12]

$$n = \frac{p}{s} + q = m + q \qquad [2]$$

Where p denotes the dimension of growth and could be 1, 2 and 3 for one, two and three-dimensional crystal growth; s is related to the process that controls the crystallization and equals 1 for processes controlled by the phase boundary reaction or 2 for the processes controlled by the diffusion; q is parameter related to nucleation and yields $q=0$ for processes where nucleation has ended before the crystal growth started, $q=1$ for the case where both processes starts simultaneously.

In order to calculate the activation energy the Arrhenius equation was employed.

Results

DTA curves of the samples obtained in isothermal conditions, at various temperatures in the range 796.5 – 816°C are shown in Fig. 1a. The curves are notable asymmetric pointing out that at least two exothermal processes occur in narrow time interval. XRD analysis revealed that gahnite, $ZnAl_2O_4$, and Zn-aluminosilicate s.s., $Zn_{x/2}Al_xSi_{3-x}O_6$, with high-quartz structure crystallize in the samples. A part of XRD scan of sample obtained by heating the sample at 802.5°C for 245 min is shown in Fig 1b.

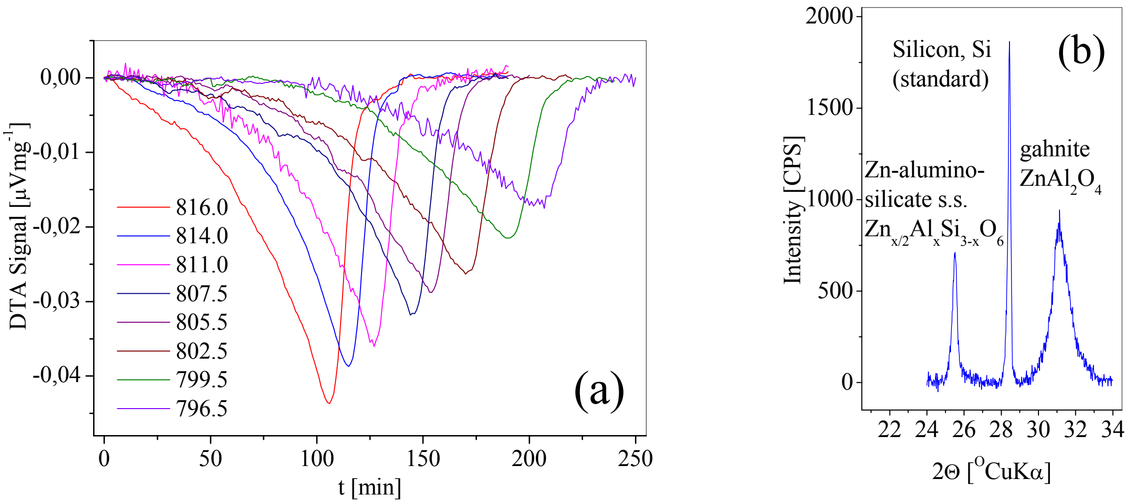

Fig. 1. (a) DTA curves of the glass samples obtained in isothermal conditions, isothermal treatment temperatures are given in the picture. (b) XRD pattern of sample isothermally treated at 803°C for 245 min (Si was added as internal standard).

The simultaneous crystallization of two phases disabled kinetic analysis using DTA data. Therefore, in order to characterize the crystallization path of the investigated system and perform the kinetic analysis, following procedure has been accomplished. The samples were isothermally treated at four temperatures: 803, 811, 816 and 820°C. The thermal treatment at each temperature has been performed for various time periods; the time at which the isothermal treatment was interrupted has been selected on the basis of DTA curves (Fig. 2a). Internal standard was added to the obtained samples and then the samples were subjected to XRD analysis. The diffraction patterns of the samples thermally treated at 803°C for various time intervals are shown in Fig 2b. In such manner a relative intensities (proportional to amounts) of two phases, after different crystallization periods have been established (Fig. 2c). Fractional conversions, α, were calculated by normalization of relative intensities (Fig. 3).

By profile fitting to JMA equation (Fig 3), with keeping Avrami exponents 4 and 3,5 for Zn-aluminosilicate and gahnite, respectively, the reaction rates and incubation times for both reactions have been calculated (Table 1). The values of Avrami exponents were selected by trial and error procedure. From the dependence of reaction rate constants on reciprocal temperature (Fig. 4) the activation energies for the crystallization processes of Zn-aluminosilicate and gahnite has been calculated to be 449±59 kJmol^{-1} for the first and 334±42 kJmol^{-1} for the second process. The comparison of differentiated JMA curves obtained by profile fitting with experimentally obtained DTA curves yield a very good match.

Discussion

As indicated by the asymmetry of DTA curves (Fig. 1a), the X-ray diffraction analysis confirmed that isothermal crystallization yields no single phase. As can be seen in Fig. 2b, two crystalline phases were identified: gahnite, $ZnAl_2O_4$, (PDF 5-669) and Zn-aluminosilicate s.s., $Zn_{x/2}Al_xSi_{3-x}O_6$ with high-quartz structure, as previously found for non-isothermally powder samples.[13] From the shift of diffraction peaks of Zn-aluminosilicate phase found in this experiment, in comparison with the literature data for $Zn_{0.75}Al_{1.5}Si_{1.5}O_6$ (PDF 32-1455)[14], it is obvious that the composition of zincaluminosilicate phase is somewhat different than that cited in literature and closer to the high-quartz solid solution, β-SiO_2, s.s., (PDF 11-252).

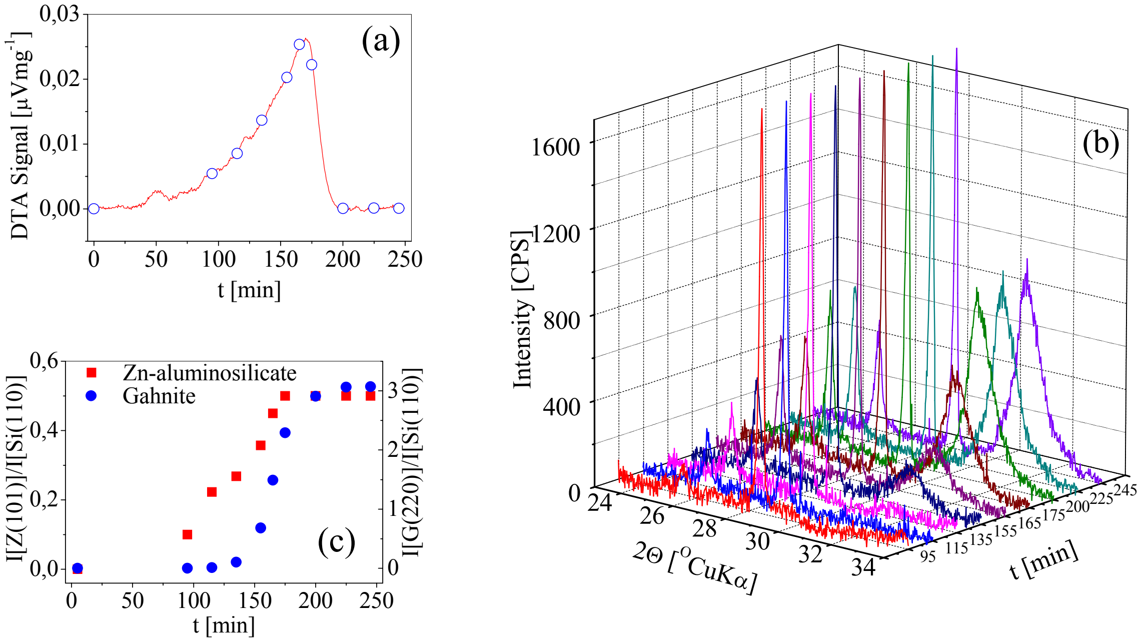

Fig. 2. (a) DTA scan of obtained in isothermal conditions at 803°C, the intervals at which the thermal treatment has been interrupted are marked with the dots. (b) XRD scans of the sample isothermally treated at 803°C for different intervals. (c) The intensity ratio for (101) line of Zn-aluminosilicate and (220) line of gahnite, respectively, and (110) line of silicon for various isothermal heat treatment intervals.

In order to characterize the crystallization behavior of the investigated system and to perform the kinetic analysis, the isothermal treatment of the samples has been interrupted after various time periods (Fig. 2a) and such obtained samples subjected to XRD analysis (Fig. 2b). XRD analyses show that the isothermal crystallization process in bulk glasses derived from ZnO-Al_2O_3-SiO_2 system proceeds in two stages (Fig. 2c). During the first stage, metastabile Zn-aluminosilicate phase crystallizes, while in the second stage the crystallization of gahnite phase occurs. It is possible that during the second process an exsolution of Zn and Al from the formed zinc-aluminosilicate phase for the formation of gahnite occurs. Some indication for the described scenario would be sudden halt of Zn-aluminosilicate crystallization process. On the other hand, the exsolution would cause shift in the Zn-aluminosilicate XRD peaks position further to pure high-temperature quartz, which is not happening. As can be seen in Fig. 2c, gahnite starts to crystallize somewhat later then Zn-aluminosilicate phase, obviously due to a slower nucleation process. However, the amount of gahnite phase formed is much greater in comparison to Zn-aluminosilicate.

A fractional conversions, α, for both reactions were calculated by normalizing intensity ratios to the maximum intensity ratio for each phase, corresponding to the longest time interval (Fig. 3).

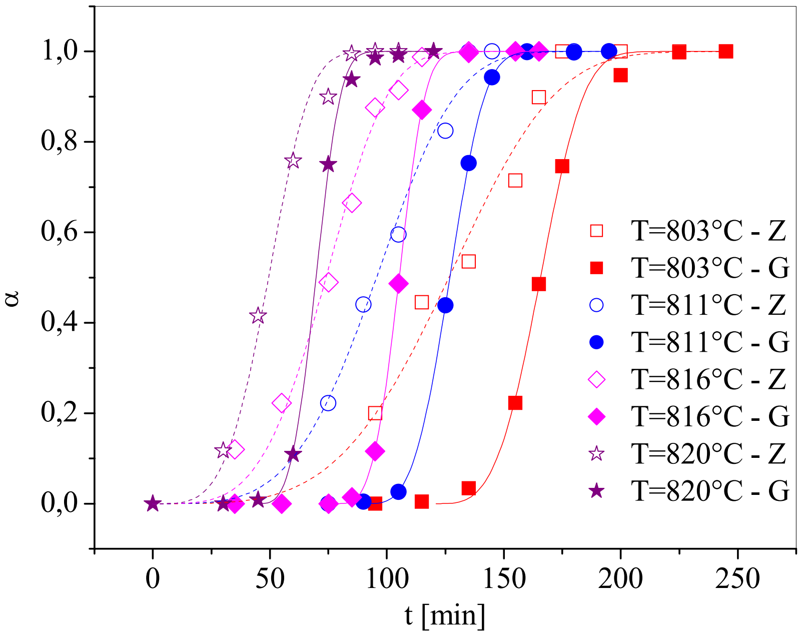

Fig. 3. Fractional conversions for the crystallization of Zn-aluminosilicate and gahnite in dependence of elapsed time and matching α-t curves obtained by profile fitting of the obtained data to JMA equation.

By profile fitting of fractional conversions, α, to JMA equation (Fig 3), the reaction rates and incubation times for Zn-aluminosilicate and gahnite have been calculated (Table 1). As can be seen in Table 1, the gahnite crystallization process proceeds far more faster than the Zn-aluminosilicate one, e.g. the Zn-aluminosilicate crystallization rate constant at 803°C yields 0,0072 min^{-1} while the gahnite crystallization rate constant at the same temperature yields 0,0202 min^{-1}. Therefore, the sudden halt of Zn-aluminosilicate crystallization process could be explained due to a consumption of substrate by faster gahnite crystallization process.

Table 1. Kinetic parameters of the samples treated isothermally at various temperatures obtained by profile fitting to JMA equation. The Avrami exponents are 4 and 3.5 for Zn-aluminosilicate and gahnite, respectively.

T / °C	k(G) / min^{-1}	k(Z) / min^{-1}	τ(G) / min	τ (Z) / min
803	0,02012	0,00721	130	30
811	0,02476	0,00955	99	23
816	0,0326	0,01233	84	18
820	0,03572	0,01645	50	12

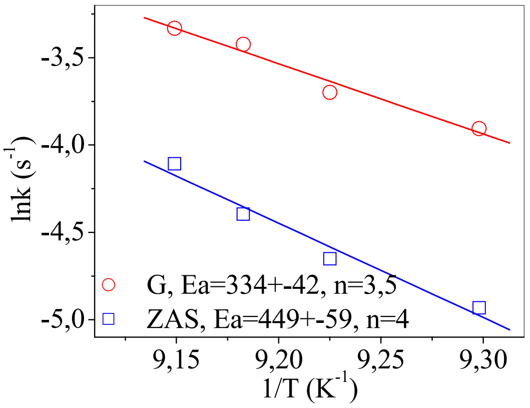

Fig. 4. The dependence of reaction rate constants for the crystallization of Zn-aluminosilicate and gahnite on reciprocal T.

According to the literature[15], in the glasses of examined system Zn-aluminosilicate phase nucleates by surface mechanism and grows two-dimensionally, while gahnite nucleates by volume mechanism and grows three-dimensionally. The obtained results for Avrami exponents are in concordance with previous findings taking into the consideration the nucleation process and the diffusion controlled growth of Zn-aluminosilicate.

From the Arrhenian dependence the activation energies for the crystallization processes of Zn-aluminosilicate and gahnite has been calculated to be 449±59 $kJmol^{-1}$ for the first and 334±42 $kJmol^{-1}$ for the second process. The obtained values of activation energies are in concordance with the values cited in literature.[13,16]

Conclusion

The bulk glass of the $ZnO-Al_2O_3-SiO_2$ system with TiO_2 as nucleating agent in isothermal conditions two phases crystallize: gahnite, $ZnAl_2O_4$, and Zn-aluminosilicate s.s., $Zn_{x/2}Al_xSi_{3-x}O_6$. The first process, Zn-aluminosilicate crystallization, is much slower than the second process, gahnite crystallization. The slow nucleation process postpones gahnite crystallization causing long induction period. After the commencing of the gahnite crystallization process sudden retardation of Zn-aluminosilicate crystallization process occurs due to an existence of concurrent reaction of a greater rate.

The activation energies for the crystallization processes in investigated glass has been determined in non-isothermal conditions and yield 449+59 $kJmol^{-1}$ for the process of Zn-aluminosilicate crystallization and 334+42 $kJmol^{-1}$ for the process of gahnite crystallization.

Acknowledgement

Ministry of science, education and sport of the Republic of Croatia is obliged for financial support.

References

1. G. H. Beall and D. A. Duke, J.Mat. Sci., 4 (1969) 340-352.
2. Z. Strnad, Glass-Ceramic Materials, Elsevier, Amsterdam, 1986.
3. G. H. Beall and L. R. Pinckney, J. Am. Ceram. Soc., 82 [1] (1999) 5-16.
4. L. R. Pinckney, U.S. Pat. 6 248 678 (2001).
5. E. Tkalčec, H. Ivanković and B. Gržeta, J. Non-Cryst. Solids, 129 (1991) 174-182.
6. J. Petzoldt Glastechn. Ber. 40 (1967) 385-395.
7. G. H. Beall, U.S. Pat. 4 874 724 (1989).
8. W. Malmendiev, U.S. Pat. 3 951 669 (1976).
9. L. R. Pinckney and G. H. Beall, Proceedings of SPIE, Inorganic Optical Materials III, Ed. A. J. Marker and M. J. Davis, San Diego, USA, Vol. 4452 (2001), 93-99.
10. A. Escardino, J. L. Amoros, A. Gozalbo, K. J. Ortis, and A. Moreno, J. Am. Ceram. Soc., 83 [12] (2000) 2938-2944.
11. W. A. Johnson and R. F. Mehl, Trans. Am. Inst. Min. (Metall.) Engs. 135 (1939) 416-425
12. S. Ranganathan, M. Von Heimendahl, J. Mat. Sci., 16 (1981) 2401-2404.
13. E. Tkalčec, S. Kurajica and H. Ivanković, J. Non.Cryst. Solids, 351 (2005) 149-157.
14. JCPDS-ICDD files
15. A. Escardino, L. J. Amoros, A. Gozalbo, M. J. Ortis, Brit. Ceram. Transactions, 98 [4] (1999) 196-199.
16. E. Tkalčec, S. Kurajica and H. Ivanković, Thermochim. Acta, 378 (2001) 135-144.

11. Savjetovanje o materijalima, tehnologijama, trenju i trošenju
11. Conference on Materials, Processes, Friction and Wear
MATRIB'06, Vela Luka, 22-24.06.2006.

OVISNOST ČVRSTOĆE MEKO UVEZANE KNJIGE O KVALITETI PAPIRA

B. Lajić, D. Babić, V. Kropar - Vančina
Contact: babic@grf.hr

Grafički fakultet Sveučilišta u Zagrebu, Getaldićeva 2, 10000 Zagreb

Sažetak: U sklopu rada ispitivana je ovisnost kvalitete sljepljivanja meko uvezane knjige o vrsti i kvaliteti papira. Ispitivano je šest vrsta papira od kojih su izrađene meko uvezane knjige. Za sljepljivanje svih knjiga rabljeno je termokol ljepilo. Rabljene su slijedeće vrste papira: papir za umjetnički tisak, mat, površinske mase 80 g/m^2; papir za umjetnički tisak, sjajni, površinske mase 100 g/m^2; papir za umjetnički tisak, mat, površinske mase 90 g/m^2; papir za umjetnički tisak, sjajni, površinske mase 80 g/m^2; papir offsetni, površinske mase 80 g/m^2 i papir offsetni, površinske mase 90 g/m^2. Karakteristike i kvaliteta svakog papira ispitane su prema ISO standardima. Meko uvezane knjige su podvrgnute statičkom ispitivanju čvrstoće knjižnog bloka. Dobiveni rezultati pokazuje ovisnost čvrstoće knjižnog bloka o kvaliteti svakog od papira rabljenih u izradbi knjiga.

Ključne riječi: čvrstoća knjižnog bloka, meko uvezana knjiga, svojstva papira

Abstract: The book block strength of flexible bound books was researched in accordance to paper quality/properties. Six various papers: two fine art matt coated, two fine art glossy coated, two uncoated offset papers, (with nominal grammage from 80 g/m^2 to 100 g/m^2) and "thermokol" adhesive were used for production of flexible bound books. Some general (caliper), surface (absorbency, Cobb for both sides) and mechanical properties (tensile strength and elongation in MD and CD) of used papers were tested according to ISO standards. Flexible bound books were submitted to statistic investigations of book block strength. Obtained results point out the dependence of the book block strength on the quality/properties of each used paper in production of books.

Key words: flexible bound book, properties of paper, strength of book block

1 UVOD

Uzimajući u obzir predpostavku kako bi sastav papira mogao imati veći utjecaj na kvalitetu slijepljenosti hrpta knjižnog bloka nego obrađenost hrpta knjižnog bloka planirana su ispitivanja šest papira različite gramature, sastava i površinske obrade.

S obzirom na potrebe današnje grafičke industrije koja je izložena izazovima nemilosrdne konkurencije, sve su češći zahtjevi za različitim vrstama i kvalitetama papira u proizvodnji knjiga.

U sklopu ovog rada nije analiziran sastava papira od kojih su izrađene meko uvezane knjige. Ispitivanja su usmjerena na poveznice nekih površinskih (upojnost pustene i sitove strane papira) i mehaničkih (prekidna sila i prekidno istezanje u uzdužnom i poprečnom smjeru papira) karakteristika papira i čvrstoće slijepljenih knjižnih blokova.

Čvrstoću slijepljenog knjižnog bloka određuje i vrsta ljepila kojom se sljepljuje knjiga. Sve meko uvezane knjige slijepljene su istim ljepilom pa je ljepilo bilo konstanta u ispitivanom sustavu meko uvezanih knjiga.

Za izradbu knjiga rabljeni su različiti papiri kako bi odredili eventualne poveznice između nekih važnih karakteristika papira i čvrstoće slijepljenih knjižnih blokova.

2 POKUSNI DIO

U sklopu rada izrađene su meko uvezane knjige, a za izradbu knjiga rabljeni su slijedeći papiri:
1. papir za umjetnički tisak, mat (površinske mase 80 g/m^2),
2. papir za umjetnički tisak, sjajni (površinske mase 80 g/m^2;
3. papir za umjetnički tisak, mat (površinske mase 90 g/m^2;
4. papir za umjetnički tisak, sjajni (površinske mase 100 g/ m^2;
5. papir, offsetni (površinske mase 80 g/m^2) i
6. papir, offsetni (površinske mase 90 g/m^2).

Određena su slijedeća svojstva papira:
debljina d [mm] (ISO 536),
upojnost, Cobb$_{(60)}$ [g/ m^2] (ISO 535),
prekidna sila F [N]
za uzdužni i poprečni smjer papira, te srednja vrijednost za uzdužni i poprečni smjer,
prekidno istezanje ε [%] (ISO 1942/2)
za uzdužni i poprečni smjer papira
za sve rabljene papire, a rezultati mjerenja nalaze se u tablici 1.

Od svih ispitivanih papira izrezane su epruvete određenih dimenzija koje su klimatizirane (ISO 187) prije konkretnih određivanja.

Debljina papira određena je pomoću mikrometra Lhomargy (ISO 536). Na slici 1 prikazan je rabljeni mikrometar.

Slika 1. Mikrometar Lhomargy

Upojnost svih ispitivanih papira određena je Cobbovom metodom, $\text{Cobb}_{(60)}$ [g/ m^2] (ISO 535), a uređaj je prikazan na slici 2.

Slika 2. Cobbov uređaj

Za određivanje prekidne sile F [N] i prekidnog istezanja ε [%] (ISO 1942/2) svih ispitivanih papira rabljena je kidalica Frank (slika 3).

Slika 3. Kidalica Frank

Čvrstoća svih knjižnih blokova meko uvezanih knjiga ispitana je Müller Martinijevim uređajem koji je prikazan na slikama 4 i5.

Slika 4. Müller Martinijev uređaj za ispitivanje čvrstoće knjižnog bloka

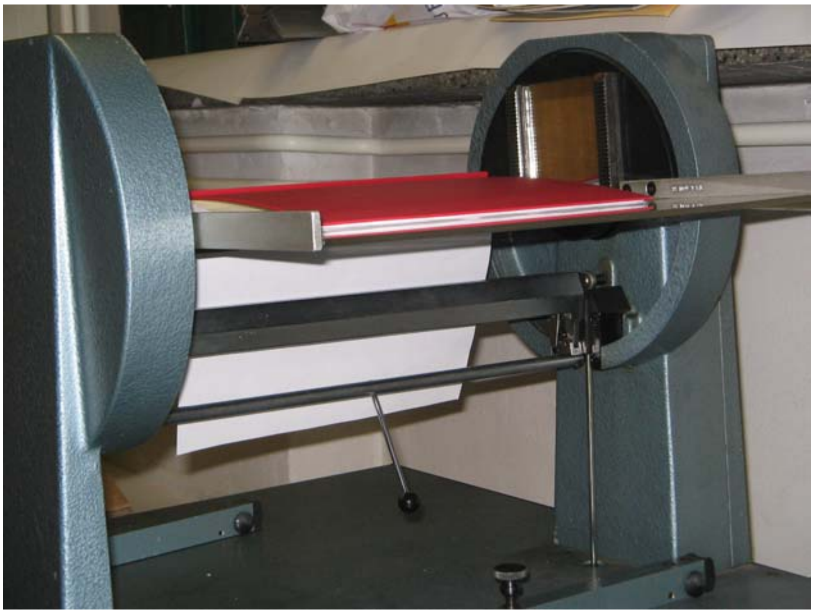

Slika 5. Ispitivanje čvrstoće knjižnog bloka

Pri ispitivanju čvrstoće slijepljenog knjižnog bloka dobiveni rezultati se uspoređuju s vrijednostima iz referentne tablice koju je izradila međunarodna udruge Adhesive Products iz Illinoisa (SAD) prema kojoj se onda daje ocjena kvalitete sljepljivanja knjižnog bloka. Tako dobivena ocjena prvenstveno je poslužila kao pokazatelj eventualnih poveznica ispitivanih karakteristika papira i čvrstoće slijepljenih knjižnih blokova.

4 REZULTATI

Tablica 1 Svojstva rabljenih papira i čvrstoća knjižnih blokova

broj uzorka	vrsta papira	d [mm]	Cobb$_{(60)}$ [g/m^2]*	F_u [N]	ε_u [%]	F_p [N]	ε_u [%]	F_{up} [N]	W [N/cm]
1	80 g/m^2 mat	x 0,0876	x 23,843	x 76,00	x 2,90	x 37,00	x 3,00	56,50	x 10,93
		σ 0,0037	σ 2,187	σ 1,00	σ 0,00	σ 2,00	σ 1,00		σ 1,13
2	80 g/m^2 sjajni	x 0,1800	x 49,723	x 91,0	x 2,50	x 42,30	x 4,66	66,65	x 11,60
		σ 0,0017	σ 5,189	σ 2,6	σ 0,00	σ 1,12	σ 0,76		σ 1,92
3	90 g/m^2 mat	x 0,0678	x 10,663	x 84,60	x 2,31	x 39,20	x 5,00	61,90	x 11,87
		σ 0,0026	σ 0,168	σ 7,67	σ 0,23	σ 0,45	σ 0,35		σ 0,92
4	100 g/m^2 sjajni	x 0,1130	x 27,550	x 110,33	x 2,33	x 48,00	x 3,50	79,15	x 11,95
		σ 0,0021	σ 2,281	σ 1,83	σ 0,29	σ 1,00	σ 0,50		σ 2,90
5	80 g/m^2 offset	x 0,0876	x 37,340	x 59,00	x 1,95	x 27,50	x 3,95	43,25	x 9,30
		σ 0,0037	σ 2,093	σ 1,73	σ 0,10	σ 1,00	σ 0,21		σ 2,62
6	90 g/m^2 offset	x 0,0962	x 24,912	x 73,25	x 2,38	x 33,25	x 3,68	53,25	x 10,48
		σ 0,0024	σ 3,560	σ 4,57	σ 0,48	σ 1,50	σ 0,39		σ 2,76

Legenda:
d - debljina papira [mm],
Cobb$_{(60)}$ - upojnost papira [g/m^2]* (srednja vrijednost za pustenu i sitovu stranu),
F_u - prekidna sila papira u uzdužnom smjeru [N],
ε_u - prekidno istezanje papira u uzdužnom mjeru [%],
F_p - prekidna sila papira u poprečnom smjeru [N],
ε_u - prekidno istezanje papira u poprečnom smjeru [%],
F_{up} - prekida sila papira [N] (srednja vrijednost za uzdužni i poprečni smjer),
W - čvrstoća knjižnog bloka [N/cm].

Papir	1	2	3	4	5	6
Cobb	23,84	49,72	10,66	27,55	37,34	24,91
F	56,5	66,65	61,9	79,15	43,25	53,25
W	10,93	11,6	11,87	11,95	9,3	10,48

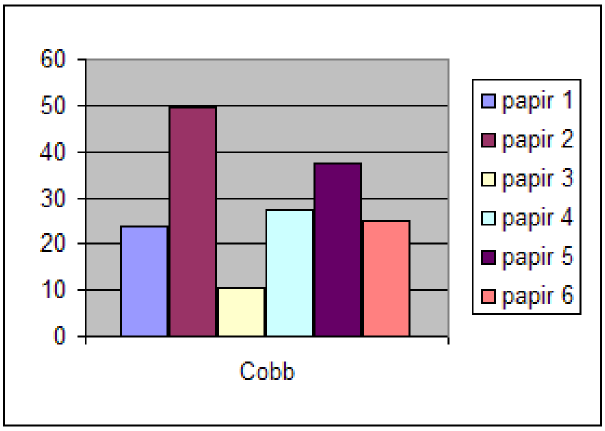

Slika 7. Grafički prikaz srednjih vrijednosti upojnosti ispitivanih papira

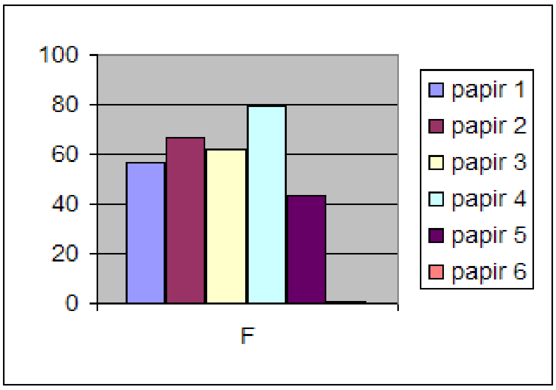

Slika 8. Grafički prikaz srednjih vrijednosti prekidnih sila u uzdužnom i poprečnom smjeru

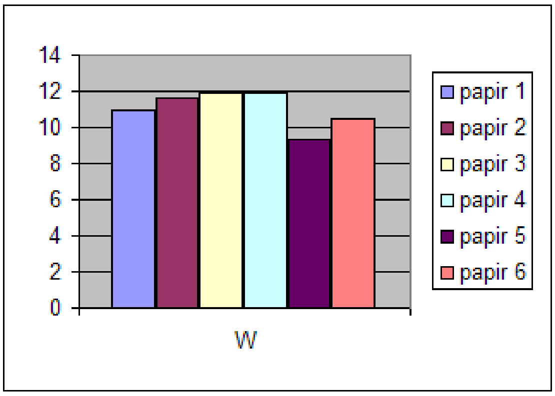

Slika 9. Grafički prikaz srednjih vrijednosti čvrstoća slijepljenih knjižnih blokova izrađenih od ispitivanih papira

Papir	1	2	3	4	5	6
Cobb	23,84	49,72	10,66	27,55	37,34	24,91
F	56,5	66,65	61,9	79,15	43,25	53,25
W	10,93	11,6	11,87	11,95	9,3	10,48

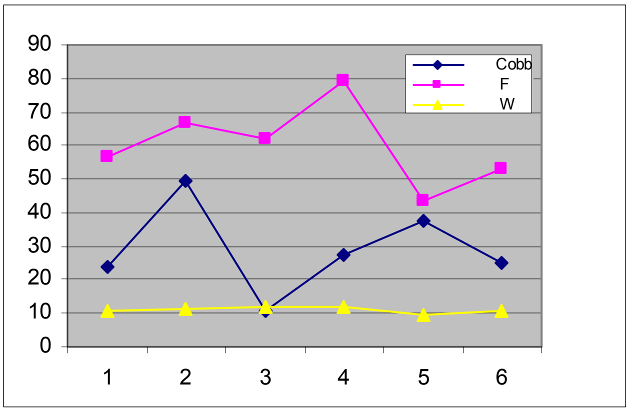

Slika 10. Grafički prikaz srednjih vrijednosti svih ispitivanja

5 RASPRAVA I ZAKLJUČCI

Ispitivanja su pokazala kako postoji poveznica između prekidnih sila papira i čvrstoće slijepljenog knjižnog bloka. Porastom srednje vrijednosti prekidnih sila u uzdužnom i poprečnom smjeru raste i čvrstoća slijepljenog knjižnog bloka (iznimka je papir br. 3). To nam pokazuje kako već samim odabirom materijala/papira možemo utjecati na kvalitetu izradbe meko uvezane knjige.

Temeljem dokazane poveznice, ovo istraživanje otvara cijeli niz daljnjih istraživanja raznih kombinacija materijala u ovisnosti o zahtjevima za određenu tehniku tiska, zatim materijala u ovisnosti o vrsti ljepila i sl. kako bi se mogao izaditi određeni naputak koji bi ovisno o zahtijevima koji se traže za određenu vrstu knjiga odredio optimalnu vrstu/kvalitetu papira za određenu tehniku tiska kao i vrstu ljepila kojim bi se onda mogle izraditi meko uvezane knjige optimalno slijepljenih knjižnih blokova.

Također nakon većeg broja ispitivanja i mjerenja preporuča se napraviti katalog odnosa ljepilo papir s čime bi se uvelike olakšao posao knjigovežnicama, ali i pripremi pri odabiru kvalitete uveza i pri izradi ponuda. Osim toga skratilo bi se i vrijeme izrade ponuda.

6 LITERATURA

[1]
F. H. Tenzer, Grundlagen der Papierverarbeitung, WEB Fachbuchverlag, Leipzig, 1966.

[2]
G. Zahn, Grundwissen für Buchbinder, Verlag Beruf & Schule, Itzehoe, 1992.

[3]
D: Babić, Istraživanje osiguranja kvalitete u grafičkoj doradi, Magistarski rad, FSB, Zagreb, 1984.

[4]
D. Babić, V. Vančina, D. Nikolić, B. Lajić, B. Lozo, Optimalni materijali i uvjeti u proizvodnji mekouvezanih knjiga, Acta Graph., **2**(90)111-116.

[5]
A. Golubović, V. Vančina, D. Nikolić, D. Babić, Istraživanje uvjeta koji osiguravaju kvalitetu slijepljenog knjižnog bloka, Acta Graph., **1**(1989)56-63.

[6]
D. Babić, Razmerje med številom nožev za reskanje in čvrstostjo broširanega knjižnega bloka, Papir, 1-2(1999)13-15.

11. Savjetovanje o materijalima, tehnologijama, trenju i trošenju
11. Conference on Materials, Processes, Friction and Wear
MATRIB'06, Vela Luka, 22-24.06.2006.

INFLUENCE OF HYDROLYSIS CONDITIONS ON CURING AND PROPERTIES OF AN EPOXY-SILANE BASED HYBRID MATERIAL

Jelena Macan, Hrvoje Ivanković
Faculty of Chemical Engineering and Technology, University of Zagreb
HR-10001 Zagreb, Marulićev trg 19, p.p. 177, Croatia
e-mail: jmacan@pierre.fkit.hr

Abstract: 3-glycidyloxypropyltrimethoxysilane (GLYMO), an organically modified methoxysilane with a reactive epoxy group linked to silicon atom through a stable Si-C covalent bond, was hydrolysed with varying amounts of water and acid or base catalyst. Reaction was followed by Fourier-transform infrared spectroscopy (FTIR), and it was found that larger content of water and acid conditions favour quick hydrolysis, while in basic conditions hydrolysis proceeds in parallel with condensation of siloxane network. After hydrolysis, epoxy groups were crosslinked with a poly(oxypropylene) diamine, Jeffamine D230, to form an organic-inorganic hybrid material, and the heat of reaction was determined by differential scanning calorimetry (DSC). Epoxy groups have remained stable during hydrolysis, and hydrolysed silanol groups can act as catalysts for the epoxy-amine reaction. Early inorganic condensation in base-catalysed systems can sterically hinder full crosslinking of the organic phase, while presence of chloride ions from acid catalyst (hydrochloric acid) adversely influences thermal stability of such hybrid materials, as determined by thermogravimetric analysis (TGA). Mechanical properties of fully cured hybrid materials were determined by nanoindentation, and glass transition temperature was determined by DSC. Systems hydrolysed with larger amounts of water show poorer mechanical properties, while the most significant improvement in mechanical properties was achieved for an acid-catalysed system.

Key words: epoxy-amine resin, mechanical properties, organic-inorganic hybrids, sol-gel

1. INTRODUCTION

Organic-inorganic hybrid materials are a class of nanocomposites with inorganic phase formed *in situ* by sol-gel process. This leads to materials with organic and inorganic phase intermingled at nano level, much more homogeneous than those prepared with hard to disperse nano-sized filler [1]. Consequently, the whole volume of hybrid material may act as an interphase, and the hybrid materials are expected to possess superior properties since they unite the qualities of both organic and inorganic phase in synergistic manner [2].

A wide range of hybrid materials can be prepared due to great flexibility of sol-gel process [3], which consists of hydrolysis and condensation of metal alkoxides. These reactions for most commonly used silicon alkoxides (alkoxysilanes) can be simplified as follows [4]:

$$\equiv\text{Si-OR} + H_2O \Leftrightarrow \equiv\text{Si-OH} + \text{ROH} \qquad (1)$$

$$\equiv\text{Si-OR} + \equiv\text{Si-OH} \rightarrow \equiv\text{Si-O-Si}\equiv + \text{ROH} \qquad (2)$$

$$\equiv\text{Si-OH} + \equiv\text{Si-OH} \rightarrow \equiv\text{Si-O-Si}\equiv + H_2O \qquad (3)$$

Here R stands for an alkyl group, usually methoxy ($-CH_3$) or ethoxy ($-C_2H_5$). Reactions of hydrolysis (equation 1) and condensation (equations 2 and 3) can be either acid or base catalysed. Acid catalysis favours the hydrolysis, while in base-catalysed systems condensation is the faster step [5].

Presence of covalent bond or hydrogen linkages between the phases increases the strength of interphase, markedly improving mechanical properties of hybrid materials [6]. The covalent bond is most commonly introduced by organically modified alkoxysilanes, since Si-C bond is resistant to hydrolysis and survives the sol-gel process intact [7]. Organic supstituent of these alkoxysilanes can contain a reactive group capable of forming the organic phase, thus creating a virtually monophasic material.

In this work, influence of hydrolysis conditions on curing and final properties of epoxy-silica organic-inorganic hybrids formed from 3-glycidyloxypropyltrimethoxysilane (GLYMO) is studied. GLYMO is an epoxy modified alkoxysilane that can undergo both sol-gel reactions of the alkoxy groups and curing of the epoxy functionality with amine, and so form a hybrid network with covalent bonds between organic and inorganic phases.

2. EXPERIMENTAL

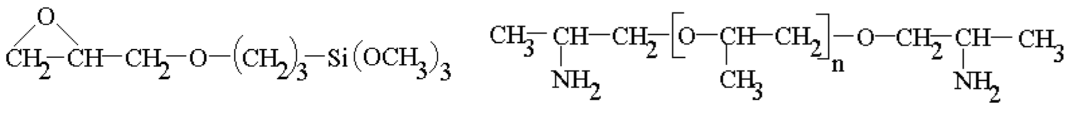

GLYMO

Jeffamine D230 (n = 1.7)

Figure 1 – Chemical formulas of starting materials

3-glycidyloxypropyltrimethoxysilane (GLYMO, 98%, Aldrich Chemicals) was used as the starting compound for synthesis of organic-inorganic hybrid materials. Poly(oxypropylene) diamine Jeffamine D230 (Huntsman Corporation) was used as a curing agent for epoxy group of GLYMO. GLYMO was hydrolysed for 3 h at 60 °C with 1.5 or 3 moles of water per mole of GLYMO, with addition of hydrochloric acid (HCl) or ammonium hydroxide (NH_4OH) as catalyst. Level of hydrolysis and condensation and stability of epoxy groups of GLYMO was determined by Fourier-transform infrared spectroscopy (FTIR), on

JASCO 615 FTIR instrument. Samples were spread on silicon wafers, and each spectrum from 4000 to 400 cm^{-1} was averaged over 16 scans at 4 cm^{-1} resolution. Jeffamine was added to hydrolysed GLYMO in a previously determined stoichiometric amount (ratio of $-NH_2$ to epoxy groups 1 : 1) [8]. Sample designations and compositions as well as conditions of cure are given in table 1.

Table 1: Sample compositions (expressed in moles per mole of GLYMO), conditions of cure and designations for all investigated systems

Jeffamine	Catalyst	Water	Curing conditions	Designation
0.5	HCl: 0.0092	1.5	7 days at RT + 24 h / 120 °C	a15
			24 h / 120 °C	AA15
		3.0	7 days at RT + 24 h / 120 °C	a30
	NH_4OH: 0.0095	1.5	7 days at RT + 24 h / 120 °C	b15
			24 h / 120 °C	BB15
		3.0	7 days at RT + 24 h / 120 °C	b30

Samples were cured at room temperature for 7 days, and then postcured at 120 °C for another 24 h. Additional samples were cured immediately at 120 °C for 24 h. Reaction of epoxy group with amine was studied by means of differential scanning calorimetry (DSC) with a heating rate of 10 K/min in temperature range 25 – 250 °C, on a Perkin-Elmer Pyris 1 calorimeter equipped with an *intercooler* cooling unit. Measurements were made immediately after mixing with Jeffamine, and again after 24 h of curing at room temperature. Heat of reaction, ΔH, was estimated from the area under the exothermic peak. Dynamic DSC experiments were also performed to determine the glass transition temperature, ϑ_g, of the completely cured material. Samples were heated to 150 °C to erase their thermal history, cooled to –50 °C and immediately reheated to 150 °C, all with the same rate of 10 K/min.

Mechanical properties of fully cured materials in form of self-standing films were determined by continuous nanoindentation testing, using Micromaterials NanoTest nanoindenter, with a maximum load of 20 mN and a load rate of 0.02 mN/s. Thermal stability of fully cured materials was determined by thermogravimetric analysis (TGA), using a Seiko SII Exstar 6000 thermobalance. Samples were heated from room temperature to 1000 °C with a heating rate of 10 K/min in a nitrogen gas flow of 250 cm^3/min.

3. DISCUSSION OF RESULTS

FTIR spectra of GLYMO hydrolysed for 3 h at 60 °C with 1.5 and 3 mol of water (figure 2) show how choice of catalyst influences the hydrolysis and condensation of alkoxy groups of GLYMO. In acid-catalysed system silanol groups, Si-OH, form immediately and in larger quantities, and the simultaneous decrease of the characteristic $-CH_3$ bands confirms that hydrolysis of alkoxy groups takes place. This is much more pronounced for system hydrolysed with 3 mol of water, regardless of catalyst used, since the abundance of water speeds up the hydrolysis. Widening of bands grouped around 1100 cm^{-1}, which are characteristic for stretching of Si-O bonds (in particular Si-O-Si and Si-O-C bridges), indicates changes due to hydrolysis and condensation of alkoxy groups. Due to overlapping of these bands, it is difficult to determine which bonds form and which disappear. A new band appears as condensation proceeds, shifting from 683 cm^{-1} to 696 cm^{-1} for fully condensed system, and it is thus ascribed to Si-O-Si bridges formed by condensation. In base-catalysed systems hydrolysis proceeds simultaneously with condensation, as silanol bands and the band at 696 cm^{-1} appear at the same time. Characteristic bands for epoxy groups do not disappear during hydrolysis, and their broadening in comparison with non-hydrolysed GLYMO can be ascribed to influence of hydrogen bonds on the stretching and bending vibrations of the epoxy ring.

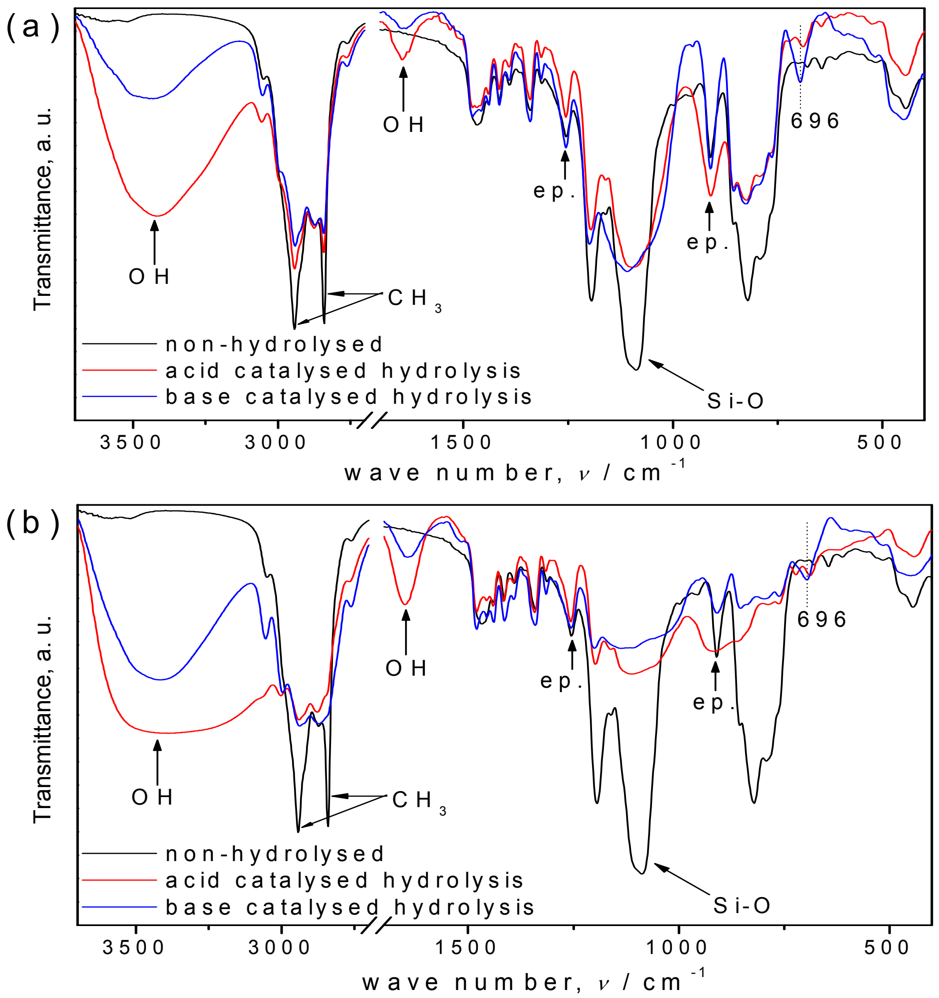

Figure 2 – FTIR spectra of GLYMO hydrolysed for 3 h at 60 °C (a) with 1.5 mol of water and (b) with 3 mol of water, compared with non-hydrolysed GLYMO

Heats of epoxy-amine reaction for hydrolysed systems are comparable with that of non-hydrolysed system (table 2), confirming that epoxy groups survive the sol-gel process intact, as concluded from the FTIR results. The only exception is b30 system, which starts to gel during homogenisation with Jeffamine due to more advanced degree of hydrolysis and condensation in comparison with other systems. As a consequence, a part of epoxy groups is trapped within the inorganic network and unable to react with amine. After 24 h of curing at room temperature all systems have hardened, but acid-catalysed systems show larger residual reactivity of epoxy groups due to a greater flexibility of less condensed inorganic network.

Mechanical properties and glass transition temperatures of hybrid materials from GLYMO hydrolysed with 1.5 mol of water are comparable to those of non-hydrolysed system (table 2). Systems hydrolysed with 3 mol of water have considerably poorer properties, presumably because excess water remains trapped within the hybrid matrix, and b30 also gels too quickly for preparation of samples for mechanical testing. Acid-catalysed systems show better properties than base-catalysed ones, presumably because the inorganic phase is much more finely dispersed and also capable of forming hydrogen linkages with the organic phase due to presence of silanol groups. Systems cured directly at 120 °C (AA15, BB15) also have better properties than comparable systems cured at room temperature (a15, b15). This can be ascribed to greater degree of crosslinking of the organic phase, which in these conditions forms more quickly than the inorganic one.

Table 2: Heat of reaction (measured given time after mixing), ΔH, Young modulus, E, hardness, H, glass transition temperature, ϑ_g, onset temperature of the main degradation step, ϑ_o, temperature of degradation rate maximum, ϑ_p, and mass fraction of residual char at 1000 °C, w, for all investigated systems

Systems	**ΔH / kJ mol^{-1}**		**E / MPa**	**H / MPa**	**ϑ_g / °C**	**ϑ_o / °C**	**ϑ_p / °C**	**w / %**
	0h	**24h**						
No hydr.	-104	--	263 ± 7	62 ± 2	17	303	374	29,97
a15	-89	-24	228 ± 5	55 ± 2	10	279	376	27,64
AA15	--	--	552 ± 6	70 ± 1	13	286	375	31,14
a30	-102	-40	141 ± 3	37 ± 1	6	293	374	29,96
b15	-106	-3	157 ± 2	46 ± 2	14	308	376	27,87
BB15	--	--	230 ± 6	52 ± 2	24	305	376	32,21
B30	-43	-3	-- -- --	-- -- --	9	300	378	27,41

Thermal stability of all hydrolysed systems is comparable to the non-hydrolysed one (table 2), with very small variation in temperature of the degradation rate maximum and the quantity of residual char at 1000 °C. Acid-catalysed systems (a15, a30, AA15) show lower onset temperatures for degradation, which is caused by the presence of chlorine from HCl catalyst that remain bound to residual amine groups within the cured material [9]. Chlorine is released by heating, and can then act as chain scission agent, catalysing the start of degradation of organic phase. Somewhat larger weight residues for systems that were immediately cured at 120 °C (AA15 and BB15, figure 3) are most likely due to facilitated evaporation of lower-weight products of sol-gel hydrolysis and residual water from the system during cure at higher temperature.

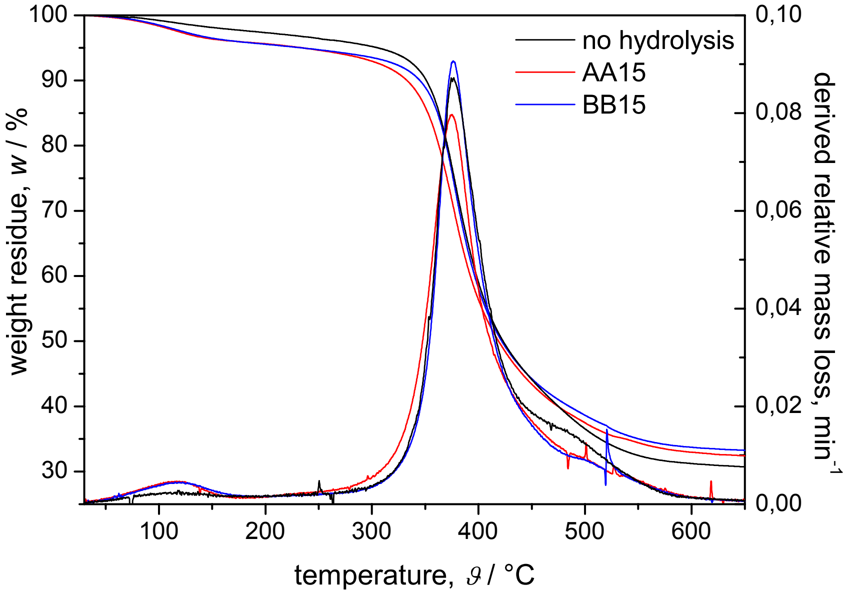

Figure 3 – Thermogravimetric curves and curves of derived relative mass loss for systems cured immediately at 120 °C (AA15 and BB15), in comparison with system prepared from non-hydrolysed GLYMO

4. CONCLUSIONS

Hydrolysis of GLYMO does not influence the stability of epoxy groups, as shown by FTIR and DSC. Acid catalysis favours quick hydrolysis of alkoxy groups, while base catalysis leads to parallel condensation and early formation of inorganic siloxane network. The early formation of the inorganic network shows detrimental influence on the reaction of epoxy groups with amine and consequently the final properties of fully cured hybrid materials. Acid hydrolysis improves the mechanical properties of fully cured materials, presumably because the inorganic phase is more finely structured and additionally linked to the organic phase by hydrogen bonds. Immediate cure of hybrid mixtures at 120 °C allows smaller molecules to evaporate more easily, which improves the final properties of the cured material. Residual chlorine from acid catalyst lowers the thermal resistance of fully cured materials.

REFERENCES

1. P. Judeinstein, C. Sanchez, *J. Mater. Chem.* **11** (1996) 511.

2. B. E. Yoldas, *J. Sol-Gel Sci. Technol.* **1** (1993) 65.

3. M. Pilz, H. Römich, *J. Sol-Gel Sci. Technol.* **8** (1997) 1071.

4. R. C. Mehrotra, in: R. Reisfeld. C. K. Jørgensen (Eds.), *Chemistry, Spectroscopy and Applications of Sol-Gel Glasses*, Springer-Verlag, Berlin 1992.

5. C. Sanchez, F. Ribot, *New J. Chem.* **18** (1994) 1007.

6. C. J. T. Landry, B. K. Coltrain, J. A. Wesson, N. Zumbulyadis, J. L. Lippert, *Polymer* **33** (1992) 1496.

7. A. B. Wojcik, L. C. Klein, *J. Sol-Gel Sci. Technol.* **2** (1994) 115.

8. J. Macan, H. Ivanković, M. Ivanković, H. J. Mencer, *J. Appl. Polym. Sci.* **92** (2004) 498.

9. L.-H. Lee, *J. Polym. Sci. A* **3** (1965) 859.

11. Savjetovanje o materijalima, tehnologijama, trenju i trošenju
11. Conference on Materials, Processes, Friction and Wear
MATRIB'06, Vela Luka, 22-24.06.2006.

REFINEMENT OF EVALUATION OF MECHANICAL PROPERTIES AND BEHAVIOUR OF SYSTEMS THIN FILM – SUBSTRATE BY CYCLIC SCRATCH TEST

Macháčková Kateřina, Štěpánek Ivo, Jiránek Ondřej, Department of Materials Science and Metallurgy, University of West Bohemia, Univerzitní 22, Pilsen, Czech Republic

Abstract: The paper is devoted by evaluation of influence properties and behaviour of basic material on fracturing of all system thin film – substrate during scratch indentation test with using different kind of indentors. The changing of kind of indentor is given by materials properties and geometry properties too, by which is changing type of stress of material system during scratch indentation test. The failures are evaluated after simple scratch test and after cyclic scratch test too with step by step evaluation of failure after every cycle of cyclic scratch test. The evaluation is dirrected on documentation of failures and mophology by light microscopy from surface and from special cross section in selective main important place of scratch too. Special x-ray fluorescent spectroscopy for measurement in small area was used for evaluation scratch too. The evaluation was directed on two systems of thin film – substrate with comparable thin film TiN, which was deposited by low voltage reactive arc evaporation in vacuum.

University of West Bohemia in Pilsen

Introduction

The scratch test methods and indentation methods at all are very important for evaluation basic mechanical properties of thin films and for more precisely evaluation of mechanical properties of systems thin film – substrate [1]. Basic properties can not give very much information about behaviour of systems thin film – substrate in real conditions and during real stress. Therefore it is important the indentation methods use for evaluation better mechanical behaviour of systems thin film – substrate during all static and scratch indentation process. It is important use indentation method for evaluation materials systems with large range of mechanical resistivity. From this point the indentation methods are developed step by step for usability on very different material systems [2].

Behaviour of surfaces of different basic materials during scratch test

At the first in this paper properties and behaviour of surfaces of basic materials are evaluated. The basic materials are tested on the surfaces prepared by metalography methods to the mirror surface and on the surfaces after etching for visualization of structures of basic materials. After metalography preparing the scratch indentation test are realised on surface of basic materials with different mechanical properties. The basic materials are steel CSN 14 220 and HSS CSN 19 830. Here is very big differences in mechanical properties. The scratch tests were provided with two different kind of indentors. Not only diamond Rockwell indentor was used. The indentors, which was used, are the standard diamond indentor Rockwell type with radius of curve of tip 0.2 mm (fig. 1a, 1c) and the indentor from sintered carbides Rockwell type with radius of curve of tip 0,5 mm (fig. 1b, 1d). Two different indentors was used for changing of stress during scratch test and possibility to use this indentation method for evaluation material with lower hardness. The conditions of scratch measurement was the same – normal force was increased from 1 to 80 N with constant rate. The results of this measurement are on fig. 1.

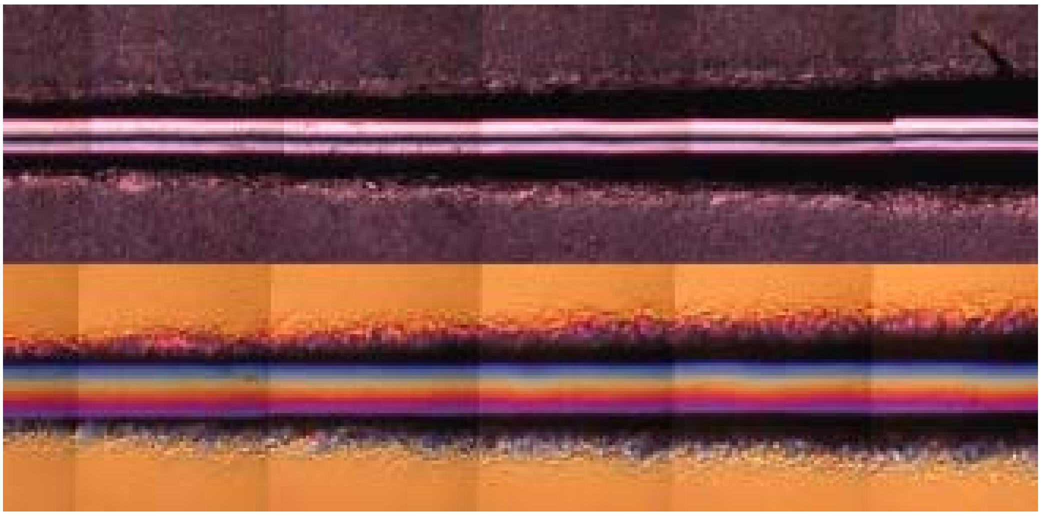

Fig 1a: The scratches in surface of basic material 14 220 – 1. etched surface, 2. polished surface – diamond indentor

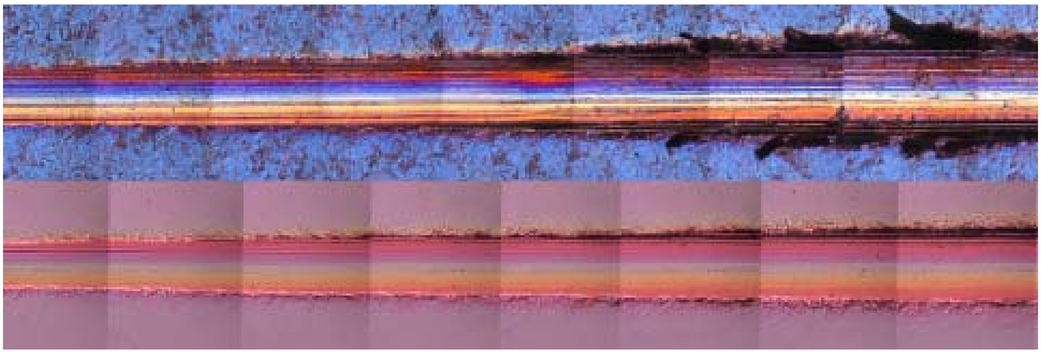

Fig 1b: The scratches in surface of basic material 14 220 – 1. etched surface, 2. polished surface – indentor from sintered carbides

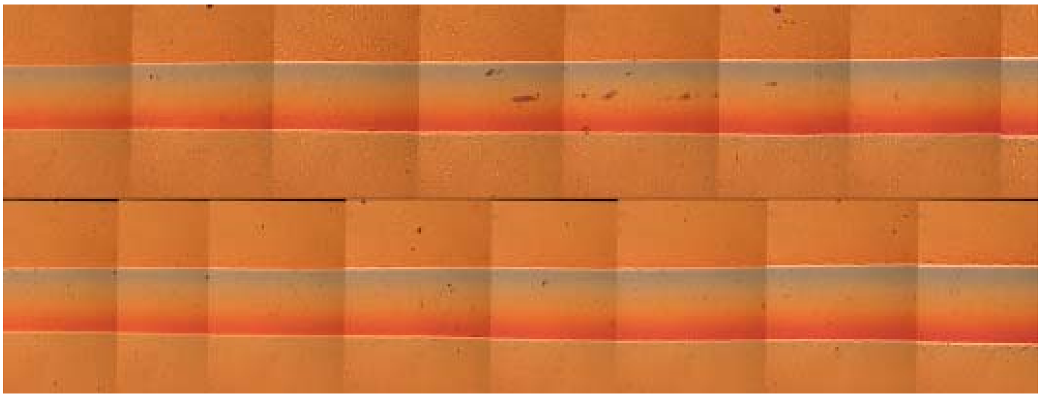

Fig 1c: The scratches in surface of basic material HSS – 1. etched surface, 2. polished surface – diamond indentor

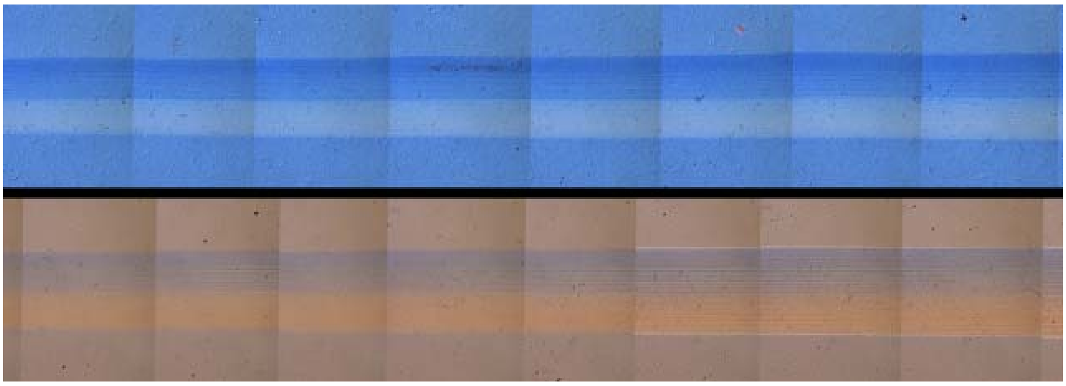

Fig 1d: The scratches in surface of basic material HSS – 1. etched surface, 2. polished surface – indentor from sintered carbides

On fig. 1 is possible to view differences between two different basic materials, two different preparation of surface – mirror type and etched type. Here is differences in deformation process, which is very important, width and depth of scratches and the others. Along the scratches the cohesive failures of basic materials are visible too. The basic material 14 220 has bigger cohesive failures then material 19 830. The cohesive failures are initiated from border of grains of structure. On materials with mirror surfaces is possible to view, that the deformation process evokes bigger cohesive failures and cracks, because the surface is modificated by grinding and polishing.

The using different type of indentors causes different type of stress. The indentor from sinteres carbides change the stress to more friction then deformation on materials

19 830. On material 14 220 the sintered carbides causes refinement of stress by deformation. During scratch test by indentor from sintered carbides on material HSS is weared indentor more then surface.

Behaviour of systems thin film substrate during scrath test

At the second in this paper properties and behaviour of systems thin film – substrate are evaluated, where the substrates are the same as above mentioned. The same conditions and the same indentors are used during measurements. Thin films are deposited by low voltage reactive arc evaporation in vacuum on both type of substrate. For good understanding of failuring of systems thin film – substrate there is important to know deformation processes and failuring and fracturing of basic materials without thin films. Therefore the scratches in surface of substrate was evaluated. On surface of substrate the cohesive failures are evaluated, deformation processes and cracks too, because these failures can influence on failuring of systems with thin films. Here is very important to know where is initiated failures. The results from scratch measurements are in fig. 2.

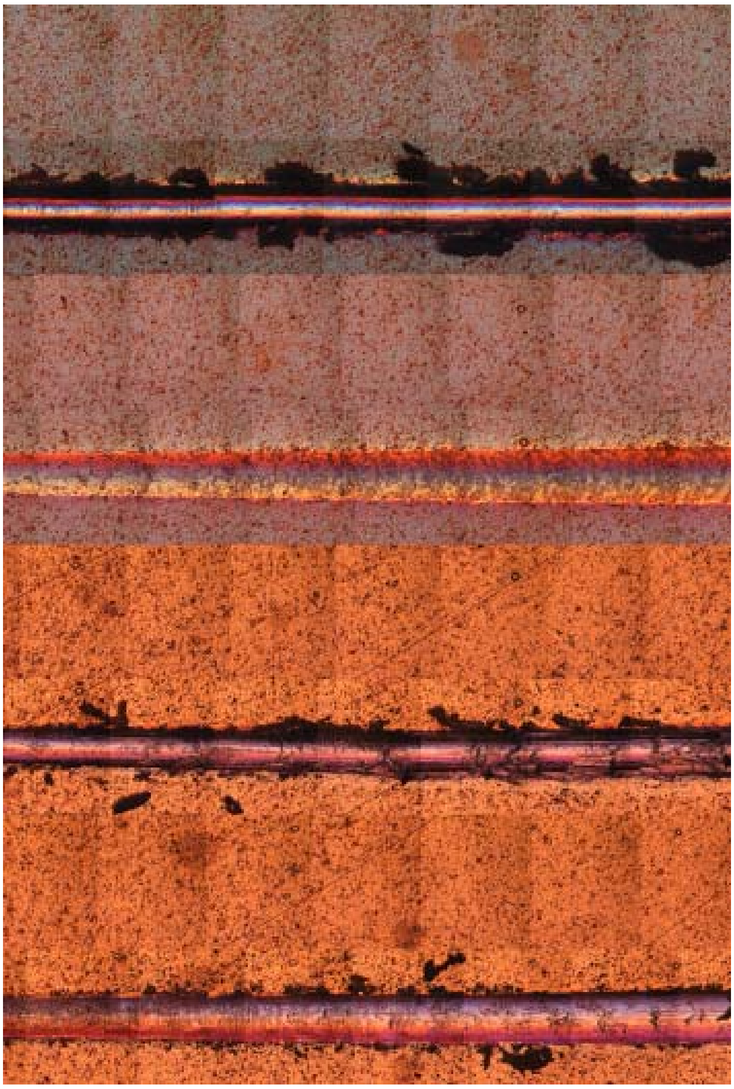

Fig 2a: The scratches in surface of systém thin film – substrate 14 220 – indentors 1. diamond 0,2, 2. diamond 0,5, 3. sintered carbides 0,2, 4. sintered carbides 0,5

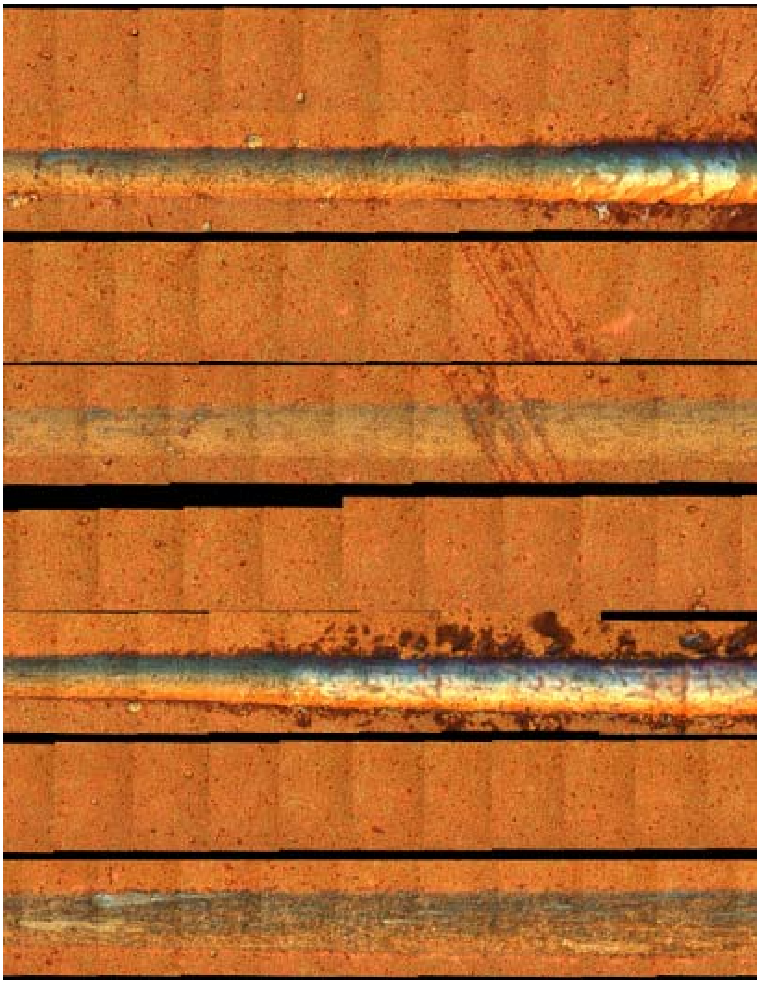

Fig 2b: The scratches in surface of systém thin film – substrate 19 830 – indentors 1. diamond 0,2 mm, 2. diamond 0,5 mm, 3. sintered carbides 0,2, 4. sintered carbides 0,5

From this fig. 2 is possible to view, what deformation processes on substrate 14 220 is the most important, because caused failuring and cracking od thin films on surfaces. Here is very big deformation. The using of indentor from sintered carbide change the stress partly from deformation stress to the friction. Here is smaller deformation process then with using diamond indentor. For evaluation this type of materials systems we prefer to use indentor from sintered carbide, which can give us possibility better understanding failuring and cracking of this type of systém thin film – substrate. The deformation process is smaller on systems thin film – substrate then on the surface of substrate before deposition process. Thin films harden surface and eliminate deformation process and expansion of failures of basic materials under thin films too. The changing on system thin film – substrate with substrate 19 830 is similar as on surface of basic material with changing type of indentor. The deformation and cohesive failures are smaller too – similar as on systém with substrate from 14 220.

Cyclic scratch tests on systems thin film substrate and surface of substrate

Cyclic scratch tests are very important as the other step for aproximation real stresses. But other expansion of this analysis need change of type of indentors, their mechanical and geometry characteristics, too. The changing of type of indentors give possibility to use this analysis for large range of properties of basic materials and systems thin film – substrate and for analysis initiation and expansion of failure and cracks step by step in other cycle. The measurement on systems above mentioned are showed on fig. 3 for basic materials and for systems thin film – substrate too. From this measurement we can analyse changing of deformation process and its expansion step by step, expansion adhesive cohesive failures. Measurements are realised with two different type of indentors above mentioned. Conditions for measurement are the same as simply scratch tests, number of maximal steps is 50.

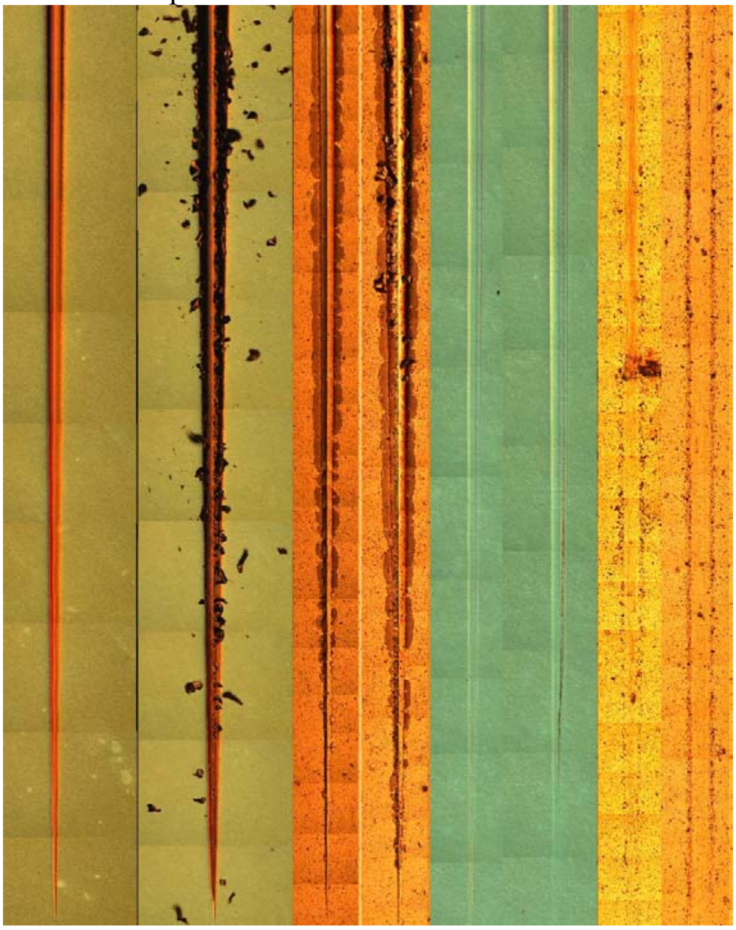

Fig 3: The scratches in surface of substrate HSS (1 scratch, after 50 cycles), in surface of systém thin film – substrate HSS (1 scratch, after 50 cycles) - indentor diamond 0,2 mm, the scratches in surface of substrate HSS (1 scratch, after 50 cycles), in surface of systém thin film – substrate HSS (1 scratch, after 50 cycles) - indentor from sintered carbides 0,5 mm

Cross section in the scratches in systems thin film – substrate and surface of substrate

Evaluation from cross section are the other analysis, which are very important for specification of importance of failures. From surface we can not specify the importance of failures, if it is to the substrate or not and if it is initiated from thin film of surface or interface. All methods, light microscopy, scanning electron microscopy and the others, has some inaccuracy. The new method for evaluation of failures is study from cross section. It is based on realisation precission cross sections in selected more important and characteristic failures. Some examples of cross sections are showed in fig. 4. From this fig. We can view, that some failures important and big from surface can not be important and not exposure of substrate from cross section analysis.

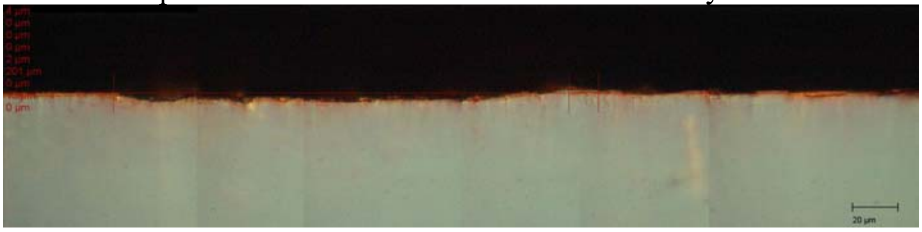

Fig. 4a: Cross section in scratch in surface of systém thin film – substrate 14 220 – indentor from sintered carbides 0,5.

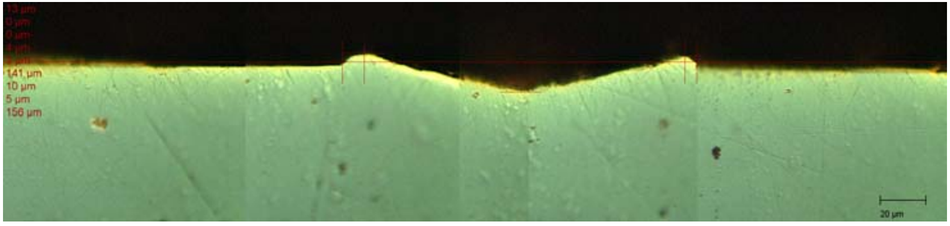

Fig. 4b: Cross section in scratch in surface of systém thin film – substrate 19 830 – indentor diamond 0,2.

Analysis of scratches by x-ray fluorescent spectroscopy on systems thin film – substrate

Here is presented result from new methods for analysis scratches in systems thin film – substrate. The special configuration of measurement by x-ray fluorescent spectroscopy with possibility to measure thin films, its thickness, informative x-ray fluorescent spectrum in very small area (collimator with diametr 0,2 mm). By this analysis we evaluate above mentioned scratches too. The result are in fig. 5. In this fig. we can view spectrums measured in scratches above mentioned step by step in different places in scratches from smaller value of normal forces to the maximal value of normal force (axis z). From this fig. 5 we can analyse from changing of spectrums, how much is weared the surface in scratches with using different type of indentor on different systems thin film – substrate.

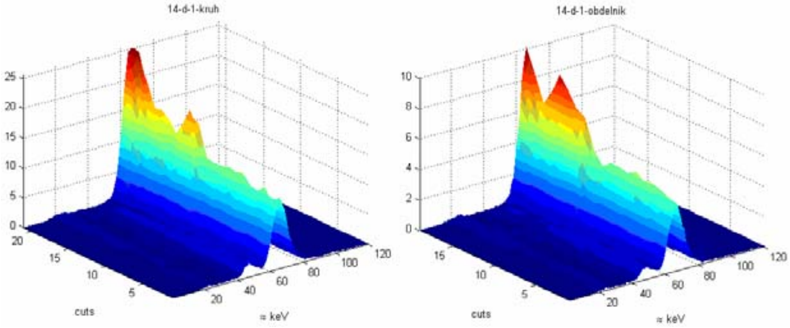

Fig. 5a: X-ray fluorescent spectrums in different places with increasing value of normal force (axis z) in scratch in surface of systém thin film – substrate 14 220 – using 2 different collimators – indentor from sintered carbides 0,5 mm.

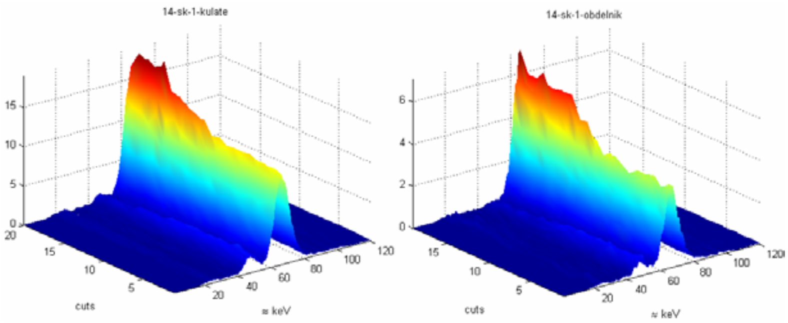

Fig. 5b: X-ray fluorescent spectrums in different places with increasing value of normal force (axis z) in scratch in surface of systém thin film – substrate HSS – using 2 different collimators – indentor from diamond 0,2 mm.

Conclusions

The scratch test indentation method can give much more information about mechanical properties and behaviour of systems thin film – substrate from initiation of failures across its expansion to the big degradation by using different type of indentor with changed material and geometry characteristic. The cyclic indentation can aproximate step by step wearing of surface with step by step mapping changes of failures. The x-ray fluorescent spectroscopy in special configuration can help with evaluation of wear in scratches and show as depth information about deformation and wear with friction. This is very interesting new analysis for evaluation results of scracth indentation. Thin films on both basic materials enhanced properties and behaviour of surfaces.

The paper is presented in the range of solution project n. FT-TA/075.

Literature

1. I.Stepanek, Complex analysis properties and behaviour systems of thin film - substrate with respect practice application of systems, proceedings of conference Matrib 2000 Vela Luka – Croatia 2000
2. I.Stepanek, Evaluation of mechanical behaviour very different kind of material and thickness of films, proceedings of conference Matrib 2002, Croatia – Vela Luka 2002

11. Savjetovanje o materijalima, tehnologijama, trenju i trošenju
11. Conference on Materials, Processes, Friction and Wear
MATRIB'06, Vela Luka, 22-24.06.2006.

UTJECAJ MIKROSTRUKTURE NA DIFUZIJSKA SVOJSTVA VODIKA U NISKOLEGIRANIM ČELICIMA

THE INFLUENCE OF MICROSTRUCTURE ON HYDROGEN DIFFUSION IN LOW ALLOY STEELS

J. Malina, A. Begić Hadžipašić, M. Malina
Sveučilište u Zagrebu, Metalurški fakultet, Hrvatska

Sažetak: Proučavao se utjecaj mikrostrukture na ponašanje čelika u interakciji s vodikom, jer zbog H-atoma apsorbiranih u metalu tijekom korozijskih procesa dolazi često do nepredvidivih lomova čeličnih konstrukcija.

Transportna svojstva apsorbiranog vodika određena su u ovom radu elektrokemijskom laboratorijskom metodom u kojoj se ispituje propusnost vodika kroz čeličnu membranu smještenu između katodne i anodne ćelije.

Iznosi dobiveni za difuzijske koeficijente vodika u ispitanim čelicima ukazuju na prisustvo brojnih mikrostrukturnih zamki koje usporavaju transport apsorbiranog vodika. Mikrostruktura s izduženim Mn-sulfidima slabi permeaciju H-atoma i usporava njihovu difuziju.

Ključne riječi: niskolegirani čelici, mikrostruktura, difuzija vodika, zamke za vodik

Abstract: The influence of microstructure on the behaviour of steels in interaction with hydrogen was studied because H-atoms absorbed in metal during the corrosion reactions are often the source of sudden cracking in steel constructions.

Transport properties of absorbed hydrogen were investigated by electrochemical laboratory method in which the permeability of hydrogen was investigated through steel membrane situated between cathodic and anodic cell.

The values obtained for diffusion coefficients of hydrogen show that number of microstructural traps are present in steels investigated. Steels having the microstructure with elongated Mn-sulfides reduce the permeability of H-atoms and delay their diffusion .

Key words: low alloy steels, microstructure, hydrogen diffusion, hydrogen traps

UVOD

Jedna od osnovnih karakteristika čelika velika je čvrstoća i široko područje primjene. Međutim, mehanička svojstva mogu se značajno promijeniti u agresivnom okolišu u kojem se tijekom korozije čelika razvija vodik i prodire u kristalnu rešetku, te dovodi do pojačane krhkosti i iznenadnih lomova. Takav korozijski napad na najrašireniji materijal današnjice [1] poznat je u literaturi kao HIC (**h**ydrogen **i**nduced **c**racking)-vodikom potaknuti lom ili HE (**h**ydrogen **e**mbrittlement)-vodikova krhkost.

Vodikova krhkost uzrokovana je djelovanjem atomarnog vodika, koji može zaostati u kristalnoj rešetki tijekom proizvodnje, prerade ili zavarivanja čelika, ali isto tako se može naknadno apsorbirati iz kapljevite faze ili plinovitog radnog medija. Pukotine u metalu nastaju kad koncentracija vodika u čeliku dostigne kritičnu razinu. Takova oštećenja ponekad su potpomognuta i napetostima u materijalu, a manifestiraju se kao krhko raspucavanje, smanjenje duktilnosti, blistering (mjehuričavost), stvaranje hidrida itd. [2].

Kako samo atomarni vodik može ući u metal, uvjeti koji omogućavaju njegov pristup površini čelika presudni su za određivanje opsega oštećenja koja se mogu pojaviti. Poznato je da visoke temperature ili izbijanje vodika nastalog korozijom omogućavaju nesmetano snabdijevanje metalne površine vodikom. Oštećenja uzrokovana vodikom ovise o mnogo faktora, a najvažniji su kemijski sastav materijala i njegova mikrostruktura te iznos naprezanja kojima je materijal izložen.

Atomarni vodik difundirati će kroz kristalnu rešetku sve dok ne dođe do barijere pri kojoj se zaustavlja daljnja migracija. Metalurški faktori, kao npr. pojava prevaljanosti, praznine u metalu i nemetalni uključci primjeri su barijera pronađenih u čeliku kroz koje vodik ne može difundirati. Kada atom pokretljivog vodika dođe do granične površine jednog od ovih diskontinuiteta, poznatih u literaturi pod nazivom «zamke», on se brzo spaja s drugim atomom i stvara molekularni vodik [3]. Neki vodikovi atomi će nakon međusobnog spajanja (rekombinacije) ostati u obliku plinovitog vodika, ali većina atoma uvijek će biti sposobna za difundiranje u metal [4]. Povećavanjem koncentracije molekularnog vodika dolazi do povećavanja tlaka i stvaranja blistera. U blizini rastućeg blistera mogu se uočiti velika neželjena naprezanja, uslijed kojih dolazi do nastajanja pukotina.

Činjenica je da su bile potrebne godine intenzivnog izučavanja o djelovanju vodika na krhkost i lom čeličnih materijala, te pronalaženje odgovarajućih testova i procedura za detektiranje i prepoznavanje ranog stadija osjetljivosti čelika prema toj vrsti oštećenja.
Zbog navedenih razloga, u ovom je radu interakcija čelika i vodika proučavana u laboratorijskim eksperimentima, koji omogućavaju navodičenje uzoraka simulirajući uvjete iz prakse.

Mikrostrukturne značajke tri uzorka čelika s različitim mehaničkim svojstvima i njihova sklonost apsorpciji vodika, ispitani su laboratorijskom metodom «vodikove difuzije» u kiselom mediju. Određena je količina vodika razvijenog u korozijskoj reakciji sa sumpornom kiselinom, te propustljivost vodika u ovisnosti o vremenu difuzije. Također je određen difuzijski koeficijent D, te volumen vodika V koji je u stacionarnom stanju difundirao kroz čeličnu membranu.

EKSPERIMENTALNI DIO

Uzorci

Radi preglednosti uvida u kvalitetu korištenih i ispitivanih materijala, u tablicama 1 i 2 su prikazani kemijski sastav ispitanih čelika te njihova mehanička svojstva.

Tablica 1. Kemijski sastav (mas. %) ispitanih čeličnih materijala.

Uzorak	**C**	**Mn**	**P**	**S**	**Si**	**Cu**	**V**	**Mo**	**Al**	**Cr**	**Ni**	**N**	**O**
	[%]	[%]	[%]	[%]	[%]	[%]	[%]	[%]	[%]	[%]	[%]	[ppm]	[ppm]
1	0.09	0.28	0.010	0.011	0.18	0.05	0.02	0.01	0.028	0.01	0.03	57	132
2	0.16	1.11	0.015	0.010	0.40	0.20	-	0.01	-	0.10	-	125	-
3	0.16	0.90	0.015	0.021	0.34	0.22	0.01	0.03	0.043	0.13	0.08	-	-

Uzorak 1 izrezan je u obliku membrane dimenzija (50×80×1) mm iz toplovaljanog lima (umireni konstrukcijski čelik oznake R St37.2 prema DIN-u 17100, odnosno S 235 JRG 2 prema EN-u 10027-2).

Uzorak 2 dimenzija (50×80×1) mm izrezan je iz trake za šavne cijevi (konstrukcijski čelik oznake St.52.3 U prema DIN-u 17100, odnosno S 355 JO prema EN- u 10027- 2).

Uzorak 3 dimenzija (50×80×1) mm izrezan je iz bešavne provodne cijevi za naftnu industriju (linepipe čelik oznake Grade B prema API 5L).

Tablica 2. Mehanička svojstva ispitanih čeličnih materijala.

Uzorak	**Granica razvlačenja R_{eH} [MPa]**	**Vlačna čvrstoća R_m [MPa]**	**Istezljivost A [%]**
1	291	408	42.0
2	411	574	34.9
3	348	514	36.1

Iz kemijskog sastava ispitanih materijala proizlazi da su to niskougljični nelegirani čelici, a relativno niski udjeli fosfora i sumpora osiguravaju im visoku čistoću. Sve uzorke karakteriziraju visoke vrijednosti maksimalne vlačne čvrstoće uz relativno niže vrijednosti za istezljivost kod čelika oznake 2 i 3.

Metode ispitivanja

Metalografska ispitivanja

U svrhu metalografskih ispitivanja uzorci su zaliveni u polimernu masu te strojno brušeni i polirani, nakon čega su nagrizani 12 sekundi u nitalu. Nakon nagrizanja, mikrostrukture su snimane na optičkom mikroskopu s digitalnom kamerom tipa Olympus DP70.

Difuzijska ispitivanja

Prodiranje atoma vodika u čelične materijale moguće je ubrzati jednostavnim laboratorijskim postupkom u kojem se uzorak stavlja kao membrana između dvije posude ispunjene odgovarajućim otopinama [5].

Eksperimentalni uređaj za elektrokemijsko praćenje difuzije vodika sastoji se od anodne (oksidacijske) ćelije i katodne ćelije za punjenje vodikom, koje su odvojene jedna od druge. Uzorak oblika membrane, odnosno tanka metalna pločica, nalazi se između ta dva prostora [6].

Oksidacijska strana membrane, tj. anodna strana uzorka podvrgnuta je postupku niklanja pri sobnoj temperaturi tijekom 55 minuta, uz gustoću struje od 0.5 A/dm^2, jer se uvjeti eksperimenta (medij i elektrodni potencijal) kontroliraju tako da je na oksidacijskoj strani membrane površina metala ili pasivna, ili otporna na koroziju.

Katodna strana uzorka se navodičava pa je ona okrenuta ka katodnom dijelu uređaja ispunjenom 2M otopinom H_2SO_4, a niklana strana je licem okrenuta anodnom prostoru ispunjenom 1M otopinom NaOH. Prije svakog mjerenja katodna strana uzorka brušena je brusnim papirima No. 100, 220, 320, 400, 500 i 600, nakon čega je uslijedilo ispiranje u destiliranoj vodi i odmašćivanje u organskom otapalu. Mjerenja su izvedena pri sobnoj temperaturi $T = 21 \pm 2$ °C.

REZULTATI I RASPRAVA

Metalografski snimci ispitanih uzoraka prikazani su na slikama 1-3. Iz slike 1 je vidljivo da uzorak 1 ima homogenu i sitnozrnatu mikrostrukturu ferita s malim udjelom perlita, a po granicama zrna zapaža se tercijarni cementit. Uzduž ispitivanog presjeka uočava se ujednačena veličina zrna (No. 9 i No. 10). Nasuprot tome, na slikama 2 i 3 vidi se da uzorke 2 i 3 karakterizira izrazito trakasta feritno-perlitna mikrostruktura, s nešto većim udjelom ferita u mikrostrukturi uzorka 3.

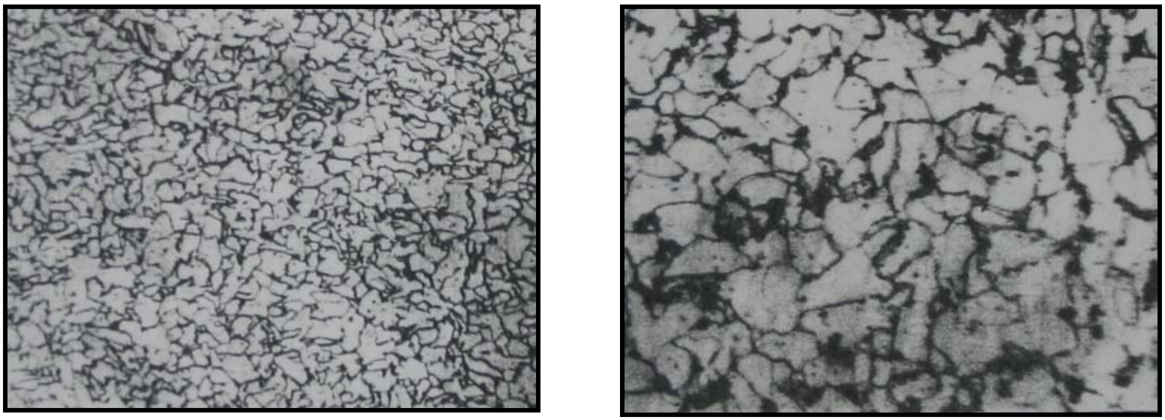

200x 500x

Slika 1. Mikrostruktura uzorka 1 kod različitih povećanja.

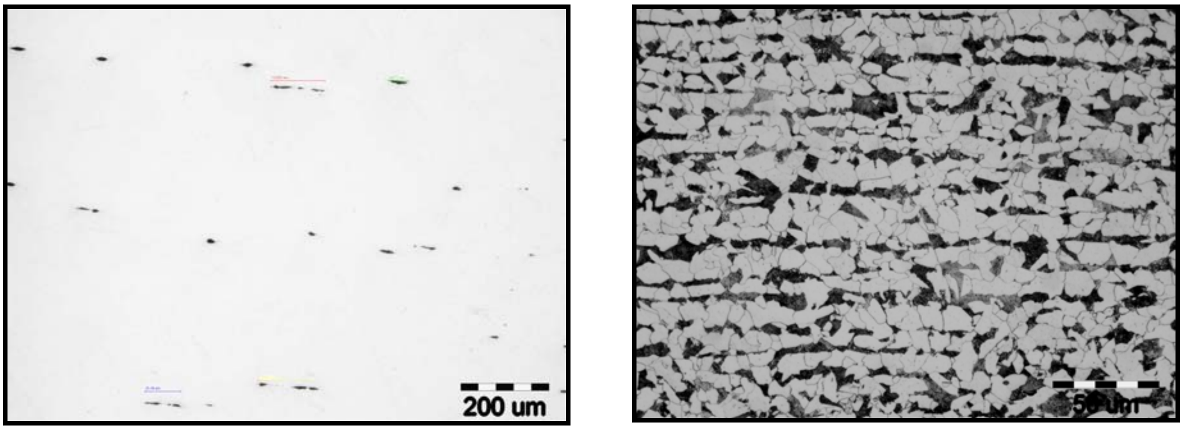

200x 500x

a) b)

Slika 2. Metalografski snimak uzorka 2:
a) bez nagrizanja-uključci
b) nagrizanje u nitalu.

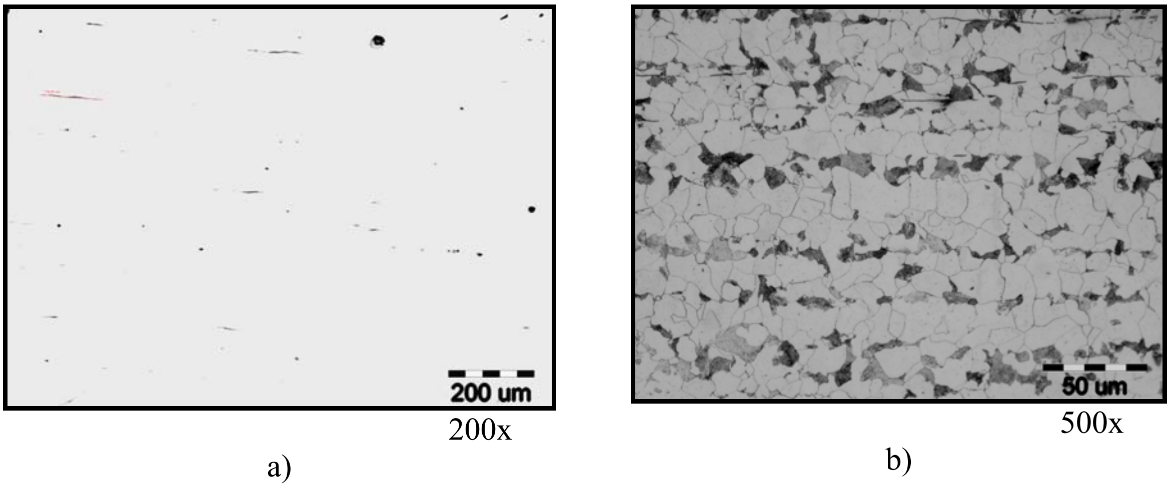

Slika 3. Metalografski snimak uzorka 3:
a) bez nagrizanja-uključci
b) nagrizanje u nitalu.

Korozijskom reakcijom ovih čeličnih uzoraka u dodiru s kiselim agresivnim medijem nastaje vodik koji prodire u metal prema shemi na slici 4. Vodik koji se stvara na ulaznoj strani membrane mjera je reaktivnosti metala, tj. njegove sklonosti koroziji, a transportna svojstva vodika kroz membranu ovise o mikrostrukturi. H-atomi koji se ne apsorbiraju u metalu za vrijeme trajanja eksperimenta, izlaze na drugu stranu membrane i tamo se, pod utjecajem primjenjenog anodnog potencijala oksidiraju u H^+-ione.

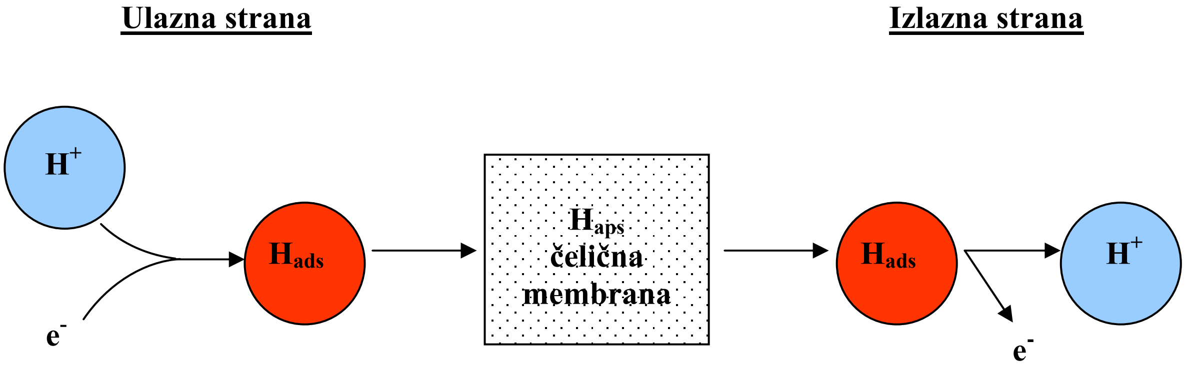

Slika 4. Shematski prikaz transporta vodika kroz čeličnu membranu.

Tijekom ispitivanja difuzije vodika kroz čeličnu membranu dobiva se na pisalu vremenski zapis ovisnosti struje oksidacije prodifundiranog vodika $I = \mathrm{f}\,(t)$. Uzimajući u obzir radnu površinu S, može se izračunati propusnost vodika P izražena u $\mu A/cm^2$ ($P = I/S$) i grafički prikazati ovisnost propusnosti vodika P o vremenu difuzije t kroz čeličnu membranu. Iz dijagrama $P = \mathrm{f}\,(t)$ određuje se stacionarna propusnost P_∞ i vrijeme t_{lag}, definirano kao vrijeme potrebno da se dostigne 63 % od stacionarne propusnosti ($0.63 \times P_\infty$). Iz dobivenih podataka i debljine membrane L, računa se difuzijski koeficijent D prema jednadžbi:

$$D = \frac{L^2}{6 \times t_{lag}} \qquad [\mathrm{cm^2/s}]$$

Prema Faradayevu zakonu izračunava se količina prodifundiranog vodika u stacionarnom stanju (F = 96 490 As/mol):

$$n(H_2) = \frac{I \times t}{z \times F \times S} \qquad [\text{mol/cm}^2]$$

Na slikama 5-7 prikazani su dijagrami provedenih eksperimenata, tj. ovisnost propusnosti vodika $P/\mu Acm^{-2}$ i vremena *t/min* uz prisustvo korištenog medija 2M H_2SO_4 i 1M NaOH. Za svaki uzorak izvedena su po tri mjerenja, a na slikama su prikazani samo prvi odzivi, jer nakon prvog mjerenja apsorbirani vodik se trajno veže u ireverzibilnim zamkama pa se u ponovljenim permeacijskim eksperimentima preostale reverzibilne zamke popune u kratkom vremenu i dolazi do brzog proboja H-atoma na suprotnu stranu čelične membrane.

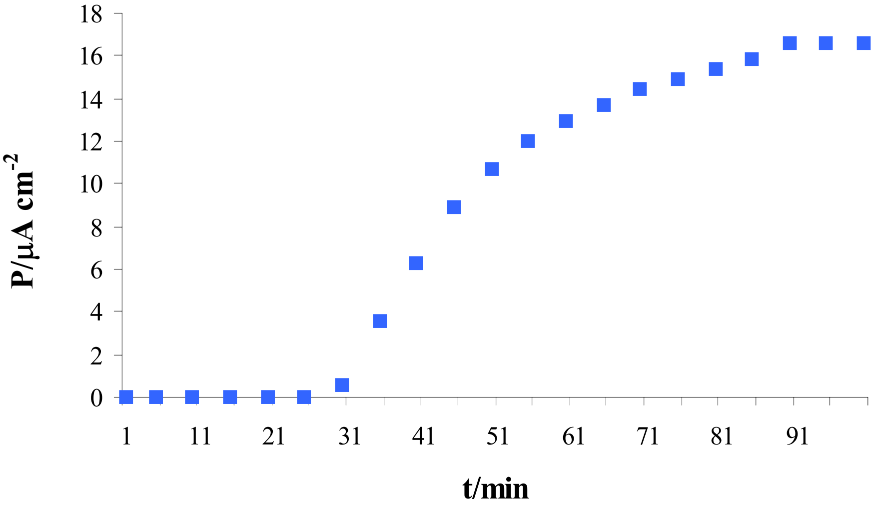

Slika 5. Propusnost vodika u ovisnosti o vremenu difuzije kroz čeličnu membranu kod uzorka 1.

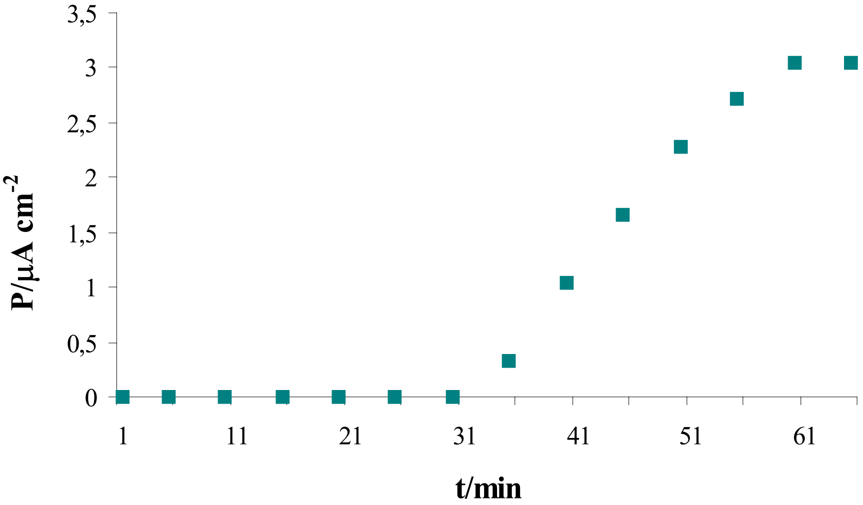

Slika 6. Propusnost vodika u ovisnosti o vremenu difuzije kroz čeličnu membranu kod uzorka 2.

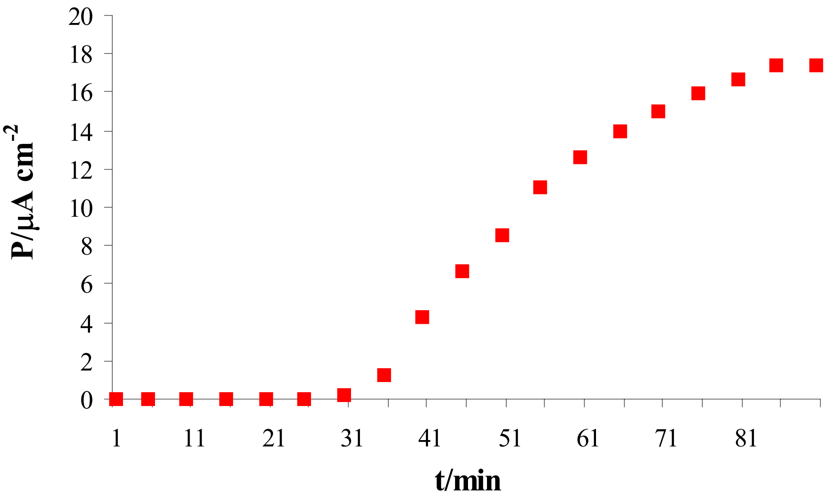

Slika 7. Propusnost vodika u ovisnosti o vremenu difuzije kroz čeličnu membranu kod uzorka 3.

Na osnovi eksperimentalnih dijagrama, izračunate su difuzijske karakteristike vodika u ispitanim čelicima. U tablici 3 prikazane su srednje vrijednosti za P_∞, t_{lag}, difuzijski koeficijent D, broj molova vodika u stacionarnom stanju n.

Tablica 3. Parametri difuzije vodika ispitanih uzoraka.

PARAMETRI	UZORAK 1	UZORAK 2	UZORAK 3
P_∞/μAcm^{-2}	16,96	2,40	17,36
t_{lag}/s	2700	2670	3270
$D \times 10^{7}$/cm^{2}s^{-1}	6,23	6,26	5,09
$n \times 10^{7}$(H_2)/molcm^{-2}	4,87	0,49	4,85
$V(H_2) \times 10^{2}$/cm^{3}cm^{-2}	1,09	0,11	1,09

Rezultati difuzijskih mjerenja prikazani na slikama 5-7 mogu se povezati s razlikama u mikrostrukturi ispitanih čelika. Tako je npr. iz slike 6 očito da vodik apsorbiran na ulaznoj strani uzorka 2 treba oko 30-tak minuta da difuzijom popuni sve zamke u mikrostrukturi i da počne proboj na suprotnu stranu membrane. Kad se sve zamke popune, na izlaznoj strani uspostavlja se stacionarni protok vodika. To se na krivulji propusnosti zapaža kao P_∞ nakon 60-tak minuta.

Kod uzoraka 1 i 3, parametri difuzije vodika s krivulje permeabilnosti na slikama 5 i 7 su drugačiji: proboj vodika počinje također nakon 30-tak minuta od početka navodičenja membrane, ali stacionarni protok vodika uspostavlja se tek nakon 90-tak minuta, jer je potrebno više vremena da se sve prisutne zamke popune.

Očito je da povećani udio ugljika u ispitanim čelicima povećava ne samo čvrstoću, već i broj zamki u kojima se apsorbirani atomi vodika mogu tijekom difuzije zadržati. Ako su zamke reverzibilne, H-atomi su labavo vezani i mogu se difuzijom kretati kroz rešetku, a iz kristalne rešetke mogu se istjerati zagrijavanjem na 112-270 ºC. Ako se pak radi o ireverzibilnim zamkama, vodikovi atomi se mogu istjerati tek pri temperaturama 305-750 ºC.

Smatra se [7] da je iznos energije veze između vodika i reverzibilnih zamki oko 0.3 eV, no u nekim je radovima određena i vrijednost od 0.7 eV za zamke tipa karbida [8]. Ipak prevladava mišljenje da vrijednost energije veze u iznosu manjem od 0.3 eV predstavlja prihvatljivu granicu za većinu reverzibilnih zamki kao što su to dislokacije, granice zrna, šupljine, intersticijski otopljeni atomi drugih metala [9-11]. Vodik koji putuje kroz mikrostrukturu čelika naziva se pokretljivi vodik (diffusible hydrogen), a sastoji se od vodika zarobljenog u reverzibilnim zamkama i vodika koji je u metalu ostao nakon proizvodnje (tzv. lattice hydrogen).

Sve eksperimentalne krivulje koje pokazuju vremenski tijek difuzije H-atoma kroz čeličnu membranu, imaju karakterističan S-oblik, ali se razlikuju po propusnosti u stacionarnom stanju. Na osnovi eksperimentalnih podataka u tablici 3 moguće je prikazati komparativni pregled permeacijskih karakteristika za sve ispitane uzorke. Dobivene krivulje prikazane na slici 8 daju ovisnost normiranog protoka atomarnog vodika $J(t)/J_\infty$ o normiranom vremenu τ $(\tau = D \times t/L^2)$. Ta će se ovisnost u daljnjem tekstu navoditi kao normirani permeacijski odziv.

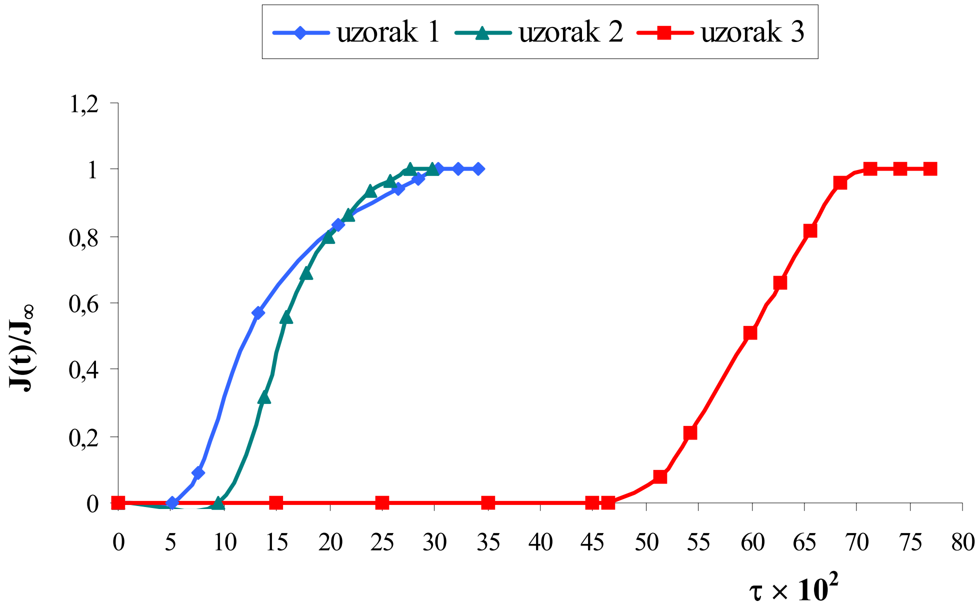

Slika 8. Komparativni dijagram ispitivanih uzoraka.

Strme krivulje normiranog permeacijskog odziva za ispitane uzorke ukazuju na to, da pored reverzibilnih zamki, u tim čelicima postoje također i ireverzibilne zamke koje apsorbirani vodik trajno vežu nakon prvog mjerenja.

Posebno niska vrijednost za propusnost vodika kod uzorka 2 (slika 6) može se povezati s nešto većim udjelom Mn i prisustvom Mn-sulfida koji su poznati kao uspješne zamke za vodik. Međutim, egzaktna korelacija difuznosti vodika i kemijskog sastava ispitanih čelika nije moguća, iako se može lakše razumjeti kad se poveže s mikrostrukturom. Stoga je na sljedećoj slici prikazana ovisnost difuzijskih koeficijenata čelika različite mikrostrukture i količine prodifundiranog vodika u stacionarnom stanju.

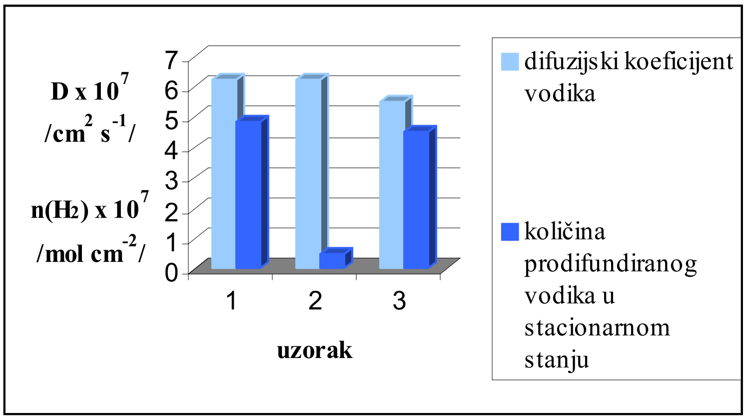

Slika 9. Komparativni prikaz uzoraka ispitivanih čeličnih materijala u ovisnosti o difuzijskom koeficijentu vodika *D* i količini prodifundiranog vodika $n(H_2)$ u stacionarnom stanju.

Uspoređujući ispitivane uzorke u ovisnosti o difuzijskom koeficijentu vodika *D* i količini prodifundiranog vodika $n\ (H_2)$, iz slike 9 je vidljivo da ispitani uzorci imaju velik difuzijski koeficijent, koji u ovom slučaju ukazuje na povećanu pokretljivost atomarnog vodika uzimajući u obzir prisustvo reverzibilnih i ireverzibilnih zamki.
Najmanja količina prodifundiranog vodika u stacionarnom stanju, izmjerena je kod uzorka rednog broja 2. Pri tumačenju ovih odnosa treba imati na umu da difuzijski koeficijent vodika u čistom željezu ima vrijednost od $D_{Fe} = 3\text{-}9,5 \times 10^{-5}$ cm^2/s [12], dok difuzijski koeficijenti za uzorke ispitane u ovom radu imaju iznos u rasponu od $3\text{-}6 \times 10^{-7}$ cm^2/s. To ukazuje na prisustvo većeg broja zamki koje usporavaju transport H-atoma kroz membranu.

ZAKLJUČAK

Nakon elektrokemijskih ispitivanja difuzije vodika provedene pri sobnoj temperaturi kod tri različita konstrukcijska čelika, može se zaključiti sljedeće:

- Propusnost vodika u ispitanim čelicima nije kontrolirana njihovim kemijskim sastavom, no može se povezati s mikrostrukturom.
- Niski iznosi za propusnost vodika kod ispitanih uzoraka ukazuju na to da njihova složena mikrostruktura ima velik broj konstituenata koji djeluju kao zamke za vodik. To mogu biti granice faza ferit/perlit, uključci, segregacije, dislokacije. Posebno niska vrijednost za propusnost vodika kod uzorka 2 (slika 6) može se povezati s nešto većim udjelom Mn i prisustvom Mn-sulfida koji su poznati kao uspješne zamke za vodik.
- Strme krivulje normiranog permeacijskog odziva (slika 8) ukazuju na to da pored reverzibilnih zamki u tim čelicima postoje također ireverzibilne zamke koje apsorbirani vodik trajno vežu nakon prvog mjerenja. U ponovljenim permeacijskim eksperimentima preostale reverzibilne zamke u kratkom se vremenu popune i dolazi do brzog proboja H-atoma na suprotnu stranu čelične membrane.
- Usporede li se s difuzijom vodika u kristalnoj rešetci željeza ($D_{Fe} = 9,5 \cdot 10^{-5}$ cm^{2}s^{-1}), difuzijski koeficijenti određeni u ovom radu su za dva reda veličine manji i ukazuju na prisustvo brojnih mikrostrukturnih zamki koje usporavaju transport apsorbiranog vodika. Prema tome, vrijednosti za *D* ($3\text{-}6 \cdot 10^{-7}$ cm^{2}s^{-1}) su u skladu s podacima iz literature za čelike sličnih mikrostrukturnih svojstava.

LITERATURA

1. T. Hara, H. Asahi, H. Ogawa, Corrosion **60** (2004) 1113-1121.
2. B. Godec, V. Grdun, Materiali in Tehnologije **35** (2001) 3-4, 181-186.
3. J. Malina, M. Malina, A. Begić Hadžipašić, Zbornik, 3. Međunarodno savjetovanje: Mehanizacija, automatizacija i robotizacija u zavarivanju i srodnim postupcima, Hrvatsko društvo za tehniku zavarivanja, Zadar, 2005, str. 119-126
4. J. Malina, J. Sefaja, Zaštita materijala **29** (1988) 1, 27-29.
5. ASTM G 148-97 (03)
6. J. Malina, Upute za Vježbe iz korozije i zaštite metala, interna skripta, Metalurški fakultet, Sisak, 2004, str. 25-30.
7. M. Brass, J. Collet-Lacoste, Acta Mater. **46** (1998) 869-879.
8. J. Malina et al, Zbornik, 9th European Congress on Corrosion, Proceedings Vol. II, Utrecht, 1989, paper No. PI-254.
9. J. Y. Lee, J. L. Lee, Phil.Mag. **A56** (1987) 293-309.
10. J. Malina et al, Metalurgija **35** (1996) 161-166.
11. J. Malina et al, Materials Science **41** (2005) 253-258.
12. E. Riecke, K. Bohnenkamp, Z. Metallkd. **75** (1984) 76-81.

UTJECAJ TROŠENJA NOŽEVA NA EFIKASNOST IZŽILJAVANJA DUHANA TIPA BURLEY

INFLUENCE TOBACCO THRESHER KNIVES WEAR ON EFFICIENCY THRESHERS OF THE BURLEY TOBACCO

Dr. sc. Vlatko Marušić, Strojarski fakultet, Slavonski Brod
Sanja Marušić, dipl. ing.,Industrijsko obrtnička škola, Slavonski Brod
Slavko Marinac
Dr. sc. Stjepan Aračić, Strojarski fakultet, Slavonski Brod

Sažetak: U fazi primarne obrade duhana tipa Burley u trešerima se pomoću noževa vrši odvajanje finog dijela lista (plojke) od rebra (nervature) tzv. izžiljavanje. Pri tome su radne površine noževa izložene trošenju. Izvršeno je ispitivanje dvije vrste zaštitnih slojeva na noževima trešera. Analiziran je utjecaj istrošenja noževa s naštrcanim slojem na kvalitetu izžiljavanja ovisno o prerađivanoj mješavini listova. Utvrđeno je da se rad s oštećenim noževima najnegativnije odražava na najkvalitetnijim frakcijama duhana – onima koje imaju najveću tržišnu vrijednost. Utvrđeno je da se primjenom naštrcanog sloja, uz pravovremenu zamjenu istrošenih noževa, efekti izžiljavanja mogu smanjiti i do 6%.

Ključne riječi:izžiljavanje duhana, noževi trešera, efikasnost

Abstract: Primary stage of Burley type tobacco in thresher machines includes separation of fine parts of tobacco leaves from the ribs, the so called "stemming". Thereby cutting edges of knives are exposed to wear by abrasive particles. Analysis has been performed of the influence of two kinds of protective layers on thresher knives on quality of stemming, depending upon tobacco leaves blend. It has been established that operation with worn knives is most negatively reflected on the most quality tobacco fractions – those having the greatest market value. It has been proved that application of spray layer instead of installation of plates made of hard metal, followed by partial exchange of worn knives can reduce tribological losses even up to 6%.

Key words: threshers of the tobacco, knives of threshering line,efficiency

1.UVOD

Nakon berbe i prirodnog sušenja na udjel 15 do 17% vlage, duhan se klasificira u razrede. Najkvalitetniji su listovi sa sredine stabljike a manje kvalitetni oni s vršnog i donjeg dijela. Donje listove je potrebno otprašiti-očistiti od čestica zemlje i pijeska. Otprašeni i klasificirani (po veličini) duhanski listovi se kondicioniraju (vodom, vodenom parom i toplim zrakom temperature oko 150ºC) te se preko dozatora dovode na liniju za izžiljavanje. Tu se na trešerima u više stupnjeva trganjem vrši izžiljavanje-odvajanje finog dijela lista (plojke)od rebra (nervature). Dimenzije trešera u I i II stupnju su 42", a u III i IV 30". Tako djelomično izžiljeni duhanski listovi se odvode na klasifikatore gdje se u 7 stupnjeva vrši razdvajanje frakcija plojke (po veličini). Neizžiljeni djelovi nakon svakog od stupnjeva odvode se na ponovno treširanje (III. stupnja). Veličina tih trešera je 36". Iz izžiljenog duhana se preko sistema sita ø5 mm izdvaja sitnjevina a potom odvaja od duhanske prašine. Izdvojena sitnjevina se mješa s prethodno izdvojenom plojkom (naknadno osušenom u tzv. redryeru). U daljnjim fazama se izdvojene frakcije suše, kondicioniraju te prešaju i pakiraju nakon čega su spremne za otpremu na daljnju finalnu doradu u cilju obrade u formu podobnu za pušenje. Također se, nakon dodatnog sušenja sistemom sita razdvajaju krupno od sitnog rebra, te je i ono nakon pakiranja spremno za otpremanje na doradu radi izdvajanja dijelova podobnih za primjenu u pripremi cigareta. U nabrojanim fazama primarne obrade duhana trošenju su najizloženiji noževi trešera na kojima se provodi i glavna faza obrade - izžiljavanje duhanskog lista. Cilj ispitivanja je utvrditi da li i koliko trošenje noževa utječe na kvalitetu izžiljavanja, što bi trebalo pomoći pri izboru postupka zaštite noževa.

2. TRIBOSUSTAV TREŠERA

2.1 Svojstva duhana tipa Burley

Kemijski sastav neizžiljenog duhana [1] prikazan je u tablici 1. Glavni sastojak duhana je nikotin. To je alakoloid koji odgovara kemijskoj formuli $C_{10}H_{10}N_2$, ima izgled bezbojne tekućine masne konstitucije, izložen na zraku i svjetlu postaje žut, a zatim posmeđi zbog fotooksidacije. Nikotin je topiv u vodi, a vrije na ~247ºC.

Tablica 1. Orjentacioni kemijski sastav neizžiljenih duhana

SASTOJAK DUHANA	UDIO IZRAŽEN ZA CIJELI LIST (%)
nikotin	0,78-4,59
celuloza	7,36-15,76
škrob	3,34
limunska kiselina	6,31
jabučna kiselina	3,2
amonijak	0,55
smola	5,6
voskovi	0,2
pektini	16,71
ukupni dušik	2,18

Ovaj sastav ovisi o položaju lista na stabljici, gnojidbi duhana, te o vrsti tla na kojemu se biljka uzgaja. Za središnji i istočni dio Slavonije karakteristične su slijedeće vrste tla : zbijeno glinena, lagano humusna i rjeđe pjeskovita.

U uvodnom je dijelu rečeno da su na stabljici naročito doljnji listovi izloženi taloženju i naljepljivanju čestica tla (uslijed kiše i vjetra). U tvornici značajna pažnja poklanja otprašivanju listova duhana u cilju uklanjanja tragova prašine i pjeska. Ovdje treba napomenuti da je pri preradi duhana iz regija gdje su tla pjeskovita, Podravina, uočeno intenzivnije trošenje noževa trešera.

Duhan je biljka koja obiluje mineralima koji mogu biti u obliku oksida, karbonskih ili mineralnih soli[1,2] Elementi koji ulaze u sastav minerala utvrđeni su analizom sastava pepela nakon sagorijevanja duhana, tablica 2.

Tablica 2. Orjentacioni sastav pepela duhanskog lista

KALIJ	KALCIJ	MAGNEZIJ	FOSFORNA KISELINA	SILICIJ	KLOR
19-29 %	27-50 %	7-15 %	2-5 %	5-18 %	0,55-9 %

Izgled duhanskog lista tipa Burley prikazan je na slici 1. Duž središnjeg dijela lista nalazi se glavno (centralno) rebro od kojeg se granaju periferna rebra (nervature). Gornja površina lista pokrivena je gustim dlačicama koje luče gume i sokove (katran). Taj se katran tijekom berbe u obliku crnih gumastih nakupina lijepi za ruke i strojeve, a pri izžiljavanju u trešerima može se lijepiti na noževe.

a)

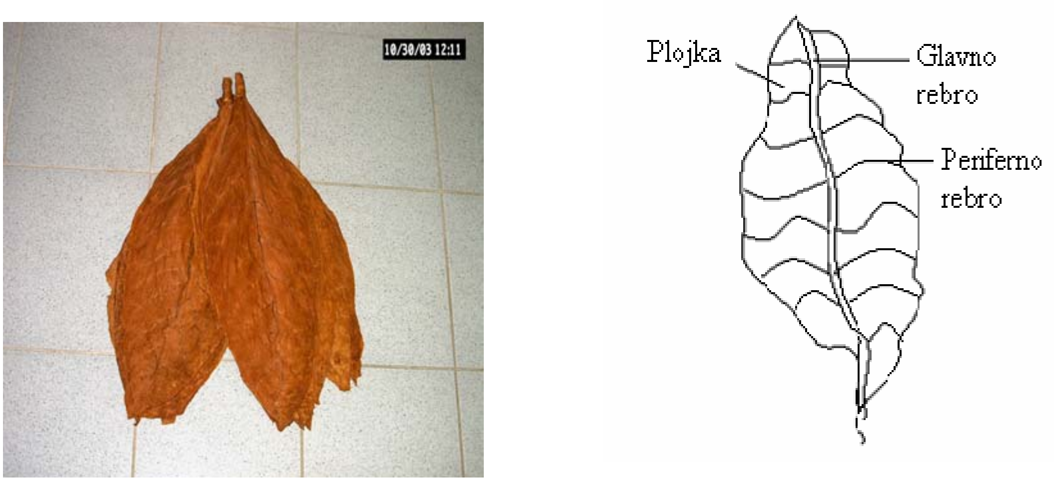

a) b)

Slika 1. Duhanski list tipa BURLY
a) suhi listovi;b) shematski prikaz položaja plojke i rebra (nervature)

Glavno i periferno rebro zbog svoje armaturne uloge sadrže jače vezivno tkivo koje nakon sušenja i gubitka vlage postaje drvenasto. Prilikom punjenja trešera listovi duhana u radni prostor padaju cijelom svojom površinom između fiksnih i rotirajućih noževa čime pružaju maksimalni otpor stroju pri trganju.

2.2 Noževi trešera

Na slici 2 dat je prikaz trešera s vidljivim rasporedom radnih dijelova u otvorenom kućištu.

Slika 2. – Izgled otvorenog trešera

Fiksni noževi tijekom rada ne mijenjaju svoj položaj, učvršćeni su sa svake strane statora trešera na bočna vrata. Postavljeni su okomito na os rotirajućeg bubnja pod međusobnim kutem 180º. Na svakoj je strani u red učvršćeno 17 fiksnih noževa.
Rotirajući noževi pričvršćeni su po obodu bubnja u 6 redova. Svaki red sadrži po 16 noževa a redovi su međusobno zakrenuti za kut od 60º, pa bubanj trešera sadrži ukupno 96 rotirajućih noževa.
Snimanjem stanja uočeno je da se noževi izrađuju s jednom od slijedeće dvije vrste zaštitnih slojeva:

1 – pločica od tvrdog metala;
2 – naštrcana prevlaka.

Na slici 3 shematski je prikazan izgled pojedinih noževa s rasporedom zaštitnih slojeva.

Fiksni nož s pločicom tvrdog metala

Fiksni nož s prevlakom

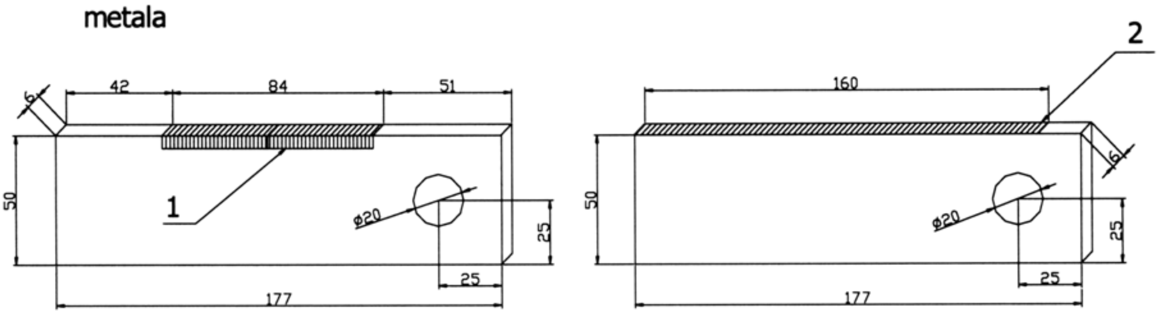

Rotirajući nož s pločicom tvrdog metala

Rotirajući nož s prevlakom

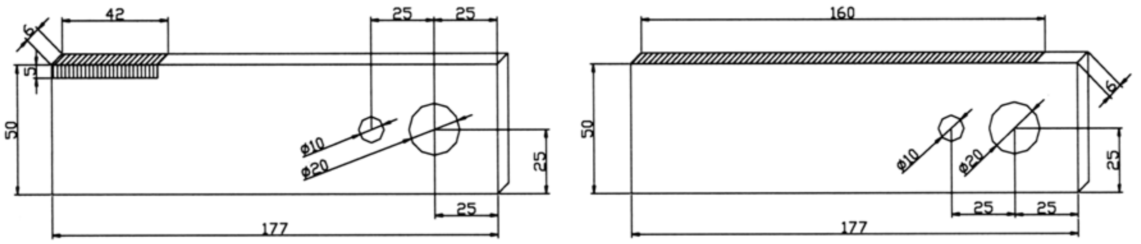

Slika3. Shematski prikaz fiksnog i rotirajućeg noža

Također je uočeno da su noževi s pločicom od tvrdog metala daleko skloniji naljepljivanju katrana nego noževi s naštrcanim slojem. Kako se postupak skidanja tih nakupina provodi udarcima metalnim sjekačem nerijetko se dogodi da pukne pločica od tvrdog metala. Na slici 4 prikazan je izgled noževa istrošenih u tijeku rada.

a) b)

Slika 4. Karakteristični izgled noževa trešera istrošenih uporabom; a)fiksni nož; b)rotirajući

3. REZULTATI ISPITIVANJA

3.1 Ispitivanje noževa trešera

Za potrebe ispitivanja strukture i tvrdoće odabrani su po jedan fiksni i rotirajući nož s pločicom tvrdog metala i s naštrcanim zaštitnim slojem[3,4].

Karakteristični makro snimci poprečnih presjeka noževa prikazani su na slici 5.a i 5.b, te shematski (s oznakom referentnog pravca za mjerenje toka tvrdoće HV 0,3) na slici 5.c.

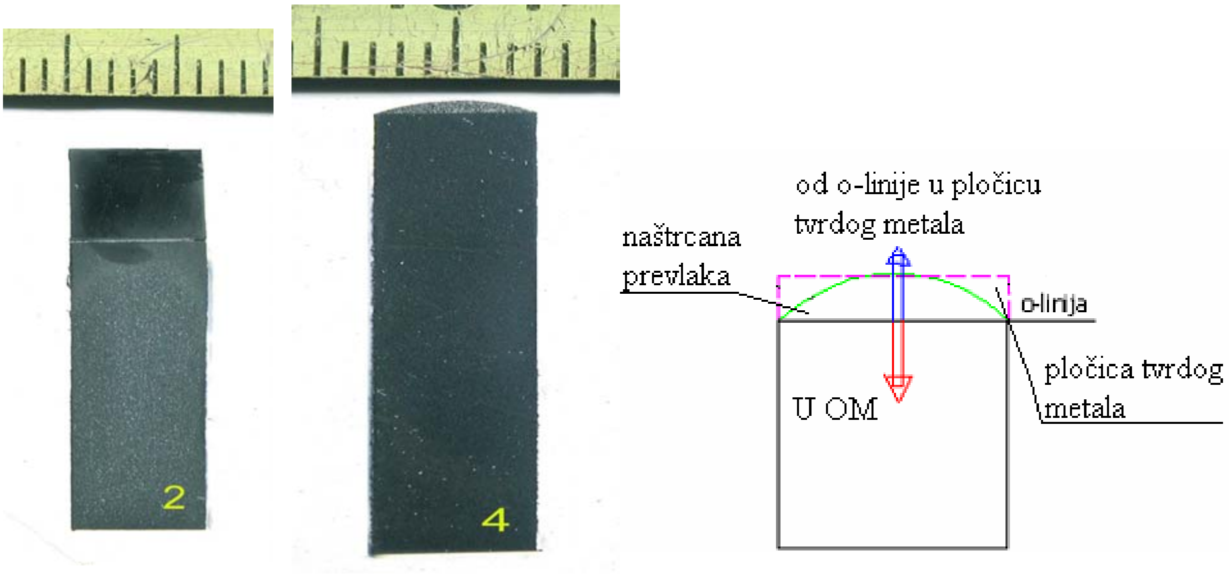

a) b) c)

Slika 5. Poprečni presjek noževa

a) makrosnimak noža s tvrdom pločicom; b) makrosnimak noža s naštrcanom prevlakom; c) shema poprečnog presjeka s označenim referentnim pravcem za mjerenje toka tvrdoće

Karakteristična mikrostruktura pločice tvrdog metala i zone spoja osnovni materijal – pločica prikazana je na slici 6.a, a noža s naštrcanim slojem na slici 6.b.

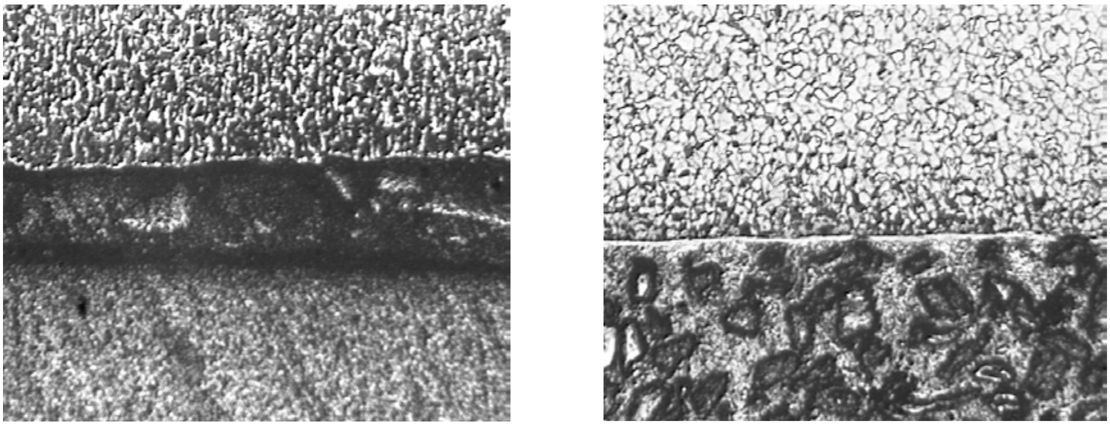

a) b)

Slika 6. Karakteristična mikrostruktura poprečnog presjeka noževa, nagriženo nitalom
a)zona spoja osnovni materijal – pločica tvrdog metala, pov. 120X
b) zona spoja osnovni materijal – naštrcani sloj, pov. 120X.

U tablici 3 prikazan je tok tvrdoće HV 0,3 od nul linije (na slici 5.c) koja je postavljena na granicu spoja osnovnog materijala sa zaštitnim slojem.

Tablica 3. Tok tvrdoće na poprečnom presjeku noževa

Rastojanje od "0" linije	TVRDOĆA HV 0,3				Rastojanje od "0" linije
	Prevlake	OM	Pločice	OM	
0,1	1238 HV	120 HV	1215 HV	214 HV	0,1
0,2	958 HV	140 HV	1350 HV	212 HV	0,5
0,3	678 HV	143 HV	1390 HV	217 HV	1,0
0,4	398 HV	134 HV	1336 HV	214 HV	1,5
0,5	118 HV	130 HV	1311 HV	216 HV	2,0
0,6	162 HV	124 HV	1363 HV	214 HV	2,5
0,7	442 HV	130 HV	1363 HV	212 HV	3,5
1,0	1238 HV	120 HV	1215 HV	214 HV	3,9

3.2 Kvaliteta izžiljavanja duhana

Da bi se došlo do spoznaje koliko trošenje noževa trešera utječe na kvalitetu izžiljavanja, provedena su istraživanja udjela pojedinih frakcija (veličine plojke) nakon obrade duhana s novim i istrošenim noževima. Kontrola izžiljavanja vršena je u tvorničkom laboratoriju standardnom metodom na za to propisanoj opremi. Standardno se preko vibrirajućih sita odvajaju tri veličine plojke (frakcije):
- prva: 1"x1",
- druga: 1/2"x1/2",
- treća: 1/4"x1/4".

Pri tome je najkrupnija frakcija ujedno i najkvalitetnija i ona na tržištu postiže najveću cijenu.
Udjeli frakcija se prate na svaku od tri moguće mješavine odbira (položaja lista sa stabljike) jer i to značajno utječe na cijenu.
Udjeli frakcija svakog uzorkovanja se zbrajaju te se izračunava prosjek postotnog udjela pojedine frakcije u kontrolnom uzorku.
Dijagramima su prikazani rezultati udjela pojedinih frakcija za svaku mješavinu i to:

- dok su noževi bili novi, neoštećeni,
- kad su noževi već bili oštećeni.

U dijagramu na slici 6 grafički je prikazan odnos postotnog udjela frakcija veličine plojke 1/2" +1" u kontrolnoj masi 12 uzoraka mješavine odbira duhana u tijeku jedne kampanje. Uočava se da se razlike u udjelu ovih frakcija pri radu s novim noževima u odnosu na rad s istrošenim, kreću u rasponu od 0 do 4,5%. Slično vrijedi i za duhansko rebro.

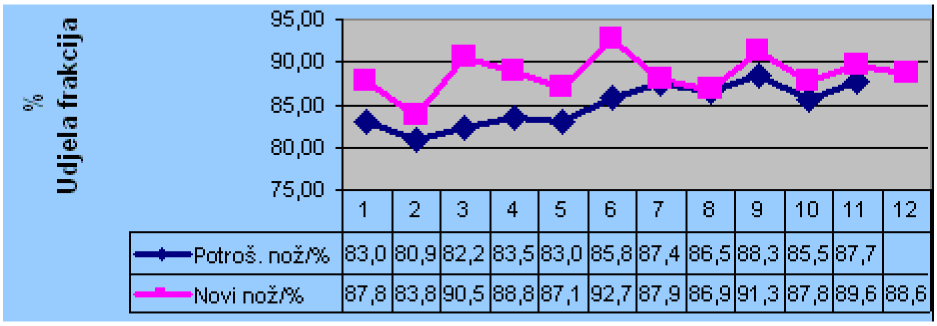

Slika 6. Udjel frakcije za veličine plojki 1/2"+1/4" kod izžiljavanja mješavine odbira duhana pri upotrebi novih i istrošenih noževa

Praćenjem udjela sitnijih frakcija (1/2"+1/4"+1")mješavine odbira utvrđeno je da on ne ovisi o intenzitetu istrošenja noževa. Treba istaći da te sitnije frakcije na tržištu postižu nižu cijenu . Dijegramom na slici 7 grafički je prikazan udjel (%) frakcija nakon izžiljavanja mješavine gornjih i srednjih listova. Uočava se da se gotovo jednaki rezultati postižu izžiljavanjem s novim i istrošenim noževima. To vrijedi kako za udjele frakcije 1/2"+1" tako i za frakcije 1/2" +1/4"+1", kao i za duhansko rebro.

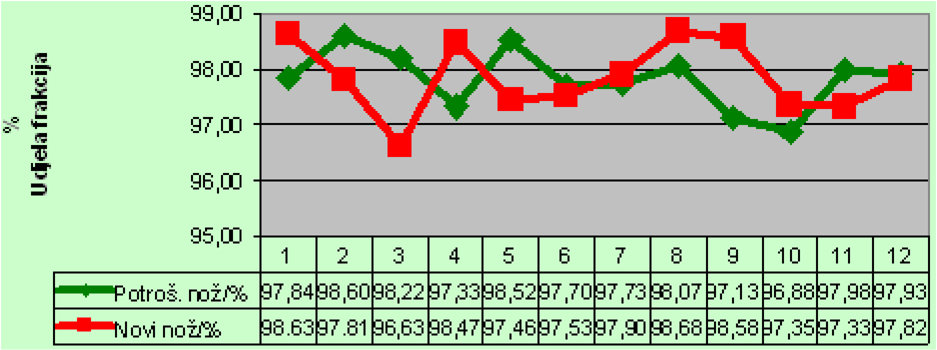

Slika 7. Udjel frakcije za veličine plojki 1/2" +1" kod izžiljavanja mješavine gornjih i srednjih listova ovisno o istrošenosti noževa

Dijagramom na slici 8 grafički je prikazan udjel (%) frakcija nakon izžiljavanja odbira mješavine srednjih i donjih listova. Uočava se da je udjel frakcija 1/2" +1" pri radu s novim noževima i do 6% veći nego pri radu s istrošenim noževima. Istovremeno je uočeno da kod sitnijih frakcija (1/2" +1/4"+1") ove mješavine, kao i kod duhanskog rebra, te razlike dosežu do najviše 1,5%.

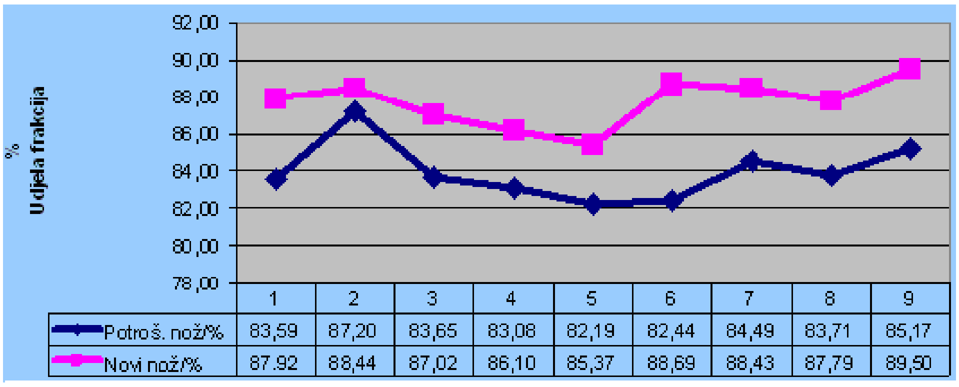

Slika 8. Udjel frakcija za veličine plojke 1/2" +1" kod izžiljavanja odbira mješavine srednjih i donjih listova pri upotrebi novih i istrošenih noževa

4. ANALIZA REZULTATA ISPITIVANJA I ZAKLJUČAK

Specifičnost položaja duhanske industrije (u kojemu se ona nalazi zbog agresivne antipušačke kampanje) ograničava mogućnost iznošenja podataka o konkretnim uštedama koje bi se postigle: I-pravilnim izborom postupka zaštite od trošenja noževa trešera; II-ispravnim definiranjem kriterija dimenzionalnog istrošenja nakon prestaje njihov funkcionalni rad.
Rezultati ispitivanja udjela kvalitetnih frakcija (1/2" +1") i frakcija nižih cijena (1/2" +1/4"+1") za tri osnovne grupe mješavina duhanskih listova ukazuje na sljedeće:

- za mješavinu duhanskog odbira razlike u udjelu kvalitetnih frakcija (1/2"+1") pri radu s novim noževima se kreće do 4,5% u odnosu na rad s istrošenim noževima,
- za mješavinu gornjih i srednjih listova ne uočava se utjecaj stupnja istrošenja noževa na udjel pojedinih frakcija,
- za mješavinu srednjih i donjih listova razlike u udjelu kvalitetnih frakcija (1/2" +1") pri radu s novim noževima se kreću do 6,25% u odnosu na rad s istrošenim noževima..

Prema dostupnim podacima [5,6] proizvodnja duhana u Hrvatskoj se kreće između 8.000 i 11. 000 tona godišnje. Za procjenu mogućih ušteda dovoljno je reći da, ovisno o tržišnim odnosima (definiraju se svake godine na početku otkupa i primarne prerade duhana), svaki postotak lošijeg izžiljavanja snižava cijenu frakcije za minimalno 2, najčešće 3, a u nekim godinama i do 4%.

5. LITERATURA

[1] Hawks S. N.Jr.,Collins W. K.: Principles of Flued-Cured Tobacco ProducUSA N.C.StateUniversity , 1987.

[2] Furney Albert Todd prof.Emeritus: Tobacco Producing a Healthy Crop USA ,North Carolina State UniversityFirst Edition ,1981.

[3] Hrgović I.:Prevlake toplinskog naštrcavanja otporne na trošenje,Tehnički fakultet –Rijeka ,1999.

[4] Novosel M., Cajner F., Krumes D.:Alatni materijali, Strojarski fakultet u Slavonskom Brodu,1996.

[5] DRŽAVNI ZAVOD ZA STATISTIKU , IND 21-Godišnji izvještaj PRODCOM, 1187/2003.

[6] DRŽAVNI ZAVOD ZA STATISTIKU , IND 21-Godišnji izvještaj PRODCOM, 1220/2004.

11. Savjetovanje o materijalima, tehnologijama, trenju i trošenju
11. Conference on Materials, Processes, Friction and Wear
MATRIB'06, Vela Luka, 22-24.06.2006.

MODIFICIRANJE POVRŠINA DIJELOVA KALUPA ZA TLAČNO LIJEVANJE ALUMINIJA

SURFACE MODIFICATION OF PARTS FOR ALUMINIUM DIE CASTING

B. Matijević, M. Stupnišek, I. Kranjčević

Faculty of Mechanical Engineering and Naval Architecture,
University of Zagreb, ZAGREB, CROATIA, bozidar.matijevic@fsb.hr

Sažetak: Dijelovi kalupa za tlačno lijevanje aluminija izloženi su kompleksnom mehanizmu trošenja te im je trajnost ograničena. Dominantni mehanizam trošenja je reakcijsko nataljenje radne površine dijelova kalupa, što ima za posljedicu česte zastoje i povećane troškove održavanja kalupa. U cilju produljenja vijeka trajanja kalupa za tlačno lijevanje aluminija primjenjuju se različiti postupci modificiranja i prevlačenja površina. Do sada često primjenjivani postupak modificiranja površina bio je postupak nitriranja u solnoj kupci (TENIFER), međutim literaturni podaci ukazuju i na djelotvornost primjene postupaka difuzijskog prevlačenja karbidnim slojem, posebice postupkom vanadiranja, zbog velike kemijske i tribološke otpornosti vanadijeva karbida.

Ključne riječi: tlačni lijev, trošenje, test uranjanja, nitriranje, vanadiranje

Abstract: Mould parts for aluminium die casting are exposed to a complex wear mechanism and therefore their life is limited. A predominant wear mechanism is the reaction-melting of the mould part working surface, which results in frequent outages and increased mould maintenance costs. In order to extend the life of moulds for aluminium die casting, different procedures of modification and surface coating are applied. So far, the most commonly used procedure has been the salt bath nitriding (the TENIFER process), but data from literature point to the efficient application of diffusion carbide coating, particularly to vanadising due to high chemical and tribological resistance of vanadium carbide.

Key words: die casting, wear, immersion test, nitriding, vanadising

1. UVOD

Tlačni lijev vrlo je raširen proces koji se koristi za visoko serijsku proizvodnju preciznih odljevaka legura nižeg tališta. Zbog visoke cijene alata za lijevanje (kalupa) obično se upotrebljava za izradu odljevaka u velikim serijama od nekoliko tisuća do nekoliko milijuna komada, debljine stjenke od 0,5 do 15 mm. Legure za tlačni lijev se baziraju na aluminiju, magneziju i cinku.

Kalupi za tlačni lijev aluminijskih legura podvrgnuti su višim radnim temperaturama i mehaničkim opterećenjima u ciklusima od 15 do 80 sekundi. Izrađuju se od alatnih čelika za topli rad koji moraju biti otporni na različite mehanizme trošenja. U tijeku lijevanja na alat djeluje čitav niz kompleksnih mehanizama trošenja koji skraćuju njegov radni vijek, a dominantni mehanizam je reakcijsko nataljenje radne površine dijelova kalupa. Reakcijom između alata i aluminijske legure nastaje tvrda i krhka intermetalna faza koja prilikom izbacivanja odljevka iz kalupa puca i djelomično ostaje na dijelovima alata. Takova slijepljena područja mogu prouzročiti nastanak tragova na odljevku i spriječiti njegovo izbacivanje što dovodi do zastoja u proizvodnji. Primjenom odgovarajućih metoda modificiranja i prevlačenja površina moguće je značajno produljiti radni vijek ovih alata i time spriječiti skupe zastoje i obustavu proizvodnje.

Odluka o primjeni određenog postupka modificiranja i prevlačenja površina dijelova kalupa za tlačni lijev ovisi o nizu utjecajnih čimbenika i proizlazi iz razmatranja uvjeta i naprezanja kalupa tijekom rada. U industriji je do sada najčešće bio primjenjivan postupak toplinske obrade kaljenjem i modificiranja površine nitriranjem u solnoj kupci. No, zbog dobrih kemijskih i triboloških svojstava karbidnih slojeva ispitivat će se mogućnost primjene difuzijskog prevlačenja karbidnog sloja postupkom vanadiranja u svrhu produljenja vijeka trajanja pojedinih dijelova alata. Eksperimentalno su uspoređeni su postupci kaljenja, nitriranja u solnoj kupki (TENIFER) i prevlačenje površine vanadiranjem. Eksperiment je proveden na uzorcima od alatnog čelika za topli rad UTOP Mo1 (Č4751) koji su uranjani u rastaljenu aluminijsku leguru za tlačni lijev.

2. TLAČNI LIJEV

Izraz "tlačni lijev " obično znači lijevanje pod visokim tlakom. To je proces u kojem se talina tlači u metalni kalup i tlak se održava sve dok se skrućivanje potpuno ne završi. Proizvod je odljevak na kojem se mogu reproducirati i najfiniji detalji unutrašnjeg oblika kalupa, a postiže se i visok stupanj točnosti odljevka. Tlačnim lijevom mogu se lijevati slitine s rasponom temperatura lijevanja od 100°C do 900°C. Ima uspješnih pokušaja lijevanja i slitina na bazi željeza. Za legure s niskim talištem (oko 420°C) upotrebljavaju se toplo komorni tlačni strojevi s metalnom pumpom potopljenom u talinu. Toplo komorni strojevi nisu primjenjivi za lijevanje slitina na bazi aluminija i bakra zbog jake toplinske erozije kojom slitina djeluje na željezo. Slitine magnezija premda s visokim talištem (oko 650°C) zbog kemijske pasivnosti prema željezu mogu se lijevati s toplom komorom, ali se ipak se najveći dio odljevaka na bazi magnezija proizvodi na strojevima s hladnom komorom. Tlačni postupak izrade odljevaka omogućuje dobivanje dovoljno glatke površine i primjenjiv je za velik broj slitina, a omogućuje postizanje dobrih mehaničkih svojstava odljevaka. Mogu se lijevati odljevci mase od dijela grama do više od 40 kg. Tlačni lijev ekonomičan je tek za velike serije odljevaka jer su instalirano postrojenje, izrada alata i usvajanje proizvodnje u usporedbi s klasičnim pješčanim lijevom vrlo skupi i zahtijevaju visok stupanj stručnog znanja [1].

2.1 Princip rada i faze tlačnog lijeva aluminija

U peć za taljenje tali se legura aluminija u bloku i povrat iz proizvodnje (škart, preljevci, uljevni kanali) u približno jednakom omjeru. U pećima se legura tali i zagrijava do temperature od 730°C - 760°C. Transport taline vrši se u transportnim loncima do peći za poček koje se nalaze uz svaki stroj. Za to vrijeme temperatura taline padne na oko 700°C. Temperatura taline u peći za poček se održava od 670°C do 690°C.

Kod suvremenih hladno komornih horizontalnih strojeva za tlačni lijev proces lijevanja se odvija u nekoliko faza. Kao što je prikazano na slici 1.

- 1. faza: prenošenje taljevine ljevačkom žlicom i ulijevanje u tlačni cilindar,
- 2. faza: popunjavanje uljevnih kanala i dovođenje taljevine do ušća u kalup,
- 3. faza: popunjavanje kalupne šupljine i podizanje tlaka do potpunog skrućivanja odljevka,
- 4. faza: otvaranje kalupa i izbacivanje odljevka,
- 5. faza: hlađenje kalupa i špricanje vodotopivim premazom.

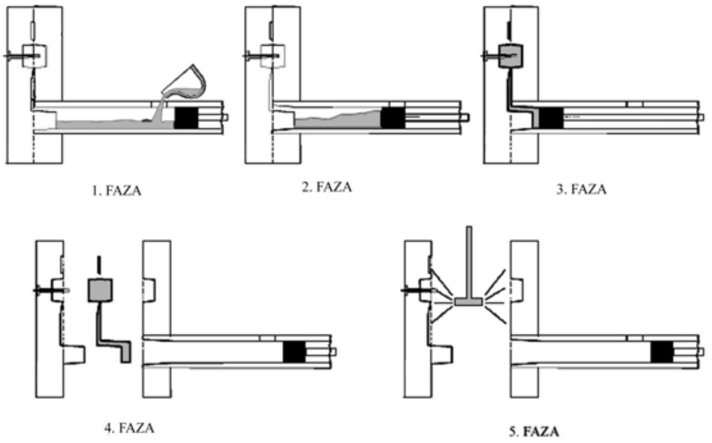

Slika 1: Faze procesa tlačnog lijeva [2]

Da bi se osigurala brzina skrućivanja odljevka kalup se prisilno hladi (vodom ili uljima). Nakon skrućivanja kalup se otvara i odljevak se pomoću izbacivača odvaja od kalupa i vadi (ručno ili manipulatorima). Trajanje ljevačkog ciklusa može iznositi od 3-90 s i ovisi o veličini odljevaka. Kalup se na početku svakog ciklusa šprica vodotopivim premazom.

2.2 Materijali kalupa za tlačni lijev

Alatni čelici za rad u toplom stanju namijenjeni su za izradbu alata koji se u radu zagrijavaju na temperature iznad 200ºC. Za vrijeme eksploatacije kalupi za tlačni lijev su izloženi brojnim toplinskim i mehaničkim utjecajima koji smanjuju vijek trajanja alata i dovode do skupih zastoja i popravaka. Tlačni lijev se uglavnom primjenjuje u velikoserijskoj proizvodnji pa kalupi moraju biti u stanju izdržati i do 150 000 ciklusa.

Neki od čimbenika kojima su kalupi izloženi za vrijeme eksploatacije su:

- visoki radni tlakovi taline u kalupu (do 700 bara),
- toplinski šokovi zbog velike razlike u temperaturi između površine (koja se trenutno zagrije na temperaturu ljevačke legure) i unutrašnjosti kalupa. Alati se još dodatno hlade vodom što pridonosi toplinskim šokovima,
- površina alata se prije ulijevanja dodatno šprica vodotopivim premazima koji imaju temperaturu 10-20ºC (ovisno o uvjetima okoliša) što uzrokuje dodatno ohlađivanje površine kalupa,
- visoka radna temperatura (najmanje 190ºC, najviše 650ºC, a na pojedinim dijelovima kalupa u trenutku ulijevanja zbog trenja i tlakova ubrizgavanja legure i do 1200ºC),

- abrazivno djelovanje taline zbog sadržaja neotopljenih konstituanata Si ili već polu skrutnutog tjestastog stanja Al legure,
- adhezija koja se javlja zbog procesa zavarivanja krutih faza materijala kalupa i legure (stvaraju se intermetalni spojevi) što dovodi do odnošenja čestica kalupa s površine ili stvaranju nataljenog sloja na površini kalupa,
- toplinski umor površine i pojava mreže pukotina koji utječu na izgled odljevka ili dovode do zaglavljenja odljevka u kalupu,
- kalupi se prije pokretanja proizvodnje griju plamenicima kako bi se doveli na početnu radnu temperaturu, pa moraju biti vatrootporni,
- zbog stalne izloženosti visokim temperaturama alatni materijali moraju bit otporni na oksidaciju (tribokoroziju),
- kalupi moraju osigurati i postojanost dimenzija zbog naglih toplinskih promjena.

Zbog prije navedenog materijal za izradu kalupa za tlačni lijev mora zadovoljiti slijedeće zahtjeve [3,4,5]:

1. visok stupanj homogenosti i sposobnost poliranja,
2. sposobnost za kovanje i mehaničku obradbu,
3. neosjetljivost prema ogrebotinama i minimalno mijenjanje dimenzija pri toplinskoj obradbi,
4. otpornost prema toplinskim šokovima,
5. otpornost prema reakcijskom nataljenju i trošenju,
6. otpornost prema kemijskim i fizikalnim utjecajima mlaza taline,
7. otpornost na oksidaciju pri povišenim temperaturama (tribokorozija),
8. otpornost na popuštanje pri visokim radnim temperaturama,
9. malu promjena dimenzija pri toplinskoj obradbi.

2.2.1 Alatni čelici za topli rad

Ova skupina čelika se koristi za izradu kalupa za tlačni lijev i spada u visokolegirane alatne čelike s udjelom legirnih elemenata >5%. Legirni elementi imaju velik utjecaj na svojstvo alatnog čelika pa prilikom izbora čelika treba voditi računa o toplinskim i mehaničkim utjecajima kojima su dijelovi kalupa izloženi za vrijeme rada. Karbidotvorci W, Mo, V, Cr povisuju otpornost na trošenje i popuštanje. V ima utjecaja na povišenje tvrdoće u toplom stanju, a Mo, Cr i Ni povisuju prokaljivost čelika. Co povećava otpornost na popuštanje jer usporava difuziju C iz martenzitne rešetke prilikom povišenja temperature. Ni povisuje žilavost i prokaljivost, a Si i Cr pogoduju otpornosti na oksidaciju pri povišenim temperaturama. Zbog nižeg udjela C ovi čelici imaju dobru žilavost i otpornost na toplinski umor. Pri izboru odgovarajućeg alatnog čelika potrebno je voditi računa o toplinskoj vodljivosti čelika ako se kalup dodatno hladi vodom jer se toplinska vodljivost snižava povišenjem udjela legirnih elemenata. Iati koji se hlade vodom trebaju biti napravljeni od Cr-Mo-V čelika, jer su oni otporniji na toplinski umor i promjenu oblika, a imaju visoku žilavost pri povišenim temperaturama.

Svojstva koja mora imati čelik za izradu kalupa za tlačni lijev su slijedeća:

- minimalni pad tvrdoće pri povišenim temperaturama,
- visoka otpornost na pucanje u toplom stanju (toplinski umor),
- mogućnost redukcije zaostalih naprezanja,
- otpornost na stvaranje reakcijskog nataljenja,
- otpornost na tribološke mehanizme (korozija, abrazija, oksidacija, erozija).

Tablica I daje pregled čelika za izradu kalupa za tlačni lijev s usporednim inozemnim oznakama te prosječnim kemijskim sastavom.

Tablica I. Preporuka za izbor čelika za izradu alata za tlačni lijev [3,4,6]

Oznaka prema DIN 17006	Oznaka prema HRN	Oznaka prema AISI	Sastav u %							
			C	Si	Mn	Cr	Ni	W	Mo	V
X38CrMoV51	Č4751 Utop Mo1	H11	0,38	1,0	0,4	5,0	-	-	1,3	0,3
X40CrMoV53	Č4753 Utop Mo2	H13	0,4	1,0	0,4	5,0	-	-	1,3	1,0
X32CrMoV33	Č9750 Utop Co2	~H10	0,32	0,3	0,3	2,8	-	-	2,8	0,5
X30WCrV41	Č6450 Utop 1	-	0,3	1,0	-	1,0	-	4,0	-	0,4
X30WCrV93	Č6451 Utop 2	H20/H21	0,3	0,25	0,3	2,85	-	9,0	-	0,4
X30CrMoW51	Č4752 Utop 3	-	0,37	0,9	0,6	4,8	-	1,4	1,5	0,2
56NiCrMoV7	Č5742 Utop ex.2	-	0,55	-	-	1,1	1,7	-	0,5	0,1

3. MEHANIZMI I INTENZITET TROŠENJA KALUPA ZA TLAČNI LIJEV

Glavnih uzroci skraćenja vijeka trajanja alata i skupih zastoja su reakcijsko nataljenje i toplinski umor površine, pa se ovim problemima pridaje veliki značaj. Cijena izrade alata u odnosu na troškove prouzročene zastojima proizvodnje i transportom alata vezanim uz popravak je relativno mala i iznosi 10% ukupnih troškova proizvodnje. Dodatne troškove proizvodnje povećava vrijeme koje se troši na zamjenu ili popravak alata. Produljenje vijeka alata je jedan od glavnih ciljeva u industriji tlačnog lijeva. Trošenje je postupni gubitak materijala s površine krutog tijela uslijed dinamičkog dodira s drugim krutim tijelom, fluidom i/ili česticama. Mehanizmi trošenja mogu se pojaviti pojedinačno ili kombinirano, a glavni mehanizmi trošenja koji utječu na vijek trajanja alata su:

- nataljenje, koje dijelimo na:
    - reakcijsko nataljenje,
    - nataljenje bez reakcije (mehaničko nataljenje),
- toplinski umor površine,
- trošenje erozijom taline (toplinska erozija),
- abrazija,
- adhezija,
- tribokorozija (oksidacija pri visokoj temperaturi),
- kavitacija.

3.1 Reakcijsko nataljenja

Jedan od značajnijih uzročnika grešaka u procesu tlačnog lijeva aluminija je nataljenje (adhezija) taline na dijelove kalupa. Ovaj fenomen se naziva reakcijsko nataljenje i lako može prouzročiti zastoj i povećanje troškova proizvodnje, a ujedno skraćuje vijeka trajanja alata. Javlja se kada rastaljena legura kemijski reagira s materijalom alata. Princip reakcijskog nataljenja moguće je objasniti afinitetom željeza i aluminija jer su oni kompatibilan tribološki par s velikom topljivosti u krutom stanju. Atomi željeza difundiraju iz površine alata, a atomi aluminija difundiraju u površinu i njihovom reakcijom dolazi do stvaranja intermetalnih faza. Reakcijsko nataljenje izgledom je isto kao i mehaničko nataljenja ali ga je puno teže odstraniti, a da se ne ošteti površina dijela alata. To je ozbiljan problem a uzrokuju ga brojni čimbenici kao što su:

- sastav aluminijske legure,
- brzina i mjesto ulaza taline,
- premazi i njihovo prianjanje,
- efekt različitih prevlaka koje su primijenjene.

Reakcijskim nataljenjem najviše stradavaju:

- ušća zbog povećanja temperature i brzine strujanja taline (veće od 50m/s),
- jezgrice zbog slabog odvođenja topline,
- klizni elementi,
- razni umetci malih dimenzija,
- izbacivači,
- površine alata na koje direktno udara mlaz taline.

Reakcijsko nataljenje također uzrokuje povećanje trenja koje ima utjecaja na silu izbacivanja odljevka (iz alata). Povećanje sile izbacivanja može prouzročiti:

- savijanje izbacivača,
- pojavu tragova na površini odljevka uslijed izvlačenja,
- deformaciju odljevka,
- promjene dimenzija odljevka.

Također je vrlo važno da se premaz koji se šprica po površini kalupa prije svakog ciklusa zadrži na površini. On stvara zaštitni sloj između površine alata i rastaljene ljevačke legure sprječavajući njezino naljepljivanje na površinu kalupa, a ujedno smanjuje silu izbacivanja odljevka. Karakteristično obilježje reakcijskog nataljenja je pojava srebrnih (aluminiziranih) područja na površini alata. Reakcijsko nataljenje s pojavom intermetalnih faza javlja se zbog reakcija u krutom stanju između ljevačke legure i alatnog čelika za vrijeme ljevačkih ciklusa. Između alatnog čelika i legure formiraju se različite intermetalne faze (Al-Fe-Si, Al-Fe i Al-Cu), a najčešća intermetalna faza je Al-Fe-Si faza kao što je prikazano na slici 2.

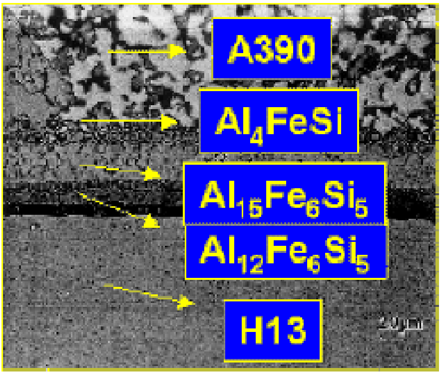

Slika 2: Prikaz različitih intermetalnih faza na presjeku čelika H13 (Č4753) [7]

Primjer nataljenog sloja na površini alata prikazan je na slici 3. na kojoj se može vidjeti da je došlo do istrošenja dijela jezgre gdje je stvoreno reakcijsko nataljenje. Ovaj dio jezgre na kojem se nalazi nataljeni sloj uležišten je u drugoj jezgri i nije dovoljno zahvaćen premazom, a zbog zračnosti dolazi i do zadržavanja aluminijske legure. Nedostatak premaza, povišena temperatura i zadržavanje legure uz površinu jezgre pogoduju stvaranju intermetalnih spojeva.

Slika 3: Reakcijsko nataljenje na jezgri alata za tlačni lijev aluminijskih radijatora s vidljivim istrošenjem površine reakcijskim nataljenjem

4.2 Toplinski umor površine

Alatni materijal je uslijed zagrijavanja i hlađenja (u toku radnog ciklusa) izložen visokim cikličkim promjenama temperature i toplinskim šokovima što uzrokuje toplinski umor materijala. Toplinski umor materijala odražava se nastankom mreža pukotina na površini alata koje dodatno pospješuju mehaničke vidove trošenja. Tokom rada povećava se broj pukotina i njihova dubina, pa alat nakon određenog vremena postaje neupotrebljiv za daljnju proizvodnju jer:

- se odljevak teško izbacuje iz alata, te se deformira ili puca,
- više ne zadovoljava kvaliteta površine odljevka.

Nakon određenog broja ciklusa lijevanja nastale pukotine se sve više šire nakon čega dolazi do odlamanja dijelova kalupa. Na slici 4. prikazan je izgled dotrajale površine dijela kalupa za izradu radijatora na kojem se vide pukotine nastale uslijed toplinskog umora materijala.

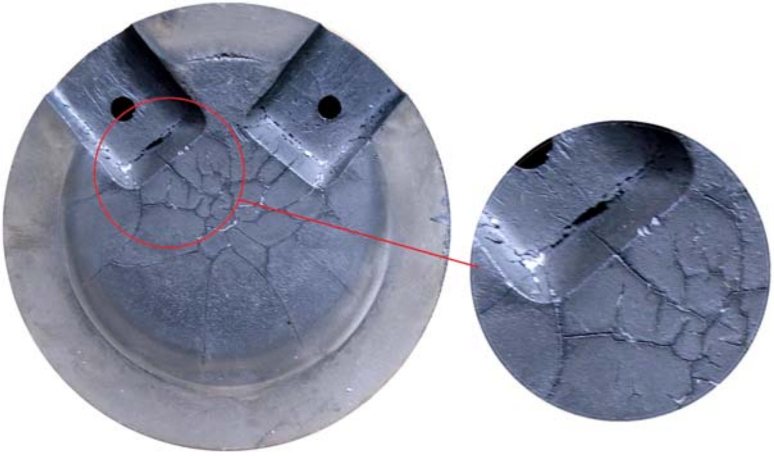

Slika 4:Toplinski umor površine na dijelu kalupa za izradu radijatora

Toplinski umor materijala najčešće se javlja:

- na područjima promjena debljine presjeka,
- na mjestima gdje su zaobljeni prijelazi,
- oko provrta gdje se nalaze izbacivači jer su takova mjesta značajni koncentratori naprezanja,
- na ušćima jer zbog suženja dolazi do povećanja brzine i temperature taline,
- na uljevnim kanalima zbog velike mase i visoke temperature taline.

Uzrok ovome mehanizmu oštećenja su napetosti koje se javljaju na radnoj površini zbog temperaturnih razlika između površine i unutrašnjosti alata. Temperatura površine kalupa gotovo trenutno postigne maksimalni iznos od 650ºC, a na pojedinim dijelovima kalupa u trenutku ulijevanja zbog trenja i tlakova ubrizgavanja temperatura površine naraste i do 1200ºC. Nakon ubrizgavanja taljevine odljevak se počinje hladiti preko radne površine, ali je sad odvođenje topline puno sporije od zagrijavanja. Skrutnuti odljevak se vadi iz kalupa i proces se ponavlja. Prije svakog ciklusa ulijevanja, temperatura površine se dodatno snižava prilikom špricanja vodo topivim premazom temperature 10-20ºC.

4.3 Trošenje alata erozijom taline

Erozija česticama je gubitak materijala s površine krutog tijela zbog relativnog gibanja (strujanja) fluida u kojem se nalaze krute čestice [8]. Erozija talinom pojavljuje se u prvoj fazi lijevanja zbog prisutnosti onečišćenja i neotopljenih konstituenata. Trajanja udaraca su općenito vrlo kratka pa se u površinu kalupa unose intenzivni i vrlo oštri tlačni udarci koji kod tvrdih metala stvaraju kružne pukotine, a kod žilavih materijala nastaje udubljenje površine uslijed plastične deformacije. Strujanje taline pod visokim tlakom preko deformirane zone uzrokuje jaka smična naprezanja i deformacije površinskih slojeva gravure kalupa. Uzastopnim ponavljanjem ovakvih deformacija dolazi do oštećenja umorom površine koje rezultira pittingom i ohrapljivanjem površine kalupa. Tvrda zrnaca nečistoća i uključaka dovode do dodatnog abrazivnog trošenja kombinacijom mehanizama odrezivanja, dubljenja, otkidanja i brazdanja. Erozija kod koje je strujanje pod malim kute u odnosu na površinu naziva se abrazivna erozija, a kad čestice udaraju površinu gotovo okomito to je udarna erozija [9]. Kod erozijskog trošenja dolazi do odnošenja površinskog sloja materijala zbog upadnog kuta taline. Veličina upadnog kuta mlaza i ulazna brzina rastaljenog materijala direktno utječu na erozijsko trošenje. Konstrukcija uljevnog sustava ima važnu ulogu prilikom smanjenja erozije talinom. Pravilnim oblikovanjem uljevnog sustava može se smanjiti upadni kut taline i time smanjiti erozijsko trošenje kalupa. Najveća erozija se javlja kod kutova upada taline na jezgre i umetke koji su između 70º i 90º. Ustanovljeno je da se erozijsko trošenje bitno smanjuje ako se površinski sloj (nitridni i karbonitridni) uspije očuvati kompaktnim tijekom radnog ciklusa jer se time izbjegava direktni kontakt taline s površinom osnovnog materijala kalupa. Erozijsko trošenje kalupa u aluminijskim talinama puno je intenzivnije nego trošenje talinama drugih obojenih metala, što se može vidjeti na slici 5.

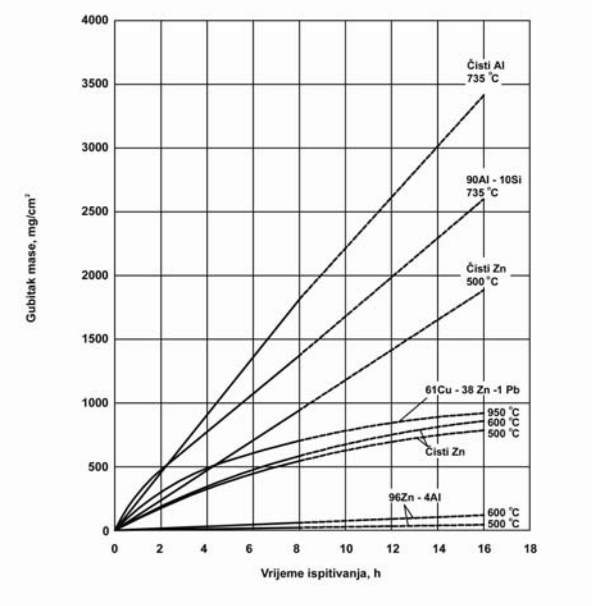

Slika 5. Erozijsko trošenje meko žarenog alatnog čelika za topli rad Č4753 (Utop Mo2) različitim talinama [9]

5. EKSPERIMENTALNI DIO

Za provođenje pokusa testa uranjanja korištena je peć za taljenje aluminija s dograđenom napravom za rotaciju uzoraka kao što je prikazano na slici 6. Test uranjanja proveden je uz rotaciju uzoraka pomoću bušilice s brojem okretaja n=2880 o/min. Temperatura taline za vrijeme testa uranjanja održavana je na 680±2ºC. Svi uzorci prije testa uranjanja bili su predgrijani na 200ºC, jer je temperatura kalupa za tlačni lijev prije svakog ciklusa ulijevanja između 190 i 250ºC, čime su simulirani uvjeti rada kalupa za tlačni lijev aluminijskih legura. Nakon završetka testa uranjanja uzorci su ohlađivani na zraku do sobne temperature. U tablici II navedene provedene toplinske obrade, oznake uzoraka i vremena trajanja uranjanja.

Slika 6: Peć s napravom za provođenje testa uranjanja

Tablica II. Pregled stanja, oznaka i trajanja uranjanja ispitivanih uzoraka

Stanje	Oznaka uzorka	Trajanje uranjanja [min]		
Kaljeno + popušteno	V8	1	4	16
	V9			
	V10			
Nitrirano TENIFER	N4	1	4	16
	N5			
	N10			
Vanadirano	V3	1	4	16
	V5			
	V7			

5.1 ANALIZA UZORAKA NAKON PROVEDENOG TESTA URANJANJA

Nakon provedenog testa uranjanja na uzorcima je ostao sloj aluminijske legure. Uzorci su zatim očišćeni pomoću otopine kositrenog klorida. Ova otopina kemijski odstranjuje leguru aluminija bez utjecaja na modificirani alatni čelik i nastale intermetalne faze između čelika i aluminija. Otopina je napravljena otapanjem 100g hidratiziranog kositar(II)klorida u 50 ml tople solne kiseline (HCl). Ova otopina je zatim razrijeđena sa 100 ml destilirane vode i dodan je 1g metalnog kositra. Nakon toga otopina je opet razrijeđena s destiliranom vodom u omjeru 1:9. Prilikom uranjanja uzoraka u otopinu dolazi do kemijske reakcije s aluminijskom legurom i na površini uzoraka nastane spužvasti talog koji se lako odstrani s mekanom četkicom, što je vidljivo na slici 7. Uranjanje u ovu otopinu ponavljano je dok reakcije otopine i aluminija nisu prestale i dok sav aluminij nije odstranjen s površine.

Slika 7: Uzorci uronjeni u otopinu za skidanje aluminijske legure s ispitivanih uzoraka

5.2 Metalografska analiza uzoraka

Nakon metalografske pripreme uzoraka provedena je analiza uzoraka koji su bili nitrirani (N10) i vanadirani (V7) a koji su bili uronjeni u aluminijsku leguru najduže trajanje testa uranjanja (16 minuta). Na slici 8. vidljivo je da je uzorak koji je bio kaljen + popušten a koji je bio u talini 16 minuta (V10) vrlo uništen pa na njemu nisu provedena metalografska ispitivanja. Metalografska pripreme se sastojala od rezanja, zalijevanja u masu, brušenja i poliranja te nagrizanja u otopinom s 3% HNO_3 razrijeđenoj u etilnom alkoholu (NITAL). Mikrostruktura slojeva snimljena je na optičkom mikroskopu OLYMPUS BH-2. Kod nitriranog uzorka korišteno je povećanje od 200:1 i 500:1 a što je prikazano na slici 8., dok su kod vanadiranog uzorka korištena samo povećanja od 500:1 i 1000:1 a mikrostruktura je prikazana na slici 9., jer je vanadirani sloj relativno tanak (oko 5μm).

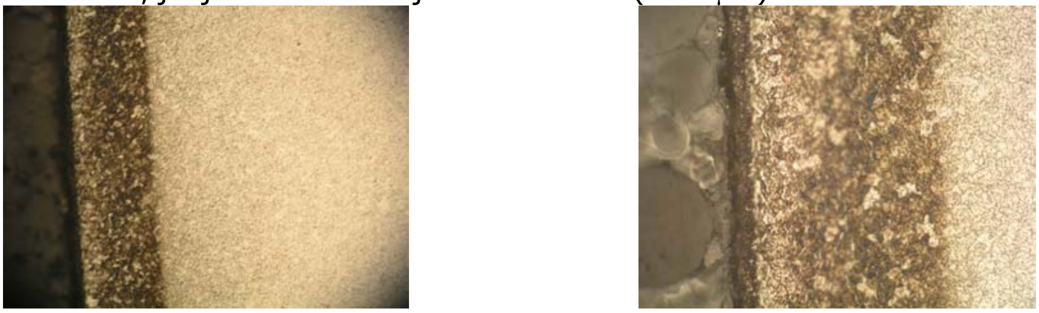

200:1 500:1

Slika 8: Mikrostruktura nitriranog uzorka nakon testa uranja u trajanju od 16 min., nagriženo u NITALU

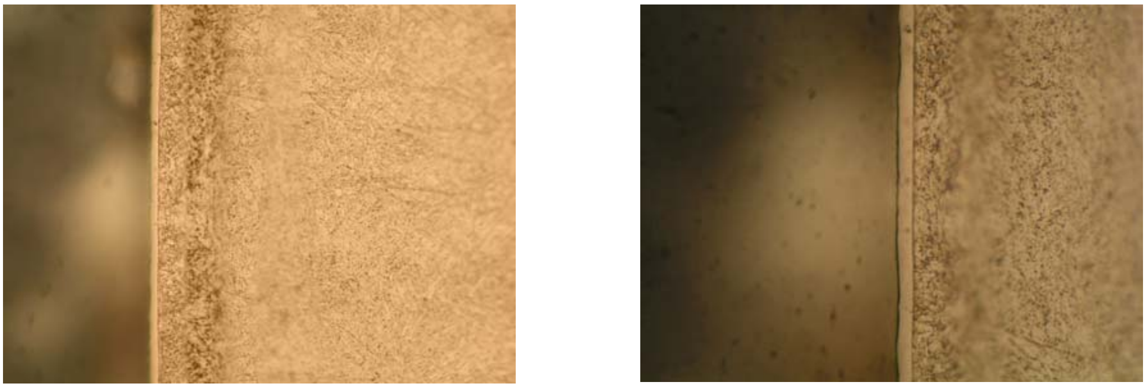

500:1 1000:1

Slika 9: Mikrostruktura vanadiranog uzorka nakon testa uranja u trajanju od 16 min., nagriženo u NITALU

Također su provedena metalografska ispitivanja primjenom elektronskog mikroskopa TESCA VEGA TS 5136 MM u Laboratoriju za materijalografiju, Fakulteta strojarstva i brodogradnje u Zagrebu. Mikrostruktura poprečnog presjeka nitriranog uzorka s parametrima ispitivanja koji je bio uronjen u rastaljenu aluminijsku leguru 16 minuta prikazan je na slikama 10. Debljina zone spojeva nitriranog sloja izmjerena je i iznosi 15 μm. Na slici 11. prikazana je mikrostruktura poprečnog presjeka vanadiranog uzorka koje su snimljene pomoću elektronskog mikroskopa uz povećanje 2000:1 i 5000:1. Izmjerena debljina vanadiranog sloja iznosila je 5 μm.

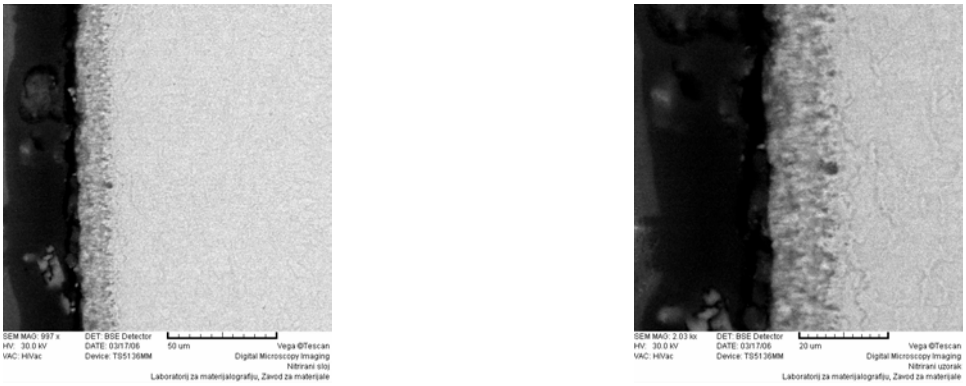

1000:1 2000:1

Slika 10: Mikrostruktura nitriranog uzorka nakon testa uranja u trajanju od 16 min., nagriženo u NITALU

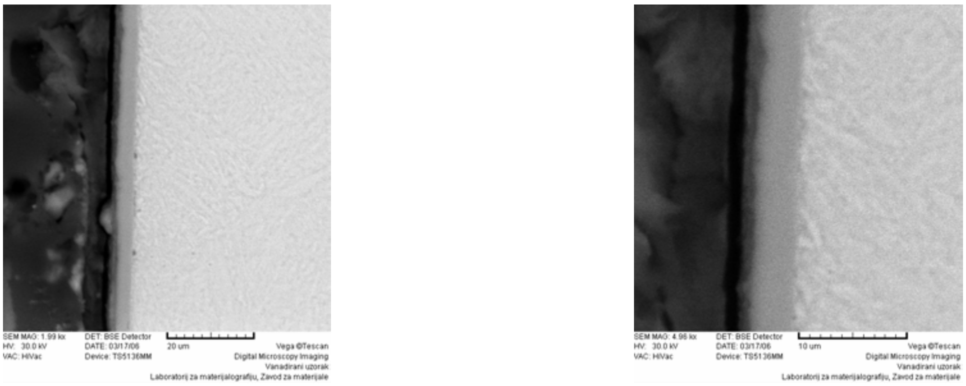

2000:1 5000:1

Slika 11: Mikrostruktura vanadiranog uzorka nakon testa uranja u trajanju od 16 min., nagriženo u NITAL

6. ZAKLJUČAK

U ovom radu su istraživani utjecaji rastaljene aluminijske legure na alatni čelik koji se upotrebljava za izradu kalupa za tlačni lijev aluminijskih legura. Test uranjanja proveden je simulacijom u Laboratoriju za ljevarstvo. Ispitivano je 9 uzoraka od alatnog čelika Č4751 (Utop Mo1), 3 uzorka za svaki postupak toplinske obradbe: kaljenje + popuštanje, nitriranje postupkom TENIFER i vanadiranje u solnoj kupki. Realni uvjeti lijevanja u tlačnom stroju simulirani su u laboratorijskim uvjetima. Ispitivani uzorci uranjani su uz rotaciju u rastaljenu aluminijsku leguru za tlačni lijev kvalitete GD AlSi12Cu2. Rotacijom uzoraka simulirano je nastrujavanje taline na površinu kalupa. Kaljeni + popušteni uzorci su imali najoštećeniju površinu (slika 8). Najbolji rezultat dobiven je kod uzoraka koji su bili obrađeni postupkom TENIFER. Na slici 9. vidi se stanje uzorka (N10) nakon 16 minuta trajanja uranjanja. Vanadirani uzorci (V5 i V7) su nakon testa uranjanja imali oštećenje samo na donjem dijelu (svega nekoliko milimetara od ruba) za koji se pretpostavlja da je oštećen zbog loše nanesenog sloja vanadijevog karbida jer su uzorci prilikom vanadiranja bili položeni na dno kupke. Preostali dio uzorka bio je bez tragova nataljenja na površini i nakon maksimalnog trajanja uranjanja u ovom testu što upućuje na to da je potrebno nastaviti istraživanje ovog postupka toplinske obradbe.

Također na slici 14., povećanje 2000:1 i 5000:1 na površini uzorka vidljiv je tanki sloj (oko 2 μm) kojeg bi uz pomoć mikro analize bilo potrebno kvantificirati.

LITERATURA

1. Grupa autora: "Ljevački priručnik", Savez ljevača Hrvatske, Zagreb 1985 .
2. Fraser Darren T.: "Soldering in High Pressure Die Casting and its Prevention by Lubricant and Oxide Layers", The University of Queensland, Australija, September 2000.
3. Katavić I.: "Ljevarstvo", Sveučilište u Rijeci, Tehnički fakultet Rijeka, Rijeka, 1993.
4. Novosel M., Cajner F.,. Krumes D: "Alatni materijali", Slavoski Brod 1996.
5. Borštner J., Letonja A., Rodić J., Černe F.: "Alatni čelici", Metabiro, Zagreb 1963.
6. Naši čelici, Železarna Ravne na Koroškem, 1982.
7. www.badgermetal.com
8. Ivušić V.: "Tribologija", Sveučilište u Zagrebu, Fakultet strojarstva i brodogranje, Zagreb, 1998.
9. Breljak I., Diplomski rad, Fakultet strojarstva i brodogradnje, Zagreb 1999.

Consolidation of Al-based particles by Equal Channel Angular Extrusion (ECAE)

J, Nagy, F, Simančík, M, Balog, K, Iždinský

Institute of Materials and Machine Mechanics, SAS, Bratislava, Slovakia

Abstract

Consolidation of Al-based particles using Equal Channel Angular Extrusion (ECAE) method as an alternative to conventionally used hot direct extrusion (DE) is presented. Two different materials were used in this study; $Al_{94}Fe_2V_4$ melt-spun ribbons (MSR) and ultra-fine 1 µm Al 99,7% powder respectively. Both are expected for structural applications requiring high strength, ductility and thermal stability at elevated temperatures above 200°C [1]. Since they cannot be consolidated at temperatures above 450°C in order to maintain optimum structure, their compaction requires high pressures often exceeding the tool limits. The experiments have shown that the pressure during ECAE of both materials was ~6 times lower if compared with pressures needed in DE at relatively low extrusion ratio of 10:1 at the same temperatures. Microhardness and density of compacts were improved after ECAE consolidation and the effect was enhanced by multiple pressing. Microstructure analyzes showed good metallurgical bonding between particles even after one ECAE pass.

1. Introduction

The extremely high tensile strengths exceeding 1 GPa accompanied with good ductility and thermal stability are expected from rapidly solidified (RS) Al-based alloys that microstructure consist of amorphous, nanocrystalline and quasicrystalline phases. However, due to limited heat flow during rapid quenching, such fine or aperiodic phases can be obtained only in thin ribbons or fine powder particles. Since the practical application of discrete particles is limited, their synthesis into bulk materials is inevitable, whereas sufficient shear deformation is required to assure sound metallic bonds. For this purpose hot extrusion is frequently used. However, the resistance against deformation of high strength materials induces extreme extrusion pressures at moderate temperatures often overtaking the limits of conventional tools [2]. Decreasing of this resistance by temperature increase is not possible in case of RS materials, since their unique structure could be ultimately destroyed. Therefore an alternative consolidation technique assuring sufficient amount of shear deformation at lower temperatures while reducing extraordinary loading of tool materials was explored. The influence of consolidation temperature, processing route and pre-compaction method was studied.

2. Experimental

The master alloy with a nominal composition of $Al_{94}Fe_2V_4$ (at. %) was prepared in vacuum induction furnace from pure elements. Rapidly solidified ribbons with a cross section of 0,02 mm x 10 mm were prepared by planar flow casting (quenching rate ~10^6 °C.s^{-1}). As-received ribbons were cryomilled and sieved into 63-125 µm particle size fractions. 1 µm Al powder (x_{50}=1,31 µm, x_{10}=0,66 µm, x_{90}=2,51 µm from Helos analyse) of technical purity 99.7 % was prepared by gas atomization (N_2 atmosphere). These were later pre-compacted using either Cold Isostatic Pressing (CIP) method or using hot direct extrusion (DE). Extrudants from Al94Fe2V4 MSR with dimensions ø10 mm x 70 mm were prepared at extrusion ratio (ER) 4:1 using flat face at extrusion temperature 450°C. The ram speed was 1,2 mm,s^{-1}. CIP pre-compacts were at first vacuumed and pressed at 200 MPa (1 µm Al powder) and 1 GPa ($Al_{94}Fe_2V_4$ MSR), respectively. Cylinders ø10 x 70 mm in dimensions were machined from CIPed green bodies. ECAE die is schematically illustrated in Fig. 1. Die consisted of two rectangular channels 12 x 12 mm in cross-section intersecting in 90° with sharp outer corner.

Cu containers with outer dimensions of 12x12x90 mm with a hole 10 mm in diameter and 70 mm in length drilled inside were used. Pre-compacted material was put into the hole and ECAE pressed at temperatures 450°C ($Al_{94}Fe_2V_4$ MSR) and 200, 250, 300, 350˚C (Al powder) respectively. Consolidation was performed by one ECAE pass and alternatively by four passes by so-called Bc route when sample is rotated by 90˚ clockwise after each pass. Measurements of density were performed in terms of Archimedes method. Mechanical properties were studied in terms of HV microhardness measurements using 10 p loading. The microstructure was characterized by light and transmission electron microscopy (TEM) using the JEOL JEM 100 C electron microscope operated at 100 kV. TEM samples were thinned electrolytically in a solution of 10 % perchloric acid, 10 % ethyleneglycol and 80 % ethanol by volume at – 50 °C.

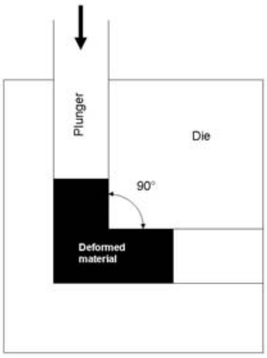

Fig. 1 Schematic illustration of ECAE die

3. Results and discussion

3.1 Experimental materials

Fig. 2 shows TEM micrographs of 1 μm Al 99,7% powder a) and $Al_{94}Fe_2V_4$ b) melt-spun ribbons in as-received state. Rounded shaped grains of Al powder are monocrystalline and no distinctive dislocations were observed. Microstructure of $Al_{94}Fe_2V_4$ MSR in as-received state is predominantly formed by α-Al grains and randomly oriented spherical icosahedral particles with diameters mostly not exceeding 100 nm. Moreover amorphous and fcc $Al_{10}V$ intermetallic phases are also present in the microstructure. Microhardness of as-received MSR was HV 275. Annealing at 100˚C resulted in increase of HV value but further increase of annealing temperature up to 500˚C caused gradual decrease of HV values below those measured on as-received MSR [2]. This was caused by transformation of high-strength metastable icosahedral phase into stable intermetallic phase and by coarsening of intermetallics.

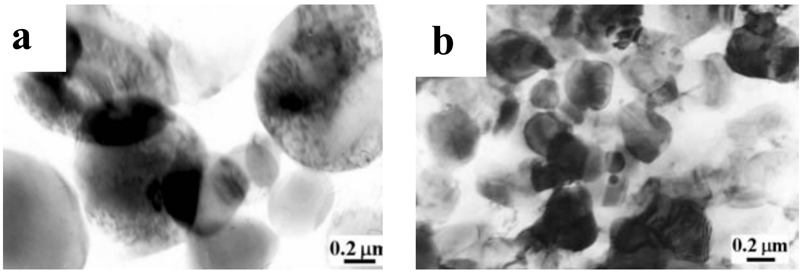

Fig. 2 TEM micrographs of 1 μm Al 99,7% powder a) and $Al_{94}Fe_2V_4$ melt-spun ribbon in as-received state b)

3.2 Consolidation

ECAE consolidation of isostatically pre-compacted (CIP) MSR was not successful. Although some places with good consolidated MSR particles were found, specimen was disintegrated and large macroscopic voids and cracks were observed. Therefore only pre-extruded MSR particles were subjected to ECAE. However in case of Al powder CIP pre-compaction was useful. Breakthrough pressures of 220 MPa for Al powder and 245 MPa for MSR were recorded during ECAE process. These values are far lower in comparison to DE with extrusion ratio 10:1 at the same temperatures where pressures achieved ~1400 MPa in case of both materials. This is presumably caused by the fact that normal stresses during ECAE are significantly reduced in contrary to DE. Tab. 1 represents the dependency of breakthrough pressure on temperature during ECAE of Al powder. As expected the highest pressure of 830 MPa was recorded during ECAE process at the lowest temperature of 200˚C. Increasing of consolidation temperature resulted in progressive decreasing of pressure up to 220 MPa at 350˚C. This is due to decrease of flow resistance of deformed material as the temperature increases.

Temperature [°C]	**200**	**250**	**300**	**350**
Pressure [MPa]	830	480	380	220

Tab. 1 Breakthrough pressures during consolidation of 1 μm Al powder via ECAE at different temperatures

Fig. 3 illustrates longitudinal cross-section of $Al_{94}Fe_2V_4$ MSR filled in Cu container subjected to 1 ECAE pass. In ideal case when friction is not considered shear would produce shear bands inclined by 45˚ [3]. In reality friction plays significant role resulting in faster flow of the top part of the specimen and much slower flow of bottom part due to enhanced friction between bottom surface of the die and the specimen. This situation is clearly seen in the front part of the specimen when the angle is about 30-35˚. The same trend was observed on Al powder compacts.

Fig. 3 Longitudinal cross-section of pre-extruded $Al_{94}Fe_2V_4$ MSR in Cu container subjected to 1 ECAE pass

3.3 Microstructure observations

TEM micrographs of Al powder after 1 ECAE pass performed at 200˚C is shown in Fig. 4 a). Microstructure consists of well-deformed grains elongated in the shear stress direction throughout the entire cross-section of the specimen. The oxides envelopes initially forming continuous cover of each grain are torn off and relatively homogeneously dispersed at grain boundaries enabling good metallic bonding between Al cores. A little finer microstructure was observed in case of consolidation at lower temperatures due to slightly higher deformation work during consolidation process. Very similar microstructure to that one achieved by ECAE of Al powder at 200 ˚C was achieved by DE at extrusion ratio 10:1 however at far higher temperature of 500˚C, Fig. 4 b). In case of multiple ECAE pressing grains became more equiaxed due to complexity of deformation mode provided by rotation of the sample. Good metallurgical bonding between particles was observed also in case of MSR however macrostructural texture was still visible as a consequence of DE pre-compaction. This trend was slightly suppressed by multiple ECAE pressing. Finer microstructure within MSR particles in comparison to as-received MSR was observed, Fig. 4 c) and d).

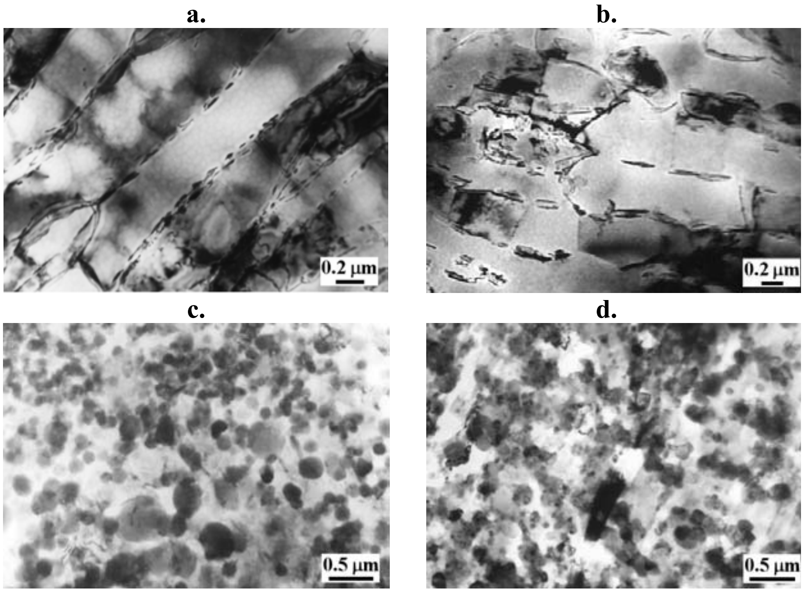

Fig. 4 TEM micrographs of Al powder processed by 1 ECAE pass at 200˚C a) and by extrusion with extrusion ratio 10:1 at 500˚C b), $Al_{94}Fe_2V_4$ MSR in as-received state c) and after 1 ECAE pass at 450˚C d)

3.4 Density measurements

The densities of Al powder compacts after 1 ECAE pressing were very close to theoretical density. Values were in the range of 2.65-2.67 g.cm^{-3} in dependence on consolidation temperature. As it was expected multiple pressing using route Bc resulted in increasing of density up to 2.7 g.cm^{-3}. Values of relative density of MSR compacts are summarized in Tab. 2 together with values of DE compacts prepared at extrusion ratio ER= 10:1. It is shown, that relative density of ECAE compacts increased by 2% and 2.4% in case of one and multiple ECAE passes, respectively, if compared to DE.

Consolidation method	**DE, ER 10:1**	**ECAE 1 pass**	**ECAE 4 passes, Bc**
Relative density [%]	89,8	91,8	92,4

Tab. 2 Relative density of Al powder compacts in dependence on consolidation method

3.5 Mechanical properties

The highest microhardness of HV 102.6 was observed on Al powder compact consolidated at the lowest temperature of 200°C. As the temperature increased the microhardness values gradually decreased up to HV 92.3 for compact consolidated at 350°C. This was caused by higher level of deformation work induced into the deformed material at lower temperature while improving the metallurgical bonding of single particles. 1 ECAE pressing of pre-compacted MSR resulted in improvement of microhardness by HV 12 and HV 7 in comparison to DE compacts prepared at ER 4:1 or ER 10:1, respectively (see Tab. 3). Multiple pressing provided further improvement of HV microhardness up to HV 96.1 (Al powder ECAE consolidated at 350°C) and HV 226 (MSR).

Consolidation method	**DE, ER 10:1**	**DE, ER 4:1**	**ECAE 1 pass**	**ECAE 4 passes, Bc**
HV microhradness	202	197	209	226

Tab. 3 HV microhardness of MSR compacts in dependence on consolidation method

4. Conclusions

- Breakthrough pressures needed for Equal Channel Angular Extrusion (ECAE) of ultra-fine 1 μm Al 99,7% powder and $Al_{94}Fe_2V_4$ melt-spun ribbons were reduced by ~6 times in comparison to direct extrusion process with extrusion ratio 10:1 at the same temperature
- This allowed successful synthesis of discrete particles of both materials into bulk profiles at much lower temperatures than usually possible with conventional extrusion process
- Well deformed particles and good metallurgical bonding between them throughout the entire cross-section were observed in compacted profiles even after one ECAE pass
- Microstructure after one ECAE pass was similar to that observed on directly extruded compacts at extrusion ratio 10:1 but was achieved at far lower temperatures
- Density and HV microhardness attained after 1 ECAE pass was higher than after conventional extrusion, whereas multiple ECAE passes using route Bc still enhanced this effect

Acknowledgement

This investigation was financially supported by Slovak Agency for S&T Support under the project APVT-51-031204. The authors thank also Slovak Centre of Excellence NANOSMART and especially P. Švec and D. Janičkovič from Institute of Physics, SAS, Bratislava for the supply of melt-spun ribbons.

References

[1] A, Inoue, H, Kimura, Mater, Sci, Eng, A 286 (2000) 1–10,

[2] J, Nagy, M, Balog, K, Iždinský, F, Simančík, P, Švec, D, Janičkovič: International Journal of Materials and Product Technology, 6129-IJMPT-08, December 2004

[3] O.N. Senkov , D.B. Miracle , J. M. Scott , S.V. Senkova, Journal of Alloys and Compounds (2003)

11. Savjetovanje o materijalima, tehnologijama, trenju i trošenju
11. Conference on Materials, Processes, Friction and Wear
MATRIB'06, Vela Luka, 22-24.06.2006.

EVALUATION OF CHANGING IN INFLUENCED AREAS AROUND MACROINDENTS ON SURFACE OF SYSTEMS THIN FILM – SUBSTRATE AND BASIC MATERIALS

Netušilová Denisa, Štěpánek Ivo, Department of Materials Science and Metallurgy, University of West Bohemia, Univerzitní 22, Pilsen, Czech Republic

Abstract: The paper is devoted by evaluation of influnced areas after macroindentation around the indents on different basic materials with and without thin film. There are evaluated changing in influenced areas and the range of influence after application thin films on surface of basic materials. The changing are documented by light microscopy from surface and special cross sections in the macroindents too. Two differet basic materials was prepared for this experiment These materials has very different mechanical properties. There are evaluated changing of plastic deformation and cohesive fracturing and its influences on fracturing all systems thin film – substrate. There are presented, what thin films enhanced properties of surface on both basic materials. The influenced areas are documented by measurement profiles of mechanical properties and behaviour in microlocations in different places around macroindents on surface and on special cross sections in macroindents in different depths of material system too. Thin films for this experiments were deposited by low voltage reactive arc evaporation in vacuum.

University of West Bohemia in Pilsen

Introduction

Thin films expand in very different applications with very different kind of stress. The most important for expansion application is predict behaviour in real stresses [1]. The expansion of application thin films need change analysis methods for giving much more information about behaviour of systems thin film – substrate. The first of all it is mechanical behaviour and changing surface properties and behaviour after mechanical, chemical and temperature stress [2]. For this evaluation the indentation method are used in very large range of value of loading from macroload to the very small loading in nanoindentation measurement. The graph dependence of information about materials systems on load give complex view about usability of indentation tests [3].

Macroindentation on surface of basic materials

At the first in this paper the measurement by macroindentation was realised. The macroindentation are used for evaluation hardness of bulk materials. For this moment the other informations are the most important for us. We prepared this measurement for analysis deformation, failures and cracks around and in indents after realisation macroindentations. We used for measurement two different kind of materials with different mechanical properties and behaviour and different structure composition. The macroindnetation is used as the type of mechanical stress – indentation stress. The first material is steel by CSN 14 220 and the second material is HSS by CSN 19 830. Here is realised measurement by value of normal force 125 kg. After measurement the indents are evaluated by light microscopy. Surface of material 14 220 was strongly deformed by plastic deformation process around the indents and indents are not regulary. On the edge of indents the cohesive failures are presented, which are given by failures expanded on the border of grains of structure. The large failures are on surface of material 14 220 then on surface of material 19 830. The surface of material 19 830 has cracks around the indents. The indents are regulary and deformation around indents is smaller then on surface of material 14 220. Cohesive failures are smaller. These deformations and failures and cracks are very important for evaluation behaviour of systems thin film – substrate with the same basic material charactristics as above mentioned. The indents are presented by fig. 1.

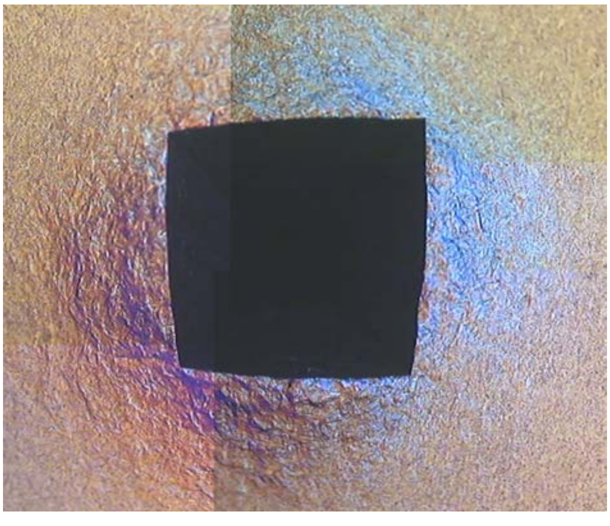

Fig. 1a: Macroindent in surface of basic material 14 220

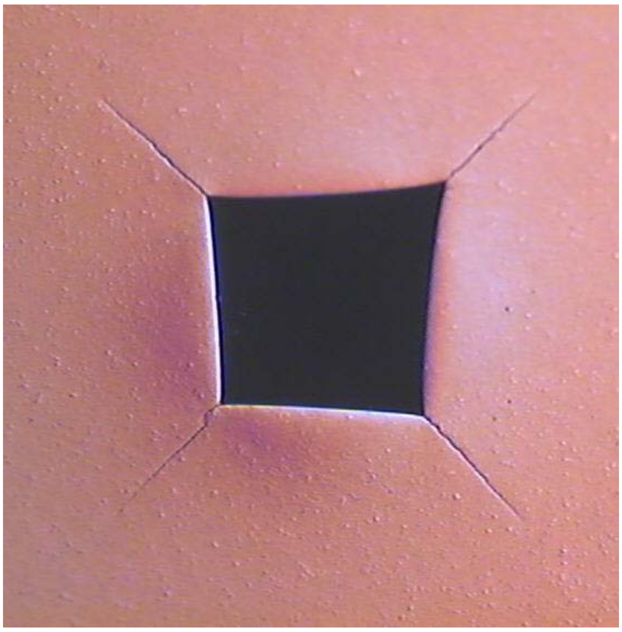

Fig.1b: Macroindent in surface of basic material HSS

Macroindentation on surface of systems thin film – substrate

At the second in this paper the measurement by macroindentation was realised on surface of systems thin film – substrate with the same substrate above mentioned. The conditions of measurement are the same as for measurement substrate without thin films. Thin films TiN was deposited by low voltage reactive arc evaporation in vacuum. The results of morphology of indents are presented in fig. 2. The fig.2 show, that thin films hardening surface of basic materials. After deposition indents are more regulary on systém thin film – substrate then on surface of alone basic material 14 220. The thin film on system with substrate 19 830 resist surface before initiation of cracks and their expansion.

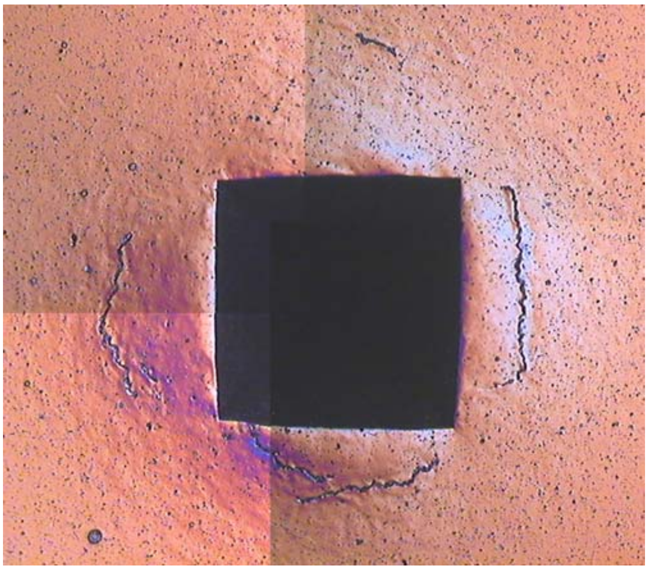

Fig. 2a: Macroindent in surface of systém thin film – substrate 14 220

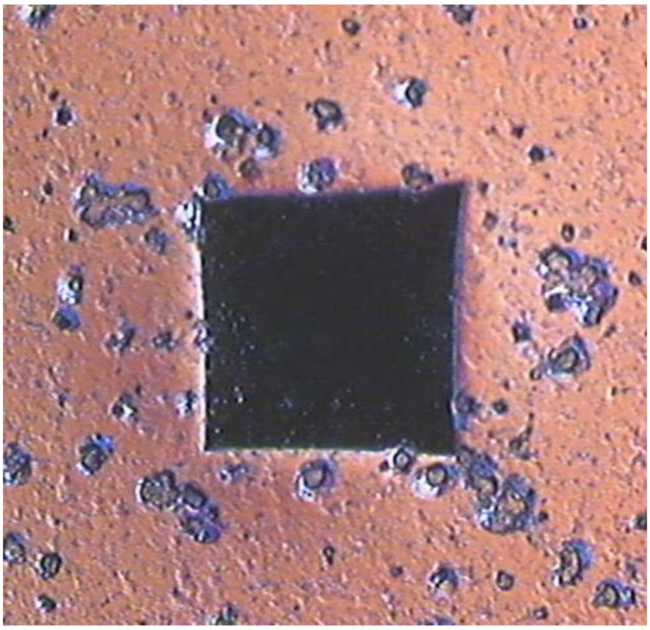

Fig. 2a: Macroindent in surface of systém thin film – substrate HSS

Evaluation of indents from cross section on systems thin film – substrate and surface of substrate

The analysis of indents not only from surface are very important . Here is very important to know, if the failures are adhesive or only cohesive in thin films or it the first cohesive failure in substrate and it cause failuring of surface thin film. We prepared cross sections in selected place of indents in systems of material above mentioned. Some cross sections are presented in fig. 3 we can to view from these fig. 3, what main deformation process is from substrate. Thin films resist surface before deformation on substrate 12 050. The thin films are not deformed after indentation significantly. Indents on surface after deposition are more regulary. Deformation process on systém thin film substrate 19 830 is smaller then on surface of basic material 19 830. The system thin film – 19 830 have not cracks, which we can view on substrate without thin films. Cohesive failures are smaller on systém with thin films at generally.

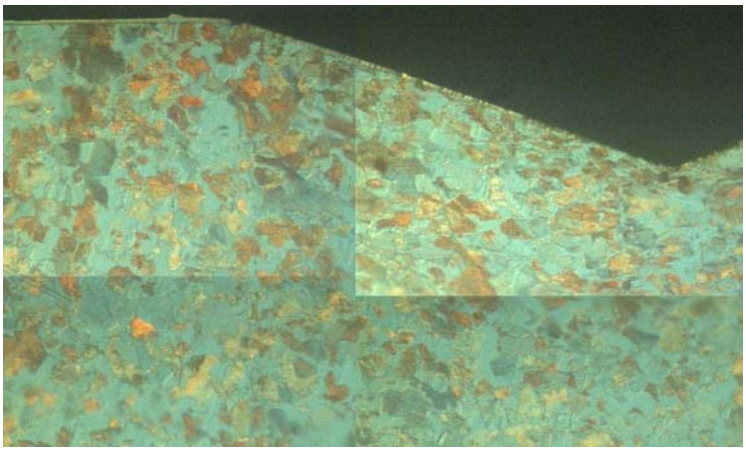

Fig. 3a: Cross section in macroindent in surface of systém thin film – substrate 12 050.

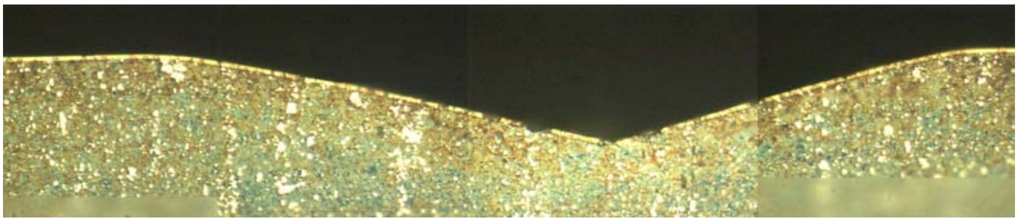

Fig. 3a: Cross section in macroindent in surface of systém thin film – substrate HSS.

Evaluation influenced area after macroindentation by nanoindentation

Main attention is given on evaluation influenced areas around the macroindents by nanoindentation measurement. The nanoindentation give possibility to measure in very small areas – microlocalities and depth of indentation is very small. We prepared measurement in different place around the macroindents from the edges to the not influenced surface of material systems on surface. The second measurement is from cross section from surface to the depth, where is not material systems influenced by macroindentation. The measurement was prepared on substrates without thin films and on systems with thin films. The results show fig. 4. changing of elastic plastic deformation in modificated places and changing nanohardness. Macroindentation increase around indents nanohardness of surface and plastic deformation of surface. This is possible to view on surface of material 14 220. The thin films decrease this differences. These results are not significantly on basic material 19 830 and system of this material with thin film. The measurement are realised in cross section too. The results from cross section (fig. 5) show depth influencing on different basic materials and different systém thin – film substrate too. The indentation curves are presented on fig. 4 and 5.

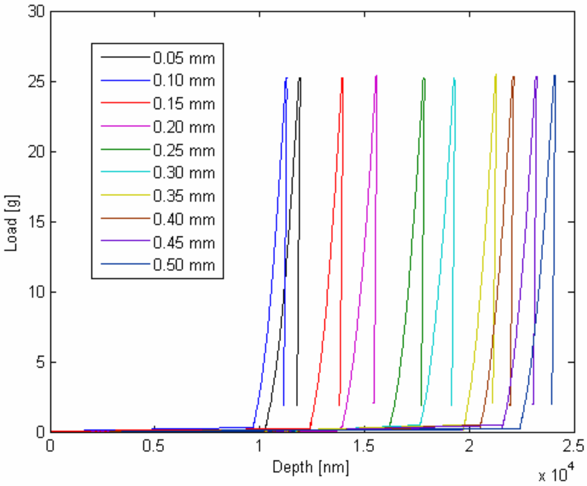

Fig. 4a: Nanoindnetation curves around macroindent in surface of basic material 14 220 – measurement on surface

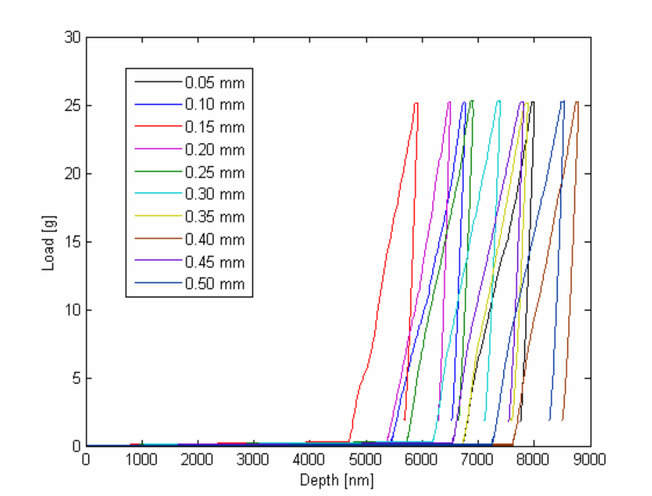

Fig. 4b: Nanoindnetation curves around macroindent in surface of system thin film – substrate 14 220 – measurement on surface

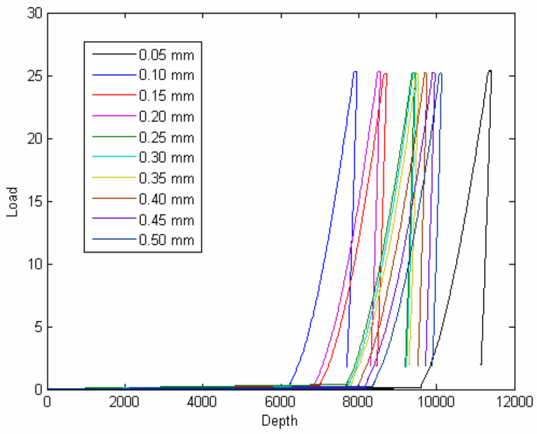

Fig. 5a: Nanoindnetation curves under macroindent in surface of basic material 14 220 – measurement in cross section

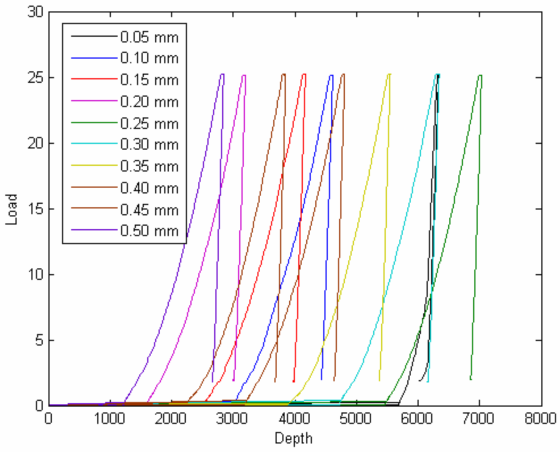

Fig. 5b: Nanoindnetation curves under macroindent in surface of systém thin film – substrate 14 220 – measurement in cross section

Conclusions

The macroindentation can aproximate some kind of mechanical stress from practice conditions. The macroindentation is used for evaluation hardness of bulk materials. The macroindentation test adheisve cohesive behaviour of systéms thin film – substrate and cohesive behaviour of surface of basic material. The properties of basic materials influence behaviour of all systems thin film – substrate during macroindentation. The substrates has large plastic deformation aroung the indents. The large it is for material 14 220. The surface of HSS after macroindnetation is failured by cracks from edge of indents. Thin films improve mechanical behaviour on both systems of thin film – substrate. In the first example thin film reduce deformation and cohesive failuring and in the second example thin film resist surface to the itiation of cracks. Influenced areas around the indents are analysed from surface and from cross section by light microscopy and local measurement on mechanical properties and behaviour aroung indents and in the depth under indents. Thin films reduce influenced areas. The nanoindentation is very good method for evaluation influenced areas. For understanding initiation of cracks and failures in systems thin film – substrate it is important provide analysis from cross section too.

The paper is presented in the range of solution project n. FT-TA/075.

Literature

1. I.Stepanek, Aproximation real stress condition with using laboratory analysis of behaviour systems thin film – substrate during combination stress, proceedings of conference Matrib 2001, Croatia – Vela Luka 2001
2. I.Stepanek, Changing mechanical properties and behaviour of systems thin film – substrate after application different stress, proceedings of conference Matrib 2002, Croatia – Vela Luka 2002
3. R.Nemec, I.Stepanek, Complex evaluation of mechanical properties of systems thin films by graph dependence measure information on value of load, proceedings of conference Matrib 2001, Croatia – Vela Luka 2001

SOUND ABSORPTION ABILITY OF ALUMINIUM CELLULAR MATERAL MAFUFACTURED VIA INFILTRATION TECHNIQUE

M. Nosko, J. Jerz, F. Simančík, R. Florek
Institute of Materials and Machine Mechanics SAS, Bratislava, Slovak Republic

Abstract:

Aim of the work is to investigate the sound absorption ability of open-cell sponge made by infiltration of sand granules with aluminium alloy. The porous structure was modified during manufacturing by variation of granule size. The sound absorption coefficient which characterizes the ability of material to absorb sound was measured by plane-wave impedance tube method.

Sound absorption ability of such sponges was attributed to viscous losses in the porous structure. It has been shown that the absorption efficiency can be successfully improved by reduction of pore size or by increase of absorber thickness as a result of more intensive dissipation of sound energy. Even better absorption performance can be achieved if smaller pores simulating perforated aluminium sheet are created at sound incident side of the sponge. Mineral wool placed behind cellular absorber can improve the sound absorption providing the permeability of the structure is relatively low. If the permeability is too high (large open area) the sound absorption ability of the sponge becomes comparable with mineral wool.

Key words: aluminium foam, sound absorption, open-cell structure

INTRODUCTION

The materials used for sound absorption applications reduce the sound intensity within the room where the sound is generated. The ability of material to absorb a sound is characterised by sound absorption coefficient α defined as the ratio of the non reflected sound intensity at the surface to the incident sound intensity.

The highly permeable materials such as open-celled polymer foams and glass or mineral wool fibres are generally used for these purposes. Flammability and evolution of toxic gases when subjected to excessive heat are the main disadvantages of polymer foams. On the other hand fibrous materials are very sensitive to erosion by shedding or fraying especially under the effects of air flow or vibration. Both types of absorbers usually require various facing materials in order to improve durability or to protect the absorber from contamination. The perforated panel often used for this purpose can provide an additional resonance effect, similarly, as it is in a case of Helmholz resonator, which is essentially a vessel in which the mass of air in the neck is driven in and out in resonance upon the stiffness of enclosed air volume [1].

The faced material itself can be constructed more sophisticated containing a plenty of small Helmholtz resonators (Fig. 1). The frequency at which the maximum sound absorption is reached can be tuned by cavity geometry.

Many studies have proposed that aluminium foams can be prospective candidates for noise control [1]. Although the recently produced aluminium foams are more expensive in comparison with the currently prevalent acoustic materials such as polymer foams and glass wool, some of them were already successfully applied for noise attenuation purposes (Fig. 2). Because of the low intrinsic damping of the rigid cell walls of most aluminium foams the noise attenuation is mostly attained via viscous losses in porous structure. To allow this mechanism to work efficiently the porous structure must be opened.

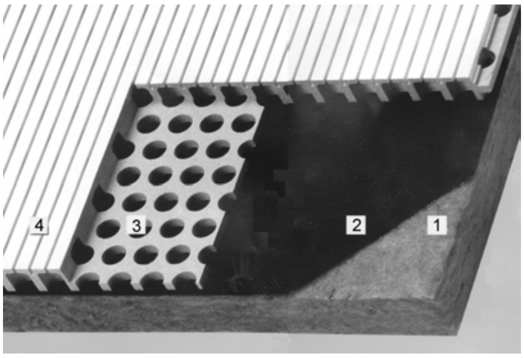

Fig. 1. Typical construction of sound absorber: thick glass fibre absorber (1), thin protective and damping foil (2), facing wood panel with resonator cavity (3) and outer design (4) [11].

However, most aluminium foams produced recently have relatively closed pores. To open them complicated and expensive techniques are necessary [1]. Therefore this study aims to characterize the sound absorption behaviour of relatively cheap open-celled aluminium sponge supplied by ACCESS - research centre of Technical University of Aachen, Germany, prepared via infiltration technique. The main objective is to investigate the ability of this sponge to attenuate noise and to suggest the conditions under which it can be applied in future sound absorbers.

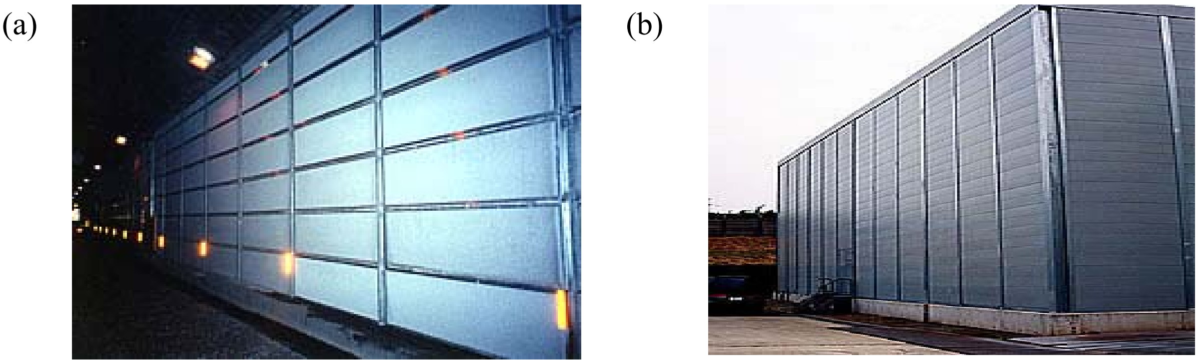

Fig. 2. Aluminium foam ALPORAS manufactured via melt route as a sound absorption material next to roads (a) and as buildings insulation (b) [2].

THEORETICAL BACKGROUND TO SOUND ABSORPTION IN ALUMINIUM FOAMS

The main parameter for good sound absorption is the permeability of the absorber. ACCESS aluminium sponge has open-celled structure with relatively thick struts. Such structure absorbs the sound energy mainly by viscous losses as the sound pressure wave pumps air in and out of the interconnected pores. The absorption efficiency depends then on the pore size distribution and on the thickness of absorber. In the case of ACCESS sponges the manufacturing process allows to adjust the optimum pore size (see Fig. 4) or even to obtain gradient pore structure in relatively easy and inexpensive way.

Fig. 3 presents the typical features of manufacturing process. The suitable mould is filled by preheated pellets made of fine grained sand then the liquid aluminium poured into the mould infiltrates them. After exposing to heat the binder in sand pellets is burning off and the loose sand is subsequently removed by mechanical vibrations leaving the pores in aluminium sponge structure. This process is very simple and allows easy modification of pore size only by changing the pellets diameter. The constant, bimodal or gradient pore size can be achieved if pellets of different diameters are filled to required sample thickness [3]. The pores are interconnected with smaller holes, which diameters are depending on contact area between adjacent pellets and can be varied by pressing of pellets prior to infiltration. The cell wall material can be widely varied and no cell structure stabilising additives are necessary [4]. However, the ligaments separating the pores are rather thick and the sponge is relatively heavy. On the other hands this allows to use it as self-bearing part of the construction.

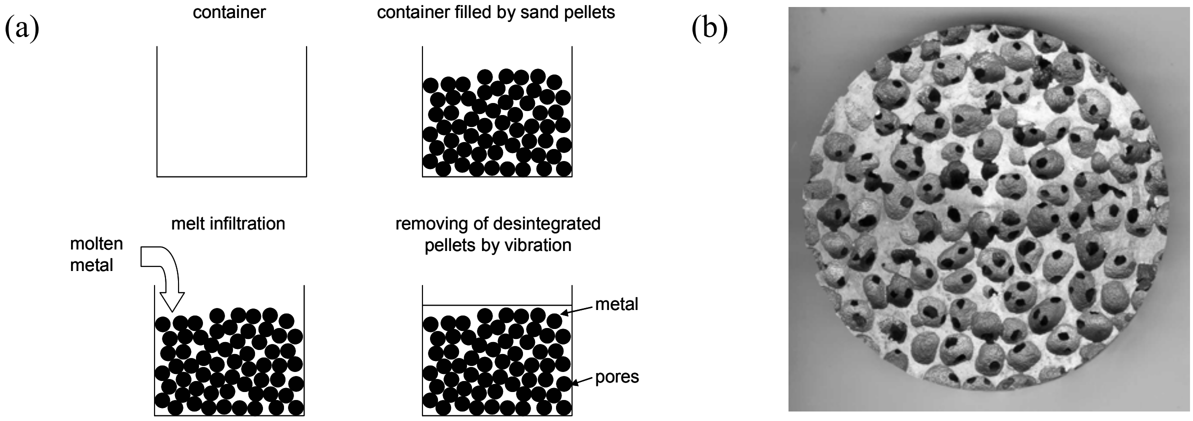

Fig. 3. (a) Infiltration process for manufacturing of open-celled aluminium sponge and (b) open pore structure with the thick ligaments between adjacent pores.

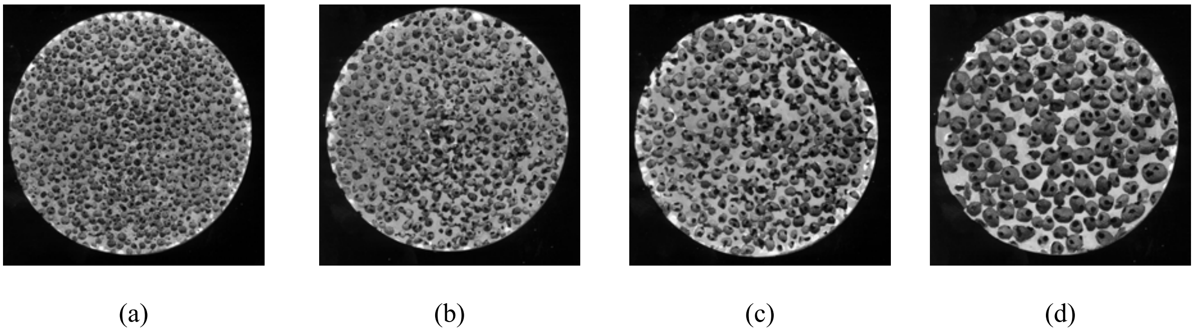

Fig. 4. Variable pore size; (a) 3-4 mm; (b) 4-5 mm; (c) 5-6 mm; (d) 6-8 mm.

EXPERIMENTAL PROCEDURE

Sound absorption of open-celled ACCESS aluminium sponge made via infiltration technique has been tested in dependence on various pore size and thickness of absorber.

In this study, the values of sound absorption coefficient have been estimated using simple impedance tube method.

Test was carried out according to ISO EN 10 534 [10]; schematic description is presented in Fig. 5. The sound is generated by load-speaker at one end of the tube and travels towards the sample which is placed at the other end. The sample is sealed to avoid the additional losses of the sound energy. The principle of measurement is to obtain pressure drop by moving the probe. Absorption coefficient is then calculated from equation:

$$\alpha = 1 - \left(\frac{p_{\max.} / p_{\min.} - 1}{p_{\max.} / p_{\min.} + 1} \right)^2 \qquad (1)$$

where $p_{max.}$ is maximum and $p_{min.}$ minimum pressure measured by moving probe. Density of samples investigated in this work is ~ 0.95 g. cm^{-3}.

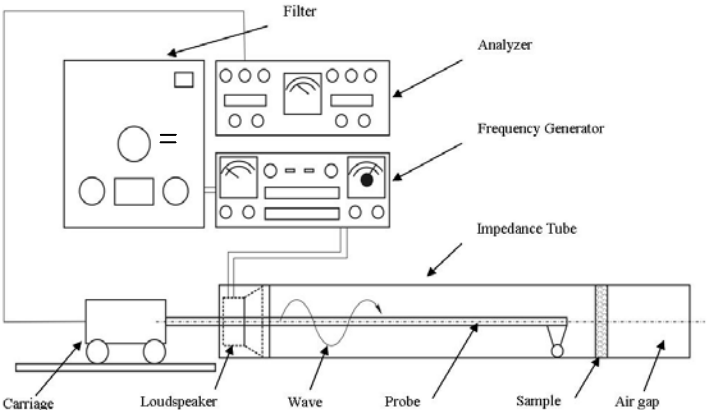

Fig. 5. Schematic description of sound-absorption coefficient measurement via impedance tube method.

RESULTS AND DISCUSSION

The absorber will be the most effective, if it is situated in a distance of a quarter wavelength from the surface. This leads to a great depth of absorber if the absorption at low frequencies is required.

As it was expected [13], the increasing thickness of absorber shifts the maximum of the sound absorption coefficient towards lower frequencies (Fig. 6).

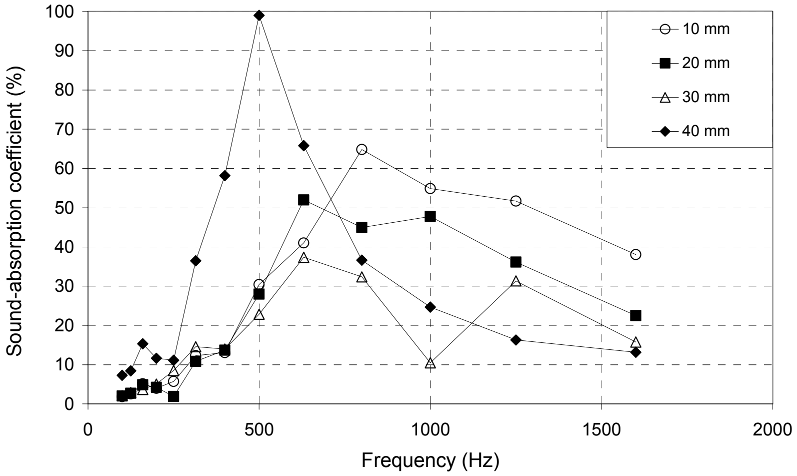

Fig. 6. Effect of the sample thickness to sound-absorption ability;
Average pore size: 4-5 mm; air gap behind the sample: 40 mm (AlSi alloy).

It is not always feasible to increase the thickness of absorber, because of the weight and cost limitations. The use of a thinner section of absorber spaced out on an equivalent air gap gives very similar results to a thick section (Fig. 7), however at significantly lower weight. Therefore, the frequency range of maximum sound absorption can be tailored by creating an optimum air gap between the absorber and rigid wall without need to increase a weight. The sound absorption can also be enhanced for wider frequency range by the combination of several foam plates with an air gap between them.

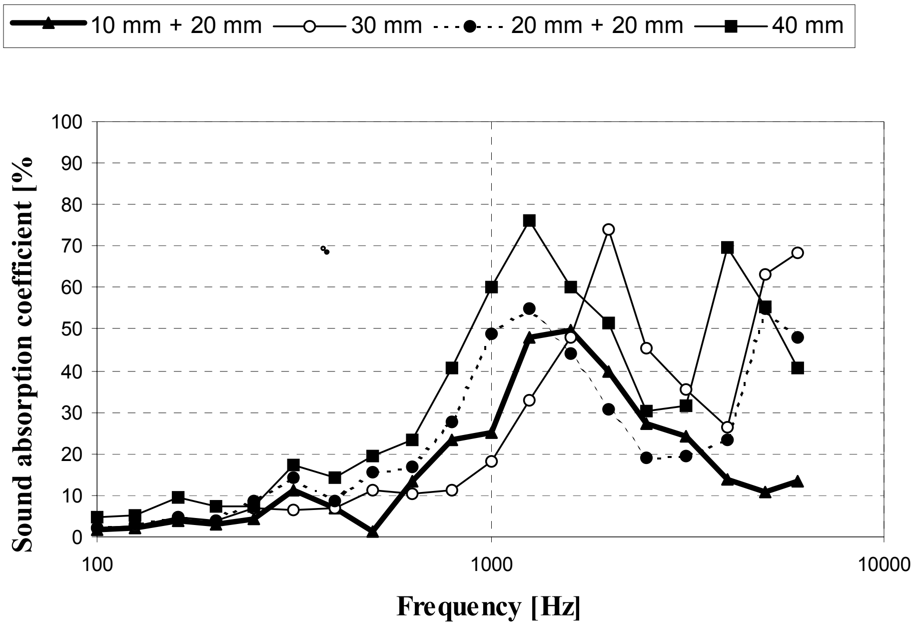

Fig. 7. Comparison of sound absorption for two designs of sound absorbing panels at two constant thickness of absorber. 1st type is the foam at given distance from rigid wall, 2nd type is thicker foam at zero distance from rigid wall.
Average pore size: 4-5 mm; (AlSi alloy).

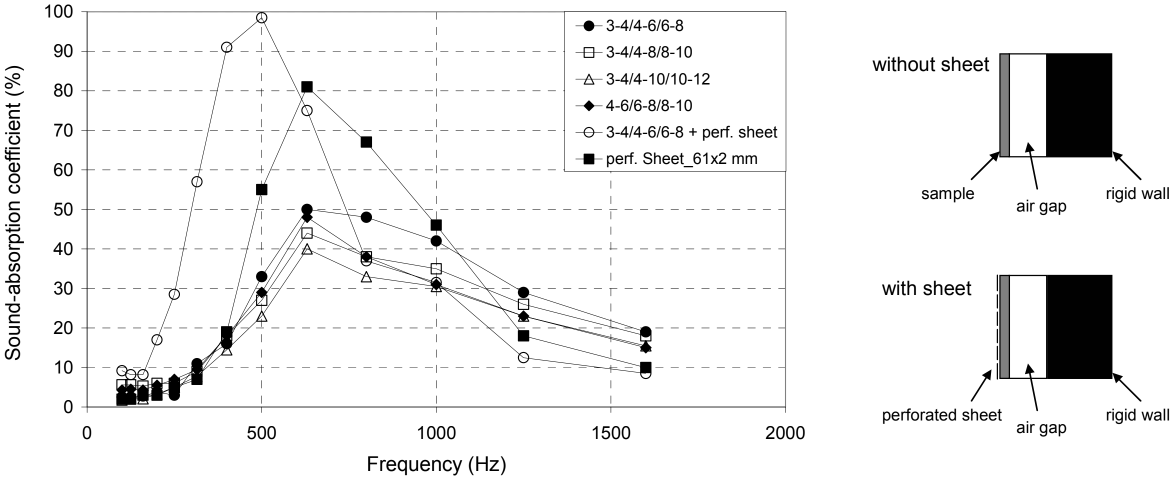

Fig. 8. Effect of different modifications of the pore size within the gradient pore structure; Sample thickness: 25 mm; air gap: 48 mm (Al); perforated sheet: 61 x 2 mm diameter, thickness: 1.5 mm.

As can be seen in Fig. 6 and 7 this sponge provides rather lower sound absorption efficiency, which can be attributed to its relatively high permeability. Fig. 8 shows, that this efficiency is not notably improved also if gradient structure (3-4/4-6/6-8) is applied, because the smallest pores (3-4 mm) are still too large to increase viscous losses. However significant improvement of absorption ability can be achieved if perforated aluminium sheet (61 holes with diameter 2 mm) is attached to incident side of the sponge. This behaviour can be explained by introduction of cavity resonator mechanism described in [6]; it is assumes that pore structure can be substituted by number of holes which with an air gap behind the sample create the cavity resonator.

Filling the air gap between aluminium sponge and rigid wall with mineral wool leads to further improvement of absorption ability as presented in Fig. 9 and Fig. 10 for gradient pore structures (3-4/4-6/6-8) with and without perforated sheet. The reason is simple. Sound energy which is not reflected or absorbed by cellular material transits the structure and is absorbed by the mineral wool. However, the sound absorption coefficient in case of structure without perforated sheet is very similar to mineral wool itself and the sponge almost does not contribute to the absorption (Fig. 9). On the other hand if the perforated sheet is used on the incident side it reflects sound wave of higher frequencies and the absorption efficiency is reduced for these frequencies.

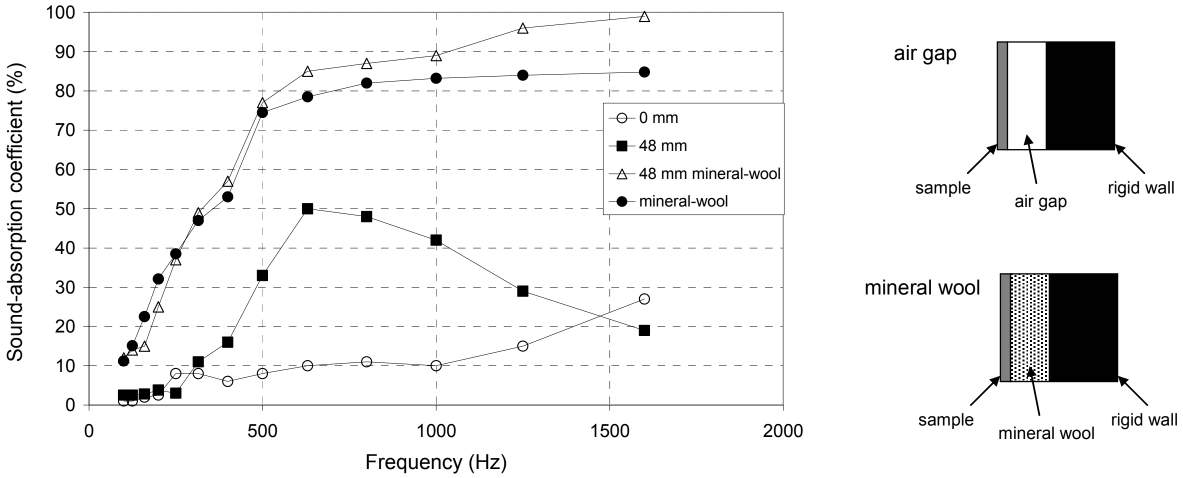

Fig. 9. Effect of different filling behind the sample; air gap is filled by mineral-wool; Thickness: 25 mm; pore size: 3-4/4-6/6-8 mm; (Al).

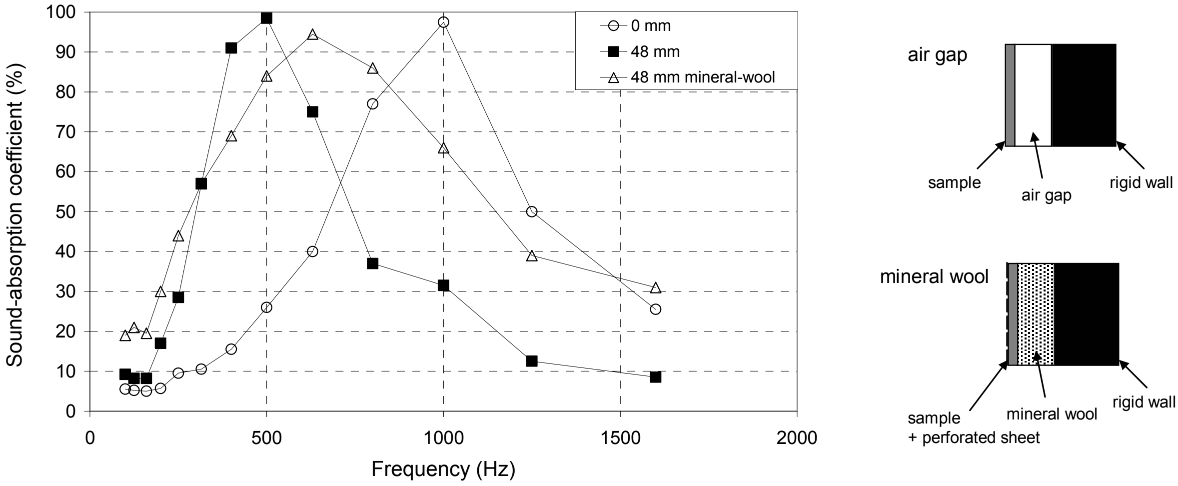

Fig. 10. Effect of different filling behind the sample; air gap is filled by mineral-wool; Thickness: 25 mm; pore size: 3-4/4-6/6-8 + perforated aluminium sheet (Al).

CONCLUSIONS

The absorption ability of open-celled aluminium sponge ACCESS manufactured via infiltration process can be adjusted to absorb required frequency range by increase of flow resistance of the structure together with introducing the air gap behind the absorber.

Increase of flow resistance can be achieved by decreasing pore size, although even minimum pore size of commercial ACCESS sponges (3-4 mm) is too large for optimum absorption efficiency. Simulation of smaller size by applying perforated aluminium sheet at the incident side of the sponge has revealed that further minimising of pore size can be beneficial for better sound absorption.

Applying the air gap between the sample and rigid wall moves the absorbed frequency range to lower frequencies. If this gap is filled with mineral wool wider range of frequencies can be efficiently absorbed, depending again on flow resistance of the structure.

Although the ACCESS aluminium sponge cannot provide a high level of sound absorption itself, it can be attractively used as a facing material, especially in combination with fibrous absorbers, provided that the structure permeability is sufficiently low. The frequency corresponding to the maximal sound absorption can be tuned by the thickness of foamed sponge or by changing of pore size.

This cellular aluminium structure additionally offers very high stiffness at low weight, is self supporting and form stable at elevated temperature, does not release toxic gases when subjected to excessive heat, possesses high durability under the effects of air flow or vibration, exhibits sufficient fire resistance and can be easily recycled.

The potential applications are expected in sterile (antiseptic, dust free) environment, in the structures where non-flammability is important (aeroplanes, hotels, commercial and industrial buildings) or in interiors under difficult conditions (elevated temperature, moisture, dust, flowing gas and vibrations).

ACKNOWLEDGEMENTS

The authors would like to thank ACCESS - research centre of Technical University of Aachen, Germany, for providing of testing material.

REFERENCES

[1] Simančík, F. - Kováčik, J.: Electrical, thermal and acoustic properties of metallic foams. In: *Handbook of Cellular Metals Production, Processing, Applications. Chapt. 5.3.* Weinheim: Wiley-VCH, 2002, p. 215-241.

[2] T. Miyoshi, M. Itoh, S. Akiyama, A. Kitahara: In. *Metal Foams and Porous Metal Structures, Ed. by J. Banhart, M.F. Ashby, N.A. Fleck, Verlag MIT Publishing,* Bremen, 1999, p. 125

[3] Grote, F.: Offenporige Metall-structuren nach dem Platzhalterfahren, Shaker Verlag, Aachen, 2003.

[4] Guiping, G. – Deping, H. – Guangji, S.: Underwater property of porous aluminum, Colloids and surfaces A, (2001), 191-194.

[5] Lu, T. J. – Chen, F. – He. D.: Sound absorption of cellular metals with semi-open cells, *Journal of accoustic society 108,* (2000) 1697.

[6] Han, F. – Seiffert, G. – Zhao, Y. – Gibbs, B.: Acoustic absorption behaviour of an open-celled aluminium foam, *Journal of physics D: Applied Physics 36,* (2003) 294-302.

[7] Ashby, M. F. and col.: Metal foam: A Design Guide. 2000, Butterworth-Heineman.

[8] Simančík, F. - Degischer, H. P. - Wörz, H.: Foamed Aluminium - Light Structural and Insulation Material, In *Euromat '95, Venice/Padua, Italy, 25. - 28. September 1995,* Assoziazione Italiana di Metallurgica, Milano, 1995.

[9] Lu, T. J. – Hess, A. – Ashby, M. F.: Sound absorption in metallic foams, *Journal of applied Physics 85,* (1999) 7528

[10] EN ISO 10534 – 1, Acoustics – Determination of sound absorption coefficient and impedance in impedance tubes - Part 1: Method using standing wave ratio, jun 2001.

[11] n'H Akustik + Design AG, Ch-6078 Lungen, 1999

[12] T. Miyoshi, M. Itoh, S. Akiyama, A. Kitahara: In. *Metal Foams and Porous Metal Structures, Ed. by J. Banhart, M.F. Ashby, N.A. Fleck, Verlag MIT Publishing,* Bremen, 1999, p. 125

[13] H. Utsumo, T. Tanaka and T. Fujikawa: *J. Accoust. Soc. Am.* 1989, 86, 637

MIKROSTRUKTURNE PROMJENE U CIJEVIMA ZA KOTRALJUĆE LEŽAJEVE

MICROSTRUCTURAL CHANGES IN BALL BEARING STEEL TUBES

V. Novosel – Radović, M. Kostelac; N. Radović*, A. Iharoš, N. Hrvatov – Crljenica, F. Šafar, K. Dužić
Valjaonica cijevi Sisak d. o. o., Željezara Sisak, 44000 Sisak, Hrvatska
*Geodetski fakultet Sveučilišta u Zagrebu, 10000 Zagreb, Hrvatska
nradovic@geof.hr

Sažetak: Tijekom valjanja, ekspoloatacije i/ ili naknadne obrade hladno valjanih čeličnih cijevi za kotraljajuće ležajeve zapažena je pojava pukotina, pucanje krajeva cijevi, neujednačene debljine stijenke i/ ili povečana ovalnost isječenih prstenova. Za iznalaženje uzroka proučavani su model uzorci, uzeti u obliku pločice 10 x 10 mm iz hladano vučene cijevi ϕ40.4 x 4.2 mm, tipa S 4146 u pojedinim fazama njene izrade od uloška do finalnog produkta. Uzeti uzorci izravno i/ ili nakon pripreme površine (*brušenjem*, *poliranjem*, *nagraizanjem*) istraživani su rentgenskom difrakcijom. Difrakcijske slike uzoraka snimane filmskom metodom (tzv. *metoda povratne refleksije*) i/ ili brojenja pomoću difraktometra s detektorom uz uporabu zračenja CoK_α. Dobivene difrakcijske su slike analizirane vizualno, te primjenom postupaka Warrena i Averbacha, te metodom komparacije.

Ključne riječi: cijevi za kotrljajuće ležajeve; mikrostrukturne promjene; rentgenska difrakcija

Abstract: To, explain the occurrence of cracks, ruptures by the tube side, uneven wall thickness and/ or pronounced oval lines of link cutting during drawing, exploitation and/ or subsequent treament of cold drawn ball bearing steel tubes an analysis of the microstructure was undertaken. Model samples were collected as 10 x 10 mm plates from a cold drawn tube, made of S 4146 steel, ϕ40.4 x 4.2 mm in diameter, at various stages of fabrication, from the finished rolled tube to the final product. The samples were examined by the method of X – ray diffraction, directly or after preparation of the surface by grinding, polishing, and etching. The X – ray diffraction patterns were recorded by means of a photographic technique known as the back reflection method and/ or by the counting technique using a diffractometer with monochromatized CoK_α radiation. The X – ray patterns were analysed visually, by the Warren – Averbach methods and by comparison.

Key words: ball bearing steel tubes, microstructural changes; X – ray diffraction

UVOD

Premda tehnologija izradi hladno vučenih čeličnih cijevi za kotrljajuće ležajeve je znana i detaljno opisana[1 – 3], ipak u fazi njihova rezanja u prstenove zapažene su anomalije, u promjeni ovalnosti prstena i/ ili debljini stijenke cijevi, pojavi pukotina i/ ili pucanja po rubovima. Pojavu anomalije Iharoš[3] tumači kao posljedicu zaostalih naprezanja, a Brusilovski i Shasho[4] strukture i distribucije karbida (tipa cementit) u površinskom sloju cijevi tijekom njene izrade. Za smanjenje veličine i broja zapaženih anomalija Kostelac[5] studira utjecaj dodatnih postupaka u izradi hladno vučenih cijevi žarenjem i/ ili ravnanjem, uporabom metoda rentgenske difrakcije i/ ili mjerenja ovalnosti obrađenih prstenova za ležajeve. Određuje vrijednost zaostalih naprezanja[6] i promatra promjene mikrostrukturnih parametara unutar stijenke cijevi detaljno opisane u ovom radu.

EKSPERIMENT

Za istraživanje mikrostrukturnih promjena u cijevima za kotrljajuće ležajeve uporabljeni su model uzorci, pripremljeni iz hladno vučene cijevi ϕ 40.4 x 4.2 mm, tipa S 4146. Uzorci su uzimani u tijeku žarenja i/ ili ravnanja hladno vučene cijevi, tablica 1. kao dijelovi cijevi.

Tablica 1.

UZORAK	ZA PRIPREMU MODEL UZORAK JE UPORABLJEN KAO
A	GOTOVA HLADNO VALJANA CIJEV
B	**A** + RAVNANA NA RAVNALICI S TRI PARA HIPERBOLNIH VALJAKA
C	**A** + RAVNANA NA RAVNALICI S JEDNIM PAROM KONKAVNO KONVEKSNIH VALJAKA
D	**A** + ŽARENA, 760°C / 5 min.
E	**D** + **B**
F	**D** + **C**

Uzeti uzorci sukcesivno su snimani po površini u smjeru valjanja cijevi i/ ili isječeni u pločice površine 10 x 10 mm uz kontinuirano hlađenje. Prije snimanja uzeti uzorci u obliku pločica su uloženi u masu; metalografski pripremljeni. Difrakcijske slike uzoraka su snimane tehnikom filma (metoda povratne refleksije) i brojenja na uređaju za difraktometriju, tipa Philips uz uporabu monokromatskog zračenja CoK_α. Dobivene difrakcijske slike su analizirane vizualno i metodom komparacije te postupkom Warrena[7] i B. L. Averbacha[8], uz uporabu modificiranog programa Popović[9]. Neki od uzoraka su istraživani na raster elektronskom mikroskopu i mikroanalizatoru, tipa Joel.

REZULTATI I RASPRAVA

Dobiveni rezultati istraživanja promjene mikrostrukturnih parametara u cijevima za kotraljajuće ležajeve su dani u obliku slika i tablica. Tako su na slici 1 dane difrakcijske slike, debyjevskog prstena 310 od Fe dobivene izravno sukcesivnim snimanjem po površini uzetih uzoraka cijevi u smjeru njena valjanja. Vizualnim uspoređivanjem difrakcijskih slika se zapaža njihova raznolikost u pojavi: točkavosti, difuznosti i/ ili cijepanju debyjevskog prstena 310 od Fe. Najveće razlike unutar mjesta snimanja su zapažene kod gotove hladno vučene cijevi, slika 1A, a najmanje kod žarene i ravnane cijevi na ravnalici valjaka slika 1F. Prema Ungaru i suradnicima[10] zapažene razlike u zabilježenim debyjevskim prstenima su posljedica razlike u mikrostrukturi, a Warrenu[11] njene nehomogene raspodjele unutar pojedninog istraživanog uzorka, a Kestensu i suradnicima[12] prisutne fragmentacije zrna.

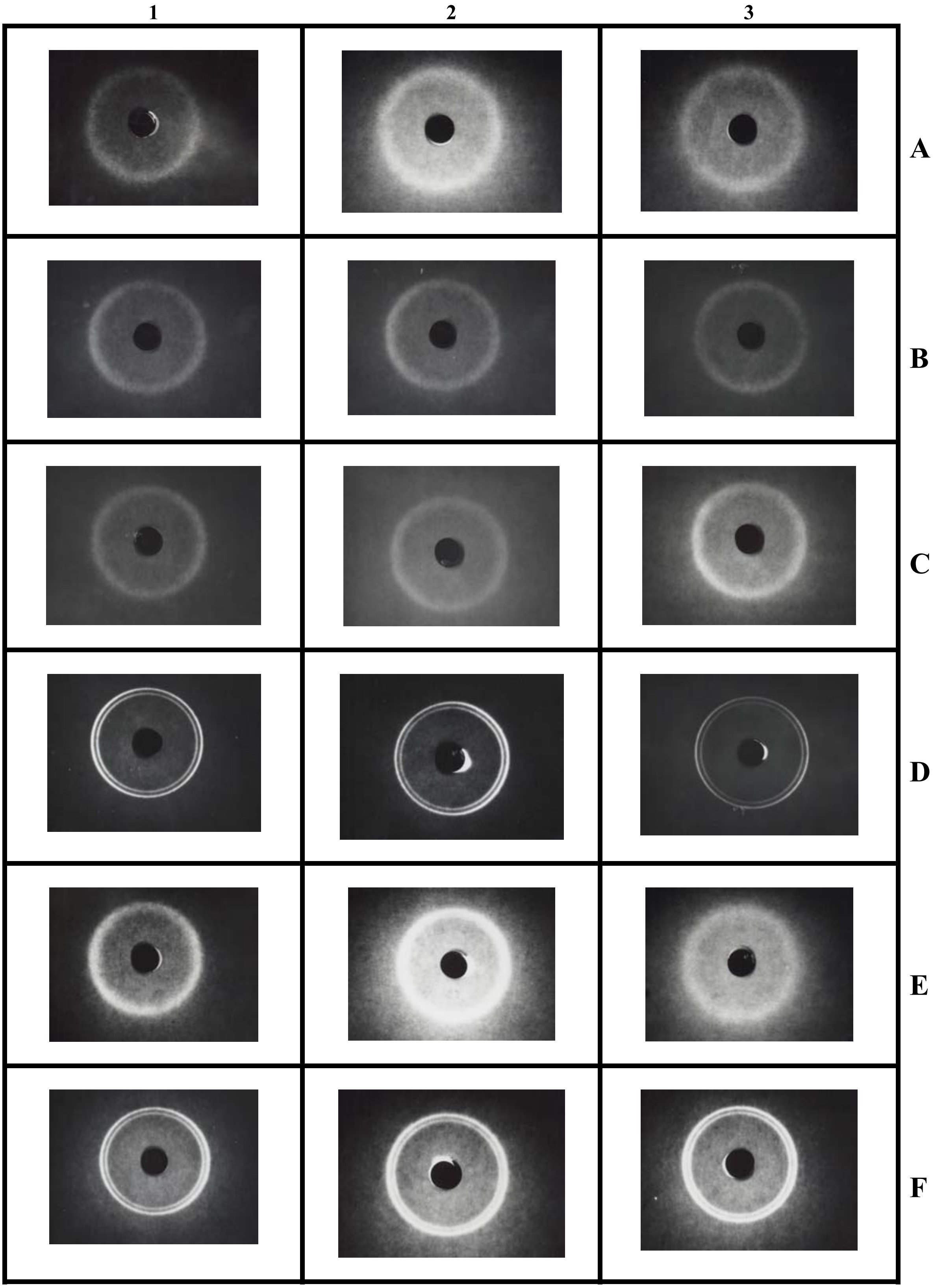

Slika 1. Promjena debyevskog prstena 310 Fe uzduž površine uzorka hladno vučene cijevi uzorka: **A**, **B**, **C**, **D**, **E**, **F** različito tretirane. **1**, **2**, **3** mjesto mjerenja unutar istraživanog uzorka.

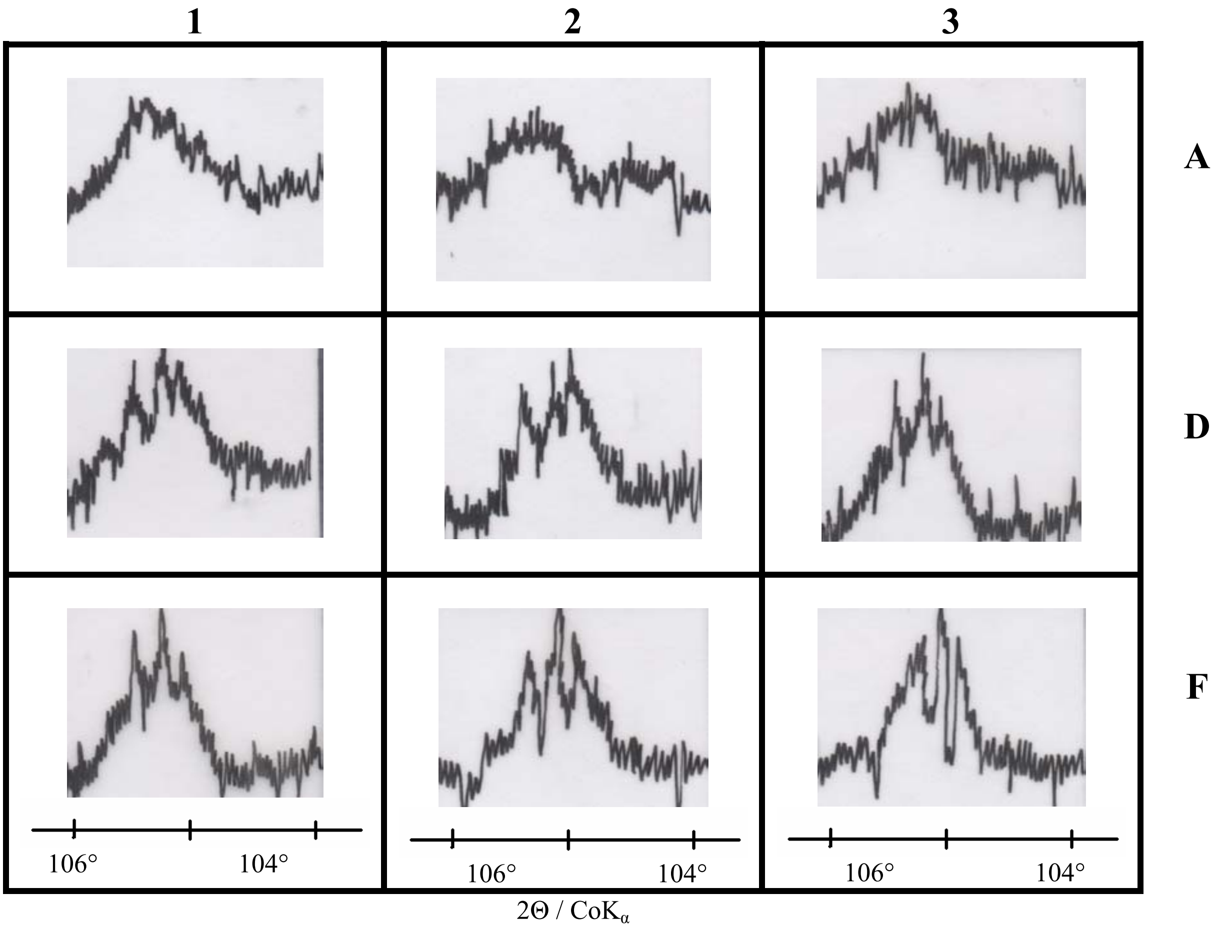

Slika 2. Promjena profila difrakcijske linije refleksa 630 $Fe_{20}C_9$ u uvjetima dodatne obrade hladno vučene cijevi: **A**, **D** i **F** na mjestu mjerenja: **1**, **2**, **3**.

Na prisutnost fragmentacije zrna upućuje zabilježeni profil difrakcijske refleksa 630 od $Fe_{20}C_9$ u kutnom području 103 do 107□2□, slika 2. Samo u uzorku F, žarenom i ravnanom na ravnalici s jednim parom konkavno konveksnih valjaka zabilježeni difrakcijski profili refleksa 630 od $Fe_{20}C_9$ su gotovo jednaki. Na slikama istraživanih uzoraka fragmentacija prenapregnutih zrna je više ili manje izražena. Također, samo u uzorku F, slika 3F ranije identificirane faze[6] na osnovi Fe – C su jednoliko distribuirane unutar njegova površinskog sloja. U uzorku A i D, slika 3A i 3D su prisutne u obliku nakupina.

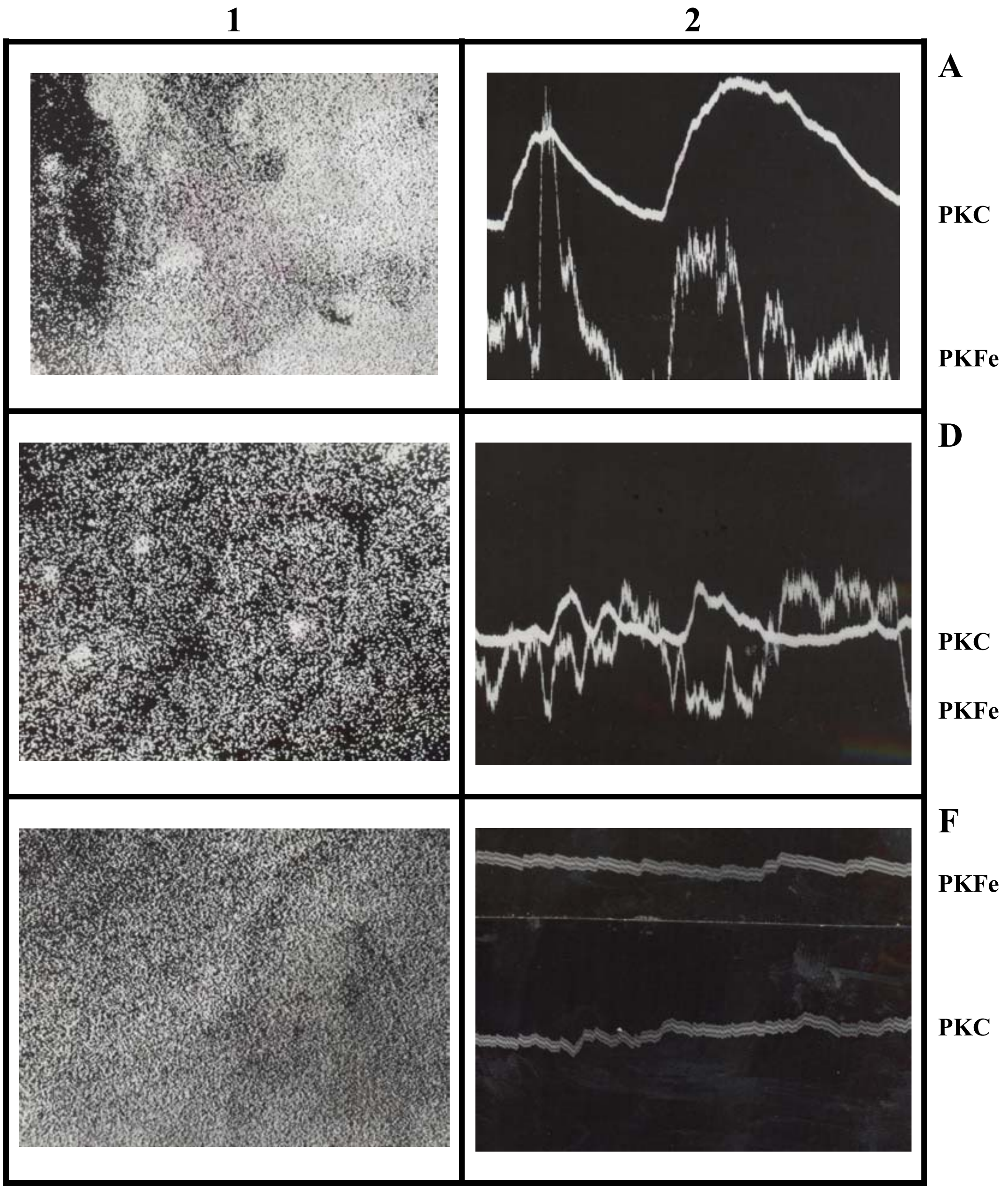

Slika 3. Elektronska snimka 1 – karakterističnog rentgenskog zračenja FeK$_\alpha$ i 2 – profila koncentracije PKFe i PKC hldano vučene cijevi uzorka: A, D i E.

Također i izmjerene širine profila difrakcijske linije na polovici visine maksimuma B$_{1/2}$ refleksa 211 od Fe korigirane za dubletno proširenje upučuju na promjene, slika 4. Izmjereni i izračunate vrijednosti B$_{1/2}$ u uzorku A s mjestom mjerenja se mijenjaju od 15 do 35 %, a u uzorku F od 1.85 do 3.70 %.

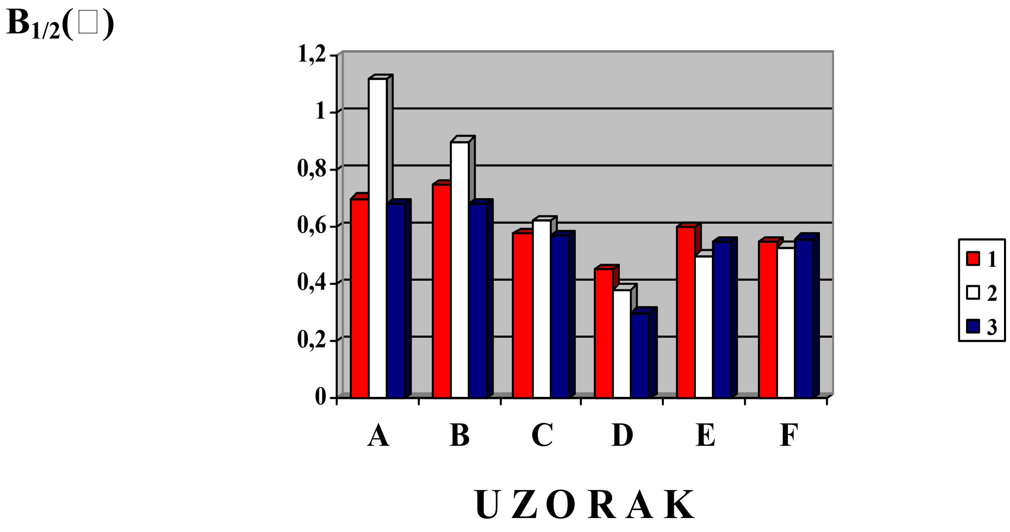

Slika 4. Histogram promjene širine na polovici visine maksimuma $B_{1/2}$ refleksa 211 od Fe korigirane za dubletno proširenje.

Na analogne promjene s izradom vučene cijevi upućuju i izračunate vrijednosti distorzije kristalne rešetke $\left\langle (\Delta L)_L^2 \right\rangle^{1/2}$ o L, slika 5. Unutar mjerenih mjesta pojedinog uzorka vrijednosti $\left\langle (\Delta L)_L^2 \right\rangle^{1/2}$ o L se mijenjaju. Najveće promjene su zapažene u uzorku A, a najmanje u uzorku F. Prema Warrenu i Averbachu[9] one su posljedica nepravilne distribucije distorzije kristalne rešetke unutar kristalita kao posljedica dodatne obrade u procesu izrade hladno vučene cijevi.

Tablica 2. Promjena stupca dužine L $\left(\overset{o}{A}\right)$ uslijed distorzije kristalne veličine $\left\langle (\Delta L)_L^2 \right\rangle^{1/2}$.

		MJESTO MJERENJA		
		1	2	3
UZORAK	DUŽINA STUPCA L, $\left(\overset{o}{A}\right)$	$\left\langle (\Delta L)_L^2 \right\rangle^{1/2} \left(\overset{o}{A}\right) \cdot 10^2$		
A	**20**	1.45	0.79	1.28
	60	1.47	1.62	1.78
	100	2.01	1.98	1.89
B	**20**	0.90	0.80	1.02
	60	1.26	1.16	1.31
	100	1.75	1.84	1.73
C	**20**	0.85	0.92	0.95
	60	1.15	1.05	1.20
	100	1.55	1.40	1.45
D	**20**	0.45	0.35	0.48
	60	0.50	0.45	0.53
	100	0.70	0.71	0.75
E	**20**	0.60	0.65	0.59
	60	1.01	0.95	0.95
	100	1.25	1.19	1.26
F	**20**	0.50	0.55	0.52
	60	0.89	0.85	0.87
	100	1.00	0.99	1.02

Za veličinu stupca L = 60 $\overset{o}{A}$ vrijednost distorzije kristalne rešetke $\langle e\rangle$, slika 5 se mijenja od 2.45 do 2.96 · 10^{-4} u uzorku A te 1.45 do 1.48 · 10^{-4} u uzorku F. Zbog toga Kostelac[4] zabilježene promjene u mikrostrukturi kao posljedicu tečenja metala, nehomogenosti deformacije i načina valjanja nastoji u izradi hladno vučenih cijevi, žarenje i ravnanje. U postupku ravnanja daje prednost uporabi ravnalice s jednim parom konveksno konkavnih valjaka. Izrezani prsteni iz tako obrađenie cijevi su upučivali na neznatne promjene ovalnosti.

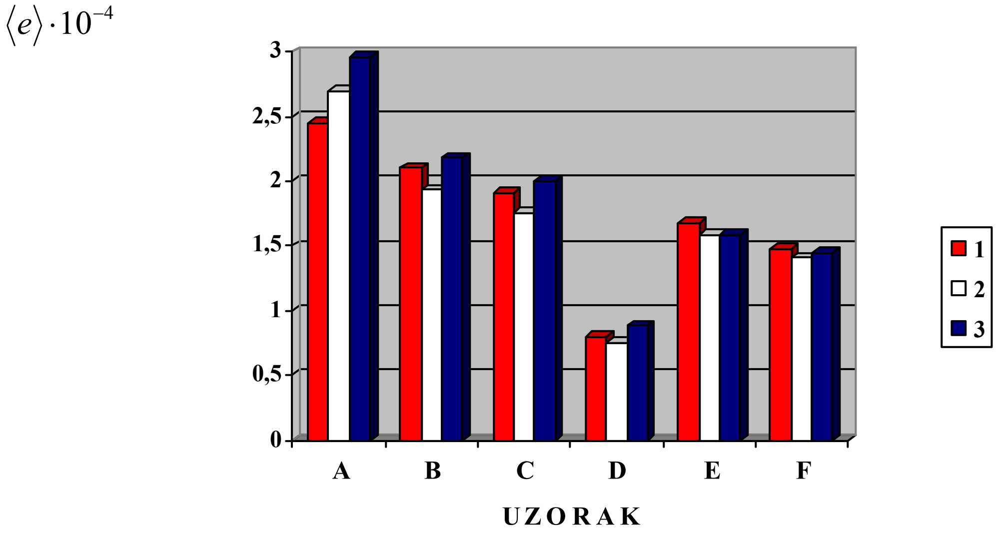

Slika 5. Promjena distorzije kristalne rešetke $\langle e_{WA}\rangle$ za L = 60 $\overset{o}{A}$ u uvjetima dodatne obrade.

ZAKLJUČAK

Izvršena su istraživanja promjene mikrostrukturnih parametara u cijevi za kotrljajuće ležajeve. Dobiveni rezultati kao difrakcijske slike: debyjevskog prstena 311 od Fe, profila difrakcijske linije refleksa 626 od $Fe_{20}C_6$, širine na polovini visine maksimuma difrakcijske linije $B_{1/2}$ refleksa koregirane za dubletno proširenje311 od Fe, promjene stupca L u $\overset{o}{A}$ uslijed distorzije $\left\langle (\Delta L)_L^2 \right\rangle^{1/2}$, te distorzije kristalne rešetke $\langle e\rangle$ upućuju da nastale promjene u mikrostrukturi posljedica su postupka izrade hladno vučene cijevi. Samo uzorci hladno vučene cijevi žareni (750□C/ 5 min) i ravnani na ravnalici parom konkavno konveksnih valjaka upućuju na homogenu raspodjelu mikrostrukturnih parametara unutar stijenke hladno vučene cijevi. Izrezani prstenovi su upučivali na neznatnu promjenu ovalnosti.

Literatura:

1. B. Iharoš; Metalurgija 14(1972) 15 – 20.
2. B. Iharoš, Metalurgija 14(1975) 25 – 34.
3. B. Iharoš, Usavršavanje tehnologije hladno vučenih cijevi (unutrašnja naprezanja u hladno vučenim proizvodima), Institut za metalurgiju Sisak, Sisak, 1977.
4. B. A. Brusilovski, A. Y. Shasho, Mat. Sci. Heat. Treat. 43(2001) 180 – 182.
5. M. Kostelac, B. Iharoš, V. Novosel – Radović, Z. Milinović, Zbornik del za IX. Posvetovanje valjarev, Slovenske željezarne, Štore, 1990., 493 – 503.
6. V. Novosel – Radović, M. Kostelax, N. Radović, N. Hrvatov – Crljenica, Metalurgija 35(1996) 151 – 155.
7. B. E. Warren, Acta Cryst. 8(1955) 483 – 486.
8. B. E. Warren, B. L. Awerbach, J. Appl. Phys. 21(1950) 595 – 598.
9. S. Popović, Analysis of X – Ray Diffraction line Brodening, D. Grdenić and B. Kamenar (edit.) Annul. Yugoslav. Cent. Crystall. JAZU, Zagreb, 21(1986) 47 – 80.
10. T. Ungar, S. Bemstorff, I. Kopaez, E. Schafler, J. Eng. Mater. Technol. 124(2002) 41 – 47.
11. B. E. Warren, X – Ray Studies of Deformed Metals, Pergamon Press, New York, 1959., 147 – 202.
12. V. Novosel – Radović, N. Radović, N. Hrvatov – Crljenica, During straightening of cold drawn tube, Bulletin of the Chech and Slovak Crystallographic Association, Vol. 5(1998)207.
13. L. Keslens, K. Verbeken, Local strain heterogeneles after cold rolling of an ultra low carbon steel, Proc. Conf. ICOTOM, Mater. Sci. Forum, 2002., 408 – 412.

EKSPERIMENTALNO ODREĐIVANJE TEMPERATURNIH POLJA METODOM TERMOVIZIJE

Mirna Nožić
Univerzitet "Džemal Bijedić"
Mašinski fakultet
Maršala Tita bb
88 104 Mostar
BiH

Himzo Đukić
Sveučilište u Mostaru
Fakultet strojarstva i računarstva
Matice Hrvatske bb
88000 Mostar
BiH

Sažetak: U radu su dati eksperimentalni rezultati dobiveni mjerenjem temperatura u procesu izvlačenja za dva referentna stanja posmatranog sistema.
Temperaturna polja na izvlakaču, prstenovima za izvlačenje, pripremcima, izratcima i rashladnom sredstvu registrovana su pomoću termovizije.
Vrijednosti temperatura u određenim tačkama elemenata sistema, izmjerene su pomoću laserskog mjernog uređaja.

Ključne riječi: Temperaturno polje, termovizija, toplota

1. UVOD

Termovizija ili infracrvena termografija, kao metod beskontaktnog mjerenja temperature, u posljednje vrijeme nalazi veliku primjenu u inžinjerskoj praksi.
Metod se zasniva na registraciji elektromagnetnih talasa iz IC dijela spektra, koje emitira posmatrani objakat i koji se manifestuju kao toplota.
Termovizijsko snimanje omogućava praćenje razvoja toplote na ključnim tačkama posmatranog objekta. Na taj način se prati rad , te pravovremeno otkrivaju i predviđaju grešake i nepravilnosti u radu mašine, odnosno postrojenja. Pregled se obavlja pomoću prenosnih kamera koje slike iz IC dijela spektra mogu zapisivati na digitalne memorijske medije. Rezultat termovizijskog pregleda je jasna slika raspodjele toplote na posmatranom objektu, koja se zove termo slika ili termogram. Konverzijom temperature u boju, uz odgovarajuću softversku podršku, termogram može biti prikazan na računaru. Personalni računari za prikaz slike u boji koriste kombinaciju tri boje: crvene, zelene i plave. Najčešće su u upotrebi “palete boja” koje višu temperaturu predstavljaju svjetlijom bojom.

2. PRIMJENA METODE ZA REGISTRACIJU I MJERENJE TEMPERATURA U PROCESU IZVLAČENJA

Eksperimentalna istraživanja, prezentirana u ovom radu, imala su za cilj dobijanje temperaturne slike u procesu dubokog izvlačenja sa redukcijom debljine zida na višestepenim alatima. Istraživanja su provedena u proizvodnim uslovima na horizontalnim mehaničkim presama, na petostepenim alatima. Zbog specifičnosti procesa izvlačenja, kretanja i zagrijavanja alata i nepristupačnosti mjerenja, temperaturna slika može se dobiti jedino beskontaktnim mjerenjem, tj. termovizijom.
Toplota u procesu se generiše deformisanjem radnog predmeta.Obzirom da se proces odvija velikom brzinom (srednja brzina deformisanja je 1.2 m/s), vrijeme jednog izvlačenja je kratko (približno 0.1 s), proces je posmatran kao idealizirani slučaj zatvorenog sistema, izolovanog u odnosu na okolinu. Snimanje i registracija temperaturnih polja u toku procesa izvršeni su za sve elemente sistema: izvlakač, prstenove za izvlačenje, pripremke, izratke i rashladno sredstvo za dva posmatrana referentna stanja. Za snimanje je korištena kamera tipa Varioscan 3022, sa mjernim područjem koje obuhvata temperaturni interval od -10°C do 1200°C. Pored termovizijskog snimanja, izvršena su i mjerenja temperatura svih elemenata sistema u početnom i konačnom stanju, pomoću laserskog uređaja.

3. REZULTATI EKSPERIMENTA

Rezultati mjerenja temperatura u početnom stanju dati su u tabeli 1. Mjerenje temperature izvlakača vršeno je na tri mjerna mjesta (na čelu , na sredini i na vrhu).

Vrijednosti temperatura elemenata sistema u stanju “1”						
Redni broj	Temperatura izvlakača T_{i1} (°C)			Temperatura pripremaka T_1(°C)	Temperatura prstenova T_{p1}(°C)	Temperatura rashladnog sredstva T_{rs1}(°C)
	Mjerna mjesta					
	1	2	3			
1	20	21	21	22	21	29
2	22	22	22	22	21	33
3	22	21	22	22	21	33

Tabela 1. Temperature elemenata sistema u stanju “1”

Termogrami na slikama 1- 4 daju prikaz temperaturnih polja na: izvlakaču, pripremcima, prstenovima za izvlačenje i rashladnom sredstvu za početno stanje (stanje “1”).

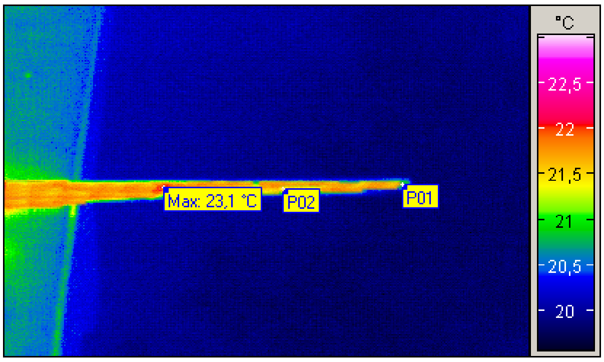

Pmax=23,1°C, P01=20,8°C, P02=21,7°C, P03=23,1°C

Slika 1. Prikaz temperaturnog polja na izvlakaču u stanju “1”

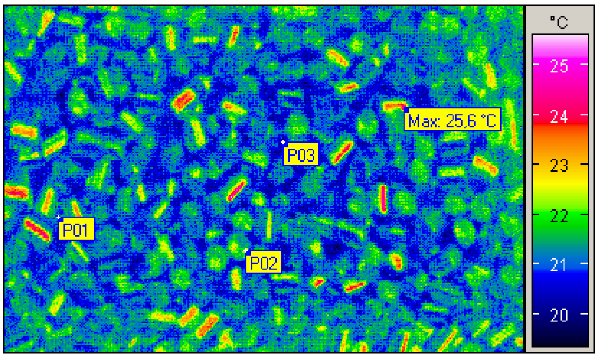

Pmax=25,6°C, P01=20,8°C, P02=21,7°C, P03=19,8°C

Slika 2. Prikaz temperaturnog polja na pripremcima u stanju “1”

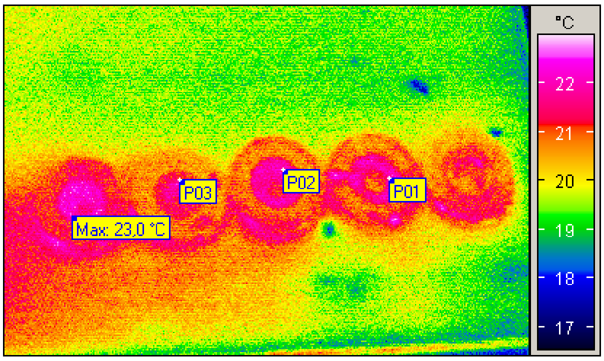

Pmax=23,4°C, P01=22,0°C, P02=21,8°C, P03=21,3°C

Slika 3. Prikaz temperaturnog polja na prstenovima za izvlačenje u stanju “1”

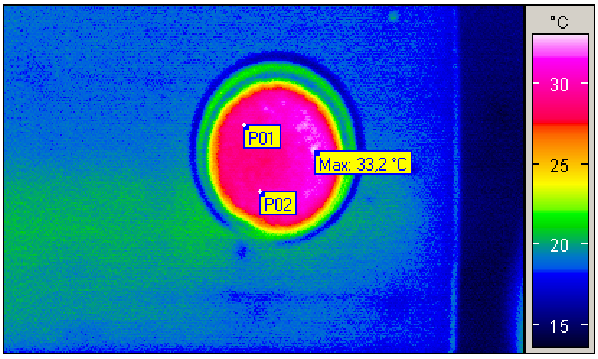

Pmax=33,2°C, P01=29,5°C, P02=29,8°C, P03=xx,x°C

Slika 4. Prikaz temperaturnog polja rashladnog sredstva u stanju “1”

U Tabeli 2. date su vrijednosti izmjerenih temperatura elemenata sistema u stanju “2”.
Izmjerene temperature prstenova date u Tabeli 2. dobivene su nakon rastavljanja alata. Obzirom da je za rastavljanje alata potrebno nekoliko minuta, u tom periodu dolazi do hlađenja prstenova, što pokazuju i rezultati mjerenja temperatura prstenova.
Stvarna temperatura prstenova mora biti usaglašena sa izmjerenim temperaturama na izvlakaču i temperaturom rashladnog sredstva.

Vrijednosti temperatura elemenata sistema u stanju “2”						
Redni broj	Temperatura izvlakača T_{i2} (°C)			Temperatura izradaka T_2(°C)	Temperatura prstenova T_{p2}(°C)	Temperatura rashladnog sredstva T_{rs2}(°C)
	Mjerna mjesta					
	1	2	3			
1	40	35	34	39	29	35
2	40	35	34	40	30	35
3	40	39	35	39	30	36

Tabela 2. Temperature elemenata sistema u stanju “2”

Slike 5 – 8 daju prikaz temperaturnih polja elemenata sistema u konačnom stanju (stanju “2”).

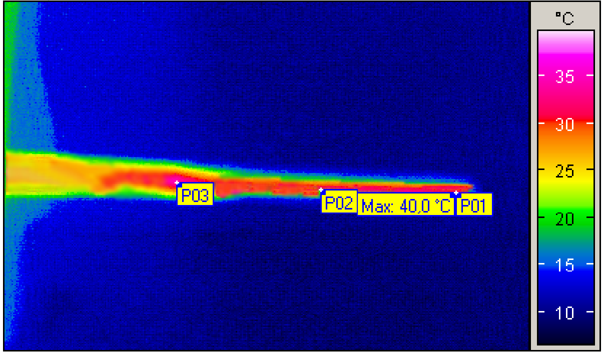

Pmax=40,0°C, P01=40,0°C, P02=35,3°C, P03=34,6°C

Slika 5. Prikaz temperaturnog polja na izvlakaču u stanju “2”

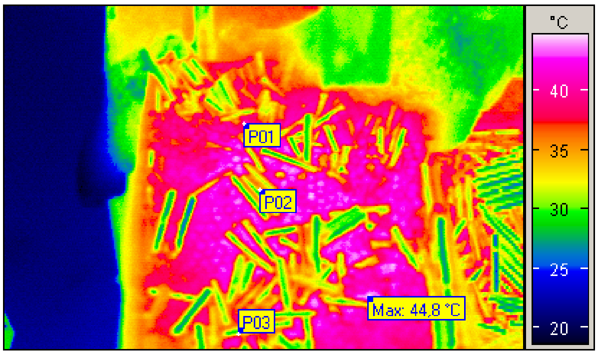

Pmax=44,8°C, P01=39,7°C, P02=33,9°C, P03=33,7°C

Slika 6. Prikaz temperaturnog polja na izratcima u stanju “2”

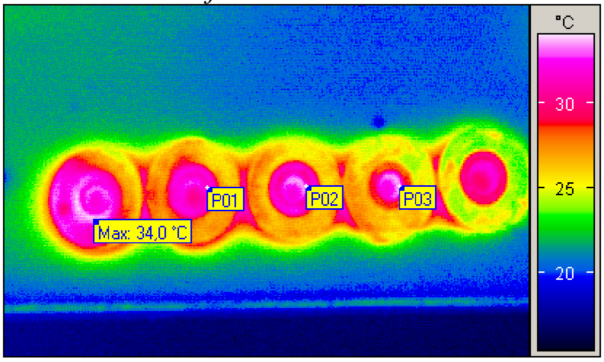

Pmax=34,0°C, P01=30,1°C, P02=30,6°C, P03=30,8°C

Slika 7. Prikaz temperaturnog polja na prstenovima za izvlačenje u stanju “2”

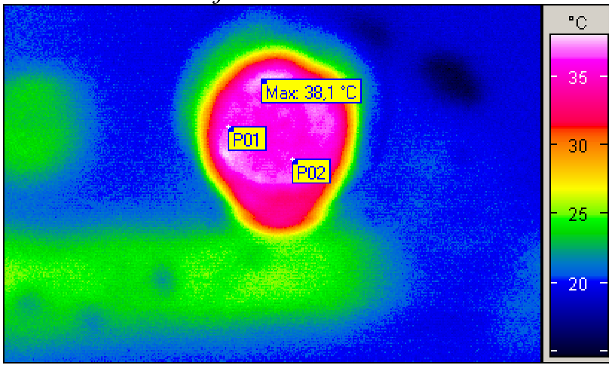

Pmax=38,1°C, P01=36,3°C, P02=36,2°C, P03=xx,x°C

Slika 8. Prikaz temperaturnog polja rashladnog sredstva u stanju “2”

4. ZAKLJUČAK

Temperaturna slika procesa izvlačenja, zbog specifičnosti procesa i problema koji se javljaju uslijed kretanja alata i nepristupačnosti mjerenja, ne može se dobiti klasičnim metodama. Termovizija omogućava brzo, lagano i jednostavno dobijanje temperaturne slike procesa. Dobiveni eksperimentalni rezultati daju izgled temperaturnih polja svih elementa sistema, sa vrijednostima u markiranim tačkama.

Poređenjem rezultata termovizije sa vrijednostima temperatura dobivenih mjerenjem pomoću laserskog uređaja, utvrđeno je dobro slaganje rezultata na izvlakaču i sredstvu za hlađenje. Niže temperature na prstenovima za izvlačenje su dobijene mjerenjem laserskim uređajem zbog rastavljanja alata nakon zaustavljanja procesa izvlačenja.

5. LITERATURA

[1] M. Nožić Prilog istraživanju pojedinačnog i ukupnog opterećenja višestepenih alata za izvlačenje sa redukcijom debljine zida, Doktorska disertacija, Mostar, 2005.

[2] M.Nožić, H.Đukić Pretvaranje mehaničke energije u toplotnu pri izvlačenju sa redukcijom debljine zida, 5th Međunarodna naučna konferencija o proizvodnom inženjerstvu “Development and modernization of production “ RIM 2005, Bihać, septembar 2005.

[3] M. Čaušević Plastična prerada metala, Svjetlost Sarajevo, 1979.

11. Savjetovanje o materijalima, tehnologijama, trenju i trošenju
11. Conference on Materials, Processes, Friction and Wear
MATRIB'06, Vela Luka, 22-24.06.2006.

PREPARATION OF HIGLY POROUS HYDROXYAPATITE CERAMICS FROM CUTTLEFISH BONE

S. Orlić, H. Ivanković, and E. Tkalčec
[1]University of Zagreb, Faculty of Chemical Engineering and Technology, Zagreb, Croatia
sorlic@fkit.hr, hivan@fkit.hr , etkalcec@fkit.hr

Abstract: Hydroxyapatite, $Ca_{10}(PO_4)_6(OH)_2$, has been widely investigated for medical purposes because it is suitable for either direct clinical use as implants or tissue-engineering applications. In this work materials were successfully produced via hydrothermal transformation of aragonite, obtained from fresh cuttlefish bones, at 200°C and high pressures. Beyond low production cost, worldwide availability and natural–biological origin of raw materials, the produced materials have ideal pore size and interconnectivity features suitable for supporting biological activities, such as bone tissue growth and vascularization. The cuttlefish bone (*Sepia officinalis L.)* from Adriatic Sea was used. The samples of cuttlebone were pretreated, boiled with NaClO in order to remove the organic phase of the bone to accelerate the conversion. The substitution of CO_3^{2-} groups predominantly into the PO_4^{3-} sites of the HAP structure was determined by FTIR spectroscopy. SEM micrographs have shown that the interconnected hollow structure with pillars connecting parallel lamellae in cuttlefish bone is maintained after conversion. Specific surface area (S_{BET}) and total pore volumes increased and mean pore size decreased by high temperature treatment.

Keywords: Scaffold, Cuttlefish bone, Hydroxyapatite, Microstructure.

Introduction

Bioceramics are a group of ceramic materials that are specially developed for use as medical and dental implants. An important member of this group is hydroxyapatite /$Ca_{10}(PO_4)_6(OH)_2$/. It is the main inorganic component of hard tissues of the bones, and it accounts for 60-70% of the mineral phase in the human bone. Due to its similarity with the mineral phase of bone has been studied for many years as implant material [1]. In recent years, particular attention was paid to the synthesis of Hap ceramic with porous morphology required for vascularization, bone cell invasion, and angiogenesis, which further improve its biomedical properties. Artificial implants of Hap are very popular for hard tissues restorations because they accelerate bone growth around the implant. Such materials should have porosity and compression strength similar to the tissues they will substitute, in order to assure bioactivity and biocompatibility [2]. The use of natural inorganic structures and materials for medical purposes has been motivated by limitations in generating synthetic materials with the requisite structure and mechanical integrity. The hydrothermal method for hydroxyapatite formation directly from corals was first used by Roy and Linnehan [3] in 1974. They reported that complete replacement of aragonite by phosphates was achieved at 270°C and 103 MPa. Kasperk and Ewers [4] prepared hydroxyapatite from calcified algae in 1986. Tkalcec et al. [5] prepared Hap hydrothermally from Adriatic shells Arca Noae in 1989. HAp derived from Indian coral using hydrothermal synthesis was developed by Sivakumar et al. in 1996 [6]. However, the resultant materials were in the form of powder and required further forming and shaping. Scaffolds of HAp from cuttlefish bones via hydrothermal transformation were first synthesized in 2005 [7].

The aim of the present work is to study the hydrothermal conversion of the aragonite (calcium carbonate) of cuttlefish bones, which is structured to combine high compressive strength with high porosity and large pore dimension, into HAp retaining its overall structure after conversion.

Materials and experimental procedure

Bone of cuttlefish (Sepia Officinalis L.) from Adriatic sea were gently cut in small pieces (about 2 cm^3) and boiled with 4% NaClO in order to remove the organic component. The samples were then sealed with the 15 mL aqueous solution of 0.6M $(NH_4)_2HPO_4$ (stoichiometrical amount) in teflon lined stainless steel pressure vessel at 200 °C for various times (1 to 48 hours). The converted HAp was washed with boiling water and dried at 110 °C. The micro-structure of boiled and hydrothermal treated (HT) cuttlefish bones were examined by scanning electron microscopy (SEM ISIDS-130). The conversion of aragonite into HAp was followed by X-ray diffraction analysis (Philips PW 1820 counter diffractometer with monochromatized Cu Kα radiation). Fourier transform infrared spectra (FTIR) were performed by attenuated total reflectance (ATR) spectroscopy for solids with a diamond crystal. Specific surface area and mean pore size were determined by nitrogen adsorption-desorption isotherms at liquid N_2 temperature on a Micromeretics ASAP 2000 instrument. The mean pore size was estimated from the desorption branch of the nitrogen adsorption-desorption isotherms by the Barrett-Joyner-Halenda (BJH) method.

Results and discussion

The specific surface area, mean pore size and total pore volume of raw cuttlefish bones and converted Hap is shown in Table 1. The monoliths about 1 cm^3 large were used for the analysis. The specific surface area, S_{BET}, of raw material is 2.5 m^{2}g^{-1}. When the samples were boiled with NaClO, incomplete removal of organic component reduced it to 0.6 m^{2}g^{-1}, but after hydrothermal treatment it increased to 9.9 m^{2}g^{-1}.

The conversion of aragonite into hydroxyapatite was followed by XRD analysis (Fig. 1) and FTIR spectroscopy (Fig. 2). The raw cuttlefish bone comprises pure aragonite which gradually converts into HAp by treatment with $NH_4H_2PO_4$ under hydrothermal conditions described above. The positions of aragonite lines correspond to JCPD file No 41-1475. The product after hydrothermal treatment was identified to be hydroxyapatite (JCPDS 09-0432).

Table 1. Specific surface area, mean pore size and total pore volume of raw cuttlefish bone and hydrothermally converted Hap

Cuttlefish bone	S_{BET} (m^{2}g^{-1})	Mean pore size (nm)	Total pore[a] volume (cm^3/g)
Raw	2.5	20	0.0134
Boiled with NaClO	0.6	26.5	0.0039
HAp 200°C/24 h	9.9	19.2	0.0489

[a] estimated using BJH desorption branch of the isotherms.

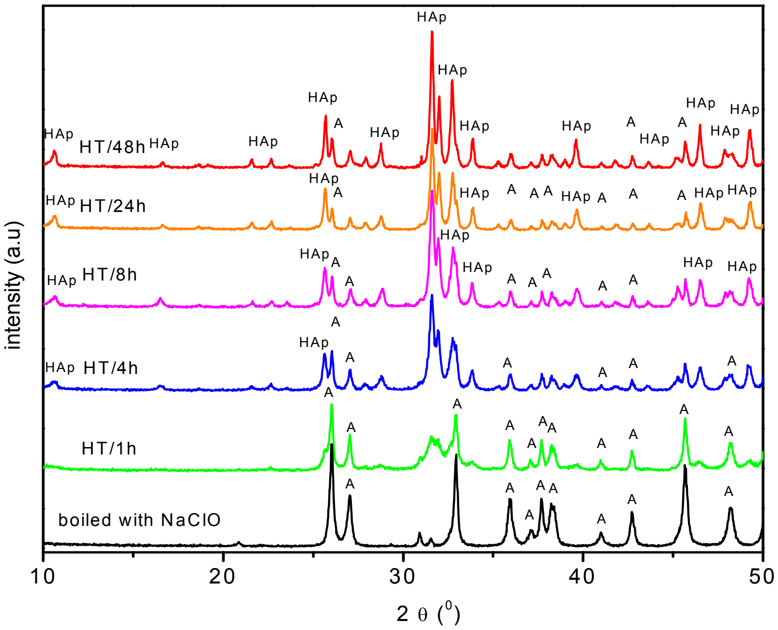

Fig. 1. XRD patterns of hydrothermally (HT) converted HAp at various times (1-48 h). The A and HAp symbols are the 2θ positions of aragonite (JCPDS 41-1475) and hydroxyapatite (JCPDS 09-0432).

XRD analysis showed that the amount of HAp increased with time but the complete conversion has not been reached even after 48 h.

In FTIR spectrum of cuttlefish bone boiled with NaClO (Fig. 2) only absorption bands of CO_3^{2-} functional groups in aragonite were seen (871, 1632, 1547, 1455, 712, 710 cm^{-1}) [8]. HT treatment at 200 °C for 1 hour caused the appearance of the bands assigned to PO_4^{3-} groups (ν_3—1085 and 1010 cm^{-1}; ν_1—960 cm^{-1}; ν_4—558 and 597 cm^{-1} and ν_2—473 cm^{-1}) The bands attributed to OH^- groups (631 cm^{-1}) and CO_3^{2-} groups substituted for PO_4^{3-}, respectively, (871 cm^{-1}, 1454 and 1414 cm^{-1}), [9] were seen in sample after HT treated at 200 °C for 8 hours. The intensities and the resolution of bands increased with the time of HT treatment. In sample treated for 48 hours the band at 1544 cm^{-1} due to the CO_3^{2-} groups substituted for OH^- [10] were also observed.

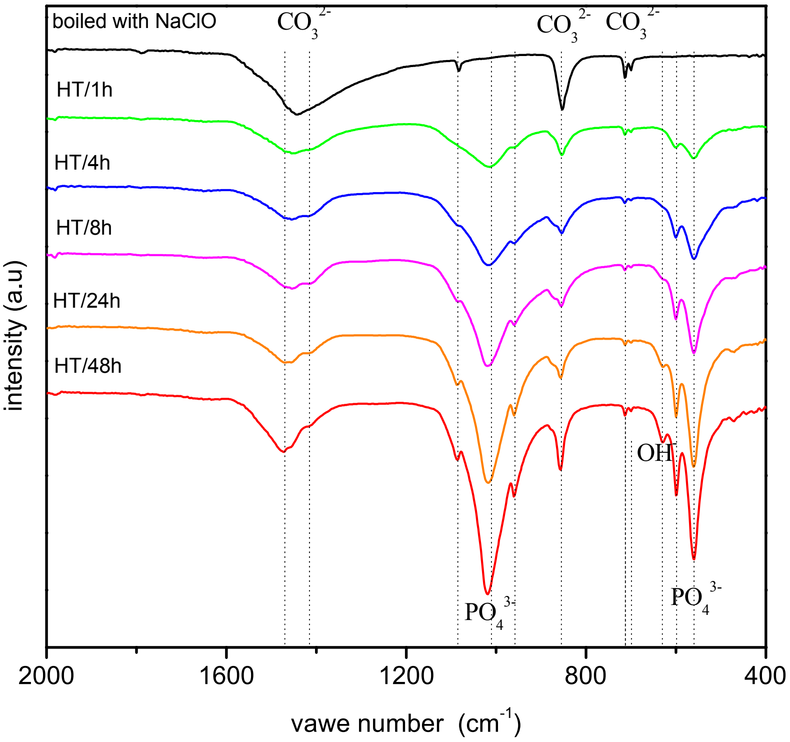

Fig. 2. FTIR spectra of cuttlefish bones boiled with 4% NaClO and hydrothermally transformed in HAp at various conditions.

Microstructure of the cuttlefish bone boiled with NaClO is shown in Fig. 3(A). The organic material enveloped the bones is partially removed by boiling. The cuttlebone (which accounts about 9 % of the animal's volume is a hollow structure, divided by parallel sheets (lamellae) which form chambers sealed from each other. The spacing of the lamellae is about 200 µm, as seen in Fig. 3(A), but it varies in different areas of the cuttlebone; usually between 200 and 600 µm. The lamellae are supported by numerous pillars which have sigmoidal cross-section. The higher magnification (insert) shows that the columns have a corrugated appearance with pore size in nanometer range.

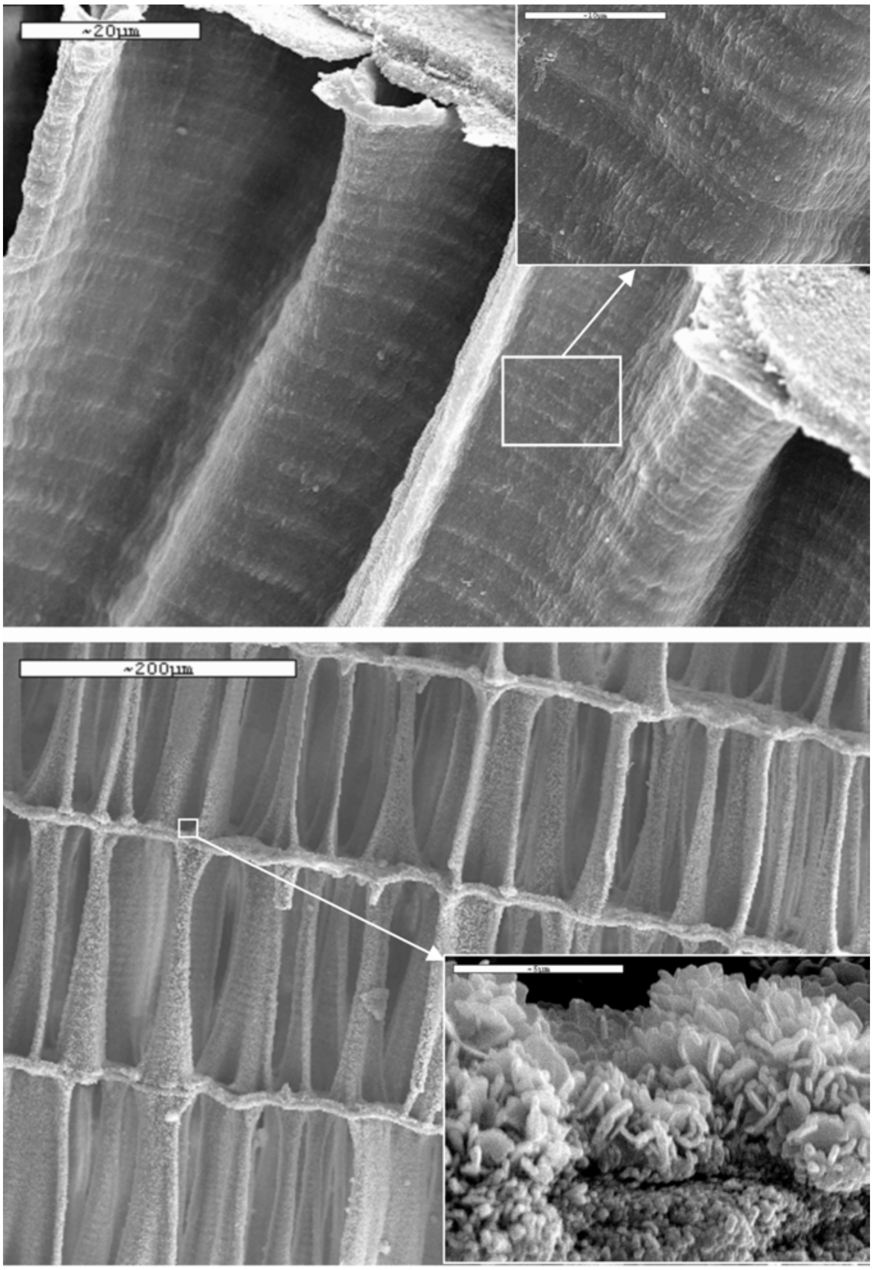

Fig. 3. SEM micrographs of (A) cuttlefish bone boiled with NaClO. The corrugated appearance of the pillars is shown in the insert. (B) the cuttlefish bone after hydrothermal conversion at 200°C/24 h showing the plate – and needle – like HAp crystals (insert). The conversion did not complete and on the surface of lamellae there is still aragonite structure.

The corresponding micro-structure converted HAp is shown in Fig. 3(B). The same hollow interconnected structure of cuttlefish bone is retained during the HT conversion. As seen at higher magnification (insert) the plate- and needle-like HAp crystals are formed. The microstructure explains the high porosity of cuttlefish bones measured by mercury porosimeter (about 90%) and is in agreement with literature [10]. the increase of S_{BET} and total pore volume decreasing the mean pore size (Table1).

Conclusion

Hydroxyapatite, $Ca_{10}(PO_4)_6(OH)_2$, has been produced via hydrothermal treatment. Aragonite samples ($CaCO_3$) from cuttlefish bone were transformed into HAp by hydrothermal reaction with $NH_4H_2PO_4$ inside sealed autoclaves at 200°C for various times (1-48 hours). FTIR spectra show the characteristic bands of Hap. Hydrothermal conversion retains the interconnected channeled structure of cuttlefish bone while altering the chemical composition from aragonite to hydroxyapatite. Plate- and needle-like crystals of HAp were formed on the surface of lamellae but there is still easy to detect aragonite structure because the reaction did not complete under specific conditions. The specific surface area (S_{BET}) and total pore volume is increased and mean pore size decreased by HT treatment.

The porosity of the cuttlefish bones is measured by mercury porosimetry to be about 90 wt% and is in agreement with literature [10].

References

[1] R.Z. Le Geros, in P.W. Brown, B. Constantz, (Ed.) Hydroxyapatite and related Materials, CRC Press, Boca Raton, 1994.

[2] L.L Hench, World Scientific, London, 1993..

[3] D.M Roy, S. K Linnehan, Nature, 274, (1974), p. 220.

[4] Ch. Kasperk, R. Evers. Zahnaertzl. Implant 2 (1986) 234.

[5] E. Tkalcec, N. Vrbos, and D. Navala, First ECERS, Vo 3 (1989) 3.37 .Ed. G. De With, R.A Terpstra and R. Metsellar, Elsevier Applied Sci.

[6] M.S Sivakumar, T. S Sampath, K.L Kuwar, K.Shanta, Rao Panduraga, Biomaterials, 17 (1996) p.1709.

[7] J.H.G. Rocha, A.F. Lemos, S. Agathopoulos, P. Valerio, S. Kannan, F.N. Oktar, J.M.F. Ferreira: Bone 37 (2005), p.850.

[8] Ch. Linga Raju, K. V. Narasimhulu, N. O. Gopal, J. L. Rao, B. C. V. Reddy, J of Molecular Structure, 608, (2002), p.201

[9] H.L. Felki, J.M. Savariault, A. Bensalah, J Alloys & Compounds, 287 (1999) p.114.

[10] E. Landi, G. Celotti, G. Logroscino,A. Tampieri, J. Eur. Ceram. Soc., 23 (2003) p. 2931.

[11] J.D. Birchall, N. L. Thomas, J. Mater. Sci., 18 (1983) p. 2081.

EVOLUTION OF NEAT OILS FOR STEEL COLD DEFORMATION PROCESSES

RAZVITAK ULJA ZA OBRADBU ČELIKA HLADNIM DEFORMIRANJEM

Ljiljana Pedišić, Marina Šviglin Marasović, Anđelko Lepušić
MAZIVA-ZAGREB Ltd., INA Group, Radnička cesta 175, Zagreb, Croatia

Abstract: Metalworking fluids for steel working processes are expected to show a high level of performance especially in control tribological effects. As producers of metalworking fluids constantly develop the products based on new facts about chemicals there is need for development of new products according to specific requirements of severe processes as are steel wire cold deformation and cutting operations.
The development of metalworking oils was very much affected by the abolishment of chlorinated paraffin widely used EP additive through "negative lists" or environmental laws. Under boundary lubrication conditions, where chlorinated-paraffin was irreplaceable EP additive for a number of years, a proper substitute is still being sought.
This paper shows the results of laboratory examinations of several functional additives and also metalworking oils, less harmful to the environment. That oil is developed for application at complex process of small pieces production from steel wire.

Key words: metalworking fluids, additives, tribological effects, deformation, steel wire

Sažetak: Od tekućina za obradbu čelika zahtijevaju se visoka radna svojstva a posebno svojstva upravljanja tribološkim učincima. Kako proizvođači tekućina za obradbu metala kontinuirano razvijaju proizvode na osnovu novih saznanja o kemikalijama, postoji potreba i za razvitkom novih proizvoda prema specifičnim zahtjevima zahtjevnih procesa kao što je obradba čelične žice operacijama hladnog deformiranja i rezanja. Na razvitak tekućina za obradbu metala uvelike je utjecala zabrana primjene klorparafina široko primjenjivanog aditiva za nošenje visokih pritisaka kroz tzv. negativne liste ili zakone zaštite okoliša. U uvjetima graničnog podmazivanja gdje je klorparafin dugo godina bio nezamjenjljiv aditiv, pravi zamjenski aditiv još uvijek se traži.
Ovaj rad prikazuje rezultate laboratorijskih ispitivanja nekoliko funkcijskih aditiva a također i ulja za obradbu metala a koji se smatraju manje štetnima za okoliš. Ovo ulje je namijenjeno za primjenu pri kompleksnom procesu proizvodnje sitnih dijelova različite geometrije iz čelične žice.

Ključne riječi: tekućine za obradbu metala, additivi, tribološki učinci, deformiranje, čelična žica

1. INTRODUCTION

At metal working operations, heat is generated between the tool and the workpiece. The cause of heat generation is friction and material resistance to the deformation created in the shear zone. The generated heat usually has a negative impact on the development of tribological effects on the tool and the workpieces [1]. High temperature and high pressures on contact surfaces cause unwanted occurrences, such as uncontrolled metal microstructure below the worked area, looses in dimension, increased tool wear, etc. The tool looses its mechanical properties, particularly its hardness, thus becoming less resistant to wear. All this leads to increased production costs. The application of proper metalworking oil considerably reduces friction of contact areas, as well as temperature in the treatment zone, tool wear, energy consumption, and finally overall metalworking costs.

The phenomenon of deformation of a metallic material is a complex collection of many processes happening simultaneously. The basic principles can be presented schematic as is shown in Figure 1. Fundamentally what occurs in individual crystals and in the lattice structure is the same for all stresses. The changes on a larger scale, in the whole sample, for example, are dependent on the method of deformation being used. Cold drawing forms metal wire from a pre-rolled or pre-drawn condition into a secondary or final shape by pulling it through precision draw dies. Cold drawing is used to form precision geometric shapes with tight dimensional tolerances. Forging is different from drawing, and bending is not the same as riveting. Production of different shape workpieces from wire is complex and requires several types of those metalworking operations.

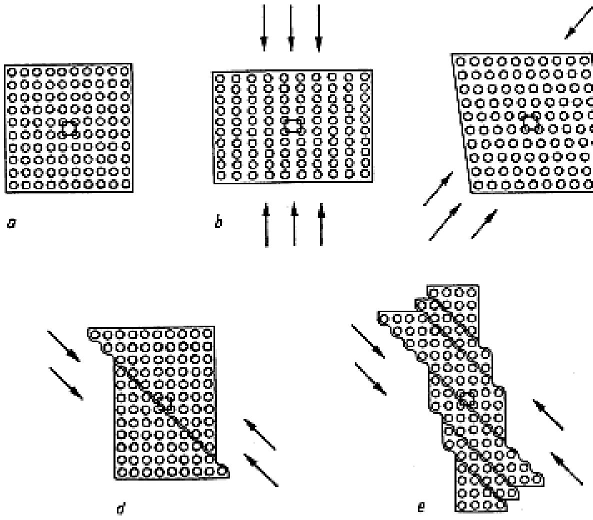

Figure 1. Change of lattice structure with deformation
a) Original state, b) Elastic deformation with vertical force applied, c) Elastic deformation with diagonal force applied, d) The beginning of plastic deformation upon a slip plane, e) Deformation proceeding upon further slip plane

2. METALWORKING FLUIDS CLASSIFICATION

Metalworking fluids, according to application form, are classified in two main types. First type are non watermiscible fluids called neat or straight oils that applied straight without additional mixing. The other types are fluids that are applied mixed with water called watermiscible fluids. For severe conditions of metalworking operations like are steel wire drawing, stamping, etc. it is recommended application of neat metalworking oils. Neat metalworking oils are recommended for metals, which are hard to machine, as well as for low working velocities.

International standard ISO 6743/7 Lubricants, industrial oils and related products (Class L) Family M (Metalworking) classified lubricants for metalworking in two main groups. First includes operations primarily needing lubrication-MH symbols, and the second operations primarily needing cooling-MA symbols. According to field of application ISO 6743/7 metalworking products are classified into eight categories as is presented in Table 1. Those are: cutting, abrasion, electro discharge machining, sheet metal forming, ironing and power spinning, wire drawing, forming and stamping, and rolling. Table 2 shows main product types, end use requirements and orientation composition of metalworking lubricants for operations primarily needing lubrication. Deutschland industry norm DIN 51385 select metalworking lubricants in three groups: non watermiscible fluids (SN), watermiscible fluids (SE), and fluids mixed with water (emulsions SEMW, solutions SESW).

In general products can be classified according to its composition, application or environmental impact like are chlorine free formulations, nitrite free, boron free, biodegradable, grinding and drawing products and others.

Table 1. Categories distribution of family M products according to field of application, ISO 6743/7

ISO-L categories	Operations							
	Cutting	Abrasion	Electro-discharge machining	Sheet metal forming	Ironing, power spinning	Wire drawing	Forming, stamping	Rolling
MHA	●		●					●
MHB	●			●	●	●	●	●
MHC	●	●		●		○	○	
MHD	●			●				
MHE	●	●		●				
MHF	●	●		●				
MHG				●		●		
MHH						●		
MAA	●			●				○
MAB	●			●		●	○	●
MAC	●			○		○		
MAD	●			●	●			
MAE	●	○						
MAF	●	○						
MAG	○	●		○			●	●
MAH	●	●					●	
MAI				●		●		

● = Main application, ○ = Possible application

Table 2. Classification of metalworking lubricants ISO 6743/7, operations primarily needing lubrication

Particular application	Product type and/or end use requirements	Symbol ISO-L	Remarks
Metal removal by cutting, abrasion or electrical discharge and metalforming by punching, deep drawing, ironing, power spinning, wire drawing, forging-hot and cold, extrusion, stamping, cold rolling	Fluid which may have anticorrosion properties	MHA	These fluids which are used undiluted may be inhibited against oxidation or may contain filers for particular forming operations
	Fluid of MHA type with friction reducing properties	MHB	
	Fluid of MHA type with extreme pressure (E.P.) properties, chemically non-active	MHC	
	Fluid of MHA type with extreme pressure (E.P.) properties, chemically active	MHD	
	Fluid of MHB type with extreme pressure (E.P.) properties, chemically non-active	MHE	
	Fluid of MHB type with extreme pressure (E.P.) properties, chemically active	MHF	
	Greases, pastes, waxes, applied pure or diluted with a fluid of MHA type	MHG	May contain a filler for particular applications
	Soaps, powders, solid lubricants, etc., and blends thereof	MHH	These products are applied without dilution

3. FORMULATION OF METALWORKING OILS

Neat metalworking oils (also known as straight oils and cutting oils) mostly consist of the base oil, mineral, natural or synthetic (60 - 98 %), and the necessary additives for improving the lubricant's properties [2]. Additives are used in the share ranging from 2-30 %, depending on application requirements. The variations in composition of lubricating oil directly affect lubricant performance.

According to its' working mechanism additives are classified into two main groups. Those are:

- polar additives, that react with physical and chemical adsorption on metal surface and
- AW/EP (antiwear and extreme pressure) additives that react chemically with metal surface building chemical compounds like sulphides, phosphides, etc.

In Table 3 are presented main types of additives for metalworking oils and typical compounds.

Table 3: Lubricant additive types and typical compounds used in metalworking oils

ADDITIVE TYPES	TYPICAL COMPOUNDS
Detergents (Metallic Dispersants)	Salicylates, Sulfonates, Phenates, Sulfophenates
Ashless Dispersants**	N-substituted long-chain alkenyl succinimides , High-molecular-weight esters and polyesters, Amine salts of high-molecular-weight organic acids, *Copolymers of methacrylic or acrylic acid derivatives containing polar groups: amines, amides, imines, imides, hydroxyl, ether, etc., *Ethylene-propylene copolymers containing polar groups as above
Oxidation and Corrosion Inhibitors	Organic phosphites, Metal dithiocarbamates , Sulfurized olefins, Zinc dithiophosphates
Antioxidants	Phenolic compounds, Aromatic nitrogen compounds. Phosphosulfurized terpenes
AW/ EP Additives ***	Organic phosphates, acid phosphates, Sulfurized olefins, Zinc dithiophosphates, Alkaline compounds as acid neutralizers, Petroleum sulfonates, Chlorinated paraffine
Surface active or polar additives***	Natural fatty oils Fatty oils and derivatives Synthetic esters

(*Also viscosity modifiers, ** Also emulsifiers, ***Also friction modifiers)

In boundary lubrication, where film thickness is of the same order of magnitude as the combined surface roughness, the interaction of lubricant component with the metal surface is important [3]. The key physical parameter of the lubricant in this lubrication regime is the coefficient of friction of the resulting boundary layer. In Figure 2 with Stribeck curve is illustrated influence of lubricant parameters (viscosity x speed/load) on friction coefficient.

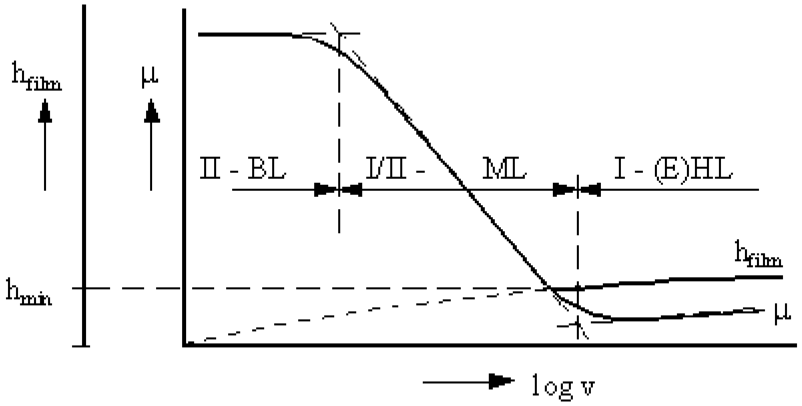

Figure 2. Stribeck lubrication curve
I - (E)HL = (Elasto)Hydrodynamic Lubrication; II - BL = Boundary Lubrication; I/II - ML = Mixed Lubrication

In boundary and mixed lubrication regimes, where load between opposite metal surfaces is very high, it is need for additive activation due to friction decreasing [4]. It is clear that is necessary to add several components to the oil to achieve higher lubricating properties in range of severe metalworking operation like are threading, cutting, stamping, etc. Characteristic for boundary lubrication is the absence of hydrodynamic pressure [5]. In mixed lubrication regime hydrodynamic pressure is build up in the lubricant when the speed increases. Characteristic for mixed lubrication is that the loading is carried by a combination of the hydrodynamic pressure and the contact pressure between the asperities of both surfaces. It is the intermediate region between boundary lubrication and hydrodynamic lubrication.

In elastohydrodynamic lubrication at high speed the hydrodynamic pressure increases such that the surface asperities are completely separated by a lubricant film. Characteristic for hydrodynamic lubrication is that the load and hydrodynamic pressure are in equilibrium. In that regime where metal surfaces are not in contact it is not necessary additive activation, and lubrication performed by low viscosity oil.

The development of metalworking oils was very much affected by the abolishment of chlorinated paraffin through “negative lists” or environmental laws [6, 7, 8]. Reduction or even complete prohibition guidelines are provided through product development and waste oil management. To save energy and resources use of mineral oils decrease and change with renewable products like are vegetable or animal oils. Under boundary lubrication conditions, where chlorinated-paraffin was irreplaceable EP additive for a number of years, a proper substitute is still being sought for example phosphorus compounds [9]. Among the possible solutions’ are overbased petroleum sulfonates [10, 11]. Dialkyl dithiophosphates are very effective in reducing the drawing force by improving the frictional properties of the lubricant [12].

4. EXPERIMENTAL

4.1. Objectives

The objective of this work is development of new metalworking oil for severe application conditions at production of small parts from wire by deformation and also cutting processes. New oil should not contain chlorinated compounds as additive. Also need perform high level of performances even higher than commonly used referent oil.

4.2. Test methods for metalworking fluid examination

Metalworking fluids are tested at the development stage and also during application at metalworking operation. For examination physical and chemical properties of additives and metalworking fluids we used standard methods like DIN, ASTM and they presented in tables with the properties [13].

Lubrication properties or anti wear and extreme pressure properties (AW/EP) of additives and metalworking fluids are tested at mechanical dynamical test machines as is shown in Table 4.

Four-ball wear test, method ASTM D 4172, describes a test method using three hard steel balls in a locked position. A fourth ball is rotated against the three stationary balls, producing a wear scar on each of the three balls. Four metal balls are placed in test fluid, heated to 75 ^{0}C. The top ball rotates at standard load (40 kg) for 60 min. After one-hour test running, scar area diameter of test balls are measured and showed as average value. This test is run at light loads. Seizure or welding usualy does not occur. Wear test is used to determine relative wear preventing properties of lubricants operating under boundary lubrication conditions.

Four-ball EP test, method ASTM D 2783, describes a similar test as the Four-ball wear test except that the loads are much higher, and load is increased till welding point. The weld load

test is a series of ten second runs where the loading is increased at specified intervals until the rotating ball seizes and welds to the other balls. The load at which the balls weld together is referred as the weld load or weld point. EP lubricant with EP additives that shows high weld point results in a high load carrying ability.
For metalworking fluids examination widely used is non standard test known as Reichert balance machine. Basic construction consists of static metal roll and rotated ring immersed in test fluid. By this method wear scar surface on test roll is measured and also specific surface pressure, MNm^{-2}. This test is running at light loads and at mixed and boudary lubrication condition. Reichert balance is apparatus that measure ability of specific load carrying capacity that occurs at metal surfaces contact.

Table 4. Operating condition of test machines for evaluation of lubricant mechanical properties

Test machine	EP-4 BALL	Wear-4 BALL	REICHERT BALANCE
Methods	ASTM D 2783	ASTM D 4172	REICHERT
Tribological elemets	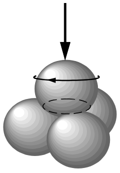		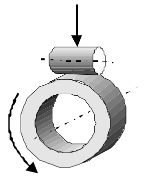
Metal	STEEL AISI-E-52 100		Steel, 100 Cr6
Diameter, mm	12.7 ball's		12.0 roll's
Speed, s^{-1}	Upper ball: 29.5	Upper ball: 20	Ring, 15
Load, N	Up to 8000	400	300
Test temperature, ^{0}C	20 ± 5	75 ± 1	20±5
Test time	10 ± 0.2 s	1 h	60 s / or 100 m sliding contact
Measured properties	Weld point, N	Wear scar diameter, mm	Wear scar surface, mm^2 Specific surface pressure, MNm^{-2}

4.3. Test metalworking oils and additives

In laboratory we mixed several new metalworking fluids in accordance to new environmental and safety requirements. For base component we used mineral oils paraffinic type with lowered aromatic molecules ($C_A < 6$ %) in combination with vegetable oil AD D and different types of additives. Additives with function of improving lubrication properties of oils are: AD B = high-sulfur content polysulfide-active (32 % S), AD C = sulfurized vegetable fatty acid ester-nonactive (10 % S), AD-PH and AD-P = phosphorus additives. As AW/EP additive for replacement of chlorinated paraffin we examined AD S4 calcium petroleum sulfonate based on natural raw material. AD Cl is chlorinated paraffine with 64 % chlorine commonly used for neat metalworking oils. The physical and chemical properties of test additives are presented in Table 5. Approximately compositions of test metalworking oils and examination results of theirs basic physical chemical properties are shown in Table 6.

Table 5. Physical and chemical properties of test additives

ADDITIVE	AD S4	AD P	AD PH
Appearance and colour	Liquid high viscous dark brown	Viscous amber liquid	Amber to light green liquid
Density, 15^0C, g/ml, ISO 3675	1.22	1.07	1.17
Sulphur content, %, X-Ray	1.4	-	20
Calcium content, %, X-Ray	15	-	-
Phosphorus content, %, ICP	-	9.5	9,5
Acid value, mgKOH/g, ISO 6618	-	350	180
TBN, mgKOH/g, ISO 3771*	400	-	-
Viscosity at 100^0C, mm^2s^{-1}, ISO 3104	75	700	14
Solubility, Water/Oil	-/+	-/+	-/+
Composition	Overbased petroleum sulphonate	Alkyl phosphate	Zinc dialkyl dithiophosphate

*TBN=total base number

Table 6: Composition of test metalworking oils and examination results of basic physical chemical properties

Composition /Test formulation	REF.	F-AM 100	F-AM-P	F-NMP-5	F-NMP-P
Base oil paraffinic type	++++	++++	++++	>> ++++	>> ++++
AD D, fatty oil natural, vegetable	++++	++++	++++	+++	+++
AD B, sulfurized oil, active	+	+++	+++	-	-
AD PH, phosphorus additive	yes	+	-	++	-
AD P, phosphorus additive	-	-	+	-	++
AD S4, petroleum sulfonate Ca	-	++	++	+++	+++
Corrosion, Cu,3h,100 ^{0}C, ISO 2160	4a	4a	4a	1b	1b
Viscosity at 40 ^{0}C, mm^2s^{-1}, ISO 3104	100	100	100	5	5

++++ = 30-50 %, +++ = 3 - 5 %, ++ = 1,5 - 2 %, + = 0.2 - 0.6 %

5. RESULTS AND DISCUSION

The examination results of additive influences on dynamical mechanical properties are presented in Figures 3, 4 and 5. Figure 3 shows weld point of additives mixtures at different concentration in mineral oil paraffinic type. The highest values shows formulations with additive AD B sulfurized active fatty ester. Polar additive AD D, vegetable fatty oil, has no influence on welding point. AD S4 shows higher values of weld point in comparison to mixtures with AD Cl (chlorinated paraffine).

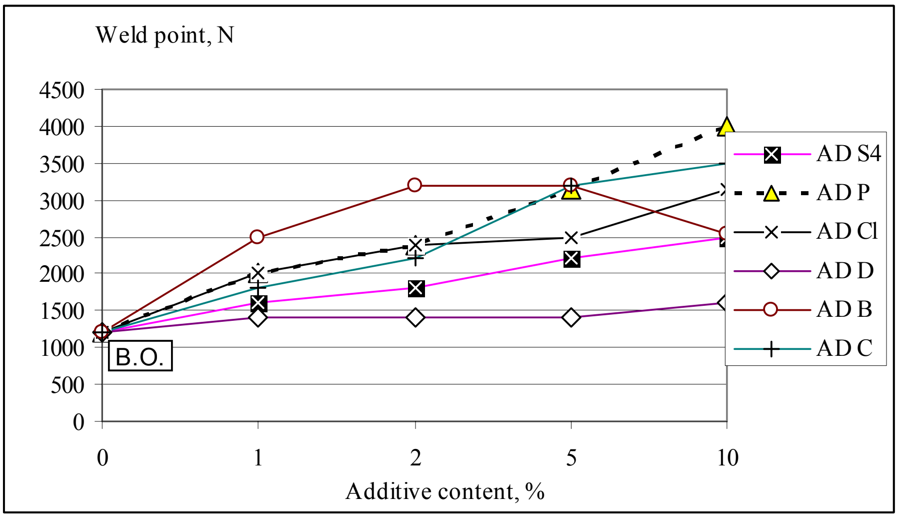

Figure 3. Influences of test additives content in base oil on Weld point, ASTM D 2783

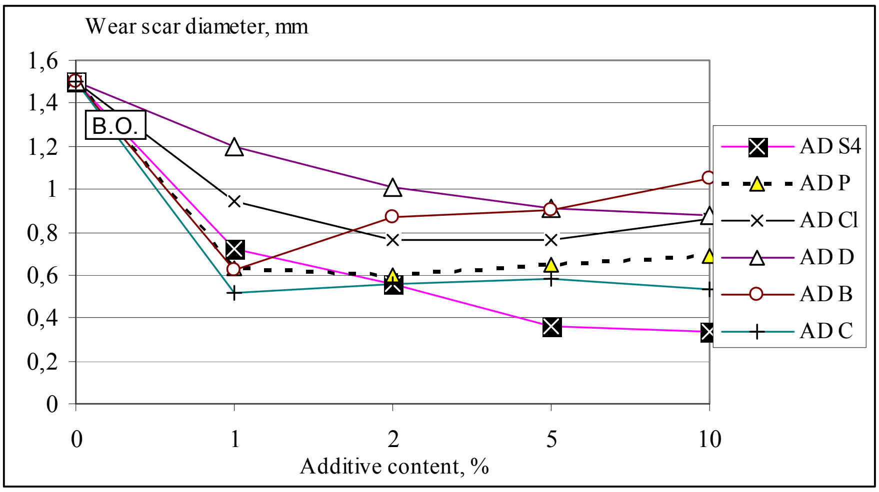

Figure 4. Influences of test additives content in base oil on Average wear scar diameter, ASTM D 4172

The results of wear test according ASTM D 4172 method are presented at Figure 4. It is obvious that all additives improve properties of base oil. At lower concentrations the best properties shows AD C and that value has no further improvement with increasing concentration. Mostly of additives show increasing wear scar diameter by increasing concentration. By increasing concentration of additives AD D and AD S4 wear scar diameter is decreased.

Additives influences on wear scar surface determined at Reichert balance test machine are presented in Figure 5. Additive AD D has no influence on this property; AD S4 has significant influence at higher concentration and all other decrease wear even at low concentration.

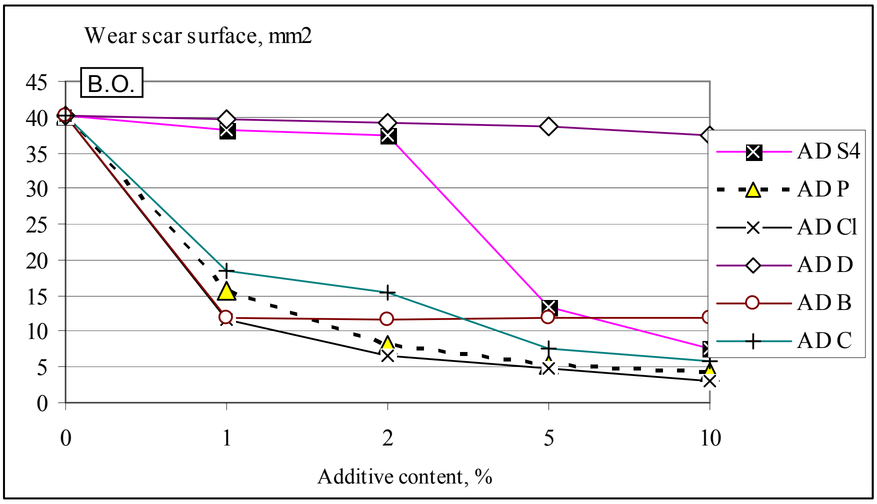

Figure 5. Influences of test additives content in base oil on Wear scar surface, Reichert test

The result of mechanical dynamical properties examination of test metalworking formulations are presented on Figures 6, 7, 8 and 9. Composition of test oils and some physical and chemical properties are shown in Table 6. In Table 7 are presented examination results of mechanical dynamical properties of final test oils. That are the best formulations produced in laboratory according to all required physical, chemical and working properties.

Table 7: Examination results of mechanical dynamical properties of test oils

Properties /Formulation	REF.	F-AM-100	F-NMP-5	F-NMP-P
Weld point, N, ASTM D 2783	8000	8000	3150	2000
Wear scar diameter, mm, ASTM D 4172	0.78	0.56	0.46	0.49
Wear scar area, mm^2, Reichert balance	2,2	2,2	9,4	15,0
Specific surface pressure, MNm^{-2} , Reichert balance	136.4	136.4	31.9	20

Basic formulation F-NMP is mineral oil inactive type with AD S4, AD D and two types of phosphorus additives, AD P and AD PH. Higher properties of load carrying capacity showed formulation based on AD PH at all tests. Basic formulation F-AM is active type metalworking oil mixed type (mineral oil and natural fatty oil) with EP (Extreme pressure) properties designed for working ferrous materials especially steel. Active type is graded according to corrosion at Cu, 100^0C, 3h (ISO 2160) minimum grade 4a and inactive corrosion grade maximum 1b. Formulation F-AM-P showed problem of components' poor compatibility through oil turbidity. Additive AD P is not compatible with natural base oil i.e. AD D, and because of that F-AM-P examination is stopped. Conventional additives that had been developed for mineral oils are not always effective for esters, synthetic or natural [14].

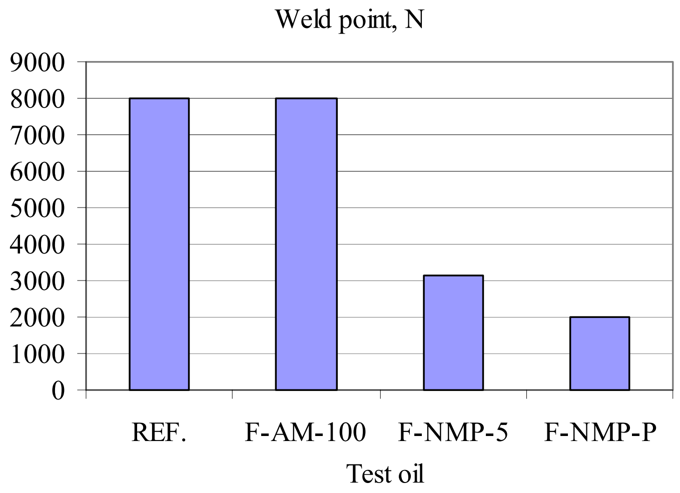

Figure 6. Weld point of test metalworking oils, ASTM D 2783

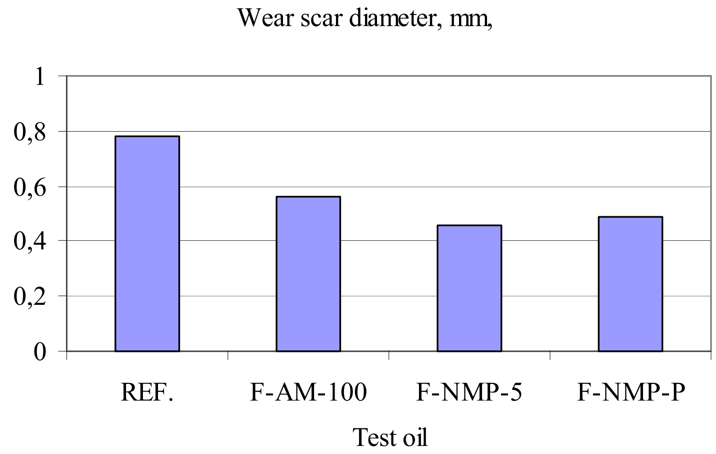

Figure 7. Wear scar diameter of test metalworking oils, ASTM D 4172

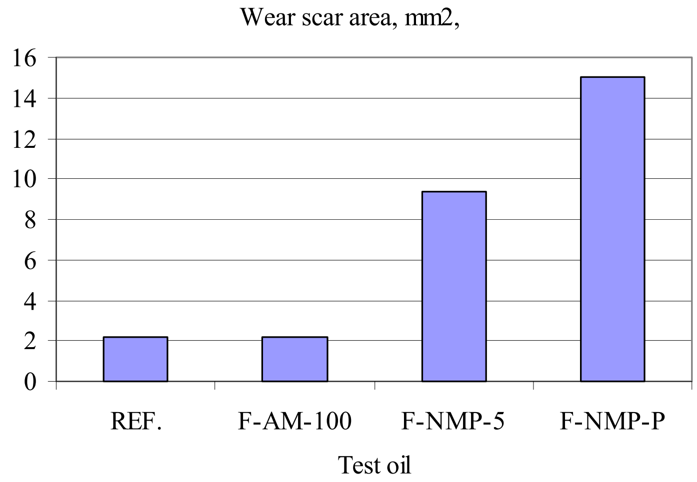

Figure 8. Wear scar area of test metalworking oils, Reichert method

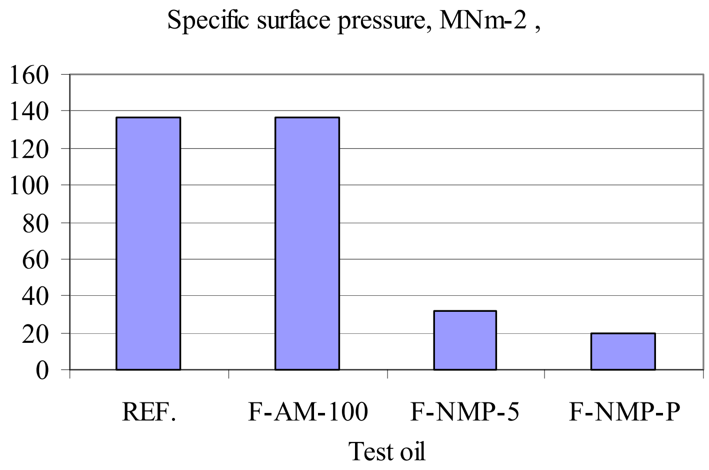

Figure 9. Specific surface pressure of test metalworking oils, Reichert method

Formulation F-AM-100 showed excellent properties at all tests. In comparison to referent oil (REF) test metalworking formulation F-AM-100 has the same and even better properties. Referent oil is mineral based with 100 cSt viscosity at 40 ^{0}C and is active type.

The numerous field tests are known for examination of lubrication properties. These methods simulate application conditions due to estimation working properties of lubricant. Generally Four-ball load carrying test is suitable for pre-evaluating lubricants for deep drawing process and has advantage over some test [5]. These methods differentiate well between lubricants having low, medium and high level of extreme pressure properties, which are essential in deep drawing where contact conditions are extremely severe [15]. By that classification it is obvious that F-AM-100 has high level of extreme pressure properties and can be used at severe wire working operations.

After satisfying laboratory test results it can be expected that formulation F-AM-100 will have the best application properties. This formulation is examined at production of different small parts with several operation types from wire drawing to cutting on multifunctional machine S2 Boltmaker, National. Material of wire is steel Č0362/Č0360, DIN QSt 36.

In drawing wire, the required deformation is accomplished by drawing the wire through the conical bore section of the die, hereby reducing the diameter through plastic deformation. During deformation, a thin film of lubricant between wire surface and die surface is essential to minimise friction, to reduce die wear, and to keep the die cool [16].

For good wire deformation, it is necessary to select a drawing die tool with the appropriate profile, designed for either ferrous or non-ferrous materials and also select the metalworking oil. It is widely accepted that wire drawing (and other processes in operation at S2 Boltmaker) involves mixed lubrication i.e. mix of hydrodynamic or full film lubrication and boundary lubrication.

New metalworking oil F-AM-100 based on additive AD S4 have good performances and even better than referent–former oil at cold deformation process and cutting that performed at S2 Bolmaker metalworking machine. It showed good cooling of tools and workpieces and also remarkable corrosion protection. As a result of good lubrication the surface finishing is excellent-it is shine, without any scratches or other unwonted phenomenon. There is no overheating of working oil, no gelling, sticking, foam is kept low and working life is extended.

6. CONCLUSION

In order to protect human health and environment and also reduce machining cost we examined several types of additives as replacement of chlorinated paraffine in metalworking oils for severe operations. Formulation F-AM-100 showed the best dynamical mechanical properties on laboratory test machines New metalworking oil contains mineral oil with lowered aromatics and also remarkable quantity of natural vegetable oil. It is active type of metalworking oil with high load carrying properties based on overbased sulfonate and without chlorinated paraffin. In laboratory and also in application at cold deformation and cutting operations of steel wire on S2 Boltmaker metalworking machine new oil showed excellent working properties.

7. REFERENCES

[1] Trent, E.M.: Metal Cutting, Second edition, Butterworths, 1984.

[2] Clason, D.L, Vinci, J. M.: Metalworking Additives - A new Approach to EP Properties, Sixth International Colloquium Tribology, Esslingen, 1988

[3] Ivusic, V.: Tribology, Hrvatsko drustvo za materijale i tribologiju (Croatian Society for materials and Tribology), Zagreb 2002

[4] Kotvis, P. V.: Overview of the Chemistry of Extreme - Pressure Additives, Lubrication Engineering, 42, 6, 1986

[5] http:/ www.tribology-abc.com

[6] Zimmerman, D.: Optimierung moderner chlorfreier nicht wassermischbarer Kuehlschmierstoffe, Mineraloel Technik, 10, 1987

[7] Mang, T.: Schmierstoffe und Umwelt - Die Schmierstoffentwicklung im Einfluss der Umweltgesetzgebung, Tribologie und Schmierungstechnik, 38 (1991) 4, 231-236

[8] DBL 6714: Liefervorschrift - Negativliste inhaltsstoffe von prozess-stoffen, 1991

[9] Schumacher, R., Zinke, H.: Tribofragmentation and Antiwear Behaviour of Isogeometric Phosphorus Compounds, Tribol. Intern. **30**, 3, 1997

[10] Hong, H., Riga, A.T., Cahoon, J. M.: Evoluation of Overbased Sulfonates as Extreme Pressure Additives in Metalworking Fluids-Part II: Lithium and Potassium Overbased Sulfonates, Lubrication Engineering, 51, 2, 1995

[11] Delfort, B., Born, M., Daoudal, B., Dixmer, F. Lallement, J.: Functionalization of Overbased Calcium Sulfonates-Synthesis and Evaluation of Antiwear and Extreme-Pressure Performances, Lubrication Engineering, 51, 12, 1995

[12] Metz, T.: Frictional Properties of Different EP Additives on Draw-Bed Test, 13th International Colloquium Tribology, Esslingen, 2002

[13] International standards ASTM, DIN, ISO

[14] Minami, I., Hasegawa, T., Memita, M.: Investigation of Antiwear Additives for synthetic Esters, Lubrication Engineering, 58, 1, 2002

[15] De Chiffre, L., Belluco, W.: Investigation of Cutting Fluid Performance Using Different Machining Operation, Lubrication Engineering, 58, 19, 2002

[16] http:/www.tecos.si/projekti/enform/indeks.htm

EFFECT OF COMPATIBILIZER EPDM-G-PS GRAFT COPOLYMERS ON PROPERTIES OF SAN/EPDM POLYMER BLENDS

UTJECAJ EPDM-g-PS GRAFT KOPOLIMERA KAO KOMPATIBILIZATORA NA SVOJSTVA SAN/EPDM POLIMERNE MJEŠAVINE

Anita Ptiček, Zlata Hrnjak-Murgić, Jasenka Jelenčić
Faculty of Chemical Engineering and Technology, Marulićev trg 19,
10000 Zagreb, Hrvatska, zhrnjak@fkit.hr

Abstract: Polymer blends offer mechanical and thermodynamic properties which are both unique and attractive for many industrial applications. There is a general agreement that the properties of polymer blends are usually controlled by the properties of the components, morphology of the blends and interaction between components in blends. Immiscibility of the most polymers today requests compatibilization with graft or block copolymers. Graft copolymers can be prepared by graft polymerization in solution or by reactive extrusion in bulk. In this work diversity in structure (various graft density and graft length) of EPDM-g-PS graft copolymers were accomplished by addition of coagent triallylcyanurate, TAC. Extracted graft copolymers were further used as compatibilizer in SAN/EPDM polymer blends which were prepared as thin films in ratio of 95/5/5 and 90/10/5. The effect of dissimilar structure of graft copolymers on miscibility in blends was followed by determination of mechanical properties, by examining morphology by scanning electronic microscopy (SEM) and by determination of surface free energy parameters. From the results it can be seen that various structure of graft copolymers has significantly effect on the miscibility of blends.

Keywords: compatibilizer, graft copolymer, in-situ polymerization, miscibility, polymer blend

Sažetak: Polimerne mješavine jedinstvenih mehaničkih i termodinamičkih svojstava zanimljive su za mnoge industrijske primjene. Krajnja svojstva polimernih mješavina uvjetovana su svojstvima komponenata, morfologijom i interakcijama između komponenata u mješavini. Većina polimera je nemješljiva i zahtijeva kompatibilizaciju što se postiže dodatkom graft ili blok kopolimera kao kompatibilizatora. Graft kopolimeri se pripremaju graft polimerizacijom u otopini ili reaktivnim ekstrudiranjem u masi. Različitost u strukturi (drugačija gustoća i duljina bočnih grana) EPDM-g-PS graft kopolimera postignuta je dodatkom koagensa trialilcijanurata, TAC. Izdvojeni graft kopolimer nadalje je korišten kao kompatibilizator u SAN/EPDM polimernim mješavinama koje su pripremljene u obliku tankih filmova u udjelima od 95/5/5 i 90/10/5. Utjecaj različite strukture graft kopolimera na mješljivost u mješavini praćen je određivanjem mehaničkih svojstava, ispitivanjem morfologije skenirajućom elektornskom mikroskopijom i određivanjem vrijednosti slobodne energije površine. Iz rezultata je vidljivo da različita struktura graft kopolimera ima značajan utjecaj na mješljivost polimerne mješavine.

Ključne riječi: graft kopolimer, in-situ polimerizacija, kompatibilizator, mješljivost, polimerna mješavina

INTRODUCTION

Polymers are rarely used for applications in their pure form and they are often mixed with other polymers and additives to alter processability and properties. The main problem that appears when polymer blends are prepared from two immiscibility and non compatible polymers is strong phase separation due to high interfacial tension and weak adhesion resulting in poor properties of blends [1-5]. Compatibility of such blends can be enhanced by the addition of pre-synthesized copolymers that can be block or graft copolymers with segment having affinity for particular of two blend components. The compatibilization aims are to achieve the desired level of dispersion, to insure strong interaction between the phases for the purposes of formation of polymer blends with good properties and maximization of the product performance. The addition of small amount of graft copolymer to an immiscible blend is possible to overcome the problem of immiscibility in polymer blends. In order to obtain different structure of graft copolymer (various graft length and graft density) use of coagents has become popular in many studies [6]. This is one of the methods to obtained diversity in the structure which provides access for tailoring the properties of graft copolymers. In this work the effect of various structures of graft copolymers on compatibility of SAN/EPDM blends was investigated. By determination of mechanical properties, by calculation of parameters of surface free energy and by examination of morphology was observed effect of dissimilar structure of graft copolymers on miscibility in blends.

EXPERIMENTAL

Materials. Polymers used in synthesis of graft copolymers and in preparation of polymer blends were ethylene-propylene-diene (EPDM, Keltan 312, DSM), containing 55 wt-% ethylene and 4 wt-% ethylidene norbornene, Mooney viscosity 33 MU, monomer styrene (St), 99.8 wt-% was supplied by DIOKI (Croatia) and coagent triallylcyanurate (TAC), 50 wt-%, (Bayer), styrene-acrylonitrile (SAN, Tyril 790, The Dow Chemical Company) with 24 wt-% AN, melt flow rate (MFR, 220^{0}C, 10 kg) was 22 g/10 min.

Preparation of samples. Graft copolymers (EPDM-g-PS) was prepared by in-situ polymerization by adding monomer styrene in toluene solution of EPDM polymer. One seria of graft copolymers was synthesized for different polymerization time (3, 7 hours) and second seria was also synthesized for different time but with addition of coagent TAC. Synthesized graft copolymer was separated from polymerization solution by Soxlet extraction in tetrahydrofurane for 8 hours. Blends were prepared from SAN, EPDM and EPDM-g-PS polymers by casting thin films of cca 1 mm from 6 wt-% toluene solution, the ratio of the components was 95/5, 90/10 and 5 phr respectively (Table 1). The SAN/EPDM blends without graft copolymer of the same composition were also prepared.

Table 1 - Composition of SAN/EPDM/EPDM-g-PS blends.

Sample	SAN/EPDM		SAN/EPDM-3*		SAN/EPDM-7*	
SAN	95	90	95	90	95	90
EPDM	5	10	5	10	5	10
EPDM-g-PS	-	-	5	-	5	-
EPDM-g-PS + TAC	-	-	-	5	-	5

*samples prepared with EPDM-g-PS graft copolymers which were synthesized for 3 and 7 hours

Characterization.

Mechanical properties. Measurements of mechanical properties (tensile strength and elongation at break) were done on prepared samples of SAN/EPDM and SAN/EPDM/EPDM-g-PS using a Zwick Testing Machine at a constant temperature of 23°C, humidity of 70% RH and crosshead speed of 1 mm/min was applied. The dimensions of specimens for tensile strength measurements were (75 x 13 x 0.5) mm and the results are average of five samples.

Scanning electron microscopy (SEM). Morphology of examined blends was characterized from a cross-section of cryogenically fractured surfaces of film samples (0.5 mm thick) using a Philips XL 30 Scanning Electon Microscope. Samples were immersed in liquid nitrogen to cool down for more 15 min and then fractured immediately. The dried samples were sputter-coated with gold prior to scanning electron microscopy examination.

Surface free energy. Measurements of surface free energy of prepared polymer blends was carried out using contact angle method on DataPhysics OCA 20 Instrument. The contact angles of standar test liquids (water, formamide and diiodometane) on the polymers have been measured at temperature T = 23°C ± 0.2 and humidity of 60% RH. Using Lewis-acid base calculation methods, parameters of surface free energy components was determined in order to evaluate the differences in polymer blends.

RESULTS AND DISCUSSION

Mechanical properties.

Pre-synthesized graft EPDM-g-PS copolymer was used as a compatibilizer in SAN/EDPM polymer blends. Graft copolymer was added in blends to enhance interactions between SAN and EPDM immiscible polymers [7, 8] through stronger interfacial bonding. Due to dissimilarity of chemical structure SAN and EPDM polymers are incompatible and immiscible and that exhibits poor mechanical properties.

Table 2 –Tensile strength and elongation at break of SAN/EDPM/EPDM-g-PS polymer blends. (T* - samples prepared with coagent TAC)

Samples SAN/EPDM/EPDM-g-PS (wt-%)	Tensile strength, σ / Nmm^{-2}	Elongation at break, ε / %
95/5	51,52	1,20
90/10	41,55	1,62
95/5/5-3	25,36	5,11
90/10/5-3	23,73	7,62
95/5/5-7	26,67	5,67
90/10/5-7	22,33	7,78
95/5/5-3T*	26,99	5,87
90/10/5-3T*	26,40	8,62
95/5/5-7T*	26,40	5,67
90/10/5-7T*	22,67	7,88

Addition of compatibilizer can improve interactions between polymers which are followed by considerable differences in values of tensile strength and elongation, namely by better mechanical properties. From the results of mechanical properties in Table 2, it can be seen that the tensile strength decrease and elongation increase with the increase of EPDM rubber and such expected behaviour is supported with many literature data. Especially, significant decrease of tensile strength is obtained in comparison to blends prepared without and with compatibilizer which are 51 Pa and cca 25 Pa, respectively. Such decrease of tensile properties we can not attributed to higher content of EPDM elastomer because for example, content of 10 wt-% EPDM in blend 90/10 gives values of 41.5 Pa for tensile strength. Such behaviour can be explained with better interactions between phases in blend.

If we now considered the effect of the structure of synthesized graft copolymers on properties of SAN/EPDM blends it can be seen that diversity in structure has influence on mechanical properties and also on morphology of SAN/EPDM 90/10 blends. Slight changes in elongation for blends in comparison to blends which is prepared with coagent TAC is observed whereas values increase of 5.11 % to 8.62 %. However, in SAN/EDPM 95/5 blends prepared with graft copolymer which contains short side branches and higher graft density are not observed significant differences in mechanical properties. For the SAN/EDPM blends 90/10/5 which is prepared with graft copolymer of short side branches with low graft density (which is synthesized for 3 hours and with coagent TAC) optimal mechanical properties are obtained.

Morphology of the SAN/EPDM blends.

Effect of various structures of EPDM-g-PS graft copolymers on morphology of SAN/EPDM blends in the composition of 90/10 can be seen on micrographs, Figure 1. Significant change of morphology of SAN/EPDM blend without compatibilizer (micrograph a)) in comparison to other blends prepared with compatibilizer (micrographs b) and c)) can be noted. It can be seen that particle size of dispersed phase on micrographs a) is significantly higher than those on micrographs b) and c).

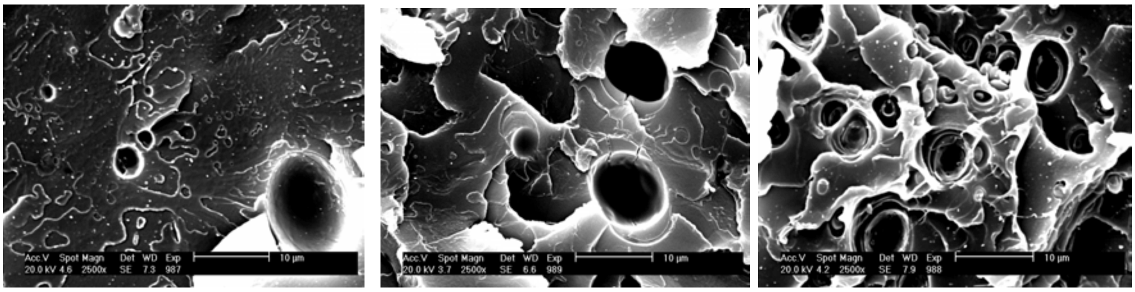

a) SAN/EPDM b) SAN/EPDM-3 c) SAN/EPDM-3-T

Figure 1 – SEM micrographs of fractured surface of SAN/EPDM/ (90/10) blends:
a) without compatibilizer; b) with 5 wt% of compatibilizer synthesized for 3 hours;
c) with 5 wt% compatibilizer synthesized for 3 hours with TAC.

Furthermore, considerable differences in distribution of particle size of dispersed phase (EPDM) for the samples prepared with and without coagent TAC, it can be seen on micrographs b) and c). Particle of dispersed phase on micrographs c) are smaller and much better distributed in the matrix than particle on micrograph b) because these two graft copolymers have different structure of the side branches. EPDM-g-PS-3 has short but dense side branches while the EPDM-g-PS-3T has short and low graft density of side branches. Such formed compatibilizer is located between two phases in blend and which is observed in blend that is prepared with graft copolymer synthesized with coagent TAC. From the micrographs it can be concluded that finer morphology is present in SAN/EPDM blends prepared with compatibilizer which is result of better interactions established between polymers which is follow by enhance of mechanical properties.

Surface free energy.

The surface free energy of the SAN/EPDM/EPDM-g-PS blends is shown in Figure 2. The results of total surface free energy for virgin SAN (Y_{total}=45.48 mJm^{-2}) and EPDM (Y_{total}=39.27 mJm^{-2}) and for their blends are calculated according to the Lewis-acid base theory. According to the results different evolution of the total surface free energy of SAN/EPDM blends is observed.

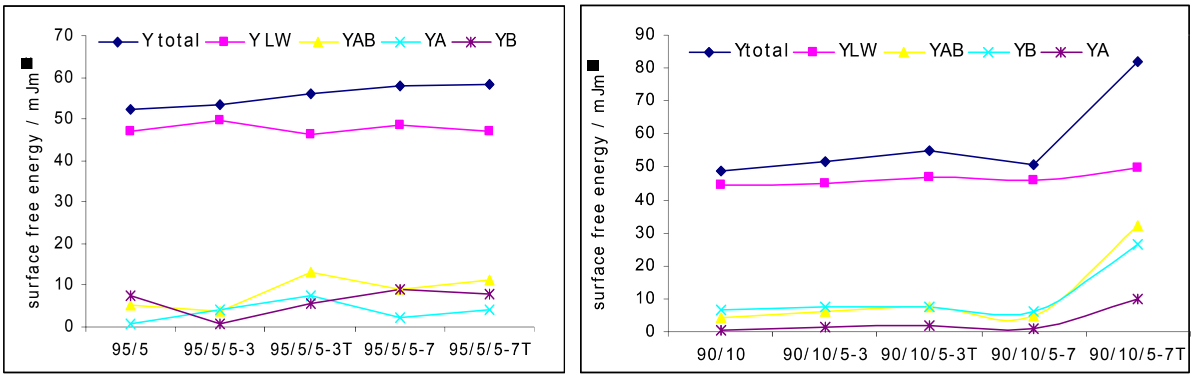

a) b)

Figure 2 – Surface free energy of SAN/EPDM polymer blends a) 95/5; b) 90/10 prepared with 5 wt% of EPDM-g-PS graft compatibilizer (synthesized for 3 and 7 hours with and without TAC) calculated according to Lewis-acid base theory.

With the Lewis-acid base method, the polymer blend surface free energy increases constantly from 52.27 mJm^{-2} for SAN/EPDM 95/5 to 58.39 mJm^{-2} for SAN/EPDM/EPDM-g-PS 95/5/5-7T. Increasing of surface free energy can be explained with different structure of side branches of used compatibilizers. The similar behavior is observed for the SAN/EPDM blends of concentration 90/10. A comprehensive insight in the Lewis acid/base surface free energy interactions can provide better understanding of the interactions and influence on physical and mechanical properties. Chemical modifications of the polymers and changes in their surface energy are of great importance for their applications [9]. The presence of acid and base active sites on the blend surfaces increases the possibility of specific intermolecular interactions with other polymers which has of significant effect on final propeties of blend.

CONCLUSIONS

From the results of mechanical properties it can be conclude that the graft copolymers significantly effects on compatibility in SAN/EPDM blends of composition 90/10. Stronger interactions in polymer blends increase thermodynamic work of adhesion at the interface and lead to improved tensile properties of blends. Better interactions between polymers are established in all SAN/EPDM blends that are prepared with graft as compatibilizer which result in finer morphology and it is followed by strongly modified mechanical properties.

LITERATURE:

1. O. Chiantore, L Trossarelli, M. Lazzari, *Polymer*, **39,**(1998**)** 2777.
2. M. M. Morimoto*, J.Appl.Polym.Sci.*, **26,** (1981) 261.
3. O. Chiantore, M. Guaita, M. Lazzari*, Polym. Deg.Stab.*, **47,**(1995) 141.
4. I. J. Hwang, M.H. Lee, B.K. Ki*, Eur.Polym.J.***, 34,** (1998**)**671.
5. C. Harrats, T. Omonov, G. Groeninckx, P. Moldenaers, *Polymer,* **45,** (24) (2004) 8115.
6. S. Mitra, A. Ghanbari-Siahkali, P. Kingshott, H.K., Rehmeier, H. Abidgaard, K. Almdal, *Polym. Degrad. Stab.* **91,** (2006), 81.
7. D. Braun, D. Yu, L. N. Andradi, B. Lőwenhaupt, G. P. Hellmann, *Macromol. Chem.*, *Macromol.Symp*. **48/49** (1991) 55.
8. D. Braun, M. Fischer, G. P. Helmann, *Macromolecules '92*, (J.Kahovec,Ed.), VSP, Zeist, (1993), p.387.
9. Q. Chao Zoua, S.L. Zhang, Q. Tang, S.M. Wang, L.M. Wu, *Journal of Chromatography A*, **1110** (2006) 140.

ADSORPCIJSKA IZOTERMA SISTEMA UGLJIČNI MATERIJAL / OTOPINA

ADSORPTION ISOTHERM OF CARBON MATERIAL / SOLUTION SYSTEM

Ankica Rađenović, Jadranka Malina
Sveučilište u Zagrebu, Metalurški fakultet, Aleja narodnih heroja 3, 44000 Sisak, Hrvatska
University of Zagreb, Faculty of Metallurgy, Sisak, Aleja narodnih heroja 3,
44000 Sisak, Croatia

Sažetak: U radu su studirana adsorpcijska svojstva, tzv. batch postupkom, nekoliko uzoraka s različitim sadržajem ugljika: aktivni ugljik, čađa, ugljen za koksiranje i visokopećni mulj. Ravnoteža sistema ugljični materijal /otopina (acetatna i citronska kiselina) opisana je Freundlichovom adsorpcijskom izotermom. Primijenjena izoterma često se rabi zbog jednostavnosti i mogućnosti opisivanja eksperimentalnih rezultata u širem koncentracijskom području.

Dobiveni rezultati mogu se koristiti u primjeni ispitanih uzoraka za uklanjanje raznih iona iz vodenih otopina.

Ključne riječi: ugljični materijal, adsorpcija, otopina, Freundlichova izoterma

Abstract: The subject of this work is batch adsorption study of samples with different carbon content: activated carbon, carbon black, coking coal and blast furnace sludge. The equilibrium in the carbon material / acid (acetic and citric) solution system is described by the Freundlich adsorption isotherm. Applied isotherm is often used since it is simple and has the ability to describe experimental results in a wide range of concentrations.

The results obtained could be useful for the application of investigated samples for the different ions removal from aqueous solutions.

Keywords: carbon material, adsorption, solution, Freundlich isotherm

UVOD

Iako poznati odavno, materijali na bazi ugljika sve češće se primjenjuju u raznim, do nedavno, nepoznatim područjima /1/. U posljednje vrijeme, intenzivnije se ispituje mogućnost njihove upotrebe kao adsorbensa za uklanjanje metalnih iona iz vodenih otopina, a naročito iz otpadnih industrijskih voda. Aktivni ugljik je jedan od najčešće korištenih ali skupih adsorbensa. Stoga su razumljiva nastojanja da se pronađu jeftiniji, no dovoljno djelotvorni adsorbensi anorganskog i organskog porijekla (drveni ugljen, lignit, tlo, zeoliti, prirodni kompost, ljuske kikirikija, oraha, koščice breskve, otpadna vuna i sl.) /2-4/. Neki industrijski nusproizvodi i otpadni materijali, kao što su troske, pepeli, prašine, muljevi, također se ispituju s ciljem proširenja područja njihove uobičajene upotrebe /5-7/.

U radu su ispitani materijali s različitim udjelom ugljika: aktivni ugljen, čađa, ugljen za koksiranje i visokopećni mulj. Praćena je adsorpcija dviju organskih (acetatna i citronska) kiselina, različitih koncentracija na navedenim materijalima. Ispitivanja su provedena statičkim ("batch") postupkom, a ravnoteža u sistemu adsorbens-adsorbirana tvar opisana je Freundlichovom adsorpcijskom izotermom.

EKSPERIMENTALNI DIO

Uzorci

Komercijalna granulirana čađa, (Č) proizvedena je uljno-pećnim postupkom s osnovnim karakteristikama: jodni broj 112,3 mg^{-1}; CTAB 113 m^{2}g^{-1}, 98,7% C, 1,0 % S; 0,28% pepela, 2,35% vlage.

Aktivni ugljik (AU) analitičke čistoće (p.a. "Carlo Erba", Milano) sadrži 83,7 % C.

Ugljen za koksiranje je mješavina (UK) ugljena ruskog (65%) i australskog (35%) porijekla s 65,25%C_{fix}, 3,05% vlage, 7,7% pepela i 0,87% S.

Visokopećni mulj (VPM), je nusprodukt industrije željeza i čelika a ima: 68% amorfne faze; 11% $CaCO_3$; 9,7% Fe_3O_4; 5% SiO_2; 3,1% $Al_2Si_2O_5(OH)_4$; 1,7% Fe_2O_3 i 1,7% $ZnCO_3$.

Veličina čestica svih uzoraka iznosila je $\leq$ 100 μm, a određena je mljevenjem u laboratorijskom mlinu "Retch"-RMO.

Adsorpcija kiselina na adsorbensima

Ispitani uzorci adsorbensa točne odvage (1g) preneseni su u tikvice i uravnoteženi tijekom 1, 8, 24 i 68 sati sa 100 ml acetatne odnosno 100 ml citronske kiseline različitih koncentracija (0,05 moll^{-1}; 0,1 moll^{-1}; 0,15 moll^{-1}; 0,25 moll^{-1}; 0,35 moll^{-1}). Nakon uravnoteženja otopina je filtriranjem odijeljena od ispitivanih uzoraka.

Adsorpcija je praćena mjerenjem koncentracije kiselina prije i nakon uspostavljanja ravnoteže na ispitanom adsorbensu (tzv. "batch" postupkom). Točna koncentracija kiselina određena je volumetrijski uz upotrebu otopine NaOH koncentracije 0,1 moll^{-1} kao titranta i fenolftaleina kao indikatora.

Sva mjerenja su provedena pri sobnoj temperaturi od 20°C.

REZULTATI I DISKUSIJA

Eksperimentalni rezultati obrađeni su Freundlichovom adsorpcijskom izotermom koja daje jednostavnu vezu između količine adsorbirane tvari po jedinici mase adsorbensa (x/m, mmolg^{-1}) i ravnotežne koncentracije adsorbirane kiseline. (C_s, mol l^{-1}). Iako su ugljični materijali kao adsorbensi i organske kiseline kao adsorbirane tvari bile u višesatnom kontaktu (1, 8, 24 i 68 sati), eksperimenti su pokazali da je ravnoteža uspostavljena već nakon jednog sata. Dobiveni rezultati su prikazani na slikama 1 i 2.

Slika 1 prikazuje rezultate ovisnosti količine adsorbirane acetatne kiseline, a slika 2 rezultate ovisnosti količine adsorbirane citronske kiseline na ispitanim ugljičnim materijalima (nakon 24 sata).

Neovisno o vrsti adsorbensa, postignuta je bolja adsorpcija acetatne u odnosu na citronsku kiselinu. Veća količina kiselina adsorbirala se iz otopina manjih koncentracija. Izuzetak je gotovo linearna ovisnost između količine adsorbirane acetatne kiseline (mmol) po jedinici mase (g) ispitane čađe (Č). Prema dobivenim rezultatima, čađa je najbolji adsorbens za acetatnu, a visokopećni mulj (VPM) za citronsku kiselinu.

Uzorci aktivnog ugljika (AU) i ugljena za koksiranje (UK) su pokazali slična adsorpcijska svojstva u oba slučaja. Naime, na uzorcima UA i UK adsorbirala se najmanja količina ispitanih kiselina.

Poznato je da uspješnost adsorpcije ovisi o vrsti adsorbensa, svojstvima njegove površine i veličini molekula koje se adsorbiraju /1/. Svi ispitani materijali sadrže ugljik, ali s različitim udjelima. Najveći maseni udjel ugljika je u čađi (98,7%), a najmanje ugljika je u visokopećnom mulju (30%).

Površinska svojstva materijala ovise o aktivnosti površinskih grupa. Na površini čađe, ugljični slojevi obično sadrže atome vodika i kisika kao i razne funkcionalne grupe (karbonilna, karboksilna, hidroksilna itd.). One su važne za adsorpcijska svojstva čađe jer predstavljaju hidrofilna mjesta na hidrofobnoj površini.

Veća koncentracija aktivnih grupa na površini čađe, u odnosu na ostale uzorke, vjerojatno je razlogom veće adsorpcije kiselina.

U radu upotrebljene, monoprotonska octena i triprotonska citronska, su organske kiseline malih molekula koje se, a naročito octena, vežu na površinu ugljičnih materijala (aktivni ugljik, čađa i ugljen za koksiranje).

Triprotonska citronska kiselina se najviše adsorbirala na uzorku visokopećnog mulja koji se sastavom razlikuje od ostalih ispitanih uzoraka. Uzorak VPM je uglavnom amorfan s najmanjim udjelom ugljika. Od kristaliničnih tvari prevladavaju oksidi željeza, kalcija, silicija i aluminija značajnih adsorpcijskih svojstava /8/.

ZAKLJUČAK

Ravnoteža sistema ugljični materijal/otopina organske kiseline opisana Freundlichovom adsorpcijskom izotermom, uspostavljena je brzo, nakon jednog sata.

Adsorpcija u sistemu ugljični materijal/otopina ovisi o vrsti uzorka, vrsti i koncentraciji adsorbirane tvari. U sistemu ugljični materijal/acetatna kiselina, najveća količina acetatne kiseline se adsorbirala po jedinici mase čađe. U sistemu ugljični materijal/citronska kiselina najveća količina citronske kiseline se adsorbirala po jedinici mase visokopećnog mulja.

Najsličniji rezultati su dobiveni praćenjem adsorpcijske izoterme aktivnog ugljika i ugljena za koksiranje čija je adsorpcijska sposobnost manja u odnosu na ostale uzorke u uvjetima provedenih ispitivanja. Veća količina kiselina se adsorbirala iz otopina manjih koncentracija.

Provedena ispitivanja daju uvid u mogućnosti korištenja čađe, visokopećnog mulja, aktivnog ugljika i ugljena za koksiranje kao potencijalnih adsorbensa u procesu uklanjanja iona iz vodenih otopina.

LITERATURA

1. M. Legin-Kolar, A. Rađenović, Ugljični materijali, Metalurški fakultet, Sisak, 2002.
2. R. W. Gaikward, EJEAFChe, **3** (2004) 4, 702-709.
3. A. Dabrowski, Advances in Colloid and Interface Science **93** (2001) 135-224.
4. T. K. Budinova, M. Gergova, N. V. Petrov, V. N. Minkova, J. Chem. Tech. Biotechnol. **60** (1994) 177-182
5. S. V. Dimitrova, D. R. Mehandgiev, Wat. Res. **32** (1998) 11, 3289-3292.
6. F. A. Lopez, M. I. Martin, C. Perez, A. Lopez-Delgado, F. J. Alguacil, Wat. Res. **37** (2003) 3883-3890.
7. F. A. Lopez, M. I. Martin, C. Perez, F. A. Lopez, Wat.Res. **32** (1998) 989-996.
8. A. Lopez-Delgado, C. Perez, F. A. Lopez, Carbon **34** (1996) 423-431.

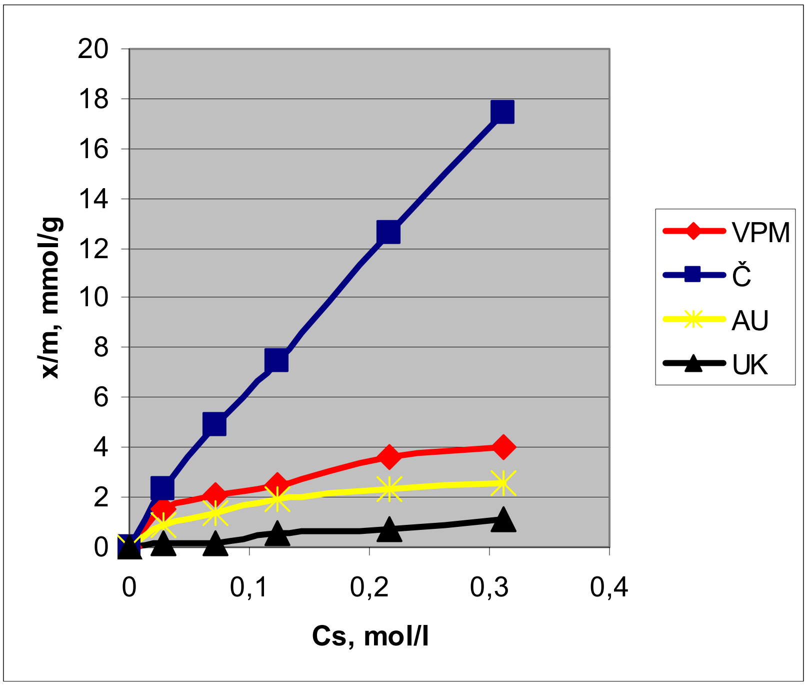

Slika 1. Ovisnost količine adsorbirane tvari (mmol) po masi (g) adsorbensa o ravnotežnoj koncentraciji adsorbirane tvari (acetatna kiselina)

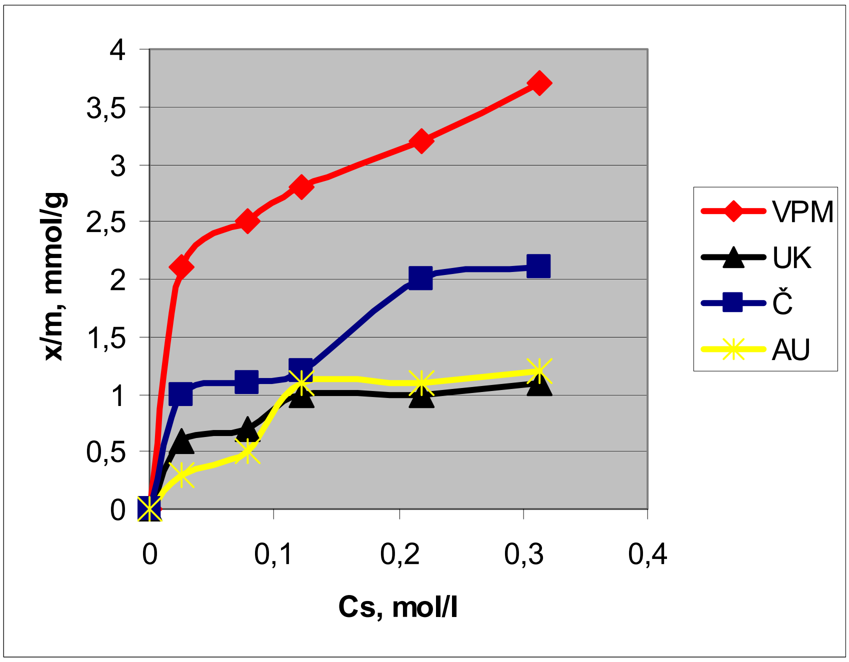

Slika 2. Ovisnost količine adsorbirane tvari (mmol) po masi (g) adsorbensa o ravnotežnoj koncentraciji adsorbirane tvari (citronska kiselina)

11. Savjetovanje o materijalima, tehnologijama, trenju i trošenju
11. Conference on Materials, Processes, Friction and Wear
MATRIB'06, Vela Luka, 22-24.06.2006.

MOLDINGS MADE FROM AMINO COMPOUNDS

Prof.dr.Nedžad Repčić
Faculty of Mechanical Engineering
University of Sarajevo
tel. 65 31 92, 65 65 62 fax. 65 30 55
e.mail: repcic@mef.unsa.ba,
Sarajevo,Vilsonovo 9, B&H

Abstract*:* Thus, PTFE bearing surfaces do not seize, even under extremely high loads. Sliding speed has a marked effect on friction characteristics of unreinforced PTFE resins; temperature has very little effect. PTFE resins have an unusual thermal expansion characteristic.A transition at 18 °C produces a volume increase of over 1%. Thus, a machined part, produced within tolerances at a temperature on either side of this transition zone, will change dimensionally if heated or cooled through the zone.

Electrical properties of PTFE, FEP, and FPA are excellent, and they remain stable over a wide range of frequency and environmental conditions. Dielectric constant, for example, is 2.1 from 60 to 10(to the 9th power) Hz. Heat-aging tests at 300 °C for six months show no change in this value. Dissipation factor of PTFE remains below 0.0003 up to 10(to the 8th power) Hz. The factor for FEP and PFA resins is below 0.001 over the same range.

Dielectric strength and surface arc resistance of fluorocarbon resins are high and do not vary with temperature. This paper discusses leading models engineering of polymers. Polymers continue to advance into engineering applications that range from automotive and aerospace to medical and electrical. There is no simple procedure for selecting the best plastic for a new application. It must be done with direct experience and knowledge of the behavior of various plastics under the real-life conditions to be encountered by a particular part after it is molded. Until this experience is acquired, a designer has little choice but to seek the advice of a reliable molder, materials manufacturer, or compounder.

Even here, there is the danger that these sources may not be aware of the many compromises a company must make internally among production, engineering, purchasing, and marketing considerations to produce a product that will sell at a profit. Also, a molder might be inclined to recommend the material that works best in his equipment, rather than the best for the application. Thus, the successful design of plastic parts that have the optimum cost/performance characteristics require learning as much as possible about many different plastics and the peculiarities of their processing.

These models are somewhat flawed as they emphasise engineering aspects, and do not stress sufficiently the 'people' aspect and the necessity for a designer to find out about all potential reactions to the solution. In spite of their tendency towards regimentation, the models clearly reflect the iterative nature of design.

Key words: plastic, engineering, application

1. INTRODUCTION

Polymers continue to advance into engineering applications that range from automotive and aerospace to medical and electrical. There is no simple procedure for selecting the best plastic for a new application. It must be done with direct experience and knowledge of the behavior of various plastics under the real-life conditions to be encountered by a particular part after it is molded. Until this experience is acquired, a designer has little choice but to seek the advice of a reliable molder, materials manufacturer, or compounder.

Even here, there is the danger that these sources may not be aware of the many compromises a company must make internally among production, engineering, purchasing, and marketing considerations to produce a product that will sell at a profit. Also, a molder might be inclined to recommend the material that works best in his equipment, rather than the best for the application. Thus, the successful design of plastic parts that have the optimum cost/performance characteristics require learning as much as possible about many different plastics and the peculiarities of their processing.

Designers used to take little interest in the molding of parts they designed. They sent the drawings to the molder in another department or another company and expected perfect parts to emerge. But design and processing have become so interrelated that this separation can no longer exist if products are to be consistently successful. Molders can usually be relied upon to detect and correct visible problems or readily measured factors such as color, surface condition, and dimensions. However, less apparent property changes are another matter. These may not show up until the moldings are in service, unless extensive testing and quality control are used. Such properties as impact strength, toughness, and chemical resistance can be diminished by improper control of processing parameters.

Close cooperation between designers and molders can eliminate disappointment and help ensure successful products. After candidate materials are selected, the design should be tested under real-life conditions involving the temperatures, loading, and environment of the anticipated service. Ideally, the test part should be molded in the shape and from the material to be used in production. In the beginning, this is costly and time consuming, but as experience is acquired, accelerated tests can be developed on simpler shapes; testing will then be more economical but just as reliable. Understanding the molding process that will produce the part is also necessary.

The process directly affects material choice, shape, tolerances, and properties of the part. For example, a container or housing can be made by injection molding, blow molding, thermoforming, or rotational molding. But each process requires a markedly different design, would use a different grade of plastic or a different plastic entirely, and would produce a component with significantly different properties. All molding processes alter the published data-sheet properties, reducing most strengths and often creating areas of stress concentrations. But each process may create stresses in different areas. Sometimes, processing conditions are so severe that there is no choice but to redesign the shape and change to a different plastic. Unfortunately, reliable data on molded strength properties may never be available because of the basic nature of plastics. Their characteristics are partly those of solids and partly those of viscous liquids, preventing the use of classical Hookean engineering formulas for calculating load distributions accurately.

Plastics are synthetic materials made from chemical raw materials called monomers. A monomer (one chemical unit) such as ethylene is reacted with other monomer molecules into long chains of repeating ethylene units, forming the polymer polyethylene. In a similar manner, polystyrene is formed from styrene monomer; polypropylene from propylene monomer; and other thermoplastic polymers from their respective monomers.

Plastics begin as a gas (monomer), approach the liquid state for forming, and end up as a solid in their finished form. They can be formed by heat, pressure, or a combination of the two. Adding reinforcements to plastics creates a different class of materials known as composites. Greater understanding of the fundamental chemistry of polymer formation has led to development of plastics with properties tailored to specific applications. Rather than refining materials found in nature, chemists can now design materials with the same elements nature uses. In fact, polymer chemists have built thousands of plastics based on only eight elements: carbon, hydrogen, nitrogen, oxygen, fluorine, silicon, sulfur, and chlorine.

2. CHEMICAL AND WEATHER RESISTANCE

Yet another way to create more variations in plastics is alloying -- an effective and economical method to improve a weak property in a base resin. Plastic alloys, also called blends or polyblends, are usually designed to retain the best characteristics of each material. Properties that have been found to be most responsive to improvement are impact strength, heat-deflection temperature, flame retardance, chemical and weather resistance, and processibility. A study by Battelle reports that research on polymer blending generates about 1,000 patents per year.

Although no totally accepted definition exists, most engineers and chemists in the plastics industry agree that a plastic alloy is identified by most of these characteristics: The combination of polymers does not depend on chemical bonds; the mixture is entirely mechanical. Thus, copolymers (some acetals and polyolefins) and terpolymers are not alloys. Nor are epoxy compounds that copolymerize with hardeners that contribute to the properties of the cured resins.The mixture has a single melt-transition temperature. At least one property or characteristic of the base polymer is improved synergistically by the addition of the other polymer(s).

The property may be physical or mechanical, or the improvement may be in processibility or cost. If synergistic improvement is not achieved, at least the best properties of all constituents are retained. Each minor component of a plastic alloy constitutes at least 5% of the mix. Many are nearer the 50:50 range. This "requirement" differs considerably from those involving metal alloys. There, only enough of an alloying element need be present to effect a change in a mechanical or physical property. The magnitude of such a change is not important. A new technology that combines incompatible polymers to form blends called interpenetrating polymer networks (IPNs) promises to provide cost/performance benefits not previously available in engineering plastics. Several companies are working on IPN development, but only a few have made developmental IPN materials available. IPNs consist of an interwoven matrix of two polymers. A typical method for producing these alloys involves crosslinking one of the monomers in the presence of the other polymer.

The need for chemical similarity between the two types of molecules is thus reduced because the crosslinking physically traps one phase within the other. The result is a structure composed of two different materials intertwined together, each retaining its own physical characteristics. The relationship is similar to that between small blood vessels and the surrounding tissue in the human body. Patented IPN technology by Shell Chemical Co. is based on the capability of the company's Kraton G thermoplastic elastomer (styrene-butadiene-block copolymer) to form stable and reproducible structures when properly mixed in the melt stage.

The blends provide properties of the individual phases of the mixture and have few or no property losses that might be expected from combining incompatible materials. The results are materials having the best performance features of both an engineering thermoplastic and a thermoplastic rubber.

Although Shell was the first to come out with injection-moldable IPNs, Allied and Du Pont are also working on similar materials. Research at Allied-Signal Corp., for example, is focused on combining the toughness of thermoplastics with the solvent resistance, heat resistance, and dimensional stability of thermoset resins. Allied researchers feel that, when the IPNs become fully commercial, they will likely be processed by reaction-injection molding (RIM), by injection molding with a postmolding oven cure, or by a sheet-molding process followed by a cure cycle.

Other current thermoplastic IPN technology is based on crystalline resins such as nylon 6, 6/6, and 6/10, PBT, acetal, and polypropylene, with silicone as the IPN. These IPNs can be further modified with reinforcements and lubricants such as glass or carbon fibers and PTFE. The silicone IPN functions as a nonmigratory silicone lubricant, release agent, and flow modifier. It also plays an important role in controlling shrinkage and warpage of resins and composites. IPNs provide excellent wear performance in gears and bearings and superior dimensional control in parts such as keyboard frames for electronic typewriters. Another way to improve the compatibility of two dissimilar polymers often involved a third material. The "compatibilizer" material is a grafted copolymer consisting of one of the principal components and a material similar to the other principal component.

The functional groups in segment A of the third material will have an affinity for the polymer produced from monomer A, and the functional groups in segment B an affinity for polymer B. The mechanism is similar to that of soap improving the solubility of a greasy substance in water. The soap contains components that are compatible with both substances.

3. INTEGRATING FEA AND MOLDING PROGRAMS

In order to reduce the number of prototypes required, designers are turning to finite-element analysis. FEA programs allow parts design and structural analysis before tooling is cut. Related software, such as moldfilling analysis and warpage programs, help to eliminate processing problems before they start.

Many of these programs depend on materials databases that organize various properties into a manageable format. Integrating FEA and molding programs with a database often optimizes the use of capital-intensive CAD/CAM equipment. Databases also enable users to conduct a fast and efficient materials search. Some degree of compromise is almost always necessary in designing plastic parts.

Impact properties of ABS are exceptionally good at room temperature and, with special grades, at temperatures as low as -40°C. Because of its plastic yield at high strain rates, impact failure of ABS is ductile rather than brittle. Also, the skin effect which, in other thermoplastics, accounts for a lower impact resistance in thick sections than in thin ones, is not pronounced in ABS materials.

ABS resins are stable in warm environments and can be decorated with durable coatings that require baking at temperatures to 71°C for 30 to 60 min. Heat-resistant grades can be used for short periods at temperatures to 110°C in light load applications.Acrylic-styrene-acrylonitrile (ASA) polymers are amorphous plastics which have mechanical properties similar to those of ABS resins. However, the ASA properties are far less affected by outdoor weathering.

ASA is a terpolymer that can be produced by either a patented, proprietary reaction process or by a graft process. Optimum results are obtained with machines having accumulators. ASA parts can be welded using thermal and spin techniques. In some cases, ultrasonic welding is possible.ASA parts also can be solvent welded using 2-butanone, dichloroethylene, or cyclohexane. ASA parts readily accept and retain print and coatings without prior surface treatment.

Vacuum metallizing by conventional methods is also possible. Applications: Building/construction -- Gutters and fittings, drain pipe and fittings, signs, mail boxes, mobile home skirting, flower boxes, and shutters.

Recreation/leisure -- Outdoor furniture, windsurfer boards, swimming pool pumps, boat hulls, pickup truck caps, and filter housings and spas. Automotive/transportation -- Exterior sideview mirror housings, grilles, drip rails, and bumper covers. Miscellaneous -- Lawn-mower components, garden-hose reels, snowmobile housings, machinery covers, and covers for outdoor lighting.

Arriving at the best compromise usually requires satisfying the mechanical, thermal, and electrical requirements of the part, utilizing the most economical resin or compound that will perform satisfactorily and be attractive, and choosing a manufacturing process compatible with the part design and material choice. Setting realistic requirements for each of these areas is of utmost importance. Probably no plastic will provide 100% of the requirements for the desired performance, appearance, processibility, and price. Selecting the best qualified material is not based simply on comparing numbers on published data sheets; such values can be grossly misleading. For example, choosing the most economical material for a part by comparing the cost per pound of various plastics is a mistake.

Some plastics weigh twice as much per cubic inch as others and so would require twice as much to fill a given cavity and cost twice as much to ship.A more meaningful comparison is cost per cubic inch. But since most expensive plastics are far stronger than the cheaper ones, cost/strength values should be analyzed as well. Paying more per pound or per cubic inch is often more economical if less material can do the job.

4. DIFFERENT CONFIGURATIONS AND DIFFERENT MOLDING PROCESSES

There is an attractive simplicity in deciding on the material with the highest ASTM test values as listed in manufacturers' data sheets. Unfortunately, this method seldom results in the best choice. First, the choice of any material should be based on the best combination of properties, not only on one property. An ideal material will have a value for each strength property just sufficient to perform properly and safely in a given application and no higher. The best material choice usually represents a trade-off among satisfactory properties, ease of processing, and cost.

It is seldom the plastic with highest values in any single category. Second, values in published data sheets represent laboratory tests, which do not duplicate real-life molding conditions. Strength of a molded plastic part is significantly affected by such processing factors as direction of flow, pressure during molding, melt temperature, thermal degradation, cooling rate, and stress concentrations. As a result, a high value listed in the data sheets for a given property can be reduced considerably by processing conditions. Because the molding variables are beyond their control, material suppliers have chosen to make simple, standardized ASTM laboratory tests that are easily reproduced.

The tests are not material performance tests for predicting real-life results over a period of time, but are actually material quality tests. They are made for the purpose of assuring a buyer that the batch he buys today is the same formulation and quality he bought last month or last year. The ASTM tests were not intended to compare one material with another on the basis of strength after molding; different configurations and different molding processes can change the values significantly.

Third, ASTM tests are essentially short-term tests with all variables fixed except the one being measured. For example, testing for tensile, flexural, or impact strength is often done at a standard rate of loading.

A short-time tensile test may show a high strength value, but if the rate of loading is reduced by 100 or 1,000 times, tensile strength can drop to as little as 20% of the short-time strength. If the loading rate is increased, the tested tensile-strength value may double or triple.

The data sheets do not show this.Plastics are also temperature sensitive; strength properties may vary by a factor of 10 over a temperature difference as little as 200°F. Since most ASTM strength tests are made at room temperature, behavior at other temperatures cannot be reliably predicted from these data. Nor can the behavior be predicted under combinations of temperature, varying loads, and changing environments outside the narrow test conditions.

5. CONCLUSION

A prototype plastic part cannot duplicate exactly the performance of an injection-molded production part unless it is molded in a production environment in a production mold. This is normally impractical, so the best that can be expected is an approximation of a production part. The fastest and most economical way to produce plastic prototypes is to machine them from slab or bar stock.

But stock forms of plastics are made by extrusion, not injection molding. Besides not having the same flow orientation of a molded part, extrusions of a given material are usually made from a higher molecular-weight grade than that used for injection molding. Consequently, properties such as impact strength, creep resistance, and chemical resistance tend to be higher in an extruded material. These differences are particularly significant in the crystalline plastics such as nylon, acetal, and polyethylene.

The variations are usually smaller in amorphous materials such as ABS, polycarbonate, and polystyrene, but even minor differences can be critical in some applications. Molding, rather than machining, of prototypes generally provides a better approximation of a production part, but here too, a number of differences in conditions can cause misleading results.Nevertheless, steel prototype molds produce parts that most nearly duplicate production parts. Although this is the most expensive prototyping method, it may be the most economical in that it provides the surest way to avoid expensive changes in production molds.

Even here, there is the danger that these sources may not be aware of the many compromises a company must make internally among production, engineering, purchasing, and marketing considerations to produce a product that will sell at a profit. Also, a molder might be inclined to recommend the material that works best in his equipment, rather than the best for the application. Thus, the successful design of plastic parts that have the optimum cost/performance characteristics require learning as much as possible about many different plastics and the peculiarities of their processing.

6. REFERENCES

[1] Neale,M.J.: Tribology Handbook, London, 1991.
[2] Barwel , F.T.: Lubrication of Bearings , Butterworths , 1996.
[3] Drozdov, I.: Trenie i iznos v ekstremalnih uslovia , Mašinostroenie , Moskva , 1996.
[4] Scheele, E. D.: Principles and Design, Prentice-Hall, USA, 1997.
[5] Walker, D.W.: Computer based information systems, Pergamon press, New York, 1998.
[6] Pahl,G., Beitz,W.: Engineering Design, Springer, Berlin,…1996.
[7] Walters, J., Nielsen, N.: Crafting Knowledge-based Systems, John Wiley, New York, 1998.
[8] Wilson, C.C., Kennedy,M.E., Trammell,C.J.: Superior Product Development, Blackwell, 1997.
[9] Katalozi i standardi: ISO, DIN, SKF, FAG, SHELL, ASME, SAE, VDI, FAM, INA, SIMRIT
[10] Web sites - http: // www. cad/cam.com / science / engineering / design / plastic

COMPACTION OF ALFE2V4 MELT-SPUN RIBBONS USING PLASTICIZER

Simancík F., Balog M., Izdinsky K., Nagy J.
Institute of materials and machine mechanics, SAS, Bratislava, SLOVAKIA

Abstract:

New approach where hard-to-deform AlFe2V4 melt-spun ribbons (MSR) were compacted into sound profiles using "non-degrading" plasticizer is shown. The plasticizer, made of 1 µm Al 99.7 % powder, enabled significant reduction of extreme loads required for extrusion of plain AlFe2V4 MSR and meanwhile improved the plasticity of extruded compacts. After extrusion plasticizer forms a "matrix" part of two-phase composite structure, which is reinforced with chopped AlFe2V4 MSR flakes. No apparent phase transformation took place even after long term annealing held at 350 °C, neither within of any compact's constituents. Unique structural stability of extruded "composites" was attributed to randomly oriented icosahedral particles, with traces of an amorphous phase and fcc $Al_{10}V$ intermetallic phase in AlFe2V4 MSR and to efficient strengthening by homogeneously distributed nano-scale dispersoids coming from broken surface oxides of original 1 µm Al powder plasticizer particles. Room temperature ductility and fracture toughness of mixture compacts were significantly improved in comparison to plain AlFe2V4 MSR compacts. Alternatively to extrusion an original approach utilizing equal channel angular pressing (ECAP) was proposed for mixture consolidation. ECAP accommodated substantial lower pressing loads than extrusion at the same pressing temperature. Obtained microstructures and mechanical properties were even slightly superior to those obtained by means of extrusion. The prepared material reproducibly attained the strength above 500 MPa at 3-4% ductility. Outstanding mechanical properties - currently superior to any conventional aluminium alloys - were attained especially at elevated temperatures (UTS ~ 300 MPa and ductility of 4-5% at 300 °C). The suggested technological approach enables real utilization of RS ribbons in bulk structural profiles, whereas most of conventional technological equipment can be used for this purpose without need of intensive new investments.

Key words: Al, rapid solidification, high strength, heat resistant, powder metallurgy, aperiodic, melt-spinning, extrusion, ECAP

1. Introduction

Potential service of high strength Al alloys at elevated temperatures (above 200 °C) cannot be fulfilled with commercial Al alloys when their high strength is based on precipitation strengthening. Herein distinctive loss of mechanical properties due to overaging effects is observed even at moderate temperatures (usually above 150 °C). This problem can be overcome by usage of rapidly solidified (RS) structures of some Al- based systems. With their enhanced structural stability considerable improvement of room and high temperature mechanical properties is enabled [1]. This is ensured mainly due to three features of RS structures: significant increase of alloying elements solid solubility, structural refinement and formation of aperiodic phases. On the other hand associated heat flow limits at least one dimension of material which can be cooled down at desired cooling rate. As a result only discrete particles or ribbons can be prepared and their consolidation into bulk structural parts is necessary. To maintain desired RS microstructures and establish good metallurgical bonding between particles the consolidation is basically circumscribed to compaction routes based on introduction of shear deformation (mostly extrusion) at moderate temperatures. However RS structures feature generally poor workability at "low" temperatures as a result of their high strength and low ductility. This leads either to improper consolidation or to the lost of mechanical properties (i.e. desired microstructures) if compaction at high temperature is used. Thus, the consolidation of high-strength RS Al based alloys is one of the most challenging technological tasks nowadays.

Al-Fe alloys are attractive for applications at temperatures beyond those normally associated with aluminum alloy use. Unfortunately, the equilibrium solubility of iron in the aluminum lattice is very low and even at high temperatures it does not exceed 0.03 at. %. Moreover these alloys cannot be strengthened using conventional precipitation hardening. Employment of RS techniques enables to make use of Al-Fe alloys potential in application where high temperature strength is of interest. For this study AlFe2V4 alloy in the form of RS melt-spun ribbons (MSR) was chosen owing to its good thermal stability at relatively high temperatures [2] as well as its promising mechanical properties [1]. Furthermore unlike other RS Al based alloys, Fe and V as relatively cheap alloying elements make the alloy prospectively competitive in potential industrial applications. Alongside to the conventional consolidation novel approach using plasticizer and/or alternatively ECAP is presented.

2. Experimental

AlFe2V4 MSR were supplied by Institute of physics SAS. Master alloys of nominal chemical compositions were prepared in vacuum induction furnace from 99.9 % pure elements. Ribbons were produced by planar flow casting onto rotating copper chill providing cooling rate ~10^6 $K.s^{-1}$. Al alloy melt was cast from the temperature of about 1150 °C. MSR had the cross-sections of ~ 0.02x10 mm. As-cast MSR were disintegrated into smaller flakes by means of cryo-chopping method where plasticity of RS MSR was retained. Chopped particles were sieved into size fraction: <63 μm, 63-125 μm, 125-200 μm and 0-200 μm. 1 μm Al powder of technical purity 99.7 %, supplied by *MEPURA G.m.bH.*, was prepared by gas atomization in N_2 atmosphere [3]. Dimensional characterization of powder was determined by means of Helos analysis and was as follows: x_{50}=1.31 μm, x_{10}=0.66 μm, x_{90}=2.51 μm. Prior consolidation were AlFe2V4 MSR + 1 μm Al 99.7 % powder mixtures homogenized for half an hour in a Turbula shaker.

Compaction was predominantly realized via conventional hot direct extrusion (DE) on pneu-hydraulical press. Extrusion ratio R = 11:1 was found as to be a good compromise wherein sufficient amount of plastic shear deformation is being induced while keeping extrusion loads low enough [4, 5]. Flat faced die design was used. No flushing, degassing and canning were carried out prior extrusion. Either loose or pre-compacted powder or mixture were filled into the preheated die (50 °C below extrusion temperature) and afterwards heated up to desired compaction temperatures for 30 min before extrusion. BN spray was used as a lubricant. To prevent the particles from pouring out through the die and meanwhile to decrease friction during extrusion, friction relief 3 mm thick Al coin was placed between the die and compacted material. Load capacity limit during extrusion was set up to the value of ~ 1.6 GPa given by limitations of tool material. The average ram speed during extrusion within chosen compaction temperature range was ~ 1 $mm.s^{-1}$ (±0.8). Alternatively to DE equal channel angular pressing (ECAP) was implemented as consolidation technique. Inlet and outlet channels of ECAP tool intersected in angle $\Phi = 90°$ and featured outer radius angle $\Psi = 0°$. Those parameters of die's design yielded equivalent strain $\varepsilon_{eq} = 1.15$ introduced during one pass through a die. Both channels were of 12x12 mm cross-section. Powders and chopped MSR were precompacted either via cold isostatic pressing or via hot extrusion done at low strains (R = 4:1). Precompacted samples were machined into cylinders with diameter of 10 mm and length of 60 mm. To decrease friction on die walls samples were placed into containers made of pure Cu. Canned samples were inserted into a die preheated to the desired compaction temperature and dwelled for 15 min prior pressing. Graphite solution was chosen as a lubricant. Load capacity limit during ECAP was set up to the value of ~ 900 MPa given by tool limitations. The average ram speed during ECAP within chosen compaction temperature range was ~1 mm.s^{-1} (±0.8).

The mechanical properties at room and at 300 °C (20 min to reach and stabilize desired temperature + 10 min dwell prior experiment) were measured on specimens with the gauge of Ø4–32 mm (tension) and Ø5.5-10 mm (compression) using ZWICK tensile machine at the cross ram speed of 1 mm.min^{-1}. Vickers microhardness measurement were performed on compacts cross section with applied load of 10 g. The unnotched fracture toughness specimens had non-standardized dimension 4x4x55 mm and were machined longitudinally to the extrusion axis. Regarding this restrictions, obtained nonstandard results of fracture toughness K_{CN} can not be compared to normalized values of K_C. Five fracture toughness specimens were machined for each extruded bar. 3-point bending dynamic mechanical analysis (DMA) experiments were performed on 2980 DMA 1.7B machine at the Technical university of Vienna. Tested PM compacts samples were of 4x1.8x50 mm dimension and two samples of each material were tested. Experiments were carried out in one cycle at the heating and cooling rate of 3 °C.min^{-1} within temperature range up to 350 °C. Frequency of 1 Hz and amplitude of 40 μm were set up. Dilatometry experiments of PM compacts were performed at the Technical University of Vienna using thermal–mechanical analysis equipment TMA 2940 CE, Thermal Instruments, USA, see details elsewhere [6].

Microstructures were characterized by means of light microscopy, transition electron microscopy (TEM) using the JEOL JEM 100 C electron microscope operated at 100 kV and scanning electron microscopy (SEM) using the JEOL JSM 5310 by 20kV. TEM foils were prepared by mechanical grinding and electrolytic etching (80 % alcohol, 10 % ethylenglycol and 10 % fluoric acid). X-ray diffraction patterns were obtained by standard XRD using Cu Kα radiation. Calorimetric signals from phase transformations were monitored by DSC using Perkin-Elmer DSC7 and by DTA using Perkin-Elmer DTA7 systems.

3. Results and discussion

3.1 Consolidation of plain AlFe2V4 melt-spun ribbons

XRD diffractions patterns of RS AlFe2V4 confirmed beside fcc-Al phase presence of icosahedral and fcc $Al_{10}V$ intermetallic phases within the structure of as-received MSR (**Fig. 1**). With increase of annealing temperature during isothermal exposures of as-received MSR, peaks of icosahedral phase gradually diminished on expense of peaks related to $Al_{10}V$ intermetallic phase which appeared to be more apparent. This structural transformation became especially profound after high temperature annealing at temperatures over 450 °C.

Devitrification of as-received AlFe2V4 MSR took place in two steps (**Fig. 2**). First exothermic reaction was associated with formation of quasicrystalline phase and its onset was found at ~ 320 °C. At the temperature of ~ 480 °C onset of $Al_{10}V$ phase formation was confirmed.

TEM observations and SAED revealed that the fine grained microstructure of as-received ribbon is predominantly formed by α-Al grains and randomly oriented icosahedral particles (**Fig. 3a**). α-Al grains are often not perfect single crystals but contain slight misorientations.

The icosahedral particles are located inside as well as in grain boundary regions of α-Al grains. Icosahedral particles are of spherical morphology with diameters mostly not exceeding the 100 nm range. Moreover, the traces of an amorphous phase as well as fcc $Al_{10}V$ intermetallic phase were confirmed to be within the MSR structure. Microstructures with presence of all phases were found to be quite heterogeneous. That was linked to mainly inconstant cooling rates operating in particular ribbon locations. The ribbon thickness varied in the 0-20 μm range and the cooling rates are expected to somehow reflect this scatter. Furthermore it is thought that the time for homogenization of molten alloy prior casting was insufficiently short to dissolve all coexisting phases (given by equipment hindrances). No dramatic changes, indicating potential phase transformations, appeared in the microstructure of thermally exposed ribbons up to a temperature of 500 °C.

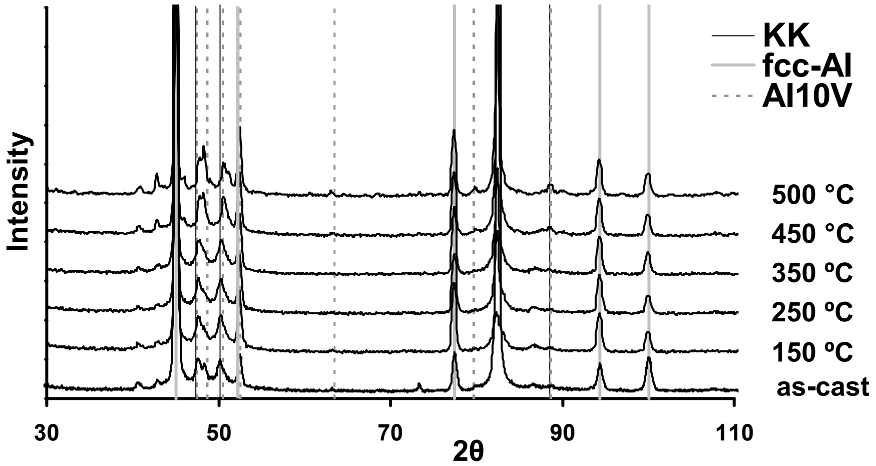

Fig. 1 XRD traces of AlFe2V4 melt-spun ribbons in as-received state and after isothermal exposures at annealing temperatures 150, 250, 350, 450 and 500 °C for 30 minutes

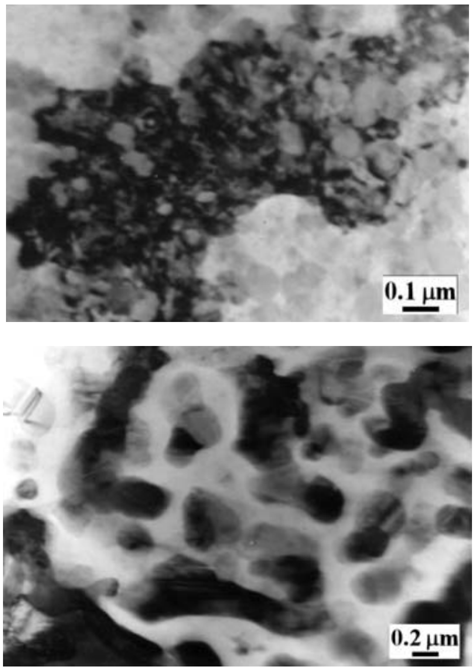

Fig. 3 TEM micrographs of as-received (upper) AlFe2V4 melt-spun ribbon (bright field image) and after annealing at 550 °C for 30 minutes (bottom)

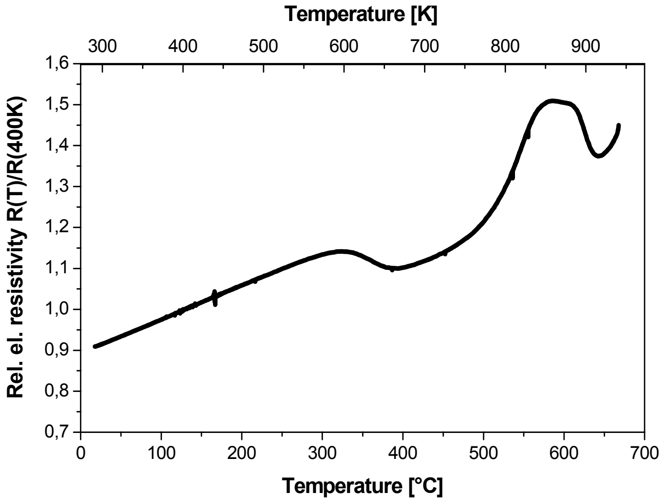

Fig. 2 Devitrification of as-received AlFe2V4 MSR (relative electrical resistivity).

The diameter of icosahedral particles did not markedly grow with increasing temperature. However, the presence of the amorphous phase was not so evident in samples that had been exposed at higher temperatures. Further increase of annealing temperature to 550 °C gave a rise to substantial grow of intermetallic $Al_{10}V$ phase (**Fig. 3b**). Consolidation of plain AlFe2V4 MSR was carried out using conventional hot direct extrusion (DE). The highest possible extrusion temperature (T_{ext}) was limited by onset of hard and brittle intermetalic phase $Al_{10}V$ formation. Excess of $Al_{10}V$ significantly depletes plasticity of MSR, makes extrusion even more difficult and eventually depletes compact's ductility and toughness. Extrusion at T_{ext} = 470 °C was established and accommodated extreme value of p_{max} = 1560 MPa (**Fig. 5**). Such high loads are technologically feasible only at laboratory level and can not be met in industry. MSR flakes defragmentation and their alignment into extrusion direction were responsible for sudden pressure drop of extrusion load after passing p_{max} value. Fraction of cryo-chopped MSR did not influence p_{max} value.

Microstructural observations revealed well deformed MSR flakes bound and arrayed into extrusion direction (**Fig. 4a**). Even though the very good metallurgical bonding between MSR particles was confirmed, the absence of deformation texture clearly revealed their poor plasticity. Though a few traces of plastic deformation within MSR namely twinning formation were observed. Lack of MSR plasticity negatively affects the material flow during extrusion and was responsible for the formation of consolidation imperfections observed predominantly in the central extrusion axis zone with less shear deformation induced (**Fig. 4b**). In agreement with annealing experiments performed on as-received MSR no new morphologies appear in the compact's microstructure after consolidation.

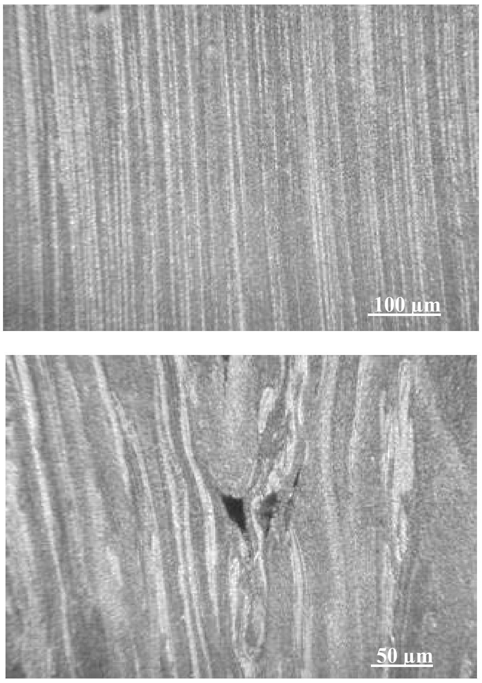

Fig. 4 Longitudinal cross-section of AlFe2V4 melt-spun ribbons extruded at T_{ext} = 470°C. Outer (upper) and central (bottom) regions of extrudate.

High compression strength of AlFe2V4 MSR compacts up to 775 MPa was determined. High strength was, however, not confirmed by subsequent more valuable tensile tests. MSR compacts prematurely failed at UTS = 548 MPa during tensile tests right after reaching yielding A = 0.2 % (**Fig. 8a**). Herein poor compact's ductility was associated with compaction imperfections. This was obviously not the case of compression tests, less sensitive to macrostructural inhomogeneities. Outstandingly high UTS of 327 MPa accompanied with significantly enhanced ductility A = 1.8 % was reached during tensile tests carried out at 300 °C (**Fig. 8b**). Relatively high Young's modulus of 96.5 GPa and 77.5 GPa determined by means of DMA analyses were confirmed at RT and 300 °C, respectively. Rather low fracture toughness of MSR compacts, wherein K_{CN} = 2 $J.cm^{-2}$ was determined, verifying the brittle character of MSR compacts. Broadest 0-200 µm fraction size of cryo-chopped MSR resulted in slightly improved ductility (at equal strengths) in comparison to narrower fractions.

3.2 Consolidation of AlFe2V4 melt-spun ribbons using "plasticizer"

To overcome the lack of plasticity new approach, where hard-to-deform AlFe2V4 MSR were compacted using "non-degrading" plasticizer made of 1 µm Al 99.7 % powder, was established. The plasticizer enabled significant reduction of extreme loads (or T_{ext}) required for extrusion of plain AlFe2V4 MSR (**Fig. 5**). Meanwhile the plasticity of extruded compacts could have been improved. After extrusion plasticizer forms a "matrix" part of two-phase composite structure, homogenously reinforced with chopped AlFe2V4 MSR flakes (**Fig. 6a**).
No apparent phase transformation took place after even long term annealing held at 350 °C, neither within of any compact's constituents. Unique structural stability of extruded "composites" was attributed to randomly oriented icosahedral particles, with traces of an amorphous phase and fcc $Al_{10}V$ intermetallic phase in AlFe2V4 MSR and to efficient strengthening by homogeneously distributed nano-scale dispersoids coming from broken surface oxides of original 1 µm Al powder plasticizer particles, see detail study of plain 1 µm Al 99.7 % compacts in [7]. Perfect metallurgical bonding was created. Interparticle fracture through MSR flakes with no pulling-out of MSR particles and no separation at the ribbon-powder interface was detected after tensile loading (**Fig. 6b**). That confirmed perfect metallurgical bonding on MSR / powder interfaces and hence proper transfer of stresses from matrix to strengthening MSR particles (**Fig. 7**).

Room temperature ductility and fracture toughness of mixture compacts were significantly improved in comparison to plain AlFe2V4 MSR compacts. The compacts reproducibly attained the room temperature tensile strength of plain MSR compacts (above ~ 500 MPa) however at significantly enhanced ductility (A ~ 4.5 %), **Fig. 8a**. Good correlation between strength values obtained from tensile and compression tests pointed out to successful consolidation of mixtures. Outstanding high temperature strength of plain MSR compacts was retained also in case of mixture compacts, where addition of plasticizer led to only marginal strength decline though at improved ductility (UTS = 281 MPa and A = 4.4 % at 300 °C for 33 wt. % of plasticizer), **Fig. 8b**.

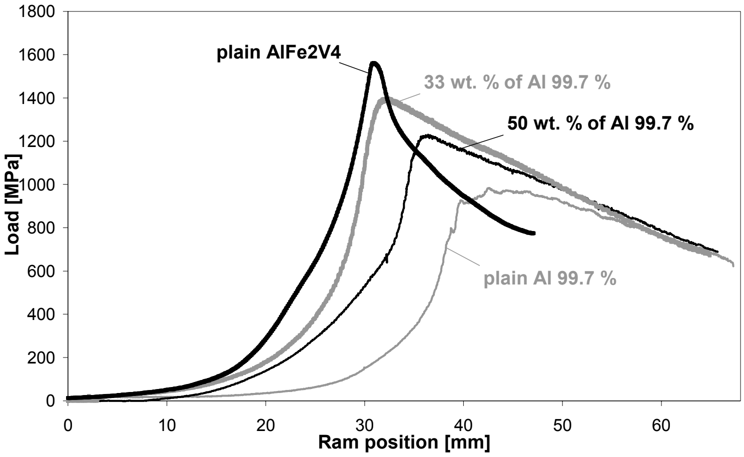

Fig. 5 Evolution of extrusion loads for AlFe2V4 MSR flakes and 1 µm Al 99.7 % powder plasticizer itself. Effect of two different amount of plasticizer admixed into AlFe2V4 MSR (T_{ext}=470 °C)

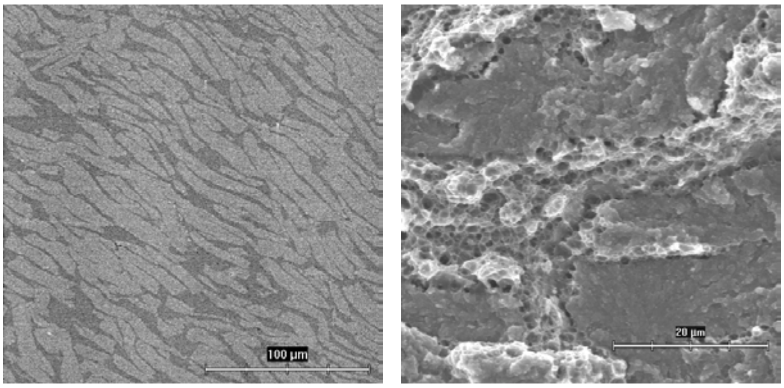

Fig. 6 Transversal cross-section micrograph (left) and fracture surface after room temperature tensile tests of AlFe2V4 MSR + 1 µm Al mixture compacts (right).
(63-200 µm MSR fraction, 33 wt.% of 1 µm Al powder, T_{ext} = 470 °C)

3.3 Consolidation using equal channel angular pressing (ECAP) technique

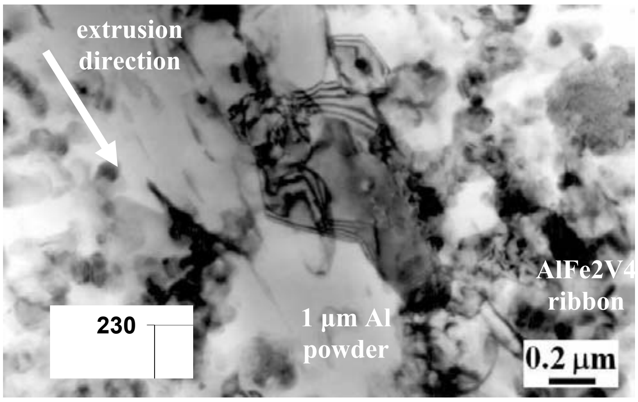

Fig. 7 TEM micrograph of AlFe2V4 MSR / 1 µm Al 99.7 % powder mixture compact (63-200 µm, 33 wt.% of Al powder, T_{ext} = 470 °C, arrow indicates extrusion direction). Bright field image of neighboring constituents

Alternatively to direct extrusion (DE) an original approach utilizing ECAP [8] technique was proposed for consolidation of AlFe2V4 MSR and ultra-fine 1µm Al 99.7 % powder mixtures. ECAP provides efficient plastic straining via simple shear where normal stresses can be minimized, what leads to significant reduction of overall loads. The experiments have shown that the pressure during ECAP of 1µm Al 99.7 % powder was almost 6 times lower if compared to pressures present during DE (R = 11:1) at the same pressing temperatures. This allowed to lower pressing temperature from 500 ˚C (DE) to 200 ˚C (ECAP) if compared for both processes carried at the same pressing load (~

800 MPa). Obtained microstructures (**Fig. 9**) and mechanical properties of ECAP compacts were identical to their DE counterparts [7]. Unlike compacts prepared via DE the ECAP brought uniform deformation throughout the entire cross-section of compacted material. Based on ECAP principles, multiple step-wise straining (finished route Bc – 4 pressings, +90° rotation) without cross-sectional changes enhanced induced deformation of powder compacts and was accompanied with further refinement and strength increase.

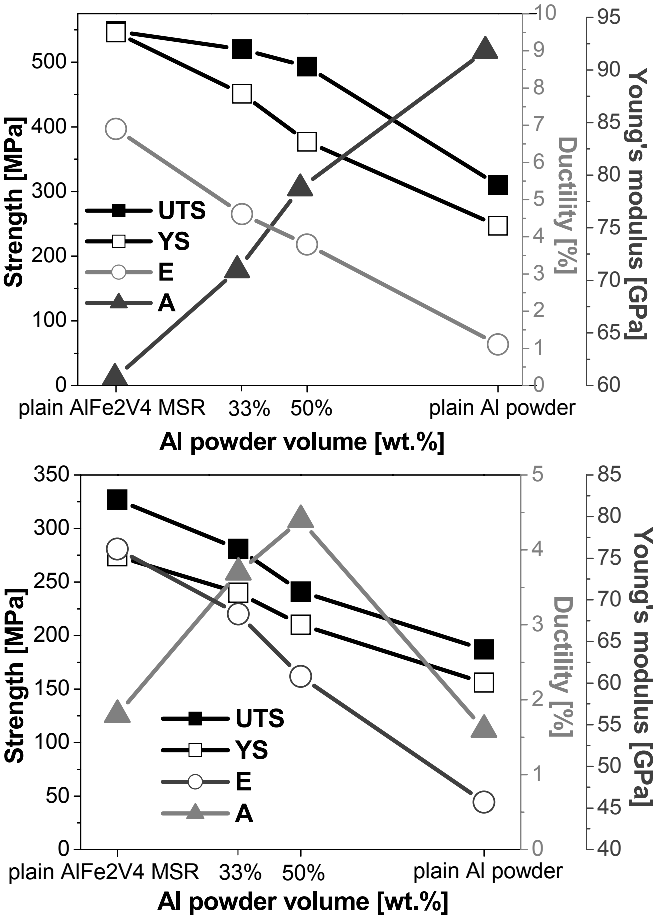

Fig. 8 Evolution of UTS, YS, A and E of extruded AlFe2V4 MSR mixture compacts in hand with increasing 1 μm Al 99.7 % powder amount obtained from room temperature tensile tests (upper) and at testing temperature 300 °C (bottom). (T_{ext} = 470 °C, 0-200 μm MSR fraction)

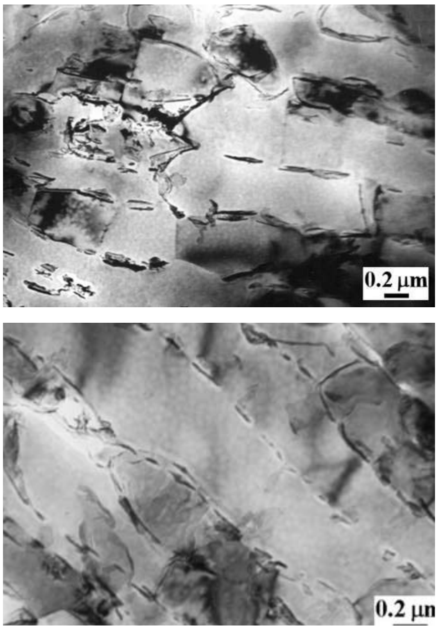

Fig. 9 The structure of compacted 1 μm Al 99.7 % powder via direct extrusion at 500 °C (upper) and ECAP at 200 °C (bottom). (TEM)

Similar consolidation behavior was observed also in a case of AlFe2V4 MSR, whereas ECAP made feasible their compaction into sound profiles even at moderate temperatures ~ 350 °C. Thus the potential of ECAP for compaction of high strength rapidly quenched materials without danger of undesired structural changes during consolidation was confirmed. Multiple pressing accommodated severe straining of compacted MSR, further densification of compacts and improvement of mechanical properties (HV), **Fig. 10**.

4. Conclusions

- to maintain desired plasticity and microstructures of rapidly solidified AlFe2V4 MSR the highest possible processing temperature was limited by formation of hard and brittle intermetalic $Al_{10}V$ phase (~ 480 °C)
- extreme pressing loads were required for consolidation of plain cryo-chopped MSR into sound compacts via conventional DE

- tensile tests of MSR compacts held at 300 °C confirmed outstanding UTS = 327 MPa at A = 1.8 %, though consolidation imperfection deteriorated plasticity (i.e. fracture toughness) of MSR compacts and led to premature failure during room temperature tensile tests
- new approach was established, wherein 1 μm Al 99.7 % powder was made use of as a plasticizer admixed into MSR yielding composites of powder matrix reinforced with MSR
- plasticizer reduced extreme loads (or T_{ext}) required for DE of plain MSR and meanwhile enhance the plasticity of extruded mixture compacts
- alternative ECAP technique showed real application potential for consolidation of discrete particles made of hard-to-work rapidly solidified Al based alloys. When compared to DE (R = 11:1) substantial decrease of pressing pressures was attained by ECAP, what enabled significant decrease of pressing temperature

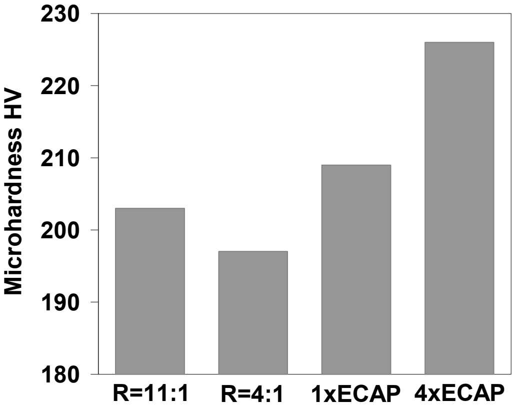

Fig. 10 Microhardness HV of compacts prepared by direct extrusion (R = 4:1 and 11:1) and by means of ECAP (1 pass and 4 passes – route Bc)

Attained mechanical properties of mixtures, especially at elevated temperatures, are currently superior to any conventional Al based alloys. The suggested technological approach enables real utilization of RS ribbons in bulk structural profiles, whereas most of conventional technological equipment can be used for this purpose without need of intensive new investments.

5. Acknowledgments

This investigation was financially supported by Slovak Agency for S&T Support under the project APVT-51-031204. The authors thank also Slovak Centre of Excellence NANOSMART and especially P. Švec and D. Janičkovič from Institute of Physics, SAS, Bratislava for the supply of melt-spun ribbons and Austrian company MEPURA GmbH for the supply of fine Al powders.

6. References

[1] INOUE A., Prog. Mat. Sci.43, 1998, p.365
[2] NAGY J., BALOG M., IZDINSKY K., SIMANCIK F., SVEC P., JANICKOVIC D., Int. J. Mat. & Product Tech, Vol.23, Nos.1/2, 2005, p.79-90
[3] MEPURA G.m.b.H., http://www.mepura.at
[4] ALTENPOHL D., Aluminium viewed from within, Aluminium-Verlag, 1982
[5] SURYANARAYANA: Nanocrystalline materials, Int. Mat. Rev., Vol.40, No.2, 1995, p.41-63
[6] HUBER T., Thermal expansion of aluminium alloys and composites. PhD thesis, Vienna University of Technology, Faculty of Mechanical Engineering, 2003
[7] BALOG M., NAGY J., IZDINSKY K., SIMANCIK F., Int. J. Mat. & Product Tech., Vol.23, Nos.1/2, 2005, p70-78,
[8] SEGAL V.M., Russ. Metall. [English Translation], 1981, 1:99

11. Savjetovanje o materijalima, tehnologijama, trenju i trošenju
11. Conference on Materials, Processes, Friction and Wear
MATRIB'06, Vela Luka, 22-24.06.2006.

PRIMJENA POSTUPKA PLINSKOG NAŠTRCAVANJA U TRIBOMEHANIČKIM SUSTAVIMA

APPLAYING OF FLAME SPRAYING ON TRIBOMECHANICAL SYSTEMS

Katica Šimunović, Goran Šimunović, Tomislav Šarić
Sveučilište Josipa Jurja Strossmayera u Osijeku
Strojarski fakultet u Slavonskom Brodu
Trg I. Brlić-Mažuranić 2, HR-35000 Slavonski Brod

Sažetak: Postupak plinskog naštrcavanja primjenjuje se često u pogonima održavanja, za obnavljanje istrošenih elemenata tribomehaničkih sustava (rukavci vratila, zaštitne čahure, brtvenice, zupčanici…), ali nije isključena niti uporaba na nove dijelove s ciljem povišenja otpornosti na trošenje i koroziju. Primjenom ovih postupaka na istrošene dijelove, ali i prilikom zaštite od trošenja novih dijelova, značajno se produljuje vijek trajanja.

Zbog velikog broja mogućih materijala slojeva i podloga na koje se slojevi mogu nanositi, postupci naštrcavanja, pa tako i plinskog naštrcavanja, danas se primjenjuju u gotovo svim granama industrije.

Jedna od prednosti postupaka naštrcavanja u odnosu na druge postupke prevlačenja je da se slojevi mogu nanositi na mjestu eksploatacije nekog dijela (tako se postupak može primijeniti, na primjer, prilikom popravaka na mostovima), primjena im nije ograničena veličinom podloge na koju se nanosi sloj, a mogu se dobiti i relativno debeli slojevi. Postupak plinskog naštrcavanja ima prilično niske troškove nanošenja slojeva.

Uz ove prednosti postoje i nedostaci, a glavni nedostatak je da je relativno loš koeficijent iskorištenja materijala za naštrcavanje, kao i velika buka, prašina i dim pri izvođenju postupka.

U radu su dane teorijske osnove, opisane su prednosti i nedostaci, te su prikazani primjeri primjene na elemente tribomehaničkih sustava.

Ključne riječi: plinsko naštrcavanje, tribomehanički sustavi, održavanje

Abstract: Flame spraying has been frequently used in maintenance workshops to regenerate worn elements of tribomechanical systems (shaft sleeves, stuffing boxes, gears, …) as well as to protect new parts from wear and corrosion. Flame spraying applied on worn tribomechanical elements as well as on new parts, has a significant influence on prolongation of service life.

Because of great number of potential coating materials and substrates, all the thermal spray technologies are applied in almost every industry branch.

One of the great advantages of flame spraying, in comparison to the other coating technologies, is application in exploitation (for example, bridge repairs); substrate dimensions are not the limiting factor, and the relatively thick coatings can be produced with low technology costs.

The most important disadvantage is the low coefficient of coating material utilization as well as noise, dust and fume.

Theoretical bases, the most important advantages and disadvantages and examples of application of flame spraying on tribomechanical systems have been presented in this paper.

Keywords: flame spraying, tribomechanical systems, maintenance

1 UVOD

U nekom realnom tribosustavu, između dvije površine u dodiru i relativnom gibanju javlja se trenje koje uzrokuje gubitak energije, te dolazi do smanjenja stupnja iskorištenja sustava [1]. Ulazna energija se dobrim dijelom troši na savladavanje sile trenja i prelazi nepovratno u toplinu. Uz gubitak energije koja se potroši na savladavanje trenja, trošenje utječe na gubitak materijala odnosno na vijek trajanja koji je određen mehanizmom tribološkog dotrajavanja [2]. Za tribološko dotrajavanje vezani su direktni i indirektni gubici. Direktni gubici odnose se na troškove održavanja (materijali za izradu rezervnih dijelova, nabava gotovih rezervnih dijelova, sredstva za podmazivanje, potrošni materijal, te utrošeni rad na aktivnosti održavanja). Indirektni gubici nastaju kao posljedica direktnih gubitaka. To su gubici uslijed zastoja i pokazano je da su u više slučajeva do sada, ovi gubici bili istog reda veličine kao i direktni gubici [2]. Osim gubitaka zbog zastoja, u indirektne gubitke ubrajaju se i kapitalne investicije koje su posljedica smanjenog vijeka trajanja opreme, kao i potrebe za podizanjem efikasnosti.

Kako bi se produljio vijek trajanja opreme, a time i smanjili direktni i indirektni gubici održavanja, poduzimaju se različite tribološke mjere, a jedna od njih može biti i primjena postupaka naštrcavanja za obnavljanje dijelova i komponenti tribomehaničkih sustava [3]. Jedan od postupaka naštrcavanja je plinsko naštrcavanje.

Plinsko naštrcavanje (engl. *flame spraying*, njem. *Flammspritzen,* rus. *gazoplamennoe nanesenie, gazovaja naplavka*) se ubraja u skupinu postupaka toplinskog naštrcavanja. Toplinsko naštrcavanje (engl. *thermal spraying*) je toplinsko-mehanički postupak prevlačenja, a postupci prevlačenja uz postupke modificiranja, čine postupke oplemenjivanja površina (inženjerstva površina) [4].

Kako se složeni sustav inženjerstva površina sastoji od tri različita podsustava, a to su podloga, sloj i postupak prevlačenja, razumljivo je i da postoje različiti pristupi istraživanju takvog složenog sustava. Kada je riječ o plinski naštrcanim slojevima, u literaturi su ispitivane različite vrste takvih slojeva, na različitim podlogama.

Istraživanja slojeva su se provodila obzirom na otpornost na trošenje i to uglavnom na abrazijsko i erozijsko trošenje [5-9]. Opći je zaključak da je većina autora došla do spoznaje da na otpornost na trošenje utječu karakteristike sloja kao što su mikrostruktura, poroznost i tvrdoća. Osobit utjecaj na trošenje imaju čestice tvrdih faza raspoređene u žilavoj matrici. Optimalna svojstva sloja se mogu postići pravilnim izborom parametara naštrcavanja kao što su omjer gorivi plin/kisik, udaljenost naštrcavanja i brzina isporuke praha.

Istraživano je i ponašanje slojeva pri djelovanju vanjskog mehaničkog opterećenja [10-14]. Postoje dva pristupa istraživanju naprezanja u sustavu podloga/sloj i to sa stajališta konvencionalne mehanike i sa stajališta mehanike loma, te je zaključeno da je za razvoj pukotine djelovanjem vanjskog opterećenja važno svojstvo lomne žilavosti sloja, debljina sloja, kao i svojstva podloge.

Pri istraživanju zaostalih naprezanja [15-20], uz eksperimentalna istraživanja razvijeni su i brojni analitički i numerički modeli. Relaksacijom zaostalih naprezanja mogu se pojaviti pukotine u sloju i na granici sustava podloga/sloj. Osobito su važna: zaostala naprezanja zbog hlađenja rastaljenih čestica u tijeku postupka naštrcavanja, naprezanja zbog faznih transformacija u sloju, naprezanja zbog hlađenja sloja i podloge na sobnu temperaturu (različiti koeficijenti toplinskog širenja materijala sloja i podloge – engl. *thermal expansion coefficient mis-match*, *CTE mis-match*), kao i naprezanja zbog plastične deformacije skrutnutog sloja.

2 O POSTUPKU PLINSKOG NAŠTRCAVANJA

Plinsko naštrcavanje je postupak koji za taljenje materijala od kojeg nastaje sloj, koristi toplinsku energiju oslobođenu izgaranjem gorivog plina u kisiku. Ubrzanje rastaljenih čestica prema podlozi postiže se pomoću plinova izgaranja ili komprimiranog zraka. Polazni materijal od kojeg nastaje sloj može biti u obliku žice, šipke ili praha. Postupkom plinskog naštrcavanja mogu se nanijeti polimerni, metalni, keramički i kompozitni slojevi.

Plinsko naštrcavanje je najstariji postupak toplinskog naštrcavanja; prvi puta se spominje u patentima švicarskog inženjera Maxa Ulricha Schoop-a (1870-1956) početkom prošlog stoljeća.

Na slici 1 shematski je prikazan postupak plinskog naštrcavanja s prahom (engl. *powder flame spraying*).

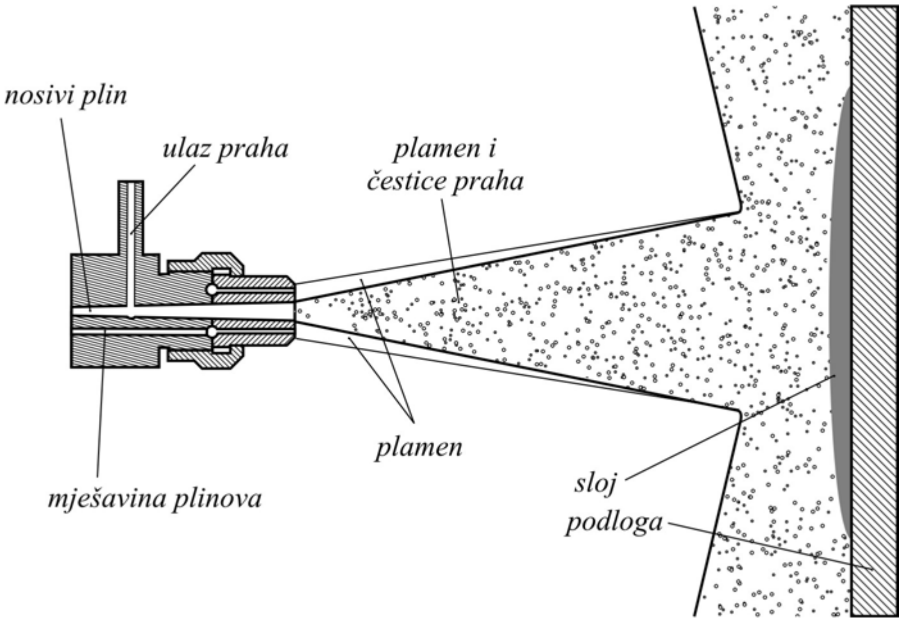

Slika 1. Shematski prikaz postupka plinskog naštrcavanja [21]

Jedna od prednosti postupaka naštrcavanja u odnosu na druge postupke prevlačenja je da se slojevi mogu nanositi na mjestu eksploatacije nekog dijela (tako se postupak može primijeniti, na primjer, prilikom popravaka na mostovima), a primjena im nije ograničena veličinom podloge na koju se nanosi sloj. Također, zagrijavanje čestica, hlađenje, skrutnjavanje i naknadna obrada nisu složeni procesi, a mogu se dobiti relativno debeli slojevi. Postupak plinskog naštrcavanja ima prilično niske troškove nanošenja slojeva.

Uz ove prednosti postoje i nedostaci, a glavni nedostatak je da je relativno loš koeficijent iskorištenja materijala za naštrcavanje, kao i velika buka, prašina i dim pri izvođenju postupka.

Pri postupku plinskog naštrcavanja, u usporedbi s plazma i HVOF naštrcavanjem, dobivaju se slojevi s više poroznosti i oksidnih uključaka, te manjom čvrstoćom prianjanja.

2.1 Hladni i topli postupak plinskog naštrcavanja

Kod *hladnog postupka* plinskog naštrcavanja, temperature na površini dodira podloge i sloja su niske (do 200°C), te je mehanička veza najčešći oblik prianjanja sloja na podlogu. Rastaljene ili djelomično rastaljene čestice materijala sloja ne tale materijal podloge prilikom dodira, nego dolazi samo do blagog zagrijavanja površine, te je to i jedna od glavnih prednosti hladnog postupka naštrcavanja. Stoga ovaj postupak obično nema utjecaja na toplinsku obradu ili kemijski sastav podloge.

Kvaliteta naštrcanih slojeva ovisit će o jačini veze (čvrstoći prianjanja, engl. *adhesive strength*) između sloja i podloge. Stoga se podloga mora prethodno pažljivo pripremiti kako bi se odstranilo onečišćenje, vlaga, korozija itd.

Nakon čišćenja površine podloge, potrebno ju je ohrapaviti, (pjeskarenjem, tokarenjem navoja, …) kako bi se osigurala dobra prionjivost. Nakon toga, postupak naštrcavanja mora što ranije započeti kako ne bi došlo do ponovnog onečišćenja podloge. U nekim slučajevima podloga se zagrijava kako bi se uklonila vlaga.

Metalurška veza između sloja i podloge stvara se kod tzv. *toplog postupka* plinskog naštrcavanja. Topli postupak plinskog naštrcavanja je postupak koji se može provesti u jednom koraku, kada imamo istovremeno naštrcavanje i spajanje (taljenje) praha (temperature su približno 1000 °C, ovisno o leguri) (slika 2) ili kada imamo prvo naštrcavanje praha, a zatim zagrijavanje plamenikom, u peći ili indukcijski, kako bi se prah vezao. To je topli postupak kod kojeg su faza naštrcavanja i faza utaljivanja razdvojene.

Toplim postupkom plinskog naštrcavanja mogu se nanositi tzv. legure sa svojstvom samotečenja (engl. *self-fluxing alloys*). Legure sa svojstvom samotečenja su složeni sustav Ni-Cr-B-Si-Fe-C čije karakteristike ovise o sadržaju i omjeru elemenata, kao i o tehnološkim parametrima taljenja i naštrcavanja.

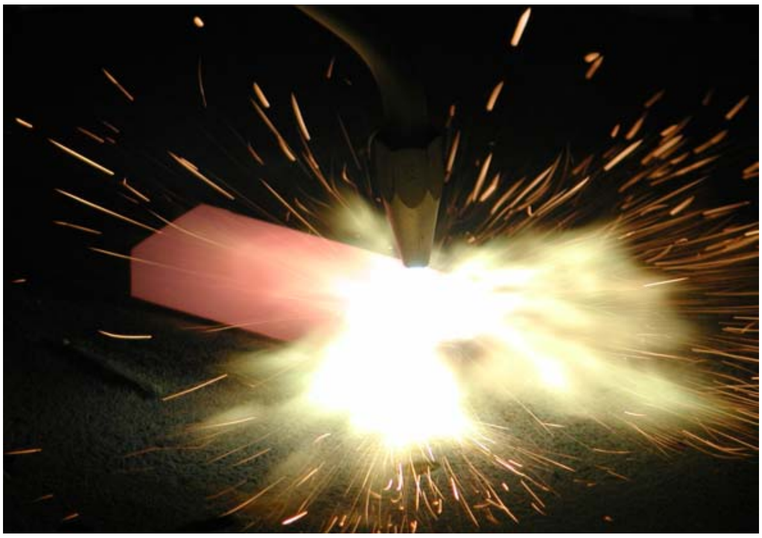

Slika 2. Topli postupak plinskog naštrcavanja [22]

3 PRIMJERI PRIMJENE PLINSKOG NAŠTRCAVANJA

U nastavku će biti opisani neki primjeri primjene.

Materijali koji se često nanose hladnim postupkom plinskog naštrcavanja su keramike. Keramički (oksidni) slojevi se zbog visoke tvrdoće i toplinske stabilnosti upotrebljavaju kao zaštitni toplinski slojevi, termalne barijere (engl. *thermal barrier coatings, TBC*) i slojevi otporni na trošenje i koroziju. Česta primjena keramičkih slojeva je za zaštitu ili obnavljanje lopatica parne turbine od nehrđajućeg čelika, koje su izložene erozijskom trošenju kapljevinom i visokim temperaturama, kao i za zaštitu ili obnavljanje rotora crpki, te cijevi u kotlovima gdje je prisutna visokotemperaturna korozija i erozija. Keramički slojevi se upotrebljavaju još i u avionskim motorima, tekstilnoj, papirnoj i grafičkoj industriji.

Slojevi od metala i legura najčešće se koriste za zaštitu od korozije u vodenim otopinama, u plinovima pri višim temperaturama, te kao vezni slojevi. Najznačajniji metali su aluminij, nikal, bakar, krom, cink i molibden. Aluminij je otporan u kiselim plinskim atmosferama (na primjer, u produktima izgaranja fosilnih goriva), kao i u slanoj vodi, te se takva vrsta slojeva može koristiti za zaštitu i popravke na mostovima ili na platformama. Veliko tehničko i ekonomsko značenje imaju i legure MeCrAlY. Te legure na osnovi kobalta, željeza ili nikla su veoma otporne na visokotemperaturnu koroziju, te se koriste u plinskim turbinama, avionskim motorima ili kao međuslojevi.

Kombinacija metalne tvrde faze s metalnom matricom tvori tvrdi metal. Za postupak naštrcavanja uglavnom se koriste tvrdi metali s volfram karbidima (WC, W_2C) i krom karbidima (Cr_2C_2) kao tvrdim fazama i kobaltom i/ili niklom kao žilavim metalnim matricama koje nose tvrde faze. Volfram karbidi se koriste s kobaltom ili niklom kao matricama, a udio je između 8 i 20%. Krom karbidi se nalaze u matricama NiCr, a udio im je od 20 do 35%. Prednost ovih slojeva u usporedbi s WC/Co slojevima je bolja stabilnost na povišenim temperaturama. WC/Co slojevi se mogu koristiti na temperaturama do 550 do 600 ^{o}C (primjer korištenja na cijevi izmjenjivača topline), a Cr_2C_2/NiCr slojevi se mogu koristiti na temperaturama do 900 ^{o}C.

Jedna od čestih primjena postupaka plinskog naštrcavanja je popravak istrošenih vratila, osobito područja ležaja. Na slici 3 prikazana je istrošena zaštitna čahura (tuljak), koja se nalazila u gumenom kliznom ležaju na vratilu vertikalne crpke u jednom energetskom postrojenju. Uslijed abrazijskog trošenja (čestice pijeska u riječnoj vodi), značajno je bio smanjen vijek trajanja čahurama, te su se morale često mijenjati. Kako su napravljene od nehrđajućeg martenzitnog Cr-Mo čelika, predstavljale su značajni trošak održavanja. Jedna od mogućih triboloških mjera za smanjenje troškova, nastalih nabavkom skupih rezervnih dijelova, je primjena postupka plinskog naštrcavanja. Često se koriste slojevi od nehrđajućeg čelika, bronce (trošenje metal-metal u kliznim ležajevima), ali i keramički slojevi.

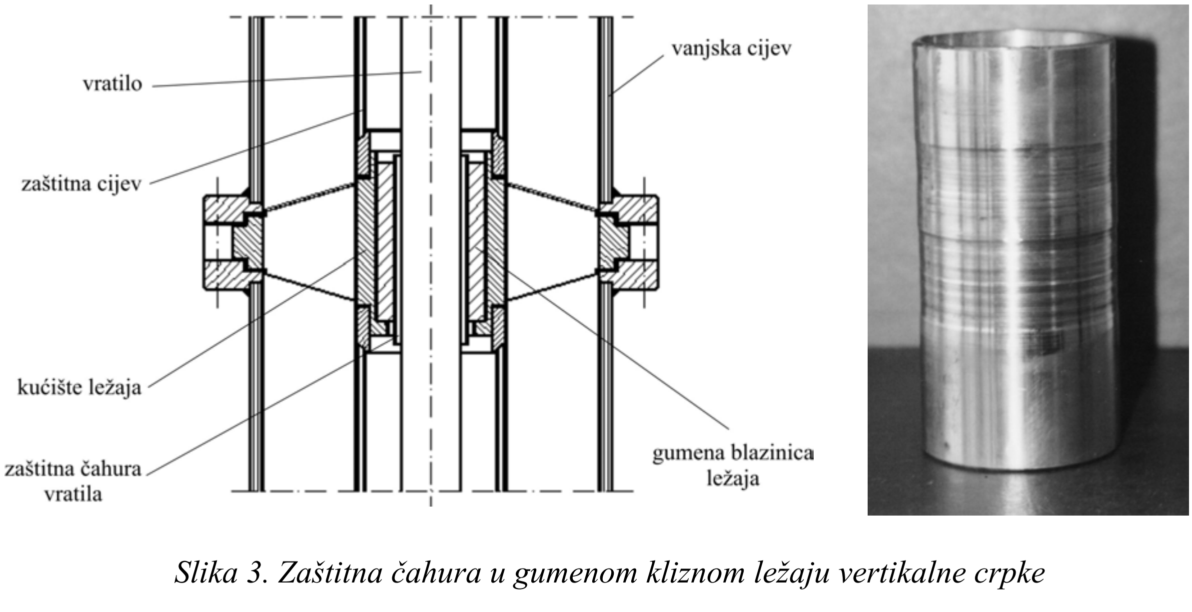

Slika 3. Zaštitna čahura u gumenom kliznom ležaju vertikalne crpke

Česta primjena postupaka plinskog naštrcavanja je i u poljoprivrednoj industriji [23] na dijelove alata za obradu zemlje, u industriji stakla, gdje materijali slojeva moraju podnijeti i visoke temperature. Tu je česta upotreba NiCrBSi legura koje mogu izdržati visoke temperature (na primjer, abrazivni medij-rastaljeno silika staklo je temperature 700^{o}C), a imaju i visoku otpornost na abrazijsko trošenje.

Plinskim naštrcavanjem mogu se nanositi i polimerni slojevi koji se sve više primjenjuju za povećanje otpornosti na koroziju i trošenje, za smanjenje trenja, za bioaktivne površine, električnu izolaciju, te u dekorativne svrhe. Dodavanjem sredstva za očvršćivanje (mineralno, organsko ili metalno) dobivaju se polimerni kompoziti s poboljšanim mehaničkim svojstvima. Danas se teži k razvoju magnetnih polimernih kompozita (s dodatkom ferita) koji bi se primjenjivali u avionskoj, automobilskoj industriji i u elektromehaničkim uređajima. Kompozitni sloj polimer/visokotemperaturna legura primjenjuje se u plinskim turbinskim motorima. Pri takvoj primjeni polimer na visokim temperaturama ispari i dobije se sloj kontrolirane poroznosti [24].

4 ZAKLJUČAK

Postupcima toplinskog naštrcavanja, pa tako i plinskog naštrcavanja, cilj je produljiti vijek trajanja elemenata tribomehaničkih sustava zaštitom od trošenja i korozije. Produljenjem vijeka trajanja istrošenih ili novih dijelova i komponenti, mogu se postići značajne uštede, jer se smanjuju direktni i indirektni gubici održavanja.

Plinsko naštrcavanje je najstariji postupak toplinskog naštrcavanja (gotovo 100 godina), ali to ne znači da se više ne koristi. Tako uz ručne postupke, danas postoje i potpuno automatizirani. Uz stalno osuvremenjivanje opreme, razvijaju se nove varijante postupaka kao i novi materijali slojeva.

5 LITERATURA

[1] V. Ivušić: Tribologija, Hrvatsko društvo za materijale i tribologiju, Zagreb, 2002

[2] R. Zgaga: Tribološki nivo proizvoda, Tribologija u industriji V(3), 1983, 67-68

[3] N. Majdandžić: Strategije održavanja i informacijski sustavi održavanja, Strojarski fakultet u Slavonskom Brodu, Slavonski Brod, 1999

[4] M. Stupnišek, B. Matijević: Pregled postupaka modificiranja i prevlačenja materijala, Zbornik radova Toplinska obradba metala i inženjerstvo površina, Zagreb, 200

[5] I. Iordanova, K.S. Forcey, B. Gergov, V. Bojinov: Characterisation of flame-sprayed pure metallic and alloyed coatings, Surface and Coatings Technology 72, 1995, 23-29

[6] J.P. Tu, M.S. Liu, Z.Y. Mao: Erosion resistance of Ni-WC self-fluxing alloy coating at high temperature, Wear 209, 1997, 43-48

[7] J. Rodriguez, A. Martin, R. Fernandez, J.E. Fernandez: An experimental study of the wear performance of NiCrBSi thermal spray coatings, Wear 255, 2003, 950-955

[8] H. Wang, W. Xia, Y. Yin: A study on abrasive resistance of Ni-based coatings with a WC hard phase, Wear 195, 1996, 47-52

[9] T. Hejwowski, A. Szewezyk, A. Weronski: An investigation of the abrasive wear of flame-sprayed coatings, Journal of Materials Processing Technology 106, 2000, 54-57

[10] M. Vijaya Babu, R. Krishna Kumar, O. Prabhakar, N. Gowri Shankar: Fracture mechanics approaches to coating strength evaluation, Engineering Fracture Mechanics 55, 1996, 235-248

[11] S.C. Gill, T.W. Clyne: Stress distributions and material response in thermal spraying of metallic and ceramic deposits, Metallurgical Transactions B21, 1990, 377-385

[12] S.R. Kim, J.A. Nairn: Fracture mechanics analysis of coating/substrate systems, Part I: Analysis of tensile and bending experiments, Engineering Fracture Mechanics 65, 2000, 573-593

[13] S.R. Kim, J.A. Nairn: Fracture mechanics analysis of coating/substrate systems, Part II: Experiments in bending, Engineering Fracture Mechanics 65, 2000, 595-607

[14] K. Holmberg, M. Matthews, H. Ronkainen: Coatings tribology – contact mechanics and surface design, Tribology International 31, 1998, 107-120

[15] I. Iordanova, K.S. Forcey: Texture and residual stresses in thermally sprayed coatings, Surface and Coatings Technology 91, 1997, 174-182

[16] J. Matejicek, S. Sampath: In situ measurement of residual stresses and elastic moduli in thermal sprayed coatings: Part 1: apparatus and analysis, Acta Materialia 51 (3), 2003, 863-872

[17] S.C. Gill, T.W. Clyne: Investigation of residual stress generation during thermal spraying by continuous curvature measurement, Thin Solid Films 250, 1994, 172-180

[18] Y.C. Tsui, T.W. Clyne: An analytical model for predicting residual stresses in progressively deposited coatings, Part 1: Planar geometry, Thin Solid Films 306, 1997, 23-33

[19] Y.C. Tsui, S.J. Howard, T.W. Clyne: The effect of residual stresses on the debonding of coatings. Part II: An experimental study of a thermally sprayed system, Acta Metallurgica et Materialia 42, 1994, 2837- 2844

[20] S. Kuroda, T.W. Clyne: The quenching stress in thermally sprayed coatings, Thin Solid Films 200, 1991, 49-66

[21] O. Knotek: Thermal spraying and detonation gun processes, in R.F. Bunshah: Handbook of Hard Coatings, Noyes Publications/William Andrew Publishing, LLC Norwich, New York, 2001

[22] K. Šimunović: Optimizacija tribomehaničkih svojstava plinski naštrcanih slojeva, doktorska disertacija, Fakultet strojarstva i brodogradnje, Zagreb, 2004

[23] S. Kralj: Navarivanje, naštrcavanje, nalemljivanje: Prednosti i nedostaci, Zbornik radova skupa Tribologija u agroindustrijskom kompleksu, Zagreb, 1993, 5-13

[24] E. Petrovicova, L. S. Schadler: Thermal spraying of polymers, International Materials Reviews 47 (4), 2002, 169-190

MICROSTRUCTURE AND HARDNESS OF Ti-BASED ALLOYS WITH Co AND Cr

Ljerka Slokar, Tanja Matković, Prosper Matković

University of Zagreb

Faculty of Metallurgy, Aleja narodnih heroja 3, 44103 Sisak, Croatia

Abstract:

In this paper the effects of cobalt and chromium additions on the microstructure and hardness of as-cast titanium-based alloys was investigated.

Ten specimens of Ti-Co-Cr alloys with titanium content ranging from 50 to 80 at. % were prepared by melting the pure elements in a laboratory arc-furnace under argon atmosphere. The microstructure of the as-cast samples was observed by optical microscope. Microphotographs were taken with digital camera and analysed with the corresponding programmes. Hardness was measured by Vickers method (HV3).

Optical microscopy shows that almost all samples have two-phases microstructure, which consists of dendritic and interdendritic region. Only one sample has a three phases microstructure. From the results of a quantitative metallography can be seen that the content of phases depends on alloy composition. Hardness measurements indicate that hardness increases with the content of dendritic phase.

Key words: Ti-Co-Cr as-cast alloys, microstructure, hardness

INTRODUCTION

Titanium and its alloys are currently the most commonly used implant materials because of many exceptional advantages, such as: biocompatibility, excellent corrosion resistance, low density and good balance of mechanical properties. On the other hand, the problems are low shear strength and wear resistance and high Young's modulus in relation to that of the bone. To solve these problems and to improve their biomechanical properties for biomedical applications, many new Ti-base alloys have been designed. For this purpose, their compositions are modified by alloying. Chromium served as stabilizer of β-phase of titanium, which has acceptable properties, and cobalt is used to strengthen these alloys /**1-3**/.

MATERIALS AND METHODS

Ten samples of Ti-Co-Cr alloys, with titanium content in the range of 50 to 80 at. %, were prepared in a laboratory arc-furnace under argon atmosphere by melting the pure elements. To achieve homogeneity, the samples in form of "buttons" (Figure 1) were melted three times by a specially constructed copper anode which was served as casting mould. In this way, cylindrical specimens with dimensions about 7x12 mm were produced directly.

Figure 1. Alloys in „buttons" form

The buttons were embedded in an epoxy resin and metallographically prepared with wet grinding on SiC paper and final polishing with Al_2O_3 water suspension. They were etched with cold solution: 50 cm^3, HCl_{conc}, 5 cm^3 $HNO_{3\,conc}$ and 50 cm^3 H_2O.

The microstructure of the as-cast alloys was observed by optical microscope Leitz, Ortholux at the magnification of 280x. Microphotographs were taken with digital camera Olympus DP11 and used for optical metallography. The programmes Olympus DP-Soft and UTHSCA Image Tool were used for quantitative analysis.

Hardness measurements were performed by Vickers method (HV3) on the equipment of Otto-Wolpert-Werke.

RESULTS AND DISCUSSION

The influences of cobalt and chromium additions on the microstructure and hardness of as-cast titanium-based alloys were examined. Ten samples of Ti-Co-Cr alloys have been prepared for this purpose. Their positions are illustrated on the isothermal section of ternary phase diagram (Figure 2).

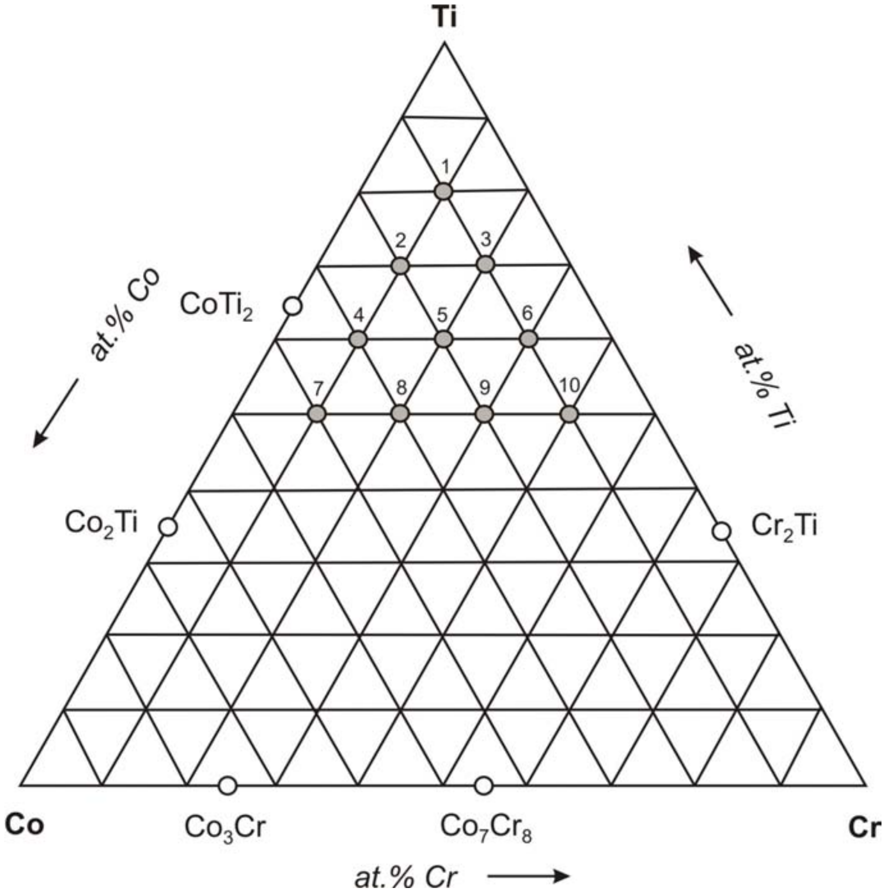

Figure 2. Compositions of experimental alloys presented on the isothermal section of ternary Co-Cr-Ti system at room temperature

Investigation of these alloys by optical microscopy shows that almost all samples have two-phases microstructure. It consists of dendritic and interdendritic region, which can be seen on microphotographs as dark and light areas (Figure 3a). Only one alloy - sample 10 has three phases microstructure (Figure 3b).

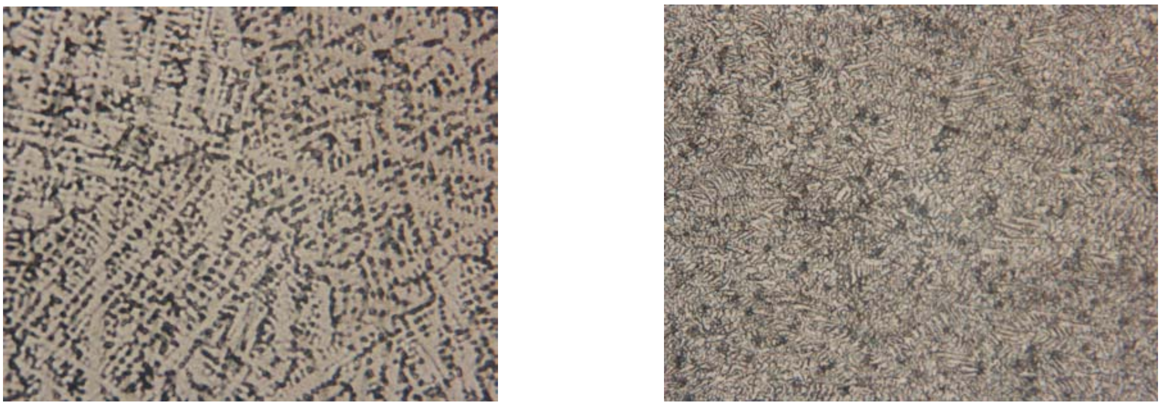

a) Sample 1, $Co_{10}Cr_{10}Ti_{80}$

b) Sample 10, $Co_{10}Cr_{40}Ti_{50}$

Figure 3. Microphotographs of as-cast $Co_{10}Cr_{10}Ti_{80}$ and $Co_{10}Cr_{40}Ti_{50}$ alloys (280x)

The results of quantitative metallography (Table 1) indicate that the phases content depends on alloy composition. So, in alloys with lower titanium content (50 at. %) the percentage of dendrites increases with increasing of chromium content and decreasing of cobalt content. Contrary to this, in alloys with higher titanium content (70 at. %) percentage of dendrites increases with increasing of cobalt content and decreasing of chromium content. On the other hand, in alloys with 60 at. % of titanium, the percentage of dendritic phase increases when the contents of chromium and cobalt are nearly the same.

Table 1. Compositions of experimental Ti-Co-Cr alloys and the results of quantitative optical metallography

Sample No.	Alloy composition, at. %	% dendrites	% interdendritic region	Average area of grains, μm^2	Perimeter of grains, μm
1	$Co_{10}Cr_{10}Ti_{80}$	68,95	31,05	42,88	35,67
2	$Co_{20}Cr_{10}Ti_{70}$	49,34	50,66	26,96	40,03
3	$Co_{10}Cr_{20}Ti_{70}$	61,47	38,35	24,14	28,56
4	$Co_{30}Cr_{10}Ti_{60}$	61,03	38,97	34,49	56,87
5	$Co_{20}Cr_{20}Ti_{60}$	60,42	39,58	40,19	47,47
6	$Co_{10}Cr_{30}Ti_{60}$	61,58	38,42	18,69	26,98
7	$Co_{40}Cr_{10}Ti_{50}$	81,50	18,50	28,08	33,08
8	$Co_{30}Cr_{20}Ti_{50}$	69,35	30,65	49,40	52,21
9	$Co_{20}Cr_{30}Ti_{50}$	64,39	35,61	34,84	48,96
10	$Co_{10}Cr_{40}Ti_{50}$	52,15	47,85	22,29	37,29

From the results of Vickers hardness measurements (Table 2) can be seen that hardness increases with the content of dendritic phase. The maximal hardness of 805 HV3 has alloy $Co_{20}Cr_{10}Ti_{70}$ with the highest percentage of dendrites, while the minimal value of hardness has alloy $Co_{40}Cr_{10}Ti_{50}$ with the lowest content of this phase.

Table 2. The results of Vickers hardness measurements

Sample No.	Alloy composition, at. %	HV3	$\overline{HV3}$
1	$Co_{10}Cr_{10}Ti_{80}$	466 475 457	466
2	$Co_{20}Cr_{10}Ti_{70}$	777 843 794	805
3	$Co_{10}Cr_{20}Ti_{70}$	554 556 563	558
4	$Co_{30}Cr_{10}Ti_{60}$	655 641 601	632
5	$Co_{20}Cr_{20}Ti_{60}$	687 675 703	688
6	$Co_{10}Cr_{30}Ti_{60}$	778 781 791	783
7	$Co_{40}Cr_{10}Ti_{50}$	345 301 345	330
8	$Co_{30}Cr_{20}Ti_{50}$	619 631 629	626
9	$Co_{20}Cr_{30}Ti_{50}$	791 789 818	799
10	$Co_{10}Cr_{40}Ti_{50}$	770 820 771	787

CONCLUSIONS

The investigations of microstructure and hardness of titanium-based alloys with cobalt and chromium additions resulted with the following conclusions:

- Optical microscopy showed that nine samples of Ti-Co-Cr alloys have similar two-phases dendritic microstructure till one sample has three phases microstructure.
- Quantitative metallography indicated that the content of dendritic phase depends on alloy composition.
- Measurements of hardness showed its dependence upon the percentage of dendritic phase.

REFERENCES

1. Y. Takada, H. Nakajima, O. Okuno, T. Okabe, *Microstructure and Corrosion Behavior of Binary Titanium Alloys with Beta-stabilizing Elements,* Dental Materials Journal 20 (1) 2001, p. 34-52
2. G. He, J. Eckert, Q. L. Dai, M. L. Sui, W. Löser, M. Hagiwara, E. Ma, *Nanostructured Ti-based multi-component alloys with potential for biomedical applications,* Biomaterials 24 (2003), p. 5115-5120
3. G. He, M. Hagiwara, *Ti alloy design strategy for biomedical applications,* Materials Science and Engineering C 26 (2006) 14-19

11. Savjetovanje o materijalima, tehnologijama, trenju i trošenju
11. Conference on Materials, Processes, Friction and Wear
MATRIB'06, Vela Luka, 22-24.06.2006.

SIMULATION OF HARDNESS DISTRIBUTION IN QUENCHED DRAWING PUNCH

B. Smoljan[1], D. Iljkic[1], G.E. Totten[2], I. Felde[3]
[1]Department of Materials Science and Engineering, Faculty of Engineering, University of Rijeka,
Vukovarska 58, 51000 Rijeka, Croatia, email: smoljan@riteh.hr
[2]Department Portland State University, Portland, USA
[3]Bay Zoltan Institute for Materials Science and Technology, Budapest, Hungary

Abstract. The modified Jominy-test was designed for prediction of hardenability of cold work tool steels i.e. high-hardenability steels and possibility of application of modified Jominy-test in computer simulation of quenching of cold work tool steels has been investigated. Because of high hardenability there are limits in application of original Jominy-specimen in computer simulation of quenching of high-hardenability steels. Prediction of hardness distribution in quenched workpieces made of cold work tool steel X 210 Cr 12 based on modified Jominy-test has been done. Modified Jominy-test can be applied in simulation of quenching of high-hardenability steel more successfully than by original Jominy-test.

Keywords: quenching, computer simulation, high-hardenability tool steels

1. Introduction

Research of numerical simulation of hardness and microstructure distribution in quenched steel specimen is one of the high priority researches in simulation of phenomenon of steel quenching.

The investigation of steel quenching suggests that choosing a proper representative of the cooling phenomenon, which is relevant for structure transformation, is one of the most important factors for a good simulation of hardening.

Mathematical model of steel quenching can be based on calculated characteristic time of cooling [1, 2]. Usually, relevant time for quenching results is the time of cooling from 800 to 500 °C, $t_{8/5}$ [3, 4]. To accept the assumption that the equal time of cooling $t_{8/5}$ of several samples indicates their equal hardness, the history of cooling of these samples must be the same or similar, i.e. their cooling curves must be similar.

By involving the time of cooling $t_{8/5}$ in the mathematical model of steel hardening, the Jominy-test results could be involved in the model.

2. Simulation of Hardness Based on Time of Cooling $t_{8/5}$ Using the JM®-Specimen

The structure transformations and hardness distribution can be estimated based on time, relevant for structure transformation. Usually, if the time of cooling $t_{8/5}$ is equal in two different specimens, i.e. quenchened workpiece and Jominy-specimen, the hardness of two these specimens are equal. In the developed computer simulation of hardenability of quenchened workpiece, the hardness at different workpiece points is estimated by the conversion of the times of cooling $t_{8/5}$ to the hardness. This conversion is provided by the relation between the time of cooling $t_{8/5}$ and distance from the quenched end of the Jominy-specimen (Figure 1) [3]. The times of cooling $t_{8/5}$ at different workpiece points can be predicted by numerical modelling using the finite volume method [5].

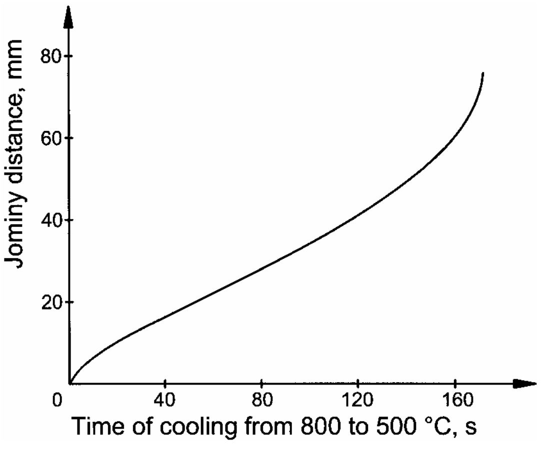

Fig. 1: Distance from the quenched end of Jominy-specimen vs. time of cooling $t_{8/5}$

For prediction of hardenability of quenchened workpiece, i.e. computer simulation of hardenability, it is necessary that the times of cooling $t_{8/5}$ for austenite decomposition in martensite, bainite, pearlite or ferrite of investigated workpiece and the times of cooling $t_{8/5}$ of Jominy-specimen are in the same range. Because of high hardenability, the times of cooling $t_{8/5}$ for austenite decomposition of most steels for tools and dies are not comparable with the times of cooling $t_{8/5}$ of Jominy-specimen and there are limits in application of original Jominy-test in computer simulation of quenching of steels for tools and dies. Figure 2 qualitatively represents austenite decomposition of some steels for tools and dies and it is visible that the times of cooling $t_{8/5}$ of austenite decomposition are ranged from 200 to 1000 s.

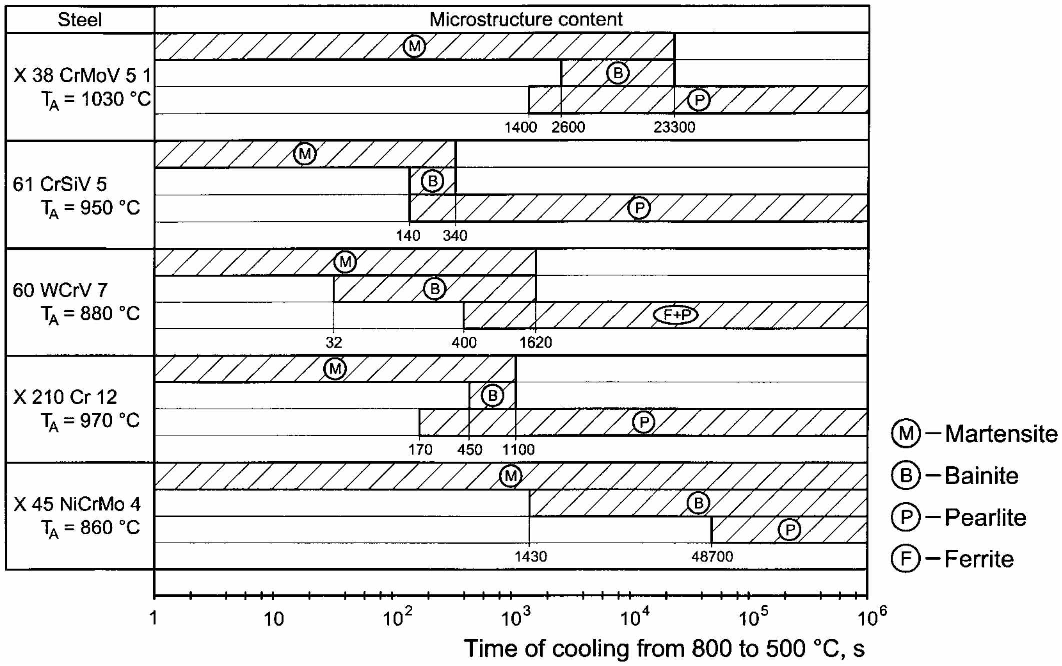

Fig. 2: Diagram for times of cooling $t_{8/5}$ for different tool steels

The time of cooling $t_{8/5}$ for bainite transformation of steels X 38 CrMoV 5 1 and X 45 NiCrMo 4 is greater then 1400 s. The time of cooling $t_{8/5}$ for pearlite transformation of steel X 45 NiCrMo 4 is greater then 45000 s. For other steels start of bainite and pearlite transformation in TTT-diagram matches the times of cooling $t_{8/5}$ in interval between 200 and 1000 s. Original Jominy-test gives the times of cooling $t_{8/5}$ up to a maximum of 200 s (Figure 1), and it is obvious that original Jominy-test is not suitable for prediction of hardenability of steels for tools and dies.

To achieve the times of cooling $t_{8/5}$ between 200 and 1000 s, the modified Jominy-specimen (JM$^{®}$-specimen) was designed for high-hardenability tool steels, i.e. steels for tools and dies. The geometry of JM$^{®}$-specimen is shown in Figure 3. Computer simulation of cooling of the JM$^{®}$-specimen has been done for cooling in air. Figure 4 shows the times of cooling $t_{8/5}$ at the depth of 0.8 mm from the surface of the JM$^{®}$-specimen at different distances from the conical tip of JM$^{®}$-specimen. Conical shape of JM$^{®}$-specimen provides a wide range of times of cooling $t_{8/5}$ at different distances from the conical tip, similar like in reference [6]. The highest cooling rates are observed at diameter of 6 mm. The lowest cooling rates are observed at diameter of 140 mm, not at maximal diameter of 144 mm as could be expected. Maximal time of cooling $t_{8/5}$ is five times longer than the maximal time given by Jominy-test.

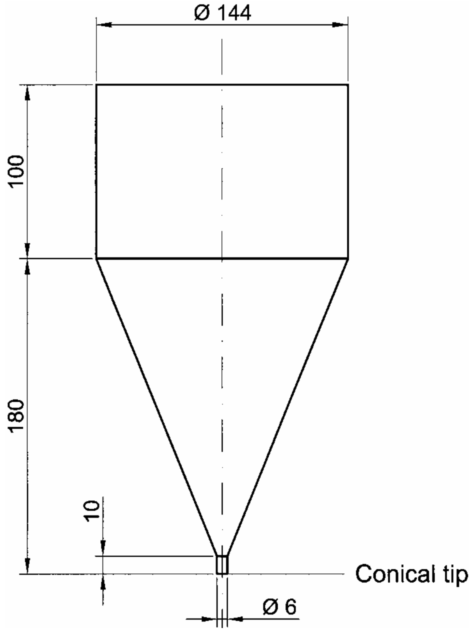

Fig. 3: Modified JM®-specimen

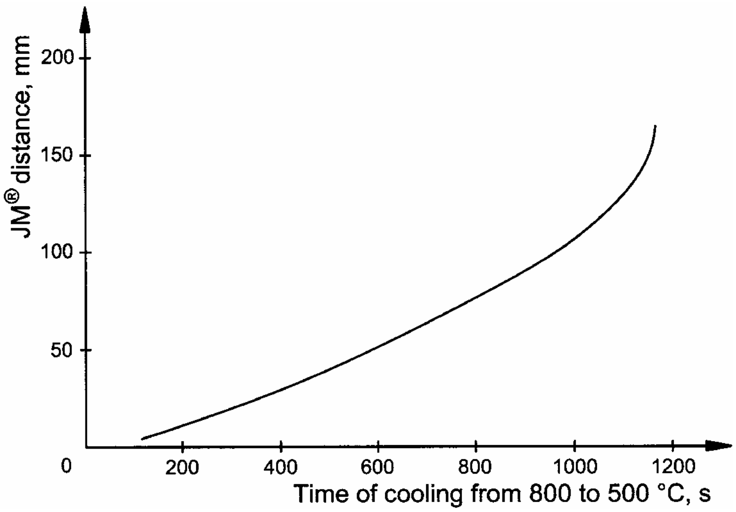

Fig. 4: Distance from the conical tip of JM®- specimen vs. time of cooling $t_{8/5}$

Based on the adequacy of reached time of cooling $t_{8/5}$ and similarity of cooling curves in investigated cylindrical specimen and JM®-specimen it can be concluded that JM®-specimen can be accepted as good potential specimen for estimation of the hardness of quenched workpieces made of steels for tools and dies [7]. The JM®-specimen can be used in computer simulation of quenching of steels for tools and dies, in similar manner as Jominy-specimen in computer simulation of quenching of structural low alloyed steels.

3. Application of JM®-test in Prediction of Hardness Distribution

Since long time of cooling of JM®-specimen (Fig. 4) it is possible by using the JM®-specimen to predict hardenability of high-hardenability tool steels.

Results of JM®-test of steel X 210 Cr 12 (austenitized at 970 °C/15 min) are shown in Table 1 and results of Jominy-test of same steel are shown in Table 2. In the Table 1 and Table 2 it is visible that much more information about hardenability of steel is possible to achieve by JM®-test.

Table 1 Results of JM®-test of steel X 210 Cr 12

JM®distance, mm	2	11	21	32	59	89	115	160
Hardness HRC	64	63	62	59	49	42	39	39

Table 2 Results of Jominy-test of steel X 210 Cr 12

Jominy distance, mm	2,5	5	10	15	20	30	40	60
Hardness HRC	64	64	64	64	64	64	63	63

Figure 5 shows the relation between JM® distance and critical diameters D_k of cylindrical specimens of different quenchants. The quenchants were with different Grossmann H value (H=5; 2; 1; 0.3; 0.2; 0.025). From Figure 5 is possible to predict the critical diameters D_k of different quenchants.

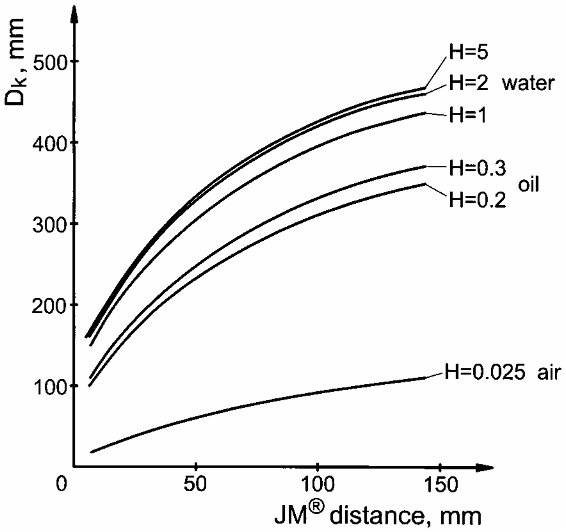

Fig. 5: JM® distance vs. critical diameters D_k

The mathematical model has been used for simulation of hardness distribution in quenched workpieces made of high-hardenability cold work tool steel [8]. Fig. 6 shows the die for which the computer simulation has been done. Because of high hardenability of investigated steel, prediction of hardness distribution has been based on JM®-test. Hardness at quenched specimen points was estimated by conversion of times of cooling $t_{8/5}$ at different workpiece points to the distance from the quenched end of JM®-specimen and of conversion of the distance from the quenched end of JM®-specimen to the relevant hardness value.

The investigation was done with the cold work tool steel X 210 Cr 12, elemental composition of investigated steel is shown in Table 3.

Table 3 Elemental composition of steel X 210 Cr 12

Elemental composition, wt.%	C	Si	Mn	P	S	Cr	Cu	Mo	Ni	V
	2.08	0.28	0.39	0.017	0.012	11.48	0.15	0.02	0.31	0.04

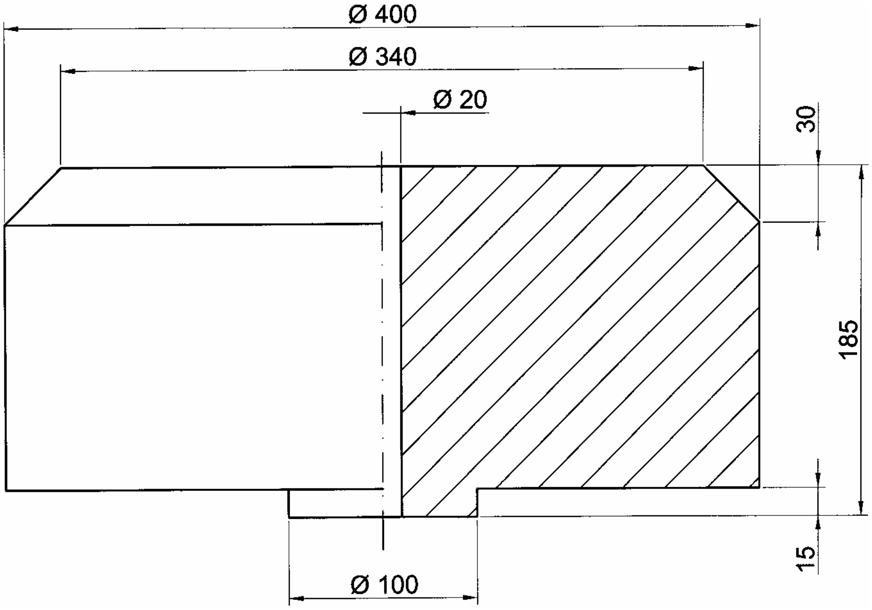

Fig. 6: Investigated die punch

Heat treatment for quenching of steel X 210 Cr 12 was heating on 980 °C for 120 min and oil quenching. The specimen has been quenched in unagitated oil with severity of quenching, i.e., Grossmann's H value equal to 0.2. JM®-results of investigated steel evaluated by the JM®-test is shown in Table 1.

Fig. 7 shows calculated results of the hardness in HRC of the quenched specimen.

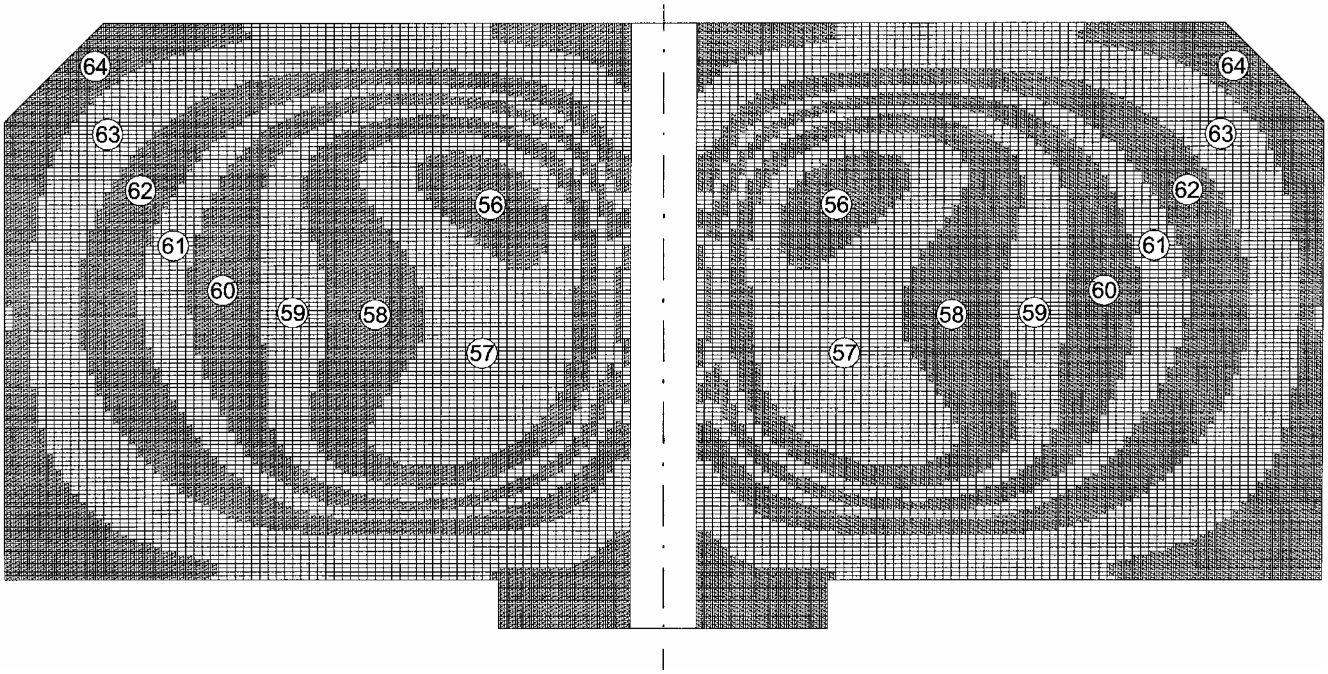

Fig. 7: Computer simulation of hardness distribution

4. Conclusion

By comparing the times of cooling $t_{8/5}$ of the JM®-specimen and the times of cooling $t_{8/5}$ required to achieve martensite microstructure in quenching of high-hardenability steels for tools and dies it is visible that the JM®-specimen is adequate for estimation of hardenability of steels for tools and dies i.e. high-hardenability steels.

Based on JM®-test, computer simulation of hardness distribution in quenched workpieces with diameter 400 mm made of high hardenability cold work tool steel X 210 Cr 12 has been done. Prediction of hardness distribution in quenched workpieces has been provided by the adequacy of reached time of cooling $t_{8/5}$ of JM®-specimen.

References

[1] B. Smoljan, The Calibration of the Heat Conductivity Coefficient in Mathematical Model of Steel Quenching, MicroCAD`99, Miscolci, 1999.

[2] B. Smoljan, The Calibration of the Mathematical Model of Steel Quenching, *Proc. of 5th World Seminar on Heat Treatment and Surface Engineering*, Isfahan, Eds. M. Salehi, ISSST and IFHT, Vol.1, 1995, pp. 709-715.

[3] A. Rose et al, Atlas zur Wärmebehandlung der Stähle I, Verlag Stahleisen, Düsseldorf, 1958.

[4] P. Mayner et al, Hardenability Concepts with Application to Steels, Metal. Soc. of AIME, New York, 1978.

[5] S. Patankar, Numerical Heat Transfer and Fluid Flow, McGrawHill Book Company, New York, 1980.

[6] Murty, N.V.S.N., “A Hardenability Test Proposal” Proceedings of the 2nd International Conference on Quenching and the Control of Distortion, 4-7 November, 1996, Cleveland, Ohio.

[7] B. Smoljan, D. Rubeša, N. Tomašić, S. Smokvina Hanza, D. Iljkić, An Analysis of Application of Modified Jominy-Test in Simulation of Cold Work Tool Steels Quenching, International Journal of Microstructure and Materials Properties, in print.

[8] B. Smoljan, Numerical Simulation of Steel Quenching, Journal of Materials Engineering and Performance, Vol.11 No. 1, February 2002, pp. 75-79.

ANALIZA TROŠENJA I OŠTEĆENJA REKONSTRUIRANIH LEŽAJA VODNIH TURBINA HE OZALJ 1

WEAR AND DAMAGE ANALYSIS OF WATER TURBINES BEARINGS IN OZALJ 1 HYDROPOWER PLANT

Prof. dr. sc. Branko Staniša, dipl.ing.
Sveučilište u Rijeci, Tehnički fakultet, Vukovarska 58, 51000 Rijeka
Mr.sc. Vladimir Tudić, dipl.ing.
Veleučilište u Karlovcu Ivana Meštrovića 10, 47000 Karlovac
Mirko Kranjčec, ing.
HEP-Proizvodnja, Pogon HE Ozalj, Nikole Tesle 2, 47280 Ozalj

Sažetak: Hidroelektrana (HE) Ozalj 1 puštena je u pogon 1908. godine za potrebe rasvjete grada Karlovca. U 1990. godini zamjenjene su dotrajale vodne turbine s novim Francisovim turbinama. Pri tome je iz ekoloških razloga izvršena rekonstrukcija i zamjena turbinskih kliznih ležaja s blazinicom od bijele kovine podmazivanih uljem, s ležajevima s blazinicom od gume podmazivanih riječnom vodom. Praćenjem pogona utvrđeno je povećano trošenje i oštećenje rukavaca ležajeva s blazinicom od gume. Zbog povećanog trošenja i oštećenja morale su se košuljice rukavaca zamijeniti daleko prije od projektnog vijeka trajanja. U ovom radu dani su rezultati istraživanja brzine i uzroka povećanog trošenja i oštećenja rukavaca. Rezultati istraživanja su pokazali da povećano trošenje nastaje zbog abrazijskog djelovanja krutih čestica u struji vode za podmazivanje ležajeva s blazinicom od gume. Predložene su mjere za smanjenje brzine trošenja i sanaciju oštećenja ležajnih rukavaca vodnih turbina HE Ozalj 1.

Ključne riječi: vodna turbina, ležajevi s blazinicom od gume, abrazijsko trošenje

Abstract: Hydro Power Plant Ozalj 1 begin with production of electricity in year 1908 for town Karlovac lighting purpose. In year 1990 all run out turbines were substituted with new Francis type turbines. Because of ecological reasons reconstruction of bearing system was made and oil supplied bearings are replaced with rubber bearings lubricated with river water. During turbines exploitation serious damage was discovered on the two axial bearings. Worn out parts has been replaced before planed period. A result of the research of run out bearing sleeves cause and speed has been presented in this paper. Investigation results suggest abrasion caused by hard particles in the stream of water used for turbine bearing lubrication. Appropriate measure and improvement steps have been proposed to prevent rapid abrasion of turbine bearings in Hydropower plant.

Key words: water turbine, rubber bearings, abrasion

1. UVOD

HE Ozalj je protočno priobalsko hidroenergetsko postrojenje smješteno na rijeci Kupi u njenom srednjem toku, blizu grada Ozlja. Sastoji se od dvije odvojene hidroelektrane HE Ozalj 1 i HE Ozalj 2. HE Ozalj 1 je smještena na desnoj obali rijeke Kupe, a nasuprot njoj na lijevoj obali je smještena HE Ozalj 2. Hidroelektrana koristi vode s oborinskog područja gornjeg i srednjeg toka rijeke Kupe površine 2190 km^2. Izgradnjom brane visine 7,5 m i dužine 77 m na prirodnoj stepenici u koritu rijeke Kupe formiran je akumulacijski bazen ukupne zapremnine 1,4 mil. m^3 i korisne zapremnine 0,55 mil. m^3. HE Ozalj 1 je jedna od najstarijih hidroelektrana u Hrvatskoj. Izgrađena je 1908. godine za potrebe rasvjete grada Karlovca. U prvoj fazi izgrađene su dvije proizvodne jedinice, a treća je izgrađena 1913., tako da je ukupna snaga hidroelektrane bila 3,3 MW godine. HE Ozalj 2 izgrađena je 1952. godine s dvije proizvodne jedinice ukupne snage 2,2 MW.

U 1990. godini zbog dotrajalosti zamjenjena su sva tri turboagregata HE Ozalj 1 sa novim agregatima. Zamjenom vodnih turbina izvršene su i rekonstrukcije na turbinskim vratilima i aksijalnom i radijalnom ležaju. Do rekonstrukcije ležajevi turbina su bili podmazivani uljem gravitacijski, bez mogućnosti nadzora brtvenja i sakupljanja ulja u turbinskim ležajevima, tako da je ulje iz ležajeva odlazilo u rijeku, što je za novije vodne turbine sa ekološkog stajališta neprihvatljivo [1, 2]. U rekonstruirane ležajeve su umjesto blazinica od bijele kovine ugrađene eko blazinice od gume podmazivane riječnom vodom. S tom rekonstrukcijom su se riješili problemi zagađivanja rijeke Kupe s uljem iz turbinskih ležaja i smanjili troškovi eksploatacije. Tijekom pogona turbina s rekonstruiranim ležajevima uočeno je povećano trošenje rukavaca ležaja, dok je trošenje blazinice od gume bilo zanemarivo. Brzina trošenja čeličnih rukavaca bila je neprihvatljiva za normalne uvjete pogona hidroelektrane, pa se je prišlo istraživanju i rješavanju tog problema.

U ovom radu dani su osnovni tehnički podaci i opis rada vodnih turbina u HE Ozalj 1. Dan je prikaz rekonstrukcije ležajeva turbine i sustava za njihovo podmazivanje riječnom vodom. Izneseni su rezultati istraživanja brzine i zakonitosti trošenja rukavaca rekonstruiranih ležajeva turbine. Istraženi su i prikazani uzroci povećane brzine trošenja ležajnih rukavaca podmazivanih riječnom vodom. Dano je rješenje za smanjenje brzine trošenja ležajnih rukavaca vodnih turbina u HE Ozalj 1.

2. OSNOVNI TEHNIČKI PODACI I OPIS RADA VODNIH TURBINA HE OZALJ 1

Prva faza HE Ozalj 1 sa dvije francisove vodne turbine puštena je u pogon 19.08.1908. godine. Druga faza od jedne francisove vodne turbine puštena je u pogon 1913. godine. Snaga generatora hidroelektrane je iznosila 3 x 750 kVA, 5 kV, 50 Hz. Strojarsku opremu isporučila je tvrtka JM VOITH iz Austrije a elektro-opremu tvrtka ELIN i FRANC PICHLER. Hidroelektrana je s ovom opremom radila do 1990. godine, kada se pojavilo puknuće rotorske lopatice na agregatu 3, nakon cca 450000 sati rada. Tada je analizom stanja odlučeno da se zamjene sva tri turboagregata sa novim tehničkim značajkama.

Nove vodne turbine je proizveo Litostroj Ljubljana, a električne generatore Končar Zagreb. Osnovni tehnički podaci vodnih turbina su [3]:

- nazivna snaga turbine	1340 kW
- instalirani protok	17 m^3/s
- neto pad	9,2 m
- brzina vrtnje	107 min^{-1}.

Na slici 1. prikazan je tlocrt strojarnice HE Ozalj 1. Iz dane slike se vidi razmještaj tri turboagregata broj 1, 2 i 3. Uzdužni presjek kroz strojarnicu HE Ozalj 1 prikazan je na slici 2.

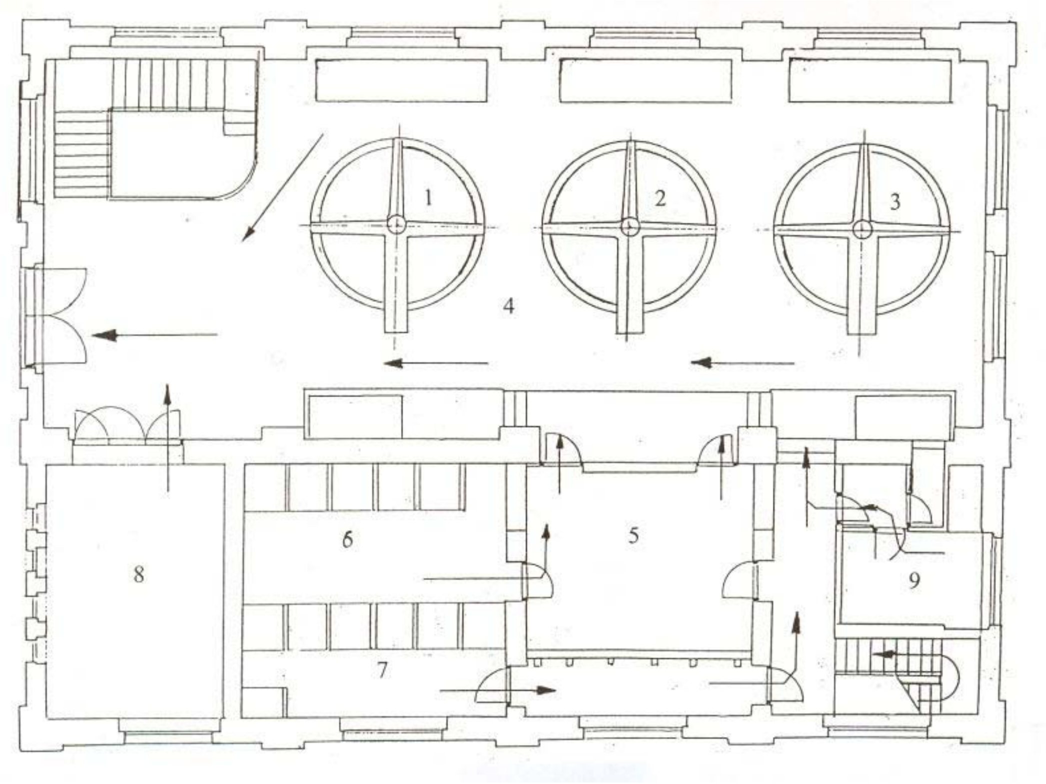

Sl. 1. Tlocrt HE Ozalj 1:
1, 2, 3-turboagregat br. 1, 2 i 3; 4- strojarnica; 5-komanda; 6, 7-10 kV i 5 kV postrojenje; 8-trafostanica; 9-pomoćna prostorija

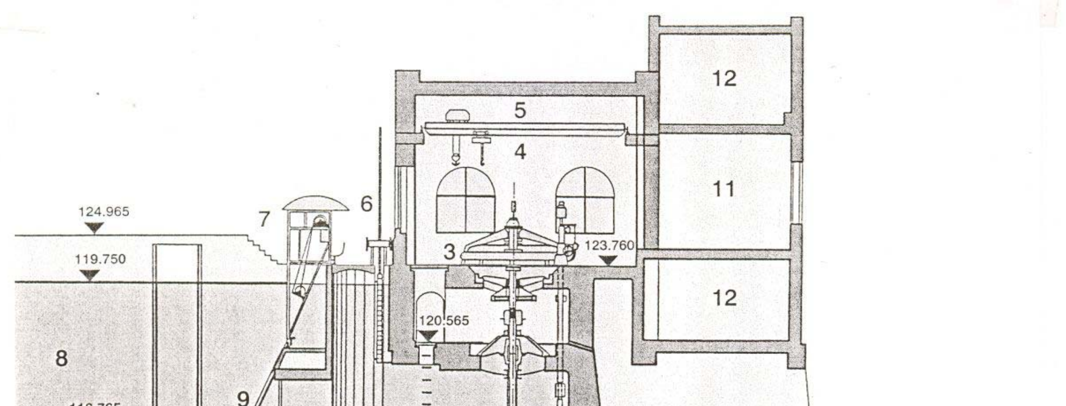

Sl. 2. Uzdužni presjek HE Ozalj 1:
1-temeljno tlo, 2-turbina, 3-generator, 4-strojarnica, 5-dizalica, 6-tablasti zatvarač 7-čistilica, 8-ulazna građevina, 9-ulazna rešetka, 10-odvodni kanal, 11-komanda, 12-pomoćne prostorije

Iz slike je vidljiv smještaj turbine i generatora, kao i dovod i odvod vode iz turbine. Generator se nalazi u strojarnici iznad turbine. Turbina i generator su spojeni krutom spojkom što ih čini jedinstvenim turboagregatom. Generator ima tri klizna ležaja. Dva ležaja su vodeća a treći je kombinirani aksijalno radijalni, tj. nosivi i vodeći ležaj. Rotor turbine ima dva radijalna vodeća ležaja, gornji i donji..

Pogonska voda ulazi u turbinu kroz ulaznu rešetku i ulazni tablasti zatvarač. Nakon pretvorbe tlačne energije u mehanički rad vrtnje rotora, voda iz turbine odlazi u odvodni kanal. Dobivenim mehaničkim radom u obliku vrtnje rotora vodne turbine pogoni se rotor generatora za proizvodnju električne energije.

Do zamjene vodnih turbina ležajevi turbine su bili s blazinicom od bijele kovine i podmazivani turbinskim uljem. Podmazivanje je bilo uljem gravitacijski bez mogućnosti nadzora brtvenja i sakupljanja ulja u turbinskom ležaju i vraćanja u spremnik ulja, već je ono odlazilo sa strujom vode, što je sa današnjeg stajališta nedopustivo. Zbog toga su se ležajevi i njihovo podmazivanje moralo rekonstruirati.

3. REKONSTRUKCIJA LEŽAJEVA VODNE TURBINE

Zamjenom vodnih turbina izvršena je i rekonstrukcija turbinskih ležaja tako da su umjesto blazinica od bijele kovine ugrađene blazinice od gume tvrdoće 80 šora za podmazivanje riječnom vodom. Na vratilu na mjestu rukavaca ležaja ugrađene su košuljice od čelika Č.4572. Ugrađen je i sustav za dovod vode za podmazivanje ležajeva. Na slici 3 dan je prikaz rekonstruiranog turbinskog vodećeg ležaja s ugrađenom blazinicom od gume. Iz slike je vidljivo kućište ležaja i ugrađena gumena blazinica za podmazivanje vodom. Prednosti podmazivanja turbinskih ležaja vodom su:

Sl. 3. Prikaz rekonstruiranog turbinskog ležaja s ugrađenom blazinicom od gume

- nema zagađivanja riječne vode uljem za podmazivanje,
- nema troškova gubitaka ulja i troškova njegove nabave,
- troškovi zamjene blazinice od gume su manji u odnosu na bijelu kovinu,
- trošenje blazinice od gume je zanemarivo.

Rekonstruirani turbinski ležaji podmazivani su riječnom vodom, koja se filtrira u automatskim filtarima, finoće mrežice 80 do 100 mikrona. Prikaz turboagregata sa shemom podmazivanja vodom rekonstruiranog gornjeg i donjeg turbinskog ležaja dan je na slici 4.

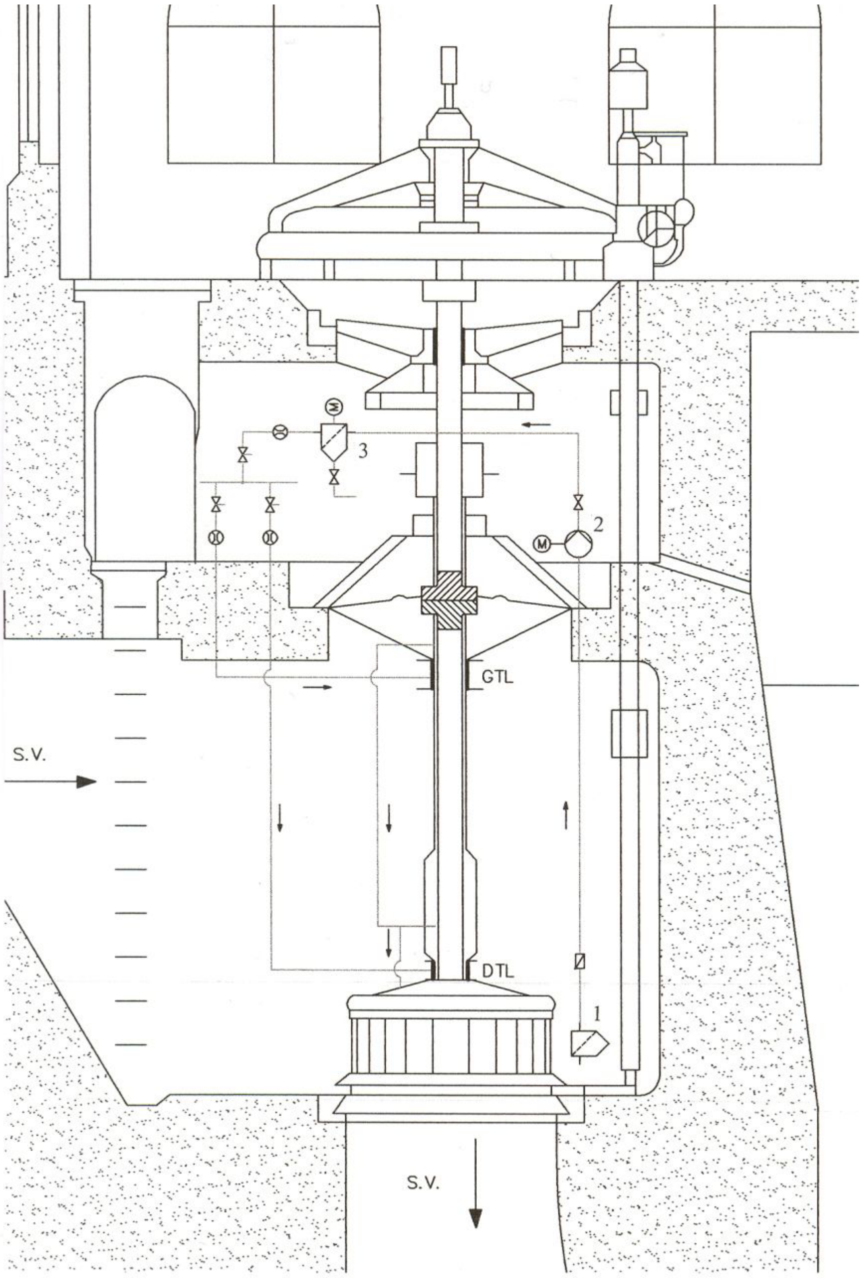

Sl. 4. Prikaz turboagregata sa shemom podmazivanja vodom gornjeg i donjeg ležaja turbine: 1-usisna košara, 2-pumpa za vodu, 3-filtar za vodu, GTL, DTL-gornji i donji turbinski ležaj

Voda za podmazivanje ležajeva se uzima u turbinskoj komori ispred ulaza u turbinu preko usisne košare u kojoj se vrši grubo čišćenje vode i pomoću pumpe tlaka 6 bar dovodi u filtar i dalje u gornji i donji ležaj s gumenim blazinicama. Za podmazivanje gornjeg i donjeg turbinskog ležaja projektom je određena količina vode po ležaju 25 do 35 l/min. Količina i tlak vode kontroliraju se vizualno u turbinskom prostoru iza razvoda rashladne vode i u komandnoj prostoriji na signalnim instrumentima.

Kao nedostatak rekonstrukcije lažajeva za podmazivanje vodom, pojavilo se je u pogonu povećano trošenje rukavaca ležaja, što je uzrokovalo povećane troškove održavanja.

Zbog toga je odlučeno da se istraži i izvrši analiza ubrzanog trošenja rukavaca, te riješi taj problem.

4. ANALIZA TROŠENJA RUKAVACA LEŽAJEVA TURBINE

Tijekom pogona turbina s rekonstruiranim ležajevima s gumenim blazinicama podmazivanim vodom uočeno je povečano abrazivno trošenje rukavaca ležaja. Pri tome je trošenje gumene blazinice bilo zanemarivo. U tijeku rekonstrukcije ležajeva očekivalo se da će biti obratno, tj. da će biti znatnije trošenje gumene blazinice u odnosu na čeličnu košuljicu rukavca ležaja. Na slici 5. dan je prikaz rukavca donjeg ležaja vratila turbine oštećenog od abrazivnog trošenja. Iz dane slike je vidljivo oštećenje rukavca u obliku dubokih abrazivnih riseva.

Sl. 5. Prikaz oštećenog rukavca ležaja vratila turbine u obliku riseva od abrazivnog trošenja

Za istraživanje brzine i zakonitosti abrazivnog trošenja i oštećenja rukavca ležaja izvršeno je praćenje oštečenja tijekom eksploatacije. Mjerenjem i praćenjem oštećenja je utvrđeno, da je prosječno trošenje rukavca linearno u iznosu 0,15 mm za 5500 sati rada. Veća brzina abrazivnog trošenja rukavca ležaja utvrđena je u proljeće i jesen u tijeku velikih voda nabujale rijeke Kupe.

Za utvrđivanje uzroka abrazivnog trošenja detaljno su pregledani oštećeni ležajevi i cijeli sustav za podnazivanje ležajeva vodom. Detaljno je pregledan i analiziran oblik oštećenja rukavca ležaja. Također je detaljno pregledano i analizirano stanje klizne površine gumene blazinice ležaja. Pregledom je na cijeloj kliznoj površini rukavca uočeno oštećenje od manjih ili mjestimično širih i dubljih abrazivnih riseva. Detaljnim pregledom gumene blazinice uočene su na njenoj kliznoj površini utisnuta sitna zrnca pijeska, koja se nisu mogla vodom isprati. Pregledom kompletnog sustava za podmazivanjem ležajeva vodom uočeno je mjestimično začepljenje mrežice filtra za vodu sa sitnim zrncima pjeska.

Analizom stanja i oblika oštećenja ležajeva utvrđeno je, da je do oštećenja rukavca došlo zbog abrazivnog djelovanja zrnaca pijeska utisnuti u kliznu površinu gumene blazinice ležaja. Utisnuta sitna zrnca pijeska u kliznu gumenu površinu blazinice ležaja pri rotaciji rukavca djeluju kao brusni papir i abrazivno ga oštećuju. Ovo abrazivno djelovanje je u proljeće i jesen veće, kada su veće količne vode nabujale rijeke Kupe i nose veće količine čestica pijeska. Tada dođu kroz filtar veće količine čestica pijeska u ležajeve i utiskuju se u kliznu površinu gumenih blazinica, te ih voda ne može isprati, pa abrazivno oštećuju rukavac.

5. MJERE ZA SMANJENJE BRZINE TROŠENJA RUKAVACA LEŽAJA TURBINE

Rekonstrukcija kliznih ležaja turbine sa zamjenom blazinica od bijele kovine podmazivanih uljem sa blazinicama od gume podmazivanih riječnom vodom pokazala je uz prednosti i nedostatke, zbog povećane brzine trošenja rukavaca. Podmazivanje ležajeva turbine sa riječnom vodom je s ekološkog stajališta prihvatljivije od podmazivanja uljem. Međutim, gumene blazinice ležajeva turbine nisu prihvatljive zbog nemogućnosti ispiranja čestica nečistoće iz gume, koje prouzrokuju abrazivno trošenje rukavca ležaja. Popravak oštećenog rukavca je daleko skuplji od popravka oštećene blazinice ležaja. Zbog toga pri trošenju ležaja zbog trenja prihvatljivije je da se troši blazinica ležaja u odnosu na rukavac.

Za smanjenje brzine trošenja rukavca ležaja turbine zamjenjene su blazinice ležaja od gume sa materijalom novilon oilon. Prikaz vodećeg ležaja turbine sa ugrađenom ležajnom blazinicom od materijala novilon oilon dan je na slici 6. Iz slike je vidljivo kućište ležaja i ugrađena blazinica od novilon oliona za podmazivanje riječnom vodom. Sustav podmazivanja ležajeva vodom i finoća filtara za vodu ostala je ista kao i sa gumenim blazinicama.

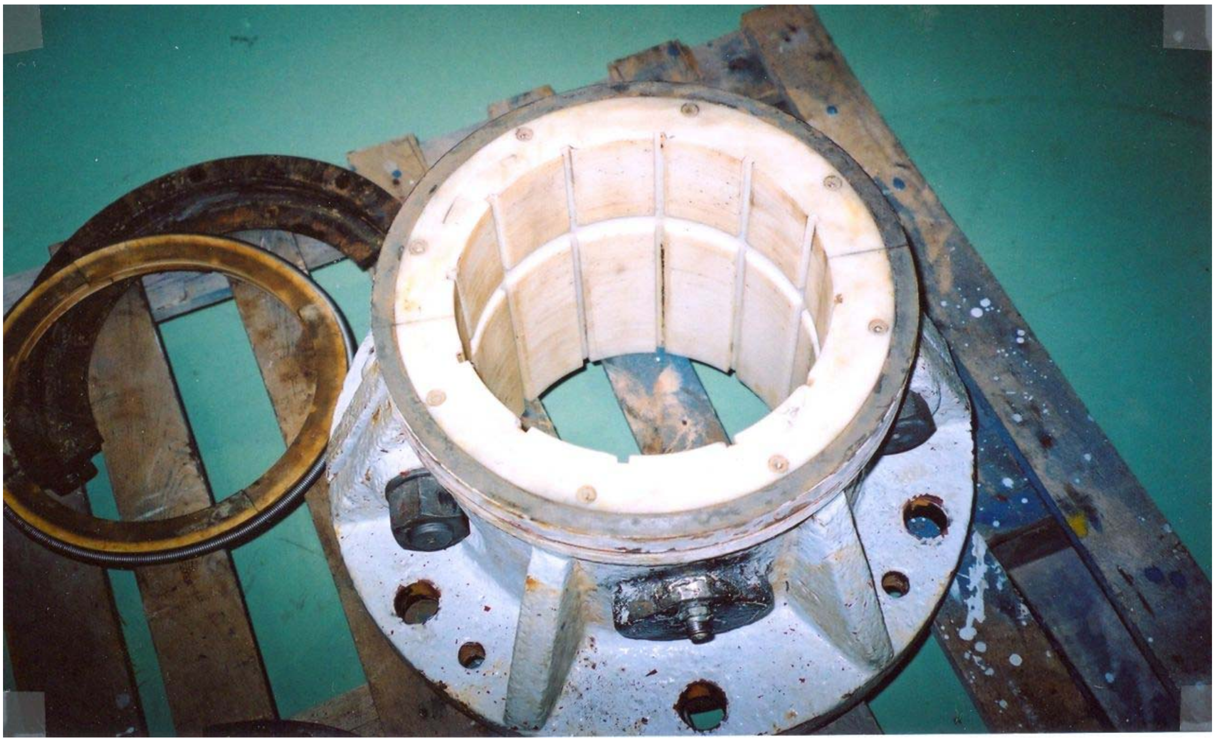

Sl. 6. Prikaz vodećeg ležaja turbine s ugrađenom blazinicom od novilon oilona

Nakon jednogodišnje eksploatacije turbine od 6000 pogonskih sati sa blazinicama ležajeva turbine od materijala novilon oilon, podmazivanih vodom, izvršena je kontrola stanja ležajeva. Mjerenjem ležajeva utvrđeno je zanemarivo trošenje blazinice i rukavca ležaja. To pokazuje da su blazinice ležajeva od materijala novilon oilon daleko povoljnije za podmazivanje riječnom vodom od gumenih. Iz toga proizlazi da je novo rješenje od materijala novilon oilon za uležištenje vratila vodnih turbina kvalitetnije i trajnije u odnosu na gumene blazinice, što će znatno smanjiti troškove održavanja.

6. ZAKLJUČAK

Na francisovim vodnim turbinama instaliranim u HE Ozalj 1 puštenoj u pogon 1908. godine, izvršena je nakon zamjene dotrajalih turbina i rekonstrukcija ekološki neprihvatljivog podmazivanja ležajeva turbinskim uljem i njegovog odlaženja u struju vode. Rekonstrukcija se sastojala od rekonstrukcije sustava za podmazivanje ležajeva i zamjeni ležajnih blazinica od bijele kovine podmazivanih uljem sa blazinicama od gume podmazivanih riječnom vodom.

Tijekom eksploatacije turbina sa rekonstruiranim ležajevima podmazivanih vodom uz niz prednosti, došlo je i do nedostatka zbog ubrzanog abrazivnog trošenja rukavaca ležaja. Istraživanjem brzine abrazivnog trošenja rukavaca utvrđeno je prosječno oštećenje 0,15 mm za 5500 sati pogona. To ubrzano trošenje rukavca ležaja uzrokavalo je povečane troškove održavanja.

Istraživanjem uzroka povećane brzine trošenja rukavaca ležajeva utvrđeno je, da je do ubrzanog trošenja došlo zbog utisnutih čestica pijeska u gumenu kliznu površinu, koje voda nije mogla isprati. Utisnute sitne čestice pijeska u gumenu kliznu površinu, koje su prošle kroz mrežicu filtara, djelovale su na rotirajući rukavac brusno i abrazivno ga oštećivale.

Za smanjenje ubrzanog trošenja rukavaca ležajeva zamjenjene su gumene blazinice sa blazinicama od materijala novilon oilon. Sustav podmazivanja vodom i filtar za vodu ostali su isti kao i sa gumenim blazinicama. Nakon jednogodišnjeg pogona od 6000 sati izvršena je kontrola blazinica i rukavaca. Mjerenjem rukavca i blazinice od novilon oilona utvrđeno je njihovo zanemarivo oštećenje.

Na temelju provedenih istraživanja i analiza može se zaključiti da je novo rješenje od materijala novilon oilon, prihvatljivije za blazinice ležajeva vodnih turbina podmazivanih riječnom vodom u odnosu na gumene blazinice. Novo rješenje će znatno smanjiti troškove održavanja vodnih turbina u HE Ozalj 1.

LITERATURA

[1] D. Horvat, "Vodne turbine", Tehnička knjiga, Zagreb, 1974.
[2] Lj. Pilić-Rabadan, "Vodne turbine i pumpe, vjetroturbine", Fakultet elektrotehnike, strojarstva i brodogradnje sveučilišta u Splitu; Split, 2000.
[3] Tehnička dokumentacija HE Ozalj 1.

COMPARISON OF MECHANICAL PROPERTIES AND BEHAVIOUR SELECTED SYSTEMS OF THIN FILM – SUBSTRATE FROM CVD, PACVD AND PVD DEPOSITION MEASURED BY INDENTATION TESTS

Štěpánek Ivo, Macháčková Kateřina, Netušilová Denisa, Černý František, Hořejš Slavomír, Department of Materials Science and Metallurgy, University of West Bohemia, Univerzitní 22, Pilsen, Czech Republic

Abstract: The paper is devoted by evaluation of properties and behaviour of different systems thin film – substrate with the same basic material, but different thin films. Thin films were deposited by different technological process. The technological processes used for this paper are classical high temperature CVD method, classical commercial PVD method and low temperature PA CVD method on different deposition equipment. There are used sometimes thin films TiN and sometimes thin films TiCN. The main attention was on evaluation mechanical properties and behaviour by indentation tests with different value of normal force and on evaluation depth profilling of chemical composition of these systems of materials. The goal is comparison of systems for possibilities to replace high temperature CVD method for some application by low temperature PA CVD with comparable or better properties and behaviour as classical commercial PVD coatings.

University of West Bohemia in Pilsen

Introduction

In this time very much different technologies of deposition thin films exist and find its utilisation in very wide range. Some technologies has advantages for low temperature during technology process and some technologies has advantages for homogeneity of deposition on areas and complicated geometry. The different technology process has differences in physical and chemical principles, properties and behaviour of prepared thin films. The most important properties are mechanical properties for application on tools, special tools, special parts of machines and the others [1].

Experimental materials

In this paper systems thin film – substrate are analysed from different technology process. The standard for experiments is high temperature CVD deposition process. Thin film is TiCN deposited on HSS substrate and after deposition the heat treatment was realised. For comparison CVD method with PVD method the deposition by reactive arc evaporation was selected. This PVD techniques represent clasical PVD thin film for comparison if the CVD method can be comparable or better then PVD. The PVD thin film is TiCN too. Deposition is on the same substrate, but the substrate before deposition is heat treatment. The most interest the thin films from low temperature deposition by PA CVD method has, because in the range one project we try to change high temperature CVD by low temperature PA CVD with advantages of high temperature CVD. In this paper three different deposition equipment was used for preparing thin films from three different collaborated company, but I can not write more information (we will used marking PA CVD 1, PA CVD 2 and PA CVD 3). Thin films TiN and TiCN was prepared by PA CVD techniques, from one DLC thin film was prepared too.

Measurement of thickness of thin films by calotest

At the first we must know thickness of thin films from used technology processes. Calotest measurement give much more information about properties and behaviour of systém thin film – substrate. The measurement are showed in fig. 1a, in which are presented result for comparison CVD, TiN thin films from PA CVD and PVD and fig. 1b – this is comparison with TiCN films from PA CVD. Here is possible analyse thickness of films, but not only thickness the resistivity to the abrasion too. From fig. 1 we can view, that CVD TiCN has sandwiches structure. The thin films from PA CVD has some interlayer on interface between substrate and thin film. The roughness of PA CVD 3 is higher then roughness of PA CVD 2. It can influence evaluation of mechanical properties and behaviour. Thin film PVD has some interlayer too. From fig.1 we can view, what the highest roughness has PA CVD 1 and here is very difficult analyse thickness and small cohesive failures. Thin films TiCN from PA CVD 2 and 3 show failures in thin films, not good resistant to the abrasion. Thickness of above mentioned thin films are in tab. 1. in the end of paper.

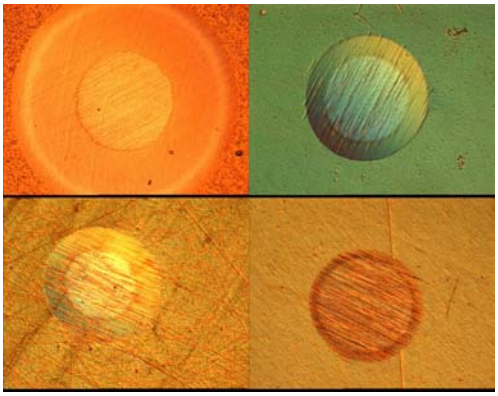

Fig. 1a: Results from calotest analysis
1. CVD. 2. TiN PA CVD 2, 3. TiN PA CVD 3, 4. PVD.

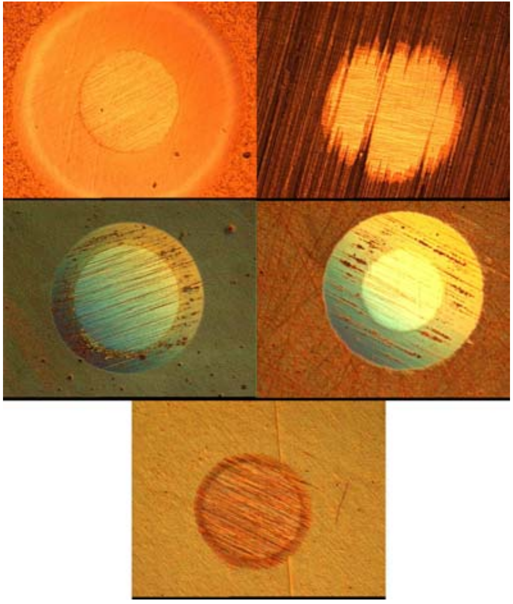

Fig. 1b: Results from calotest analysis
1. CVD. 2. TiCN PA CVD 1, 3. TiCN PA CVD 2, 4. TiCN PA CVD 3, 5. PVD.

Nanoindnetation on systems thin film – substrate

At the second we analyse mechanical behaviour during nanoindentation. We realised measurement with the similar conditions – maximal load was 200 g – for analysis modificated substrate under thin film, 25 g – for analysis systems thin film – substrate and 2 g – for analysis thin films without influences from substrate [2]. The results from measurement are in fig. 2 and 3. Here is presented nanoindentation curves – dependence depth indentation and normal force during loading, time delay and unloading.

Thin film CVD influence indentation with maximal load 200 g, because thickness is very large in comparison other thin films. Here is possible view changing in slope of indentation curves and rate between elastic and plastic deformation. Thin film PVD influence indentation with maximal load 200 g, because this thin film has large nanohardness and good adhesive cohesive behaviour. The other films not influence this measurement and nanoindentation curves are similar as on substrate (fig. 2). The indentation curves with maximal load 25 g show similar results as above mentioned for

200 g (fig. 2). The adheisve cohesive failures is not possible to view here. For this loading mechanical behaviour all systems is good. The nanohardness of thin films is analysed from indentation curves with maximal load 2 g (fig. 3). Nanohardness is presented in tab.1

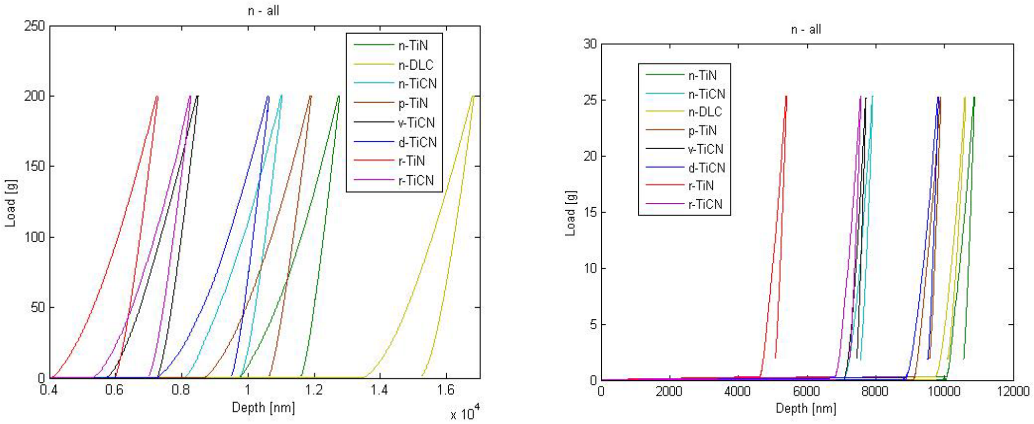

Fig. 2: Nanoindentaion curves – 1. for maximal load 200 g, 2. for maximal load 25 g.
CVD – v TiCN, PVD – p TiN, PA CVD 1 – d, PA CVD 2 – r, PA CVD 3 – n

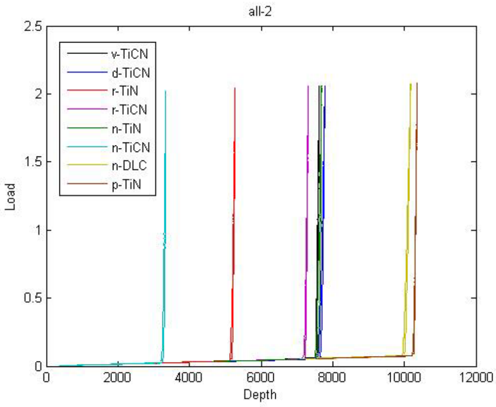

Fig. 3: Nanoindentaion curves for maximal load 2 g.
CVD – v TiCN, PVD – p TiN, PA CVD 1 – d, PA CVD 2 – r, PA CVD 3 – n

Static indentation on systems thin film substrate

At the third we analysed resistance to the static indentation. The measurement was realised on macroscratch tester REVETEST in mode of static measurement. The maximal load was setup on 30 N, 60 N and 90 N. In the fig. 4 are presented resulted indents on CVD, TiN PA CVD 2 and 3 and PVD at the first and CVD, TiCN PA CVD 1, 2, 3 and PVD at the second. The most expressive is failures on system with TiN thin film PA CVD 2 and deformation on system with TiN thin film PA CVD 3 for the first image (fig. 4). In the second image (fig. 4) the largest deformatin is on systém with TiCN PA CVD 1 (therefore thickness is very small). On the systém with TiCN PA CVD 2 the cracks increase around indents and the cohesive failures expands on systém with TiCN PA CVD 3.

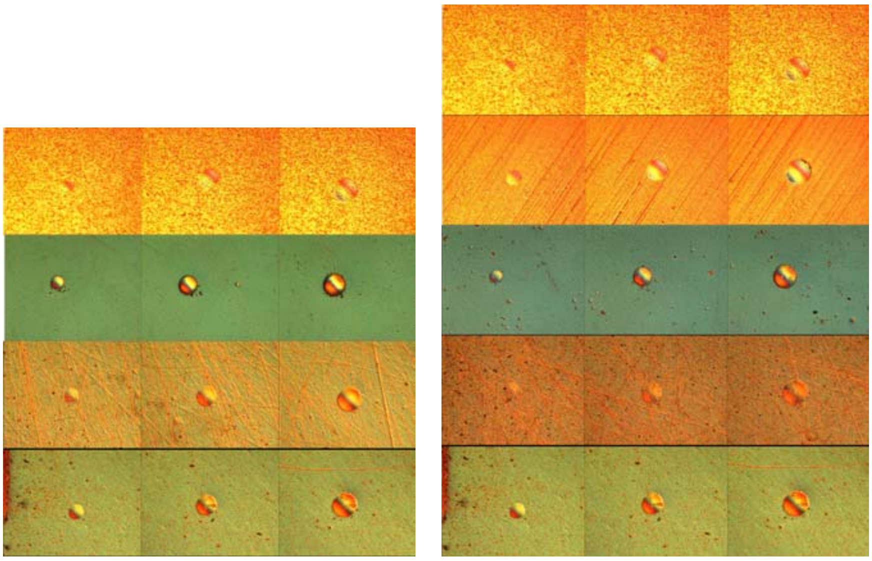

Fig. 4: Indents after static indentation with value of load 30, 60 and 90 N. 1. – comparison CVD, TiN PA CVD 2, TiN PA CVD 3, PVD, 2. comparison CVD, TiCN PA CVD 1, TiCN PA CVD 2, TiCN PA CVD 3, PVD.

Scratch indentation tests on systems thin film – substrate

At the fourth we evaluate adhesive cohesive failures [3] after scratch tests prepared on all systems of thin film – substrate. The scratch test was realised with the same conditions for all systems. The conditions of measurement was increased normal force from 1 N to 80 N with constant rate of normal force and constant rate of holder with samples. The results of scratch tests are in fig. 5 and fig. 6 similar as static indentation in fig. 4. Here is only part of scratches from 40 N to 80 N. The best is the systém with CVD and PVD thin film. The systém with TiN PA CVD 2 has cohesive failures on the edge of scratch. Here is very big differences between TiN and TiCN thin films prepared by PA CVD at all. TiCN thin films (namely PA CVD 2 and 3) are the largest cohesive failures on the edges of scratches. The cohesive failures change to the adhesive with increased normal force. The TiCN PA CVD 1 has smaller cohesive failures because thickness is much more smaller. From this measurement the results is - comparable can be only TiN from PA CVD 3.

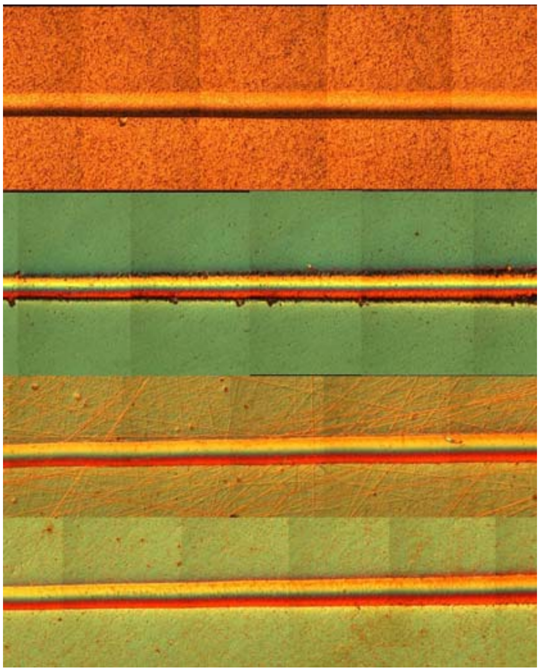

Fig. 5: Scratches with value of normal force from 40 to 60 N – CVD, TiN PA CVD 2, TiN PA CVD 3, PVD.

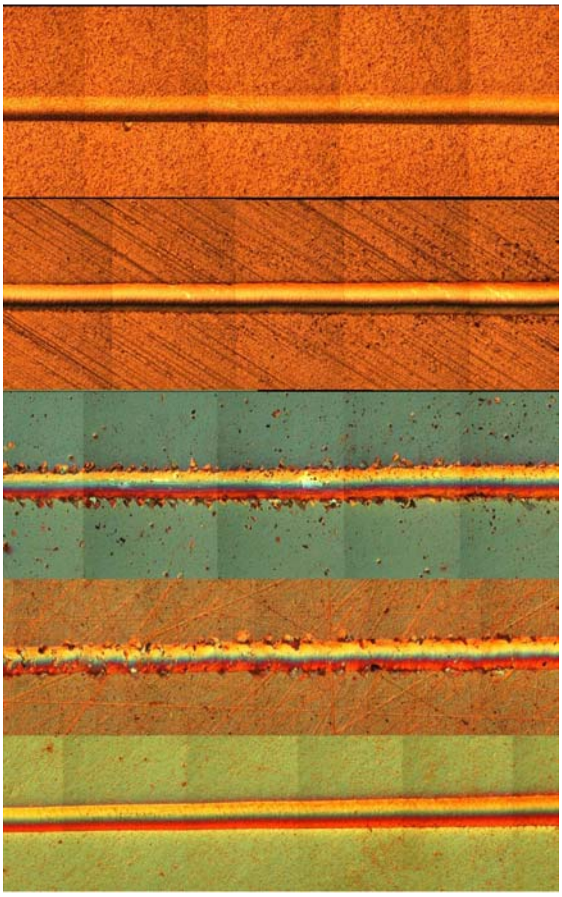

Fig. 6: Scratches with value of normal force from 40 to 60 N – CVD, TiCN PA CVD 1, TiCN PA CVD 2, TiCN PA CVD 3, PVD.

Depth profile of chemical composition of systems thin film – substrate

At the fifth we measure depth profile of chemical composition on all systems by GDOES method. The result are in fig. 7. The TiN thin films has similar depth profile of chemical composition. The TiCN has very bid differences in chemical composition in depth. CVD thin film has local maximum of carbon and minimum of nitride, PVD thin film has composition from multilayer, TiCN from PA CVD 3 has gradient composition of carbon and nitride, PA CVD 2 has local minimum of nitride and PA CVD 1 gradient composition of nitride, carbon and titanium. Here is possible to view differences in thickness too.

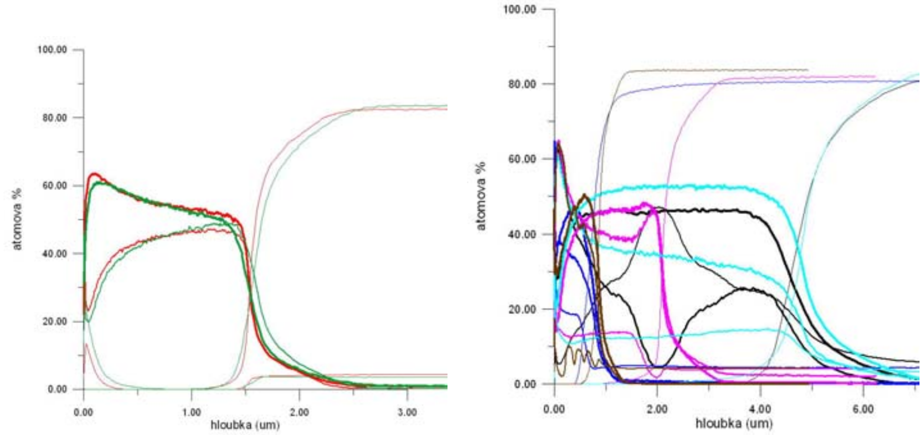

Fig. 7: Depth profile of chemical composition of systems thin film – substrate – 1. TiN – substrate, 2. TiCN – substrate.

Conclusions

There are compared different systems thin film – substrate from different technology process – high temperature CVD, PVD and low temperature PA CVD. For comparison the indentation measurement was provided by static indentation with different range of normal force used and scratch indentation too. From this analysis are results tab. 1 with numbers characterize differences between systems thin film – substrate and complex evaluation of properties and behaviour during indentation stress and initiation and expansion of failures and cracks and study of adhesive cohesive failures around and in scratches and indents too. From analysis is clear what only simply number not characterize correctly evaluated systéms of materials and can not give view about behaviour (namely critical force from scratch test) in real conditions and is very different then complex evaluation adhesive cohesive behaviour. From all analysis we can say, what near to comparable with PVD thin film is TiN from PA CVD prepared in third collaborated company. The systems of thin film – substrate from different technology process are very different. Differences are in roughness, thickness, nanohardness, depth profile chemical composition and mechanical resist to the scratch and static indentation stress and it is very difficult compare these systems of materials.

The paper is presented in the range of solution project n. FT-TA/075.

process		CVD	PACVD1	PACVD2		PACVD3			PVD
Thin film		TiCN	TiCN	TiN	TiCN	TiN	TiCN	DLC	TiCN
Nanohardness [DHV]	200 g	1025	650	871	740	830	920	710	740
	25 g	2170	1170	1748	1560	1630	1470	1270	1720
	2 g	2710	2150	2680	2420	2560	2610	2040	2790
Thickness [µm]	calotest	12.7	1.5	2.2	2.7	2.1	5.2	3.3	1.3
	GDOES	4.3	0.9	1.4	2.1	1.4	4.7		0.9
Critical normal force [N]	The first failure	44	16	24	8	14	11	18	7
	significant failure	75	38	31	18	31	31	19	39
	Total exposure substrate		58	48	31	56	38	37	58

Tab. 1: Basic mechanical properties – nanohardness, thickness and critical forces

Literature

1. I.Stepanek, Correlation between deposition parameters and method for evaluation properties and behaviour system of thin film - substrate, proceedings of conference Matrib 2000 Vela Luka – Croatia 2000

2. R.Nemec, I.Stepanek, Complex evaluation of mechanical properties of systems thin films by graph dependence measure information on value of load, proceedings of conference Matrib 2001, Croatia – Vela Luka 2001

3. I.Stepanek, Evaluation of mechanical behaviour very different kind of material and thickness of films, proceedings of conference Matrib 2002, Croatia – Vela Luka 2002

11. Savjetovanje o materijalima, tehnologijama, trenju i trošenju
11. Conference on Materials, Processes, Friction and Wear
MATRIB'06, Vela Luka, 22-24.06.2006.

COMPLEX EVALUATION OF MECHANICAL PROPERTIES AND BEHAVIOUR OF HIGH AND LOW RESISTIVITY SYSTEMS THIN FILM – SUBSTRATE BY INDENTATION TESTS

Štěpánek Ivo, Macháčková Kateřina, Department of Materials Science and Metallurgy, University of West Bohemia, Univerzitní 22, Pilsen, Czech Republic

Abstract: The paper is devoted by complex view on evaluation of mechanical properties and behaviour of systems thin film – substrate for very different systems of materials from point of view resistivity to the indentation stress and evaluation results of indentation tests realised on these materials. The evaluation is dirrected on indentation tests statical and scratch with big range of acted normal force. The measurement is refining at the first for evaluation low resistivity systems and at the second for evaluation initiation and expansion fractures. There are developed methods for simulation and analysis wear and resistant during repeated stress with the help cyclic static indentation and scratch indentation tests. The refining of analysis is reached by different geometry and material of indentors and by changing value of normal force. Indents and scratches are evaluated by light microscopy. The influenced area is documented by nanoindentation measurements from surface and from special cross sections in the indents too. Scratches are documented by special local x-ray fluorescent spectroscopy for getting information about step of wear and degradation.

University of West Bohemia in Pilsen

Introduction

The rapidly increased application of thin films and requirement on behaviour in application on special tools, special parts of machine and for special application in different processes with very different kind of stresses need modification standard and developing new methods for evaluation properties and behaviour of systems thin film – substrate. In this time very much method exists for analysis basic properties of thin films, but analysis for comlex understanding behaviour of systems thin film – substrate in aproximately real conditions are not standardized yet. Basic properties do not give information, which can give possibility to predict behaviour in practise conditions, reliability and lifetime.

Evaluation by static indentation tests of systems thin film – substrate

Some our papers solute problem application of indentation measurement on very different kind of systems thin film – substrate. Much more information about materials systéms we can get from graph of dependence rate of information about materials systems and value of loading acted on surface of materials. The standard methods of analysis give possibility to use indentation method for evaluation very close range of materials systems (systems thin film - substrate). Informations about material systems from indentation are given not only by value of loading, thickness of thin films and homogeneity of surface, but the resistivity of material systems is very important too. The macrohardness is evaluated on bulk material, microhardness is evaluated in large locality, large structure components, thick films and thin films with larger thickness, where basic material properties not influence reasult of measurement. Nanohardness is evaluated on thin films, in microlocality, smaller structure components, for evaluation depth profile mechanical properties, mapping of mechanical properties in areas. Setup of the load for evaluation adhesive cohesive is given by thickness of thin films, by size of grains of structure components. The resistivity of material systems is very important for seting of value of load too. If the resistivity of systems of materials is very low, then nanoindentation curves catches adhesive cohesive failures and cracks (fig. 1), which are documented by light microscopy on fig. 3, 4 and 5. Bad adhesion can results as incresing elastic deformation or plastic deformation too (fig. 2). Nanoindentation measurement is useful for evaluation not only nanohardness but for evaluation rate of elastic and plastic deformation, resistance to the indentation stress, fracturing and failuring of surface and for the others.

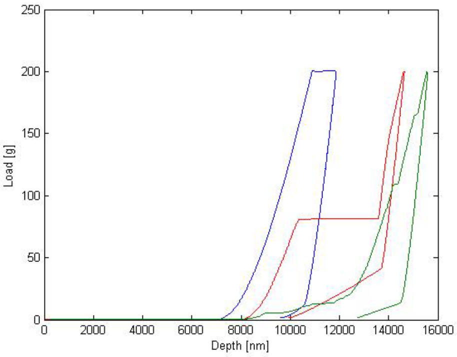

Fig. 1: Nanoindentation curves influenced by failures and cracks give results with stairs on curve or as big plastic deformation or as multilayer system.

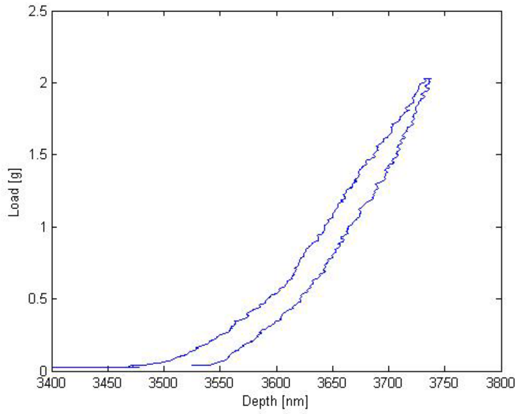

Fig. 2: Nanoindentation curve influenced by bad adhesion thin film to the substrate give result as very elastic material.

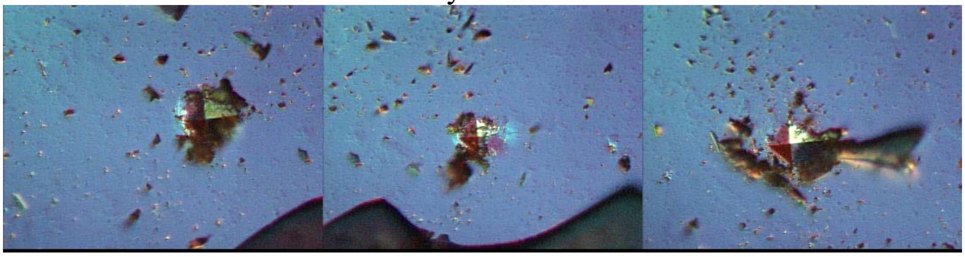

Fig. 3: Examples of failures around the indents after nanoindentation with maximal load 200 g – the indents we can not evaluate for microhardness.

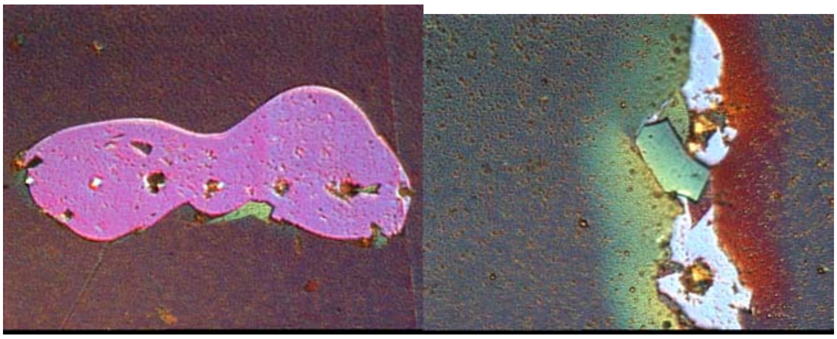

Fig. 4: Examples of failures around the indents after nanoindentation with maximal load 200 g – here is very large failure around indents

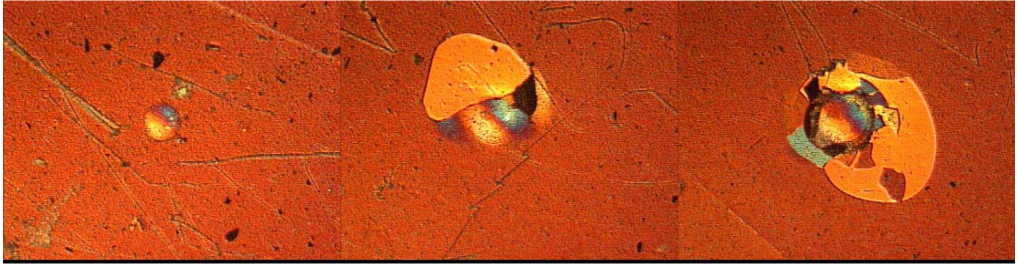

Fig. 5: Indents from static indentation measurement on surface with thin film with normal force 30, 60 and 90 N

Evaluation by scratch indentation tests of systems thin film – substrate

In the base the scratch test enable evaluation of adhesion of thin films to the substrate. The adhesion by standard methods evaluate as establishing critical normal force for exposure substrate. The critical force is established from morphology of scratch. The second method for establishing critical force is from dependence signal of acoustic emission signal on value of normal force in measurement with increased normal force. The third method for establishing critical force is from dependence of coefficient of friction on value of normal force. If we establish critical normal force by all above mentioned methods on different systems of thin film – substrate we can get results what the critical forces are very different. Coefficient of friction is dependence on wear and failure of indentor and acoustic emission too. The signal of acoustic emission depend on surface preparation, modification and properties of basic materials. Evaluation failures in scratches is very difficult and unreliability and subjective. The most important the evaluation behaviour of systems thin film – substrate and all failures and cracks are more important and give much more information about properties and behaviour of systems thin film – substrate. The deformation and cohesive failures of substrate influence behaviour all systém thin film – substrate, therefore it is important analyse behaviour of surface of basic material before deposition for understanding deformation process and failures, which can influence degradation all systém of thin film – substrate. Some results of comparison behaviour surface of substrate and systém thin film – substrate is showed in fig. 6.

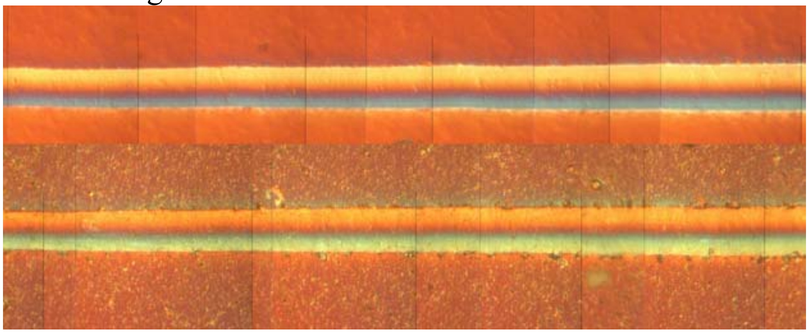

Fig. 6a: Part of scratch in surface of basic material HSS and in surface of systém thin film – substrate HSS – the same conditions for measurement

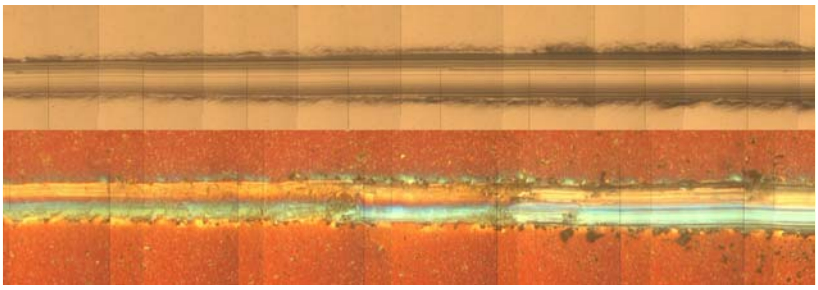

Fig. 6b: Part of scratch in surface of basic material VT6 and in surface of systém thin film – substrate VT6 – the same conditions for measurement

Change of sensitivity of measurement by scratch indentation tests

The standard method of evaluation of scratch tests enable analyse only close range of material systems with good mechanical resistivity, high microhardness of basic materials, better adhesive cohesive behaviour of thin films and cohesive behaviour of substrate. The large range of application thin films need using of analysis by scratch test in wide rande of properties and behaviour of systems thin film – substrate and substrate. We must change sensitivity of measurement by scratch indentation. More resistivity materials systems need more drastic scratch indentation. On the other side less resistivity material systems need refinement of scratch indentation tests. The refinement is possible realise by changing of range of normal force to the smaller normal force with using different type of equipment. We can use microscratch tester or nanoscratch tester for evaluation less resistivity systems of materials or systems thin film – substrate with smaller thickness or multilayers and similar or if we want to analyse initiation of failures and cracks. Other method for refinement is using different type of indentors. Changing of materials and geometry characteristic of indentors give possibility to use scratch test method for analysis different material systems, change main type of degradation, change deformation process and friction between indentor and surface of tested material. In fig. 7 we can analyse deformation by scratch test, wear by friction, deformation of basic material, all systém thin film – substrate, smaller and bigger failures and its initiation and other expansion with increasing normal force.

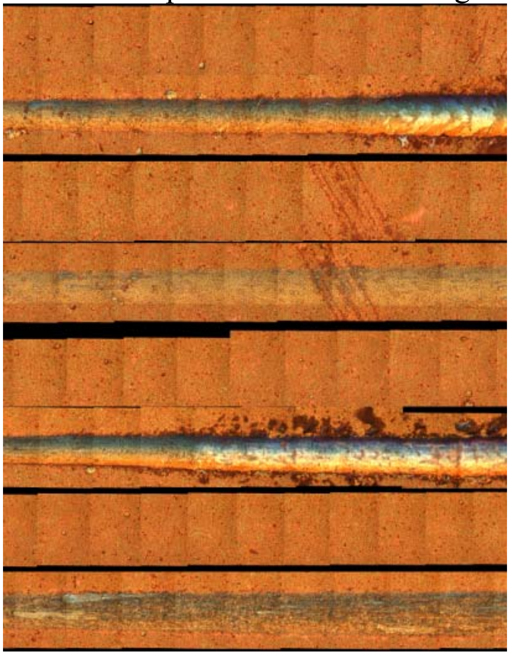

Fig 7: The scratches in surface of systém thin film – substrate 19 830 – indentors 1. diamond 0,2 mm, 2. diamond 0,5 mm, 3. sintered carbides 0,2, 4. sintered carbides 0,5

Evaluation resistivity to the expansion of failures by scratch test

If we refine the scratch analysis we give other expansion of utilization this analysis method. We can analyse resistivity of systems thin film – substrate with using different normal force, different type of indentors. This method give information about resistivity to the different type of stress – deformation and friction and combination. The other aproximation of real stress and step by step changing of failures during indentation stress we can get by cyclic scratch indentation tests. The cyclic scratch indentation measurement enable evaluate initiation of failures and cracks and its expansion with increasing of number of cycles. By this we can analyse wear resistant of systém thin film – substrate. By using different type of indentors we can analyse wear resistant of less resistant systems of materials and more resistant systems of materials too. Some example of measurement by scratch test on less resistant systém is presented on fig. 8. The systém thin film – substrate steel CSN 14 220 is degradate mainly by deformation process of substrate, if we use diamond indentor Rockwell type with radius of tip 0,2 mm. The measurement with indentor from sintered carbides with radius of tip 0,5 mm give smaller deformation and here is possible better analyse resistant to the friction. I we use sintered carbides for evaluation systém thin film – substrate with HSS substrate we can view, what wear is given by friction and here is very big wearing and failuring of indentor too.

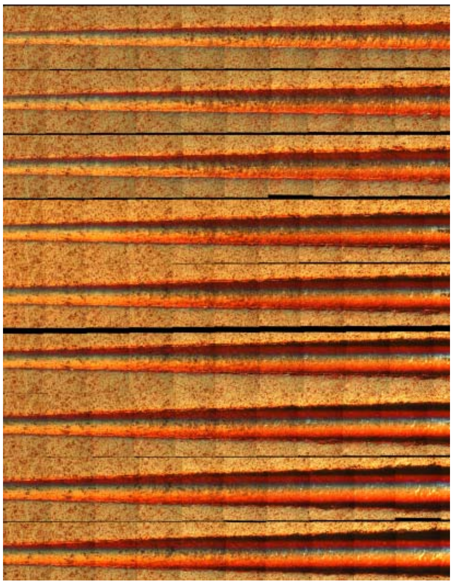

Fig 8: The scratches in surface of systém thin film – substrate 14 220 after cyclic scratch indentation – 1 cycle, 2 cycles, 3 cycles, 5 cycles, 7 cycles, 10 cycles, 15 cycles, 22 cycles, 30 cycles – indentor diamond 0,5 mm

Analysis of wear and fracturing in scratches with depth sensitivity

Evaluation of results of scratch test is realised mainly by light microscopy with using polarisation and Nomarsky differential contrast too (different magnification). The other evaluation is give by analysis acoustic emission signal and coefficient of friction in dependence on acted normal force. Deformation process and failuring and wearing in the scratches is evaluated very difficult. We can analyse scratch by scanning electron microscopy by secondary electrons and backscattered electrons, which give some interesting information too, because here is higher depth sharpness and sensitivity to atomic weigh. For evaluation critical force we can use EDX analysis method in selective places [2]. The method SEM and EDX are interesting but not operative. The new method, which we try to use for evaluation of scratches is special x-ray fluorescent spectroscopy. The configuration of equipment CMI 950 for analysis by x-ray fluorescent spectroscopy is special for analysis thin films, its chemical composition after calibration and thickness of thin films after calibration too. The settign of special collimators give possibility to provide analysis from very small area and give possibility to measure in special places, which are the most important. By this equipment we can measure on selective parts of tools, some parts of machines and the others. The measurement by x-ray fluorescent spectroscopy is non destructive. The parameters of equipment CMI 950 are very interesting for using for analysis of scratches. The area of analysis is small but not enough for analysis smaller failures. The area of analysis is enough for analysis wear after scratches for evaluation of reduction of thin films in the scratches. We provide measurement in different places in scratches with different acted normal force. The results of the measurement are in fig. 9 and fig. 10 on different systems thin film – substrate and failured by different type of indentor. The fig. 9 and fig. 10 illustrate very good reduction of thin films in scratches with increasing of normal force. Here is possible to view changing of wear with using different indentor on different systems thin film – substrate.

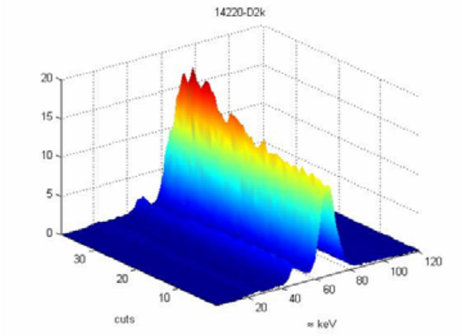

Fig. 9: X-ray fluorescent spectrums in different places with increasing value of normal force (z axes) in scratch in surface of systém thin film – substrate 14 220 – indentor from diamond with radius of tip 0,2 mm.

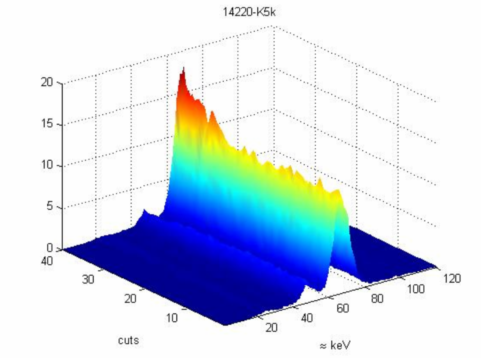

Fig. 10: X-ray fluorescent spectrums in different places with increasing value of normal force (z axes) in scratch in surface of systém thin film – substrate 14 220 – indentor from sintered carbides with radius of tip 0,5 mm.

Evaluation of deformation and failuring in scratches in cross sections

The other analysis, which give us very interesting information and which give the most important information about importance of failures and cracks, are analysis from special sensitive cross section in selective places with characteristic and more important failures [3]. Fig. 11 represent the important failures, which is not possible right evaluate from observation from only surface. The first failure is large from surface, but from cross section the failure not significant. The second failure from cross section show only reduction of thin film but not exposure of substrate. The other failure show, what initiation for failuring is deformation of substrate under thin film. From this examples it is clear, that cross section is very important for evaluation special failures.

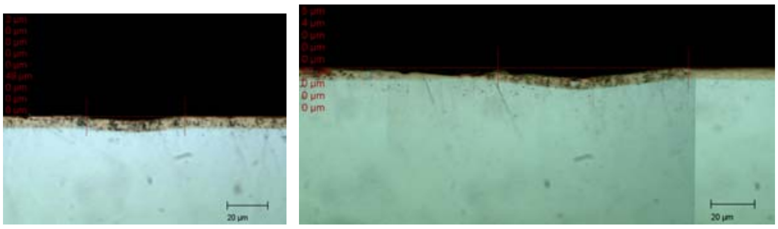

Fig. 11a: Cross section in selective places in scratch in systém thin film (TiN) – substrate HSS.

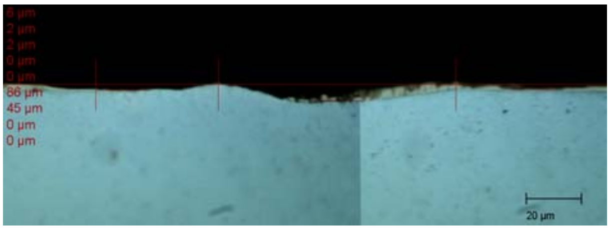

Fig. 11b Cross section in selective places in scratch in systém thin film (TiN) – substrate HSS.

Conclusions

The standard method of evaluation by static indentation and scratch indentation measurement give information about basic mechanical properties of special part of materials systems with good mechanical resistivity of basic materials and thin films too. The measurement give only basic information about hardness, microhardness, adhesion and the others. Practice application of systéms thin film substrate need much more information about mechanical properties and behaviour too. The analysis by indentation are changed for evaluation not only mechanical properties but mechanical behaviour during indentation process and initiation and expansion failures and cracks too. By complex analysis by indentation we can get information about initiation failures, expansion failures and wear after indentation process. By refinement of measurement changing range of value of acted force or type of indentor and mode of measurement we can use these methods for evaluation less mechanical resistivity materials and more mechanical resistivity materials too based on concrete example. The evaluation by x-ray fluorescent spectroscopy and abalysis from cross section help to understand more of mechanism of failures, its initiation and its expansion in next indentation stress.

Literature

1. R.Nemec, I.Stepanek, Graph dependence measure information on size load at statical indentation tests, proceedings of conference Matrib 2000, Croatia – Vela Luka 2000
2. I.Stepanek, Method for complex evaluation of properties and behaviour systems of thin film – substrate, proceedings of conference Matrib 2000, Croatia – Vela Luka 2000

3. Štěpánek, I., Kavinová, M., Hrdý, M.: Evaluation of macroindentation statical and scratch tests in cross section in systems thin films – substrate, proceedings of conference 2004, Croatia 2004

11. Savjetovanje o materijalima, tehnologijama, trenju i trošenju
11. Conference on Materials, Processes, Friction and Wear
MATRIB'06, Vela Luka, 22-24.06.2006.

EVALUATION OF CHANGING OF MECHANICAL BEHAVIOUR BY NANOINDENTATION TESTS IN DIFFERENT MODES OF MEASUREMENT OF POLYMER MATERIALS AFTER TEMPERATURE AGEING

Tengler Marek, Štěpánek Ivo, Netušilová Denisa, Department of Materials Science and Metallurgy, University of West Bohemia, Univerzitní 22, Pilsen, Czech Republic

Abstract: The paper is devoted by evaluation of surface films of materials, which not created by deposition processes, but step by sted degradation process. The methods of analysis mechanical properties and behaviour of systems thin film – substrate by indentation tests with different value of normal force are modified for evaluation of these materials. Very interesting and important information from nanoindentation measurement is indentation curve, which bring information about all indentation process during loading, time holding and unloading. Indentation curve is influenced by inhomogeneity in different depth. There are used evaluation by different modes of measurements for capture changing during degradation process. The cyclic modes are used too, which bring much more information about changing behaviour during repeated indentation stress. There are presented measurement of polymer materials before and after thermal stress, thermal ageing.

University of West Bohemia in Pilsen

Introduction

The methods for analysis of properties and behaviour thin films respectively systems thin film – substrate are developed for better undestanding of behaviour of systems thin film – substrate in real conditions. Here is very important not only analyse basic properties, but also behaviour during different stress. We must analyse initiation of failures and cracks, adhesive cohesive failures and its other expansion during repeated stress. Thin films are prepared by very different methods on surface of basic material. Thin films can be created by modification process in surface of basic materials too. In the end thin films on surface can be created by degradation process too. From this point of view it is very important prepare methods for analysis these special material systems too.

Nanoindentation method of evaluation mechanical properties and behaviour of surfaces of materials

The nanoindnetation method bring much more information about mechanical properties and mechanical behaviour of surfaces of materials [1]. The standard measurement is in mode 2. It is measurement of indentation curves during loading, time holding and unloading – dependence of actual depth indentation and actual normal force. From this measurement we can analyse not only nanohardness, but here is possible analyse behaviour of material systems during all indentation process. Indentation curves bring information about nanohardness, elastic plastic deformation, failures and cracks (fig. 1 and fig. 2) too and the others. Indentation curves bring information from different depth of materials too. Setup of conditions of measurement give very large possibility. The setup conditions are maximal load, rate of loading, time holding and depth of indentation.

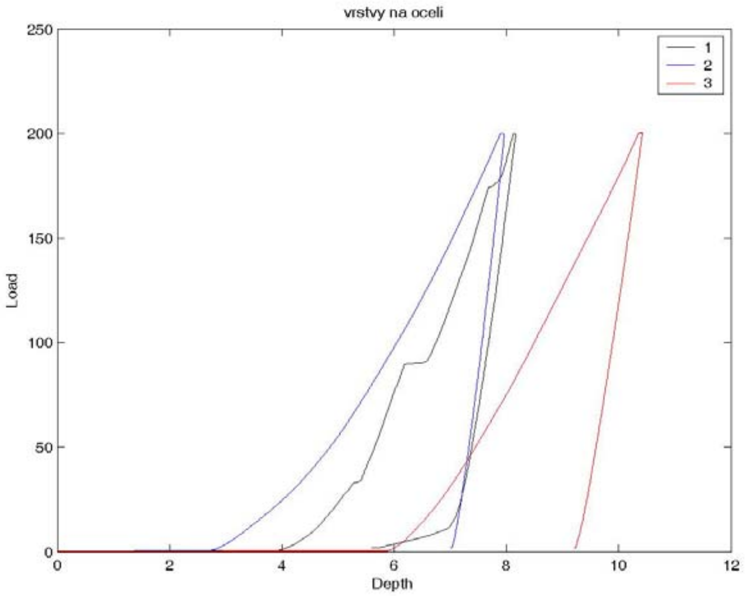

Fig. 1: Nanoindentation curves influenced by failures and cracks.

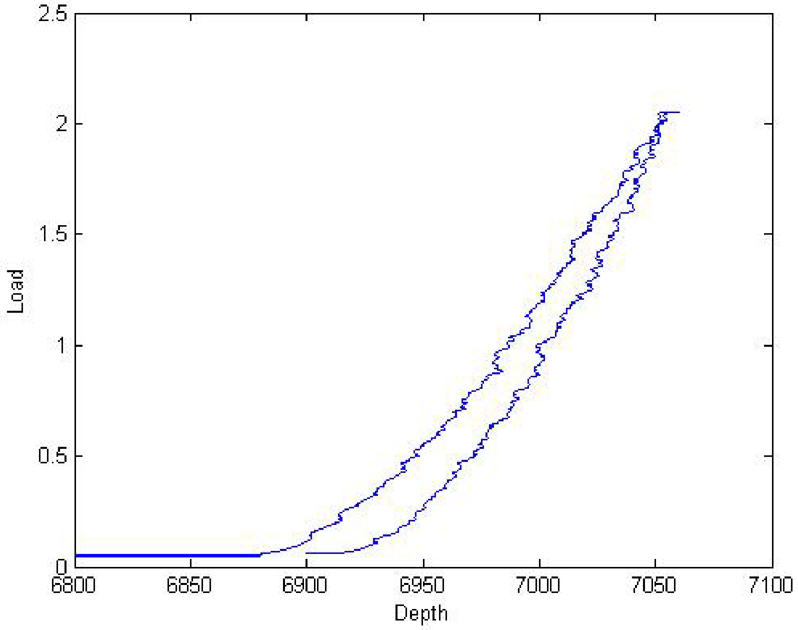

Fig. 2: Nanoindentation curve influenced by bad adhesion thin film to the substrate.

Nondestructive nanoindentation method of measurement

The analysis by nanoindentation are realised with very small loading and not evaluated here indents but indentation curves – dependence of depth of indentation and loading. Indents are very small and it give possibility to take this method as nondestructive. We can measure on real parts without destruction [2]. We can use this method as controling method after some exposition in real conditions, step by step changing during some stress – after corrosion, temperature stress, mechanical stress and the others [3]. The measurement is sensitive on changing properties and behaviour to the depth of material.

Sensitivity of simple indentation on inhomogeneity in the depth of materials

The indentation curves are sensitive on inhomogeneity in the depth of material systems. Small value of loading give possibility analyse surface of materials. In the example of systém thin film – substrate we can analyse surface of systems by very small loading about 0,05 g, thin films are analysed with loading in dependence on thickness and mechanical properties about 1, 2, 5 and 10 g. If we can know changing of mechanical properties of basic material after deposition or modification proces or degradation process, we must setup loading on value 200 g (fig. 3) or large. The similar it is if we want analyse changing in the depth after different step of degradation or modification processes. Fig. 3 and fig. 4 show changing of indentation curves with different maximal load setup on system thin film – substrate. Fig. 5 – 7 show changing of nanoindeetation curve on surface of polymer material with different maximal load (1g, 0,1 g and 0,02 g).

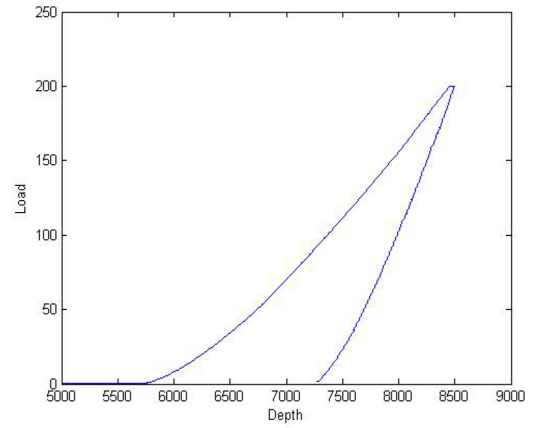

Fig. 3: Nanoindentation curve on system thin film (TiN) – substrate (HSS) with maximal load 200 g.

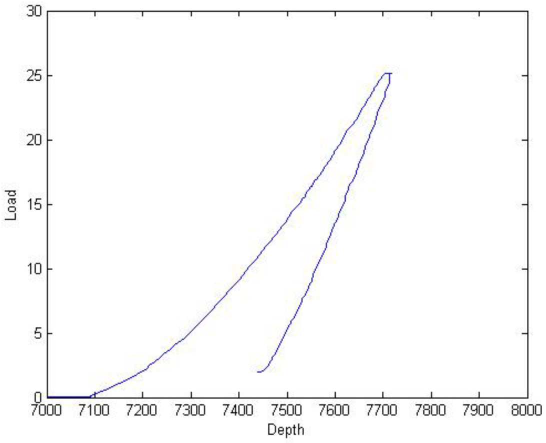

Fig. 4: Nanoindentation curve on system thin film (TiN) – substrate (HSS) with maximal load 25 g.

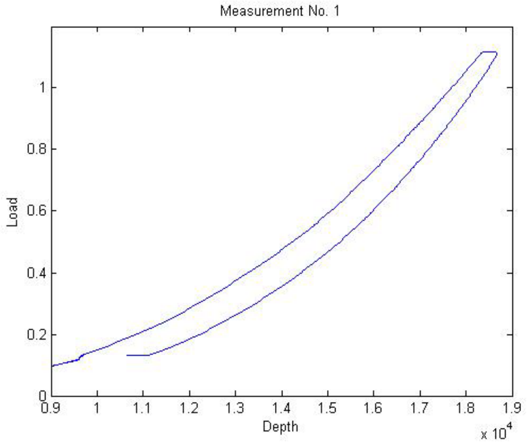

Fig. 5: Nanoindentation curve on surface of polymer material with maximal load 1 g.

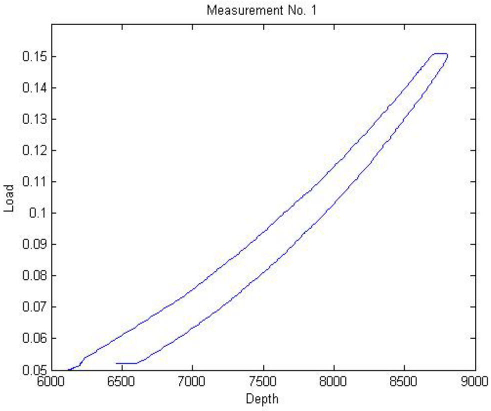

Fig. 6: Nanoindentation curve on surface of polymer material with maximal load 0,1 g.

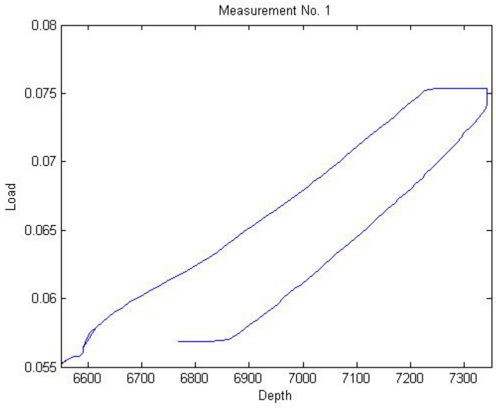

Fig. 7: Nanoindentation curve on surface of polymer material with maximal load 0,02 g.

Sensitivity of cyclic nanoindentation on changing of material properties in the depth

Cyclic nanoindentation measurement give possibility to analyse much more information not only nanohardness and changing rate of elastic plastic deformation process but also changing properties in the different depth, changing properties and behaviour after step by step or cyclic loading in the same places. This method give possibility analyse hardening of surface and creep of materials, because this changing is catched in nanoindentation curves. We can use two different modes of cyclic nanoindentation measurement. At the first it is mode, in which loading is realised repeatedly in the same places with the same maximal load, the same time holding, rate of loading (fig. 8 and fig. 9). Maximal number of cycle of one measurement is 250. The second mode is mode, in which is step by step increased loading – maximal loading is recalculated on maximal 20 steps (fig. 10 and fig. 11). Then measurement is running to the step by step increased loading from 0 to twentieth of maximal loading, next step to the second twentieth of maximal load and so on. This measurement give us possibility to view changing mechanical properties and behaviour during step by step changing indentation depth. The fig. 10 and 11 show examples measurement on polymer material in this modes with different maximal load. Here is possible to view, what curves are changed after step by step indentation and with deeper indentation.

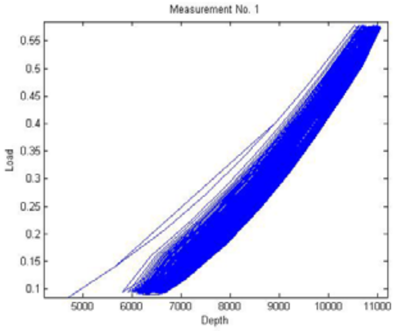

Fig. 8: Cyclic nanoindentation curve – mode 4 on surface of polymer material with maximal load 0,5 g.

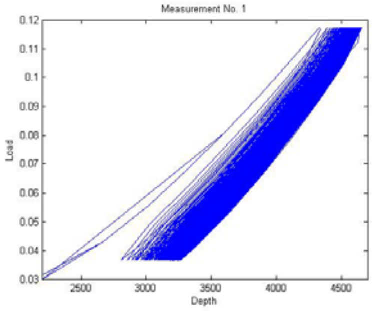

Fig. 9: Cyclic nanoindentation curve – mode 4 on surface of polymer material with maximal load 0,1 g.

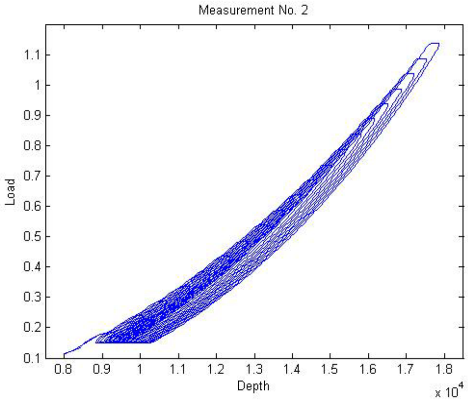

Fig. 10: Cyclic nanoindentation curve – mode 7 on surface of polymer material with maximal load 1 g.

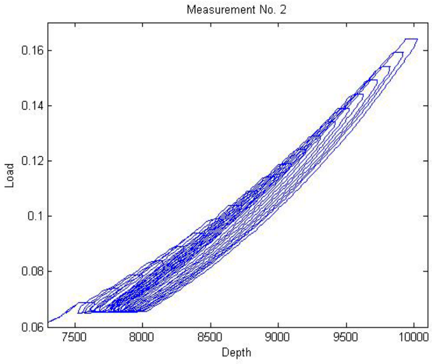

Fig. 11: Cyclic nanoindentation curve – mode 7 on surface of polymer material with maximal load 0,1 g.

The first experiments for evaluation of degradation process by nanoindentation

In this parts we present the first experiment of measurement on surface of polymer material before and after temperature ageing. At the first here is presented indentation curves before degradation process with different maximal load during measurement (fig. 12 and fig. 14). This material is strongly elastic with very small value of nanohardness. At the second here is presented indentation curves after temperature ageing (fig. 13 and fig. 15) with maximal load similar as for examples before ageing. The results show, what after temperature stress is changed rate of elastic and plastic deformation process and from slope it is possible to view changing of nanohardness.

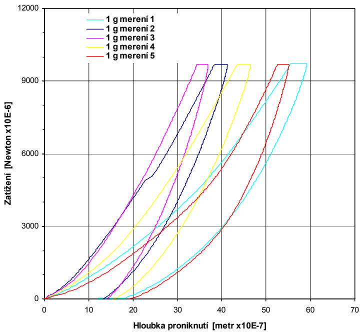

Materiál Polidan teplotně neovlivněný.
Indentační zatížení 1g MOD 2.

Fig. 12: Nanoindentation curves on surface of polymer material with maximal load 1 g.

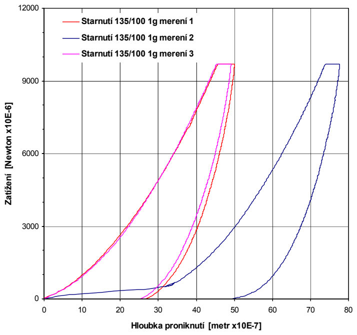

Materiál Polidan uměle zestárnutý při 135°C / 100 hod.
Indentační zatížení 1g MOD 2.

Fig. 13: Nanoindentation curves on surface of polymer material with maximal load 1 g after temperature stress.

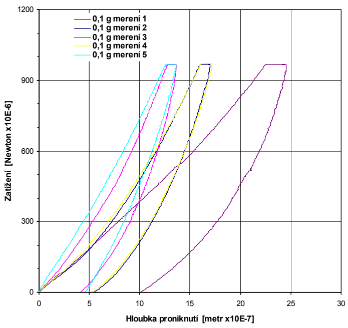

Materiál Polidan neovlivněný teplotním stárnutím.
Indentační zatížení 0,1g MOD 2.

Fig. 14: Nanoindentation curves on surface of polymer material with maximal load 0,1g.

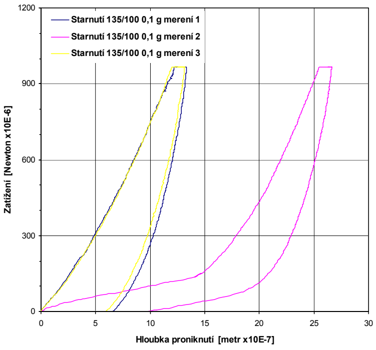

Materiál Polidan uměle zestárnutý při 135°C / 100 hod.
Indentační zatížení 0,1g MOD 2.

Fig. 15: Nanoindentation curves on surface of polymer material with maximal load 0,1g after temperature stress.

Conclusions

The nanoindentation techniques and indentation measurement at all can has much more application then only for measurement hardness, microharness, nanohardness and adhesion. The nanoindentation bring information about elastic plastic deformation, resistivity to the local indentation and the others. The nanoindentation can give information about depth profile mechanical properties and behaviour from simple measurement with increasing value of load, cyclic measurement can bring more complex information about behaviour of surface of materials. The optimalised method for evaluation by nanoindentation give possibility to evalute not only created by deposition thin films but thin films created by modification and degradation process too. The nanoindnetation is non destructive method for analysis properties and behaviour and is very useful for analysis on special places before and after some stress for control changing properties and behaviour. One of the way is using this method for evaluation changing properties and behaviour of surface polymer materials with depth sensitivity after temperature ageing process.

Literature

1. R.Nemec, I.Stepanek, Graph dependence measure information on size load at statical indentation tests, proceedings of conference Matrib 2000, Croatia – Vela Luka 2000
2. R.Nemec, I.Stepanek, J.Michalek, Special measurements of mechanical properties in microlocation in comparison with measurement thin films, proceedings of conference Matrib 2001, Croatia – Vela Luka 2001
3. I.Stepanek, Aproximation real stress condition with using laboratory analysis of behaviour systems thin film – substrate during combination stress, proceedings of conference Matrib 2001, Croatia – Vela Luka 2001

11. Savjetovanje o materijalima, tehnologijama, trenju i trošenju
11. Conference on Materials, Processes, Friction and Wear
MATRIB'06, Vela Luka, 22-24.06.2006.

ANALIZA VARIJACIJA MIKROSTRUKTURE NODULARNOG LIJEVA U LIJEVANOM ISPITNOM UZORKU

ANALYSIS OF MICROSTRUCTURE VARIATIONS OF NODULAR CAST IRON IN CAST TEST SAMPLE

K. Terzić1), Z. Glavaš1), F. Unkić1)
1) Metalurški fakultet Sisak, Aleja narodnih heroja 3, 44103 Sisak

Sažetak: Referentni uzorci za ispitivanje mehaničkih svojstava željeznih ljevova najčešće se dobivaju iz odvojeno lijevanih ispitnih uzoraka (tzv. „Y-probi“) lijevanih u jednokratne kalupe sukladno propisanim normama. Obzirom na konfiguraciju lijevanog ispitnog uzorka, pokazalo se potrebnim istražiti varijacije u mikrostrukturi ovisno o mjestu uzimanja uzorka, a samim tim i utjecaj mjesta uzimanja uzorka na dobivene vrijednosti mehaničkih svojstava. Ustanovljeno je da se udio ferita, kao i broj grafitnih nodula/mm^2 u lijevanom ispitnom uzorku smanjuje s približavanjem mjesta uzimanja uzorka toplinskom centru i najveći je u donjem, perifernom dijelu uzorka. Mikrostruktura lijevanog ispitnog uzorka pod jakim je utjecajem toplinskih gradijenata, što može imati za posljedicu varijacije mehaničkih svojstava obzirom na mjesto uzimanja uzorka.

Ključne riječi: nodularni lijev, mikrostrukturna svojstva, lijevani ispitni uzorak, tvrdoća

Abstract: Standard test samples for examination of cast iron mechanical properties are most often obtained from separately cast test samples („Y-block“). Cast test samples („Y-block“) are obtained by melt pouring in green sand moulds according to norms. Regarding to the configuration of cast test sample, it is necessary to examine variations in microstructure depending on place of sample taking, and its influence on assigned values of mechanical properties. In this paper shown is that ferrite share and number of graphite nodules/mm^2 in cast test sample decrease with approach place of sample taking to thermal center of sample. Ferrite share and number of graphite nodules/mm^2 are biggest in lower, periphery part of cast test sample. Thermal gradients have strong influence on microstructure of cast test sample, which could conduce variations in mechanical properties depending on place of sample taking.

Key words: nodular cast iron, microstructure properties, cast test sample, hardness

UVOD

Osnovna karakteristika nodularnog lijeva je izlučivanje grafita u tzv. nodularnom obliku sukladno HRN EN 945 ("Željezni lijev – označivanje mikrostrukture grafita") [1]. Prema ovoj normi nodularni grafit označava se kao oblik VI. Klasifikacija nodularnog lijeva provodi se prema HRN EN 1563 [2]. U odnosu na konkurentne materijale, prije svega sivi i vermikularni lijev, nodularni lijev posjeduje relativno visoku granicu razvlačenja visoko istezanje i udarnu žilavost. Vlačna čvrstoća nodularnog lijeva je na nivou vrijednosti vlačne čvrstoće čeličnog lijeva [3-5]. Zbog povoljne kombinacije svojstava, nodularni lijev ima danas široku primjenu: u industriji motornih vozila, industriji motora, metalurškoj industriji, gradnji cjevovoda i proizvodnji armatura, industriji tekstilnih strojeva, kemijskoj industriji itd.

Mehanička svojstva željeznih ljevova najčešće se određuju na ispitnim (normiranim) uzorcima koji se dobivaju strojnom obradom iz lijevanih ispitnih uzoraka, (tzv. „Y-probi"). Lijevani ispitni uzorci dobivaju se lijevanjem taljevine u odvojene kalupe, najčešće izrađene od svježe kalupne mješavine. Norma HRN EN 1563:1997 propisuje oblik i dimenzije lijevanih ispitnih uzoraka. Budući da lijevani ispitni uzorak ima oblik slova Y, odnosno naglašene varijacije u dimenziji, može se očekivati da postoje i varijacije u mikrostrukturi po visini uzorka zbog različitih toplinskih gradijenata [6]. Poznato je da brzina hlađenja (toplinski gradijenti) ima značajan utjecaj na mikrostrukturna svojstva nodularnog lijeva [7 - 9]. Različite mikrostrukturne karakteristike mogu rezultirati i različitim vrijednostima mehaničkih svojstava, što može u konačnici rezultirati odstupanjem od normom propisanih mehaničkih svojstava.

U okviru ovog rada analizirana je varijacija mikrostrukture nodularnog lijeva u lijevanom ispitnom uzorku glede mjesta uzimanja ispitnih uzoraka.

METODOLOGIJA ISPITIVANJA

Taljevina nodularnog lijeva izrađena je u ljevaonici i tvornici armatura „MIV" d.d. u Varaždinu. Nakon taljenja u kupolnoj peći, taljevina se prenosi u mrežno–frekventnu indukcijsku peć gdje se provodi korekcija temperature, homogenizacija i eventualna korekcija kemijskog sastava. Pripremljena bazna taljevina prenosi se potom u receptor.

Obrada taljevina provedena je "Osmosa" postupkom. Poslije obrade taljevina predlegurom na bazi magnezija uzima se uzorak za određivanje kemijskog sastava obrađene taljevine i lijeva se ispitni uzorak, tzv. "Y – proba" sukladno HRN EN 1563:1997.

Iz odlivenog ispitnog uzorka („Y-probe") isječen je segment debljine 20mm po čitavoj visini. Isječeni segment podijeljen je na 7 dijelova prema slici 1. Svaki dio je zasebno analiziran.

Metalografska ispitivanja (određivanje udjela ferita i perlita, stupnja nodularnosti, broja nodula/mm^2) provedena su na Metalurškom fakultetu u Sisku pomoću svjetlosnog metalografskog mikroskopa s digitalnom kamerom (Olympus GX 51) i sustava za automatsku obradu slike (AnalySIS® Materials Research Lab) uz povećanje 100 puta. Kriterij koji određuje česticu uzima u obzir sve čestice čija je površina $\geq 100 \mu m^2$. Ako čestica zadovoljava kriterij da je 4 x površina čestice/najduža dimenzija između 1,4 – 3,2, smatra se nodulom.

Ispitivanja tvrdoće provedena su prema HRN EN 6506-1:1999. Tvrdoća ispitivanih uzoraka određena je na tvrdomjeru "Amsler Otto Wolpert Dia Testor 2Rc" po Brinell metodi s promjerom kuglice 2,5 mm uz opterećenje 187,5 kg i vrijeme utiskivanja 15 s, u ljevaonici "Dalit Corp." d.d.

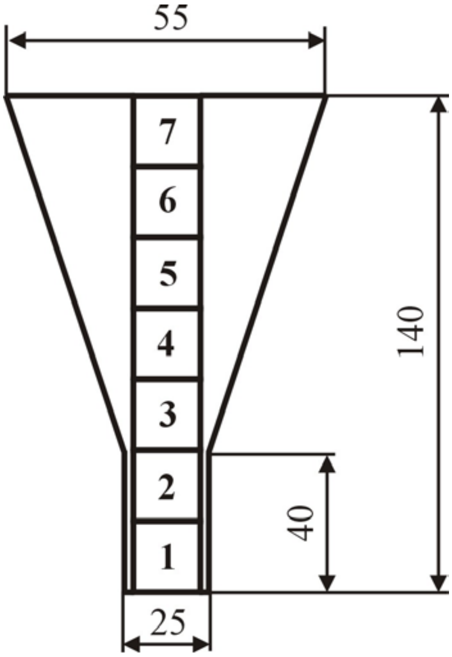

Slika 1. Shema uzimanja uzoraka iz „Y-probe“. Dimenzije „Y-probe“ dane su u mm i sukladne su HRN EN 1563:1997. Dužina „Y probe“ iznosila je 160 mm

REZULTATI I DISKUSIJA REZULTATA

Kemijski sastav taljevine iz koje je odliven standardizirani ispitni uzorak („Y-proba“) prikazan je u tablici 1.

Tablica 1. Kemijski sastav taljevine iz koje je odliven standardizirani ispitni uzorak („Y-proba“)

Element	***C***	***Si***	***Mn***	***S***	***P***	***Cu***	***Mg***
%	3,70	2,75	0,14	0,003	0,02	0,041	0,030

U cilju dobivanja što vjerodostojnijih podataka o mikrostukturi, na svakom uzorku provedeno je 15 mjerenja. Rezultati mikrostrukturnih ispitivanja i ispitivanja tvrdoće prikazani su u tablici 2. Shodno prethodno navedenom, udio ferita i perlita, stupanj nodularnosti i boj nodula/mm^2 prikazan je kao srednja vrijednost 15 mjerenja. Na slikama 2 – 8 prikazane su metalografske snimke mikrostrukture za svaki uzorak u ne nagriženom i nagriženom stanju pri povećanju 100x.

Iz tablice 2 i sa metalografskih snimki (slike 2 – 8) vidljivo je da je udio ferita u mikrostrukturi najveći kod uzorka br. 1, a najmanji kod uzorka br. 4. Od uzorka br.4 prema uzorku br. 7 vidi se ponovo lagani trend porasta udjela ferita u mikrostrukturi. Dobiveni rezultati suprotni su očekivanjima, jer gledajući u odnosu na mjesto toplinskog centra bilo bi za očekivati porast udjela ferita od periferije prema smjeru toplinskog centra.

Tablica 2. Rezultati mikrostrukturnih ispitivanja standardiziranog lijevanog ispitnog uzorka („Y-proba“)

Broj uzorka	***Udio ferita, %***	***Udio perlita, %***	***Broj nodula/mm***^{2}	***Nodularnost, %***	***Tvrdoća, HBW***
1	87,42	12,58	139	72,0	168
2	84,23	15,77	118	71,0	167
3	74,58	25,42	83	70,0	175
4	71,85	28,15	77	66,0	178
5	72,44	27,56	94	70,0	178
6	75,23	24,77	114	71,0	180
7	75,96	24,04	132	72,0	183

Razlog ovakve strukture lijevanog ispitnog uzorka treba tražiti u broju nodula/mm^2. Iz tablice 2 vidljivo je da se shodno promjenama udjela ferita u mikrostrukturi mijenja i broj nodula/mm^2, odnosno da promjena broja nodula/mm^2 ima isti trend kao promjena udjela ferita u mikrostrukturi. Razlog za to je činjenica da je brzina hlađenja veća u donjim dijelovima Y-probe i da opada u smjeru toplinskog centra. Zbog toga u donjim dijelovima Y-probe nastaje veći broj nodula manjeg promjera. Veća gustoća grafitnih nodula omogućava kraće putove difuzije ugljika iz austenita na grafitne nodule i samim tim veći udio ferita u mikrostrukturi. Sporije hlađenje rezultira manjim brojem nodula većeg promjera. Pravilnim cijepljenjem taljevine mogu se smanjiti navedene razlike u mikrostrukturi.

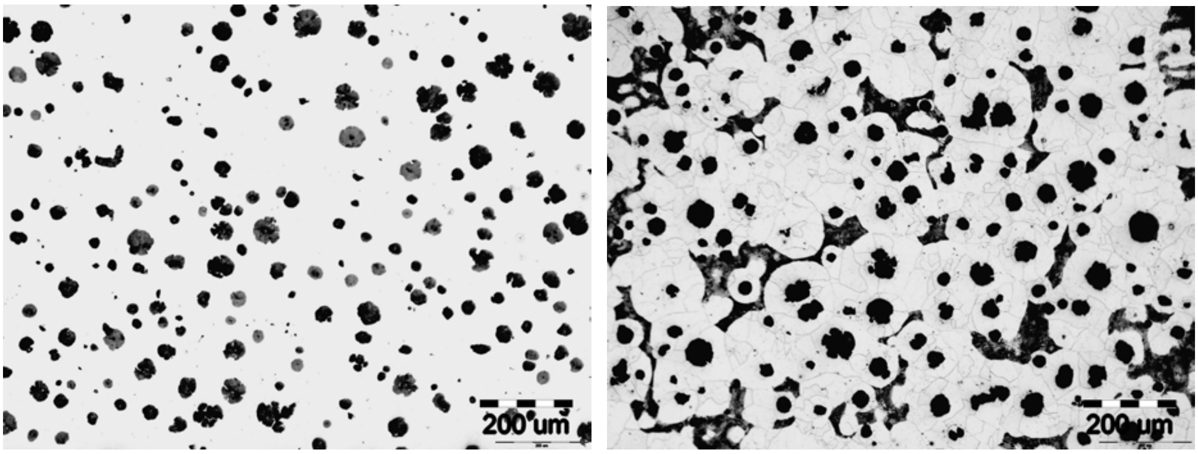

a) ne nagriženo stanje

b) nagriženo stanje

Slika 2. Metalografske snimke mikrostrukture uzorka br.1 pri povećanju 100x: a) ne nagriženo stanje, b) nagriženo stanje (nital)

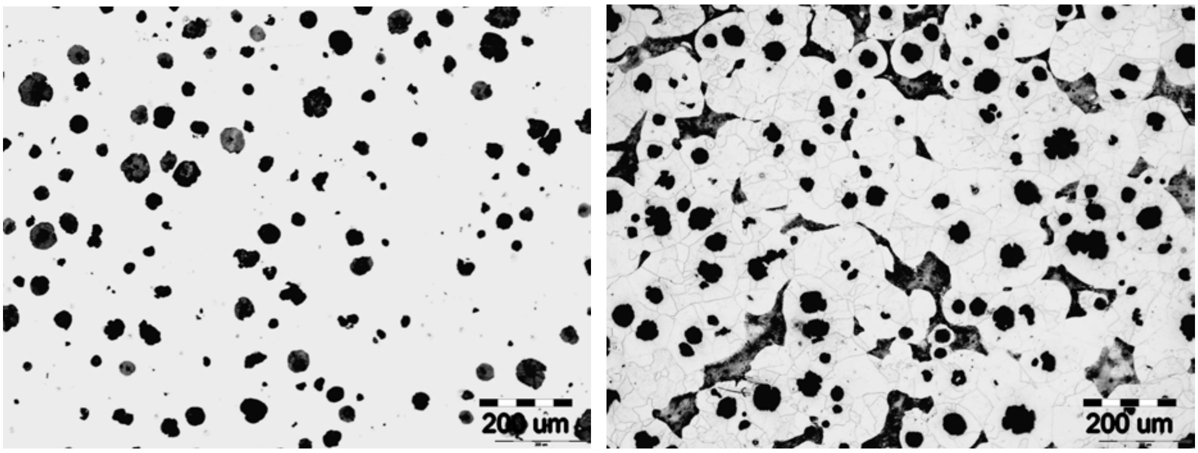

a) ne nagriženo stanje

b) nagriženo stanje

Slika 3. Metalografske snimke mikrostrukture uzorka br.2 pri povećanju 100x: a) ne nagriženo stanje, b) nagriženo stanje (nital)

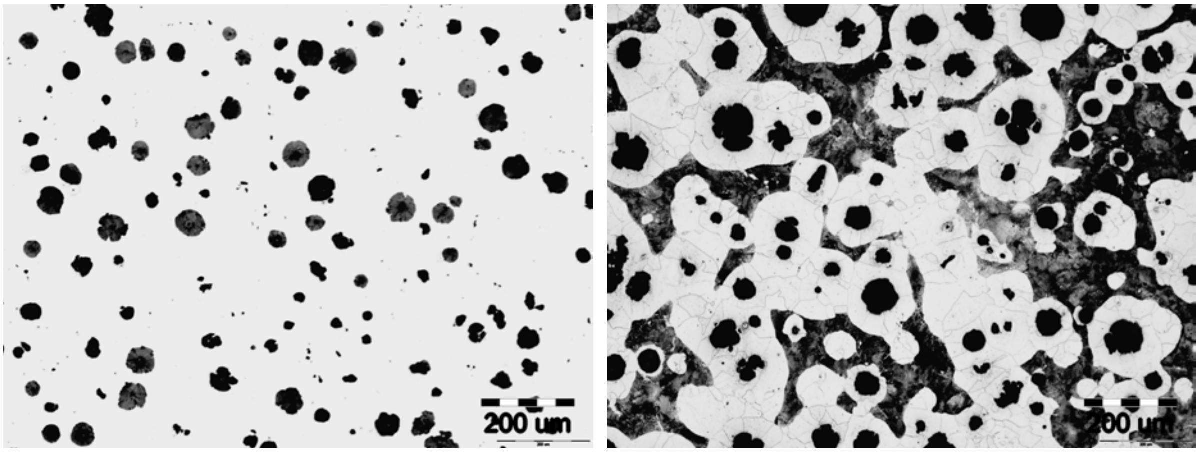

Slika 4. Metalografske snimke mikrostrukture uzorka br.3 pri povećanju 100x: a) ne nagriženo stanje, b) nagriženo stanje (nital)

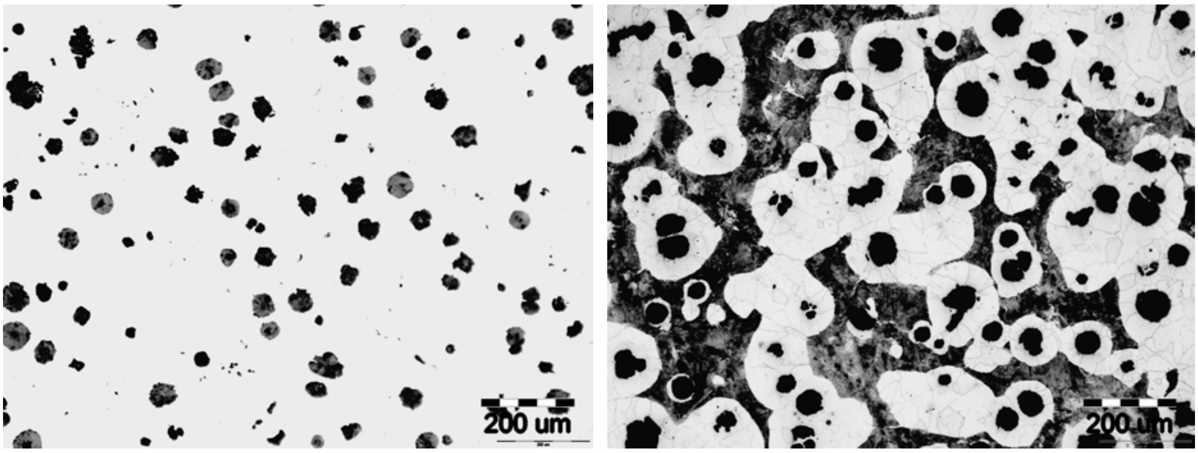

Slika 5. Metalografske snimke mikrostrukture uzorka br.4 pri povećanju 100x: a) ne nagriženo stanje, b) nagriženo stanje (nital)

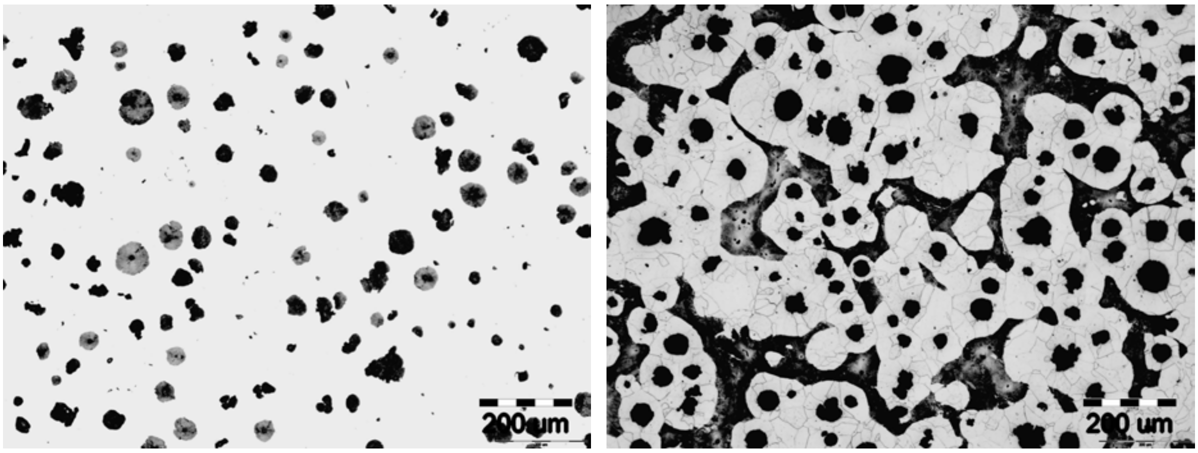

Slika 6. Metalografske snimke mikrostrukture uzorka br.5 pri povećanju 100x: a) ne nagriženo stanje, b) nagriženo stanje (nital)

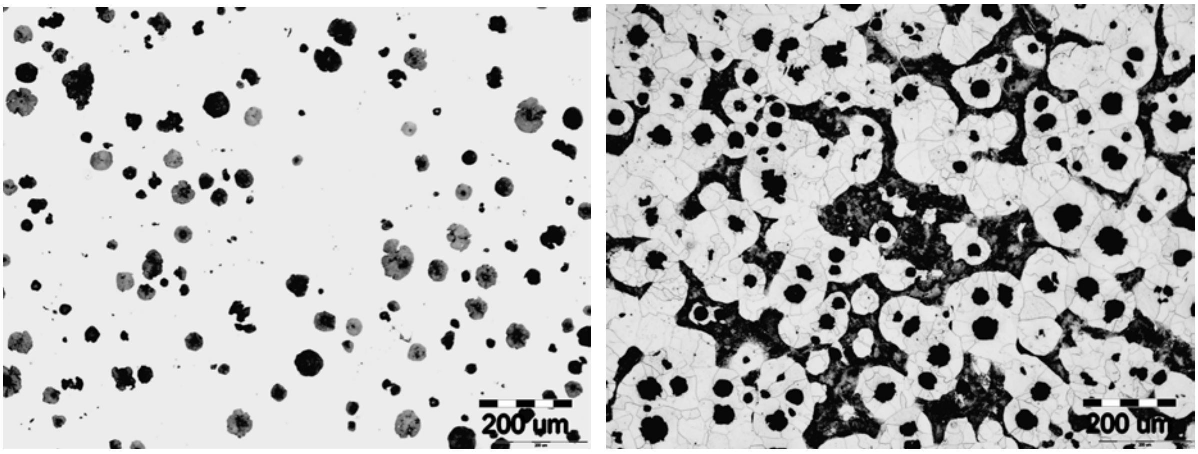

Slika 7. Metalografske snimke mikrostrukture uzorka br.6 pri povećanju 100x: a) ne nagriženo stanje, b) nagriženo stanje (nital)

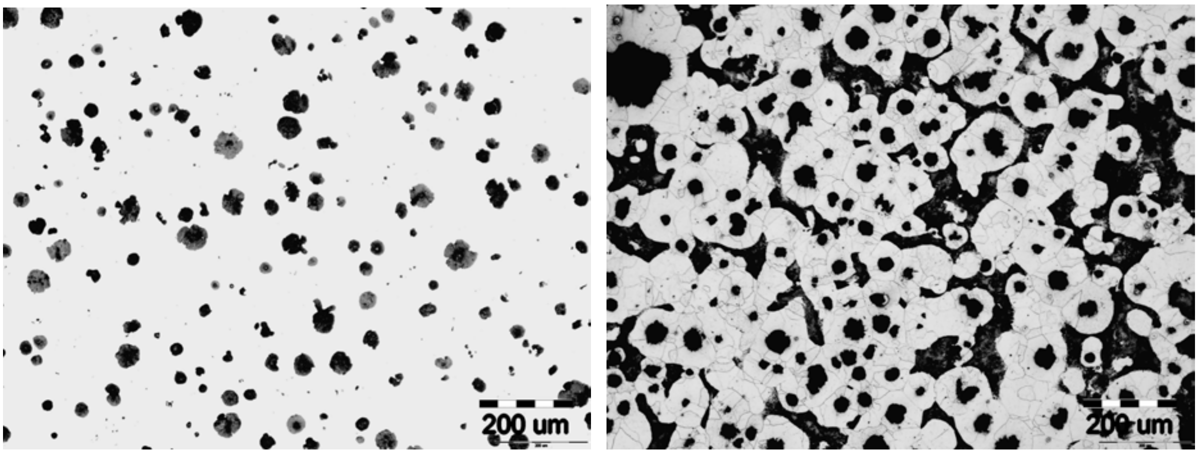

Slika 8. Metalografske snimke mikrostrukture uzorka br.7 pri povećanju 100x: a) ne nagriženo stanje, b) nagriženo stanje (nital)

Obzirom da postoje varijacije u mikrostukturi lijevanog ispitnog uzorka, može se očekivati da će postojati i razlike u dobivenim vrijednostima mehaničkih svojstava ovisno o mjestu uzimanja uzorka. U tu svrhu na ispitivanim uzorcima iz „Y-probe“ određena je tvrdoća. Dobiveni rezultati mjerenja tvrdoće prikazani su u tablici 2 i predstavljaju srednju vrijednost 5 mjerenja. Može se vidjeti da je tvrdoća uzoraka uzetih iz donjeg, tanjeg dijela „Y-probe“ (uzorci 1 i 2) manja u odnosu na tvrdoću uzoraka uzetih iz gornjeg dijela „Y-probe“ (uzorci 3 - 7), što je prije svega povezano s većim udjelom ferita u mikrostrukturi. Pored toga vidljivo je da pri sličnim udjelima perlita, odnosno ferita u mikrostrukturi, veće vrijednosti stupnja nodularnosti rezultiraju višim vrijednostima tvrdoće.

ZAKLJUČAK

Na osnovu eksperimentalnog istraživanja varijacija mikrostrukture nodularnog lijeva u lijevanom ispitnom uzorku glede mjesta uzimanja uzorka i dobivenih vrijednosti tvrdoće utvrđeno je:

- mehanička svojstva nodularnog lijeva usko su povezana s mikrostrukturom, prije svega, oblikom, raspodjelom i veličinom izlučenog grafita te vrstom metalne osnove (udio ferita, odnosno perlita) kao i prisustvom nekih drugih mikrostrukturnih konstituenata (npr. karbida, karbonitrida, fosfidnog eutektika itd.),
- za razliku od sivog lijeva, kod nodularnog lijeva metalna osnova ima dominantan utjecaj na mehanička svojstva,
- udio ferita kao i broj grafitnih nodula/mm^2 u lijevanom ispitnom uzorku, tzv.“Y-probi“ smanjuje se s približavanjem toplinskom centru i najveći je u donjem, perifernom dijelu Y-probe,
- mikrostruktura Y-probe pod jakim je utjecajem toplinskih gradijenata što ima za posljedicu varijacije mehaničkih svojstava obzirom na mjesto uzimanja uzoraka,
- pri sličnim udjelima perlita, odnosno ferita u mikrostrukturi, veće vrijednosti stupnja nodularnosti rezultiraju višim vrijednostima tvrdoće.

LITERATURA

[1] Državni zavod za normizaciju i mjeriteljstvo, HRN EN 945:2002, Zagreb 2002.

[2] Državni zavod za normizaciju i mjeriteljstvo, HRN EN 1563:1997, Zagreb 1997.

[3] The Sorelmetal Book of Ductile Iron, Rio Tinto Iron & Titanium Inc., Montreal, Canada, 2004.

[4] I. C. H. Hughes, Ductile Iron, in Metals Hadbook, .Ninth Edition, vol.15 Casting ASM International, Metals Park Ohio, 1988.

[5] R. Elliott, Cast Iron Technology, Butterworths, London, 1988.

[6] R. Hummer, H. Kerber, H. Bühring-Polaczek, Aussagekraft der Eigenschaften Getrennt Gegossener Probestücke Über die Tatsächlichen Eigenschaften des Gußstückes aus GJS, Zbornik radova 3. međunarodnog savjetovanja ljevača, Suvremeni postupci proizvodnje odljevaka od željeznog lijeva, ur. F. Unkić, Sisak, 11 i 12 listopad 2000, 39-53.

[7] D.M. Stefanescu, R.J. Warrick, L.R. Jenkins, G. Chen, F. Martinez, Influence of the Chemical Analysis of Alloys on the Nodule Count of Ductile Iron, AFS Transactions **93**(1985), 835-848.

[8] D. Venugopalan, A. Alagarsamy, Effects of Alloy Additions on the Microstructure and Mechanical Properties of Commercial Ductile Iron, AFS Transactions **98**(1990), 395-400.

[9] R.W. Heine, Nodule Count: The Benchmark of Ductile Iron Solidification, AFS Transactions **101**(1993), 879-884.

11. Savjetovanje o materijalima, tehnologijama, trenju i trošenju
11. Conference on Materials, Processes, Friction and Wear
MATRIB'06, Vela Luka, 22-24.06.2006.

XRD AND TGA INVESTIGATION OF HARDENED CEMENT PASTE DEGRADATION

Neven Ukrainczyk[1*], Marko Ukrainczyk[2], Juraj Šipušić[1], Tomislav Matusinović[1]
[1]Faculty of Chemical Engineering and Technology, University of Zagreb, Marulićev trg 19, HR-10 000 Zagreb, Croatia
[2]Institut Ruđer Bošković, Bijenička 54, HR-10 000 Zagreb, Croatia

Abstract: It is generally recognized that the environmental degradation of the concrete infrastructure is a serious, large scale and costly problem in many parts of the world. In this paper a deterioration of concrete by leaching of hardened cement paste due to aggressive water action is considered.

Concrete from a hydro-electric power plant's pipeline 30 years old was characterized with X-ray diffraction (XRD), and thermogravimetric analysis (TGA/DTA). The study highlights the capabilities of the methods for the analysis of concrete towards the determination of hardened cement paste degradation. On the basis of a visual survey of drilled cores, a number of representative spots were selected for detailed testing and verification of visual estimates.

The methods ascertain a leach of hardened cement paste on samples taken from a surface concrete cover layer of few millimetres, and from flaws like cracks, segregations or cold joints. On these samples XRD results showed small quantity of ettringite, calcium carboaluminate hydrate and Friedel's salt, and a complete leach of portlandite, while TGA results indicated small quantities of hydrates. Samples taken from flawless inside of concrete layer showed expected quantities of hydrates for the concrete.

Keywords: X-ray diffraction, thermogravimetric analysis, concrete, degradation.

.

1 Introduction

Contrary to common belief, concrete is a complex composite material, whose structure and properties can change over time. It is generally recognized that the environmental degradation of the concrete infrastructure is a serious, large scale and costly problem in many parts of the world.

The concrete structures are designed and built for a service life, which is defined by the designer and is controlled by the manufacturer. For this period of time, the structure should not be so deteriorated that it does not fulfill any more its functions. In this paper a deterioration of concrete by leaching of hardened cement paste due to aggressive water action is considered.

Waters which are acid owing to the presence of organic acids and carbon dioxide do not normally produce more than a surface attack on mass Portland cement concrete, though with the more acid waters over long period of years the action may penetrate to a depth of few centimeters. If, however, there exists a considerable hydrostatic pressure tending to force the water through a concrete mass the action may become much more serious. The destructive effect on thin-walled concrete products like pipes may also be severe.

Pure water dissolves lime to the extent of about 1.2 g/L and is also capable of leaching out lime from set cement compounds. When carbon dioxide is present in the water in a free state it increases the aggressive action of the water. Initially it reacts with the lime to form insoluble calcium carbonate, but on further action the much more soluble calcium bicarbonate is formed. A solution of calcium bicarbonate alone in water will not dissolve further quantities of calcium carbonate, and if it reacts with lime the insoluble calcium carbonate is formed [2].

In water conduits built in Scotland in connection with a hydro-electric power scheme [2] was found that the surface of the concrete became attacked and the aggregate exposed within less than one year's exposure to waters of an average pH of about 6.8. After a period of years the coarse aggregate near the surface became loose and commenced to be washed out. In other constructional work on similar schemes in Scotland a lining of calcium aluminate cement concrete has been applied to aqueducts and pressure tunnels. Pozzolanic cements, and some Portland blastfurnance cements, are rather more resistant to attack than Portland cement, but concretes made with them still suffer gradual surface erosion when exposed to running water, or leaching if the concrete is permeable.

Considerable trouble has been experienced in the Scandinavian countries with large concrete dams exposed to pure or acid mountain waters [2]. A dam is subjected to a one-sided pressure by water and, if the concrete is permeable, water will continuously permeate through the mass. With waters which are not very pure and have little solvent action the pores in a concrete mass often slowly seal up, but when the water has a marked solvent action lime is gradually removed from the concrete which becomes progressively more porous.

Concrete pipes and similar thin-walled concrete units require rather special consideration in regard to their resistance to chemically destructive agents.

Particular attention has been paid in Sweden to the attack of concrete pipes by acid waters containing free carbon dioxide [2]. Concrete pipes of sound quality could be used, it was concluded, unless the subsoil water had a very low content of bicarbonates of lime and magnesia (a very low temporary hardness), or had a rather high content of aggressive carbonic acid, and the circulation of the water at the same time was considerable [2].

In this paper 30 years old concrete from a pipeline that leads water from a reservoir (lake) to the turbine of the hydro-electric power plant was characterized with X-ray diffraction (XRD), and thermogravimetric analysis (TGA/DTA). The study highlights the capabilities of the methods for the analysis of concrete towards the determination of hardened cement paste degradation.

2 Sample preparation

Firstly, a visual survey of the pipeline water conduits in connection with a hydro-electric power scheme was conducted with categorization of flaws on the basis of outward appearance and samples were taken drilling a core, **Figure 1 - 4**. On the basis of a visual survey of drilled cores, a number of representative spots were selected for detailed testing and verification of visual estimates. Samples were taken from a *surface* concrete cover layer of few millimetres, and from flaws like *cracks*, *segregations* or *cold joints*. Samples were taken from these representative spots by carefully scraping and drilling concrete in powder. Powder samples were stored in sealed bags to prevent carbonation. Before analyses powder was additionally grind in corundum crucible.

3 Thermogravimetric analysis

Eight samples were analyzed by thermogravimetric analysis (TG/DTA). The samples were taken in a ceramic crucible and heated from room temperature to 950 °C in thermoanalyzer TG – 50 Mettler (procesor TC 11, TA 4000) at a heating rate of 10 °C min^{-1} using air as a medium under static condition. Alumina powder was used as the reference material. TG and DTA were done simultaneously. The samples were dried at 105 °C in oven and cooled to room temperature before performing TG/DTA analysis.

Table 1. TG/DTA resultes for four characteristic samples.

Sample	Temperature range (°C)	Peak temperature (°C)	Weight loss (%)
Flawless 10+375 D=24	29 - 100	35	0,72
	100 - 350	138	2,37
	400 - 460	431	0,74
	506 – 896	805	33,17
Surface 0+210	26 - 80	38	0,86
	82 - 400	365	4,41
	400 - 496	445	0,46
	496 - 892	779	36,73
Segregation 3+342	28 - 100	36	1,01
	520 - 860	799	41,79
Crack 0+250	25 -99	42	0,95
	100 - 210	105	0,25
	450 - 857	800	35,16

Table 2. $Ca(OH)_2$ and $CaCO_3$ estimated by TG/DTA.

Sample	$Ca(OH)_2$ (%)	$CaCO_3$ (%)
Flawless 0+375 D=24	0,49	75,34
Surface 0+210	0,23	83,42
Segregation 3+342	0	94,95
Crack 0+250	0	79,91

The total weight losses of samples due to heating from 25 °C to 950 °C were between 40 % and 47%. The TG/DTA results are presented in **Table 1**, as weight loss with respective temperature range and peak temperature for the four characteristic samples. The four characteristic endothermic effects are noticed. The first effect, in temperature range from 25 to 100 °C is due to evaporation of surface adsorbed water because samples adsorbed water from air during its cooling to the room temperature after drying at 104 °C. The second endothermic effect, in temperature range from 100 to 350 °C, is attributed to the dehydration of C–S–H and ettringite and calcium aluminate hydrate [1]. The temperature at which these compounds lose water depends upon the available CaO:SiO_2 ratio in the hydrated cement matrix. The third effect, with peak temperature between 430 i 460 °C, indicates the decomposition of $Ca(OH)_2$ formed during hydration. The $Ca(OH)_2$ was estimated from the weight loss measured from the TG curve between the initial and final temperature of the corresponding TG peak by considering the following decomposition reaction (**Table 2**):

$$Ca(OH)_2\ (s) \rightarrow CaO\ (s) + H_2O\ (g) \tag{1}$$

Finally, an endothermic around 790 °C indicates the decarbonation of calcium carbonate in the hydrated compound. The $CaCO_3$ was estimated from the weight loss by considering the following decarbonation reaction **(Table 2)**:

$$CaCO_3\ (s) \rightarrow CaO\ (s) + CO_2\ (g) \tag{2}$$

It can be seen from **Table 1** that ettringite, C-S-H gel and calcium aluminate hydrate are not present in sample *Segregation 3+342*. Ettringite, C-S-H gel and calcium aluminate hydrate are present in small quantity in sample *Crack 0+250,* whereas they can be found in more quantity in samples *Flawless 10+375 D=24* and *Surface 0+210* (**Table 1**). Moreover, it is evident from **Table 2,** that calcium hydroxide is not present in samples *Segregation 3+342* and *Crack 0+250.*

4 X-ray diffraction analysis

The powder method of X-ray diffraction was adopted in the present study. For this, a Phillips diffractometer PW1730 with a X-ray source of Cu Kα radiation (λ = 1.5418 Å) was used. The scan step size was 0.02^o, the collection time 1s, and in the range 2Θ CuKα from $5^{\ o}$ to $50(65)^o$. The X-ray tube voltage and current were fixed at 40 kV and 30 mA respectively.

Although X-ray diffractometry does not provide any reliable quantitative information, the technique is sensitive. An on-line search of a standard database (JCPDS database) for X-ray powder diffraction pattern enables phase identification for a large variety of crystalline phases in a sample [3].

Figure 1 – 4 illustrate the XRD diffractograms for investigated samples. Each figure presents comparatively diffractograms of a sample taken from a *flawless* concrete spot (black top line) and a *surface* concrete cover layer of few millimeters, or from flaws like *cracks*, *segregations* or *cold joints* (green bottom line). The symbols on figures indicate the positions and peak intensities of the powder diffraction standard from JCPDS database. In samples *Flawless 3+342* and *Segregation 3+342*, **Figure 1**, XRD analysis indicates predominance of calcite [$CaCO_3$] and dolomite [$CaMg(CO_3)_2$] peaks. In both samples Quartz [SiO_2] is identified.

In sample *Flawless 3+342* diffraction peaks indicate presence of portlandite [$Ca(OH_2)$], ettringite and carboaluminate hydrate and Friedel's salt (overlap near 2Θ = $11^{\ o}$). However, sample *Segregation 3+342* shows no diffraction peak of portlandite [$Ca(OH_2)$], and small quantity of ettringite, calcium carboaluminate hydrate and Friedel's salt (chloroaluminates) is identified.

In samples *Flawless 10+375* and *Crack 10+375*, **Figure 2**, *Flawless 10+250* and *Crack 10+250*, **Figure 3**, *10+210 D=11cm* and *Surface 10+210*, **Figure 4**, XRD analysis indicates predominance of calcite [$CaCO_3$] peaks. In all *Flawless* samples diffraction peaks indicate presence of portlandite [$Ca(OH_2)$], ettringite and carboaluminate hydrate and Friedel's salt. However, in both *Crack* samples and sample *Surface* XRD analysis shows no diffraction peak of portlandite [$Ca(OH_2)$], and small quantity of ettringite, calcium carboaluminate hydrate and Friedel's salt is identified. In all samples small quantity of Quartz [SiO_2] is identified.

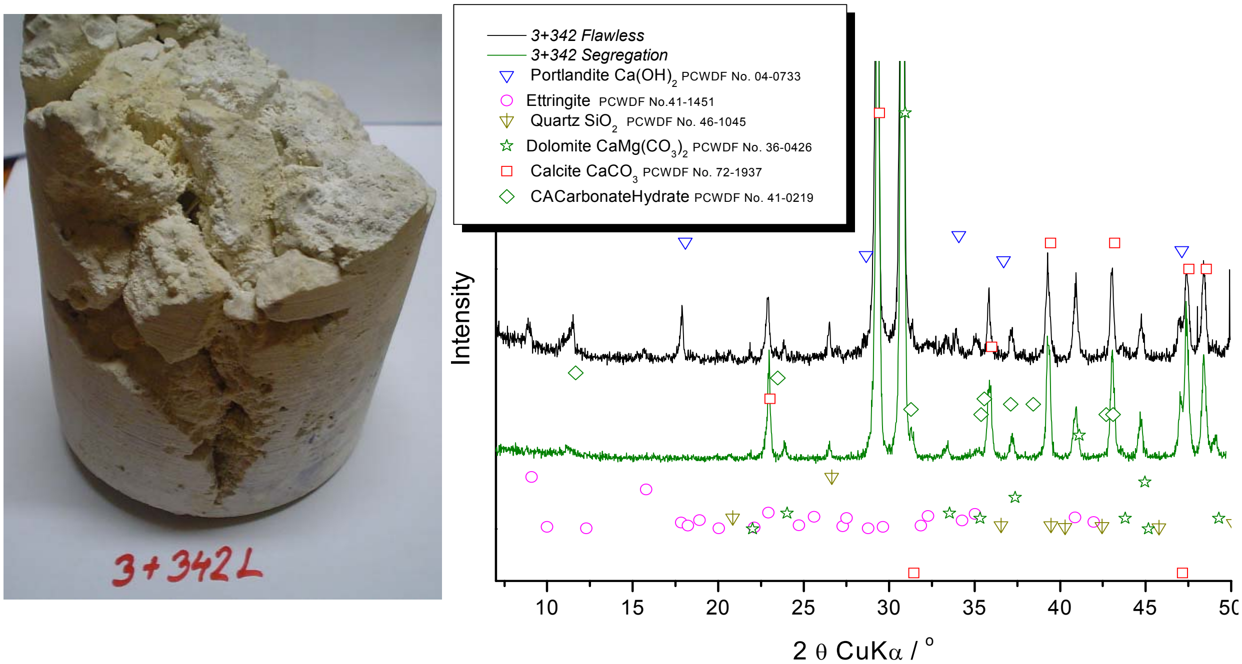

Figure 1. Photo and XRD diffractograms for samples *Flawless 3+342* and *Segregation 3+342*.

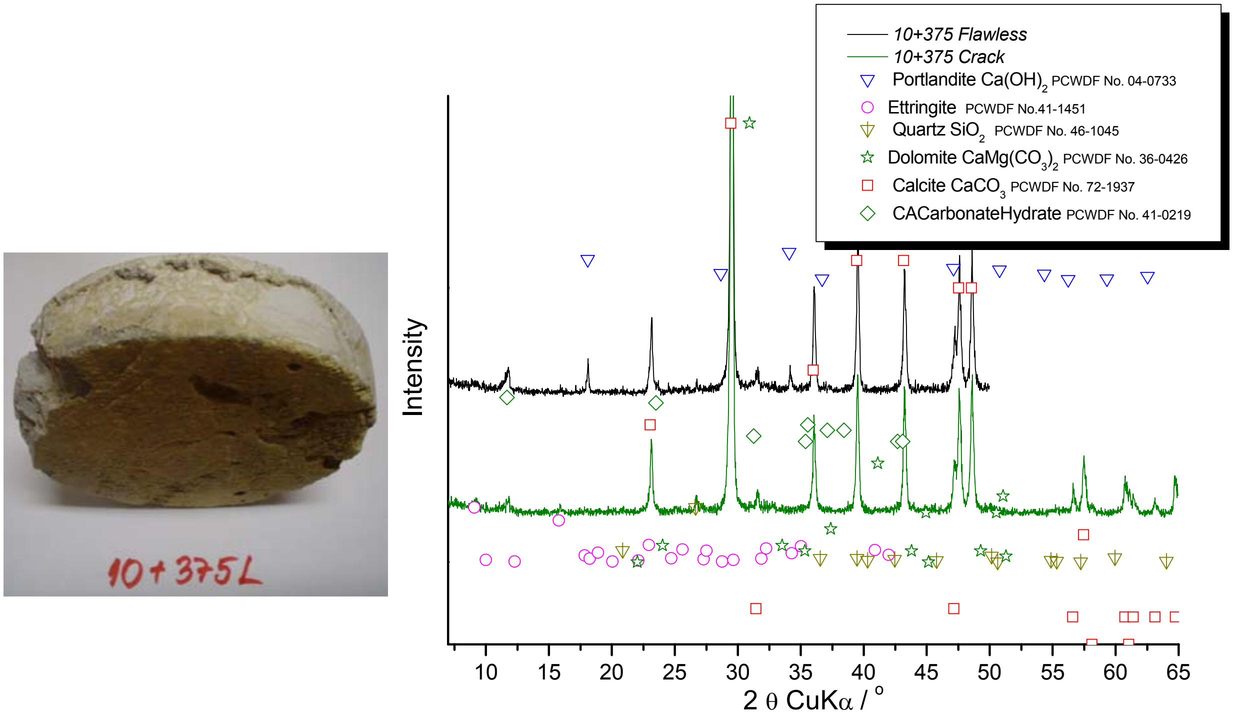

Figure 2. Photo and XRD diffractograms for samples *Flawless 10+375* and *Crack 10+375*.

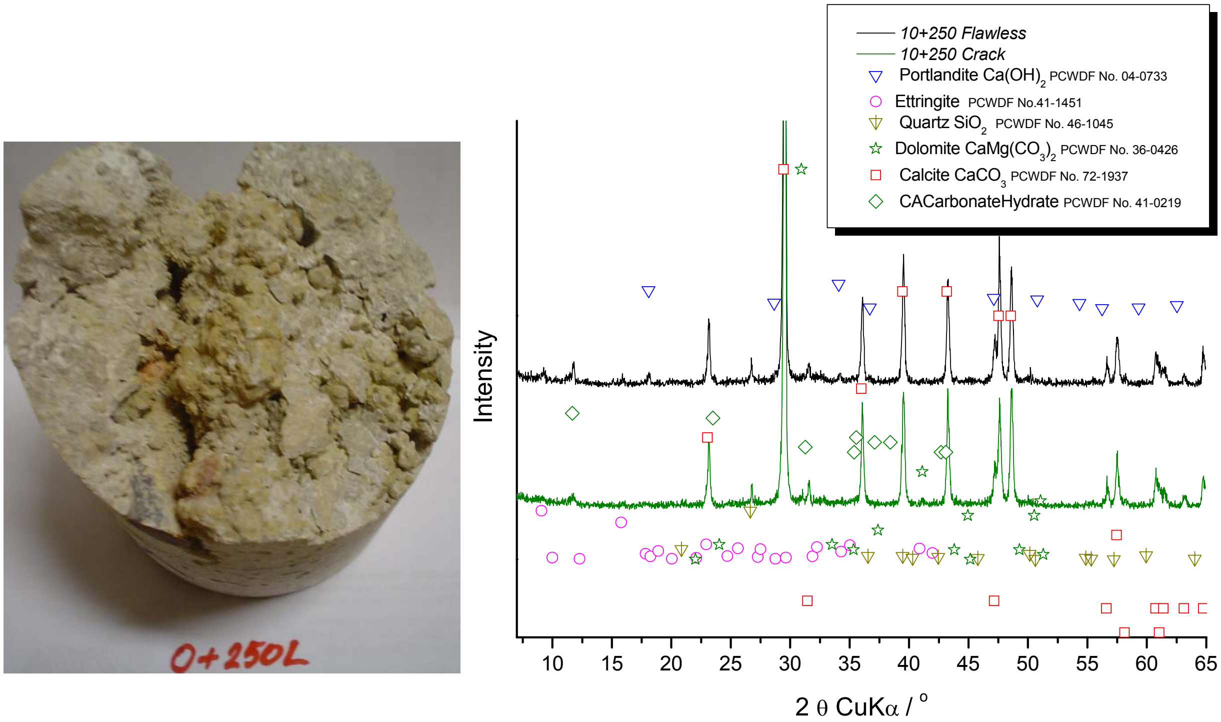

Figure 3. XRD diffractograms for samples *Flawless 10+250* and *Crack 10+250*.

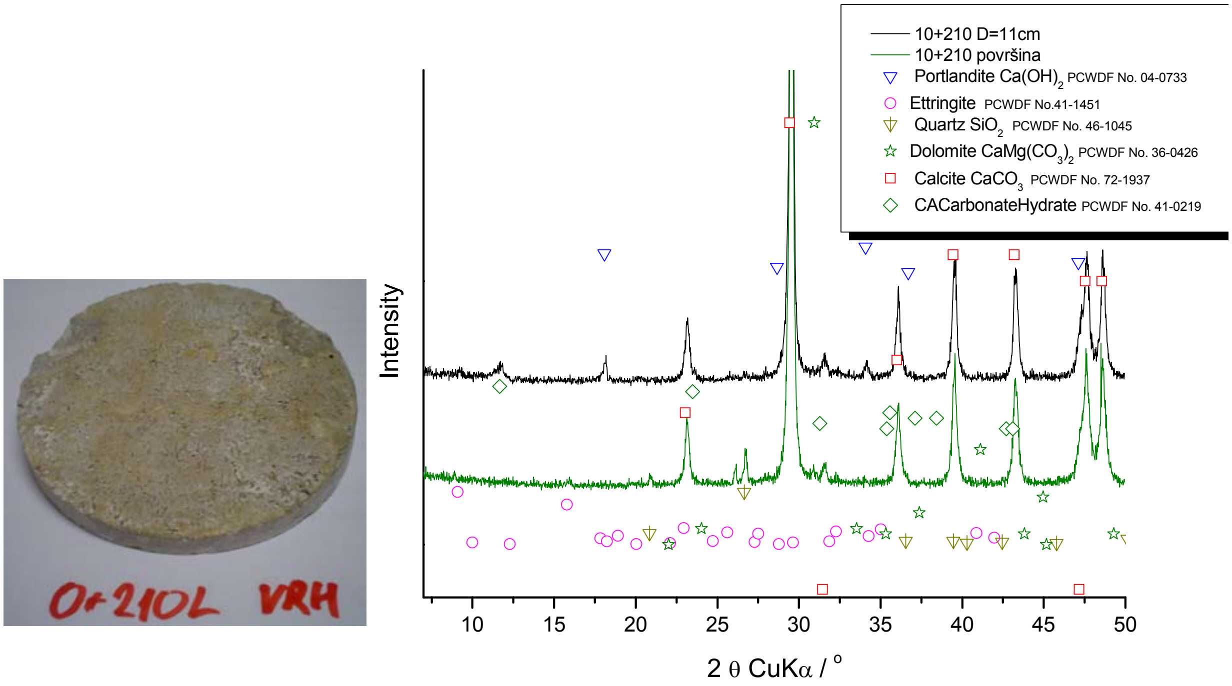

Figure 4. Photo and XRD diffractograms for samples *10+210 D=11cm* and *Surface 10+210*.

5 Conclusion

Concrete from a hydro-electric power plant’s pipeline 30 years old was characterized with X-ray diffraction (XRD), and thermogravimetric analysis (TGA/DTA). The study highlights the capabilities of the methods for the analysis of concrete towards the determination of hardened cement paste degradation. The methods ascertain a leach of hardened cement paste on samples taken from a surface concrete cover layer of few millimetres, and from flaws like cracks, segregations or cold joints. On these samples XRD results showed small quantity of ettringite, calcium carboaluminate hydrate and Friedel's salt, and a complete leach of portlandite, while TGA results indicated small quantities of hydrates. Samples taken from flawless inside of concrete layer showed expected quantities of hydrates for the concrete.

6 References

1. Vedalakshmi R., Sundara Raj A., Srinivasan S., Ganesh Babu K.: Quantification of hydrated cement products of blended cements in low and medium strength concrete using TG and DTA technique, Thermochimica Acta 407, 49–60, 2003.
2. F.M. Lea, The Chemistry of Cement and Concrete, 3rd Ed., Edward Arnold, London, 1970. ISBN: 0-7131-2277-3
3. V.S. Ramachandran, Thermal Analysis, in: Handbook od analytical techniques in concrete science and technology, V.S. Ramachandran and J.J. Beaudoin, Eds., Noyes Publications, New Jersey, 2001. ISBN: 0-8155-1437-9

11. Savjetovanje o materijalima, tehnologijama, trenju i trošenju
11. Conference on Materials, Processes, Friction and Wear
MATRIB'06, Vela Luka, 22-24.06.2006.

POVRŠINSKA OŠTEĆENJA GLAVE ŽELJEZNIČKIH TRAČNICA U EKSPLOATACIJI

SURFACE DAMAGES TO HEAD OF RAILWAY RAILS CAUSED BY OPERATION

Ivan Vitez, Ivica Kladarić, Vladimir Pecić
Strojarski fakultet Slavonski Brod, Sveučilišta J.J. Strossmayera u Osijeku,
Trg I.B. Mažuranić 2, HR-3500 Slavonski Brod
Tomislav Hozjan
HŽ – Infrastruktura, Građevinski poslovi,
Tomislavov trg 11, HR-10000 Zagreb

Sažetak: Povećanje obima željezničkog prometa, veća osovinska opterećenja, veće brzine i nova generacija željezničkih vozila povećali su opterećenja željezničkih tračnica naročito u krivinama. Željeznice najviše danas koriste kao standardnu opremu za kolosjeke tračnice iz čelika 260 (900A) i u vrlo ograničenom obimu tračnice iz čelika 260 Mn (900B). Ni tračnice iz ovih vrsta čelika nisu pošteđene od problema koji se pojavljuju u krivinama s vrlo malim polumjerima i/ili s visokim opterećenjima. To su problemi s rubnim i vertikalnim trošenjem glava željezničkih tračnica.

U ovom radu obrađeno je nekoliko tipičnih površinskih oštećenja na glavama željezničkih tračnica koja nastaju u eksploataciji, kao što su: ljuštenje, pukotine "head checks", poprečne i uzdužne pukotine i sl. prema novim propisima i preporukama (Katalog oštećenja UIC 712R, Preporuke za uporabu vrsta čelika za tračnice UIC 721 R i Postupak s oštećenjima tračnica UIC 725 R).

Ključne riječi: željezničke tračnice, površinska oštećenja glave, pukotine, katalog, preporuke, postupak.

Abstract: Increases in railway traffic, greater axleloads, higher speeds and introduction of new generations of rolling stock have increased the loads on rails in curves especially. Most railways today opt as standard equipment for their track steel grades 260 (R0900A) and to a very limited degree 260 Mn (R0900B). Neither rails of steel grades 260 and 260 Mn are not exempt from the problems that arise in curves small and very small radii and/or heavy loadings. That are lateral and vertical wear problems arise later on heads of railway rails.

This paper elaborate a number of typical near – surface defects on heads railway rails caused by operation such as shelling, head checks, horizontal and vertical cracking etc. according to new regulations and recommendations (Catalogue of Rail defects UIC 712 R, Recommendations for the use of the rail grades UIC 721 R and Treatment of rail defects UIC 725 R).

Key words: railway rails, near-surface defects on head, cracks, catalogue, recommendations, treatment

1. UVOD

U suvremenim uvjetima eksploatacije željezničke tračnice su izložene kako porastu brzina i osovinskog opterećenja, tako i porastu zaostalih naprezanja od zavarenih kolosijeka. Zato su moderna tehnologija proizvodnje željezničkih tračnica i navedeni zahtjevi u okviru Europske unije dali sasvim novi pogled na filozofiju i sadržaj novih europskih standarda za proizvodnju i isporuku željezničkih tračnica (serija EN 13674 i druge preporuke). Novi zahtjevi na tračnice su specificirani uglavnom u novom europskom standardu EN 13674-1/2004. kroz kvalifikacijske kriterije i prijamna ispitivanja s nizom novih složenih kriterija i ispitivanja, kao što su: lomna žilavost, brzina rasta pukotine umaranja, ispitivanje umaranjem, ispitivanje zaostalih naprezanja, mikrostrukture, dekarbonizacije, oksidne čistoće, tvrdoće itd. [1].

Rastućim opterećenjima kolosijeka i povećanim zahtjevima na kvalitetu proizvođači su uspješno odgovorili sa:

- porastom mase tračnica po dužnom metru s 45 do 77 kg/m. U novije vrijeme se u Europi koriste sve više tračnice tipa 60E1 (stara oznaka UIC 60) umjesto tipova 46E1 do 56E1 iz raznih vrsta čelika za tračnice. Ukupno ima 21 profil tračnica u standardu EN 13674-1 [2];
- porastom vlačne čvrstoće čelika za tračnice s 700 do 1300 MPa kod prirodno-tvrdih tračnica (bez toplinske obradbe) s izmjenom sadržaja legirnih elemenata;
- povećanom čistoćom čelika za tračnice kroz smanjivanje dopuštenih sadržaja štetnih primjesa fosfora i sumpora s 0,050 na 0,030% S, odnosno 0,025% P maksimalno i sl.;
- proizvodnjom sve duljih tračnica s 12 do 120 m, zbog manjeg broja zavara [1 do 5].

2. ZAHTJEV EUROPSKOG STANDARDA EN 13674-1

Gdjegod je to moguće koristi se standard za osiguranje kvalitete EN ISO 9001 i zadnja dokazana tehnologija proizvođača. Dva glavna dijela prijedloga EN su: kvalifikacijska i prijamna ispitivanja. Kvalifikacijska ispitivanja traže i neka svojstva kojih nije bilo u prethodnim nacionalnim ili internacionalnim normama (kao npr. lomna žilavost K_{Ic}). Prijamna ispitivanja kontroliraju propisana svojstva koja osiguravaju proizvodnju željezničkih tračnica visoke kvalitete i zahtjeve željezničkih uprava. Načelno je prijamni kriterij utemeljen na izmjerenim vrijednostima tvrdoće, po kojima su uvedene i nove oznake vrsta čelika za željezničke tračnice [1, 2].

U tablici 1 dane su vrste čelika za tračnice, raspon tvrdoća, lomne žilavosti, oznake i vlačna svojstva.

Tablica 1. Vrste čelika, rasponi tvrdoća, lomne žilavosti, oznake i vlačna svojstva

Vrste čelika	Rasponi tvrdoća, HBW	Lomna žilavost, K_{IC} (MPa $m^{1/2}$) minimalne vrijednosti		Opis	Oznaka na vratu	R_m min. MPa	Istezljivost min. A_5, %
		pojedinačna	srednja				
200	200-240	30	35	C-Mn		680	14
220	220-260	30	35	C-Mn	—	770	12
260	260-300	26	29	C-Mn	═	880	10
260 Mn	260-300	26	29	C-Mn	═	880	10
320 Cr	320-360	24	26	1 %Cr	≡	1080	9
350 HT	350-390	30	32	C-Mn s TO[1]	═——	1175	9
350 LHT	350-390	26	29	niskolegirano s TO[1]	≡——	1175	9
[1] s toplinskom obradom							

3. PODACI IZ KATALOGA OŠTEĆENJA UIC 712 R

Klasifikacija lomova i oštećenja na željezničkim tračnicama provedena je po katalogu UIC 712R/2002 sa brojem od najviše četiri znamenke, kod kojeg označava:

– ***Prva znamenka***
1. greške na krajevima tračnica,
2. greške u sredini tračnice,
3. greške izazvane opterećenjima,
4. greške zavarivanja i navarivanja.

– ***Druga znamenka***
1. prvobitni položaj greške u presjeku tračnice,
2. vrstu zavara, ako se radi o greškama zavarivanja i navarivanja.

– ***Treća znamenka***
1. orjentacija greške u slučaju loma,
2. vrsta greške u slučaju oštećenja,
3. uzrok greške u slučaju oštećenja tračnice,

– ***Četvrta znamenka***

Ova znamenka prema potrebi dozvoljava dodatnu klasifikaciju prema tipovima greški.

U tablici 2 dana je podjela grešaka na glavi željezničkih tračnica [4].

Tablica 2. Podjela grešaka na glavi željezničkih tračnica

	Oznaka (UIC) i naziv greške
Greške na krajevima tračnica	**112** Horizontalne pukotine
	113 Vertikalne uzdužne pukotine
	121 Površinske greške
	122 Ljuštenje vozne površine
	123 Nagnječenje
	124 Mjestimično udubljenje
	125 Oštećenje klizanjem
Greške na sredini tračnice	**211** Postupno stvaranje poprečne pukotine (ovalna pjega)
	212 Horizontalne pukotine
	213 Vertikalne uzdužne pukotine
	220 HABANJE
	2201 Valovito habanje sa kratkim valovima
	2202 Valovito habanje sa dugim valovima
	2203 Abnormalno bočno habanje
	2204 Abnormalno habanje vozne površine
	221 POVRŠINSKE GREŠKE
	2211 Otisak uvaljanosti
	2212 Žlijeb ili brazda
	2213 Fina uzdužna pukotina
	222 LJUŠTENJE
	2221 Ljuštenje vozne površine
	2222 Ljuštenje rubova vozne površine
	2223 Head checking/Ljuskanje vozne površine
	223 Gnječenje sa ili bez hrapavosti
	224 Mjestimično udubljenje vozne površine
	225 OŠTEĆENJE KLIZANJEM
	2251 Oštećenje samo uzrokovano jednim klizanjem
	2252 Oštećenje ponavljanog klizanja
	227 Zadebljanje/Pukotine i lokalna udubljenja vozne površine
Greške nastale oštećenjem tračnice	**301** Razna oštećenja
Greške zavarivanja i navarivanja	**411** Poprečne pukotine (kod električnog tupog zavarivanja)
	421 Poprečna pukotina (aluminotermijsko zavarivanje)
	471 Poprečna pukotina u glavi tračnice (navarivanje)
	472 Odvajanje ili ljuštenje navarenog dijela
	481 Poprečna pukotina u glavi tračnice na mjestu zavarivanja električnog tračničkog prespoja (različita zavarivanja)

Kraći opisi grešaka ljuštenja (broj 222) i "head checks" (broj 2223) slijede:

Ljuštenje je oštećenje tračnice koje se javlja u sljedećim oblicima:

- *Ljuštenje vozne površine* može dostići dubinu od nekoliko milimetara, a predhodi mu pseudo-valovita deformacija vozne površine. Ljuske mogu biti različitih oblika a najčešće su trokutastog ili trapezoidnog oblika. Ove greške otkrivaju se vizualnim promatranjem i sa ultrazvučnim ispitivanjem vozne površine,
- *Ljuštenje rubova vozne površine (iskrzanost)* je oštećenje koje se javlja na voznom rubu tračnice. Prvo nastaju uzdužne pukotine i nepravilno raspoređene duguljaste crne mrlje, a pucanjem ovih mrlja nastaju ljuske koje se odvajaju. Na mjestima gdje pukotine dođu do površine tračnice nastaje iskrzanost. Ova greška javlja se na tračnicama u krivinama koje se podmazuju radi spriječavanja bočnog trošenja. Također se otkrivaju vizualnim i ultrazvučnim ispitivanjem [4].

Head checks su ljuskave vrlo tanke površinske pukotine koje se primjećuju pretežno na tračnicama u krivinama. One se stvaraju pod kutom od oko 45° u pravcu vožnje. Razmak između pukotina može varirati ovisno o lokalnim uvjetima i kakvoći materijala tračnice, a obično se kreće od 2 do 7 mm. Nastaju uslijed fenomena kontaktnog umaranja pri kotrljanju (rolling contact fatigue – RCF) [7, 8, 9].

Head checks oštećenja javljaju se u sljedećem obliku:

- *Head checks sa ljuskama* su pukotine unutar glave tračnice koje napreduju pod kutom od 10° do 15° do maksimalne dubine koja u nekim slučajevima iznosi nekoliko milimetara. Ove pukotine napreduju paralelno sa voznom površinom tračnice, a završavaju na voznom rubu tračnice uzrokujući ljuskanje,
- *Head checks u obliku dugačke uzdužne pukotine* koja završava na vrhu uzdužne osi tračnice. Uz ovakav oblik *head checks* oštećenja javljaju se male jamice tamnog izgleda, a često dolazi do proširenja vozne površine. Ako se ove pukotine pojavljuju periodično može doći do višestrukih lomova uslijed kontaktnog umaranja. Vrlo ih je teško otkriti u ranoj fazi i predvidjeti njihovu propagaciju,
- Ova oštećenja se otkrivaju vizualnim promatranjem i ultrazvučnim ispitivanjem, a u novije vrijeme sve češće se koristi ispitivanje vrtložnim strujama [4, 6].

Zbog sve izraženijeg razvoja *head checks* oštećenja u krivinama, skretnicama i na pružnim prijelazima a koja su uzrokovana prevelikim opterećenjem kontaktnog područja Europska unija je pokrenula projekt "InfraStar". Zadatak ovoga projekta je razviti tračnicu sa jednim dodatnim slojem na voznoj ivici glave tračnice, te na taj način otkloniti preopterećenje kontaktne zone tj. spriječiti nastanak head checks oštećenja. U ovaj projekt uključeni su Sveučilište iz Sheffielda te tvrtke Duroc iz Švedske, Corus iz Francuske i mnogi drugi. Nakon mnogobrojnih analiza inženjeri Duroca usredotočili su se na laserskoj tehnologiji "oklopljavanja" tj. nanošenja dodatnog sloja na vozni rub (slika 1) te su za ispitivanja pripremili dva prototipa materijala (Duroc 222 i Duroc 508) koji su uspješno testirani u laboratorijima Sveučilišta u Sheffieldu [9].

a) b) c)

Slika 1. Izgled tračnice sa laserski nanešenim slojem
a) vozna površina tračnice (mjesto kontakta)
b) laserski nanešeni sloj (bijeli) na glavi tračnice
c) postupak laserskog nanošenja dodatnog sloja

Durocova tehnologija laserskog nanošenja dodatnog sloja zasniva se na površinskom postupku sa kojim se legura sa keramičkim dodatcima nanosi na voznu ivicu. Ova legura može biti primijenjena u svrhu proizvodnje posebnog materijala za tračnice. Ova tehnologija laserskog nanošenja sloja razvijena je prije više od 10 godina, a prvi puta se primjenjuje na čelike za tračnice. Debljina sloja je oko 3 mm, a širina 17-24 mm. Nakon 18 mjeseci uporabe boljim se pokazao sloj Duroc 222 širine 24 mm [9].

4. PODACI SA PRUGA HŽ

Oštećenje tipa "head checks" (slika 2) uočeno je i na skretnicama Hrvatskih željeznica prije nekoliko godina [10].

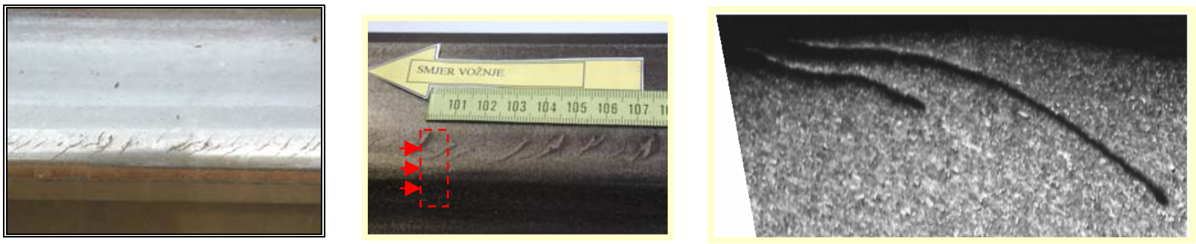

a) b) c)

Slika 2. Oštećenje tipa "head checks" na voznim rubovima tračnice
a) izgled oštećenja na rubu glave tračnice (kutovi oko 20°)
b) makrografski prikaz razvoja pukotine (20x)
c) makrografski izgled razvoja pukotine u dubinu (do 1,23 mm, x20)

Vizualna praćenja i mjerenja oštećenja tipa "head checks" na skretnicama provedena su na dionici pruge Hrvatskih željeznica od kolodvora Strizivojna – Vrpolje do kolodvora Novska. Analizirajući oštećenja definirana su mjesta na kojima se ona javljaju na pojedinim skretnicama.

Na slici 3 shematski je prikazana skretnica sa označenim mjestima pojavljivanja oštećenja tipa "head checks", a na slici 4 dan je histogramski prikaz 22 lokacije na kojima je uočeno 127 oštećenja tipa "head checks" (UIC 2223).

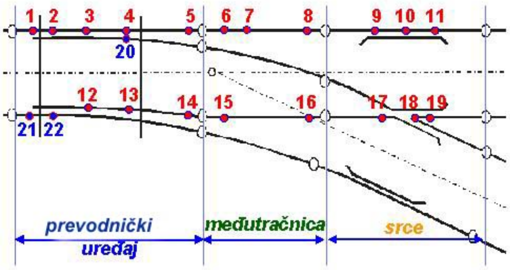

Slika 3. Mjesta pojavljivanja oštećenja tipa "head checks" na skretnicama

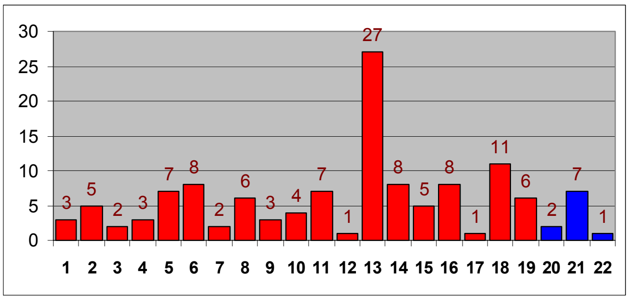

Slika 4. Broj oštećenja tipa "head checks" na pojedinim lokacijama

5. ZAKLJUČAK

Suvremeni uvjeti eksploatacije željezničkih tračnica s povećanim brzinama i osovinskim opterećenjima dovode do porasta zaostalih naprezanja i različitih površinskih oštećenja na glavama tračnica. Iako su znatno pooštreni uvjeti prijama i isporuke tračnica u EN 13674-1 u eksploataciji nastaju oštećenja u obliku vrlo sitnih pukotina tipa "head checks" i sl. koje je teško otkriti i pratiti u prvoj fazi, kao i sanirati, jer mogu dovesti i do lomova uslijed kontaktnog umaranja. Takva oštećenja danas predstavljaju do 30% od ukupnog broja oštećenja glave tračnica.

U Europi se već godinama radi na otkrivanju i sanaciji takvih površinskih oštećenja na glavama željezničkih tračnica, a u RH je problematika također otkrivena prije nekoliko godina i na HŽ se poduzimaju potrebite mjere za saniranje problema i osiguranje pouzdanosti željezničkog prometa.

Zahvalnost:

Ovaj rad je urađen u okviru projekta "Usvajanje tehničke dijagnostike i rješavanje problematike održavanja tračnica na prugama HŽ", a prikazani rezultati su nastali u okviru programa TEST – Tehnologijski istraživačko-razvojni projekti uz potporu Ministarstva znanosti, obrazovanja i športa RH.

LITERATURA

[1] Vitez I., Kladarić I., Pecić V.: Novi zahtjevi na svojstva čelika za željezničke tračnice, 9. Savjetovanje MATRIB'04, Vela Luka 2004., 333-337.

[2] Vitez I., Hozjan T.: Usporedba normi o svojstvima čelika za željezničke tračnice, Građevinar 55 (2003.)5, 279-284.

[3] Vitez I., Krumes D., Marušić V.: Važnost lomne žilavosti za kvalitetu željezničkih tračnica, 4. Naučno-stručni skup "Quality 2005", Fojnica 2005., 413-420.

[4] *** Code UIC 712 R:2002 / Catalogue of Rail Defects.

[5] *** UIC Draft Leaflet 721R:2003 – Recommendation for the use of rail steel grades.

[6] *** UIC Draft Leaflet 725R:2005 – Treatment of rail defects.

[7] Thomas H.-M., Junger M., Hintze H., Krull R., Rühe S.: Pioneering Inspection of Railroad Rails with Eddy Currents, http://www.ndt.net/article/wcndt00/papers/idn796/idn796.htm,

[8] Hiensch M.: Two-material rail combats rolling contact fatigue, www.railwaygazette.com,

[9] Hiensch M., Larsson P.-O., Nilsson O., Levy D., Kapoor A., Franklin F., Nielsen J., Ringsberg W.J., Josefson L.B.: Development of a Two-Material Rail for RCF and Noise Control, http://infrastar.shet.ac.uk,

[10] Pollak B, Bajić G.-A.: Posebna oštećenja tračnica na skretnicama, Građevinar 54 (2002) 8, 465-471

11. Savjetovanje o materijalima, tehnologijama, trenju i trošenju
11. Conference on Materials, Processes, Friction and Wear
MATRIB'06, Vela Luka, 22-24.06.2006.

UTJECAJ POVIŠENE TEMPERATURE NA KUGLIČARENU ALUMINIJEVU SLITINU AlMg4.5Mn

THE ELEVATED TEMPERATURE INFLUENCE ON THE SHOT-PEENED SURFACE OF ALUMINUM ALLOY 5083

Authors: **Dražen Živković** Eng.D., Associate Professor, University of Split, Faculty of Electrical Engineering, Mechanical Engineering and Naval Architecture, Republic of Croatia
Boris Anzulović, Eng.D. Full Professor, University of Split, University Centre for Vocational Studies, Republic of Croatia
Boris Stipaničev, Mechanical Engineer, University of Split, Faculty of Electrical Engineering, Mechanical Engineering and Naval Architecture, Republic of Croatia

Sažetak: Ovaj rad bavi se utjecajem povišene temperature na kugličarenu površinu aluminijeve slitine AlMg4.5Mn. Kugličarenje rezultira povoljnijim stanjem naprezanja u površinskom sloju metala. Nakon izrade uzoraka, isti su izloženi različitim povišenim temperaturama. Po završetku toplinske obrade, na istim je provedena kontrola granice plastičnosti i vlačne čvrstoće. Rezultati dobiveni ispitivanjem ukazuju da povišena temperatura ima utjecaja na kugličareni metal, ali da temperature kojima su izloženi uzorci nisu u potpunosti poništile željeni efekt kugličarenja.

Ključne riječi: AlMg4.5Mn, kugličarenje, povišena temperatura.

Abstract: The paper deals with the elevated temperature influence on shot-peened surface of 5083 aluminium alloy. Shot-peening introduces the compressive stress in the surface layer of the metal, changing the resulting tensile residual stresses. After the specimen had been exposedto the elevated temperature, the yield and the tensile strength were tested. The test results indicate that elevated temperature treatment is significant on the shot-peened of AA 5083, although the positive effect of peening is not entirely gone.

Key words: AA 5083, shot peening, elevated temperature.

1. INTRODUCTION

Nowadays, the global development trends are more concentrated on the structures made from aluminum alloys. The increasing usage of Al-alloys is based upon the new technologies of treatment, good mechanical properties as well as on their excellent corrosion resistance.

In the modern engineering practice the majority of large aluminum structures are welded. The fatigue strength of welded structures follows the same general rules that apply to other types of fabricated assemblies. The fatigue strength is governed by the peak stresses at points of stress concentration rather than by nominal stresses. Anything that can be done to reduce peak stresses, by eliminating stress raiser will tend to increase the life of welded assemblies that are subjected to repeated loadings. Residual stresses in welded joints are obtained by local thermal expansion, plastic deformation and subsequent shrinkage on cooling. In the region near the weld (the heat affected zone), the resulting tensile residual stresses have a magnitude approaching the yield strength.

Welding stresses significantly reduce the fatigue strength of aluminium alloy welds, particularly butt welds. As the heat treatments to relieve these stresses are impractical for many of large welded assemblies, shot-peening can and should be considered as an alternate method of improving the fatigue strength.

In one of the previous papers [1] it was pointed out that shot-peening is the most acceptable treatment for increasing the fatigue life of aluminium welded joints, especially in the case of hot crater crack appearance.

According to the literature [2], the elevated temperature exposure of aluminium alloys, prolonged heating and temperature cycling, leads to the significant changes of yield and ultimate tensile strength. For the alloys of the *5xxx* series, those with magnesium contents greater than *3,0 wt%,* such as *5083,* contain a continuous film of anodic Al_2Mg_3 along the grain boundaries rather than in a solid solution within the grains (*Hatch, 1984*) [3]. This decreases the toughness, the ability of a material to withstand an impact, by making the alloy brittle. The most detrimental precipitates form at room temperature in heavily cold worked material. Those precipitates form over a number of years, or after prolonged exposure to slightly elevated temperatures of 65^oC to 180^oC like those found near the engine and exhaust system of ship. So, this paper deals with the elevated temperature influence on the shot-peened surface of *5083* aluminium alloy. The *AA 5xxx* series are the most resistant and most widely used because of their favourable strength and good weldability.

2. SHOT-PEENING

The fatigue strength of aluminum alloy welds can be increased by the cold working of high velocity stream of shot media upon the exposed surface layers of metallic parts under the controlled conditions [4, 5]. When individual particles of shot in the high velocity stream contact the metal surface, they produce slightly rounded depressions in the surface. The metal beneath this first layer is not plastically deformed. The stress distribution that has developed in the metal surface, has induced residual compressive stress parallel to the surface, while the metal beneath has reaction - induced tensile stress.

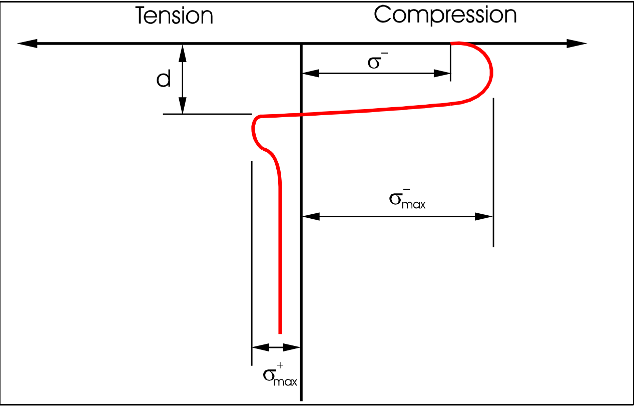

σ^- - *The surface compressive stress,*

$\sigma^-_{\mathbf{max}}$ - *The maximum compressive stress (usually found slightly below the surface – often taken to be 25% of the thickness),*

d - *The depth at which the residual stress becomes negative,*

$\sigma^+_{\mathbf{max}}$ - *The maximum tensile stress*

Figure 1. "Characteristic residual stress profile created by shot-peening"

3. MATERIAL AND TREATMENT

3.1. Material

The specimens were made from *5083* Al-alloy plate. This alloy is usually used as marine material, because of its excellent corrosion resistance in the sea water. Also it has good mechanical properties (*R_m is from 275 to 310 MPa, $R_{0,2}$ is about 200 MPa*) [6]. The testing of the tensile strength was provided in the *Laboratory for Mechanical Testing (LMT), Department for Materials, Faculty of Mechanical Engineering and Naval Architecture, University of Zagreb – Republic of Croatia.* The testing results were: *R_m = 280 MPa, $R_{0,2}$ = 196 MPa.*

The chemical composition of specimen metal is given in *Table 1.*

Table 1. "Chemical composition"

Specimen material	***Chemical element (wt %)***							
	Cr	***Cu***	***Fe***	***Mg***	***Mn***	***Si***	***Ti***	***Zn***
5083	0,11	0,02	0,38	4,75	0,58	0,17	0,021	0,01

The table shows the weight percentage of alloying elements, and the rest is aluminum. This chemical composition control is provided by the *Laboratory for Chemical Analysis – "Aluminum Industry" - Šibenik (Croatia).*

3.2. Specimen shape

The strips from the 5083 alloy sheet were cut out. The strips were *35 mm* wide and *210 mm* long. After milling, the additional rasping of the specimen edges was carried out. The shape and dimensions of the specimen were defined towards possibilities of the test machine, and are shown on *Fig. 2.*

According to the *Central Composite Plan (CCP)* thirteen (13) specimens for the experimental work were conducted. All the specimens had been shot-peened and exposed to the elevated temperatures. Figure *4* shows the specimen shape and dimensions.

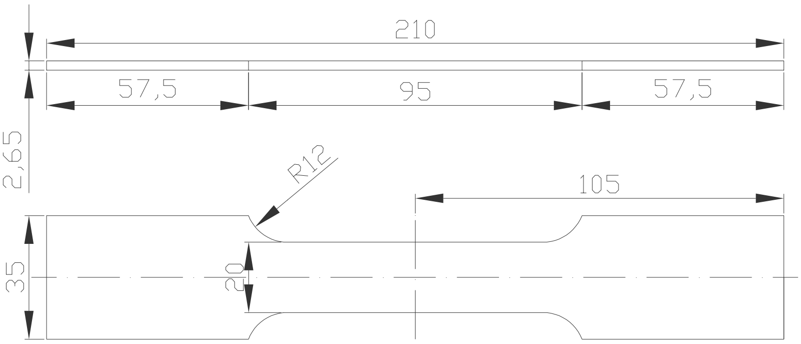

Figure 2. "The specimen shape and dimensions"

3.3. Shot-peening

The 13 specimens had been shot-peened from the both sides by *Almen* intensity of *1,0 N2.* The shot impact angle was 90^o. The shot-peening parameters were defined according to the norms SAE J422/J433, and are shown in *Table 2.*

Table 2. "The shot-peening parameters"

The air pressure at the nozzle input	*4 bars*
The distance form nozzle to specimen surface	*90 mm*
The impact angle	90^0
The time of shot exposure	*60 seconds*
The media type	*S 390**
The obtained surface coverage	*96%*

**Manufacturer "Wheelabrator Corporation"*

Figure 3. "The shot-peened specimen surface"

3.4. Elevated temperature exposure

The second level equation of *CCP* needs two input parameters. So, for this purpose the temperature and time were chosen as variables. The yield strength and the tensile strength were observed as output results.

There were three chosen basic temperatures: 70^o *C*, 100^o *C* and 130^o *C*. The additional two temperatures *(*58^o *C* and 142^o *C)* were calculated according to the *CCP.* Similarly there were three expose time periods chosen: *20, 40* and *60 minutes.* The additional two time periods *(12* and *68 min.)* were calculated according to the *CCP.* The input parameters are shown in the *Table 3.*

Table 3. "Input parameters CCP"

INPUT VARIABLES	TEMPERATURE X_1 (^oC)	TIME PERIOD X_2 *(minutes)*
minimum (-1)	*70*	*20*
medium (0)	*100*	*40*
maximum (1)	*130*	*60*
$X^{1,2}$ *kod (-1,414)*	*58*	*12*
$X^{1,2}$ *kod (1,414)*	*142*	*68*

The shot-peened specimens were treated according to the parameters shown in table *4*.

Table 4. "Treated specimens"

The number of specimens	***Temperature*** ***(^oC)***	***Time exposure (min)***
4	*70*	*20*
	70	*60*
	130	*20*
	130	*60*
4	*58*	*40*
	142	*40*
	100	*12*
	100	*68*
5	*100*	*40*
	100	*40*
	100	*40*
	100	*40*
	100	*40*

4. TENSILE TESTING

The tensile strength tests were conducted in the *Laboratory for Mechanical Testing* in the *"Aluminum Industry" - Šibenik*. The tensile testing machine was *60 kN* measuring range, and it is shown on the *Figure 4*.

Thirteen peened and heated specimens were tested. Additional two specimens were also tested. One of them was only shoot-peened, and the other was completely untreated. The tensile test results are given in the *Table 5*.

Figure 4. "The Tensile Testing Machine"[1]

Table 5. "Tensile test results"

Treatment	Specimen number	Cross section A [mm²]	Temp. T [°C]	Time exposure t [min]	Yield strength $R_{0,2}$ [MPa]	Tensile strengrh R_m [MPa]	Strain [%]
U	B	52,48	room	/	154	310	28
P	0	55,33	room	/	192	309	20
P+H	1	52,22	70	20	180	309	23
P+H	2	53,53	70	60	172	307	20
P+H	3	54,15	130	20	168	307	26
P+H	4	54,11	130	60	170	306	25
P+H	5	54,81	58	40	172	307	25
P+H	6	54,52	142	40	166	305	24
P+H	7	54,60	100	12	169	310	24
P+H	8	54,99	100	68	180	310	25
P+H	9	54,44	100	40	177	309	24
P+H	10	54,82	100	40	167	307	24
P+H	11	52,54	100	40	173	311	24
P+H	12	53,41	100	40	181	309	23,6
P+H	13	53,75	100	40	172	307	23

B – the basic metal, P – shot-peened, H – heated, U - untreated

5. RESULT ANALYSIS

The yield strength results indicate significant differences between the shot-peened specimens and specimens that were additionally thermal treated. By the second level *CCP* the test results are mathematically analyzed and associated with two input variables (temperature and exposure time). The shot-peened specimen has nearly *40 MPa* higher yield strength compared with the unpeened specimen. The plots of interaction between yield strength, temperature and exposure time is shown on *Figure 5.*

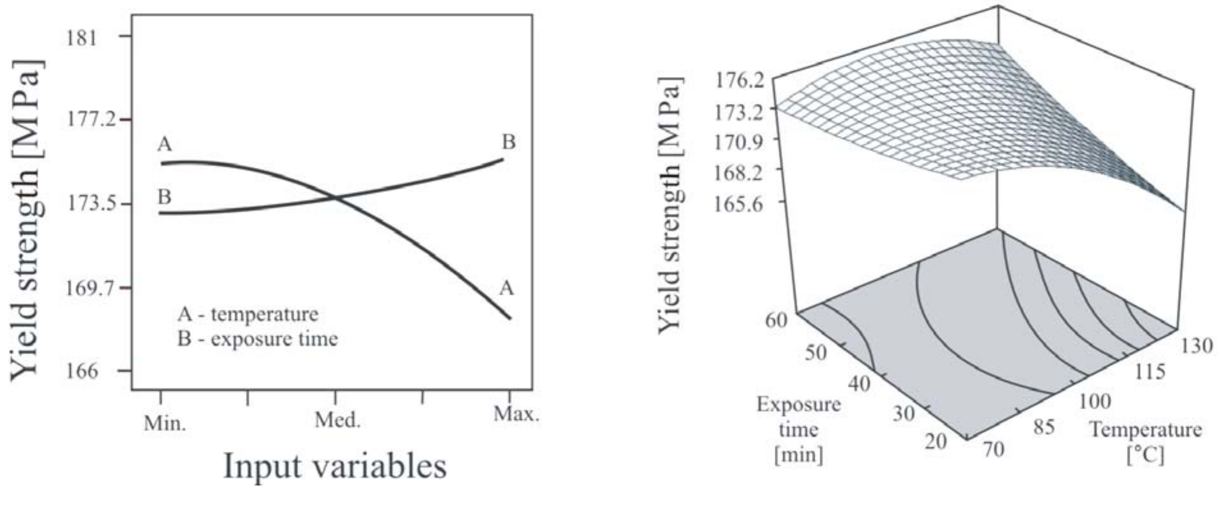

Figure 5. "2D and 3D plots of yield strength, temperature and exposure time"

Additional thermal treatment decreased the yield strength of the specimen, but it is also obvious that thermal treatment had not set aside all shot-peened effects. The most significant effect of elevated temperature is registered with the specimen that was *40* minutes exposed to temperature of *142°C*. But, in this case also the benefits of shot-peening are not entirely gone.

The tensile strength results indicate that there are no significant effects caused by shot-peening and elevated temperature on *AA 5083* test specimens. By *CCP* the obtained results are calculated and plotted on *Figure 6.*

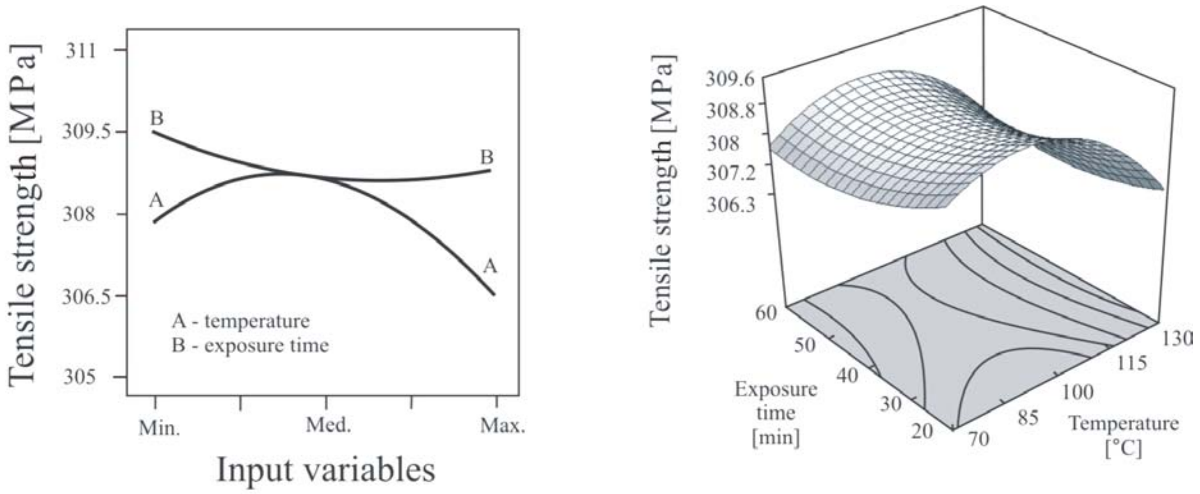

Figure 6. "2D and 3D plots of tensile strength, temperature and exposure time"

6. CONCLUSION

The goal of this work was the analysis of the mechanical properties of the shot-peened *AA 5083* specimen*,* after it had been exposed to the elevated temperatures. At the end of experimental work and result analysis, it may be concluded:

- although the deformation of the specimen is in the elastic area, shot-peening significantly affects the yield strength of *AA 5083;*
- the exposure to the elevated temperature decreased the yield strength of shot-peened *AA 5083,* but it had not set aside all shot-peened effects;
- shot-peening and elevated temperature exposure had not affected the tensile strength of *AA 5083* specimens. Achieved deformations, during tensile test, were in the plastic area, so the advantageous effects of shot-peening had entirely gone.

7. LITERATURE

1. Živković, D., Anzulović, B., ***The influence of shot-peening intensity on fatigue behavior of aluminum alloy welds with crater hot-crack,*** Conference on Materials, Processes, Friction and Wear (MATRIB), 2002, Vela Luka, Croatia, (p. 253 – 259).
2. Brown, S. (1999), ***Feasibility of Replacing Structural Steel with Aluminium Alloys in the Shipbuilding Industry,*** University of Wisconsin at Madison, (p. 1-15). www.elvis.engr.wisc.edu:16080/UER/uer99/author1/content.html
3. Kent, R.K., Baggerly, R. (2000), MDE Engineers, Inc., *Intergranular Corrosion, (p.*777-785).
4. Delić, D. (2004), ***Utjecaj mora na kugličarenu aluminijevu slitinu AlMg4.5Mn,*** Diplomski rad, Fakultet elektrotehnike, strojarstva i brodogradnje, Sveučilište u Splitu.
5. Živković, D. (1999), ***Utjecaj toplinskih pukotina i kugličarenja na dinamičku izdržljivost zavarenih aluminijskih konstrukcija,*** doktorska disertacija, Fakultet elektrotehnike, strojarstva i brodogradnje, Sveučilište u Splitu.
6. www.aluminium.matter.org.uk/aluselect/

institute of materials & machine mechanics

slovak academy of sciences

Address:	Racianska 75 831 02 Bratislava 3 Slovakia
Tel.:	+ 421 – 2 – 44 25 47 51
Fax:	+ 421 – 2 – 44 25 33 01
E-mail:	ummssekr@savba.sk

http://www.umms.sav.sk

Research activities

Advanced materials

- metal matrix composites
- metallic foams
- intermetallics
- nanostructured materials
- coatings

Technologies

- pressure infiltration
- foaming of aluminium and zinc alloys
- hot and cold isostatic pressing
- powder metallurgy
- directional solidification
- Equal Channel Angular Pressing
- vacuum hot pressing
- thermal spraying (plasma, gas)
- magnesium recycling
- vacuum deposition
- PVD, CVD, electrolytic coatings

Structural analysis

- electron microscopy, SEM, TEM
- EDX-microanalysis
- light microscopy, microhardness measurement
- metallography, ion milling, etching
- X-ray analysis, diffraction
- DTA, thermogravimetry
- mass spectroscopy
- surface tension

Testing of properties

- mechanical properties (tension, compresion, bending, torsion)
- fatigue
- creep
- wear (adhesion, abrasion)
- surface roughness measurement
- acoustic emission
- thermal and electrical conductivity

Mechanics

- vibration and noise control
- fatigue endurance of materials and structures
- static and dynamic stress analysis

Published scientific journals

Strojnícky časopis
JOURNAL OF MECHANICAL ENGINEERING

KOMAAW
KOVOVÉ MATERIÁLY
METALLIC MATERIALS

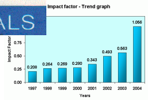

Centre of excellence SAS

- Centre of nanocrystalline materials (NANOSMART)

Centre of SAS - MULTIDISK

Common utilisation of expensive equipments for research of nanocrystalline materials

NanoSci-ERA

- Nanoscience in the European Research Area

Coordination action of 6th FP EU
(15 partners from 11 European countries)

Research achievements

Heat sinks based on copper matrix composites

- copper matrix composites reinforced by tungsten wires developed for application in fusion reactor ITER

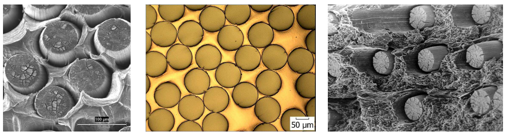

Composite material W-fibre / Cu-matrix

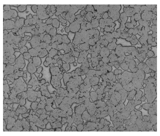

W-particles infiltrated by Cu

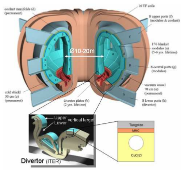

Fusion reactor ITER

- composite materials based on highly graphitised carbon fibres embedded in copper matrix for use in applications, where extreme heat fluxes combined with tailored CTE are the main requirements (heat sink materials for electronic devices)

Under development within the Integrated Project of 6th FP EU ExtreMat
New Materials for Extreme Environments
(38 partners from 11 European countries)

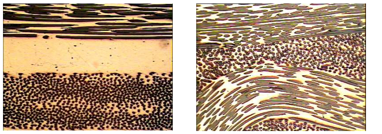

Cu-matrix / C-fibre composite made by diffusion bonding of copper coated continuous carbon fibres

Woven fabrics made from Cu-coated C-fibres

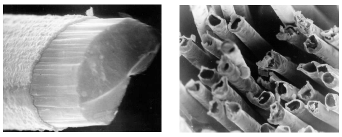

Copper coated C-fibres

Intermetallic alloys

Ti-Al based intermetallic alloys with improved creep resistance up to 1000°C and substantial weight reduction in comparison with Ni-based superalloys applicable for turbine and compressor blades, vane support rings, automotive exhaust valves, turbocharger wheels etc.

Under development within the Integrated Project of 6th FP EU: IMPRESS
Intermetallic Materials Processing in Relation to Earth and Space Solidification
(45 partners from 15 European countries)

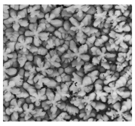

Ti-Al based intermetallic alloy

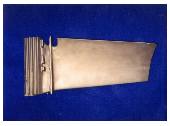

Turbine blade made from Ti-Al based intermetallic alloy

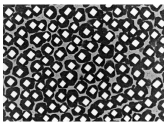

Intermetallic alloy Ni_3Al

Aluminium foams

- PM prepared Al foams (co-operation with **Alulight** GmbH Ranshofen, Austria)

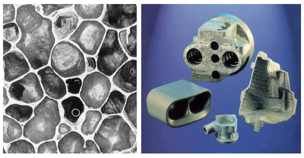

Complex-shaped castings

Panels, plates and sandwiches

Reinforced Al foam profile

Stiffener of suspension part

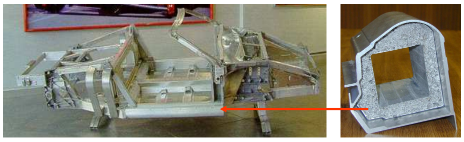

Hollow car frame Ferrari with aluminium foam stiffener

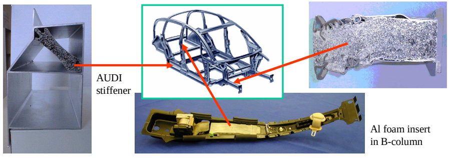

- **ALPORAS** foams
(co-operation with Gleich GmbH Kaltenkirchen, Germany)

Marble floor panel heated by Al foam heater

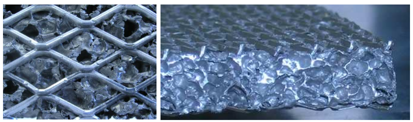

ALPORAS foams reinforced by expanded Al sheet

Foam cored casting

Graphite infiltrated by copper or antimony

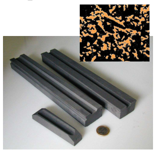

Graphite infiltrated by copper
Electrical sliding contacts for electric trains and trolleybuses
Cooperation with Elektrokarbon Topoľčany, Slovakia

Graphite infiltrated by antimony
Rotary sealing rings

Autoclave for gas pressure infiltration

- max. temperature 1300°C
- max. pressure 10 MPa
- max. size of infiltrated sample: Ø 240 mm × 400 mm

Plasma prayed coatings

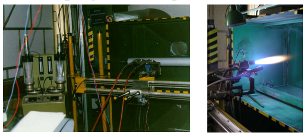

Equipment for plasma spraying of metallic and ceramic coatings

Plasma sprayed Al_2O_3 + TiO_2 coating with increased wear resistance for textile industry

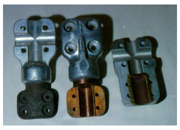

Plasma sprayed contact coating with improved electroconductivity

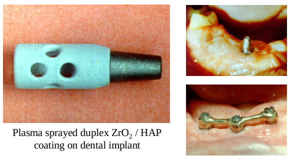

Plasma sprayed duplex ZrO_2 / HAP coating on dental implant

Metal matrix composites for structural applications

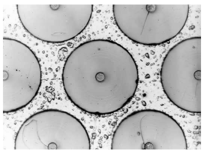

Composite Al-matrix / continuous boron fibres made by diffusion bonding of imprinted monolayers

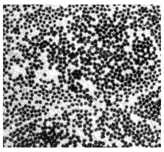

Mg-Li-matrix / continuous carbon fibres

	Al / B	Mg-Li / C
Density:	2.65 g/cm³	1.64 g/cm³
Longitudinal Young`s modulus:	245 GPa	80 GPa
Strength:	1178 MPa	680 MPa

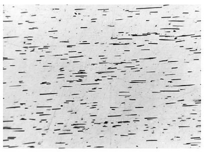

Short C-fibre /Al-matrix composite made by hot extrusion of powder mixture

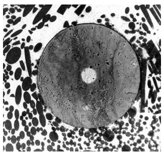

MgLi-matrix / TiB_2 and Saffil fibres

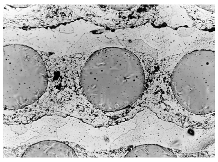

Al-matrix / Maraging wire composite made by diffusion bonding of plasma sprayed monolayers

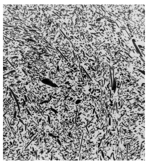

MgLi-matrix / Saffil fibres prepared by pressure infiltration

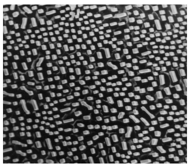

Composite Ni-Al-Mo-X prepared by directional solidification

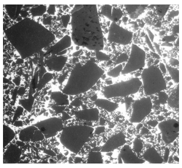

Al-matrix composite reinforced with Al_2O_3 particles prepared by pressure infiltration

Aluminium alloys prepared by PM

Automotive component made by hot extrusion of Al alloy powder (Camphasing Adjusment System produced by SAPA Profily a.s. for BMW)

Nanostructured high strength aluminium profiles

"bottom-up" approach - to tailor desired properties on nano-scale level followed by non-degrading consolidation procedures

RS, Melt-spinning — Cryogenic chopping — Compaction by hot extrusion

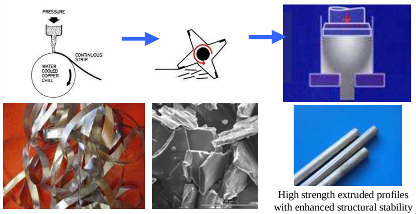

Melt-spun ribbons

Cryo-chopped flakes

High strength extruded profiles with enhanced structural stability at high temperatures